

UNIVERSITÀ VITA-SALUTE SAN RAFFAELE

**CORSO DI DOTTORATO DI RICERCA INTERNAZIONALE
IN MEDICINA MOLECOLARE**
Curriculum in Neuroscienze e Neurologia Sperimentale

**TRACKING AND PREDICTING
NEURODEGENERATION SPREADING IN
SPORADIC AND GENETIC
PRESENTATIONS OF THE ALS/FTD
CONTINUUM**

DoS: Prof.ssa Federica Agosta
Second Supervisor: Prof. Martin Turner

Tesi di DOTTORATO DI RICERCA di Edoardo Gioele Spinelli
Matr. 013831
Ciclo di Dottorato XXXIV
SSD MED/26

Anno Accademico 2020/2021

Federica Agosta

CONSULTAZIONE TESI DI DOTTORATO DI RICERCA

Il/la sottoscritto/I SPINELLI EDOARDO GIOELE

Matricola / *registration*
number 013831

natA_ a/ *born at* MILANO (MI)

il/ *on* 19/12/1987

autore della tesi di Dottorato di ricerca dal titolo / *author of the PhD Thesis entitled*

TRACKING AND PREDICTING NEURODEGENERATION SPREADING IN

SPORADIC AND GENETIC PRESENTATIONS OF THE ALS/FTD CONTINUUM

- AUTORIZZA la Consultazione della tesi / *AUTHORIZES the Consultation of the thesis*
- NON AUTORIZZA la Consultazione della tesi per 12 mesi /*DOES NOT AUTHORIZE the Consultation of the thesis for 12 months*

a partire dalla data di conseguimento del titolo e precisamente /*from the PhD thesis date, specifically*

Dal / *from*/...../..... Al / *to*/...../.....

Poiché /*because*:

l'intera ricerca o parti di essa sono potenzialmente soggette a brevettabilità/ *The whole project or part of it might be subject to patentability;*

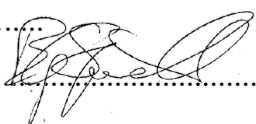
ci sono parti di tesi che sono già state sottoposte a un editore o sono in attesa di pubblicazione/ *Parts of the thesis have already been submitted to a publisher or are in press;*

la tesi è finanziata da enti esterni che vantano dei diritti su di esse e sulla loro pubblicazione/ *the thesis project is financed by external bodies that have rights over it and on its publication.*

Si rende noto che parti della tesi sono indisponibili in relazione all'utilizzo di dati tutelati da segreto industriale **(da lasciare solo se applicabile)** /*Please Note: some parts of the thesis are not available in relation to the norm of the use of information protected by trade secret (To leave only if applicable)*

E' fatto divieto di riprodurre, in tutto o in parte, quanto in essa contenuto / *It is not allowed to copy, in whole or in part, the data and the contents of the thesis*

Data /Date 31/01/2022

Firma/Signature..........

DECLARATION

This thesis has been composed by myself and has not been used in any previous application for a degree. Throughout the text I use both 'I' and 'We' interchangeably.

All the results presented here were obtained by myself, except for:

- 1) Agosta et al., *Eur J Neurol.* 2019; Spinelli et al., *Hum Brain Mapp.* 2019; Spinelli et al., *Neuroimage Clin.* 2020; Basaia et al., *Neurology* 2020; Canu et al., *Neurology* 2020; Cividini et al., *Neurology* 2021; Spinelli et al., *Neurology* 2021; and the preliminary study reported in Chapter 4.2. Patient recruitment has been performed by Dr. Riva, Dr. Magnani and collaborators, Department of Neurology; genetic analysis by Dr. Riva and collaborators; and the MRI acquisition by Prof. Falini and collaborators, Department of Neuroradiology, San Raffaele Scientific Institute, Vita-Salute San Raffaele University, Milan, Italy.

- 2) Spinelli et al., *Hum Brain Mapp.* 2019; Basaia et al., *Neurology* 2020; Spinelli et al., *Neurology* 2020; and the preliminary study reported in Chapter 4.2. Contribution to patient recruitment and genetic analysis has been performed by Prof. V. Silani and collaborators, Department of Neurology and Laboratory of Neuroscience, IRCCS Istituto Auxologico Italiano, Milan, Italy; Prof. A. Chiò and collaborators, Rita Levi Montalcini Department of Neuroscience, ALS Center, University of Turin, Turin, Italy; Dr. P. Caroppo and collaborators, Fondazione IRCCS Istituto Neurologico Carlo Besta, Unit of Neurology 5 - Neuropathology, Milan, Italy; Dr. L. Tremolizzo and collaborators, Neurology Unit, "San Gerardo" Hospital and University of Milano-Bicocca, Monza, Italy; Prof. G. Sorarù and collaborators, Department of Neuroscience, University of Padova, Padova, Italy; Dr. Francesca Trojsi and collaborators, Università degli Studi della Campania "Luigi Vanvitelli", Naples, Italy.

- 3) Canu et al., *Neurology* 2020. Contribution to patient recruitment and MRI acquisition has been performed by Prof. Gorno-Tempini and collaborators, Memory and Aging Center, University of California, San Francisco, California, USA.

4) Preliminary study reported in Chapter 4.2. Contribution to patient recruitment has been performed by Dr. K. Josephs and collaborators, Department of Neurology, Mayo Clinic, Rochester, Minnesota, USA; and MRI acquisition by Dr. J. Whitwell and collaborators, Department of Radiology, Mayo Clinic, Rochester, Minnesota, USA.

All the studies reported here, except for Chapter 4.2., have been published (Agosta et al., *Eur J Neurol.* 2019; Spinelli et al., *Hum Brain Mapp.* 2019; Spinelli et al., *Neuroimage Clin.* 2020; Basaia et al., *Neurology* 2020; Canu et al., *Neurology* 2020; Cividini et al., *Neurology* 2021; Spinelli et al., *Neurology* 2021).

The studies reported in Basaia et al., *Neurology* 2020 and Cividini et al., *Neurology* 2021 are the results of a joint effort with Dr Camilla Cividini, another PhD candidate at University Vita-Salute San Raffaele. Although study design and manuscript drafting were performed by both candidates, Dr Cividini (bioengineer) was mostly focused on developing and performing MRI post-processing and statistical analysis, whereas I gave my contribution as a neurologist for data acquisition and analysis and critical interpretation of results in a clinical context.

All sources of information are acknowledged by means of reference.

ACKNOWLEDGMENTS

These three years of PhD have been for me a very intense period of learning and development, both personally and professionally, despite the COVID pandemic and its consequences. First of all, I would like to thank all the people that have supported and helped me through all these years.

I would like to express my sincere gratitude to Prof. Massimo Filippi for giving me the opportunity to attend a PhD program in his laboratory and for his precious guidance during these years, both in the clinical and in the research fields.

A special thanks goes to Prof. Federica Agosta, who trusted and encouraged me in several occasions, giving me many opportunities throughout these years of close collaboration. Her support, guidance and insightful comments have been extremely helpful to become, one day at a time, a true physician scientist.

I thank Prof. Martin Turner for his supervision and interest to my PhD project.

I thank Prof. Andrea Falini and his team for their precious collaboration.

I thank Dr. Riva, Dr. Magnani, Dr. Caso and all external collaborators for their fundamental contribution for the accomplishment of the studies reported in this dissertation.

My special thanks to each of my colleagues and friends at the Neuroimaging Research Unit. Thanks to my PhD companions Camilla and Veronica, for the reciprocal help and for sharing the moments of anxiety. Thanks to Silvia, Elisabetta, Elisa, Michela, Gigi, Etta, Gardo, Giordano, Giulia, Massimo, Davide, Alma, Pietro, Noemi and all the people who dedicated their efforts to create such a good working environment and made these years so much fun.

Thanks to my family, for their continued support and encouragement throughout all my (27!) years of education. Thanks to Alessandro, for being the most unexpected surprise, right when the world was turned upside down.

*The scientist is not a person who gives the right answers,
he is one who asks the right questions.*

Claude Lévi-Strauss
The Raw and the Cooked (1964)

ABSTRACT

Neurodegenerative diseases are associated with the accumulation of toxic proteins in the human brain. A growing body of evidence suggests that such proteins can propagate in the brain in a prion-like fashion through the connections between neurons. The most recent evidence suggest that the clinical picture of each neurodegenerative disease might largely depend on the damage of the anatomical pathways connecting the different regions of the brain. Magnetic resonance imaging (MRI) advanced techniques, particularly diffusion tensor (DT) imaging and resting state functional MRI (RS-fMRI), allow exploring the role of network alterations in these disorders.

In this dissertation, I explored network connectivity alterations in the wide spectrum of clinical presentations due to frontotemporal lobar degeneration (FTLD), including not only a range of purely cognitive disorders (i.e., frontotemporal dementia [FTD] variants), but also motor neuron disease (MND), such as amyotrophic lateral sclerosis (ALS). The overlap between ALS and FTD has been suggested not only by the presence of mixed clinical presentations, but also by common pathological and genetic determinants. In the studies here reported, volumetric techniques, DT MRI, RS-fMRI and novel connectomic approaches were employed to explore converging and diverging brain network signatures across the ALS/FTD continuum.

The analysis of grey matter volumes and white matter DT MRI alterations in patients with MND revealed useful structural MRI markers of motor and cognitive progression, as well as prognostic indicators of a subsequent benign or aggressive disease course, which might be used to predict time to the development of clinical milestones. Moreover, a combined analysis of structural and functional connectomics showed extensive network reorganization both in motor and extra-motor brain regions of MND patients. When examining in detail cognitive FTD phenotypes, for each variant, we showed characteristic volumetric MRI signatures and patterns of functional network reorganization propagating from the corresponding disease epicenter. Finally, we provided further evidence supporting the notion of a continuum across FTD and MND, both in sporadic and in genetic presentations of FTLD.

Taken together, our studies suggest that the assessment of network connectivity in the ALS/FTD spectrum is useful in improving our understanding of the mechanisms that link protein deposition and consequent neuronal damage to motor and cognitive symptoms in

these patients. A more profound knowledge of such mechanisms will allow a better stratification of patients and an improved prognostic definition that will be vital in future clinical trials with disease modifying drugs.

TABLE OF CONTENTS

1. GENERAL INTRODUCTION.....	5
1.1. THE SPECTRUM OF FRONTOTEMPORAL LOBAR DEGENERATION.....	5
1.1.1. <i>Epidemiology</i>	6
1.1.2. <i>Clinical presentations of the ALS/FTD continuum</i>	7
a. Behavioral variant of frontotemporal dementia (bvFTD).....	7
b. Primary progressive aphasia (PPA)	10
c. Motor neuron disease (MND).....	15
1.1.3. <i>Neuropathology</i>	17
1.1.4. <i>Genetics</i>	20
1.1.5. <i>Neuroimaging</i>	21
a. bvFTD	21
b. PPA	23
c. MND	25
1.1.6. <i>Treatment</i>	26
a. FTD presentations.....	26
b. MND	28
1.2. GENETIC FTL D: CHARACTERISTIC CLINICAL AND NEUROIMAGING FEATURES	29
1.2.1. <i>C9orf72</i>	29
1.2.2. <i>GRN</i>	31
1.2.3. <i>MAPT</i>	34
1.2.4. <i>Other mutations</i>	37
1.3. MRI ADVANCED TECHNIQUES: APPLICATIONS TO FTL D.....	39
1.3.1. <i>Structural volumetric MRI</i>	39
a. FTD presentations.....	39
b. MND	41
1.3.2. <i>Diffusion tensor MRI</i>	43
a. FTD presentations.....	43
b. MND	45
1.3.3. <i>Resting-state functional MRI</i>	46
a. FTD presentations.....	46
b. MND	47
1.3.4. <i>MRI connectomics</i>	48
a. FTD presentations.....	50
b. MND	51
2. AIMS OF THE WORK	90
3. NEUROIMAGING PROGRESSION MARKERS IN MOTOR NEURON DISEASE	93
3.1. SURVIVAL PREDICTION MODELS IN MOTOR NEURON DISEASE	93
3.2. BRAIN MRI SHOWS WHITE MATTER SPARING IN KENNEDY’S DISEASE AND SLOW-PROGRESSING LOWER MOTOR NEURON DISEASE	138
3.3. STRUCTURAL MRI OUTCOMES AND PREDICTORS OF DISEASE PROGRESSION IN AMYOTROPHIC LATERAL SCLEROSIS.....	165
3.4. STRUCTURAL AND FUNCTIONAL BRAIN CONNECTOME IN MOTOR NEURON DISEASES: A MULTICENTER MRI STUDY	200

4. TRACKING NEURODEGENERATION IN FRONTOTEMPORAL DEMENTIA VARIANTS	256
4.1. SPEECH PRODUCTION DIFFERENCES IN ENGLISH AND ITALIAN SPEAKERS WITH NON-FLUENT VARIANT PPA	256
4.2. FUNCTIONAL CONNECTIVITY REARRANGEMENTS PROPAGATING FROM DISEASE EPICENTERS IN FRONTOTEMPORAL LOBAR DEGENERATION VARIANTS	279
5. NEURODEGENERATION PATTERNS ACROSS THE ALS/FTD CONTINUUM	325
5.1. STRUCTURAL MRI SIGNATURES IN GENETIC PRESENTATIONS OF THE FRONTOTEMPORAL DEMENTIA/MOTOR NEURON DISEASE SPECTRUM	325
5.2. AMYOTROPHIC LATERAL SCLEROSIS-FRONTOTEMPORAL DEMENTIA: SHARED AND DIVERGENT NEURAL CORRELATES ACROSS THE CLINICAL SPECTRUM	385
6. GENERAL DISCUSSION	429
7. ADDITIONAL PUBLICATIONS	438

ACRONYMS AND ABBREVIATIONS

AD=Alzheimer's disease

ALS=Amyotrophic Lateral Sclerosis

axD= Axial Diffusivity

bvFTD=Behavioral Variant Of Frontotemporal Dementia

CBS=Corticobasal Syndrome

CNS=Central Nervous System

CSF=Cerebrospinal Fluid

CST=Corticospinal Tract

CT=Computed Tomography

C9orf72=Chromosome 9 Open Reading Frame 72

DMN=Default-Mode Network

DT=Diffusion Tensor

EEG=Electroencephalography

FBI=Frontal Behavior Inventory

fMRI=Functional Magnetic Resonance Imaging

FA=Fractional Anisotropy

FTD= Frontotemporal Dementia

FTLD=Frontotemporal Lobar Degeneration

FTLD-FUS=FTLD Associated With Fused In Sarcoma Protein Inclusions

FTLD-tau=FTLD Associated With Tauopathy

FTLD-TDP=FTLD Associated With TDP-43 Inclusions

FTLD-U=FTLD Associated With Ubiquitin Inclusions

FUS=Fused In Sarcoma

GM=Grey Matter

GRN=Granulin precursor (progranulin)

IFOF=Inferior Fronto-Occipital Fasciculus

ILF=Inferior Longitudinal Fasciculus

LMN=Lower Motor Neuron

lvPPA=Logopenic Variant of Primary Progressive Aphasia

MAPT=Microtubule Associated Protein Tau

MCI=Mild Cognitive Impairment
MD=Mean Diffusivity
MMSE=Mini Mental State Examination
MND=Motor Neuron Disease
MRI=Magnetic Resonance Imaging
NCI=Neuronal Cytoplasmic Inclusions
nfvPPA= Non-Fluent/agrammatic Variant of Primary Progressive Aphasia
PET=Positron Emission Tomography
PD=Parkinson's Disease
PiD=Pick's Disease
PLS=Primary Lateral Sclerosis
PMA=Progressive Muscular Atrophy
PPA=Primary Progressive Aphasia
PSP=Progressive Supranuclear Palsy
radD=Radial Diffusivity
ROI=Region Of Interest
RS=Resting State
SBM=Surface Based Morphometry
SN=Saliience Network
SvPPA=Semantic Variant of Primary Progressive Aphasia
SLF=Superior Longitudinal Fasciculus
SOD1=Superoxide Dismutase 1 Gene
TBK1=TANK Binding Kinase 1
TBSS=Tract-Based Spatial Statistics
TDP-43=TAR DNA-Binding Protein 43
UMN=Upper Motor Neuron
VBM=Voxel-Based Morphometry
WM=White Matter

1. GENERAL INTRODUCTION

1.1. The spectrum of Frontotemporal Lobar Degeneration

The term frontotemporal lobar degeneration (FTLD) encompasses a group of neurodegenerative disorders characterized by a predominant degeneration of the frontal and/or temporal lobes of the brain. The highly heterogeneous clinical, neuropathological and genetic characteristics of FTLD presentations complicate and often delay their diagnosis and make up the greatest challenge in the study of these diseases. As will be illustrated in this Introduction, FTLD can manifest with a very miscellaneous range of behavioral derangements (which can be easily misdiagnosed as psychiatric disorders and postpone by many years the correct diagnosis) and/or speech dysfunctions, which can be mainly distinguished into two variants: a behavioral variant of frontotemporal dementia (bvFTD); and a language variant, termed primary progressive aphasia (PPA). The latter, according to the characteristics of the speech impairment, can be further subclassified into non-fluent/agrammatic variant PPA (nfvPPA), semantic variant PPA (svPPA) and logopenic variant PPA (lvPPA). However, as will be better clarified in the following chapters, since lvPPA is mostly characterized by Alzheimer's disease (AD) pathology, this variant will not be addressed in this dissertation (Gorno-Tempini, Hillis et al., 2011).

Furthermore, some forms of FTLD overlap with or progress to full-blown motor neuron disease (MND), with amyotrophic lateral sclerosis (ALS) as the most common presentation. Increasing clinical, neuroimaging, genetic and neuropathologic evidence supports the concept that FTLD and ALS are overlapping multisystem disorders. While 10-15% of ALS cases fulfil criteria for bvFTD/PPA (collectively referred to as "frontotemporal dementia" [FTD]), features of MND appear in approximately 15% of FTD patients during the progression of the disease (Ling, Polymenidou et al., 2013). Neuroimaging studies in ALS have consistently reported extramotor cortical involvement in this disease and similarities in patterns of regional cortical volume loss have also been identified in cognitively intact ALS patients and those with ALS-FTD, providing further evidence of a neuroanatomic "continuum" between these two disorders (Ling et al., 2013). Converging evidences come from genetic studies as well. The hexanucleotide repeat expansion in C9orf72 is the most common mutation in inherited forms of ALS (40%) and FTD (25%), and in a significant number of sporadic ALS (5%–20%) and FTD

(6%) cases, and explains the majority of the overlap of these two conditions (Majounie, Renton et al., 2012). Moreover, mutations in the TARDBP gene have been found to be causative for both ALS and FTD (Lattante, Ciura et al., 2015), confirming the existence of shared susceptibility genes among these conditions.

In this context, the investigation of common genetic risk factors has enabled to partially unravel the role of altered cellular pathways, such as nucleocytoplasmic transport dysfunction, in the pathogenesis of these conditions (Jovicic, Paul et al., 2016). The overlap among ALS and FTD has been further confirmed by pathological studies, where hyperphosphorylated TDP-43 inclusions have been observed in neurons and glial cells of nearly half of bvFTD cases as well as the majority of ALS patients (Ferrari, Kapogiannis et al., 2011). In conclusion, a growing body of evidence challenges the traditional view of ALS as a pure motor disease. In particular, advances in neuroimaging, neuropathology and genetics have allowed to recognize ALS and FTD as part of a complex disease continuum instead of separate nosographic entities.

All the aforementioned features make the spectrum of FTLN a complex chapter in the field of neurodegenerative diseases, which demands, on one hand, a multimodal approach to achieve an accurate diagnosis, and, on the other hand, a multidisciplinary team for the management of affected patients. In an era in which no effective disease-modifying treatment has yet been approved for FTLN presentations, neuroimaging plays a fundamental role in picking up the correct diagnosis among the magnitude of differentials, in following disease progression longitudinally, and in providing useful biomarkers to be possibly employed in clinical trials. All these aspects will be elucidated in the present Introduction.

1.1.1. Epidemiology

In patients younger than 65 years, FTLN is the second most common cause of neurodegenerative dementia after Alzheimer's disease (AD), accounting for 10.2% of cases (Van Mossevelde, Engelborghs et al., 2018). Overall, estimates of the prevalence of FTLN reach 461 cases per 100,000 individuals (Hogan, Jette et al., 2016). The incidence of FTLN is estimated to range from 1.6 to 4.1 new cases per 100,000 individuals annually (Coyle-Gilchrist, Dick et al., 2016, Knopman & Roberts, 2011). Age of onset typically varies between 45 and 65 years, but patients aged 30 or older than 65

have been reported in the literature as well (Snowden, Neary et al., 2004) so that individuals with an age outside the aforementioned range should not be excluded a priori for a diagnosis of FTLD, even though psychiatric diseases can be encountered more frequently in younger patients and other types of dementia (i.e. AD, vascular dementia) are more common in the elderly.

A systematic review of 26 studies on FTLD prevalence highlighted that men and women are equally affected (Hogan et al., 2016). When disease subtypes are stratified and the prevalence of each variant is analyzed, 60% of patients have bvFTD, whereas language variants account for the remaining 40% (Onyike & Diehl-Schmid, 2013).

FTLD is likely underdiagnosed among non-neurologists, since its symptoms can be easily mistaken for psychiatric manifestations. Therefore, these data should be carefully considered in light of a possible underestimation.

1.1.2. Clinical presentations of the ALS/FTD continuum

As previously stated, one of the main peculiarities of FTLD is the wide range of clinical presentations that can be associated with the pathognomonic frontotemporal atrophy. Here below, the different clinical variants of this pathological continuum will be addressed in detail.

a. Behavioral variant of frontotemporal dementia (bvFTD)

Patients affected by the behavioral variant of frontotemporal dementia show a progressive decline in their social skills, planning and higher-level thinking, which are mainly secondary to executive dysfunction and changes in behavior.

Other cognitive areas such as episodic memory and visuospatial functions are generally preserved, at least in the early stages of the disease (Woollacott & Rohrer, 2016). Patients usually lack insight of their symptomatology and show indifference or annoyance when brought to medical attention. Indeed, in the majority of cases it is relatives, friends or coworkers who report a problem and encourage the patient to seek medical attention. The majority of initial complaints regards odd behaviors or increasingly poor performances at work. Indeed, people who are closest to the patient report interpersonal and social dysfunctions rather than true memory issues (differently from what patients affected by AD or mild cognitive impairment, i.e. MCI, usually

complain). Nonetheless, sometimes patients may report ‘poor memory’, which almost inevitably can lead to a misdiagnosis of AD or stress-related issues or depression, especially when evaluated by non-specialist medical personnel or diagnostic work-up is not backed by imaging support. Generally speaking, this is avoided by a careful anamnestic background, especially of the accompanying relative, which will reveal the true nature of the cognitive issues, which may be erroneously perceived as memory impairment by the patient himself.

As already mentioned, the diagnosis of bvFTD remains quite challenging: in many cases it can be simply missed and patients dismissed as ‘normal’, while others might actually be misdiagnosed (the most common misdiagnoses being AD and psychiatric pathologies)

(Mendez, Shapira et al., 2007b). Henceforth, early and accurate diagnosis of bvFTD plays a fundamental role and has implications at different levels, including heritability (Baker, Mackenzie et al., 2006, Kumar-Singh & Van Broeckhoven, 2007), prognosis (Chow, Hynan et al., 2006, Rascovsky, Salmon et al., 2005), therapeutics (Ljubenkov & Boxer, 2021) and environmental management of patients (Shinagawa, Nakajima et al., 2015).

The most recent diagnostic criteria for bvFTD (Rascovsky, Hodges et al., 2011) were developed in 2011 by the Frontotemporal Dementia Consortium (FTDC). They replaced the already existing consensus criteria published in 1998 (Neary, Snowden et al., 1998), which notwithstanding their clinical utility had shown, in time, some limitations such as the ambiguity of behavioral descriptors and inflexibility in their application. The novel criteria finally clarified the key features of behavioral changes that can be assessed in those patients, while recognizing that other types of cognitive impairment, such as episodic memory loss, can be affected albeit less commonly. Revised criteria divide the diagnosis of bvFTD into ‘*possible bvFTD*’, ‘*probable bvFTD*’ and ‘*bvFTD with definite frontotemporal lobar degeneration*’.

According to these internationally validated criteria, patients with *possible bvFTD* require three out of six clinically discriminating features, which include disinhibition, apathy/inertia, loss of sympathy/empathy, perseverative/compulsive behaviors, hyperorality and dysexecutive neuropsychological profile. For patients to be categorized as having a *probable* form of bvFTD instead, functional disability and characteristic

neuroimaging data must be present too. Eventually, the presence of histopathological confirmation or, alternatively, of a mutation, makes up the diagnosis of *definite* bvFTD.

Current criteria are listed in the following table (Rascovsky et al., 2011):

Behavioural variant of Fronto Temporal Dementia
To meet criteria for bvFTD the patient must show progressive deterioration of behaviour and/or cognition by observation or history (as provided by a knowledgeable informant).
<i>II. Possible bvFTD</i>
Three of the following behavioural/cognitive symptoms (A–F) must be present to meet criteria. Ascertainment requires that symptoms be persistent or recurrent, rather than single or rare events.
A. At least one of the following early behavioural disinhibition’s signs: <ul style="list-style-type: none"> A.1. Socially inappropriate behaviour A.2. Loss of manners or decorum A.3. Impulsive, rash or careless actions
B. At least one of the following early signs apathy or inertia: <ul style="list-style-type: none"> B.1. Apathy B.2. Inertia
C. At least one of these early signs of loss of sympathy or empathy: <ul style="list-style-type: none"> C.1. Diminished response to other people’s needs and feelings C.2. Diminished social interest, interrelatedness or personal warmth
D. At least one of these early perseverative, stereotyped or compulsive/ritualistic behaviour signs <ul style="list-style-type: none"> D.1. Simple repetitive movements D.2. Complex, compulsive or ritualistic behaviours D.3. Stereotypy of speech
E. At least one of the following hyperorality and dietary changes: <ul style="list-style-type: none"> E.1. Altered food preferences E.2. Binge eating, increased consumption of alcohol or cigarettes E.3. Oral exploration or consumption of inedible objects
F. Neuropsychological profile: executive/generation deficits with relative sparing of memory and visuospatial functions <ul style="list-style-type: none"> F.1. Deficits in executive tasks F.2. Relative sparing of episodic memory F.3. Relative sparing of visuospatial skills
<i>III. Probable bvFTD</i>
All of the following symptoms (A–C) must be present to meet criteria.
A. Meets criteria for possible bvFTD
B. Exhibits significant functional decline (by caregiver report or as evidenced by Clinical Dementia Rating Scale or Functional Activities Questionnaire scores)
C. At least one of the following imaging results consistent with bvFTD: <ul style="list-style-type: none"> C.1. Frontal and/or anterior temporal atrophy on MRI or CT C.2. Frontal and/or anterior temporal hypoperfusion/hypometabolism on PET/SPECT
<i>IV. Behavioural variant FTD with definite FTL D Pathology</i>
Criterion A and either criterion B or C must be present to meet criteria.

<ul style="list-style-type: none"> A. Meets criteria for possible or probable bvFTD B. Histopathological evidence of FTLD on biopsy or at post-mortem C. Presence of a known pathogenic mutation
V. Exclusionary criteria for bvFTD
<ul style="list-style-type: none"> A. Pattern of deficits is better accounted for by other non-degenerative nervous system or medical disorders B. Behavioural disturbance is better accounted for by a psychiatric diagnosis C. Biomarkers strongly indicative of AD or other neurodegenerative process

In cases in which the pattern of deficits is better accounted for by other non-degenerative nervous system or medical disorders or the behavioral disturbance is better accounted for by a psychiatric diagnosis, then bvFTD should be excluded in the differential diagnosis. The same applies to cases in which cerebrospinal fluid (CSF) biomarkers or serum biomarkers are strongly indicative of AD or other neurodegenerative processes.

Both the 1998 (Neary et al., 1998) and the revised FTDC criteria (Rascovsky et al., 2011) rely on the presence of distinct clinical features for the diagnosis of bvFTD. The most striking difference is that the 1998 criteria required the presence of all five core diagnostic features: insidious onset and gradual progression, early decline in personal and social interpersonal conduct, emotional blunting and loss of insight. Nevertheless, it is important to take into account that, notwithstanding the fact that individual core features are common at presentation, these are not always concomitantly present.

b. Primary progressive aphasia (PPA)

The key feature of PPA is a progressive and insidious language decline affecting at least one among: speech production; object naming; syntax; or word comprehension. Notwithstanding the fact that other cognitive or behavioral impairments can emerge later in the course of the disease, language must be the first and the most impaired domain throughout the disease duration (Mesulam, 1982, Mesulam, 2003).

As in bvFTD, also in the case of PPA a series of criteria have been released throughout the last decades. The first ones were published by Mesulam *et al.* in 1982 and then updated in 2003 (Mesulam, 1982, Mesulam, 2003); however, the most updated and currently used are those published by Gorno-Tempini *et al.* in 2011 (Gorno-Tempini et al., 2011). Three criteria must be fulfilled by patients in order to be defined as suffering from PPA:

1. The most prominent clinical feature is difficulty with language (i.e., aphasia);
2. These deficits are the principal cause of impaired daily living activities;
3. Aphasia should be the most prominent deficit at symptom onset and for the initial phases of the disease.

Once the diagnosis of PPA is formulated, then patients can be categorized in one of the three subvariants of the syndrome: svPPA, nfvPPA and lvPPA.

Due to the high heterogeneity of both imaging and biological features of PPA, these findings have also been incorporated in the classification system, as will be displayed in the next Chapters.

PPA is characterized by heterogeneous neuropathological causes. Indeed, most patients with PPA have tau-positive FTLN, ubiquitin/TDP43-positive FTLN (Hodges, Davies et al., 2004, Spinelli, Mandelli et al., 2017) or AD pathology (Forman, Farmer et al., 2006). Nonfluent aphasia is most often linked to tau-positive pathology (Mesulam, Wicklund et al., 2008, Spinelli et al., 2017), semantic dementia to ubiquitin-positive, TDP43-positive pathology (Hodges et al., 2004, Spinelli et al., 2017), while the logopenic variants to AD pathology (Spinelli et al., 2017), as also demonstrated by amyloid PET and CSF biomarkers of AD (Bergeron, Gorno-Tempini et al., 2018).

Classification of PPA into one of the variants may occur at three levels: clinical, imaging-supported, or definite pathologic diagnosis. It is important to stress is that the clinical criteria for each variant must be met, as imaging only plays a supportive role in the diagnosis.

When classifying PPA patients in the different variants at a clinical level, the main language domains considered are speech production features (grammar, motor speech, sound errors and word-finding pauses), repetition, single-word and syntax comprehension, confrontation naming, semantic knowledge and reading/spelling.

Semantic variant PPA (svPPA). According to the criteria, in order to make a clinical diagnosis of semantic variant PPA, the features reported in the following table must be present (Gorno-Tempini et al., 2011):

Semantic variant PPA
<i>I. Clinical diagnosis of semantic variant PPA</i>
Both of the following core features must be present: 1. Impaired confrontation naming 2. Impaired single-word comprehension
At least 3 of the following other diagnostic features must be present: 1. Impaired object knowledge, particularly for low frequency or low-familiarity items 2. Surface dyslexia or dysgraphia 3. Spared repetition 4. Spared speech production (grammar and motor speech)
<i>II. Imaging-supported semantic variant PPA diagnosis</i>
Both of the following criteria must be present: 1. Clinical diagnosis of semantic variant PPA 2. Imaging must show one or more of the following results: a. Predominant anterior temporal lobe atrophy b. Predominant anterior temporal hypoperfusion or hypometabolism on SPECT or PET
<i>III. Semantic variant PPA with definite pathology</i>
Clinical diagnosis (criterion 1 below) and either criterion 2 or 3 must be present: 1. Clinical diagnosis of semantic variant PPA 2. Histopathologic evidence of a specific neurodegenerative pathology (e.g., FTLT-tau, FTLT-TDP, AD, other) 3. Presence of a known pathogenic mutation

Notwithstanding the fact that naming problems are present also in other variants of PPA or in other neurodegenerative conditions causing aphasia, in the semantic variant the disturbance is severe, especially when compared to other language domains, which are instead relatively spared. Impaired single-word comprehension is one of the major features of the disease and stands true especially for low-frequency items (e.g. “crocodile” vs. the more familiar/frequent “dog”). Poor comprehension of single words is usually the first manifestation of a widespread semantic memory impairment that causes deficits in both object knowledge and person recognition (prosopagnosia).

Semantic deficits usually regard most categories (i.e., tools, animals, people), even if rarer cases have been described in the literature with prominent, if not selective, deficits for people and animals (Evans, Heggs et al., 1995, Gainotti, 2007).

Others describe patients with worse performance with concrete object concepts as compared to abstract concepts (Yi, Moore et al., 2007). These cases are generally

associated with predominant right temporal atrophy and early behavioral changes, including loss of empathy and compulsions (Seeley, Bauer et al., 2005).

Surface dyslexia and dysgraphia are features usually encountered in semantic variant PPA and refer to deficits in reading and writing, respectively, words with “irregular” or atypical relationship between spelling and pronunciation, such as “sew”, which patients usually read as /su/, instead of /səʊ/, by a process of “regularization” of such words (Wilson, Ogar et al., 2009).

It is important to emphasize that these patients do not have any impairment in repetition and motor speech, even when semantic deficits are prominent. Even if language production is generally grammatically correct, patients can make some “paragrammatic” errors, such as substituting less appropriated closed class words (i.e. “I know what they’re doing but I can’t think the words what they’re doing”) (Meteyard & Patterson, 2009).

Non-fluent/agrammatic variant PPA (nfvPPA). The nonfluent/agrammatic variant of PPA is also known with other names, such as progressive nonfluent aphasia. All the aforementioned nomenclatures define the same disease.

Like svPPA, a diagnosis of nfvPPA can be made at a clinical, imaging and pathologic level. Also in this case, imaging plays a supportive role and clinical criteria have to be fulfilled, as reported in the following table (Gorno-Tempini et al., 2011):

Nonfluent/agrammatic variant PPA
<i>I. Clinical diagnosis of nonfluent/agrammatic variant PPA</i>
At least one of the following core features must be present: 1. Agrammatism in language production 2. Effortful, halting speech with inconsistent speech sound errors and distortions (apraxia of speech)
At least 2 of 3 of the following other features must be present: 1. Impaired comprehension of syntactically complex sentences 2. Spared single-word comprehension 3. Spared object knowledge
<i>II. Imaging-supported nonfluent/agrammatic variant diagnosis</i>
Both of the following criteria must be present: 1. Clinical diagnosis of nonfluent/agrammatic variant PPA 2. Imaging must show one or more of the following results: a. Predominant left posterior fronto-insular atrophy on MRI or b. Predominant left posterior fronto-insular hypoperfusion or hypometabolism on SPECT or PET
<i>III. Nonfluent/agrammatic variant PPA with definite pathology</i>
Clinical diagnosis (criterion 1 below) and either criterion 2 or 3 must be present:

1. Clinical diagnosis of nonfluent/agrammatic variant PPA
2. Histopathologic evidence of a specific neurodegenerative pathology (e.g., FTLT-tau, FTLT-TDP, AD, other)
3. Presence of a known pathogenic mutation

Agrammatism and effortful speech are the main criteria that define nfvPPA. Agrammatism is characterized by short, simple phrases and omissions of grammatical morphemes such as function words (i.e., conjunctions, prepositions, pronouns etc.) or inflections (e.g., the genitive 's, the plural -s, the third person singular -s, the comparative -er etc.). Effortful speech instead refers to slow, labored speech production. Generally, a main manifestation of these patients consists in the so-called apraxia of speech (i.e., articulation planning deficit), which can be the initial sign of the disease. Patients with nfvPPA usually make a series of inconsistent speech sound errors, the most common being distortions, deletions, substitutions, insertions or transposition of speech sounds. Usually, they are aware of their difficulties. Prosody is also disrupted, and the rate of speech is markedly reduced too (Ogar, Dronkers et al., 2007). Before apraxia of speech or agrammatism become clearly evident, effortful speech and production errors can nevertheless be detected; in this case, a written production test (such as a written description of a picture) or syntax comprehension tasks can often reveal early grammatical errors (Ogar et al., 2007).

For what concerns additional diagnostic criteria, deficits in syntax comprehension are evidenced by difficulties in sentence comprehension, which initially may be limited to the most difficult syntactic constructions, such as negative passives or objective relative clauses (e.g., “The car that the truck hit was green”) (Pelle, Troiani et al., 2008).

A feature nfvPPA shares with svPPA is the impairment in comprehension. However, in the nonfluent presentation, the impairment is clearly influenced by grammatical complexity of the sentence (Knibb, Woollams et al., 2009). Furthermore, nfvPPA patients usually present spared object knowledge and single-word comprehension, another feature that help physicians in determining differential diagnosis.

As noted above, an imaging-supported diagnosis of nfvPPA requires both clinical diagnosis of nfvPPA, and atrophy and/or hypometabolism of left posterior fronto-insular brain regions (in particular, the inferior frontal gyrus, insula, premotor and supplementary motor areas) (Wilson, Dronkers et al., 2010).

It is known that patients with nfvPPA have a tendency to progress to a syndrome that encompasses both pyramidal and extrapyramidal motor problems, compatible with a diagnosis of motor neuron disease (MND), corticobasal syndrome (CBS) or progressive supranuclear palsy (PSP) (Ulugut, Stek et al., 2021). Henceforth, a clinical diagnosis of pure nfvPPA should be limited to those patients who do not show motor symptoms that impair daily activities (e.g. generalized rigidity or tremor). Still, the presence of mild apraxia or slowing of fine finger movements does not exclude a PPA diagnosis.

c. Motor neuron disease (MND)

MND is a neurodegenerative disorder with a highly heterogeneous clinical onset and progression. Amyotrophic lateral sclerosis (ALS) is the prototypical presentation of MND and is characterized by the progressive degeneration of upper (UMN) and lower motor neurons (LMN) in the cerebral cortex, brainstem and spinal cord (Taylor, Brown et al., 2016). From a clinical standpoint, patients with MND greatly differ in terms of site of onset, differential UMN and LMN involvement, degree of extra-motor – particularly, cognitive – impairment, and disease progression, configuring a wide spectrum of syndromes partially overlapping with FTD, with different prognostic impact at the individual level (Swinnen & Robberecht, 2014).

As previously noted, FTD and MND are increasingly perceived along a clinicopathological continuum with shared fundamental biology. Patients with FTD who later develop MND are usually diagnosed with FTD-MND (or FTD-ALS), while those with initial MND and symptoms that later fit criteria for bvFTD or PPA are labelled as MND-FTD (or ALS-FTD). Still, notwithstanding the fact that 10-15% of patients with FTD develop MND, an even higher percentage (60%) has ‘subclinical’ evidence of MND with either electromyogram (EMG) evidence of motor neuron disruption or subtle MND-like clinical signs, such as fasciculations (Van Langenhove, Piguet et al., 2017). Conversely, while 10-20% of MND patients meet diagnostic criteria for FTD, approximately 50% develop cognitive or behavioral impairment, termed MNDci and MNDbi, respectively (Strong, Abrahams et al., 2017). In order to match a diagnosis of ALS, patients must manifest a combination of both upper motor neuron (UMN) and lower motor neuron (LMN) degeneration either clinically or at EMG. Based on the criteria

elaborated in a consensus meeting recently held in Gold Coast (Australia) (Hannaford, Pavey et al., 2021, Shefner, Al-Chalabi et al., 2020), a diagnosis of ALS requires at least:

- progressive motor impairment, as documented by history or clinical assessment, preceded by preserved motor abilities;
- presence of UMN and LMN signs in at least one body region (with UMN and LMN signs noted in the same body region if only one body region is involved) or LMN dysfunction in at least 2 body regions;
- exclusion of other disease etiologies.

Of the various MND phenotypes that can be appreciated in FTD patients, the most common is ALS, even though pure LMN (primary muscular atrophy) or UMN (primary lateral sclerosis) involvement can also be appreciated in a minority of cases (Devenney, Foxe et al., 2015). Early bulbar dysfunction (progressive bulbar palsy [PBP]) is observed more frequently in FTD-MND than in isolated ALS and patients with FTD-MND show the shortest survival among individuals with FTD syndromes, since the course of the disease can be very aggressive, with acceleration at the onset of MND (Elahi, Marx et al., 2017).

Generally speaking, the majority of MND patients show various degrees of executive or behavioral dysfunction (Vinceti, Olney et al., 2019). The cognitive profile of the FTD-MND spectrum is most often described by social cognition and behavioral disturbances or, alternatively, by executive dysfunction, which is compatible with a diagnosis of bvFTD (Phukan, Pender et al., 2007).

Similar to bvFTD, also PPA patients may develop clinical features of MND (although, in some cases, without fully meeting diagnostic criteria). For instance, these patients may develop mild muscular wasting or fasciculations, as it has been reported by one study (Burrell, Kiernan et al., 2011). Most cases of PPA-MND are nvPPA, while MND in typical svPPA is rare. As speech and motor impairments belong to the same spectrum of FTLD, also some MND patients may develop language impairment, even if not fully meeting criteria for PPA. In these patients, due to the presence of dysarthria, it may be challenging to discern the presence of aphasia, which indeed can be under-reported. According to a study, language dysfunction may be present in up to 43% of MND patients, to different extents (Taylor, Brown et al., 2013).

1.1.3. Neuropathology

As previously noted, three different pathologies can be associated with FTLD. 90-95% are either FTLD-tau or FTLD-TDP, caused by intracellular aggregates of tau or transactive response (TAR) DNA binding protein 43 (TDP-43), respectively, while the remaining 5-10% of cases are FTLD-FUS, caused by intracellular FUS (fused in sarcoma) inclusions (Mackenzie & Neumann, 2016, Mackenzie, Neumann et al., 2010, Neumann, Rademakers et al., 2009, Neumann, Sampathu et al., 2006).

Although virtually any FTLD-related pathology may underlie each clinical phenotype, there are some relevant clinico-pathological associations. Indeed, neuropathological studies identified cytoplasmic inclusions of TDP-43 as the molecular hallmark in up to 98% of MND cases (Neumann et al., 2006), following a progressive spreading pattern from the motor cortex that has been classified into 4 sequential stages (Brettschneider, Del Tredici et al., 2013). Similarly, approximately 90% of individuals with svPPA have FTLD-TDP type C pathology (Spinelli et al., 2017). By contrast, bvFTD can be associated with all molecular subsets. According to a recent clinicopathological study, 60% of cases of bvFTD show TDP-43 aggregates, 30% show some subtype of FTLD-tau pathology, while the remaining 10% show FTLD-FUS pathology (Perry, Brown et al., 2017).

Here below, each neuropathological subtype of FTLD will be addressed, starting from its hallmark protein aggregate.

FTLD-tau. Tau is a protein encoded by the microtubule-associated protein tau (*MAPT*) gene, located on chromosome 17q21.31. *MAPT* mRNA undergoes the process of alternative splicing, leading to production of six tau isoforms, which are expressed in different areas across the brain (Elahi and Miller, 2017). Tau binds to and stabilizes microtubules, which are fundamental for cellular structure and function. In neurodegenerative disorders, the normally phosphorylated tau becomes aberrantly hyperphosphorylated, so that it dissociates from microtubules and forms aggregates within neurons and glia. Disorders in which tau pathology is considered the major contributing factor to neurodegeneration are referred to as “primary tauopathies” (which include both FTLD-tau and AD pathologies).

Exon 10 of MAPT is alternatively spliced to generate tau species with either three or four conserved ~32 amino acid repeats in the microtubule binding domain of tau protein (Andreadis, 2012), referred to as 3R and 4R tau. Pick disease (PiD) is a typical 3R tauopathy; CBD, PSP, argyrophilic grain disease, and multisystem atrophy with globular inclusions belong to 4R tauopathies. All these are subtypes of FTLD-tau pathology. By contrast, in AD pathology, neurofibrillary pathology is composed of an equimolar ratio of 3R and 4R tau.

FTLD-TDP. TAR DNA-binding protein 43 (TDP-43) is encoded by the *TARDBP* gene, which is located on chromosome 1p36.22. This protein is found in the nucleus, where it regulates different steps of protein production, from DNA transcription to RNA stabilization, translation and splicing. *TARDBP* mutations typically cause ALS but are also, in rare cases, implicated in FTD with TDP pathology. The TDP-43 C-terminus contains a prion-like domain that allows the formation of TDP-43 oligomers. Furthermore, it is a hotspot of disease-causing mutations in ALS. TDP-43 pathology is subclassified according to patterns of TDP-43-containing neuronal cytoplasmic inclusions and dystrophic neurites in diseased neurons. Five FTLD-TDP subtypes have been documented (Van Mossevelde et al., 2018):

- Type A: characterized by crescentic to oval/ring-like neuronal cytoplasmic inclusions and many short dystrophic neurites involving superficial neocortical layers. Lentiform neuronal intra-nuclear inclusions and oligodendroglial (oligo) inclusions may also be observed. Common phenotypic presentations of FTLD-TDP Type A include bvFTD and nvPPA; this pathological alteration is commonly associated with *GRN* and *TBKI* (TANK binding kinase 1) mutations, less commonly to *C9orf72*;
- Type B: characterized by neuronal cytoplasmic inclusions affecting superficial and deep neocortical layers with a paucity of dystrophic neurites. Oligodendroglial inclusions may be observed. The most common phenotypic presentations associated with FTLD-TDP Type B is bvFTD with or without MND. At a genetic level, it is associated with *C9orf72* mutations and *TBKI* mutations;
- Type C: characterized by long dystrophic neurites predominantly in superficial layers with a paucity of neuronal cytoplasmic inclusions. It is clinically correlated with svPPA and bvFTD, while it has no specific genetic association;

- Type D: characterized by frequent lentiform neuronal intranuclear inclusions with short dystrophic neurites. Clinically, it is associated with inclusion body myopathy with early-onset Paget disease and FTD (IBMPFD) – ALS. Genetically, it is caused by *VCP* mutations;
- Type E: characterized by granulofilamentous neuronal inclusions and very fine, dot-like neuropil aggregates affecting all neocortical layers in addition to curvilinear oligodendroglial inclusions in the white matter. It is clinically expressed as bvFTD.

In 2013, Brettschneider et al. (Brettschneider et al., 2013) demonstrated how the propagation of TDP-43 in ALS appears to spread from the motor regions to a much distributed CNS involvement. Based on 76 ALS autopsies, they recognized four different stages of the spreading of the lesions:

- Stage 1: ALS cases with the lowest burden of TDP-43 pathology are characterized by lesions in the agranular motor cortex, brainstem motor nuclei of cranial nerves V, VII, and X-XII, and spinal cord α -motoneurons. TDP-43 immunoreactive inclusions are present also in oligodendrocytes of the cortex, subcortical white matter and among corticobulbar and corticospinal projections.
- Stage 2: increasing burdens of pathology shows involvement of the prefrontal neocortex (middle frontal gyrus), brainstem reticular formation, precerebellar nuclei, and the red nucleus. The oligodendroglial involvement is seen along projections from precerebellar nuclei to the cerebellum.
- Stage 3: TDP-43 pathology involves also the prefrontal (gyrus rectus and orbital gyri) and then postcentral neocortex and striatum. The lesions, mostly involving long-axoned cortical pyramidal cells, are frequently accompanied by TDP-43 immunoreactive oligodendrocytes in the cortex and relative subcortical white matter.
- Stage 4: these are the cases with the greatest TDP-43 burden, which can be found in anteromedial portions of the temporal lobe, including the hippocampus.

In 2014, Brettschneider et al. (Brettschneider, Del Tredici et al., 2014) demonstrated how the propagation of TDP-43 in bvFTD spread from frontal to other regions, based on 60 patients' autopsies. According to their findings, it is possible to describe 4 patterns indicative of sequential dissemination of TDP-43 in bvFTD:

- Pattern I: cases with the lowest burden of pathology are characterized by widespread TDP-43 lesions in the orbital gyri, gyrus rectus, and amygdala.

- Pattern II: cases with increasing burden of pathology show TDP-43 lesions emerging in the middle frontal and anterior cingulate gyrus as well as in anteromedial temporal lobe areas, superior and medial temporal gyri, striatum, red nucleus, thalamus, and precerebellar nuclei.
- Pattern III: more advanced cases show involvement of the motor cortex, bulbar somatomotor neurons, and the spinal cord anterior horn.
- Pattern IV: characterized by TDP-43 lesions in the visual cortex.

FTLD-FUS. Fused in sarcoma (FUS) is an RNA-binding protein involved in splicing and nuclear export of mRNA. It is located on chromosome 16p11.2. Mutations in *FUS* have been associated not only to FTLD but also to Ewing sarcoma and other soft tissue tumors. FTLD-FUS features three subtypes:

- Atypical FTLD with ubiquitinated inclusions;
- Basophilic inclusion body disease, associated with juvenile ALS;
- Neuronal intermediate filament inclusion disease, which tends to rapidly progress.

1.1.4. Genetics

As it can be appreciated from the diagnostic criteria that have been reviewed in **Paragraph 1.1.2**, a definite diagnosis of FTLD relies on the underlying neuropathology, as noted on autopsy or – in rare cases – biopsy. Alternatively, the presence of a known pathogenic mutation must be demonstrated. There is indeed a strict interconnection between genetics and pathology. Genetics play a major role in FTLD, as up to 43% of patients have a positive family history (at least one affected first-degree family member with dementia, ALS or parkinsonism). Furthermore, between 10% to 27% of patients carry an autosomal dominant form of the disease (Rohrer & Warren, 2011, Seelaar, Rohrer et al., 2011). Different phenotypic and imaging characteristics for each mutation will be further addressed in the dedicated **Chapter 1.2**. Here below are listed the most common FTLD-causative mutations, which affect genes encoding for:

- Chromosome 9 open reading frame 72 (*C9orf72*);
- Progranulin (*GRN*);
- Microtubule-associated protein tau (*MAPT*).

More rarely, mutations can also affect a wide variety of other genes, including:

- TANK-binding kinase 1 (*TBKI*);
- Fused in sarcoma (*FUS*);
- Transactive response (TAR) DNA binding protein 43 (*TARDBP*);
- Superoxide dismutase 1 (*SOD1*).

Given the high heterogeneity in clinical presentations of FTLD molecular pathologies, it is very difficult to predict pathology *ante mortem*. However, familiar FTLD denotes an exception, as the affected genes disclose the causative pathology. Indeed:

- Mutations in the *C9orf72*, progranulin (*GRN*), valosin-containing protein (*VCP*), TANK-binding kinase 1 (*TBKI*) and *TARDBP* are associated with TDP-43 pathology;
- *MAPT* mutations are consistently associated with FTLD-tau pathology;
- *FUS* mutations are associated with FUS pathology.

1.1.5. Neuroimaging

While CT scan can be helpful to exclude other pathology involving the frontotemporal region (e.g., meningiomas, vascular disease, etc.), MRI is the method of choice to demonstrate (early) atrophy of the frontal and temporal lobes in patients with suspected FTLD. Coronal images are particularly relevant, as they facilitate the assessment of asymmetry in the temporal lobe structures. In complementarity with MRI that shows structural alterations, PET with ¹⁸F-fluorodeoxyglucose tracer (FDG-PET) is capable of showing functional deficits in terms of glucose hypometabolism in pathognomonic regions of FTLD (Dukart, Mueller et al., 2011, Morbelli, Ferrara et al., 2016).

a. bvFTD

bvFTD is characterized by atrophy of the frontal and temporal lobes, which can be better appreciated on T1-weighted images of an MRI scan. bvFTD is generally characterized by frontotemporal atrophy that shows an antero-posterior gradient with involvement of medial orbitofrontal, anterior cingulate, insular and anterior temporal cortices and relative sparing of the parietal and occipital lobes (Perry, Graham et al., 2006, Seeley, Crawford et al., 2008). Furthermore, atrophy, although commonly bilateral, is generally asymmetrical (Perry et al., 2006, Seeley et al., 2008). In order to exclude concomitant vascular disease as well as to assess subcortical white matter changes described in bvFTD it is important to analyze T2-weighted and FLAIR images. The first areas to be affected

by atrophy is the orbitofrontal cortex, which undergoes sulcal widening, followed by the mesiofrontal cortex. As the disease progresses, the dorso-lateral prefrontal cortex also gets involved by the atrophic process. Other key findings in bvFTD include bilateral hippocampal and amygdalar atrophy, which are again generally asymmetrical. However, also the striatum (Boccardi, Sabattoli et al., 2005, Seeley et al., 2008), thalamus (Seeley et al., 2008) and brainstem (Chao, Schuff et al., 2007, Seeley et al., 2008) are involved. Importantly, medial temporal lobe is majorly affected anteriorly (i.e. the amygdala is more atrophic than the hippocampus), while the posterior hippocampus is generally spared.

Such pattern is consistent across studies and has shown high sensitivity and specificity in differentiating bvFTD from AD (Schroeter, Raczka et al., 2007), which typically shows an opposite postero-anterior gradient of brain atrophy. The presence of frontal and/or anterior temporal atrophy (as an alternative to hypoperfusion/hypometabolism in the same brain areas) is necessary to make a diagnosis of probable bvFTD according to the current criteria (Rascovsky et al., 2011), and has shown to provide greatly increased specificity in path-proven cases (up to 95%, compared with 82% when only clinical criteria of possible bvFTD were considered) (Harris, Gall et al., 2013). However, despite such consistency at the group level, great heterogeneity of MRI findings exists among individuals, as different cases show variable degree of hemispheric asymmetry, predominance of frontal versus temporal lobe atrophy and extent of posterior cortical involvement (Schroeter, Laird et al., 2014).

Early on in the course of the disease, structural imaging generally results normal. Furthermore, although many patients will show frontotemporal atrophy later in the course of the disease, there is a subset of patients for which the advancement of clinical behavioral symptoms is not longitudinally matched by findings of atrophy (Davies, Kipps et al., 2006, Kipps, Davies et al., 2007). Some of these cases are likely to be non-neurodegenerative phenocopies (such as primary psychiatric disorders), which is why serial longitudinal imaging is very helpful in the differential diagnosis (Josephs, Duffy et al., 2006). Abnormalities of the WM are considered as key neuropathological underpinnings of FTLT (Mackenzie & Neumann, 2016, Neumann, Kwong et al., 2007), although they usually occur at a microstructural level that can be detected only using advanced MRI techniques (i.e., diffusion tensor [DT] MRI) (see **Chapter 1.3**).

The use of PET with ^{18}F -fluorodeoxyglucose (FDG-PET) enables visualization of alterations in brain metabolism that may precede grey matter atrophy in FTD, as well as in other forms of dementia (Dukart et al., 2011, Morbelli et al., 2016). In particular, bvFTD is characterized by (often asymmetrical) low glucose metabolism at the level of the orbitofrontal cortex, anterior temporal poles and basal ganglia (Grimmer, Diehl et al., 2004, Ishii, Sakamoto et al., 1998, Jeong, Cho et al., 2005). PET scans represent a valid alternative to structural MRI to make a diagnosis of probable bvFTD according to the current criteria (Rascovsky et al., 2011), possibly indicating frontal and temporal alterations that precede the development of grey matter atrophy (Morbelli et al., 2016). The most severely impaired regions are the medial frontal cortex, the frontolateral and anterior temporal cortices. Such characteristic pattern of hypoperfusion or hypometabolism on PET scans has demonstrated to greatly increase the sensitivity of detecting bvFTD, compared with clinical diagnosis alone (Mendez et al., 2007b). This pattern of hypometabolism characterizes both patients with early symptoms of bvFTD but also individuals a few years before conversion into FTD (Morbelli et al., 2016). These findings of hypometabolism differentiate patients affected by bvFTD from patients affected by other types of dementia or HC with both a sensitivity and specificity of 80-95% (Buhour, Doidy et al., 2017, Diehl-Schmid, Grimmer et al., 2007, Vijverberg, Wattjes et al., 2016). Still, some false negative results have been reported in patients affected by some primary psychiatric disorders, hence future quantitative assessment metabolic patterns with PET are needed in order to increase the diagnostic value of this technique.

b. PPA

On MRI, nfvPPA is characterized by heterogeneous findings including atrophy of a number of regions in the dominant (left) hemisphere, although classically the most affected region in the left perisylvian one, particularly the left inferior frontal (Broca's area) and insular cortices (Gorno-Tempini, Dronkers et al., 2004, Rogalski, Cobia et al., 2011). As language deficits worsen, ipsilateral anterior frontal, lateral temporal and anterior parietal lobes show increasing atrophy, and posterior frontal and temporal lobe structures in the right hemisphere also get involved (Rogalski et al., 2011, Rohrer, Warren et al., 2009). Variation between patients likely reflects heterogeneity in the

neurolinguistic deficits of nfvPPA. Moreover, bilateral atrophy of the basal ganglia, thalamus, and amygdala has been observed in nfvPPA patients (Garibotto, Borroni et al., 2011, Gorno-Tempini et al., 2004). Although left hippocampal atrophy has also been reported, this is typically less severe relative to AD patients (van de Pol, Hensel et al., 2006).

For what concerns differences according to pathology, nfvPPA patients with tau pathology have more severe temporal lobe atrophy than other forms, while those with TDP-43 pathology show notable atrophy in the left lateral temporal lobe (Josephs et al., 2006, Whitwell, Weigand et al., 2012).

svPPA is characterized by left greater than right temporal lobe atrophy. Atrophy is mainly temporal anterior (temporal pole), with an antero-posterior gradient, affecting also the lateral and ventral temporal surfaces, as well as the anterior hippocampus, amygdala and fusiform gyrus (Galton, Patterson et al., 2001, Gorno-Tempini et al., 2004, Mummery, Patterson et al., 2000, Rosen, Gorno-Tempini et al., 2002). The anterior temporal lobe can be defined by having a knife-edge or ‘razorback’ atrophy, which can be appreciated at both coronal and axial views. Temporal lobe atrophy is mainly inferior as it mainly affects the fusiform gyrus, while it spares the superior temporal gyrus (Boxer & Miller, 2005, Collins, Montal et al., 2017).

Semantic patients may have hippocampal atrophy that is at least as severe as that seen in AD patients, although predominantly located in the anterior regions (Chan, Fox et al., 2001b, Galton et al., 2001, van de Pol et al., 2006). These features come very helpful when used to differentiate nfvPPA from AD. Although the most common variant of svPPA displays left greater than right temporal lobe atrophy, the opposite pattern can be observed less frequently in cases showing significant overlap with the right temporal variant of bvFTD (Josephs, Whitwell et al., 2009). As the disease progresses, greater atrophy of posterior and superior temporal, frontal (orbitofrontal, inferior frontal and cingulate gyri), and insular regions can be detected (Brambati, Rankin et al., 2009, Rohrer et al., 2009).

In a similar way to bvFTD, the assessment of atrophy patterns on conventional MRI has been included in the current diagnostic criteria of PPA clinical variants (Gorno-Tempini et al., 2011), as a possible method to make an “imaging-supported” diagnosis. Furthermore, differential atrophy of the left temporal pole and pars opercularis of the

inferior frontal gyrus was shown to aid in the discrimination between nfvPPA and svPPA (Agosta, Ferraro et al., 2015a). However, initial distinctive neuroanatomical features can be very subtle in the early phase of the disease or may be lost as degeneration progresses and converges over time (Rogalski et al., 2011, Rohrer et al., 2009).

When evaluating functional alterations showed by FDG PET imaging, the patterns of focal hypometabolism vary between clinical variants of PPA, mirroring the structural changes described previously. svPPA is characterized by asymmetrical temporal hypometabolism, more marked on the left side (Drzezga, Grimmer et al., 2008, Nestor, Fryer et al., 2006, Rabinovici, Jagust et al., 2008), while nfvPPA is associated with a greater variability in hypometabolic patterns of the left inferior frontal gyrus, dorsolateral frontal cortex, anterior cingulate cortex, insula and – occasionally – parietal cortex (Cerami, Dodich et al., 2017). Involvement of bilateral caudate nuclei and thalami has also been reported (Pernecky, Diehl-Schmid et al., 2007).

A PET study of non-fluent patients demonstrated that a pattern of bilateral temporoparietal involvement is predictive of AD pathology, while a unilateral (left) temporoparietal cortex hypometabolism/perfusion was seen in cases with FTLN pathology; on the contrary, a bilaterally normal temporoparietal cortical perfusion or metabolism was predictive of FTLN pathology (Nestor, Balan et al., 2007). A study comparing svPPA and very early AD patients using structural MRI and FDG-PET revealed hippocampal atrophy and hypometabolism in both groups; however, AD patients showed a strikingly reduced metabolism of the posterior cingulate cortex, which was not detected in those with svPPA (Nestor et al., 2006).

c. MND

Part of the following paragraph has been published in Agosta F, Spinelli EG, Filippi M. Expert Rev Neurother. 2018 May;18(5):395-406, doi: 10.1080/14737175.2018.1463160. Historically, MRI has been used to exclude structural abnormalities that can mimic clinical UMN and LMN damage, both in the brain (e.g., vascular lesions, multiple sclerosis, tumors) and the spinal cord (e.g., radiculopathy, myelopathy, syringomyelia). Since the last decade of the 20th century, some observations led to the definition of MND-related MRI alterations, which are detectable on conventional imaging. Corticospinal tract (CST) hyperintensity on T2-weighted, proton density or fluid-attenuated inversion

recovery (FLAIR) sequences of brain MRI has been described in a highly variable proportion of ALS cases, ranging from 15% to 76% across different cohorts (Filippi, Agosta et al., 2010). A hypointense rim in the precentral gyrus can also be observed on T2-weighted images of patients with ALS (Filippi et al., 2010). However, these findings are neither sufficiently sensitive nor specific for ALS. For example, increased T2-signal intensity in the CST has also been shown in healthy individuals and patients with hepatic failure (Filippi et al., 2010). Therefore, the visual assessment of these alterations on brain MRI is currently not recommended for making a firm diagnosis of ALS (Filippi et al., 2010). Only recently, the application of quantitative approaches to assess FLAIR hyperintensity in the CST has been suggested to provide some benefit for the diagnosis of ALS, particularly in those subjects with greater UMN damage (Fabes, Matthews et al., 2017).

CST involvement can also be detected using conventional MRI of the spinal cord, as T2 and T1 hyperintensities have been shown in the anterolateral columns of the cervical cord of patients with ALS (Filippi et al., 2010). Cord hyperintensities provided higher specificity compared with intensity alterations on brain MRI (Filippi et al., 2010). In this context, preliminary findings using ultra-high field (7 Tesla) MRI has recently shown some potential to detect signal abnormalities in the spinal CST of ALS patients with high accuracy (Cohen-Adad, Zhao et al., 2013).

1.1.6. Treatment

a. FTD presentations

There are currently no approved treatments for FTD. Indeed, off-label pharmacological and behavioral modification techniques are generally used to manage symptoms (Olney, Spina et al., 2017).

Treatments that have received approval for AD did not show any benefit in FTLD syndromes. On the contrary, there is evidence in literature that acetylcholinesterase inhibitors actually make symptoms in bvFTD worse (Kimura & Takamatsu, 2013, Mendez, Shapira et al., 2007a). Memantine, which has a different mechanism of action as compared to acetylcholinesterase inhibitors, has been tolerated by patients with FTD but has showed no improvements in behavior or cognition in a double-blind, placebo-

controlled trial (Boxer, Knopman et al., 2013, Vercelletto, Boutoleau-Bretonniere et al., 2011).

FTD behavioral symptoms can be somehow controlled with serotonin selective reuptake inhibitors (SSRIs) (Ikeda, Shigenobu et al., 2004). Indeed, a small randomized, placebo controlled double blinded trial with trazodone (a drug belonging to the class of SSRIs) demonstrated improvement in Neuropsychiatry Inventory (NPI) scores of bvFTD patients (NPI is a test that assesses psychiatric symptoms in 10 different domains, namely Delusions, Hallucinations, Agitation, Dysphoria, Anxiety, Apathy, Irritability, Euphoria, Disinhibition and Aberrant motor behavior) but not in Mini-Mental State Examination (MMSE, a 30-points questionnaire which analyses different categories including Orientation to time, Orientation to place, Registration, Attention and calculation, Recall, Language, Repetition and Complex commands) (Folstein, Robins et al., 1983).

Due to their important side effects in increasing vulnerability to the development of extrapyramidal symptoms, atypical antipsychotics should be used with caution. Indeed, they have a black box warning for their use in the elderly (Pijnenburg, Sampson et al., 2003). Mood stabilizers instead have found little evidence of benefit in patients with FTLN (Cruz, Marinho et al., 2008). Oxytocin also has been proposed as a potential drug targeting emotional changes in FTD. A small study showed mild improvement at NPI score after its use (Jesso, Morlog et al., 2011).

Non-pharmacological therapies also play a major role to treat FTD. Most importantly, patients' symptoms can improve simply with caregiver education about behavioral, environmental and physical techniques to minimize or redirect unwanted behaviors (Merrilees, 2007). Furthermore, physical exercise has been demonstrated to delay cognitive decline. Indeed, it should be recommended to all FTD patients that can tolerate it (Cheng, Chow et al., 2014). Furthermore, patients with nfvPPA, svPPA or other language deficits may benefit from speech therapy (Kortte & Rogalski, 2013).

Although there are no approved treatments for FTLN, novel clinical trials are started every day targeting specific mechanisms and pathology. Unfortunately, the complexity of FTLN phenotypes represents an important challenge for clinical trial design, as well as in the definition of outcome measures, notwithstanding the fact that FTLN disorders are also considered rare diseases (less than 200.000 affected in the US) (Boxer, Gold et al., 2020). There have been few randomized, placebo-controlled trials in FTLN (Tsai &

Boxer, 2016), which have demonstrated the feasibility of using behavioral questionnaires, cognitive scales and functional activity ratings as outcome measures. Still, no study to date has yielded evidence of disease modifying therapeutic efficacy. Most probably, this was due to the fact that previous trials did not consider clinical, etiological and imaging heterogeneity between patients carrying the same molecular diagnosis or sample sizes were inadequate and participants too advanced in the course of the disease to demonstrate any benefit.

The two largest industry-sponsored trials in bvFTD (NCT01626378) and FTLD due to progranulin gene mutations (FTLD-GRN; NCT02149160) still haven't been published. However, despite these challenges, new treatments targeting tau gain of function, progranulin haploinsufficiency and chromosome 9 open reading frame 72 (*C9orf72*) hexanucleotide repeat expansions are progressing in clinical development for FTLD and related disorders.

b. MND

Currently, no curative treatment is available for MND, and disease-modifying options are limited. Only two drugs, namely riluzole and edaravone, have been approved for the treatment of ALS. Riluzole is thought to reduce glutamate-induced excitotoxicity, whereas edaravone is a potent free radical scavenger. Both drugs act by preventing oxidative stress from inducing motor neuron death. However, they have been shown to slow ALS progression only to a modest degree (Bensimon, Lacomblez et al., 1994, Writing & Edaravone, 2017).

Current European guidelines (Diagnosis, Management of Amyotrophic Lateral et al., 2012) recommend oral treatment with riluzole 50 mg twice daily for ALS patients. Patients most likely to benefit from this therapy are those with definite or probable ALS with symptoms present for less than 5 years, a forced vital capacity of 60% or more at pulmonary function tests, and no tracheostomy (Bensimon et al., 1994, Lacomblez, Bensimon et al., 1996). To date, riluzole is the only drug which has shown any impact on survival (Lacomblez et al., 1996).

Edaravone (60 mg) is administered by very slow intravenous infusion (60 minutes) in 28-day cycles. This drug has been shown to slow down the loss of physical function in ALS patients by 33% as compared to placebo, in a selected population of patients with

mild to moderate impairment (i.e., scoring at least 2 points on all 12 items of ALSFRS-R), forced vital capacity of 80% or more, definite or probable ALS according to the revised El Escorial criteria, and disease duration of 2 years or less (Writing & Edaravone, 2017). However, the long-term effects of edaravone on ALS patients, including its impact on survival, remain unclear.

There was a huge time lag between the first approval of riluzole (1995) and the recent approval of edaravone (2017). Over these 22 years, more than 60 molecules have been investigated as a possible treatment for MND, but none of these reached approval for clinical use (Petrov, Mansfield et al., 2017). It has been suggested that the difficulty to enroll patients in early phases of the disease using current diagnostic tools, together with the well-known disease heterogeneity, might explain the high failure rate of pharmacological trials in MND (Katyral & Govindarajan, 2017).

Motor physical rehabilitation, ventilator support and feeding support also have a significant impact on the assistance of MND patients (Diagnosis et al., 2012).

1.2. Genetic FTLD: characteristic clinical and neuroimaging features

1.2.1. C9orf72

In 2011, an expansion of the hexanucleotide G₄C₂ repeat in the proximal regulatory region of *C9orf72* was identified as a frequent cause of genetic cases of both FTD and ALS (Renton, Majounie et al., 2011). What is known about *C9orf72* is that it is transcribed into three different transcripts that encode for two protein isoforms, whose function remains largely uncharacterized. It is thought that *C9orf72* is expressed at the presynaptic terminal of neurons, where it plays a role in many processes involving RNA. The hexanucleotide repeat generally comes in 2-24 copies in healthy individuals, while patients can carry expansions of over 1,000 repeats. The pathognomonic mechanism of the expansion still remains largely unknown, with different hypothesis advanced in the course of the years, including haploinsufficiency, gain of protein function and gain of RNA function. The protein-mediated mechanism of cellular harm is characterized by toxic accumulation of dipeptide repeat proteins that are translated from the G₄C₂ repeat through unconventional repeat-associated non-ATG translation, while the RNA-mediated

mechanism features toxic effects derived from sense and antisense RNA foci generated from the expanded repeat (Gendron, Bieniek et al., 2013).

C9orf72 repeat expansion is the most common genetic cause of FTD and ALS. It is indeed found in 4-19% of individuals with FTD (Boeve, Boylan et al., 2012, Mahoney, Beck et al., 2012, Whitwell et al., 2012), 11% individuals with ALS (Cooper-Knock, Hewitt et al., 2012) and in 17-28% of patients with FTD-ALS (Boeve et al., 2012), depending on the population. However, individual clinical presentations of *C9orf72* expansion carriers are very heterogeneous, even within the same family (Hsiung, DeJesus-Hernandez et al., 2012, Van Mossevelde, van der Zee et al., 2017). Furthermore, apart from FTD and ALS, *C9orf72* repeat expansion has also been documented in cases of AD, Parkinson's disease (PD), Huntington disease phenocopy and several other conditions (Cacace, Van Cauwenberghe et al., 2013, Harms, Benitez et al., 2013, Hensman Moss, Poulter et al., 2014, Majounie, Abramzon et al., 2012). According to several studies, 65% of patients carrying the expansion expresses the bvFTD phenotype of the disease (Chio, Borghero et al., 2012, DeJesus-Hernandez, Mackenzie et al., 2011, Gijssels, Van Langenhove et al., 2012, Renton et al., 2011, van der Zee, Gijssels et al., 2013). Different studies report discordant data about the first behavioral alteration of these patients: some studies report a predominance of disinhibition at the beginning of the disease (Mahoney et al., 2012, Van Langenhove, van der Zee et al., 2013), while others report apathy as the first presentation (Kaivorinne, Bode et al., 2013, Simon-Sanchez, Dopper et al., 2012, Snowden, Rollinson et al., 2012). When patients with pure FTD are compared to those with FTD-MND, what emerges is that disinhibition seems more frequent than apathy if MND is associated with dementia (36% versus 18%), while none of the patients with pure FTD presents disinhibition and 50% presents with apathy (Sha, Takada et al., 2012).

Up to 30% of patients with the expansion can be diagnosed with PPA, most often nfvPPA (Murray, DeJesus-Hernandez et al., 2011). Still, the percentage of patients with the expansion who exhibits speech and language difficulties is much higher (84%) (Kaivorinne et al., 2013). Most of these patients exhibit features of dynamic aphasia (i.e. reduced generation of propositional speech). Furthermore, features of parietal lobe dysfunction such as apraxia and dyscalculia have been reported in 57% and 38% of patient with *C9orf72* expansion, respectively (Mahoney et al., 2012).

A rather common characteristics of patients carrying the expansion is the occurrence of psychiatric symptoms such as anxiety, psychosis, delusions and hallucinations. These occur in 21-56% of mutated patients as compared with < 18% sporadic bvFTD cases (Galimberti, Reif et al., 2014, Kertesz, Ang et al., 2013). Psychosis is sometimes the first symptom to occur in *C9orf72* expansion carriers, even years before manifestation of other symptoms. Still, primary psychiatric patients with schizophrenia or schizoaffective disorder rarely or never carry the expansion (Galimberti et al., 2014, Huey, Nagy et al., 2013).

Parkinsonism is reported in up to 40% of *C9orf72* expansion carriers with FTD (with or without MND) (Bourinaris & Houlden, 2018). Akinesia and rigidity are the most striking features in these patients. However, several studies have not reported an increase in the incidence of parkinsonism in mutated subjects as compared to sporadic ones and *C9orf72* expansions have not been demonstrated to contribute to the risk of PD, are rarely identified in patients diagnosed with PD and even absent in autopsy-confirmed PD (Nuytemans, Inchausti et al., 2014, Theuns, Verstraeten et al., 2014).

Disease onset in expansion carriers occurs between the ages of 27-80 years (with an average onset age between 49.8-63.9 years, depending on the cohort) (Van Langenhove et al., 2013, Van Mossevelde et al., 2017). No significant difference in age of onset has been reported in between the two groups, except for three studies in which *C9orf72* expansion carriers (with FTD, FTD-MND or ALS) developed disease earlier than noncarriers (Sha et al., 2012, van Rheenen, van Blitterswijk et al., 2012).

Atrophy in *C9orf72* mutated patients has variable patterns, but is usually symmetric and diffuse, with involvement of frontotemporal regions, often including also parietal and occipital lobes (Whitwell et al., 2012). Several studies have reported that, compared to non-carriers, *C9orf72* expansion carriers exhibit a considerable atrophy at the level of the thalamus and/or cerebellum (Irish, Devenney et al., 2013, Mahoney et al., 2012, Mahoney, Ridgway et al., 2014, Sha et al., 2012). Some studies have also suggested that severe atrophy of the precuneus can discriminate between sporadic and *C9orf72* FTD (Devenney, Hornberger et al., 2014, Irish et al., 2013, Whitwell & Josephs, 2012, Whitwell et al., 2012).

1.2.2. GRN

There are over 70 known pathogenic mutations affecting *GRN*. The majority of these result in a loss of function caused by either the production of aberrant *GRN* transcripts (secondary to frameshift, nonsense or splice mutation), which are largely degraded, or by prevention of translation (e.g. mutation in the translation initiation codon), which results in a decreased *GRN* expression of up to 50%. Therefore, in these cases a mechanism of *GRN* haploinsufficiency leads to the development of an FTLD syndrome. A subgroup of missense mutations instead exerts its pathogenic effect in altering the structure and stability of *GRN*, resulting in partial haploinsufficiency (van der Zee, Le Ber et al., 2007). *GRN* is an 88 kDa glycoprotein composed of 7.5 cysteine-rich granulin domains. These can be cleaved into 6kDa units that go under the name of granulins. *GRN* is expressed by both neurons and microglia, at increasing concentrations with age (Petkau & Leavitt, 2014). Both *GRN* and granulins are involved in neuroinflammation, neurite outgrowth, stress response, lysosome biology and synapse biology (Petkau & Leavitt, 2014).

After *C9orf72*, pathogenic mutations in *GRN* are the second most prevalent genetic cause of FTLD-TDP (Van Mossevelde et al., 2018). They cause 1-2% of FTD, 4-26% of familial FTD, 21-25% of autopsy-confirmed FTLD-TDP and 56% of familial FTLD-TDP (Beck, Rohrer et al., 2008, Le Ber, Camuzat et al., 2008, Pickering-Brown, Rollinson et al., 2008). Loss-of-function mutations in *GRN* cause heterogeneous neurodegenerative diseases, even among relatives carrying the same mutation. The majority of individuals carrying a mutation in *GRN* is diagnosed with FTD, bvFTD being more frequent than PPA (Josephs, Ahmed et al., 2007, Sassi, Capozzo et al., 2016). Still, PPA (and more specifically nvPPA) is more common in individuals carrying a *GRN* mutation as compared to those with sporadic FTD (Van Mossevelde, van der Zee et al., 2016). *GRN* mutations can also be associated with presentations resembling AD, PD, dementia with Lewy bodies and CBS (Chen-Plotkin, Martinez-Lage et al., 2011, Kelley, Haidar et al., 2010, Mesulam, Johnson et al., 2007, Pires, Coelho et al., 2013, Puoti, Lerza et al., 2014, Spina, Murrell et al., 2007).

Most of the patients with a *GRN* mutations at neuropsychological testing exhibit executive dysfunction. In the first stages of the disease, up to 33% of patients show episodic memory deficits of the hippocampal type that resemble AD or MCI (Whitwell, Weigand et al., 2011). On the other hand, behavioral symptoms develop early in 75% of patients with a *GRN* mutation, but it is comparable to the percentage of patients affected

by sporadic FTD (Whitwell, Jack et al., 2007). Apathy and social withdrawal are the main behavioral symptoms developed by *GRN* mutated patients, which rarely show disinhibition. Language impairment is present at first evaluation in 20-91% mutated patients, depending on the population, while it is only appreciated in 20-23% of noncarriers (Chen-Plotkin et al., 2011).

In individuals developing PPA, nfvPPA is the most common variant. Still, a *GRN*-mutation-associated PPA variant has also been proposed, including elements of both nfvPPA and lvPPA (Rohrer, Crutch et al., 2010). Indeed, some individuals with *GRN* mutation can be diagnosed with lvPPA (Josephs, Duffy et al., 2014, Kim, Ahmadian et al., 2016). In most instances, lvPPA is characterized by AD pathology. Still, a lack of amyloid-beta deposition in a lvPPA patient is strongly suggestive of *GRN* mutation. nfvPPA in *GRN* mutated patients is characterized by impoverished propositional speech, severe anomia, prolonged word-finding pauses, impaired speech repetition, which is most marked for sentences and impaired verbal short-memory (Caso, Villa et al., 2012, Milan, Napoletano et al., 2017). Single-word comprehension is sometimes spared despite impaired comprehension of grammatically complex sentences. Carriers of *GRN* mutations also show phonemic and semantic paraphasias and make grammatical errors (even though it is quite hard to assess the latter, owing to the scarcity of spontaneous speech) (Rohrer et al., 2010). On the other hand, progressive apraxia of speech is extremely rare in these patients (Flanagan, Baker et al., 2015). If a clear diagnosis of PPA cannot be done, the language impairment mainly features mild anomia or decreased speech output consistent with dynamic aphasia.

Parkinsonism also occurs more frequently in *GRN* FTD patients as compared to other forms of FTD, with a percentage of 30-90% of cases, depending on the population (Spina et al., 2007). Conversely, mutated patients less commonly show pyramidal signs and concomitant MND is indeed rare (Kuuluvainen, Poyhonen et al., 2017). Furthermore, only patients with missense *GRN* mutations with unknown pathogenicity have been described in patients carrying a MND phenotype or in patients with FTD and a positive family history of MND (Schymick, Yang et al., 2007, Sleegers, Brouwers et al., 2008).

Age of onset ranges between 35 and 88 years, with an average of 53.3-64.5 years, depending on the cohort (Chiang, Rosvall et al., 2008). Disease duration shows an average of 5-7 years, ranging from 1 to 20 years. In the majority of studies, both age of

onset and disease duration were comparable between carriers and noncarriers. Still, in a few series, an earlier onset (Premi, Formenti et al., 2014) or a shorter disease duration were observed in carriers.

At neuroimaging, the most striking feature of *GRN* mutation carriers is an extremely widespread and severe brain atrophy and neuronal loss. Furthermore, whole-brain atrophy rate is faster as compared to noncarriers. The pattern of both atrophy and functional impairment is remarkably asymmetric in *GRN* mutated patients, which however do not show a dominant hemisphere. Frontotemporal regions are mainly affected (Whitwell, Jack et al., 2009b), but the pattern of atrophy characterizing *GRN* mutations includes early involvement of parietal lobes. Furthermore, according to some studies, atrophy of the right lateral parietal lobe is predictive for *GRN* mutations. Another feature of these patients is the presence of white matter hyperintensities in the atrophied regions (Caroppo, Le Ber et al., 2014, Paternico, Premi et al., 2016, Pietroboni, Fumagalli et al., 2011). Neuropathological studies have suggested that these WM hyperintensities might not be vascular in origin, but rather associated with prominent microglial activation (Woollacott, Bocchetta et al., 2018).

For what concerns *GRN* patients presenting with lvPPA, neuroimaging findings are markedly asymmetric with a relatively preserved right hemisphere and a majorly involved left anteromedial temporal and medial prefrontal cortices; this helps distinguishing them from patients with AD pathology, which instead show greater involvement of the right temporoparietal and frontal lobes (Whitwell, Boeve et al., 2015).

1.2.3. MAPT

Part of the following paragraph has been published in Agosta F, Spinelli EG, Filippi M. Expert Rev Neurother. 2018 May;18(5):395-406, doi: 10.1080/14737175.2018.1463160.

The *MAPT* gene, located on chromosome 17q21, encodes for the tau protein, which in its 4R isoform accumulates in both neurons and glial cells, causing FTLD. Henceforth, FTLD-tau can be defined as a tauopathy affecting white and grey matter in the absence of amyloid beta deposition. FTLD due to *MAPT* mutations affects men and women equally. The average age of onset of the disease is 49 years, with a range from the early 20s to the late 70s, which is a presentation similar to sporadic FTLD. The average life expectancy at symptom onset is of 8.5 years (ranging from 1.5 to 26 years) (Reed,

Wszolek et al., 2001, Wszolek, Krygowska-Wajs et al., 2003). Disease phenotype differs significantly in patient with the same *MAPT* mutation, both within and between families (Bugiani, Murrell et al., 1999, Forman, 2004). It is still unknown to which extent genetic modifiers and/or environmental factors contribute to the phenotypic variability in clinical presentation.

The vast majority of mutations affecting *MAPT* encoding region occur in the microtubule-binding domain repeats, resulting in a mutant tau protein with a reduced ability to interact with microtubules (Dayanandan, Van Slegtenhorst et al., 1999). These mutations occur in exons 9-13 in almost every case. On the other hand, most intronic mutations are clustered in the 5'-splice site of the intron following exon 10. The primary effect of mutations at the level of coding region is equivalent to a partial loss of function. The consequence of the mutation is expressed at the RNA level, where it results in the overproduction of wildtype 4R tau, which interacts more strongly with microtubules than 3R tau (Goedert & Jakes, 1990). This overproduction of 4R tau results in excess of tau over available binding sites on microtubules, leading to cytoplasmic accumulation of unbound 4R tau, which results cytotoxic.

At a clinical level, the onset of MAPT FTD is generally insidious (Greaves & Rohrer, 2019). However, patients with a fully developed clinical syndrome usually show at least two of the three cardinal symptoms, which include behavioral and personality disturbances, cognitive impairment and/or motor dysfunction, usually as extrapyramidal/parkinsonisms. Even at a clinical level, a substantial heterogeneity exists, even in individuals carrying the same mutation (either in different families or in the same family) (Greaves & Rohrer, 2019). Among the behavioral and personality disturbances, disinhibition, apathy, loss of empathy, emotional flatness, impulsive and/or compulsive behavior, lack of regard for personal hygiene, hyperorality and in some cases verbal/physical aggressiveness are the major symptoms that can be encountered. In the cognitive sphere, instead, at the beginning of the disease patients usually demonstrate inattention and executive dysfunction (e.g. difficulty in initiating or completing activities or tasks), disorganization, impaired judgement and decision making with a relative preservation of memory, visuospatial function and orientation. Henceforth, those patients generally fulfill criteria for bvFTD (Greaves & Rohrer, 2019). When patients or their relatives report episodes of memory loss in daily life, this is often a reflection of the

effects of attentional or executive dysfunction on either encoding or retrieval. Still, it is important to consider that some *MAPT* patients can sometimes present with a profound amnesic syndrome (Reed, Grabowski et al., 1997). In literature, also cases of *MAPT* FTD patients with a diagnosis of semantic dementia exist, even if it is usually associated with behavioral derangements as well (Pickering-Brown et al., 2008). Furthermore, in an individual carrying the V363I substitution, other characteristics of semantic dementia have been described, including anomia and right temporal lobe atrophy (Bessi, Bagnoli et al., 2010). Henceforth, behavioral derangements are not the only hallmark of *MAPT* FTD and patients may display disorders at the level of semantic memory as well.

Progressive nonfluent aphasia can be appreciated in the initial stages of the disease (Munoz, Ros et al., 2007) even though patients more commonly develop adynamic aphasia, which is characterized by a very poor speech as they lose the ability to generate language. Later in the course of the disease, deterioration of memory, orientation and visuospatial function develop, as well as echolalia (i.e. meaningless repetition of another person's spoken words), palilalia (i.e. automatic repetition of one's own words or syllables) verbal and vocal perseveration (Greaves & Rohrer, 2019). Eventually, progressive dementia encompassing different cognitive domains develops and patients generally become mute.

MRI of patients with *MAPT* mutations reveal atrophy of the frontal and/or temporal lobes with occasional involvement of the parietal lobes. This is accompanied by enlargement of the lateral ventricles (Boeve, Tremont-Lukats et al., 2005, Dumanchin, Camuzat et al., 1998, Murrell, Spillantini et al., 1999, Whitwell, Jack et al., 2009a, Whitwell et al., 2009b, Yasuda, Yokoyama et al., 2000). In the majority of patients, cortical atrophy is relatively symmetrical. Furthermore, T2-weighted images may highlight accumulation of paramagnetic substances (iron) at the level of mesencephalic nuclei as well as increased T2-weighted signal changes in the WM. When comparing *MAPT* mutations to other FTD-causing mutations, patients affected by *MAPT* present a relatively symmetric atrophy of the anterior temporal lobe, accompanied by lesser atrophy of the orbitofrontal and lateral prefrontal cortices. When *MAPT* mutation affects the splicing of exon 10, patients preferentially show medial temporal lobe atrophy, as opposed to mutations affecting the coding region, which are most commonly associated with lateral temporal lobe involvement (as different tau isoforms, 3R and 4R will be

produced). Both rates of atrophy and sequences of anatomical involvement are highly variable in hereditary tauopathies, even in individuals carrying the same mutation; this is the main reason why being able to correlate structural brain imaging and biology would be unlikely. Longitudinal studies have suggested that *MAPT* mutations are associated with an atrophy rate which is intermediate between those of *GRN* and *C9orf72* (Mahoney et al., 2012, Whitwell, Jack et al., 2011a).

1.2.4. Other mutations

TBKI. Mutations in these gene have been identified for the first time in 2015 in an ALS cohort and, subsequently, in patients with FTD as well (Cirulli, Lasseigne et al., 2015, Freischmidt, Wieland et al., 2015, Gijselinck, Van Mossevelde et al., 2015, Pottier, Bieniek et al., 2015). Loss of function mutations have been associated with the development of symptoms. These lead to the degradation of *TBKI* transcript, with a net 50% reduction in its production. Gene deletions have also been described in these patients (van der Zee, Gijselinck et al., 2017). *TBKI* belongs to I κ B kinase family and has a role in autophagy, neuroinflammation and phosphorylation of different substrates. *TBKI* mutations represent 0.4-3.4% of ALS cases, 0.2-1.3% of FTD cases and 3.3-4.5% of FTD-ALS cases (Gleason, Ordureau et al., 2011, Weidberg & Elazar, 2011). More than 50% of *TBKI* mutated patients has a diagnosis of MND (mainly ALS), while 25% of them has pure FTD and the remaining percentage is affected by a combination of MND and FTD or unspecified dementia (Borghero, Pugliatti et al., 2016, Kim, Oh et al., 2017, Tsai, Liu et al., 2016, Williams, McCann et al., 2015). Of the patients with FTD, over 60% has a diagnosis of bvFTD. To date, very few detailed phenotype descriptions exist in literature and different cohorts have displayed diverse features. None among either the behavioral or the language and speech impairments has resulted to be clearly predominant.

At the level of neuroimaging, the majority of *TBKI* mutated patients display cortical atrophy at the level of frontal and temporal lobes, while 25-30% patients present medial temporal lobe or hippocampal atrophy (Van Mossevelde et al., 2018). On the other hand, functional neuroimaging has showed parietal involvement in up to 60% of patients, which was not however correlated to the presence of symptoms of parietal dysfunction. Furthermore, in 69% and 89% of patients, an asymmetric pattern of atrophy and

functional impairment has been described, respectively, with left hemisphere being more affected. Mesencephalic and cerebellar atrophy has also been described in *TBKI* mutated patients, but a larger cohort of subjects would be necessary to confirm this finding (Van Mossevelde et al., 2018).

FUS. The product of this gene is an RNA-binding protein involved in splicing and nuclear export of mRNA. Mutations in this gene have also been associated with Ewing sarcoma and other soft tissue tumors. Patients generally display ALS, but a minority can develop bvFTD, FTD-MND or PPA phenotypes. Recently, a specific phenotype related to sporadic FTLD-FUS pathology has emerged, which is characterized by a very young onset (22–46 years), prominent caudate atrophy, and clinical features of marked obsessiveness, social withdrawal, hyperorality often with pica and ritualistic behaviors. The cognitive profile instead is characterized by subcortical executive dysfunction in the absence of cortical language, perceptual and praxis impairments.

TARDBP. Mutations in this gene account for 4-6% of familial ALS cases, 1% of ALS sporadic cases, a small proportion of cases with combined FTD-MND and can also present with a broad phenotype that includes parkinsonian featured or overlap syndrome of MND/PSP (Chio, Calvo et al., 2010, Moreno, Rabinovici et al., 2015, Rutherford, Zhang et al., 2008). It is very rare to find cases of *TARDBP* mutations associated with pure FTD (< 20 cases identified). Age of onset has a wide range (29-77 years) (Borroni, Bonvicini et al., 2009, Gelpi, van der Zee et al., 2014, Gitcho, Bigio et al., 2009).

SOD1. According to a UK study carried out in 2009 (Wicks, Abrahams et al., 2009) that analyzed cases of familial ALS, *SOD1* mutations accounted approximately for 20% of cases. Patients with this mutation had a longer disease duration as compared to other genetic ALS patients. Cognitive abnormalities were less evident in patients with *SOD1* mutations as compared to either other genetic or sporadic ALS cases and they lacked any sign of behavioral dysfunction, which were instead more evident in non-*SOD1* familial ALS. Still, *SOD1* patients showed higher levels of emotional lability overall, which apparently occurred independently of cognitive impairment, notwithstanding the fact that the latter can be associated with aspects of cognitive dysfunction (Wicks et al., 2009).

Another study (Agosta, Spinelli et al., 2018b) described patients with *SOD1* ALS as having a longer disease duration and slower functional decline as compared to sporadic ALS patients. Furthermore, the two groups showed similar cognitive profiles. Furthermore, according to a recent Italian study, *SOD1* mutations correlate with flail leg phenotype and were less frequent in bulbar phenotype (Chio, Moglia et al., 2020). At conventional MRI, *SOD1* ALS patients do not display any cortical or white matter alteration relative to healthy controls. As showed in following chapters, advanced neuroimaging techniques are indeed needed to unravel subtle differences in these two groups of patients.

1.3. MRI advanced techniques: applications to FTLD

1.3.1. Structural volumetric MRI

The majority of imaging studies in FTLD used volumetric T1-weighted MRI to investigate atrophy in gray matter (GM) structures, both cortical and subcortical. Brain volume, rate of brain atrophy or the volumes of different regions of interest (ROIs) can be quantified with this technique. By applying several post-processing analytical techniques, investigation of changes voxel-by-voxel (voxel-based morphometry, VBM) or measurement of cortical thickness (using software like FreeSurfer) can be done on T1-weighted images.

a. FTD presentations

At a single-patient level, a semiquantitative assessment of atrophy can be performed by using visual rating scales. This is done by dementia experts and has yielded good diagnostic accuracy in the discrimination between AD and FTD and a specificity of 81% (Harper, Fumagalli et al., 2016). Indeed, several studies have assessed the discriminatory power of atrophy patterns to distinguish FTLD from AD. In fact, FTD is associated with greater atrophy in the frontal, insular, anterior cingulate cortices and striatum, whereas AD is characterized by a more severe damage to the posterior cingulate, precuneus, and occipital regions (Agosta, Canu et al., 2012a). Studies that compared bvFTD with typical and atypical AD presentations (i.e., early-onset AD, or AD cases with prominent behavioral or language deficits) indicated that, independent of clinical phenotype, cortical

thinning of the anterior temporal and frontal lobes is suggestive of an FTD diagnosis, whereas atrophy of the posterior cingulate gyrus, parietal lobe, and frontal pole indicates AD pathology (Canu, Agosta et al., 2017, Lehmann, Rohrer et al., 2010, Whitwell, Jack et al., 2011b).

Also at a molecular level, variability in the atrophy pattern can be used in order to suggest the underlying pathology of FTD presentations. Indeed, within FTLT-tau, Pick's disease (PiD) is characterized by early severe, asymmetric fronto-insular atrophy that extends into the anterior temporal lobes (Murray, Kouri et al., 2014), whereas patients with bvFTD due to CBD show relative sparing of the fronto-insular and temporal structures and greater atrophy of the parietal lobes (Rankin, Mayo et al., 2011). Basal ganglia atrophy is more evident in CBD than in PSP (Josephs, Lin et al., 2008), whereas cases with PSP pathology show preferential involvement of the brainstem and degeneration of the superior cerebellar peduncle (Boxer, Geschwind et al., 2006, Josephs, Whitwell et al., 2008, Santos-Santos, Mandelli et al., 2016). Of the four subtypes of FTLT-TDP pathology, types A and B are most commonly observed in bvFTD cases (Perry et al., 2017). Type A is usually found in bvFTD patients with *GRN* mutations, who typically show asymmetric atrophy extending into the parietal lobes with relative sparing of the cerebellum (Bocchetta, Cardoso et al., 2016, Whitwell et al., 2015). FTLT-TDP type B pathology is often observed in FTD cases with concurrent motor neuron disease (FTD-MND) and is associated with predominant symmetrical atrophy of the frontal lobes and involvement of the insula and the anterior temporal lobe (Rohrer & Rosen, 2013). FTLT-TDP type C is the prevalent underlying pathology of svPPA and the right temporal variant of bvFTD (Karageorgiou & Miller, 2014). Finally, FTLT-FUS typically presents with severe atrophy of the caudate nuclei (Lee, Seeley et al., 2012).

An alternative approach to volumetric MRI analysis involves the use of serial registration scanning to quantify changes in brain volume over time. Relying on the detection of in brain volume changes in the same subject, this technique avoids the problem of interindividual variability in whole-brain size (Chan, Fox et al., 2001a). Only a few MRI studies have attempted to delineate the longitudinal anatomical progression of FTLT, and all of them agree that longitudinal rates of change are largest in the regions that are already most involved at baseline. More specifically, bvFTD patients show greater atrophy rate in the frontal lobes (Krueger, Dean et al., 2010), whereas svPPA

patients show the greatest longitudinal volume loss in the temporal lobes (Krueger et al., 2010). One study assessing longitudinal atrophy changes in nvPPA (Whitwell, Anderson et al., 2004) identified a significant cluster in a small area adjacent to the most medial extent of the left sylvian fissure. Taken as a whole, FTLD patients show increased rates of volume loss in frontal, temporal and parietal regions and a significant expansion of the lateral and third ventricles, bilaterally, compared with controls (Whitwell et al., 2004), with an annualized percent change of -1.6% for whole brain volume and 11.6% for ventricular volume (Knopman, Jack et al., 2009). bvFTD patients show a significantly higher mean atrophy rate [3.7%, standard deviation (SD) 2.5%], compared with both PPA patients (2.5%, SD 1.0%) and AD patients (2.4%, SD 1.0%) (Chan et al., 2001a). Nonetheless, this difference is reduced when atrophy rates in the most involved lobes are compared: 6.3% of atrophy rate in the left frontal lobe and 6.1% in the right frontal lobe for bvFTD patients as opposed to 5.9% in the left temporal lobe and 4.8% in the right temporal lobe for svPPA patients (Krueger et al., 2010). No correlation was found between atrophy rate and either age and gender (Chan et al., 2001a) or baseline brain volume and baseline atrophy (Knopman et al., 2009).

b. MND

Part of the following paragraph has been published in Agosta F, Spinelli EG, Filippi M. Expert Rev Neurother. 2018 May;18(5):395-406, doi: 10.1080/14737175.2018.1463160.

In MND syndromes, initial volumetric studies showed diverging results, with some reporting focal atrophy in motor/premotor regions (Agosta, Pagani et al., 2007, Turner, Hammers et al., 2007), and others reporting no significant atrophy (Abrahams, Goldstein et al., 2005), most likely as a consequence of variable image processing pipelines and statistical approaches. A meta-analysis including 638 ALS patients showed significant volume loss of the right precentral gyrus and bilateral inferior frontal cortex (Shen, Cui et al., 2016). Volumetric studies have also shown diverging atrophy patterns characterizing specific clinical presentations. For example, ALS patients with bulbar and limb onset showed different GM involvement within the motor strip, consistent with their clinical disability (Bede, Bokde et al., 2013). Patients with ALS and FTD have shown the most severe atrophy involving widespread frontotemporal cortical areas and the caudate nucleus (Lillo, Mioshi et al., 2012, Masuda, Senda et al., 2016), although significant GM

loss in extensive cortical and subcortical regions - including the caudate nucleus – has been observed also in patients with subtle cognitive and/or behavioral impairment (Alruwaili, Pannek et al., 2017).

A consistent cortical thinning has also been shown in the primary motor areas of ALS patients (Agosta, Valsasina et al., 2012b, Verstraete, van den Heuvel et al., 2010), with additional involvement of extra-motor cortical regions that was particularly severe in those with cognitive or behavioral impairment (Agosta, Ferraro et al., 2016, Schuster, Kasper et al., 2014a). Focal cortical alterations of the motor areas were found to mirror specific clinical presentation (Schuster, Kasper et al., 2013). Significant associations were observed between primary motor cortical thinning over one year and the progression of clinical disability (Kwan, Meoded et al., 2012). Cortical motor thinning is likely specific to UMN degeneration, as studies that aimed to assess its presence in prevalent LMN involvement and ALS-mimic syndromes showed negative results (Spinelli, Agosta et al., 2016, Walhout, Westeneng et al., 2015). One longitudinal MRI study demonstrated a significant worsening of cortical thinning from the primary motor cortex to frontal, temporal, and parietal regions (Schuster, Kasper et al., 2014b). Such extra-motor cortical damage and its pattern of progression is consistent with postmortem studies that have recently led to the development of a pathological staging system of ALS (Brettschneider et al., 2013), supporting this model *in vivo*.

Recent studies have applied VBM or cortical thickness approaches to the specific assessment of subcortical structures. Notably, the caudate nucleus, nucleus accumbens (Bede, Elamin et al., 2013), and thalamus (Menke, Korner et al., 2014) were found to be involved in patients with ALS, consistent with neuropathological studies (Brettschneider et al., 2013). Volume loss in the basal ganglia has also been shown to correlate with shorter survival in ALS patients (Westeneng, Verstraete et al., 2015). Cerebellar involvement shown by neuroimaging studies (Tan, Devenney et al., 2014) is also in line with findings from *postmortem* studies (Brettschneider et al., 2013). Cerebellar atrophy has been shown to affect predominantly the inferior lobules and vermis in ALS patients with motor symptoms and the superior lobules and crus in patients with cognitive and neuropsychiatric symptoms (Tan et al., 2014).

1.3.2. Diffusion tensor MRI

Diffusion tensor magnetic resonance imaging (DT MRI) allows to evaluate white matter (WM) structures by measuring microstructural integrity. It is able to determine the rate of diffusion of water molecules in different directions in the CNS parenchyma, which reflect pathological changes in microstructure. For example, an increase in radial diffusivity (radD) is associated with myelin breakdown, while a decrease in fractional anisotropy (FA, a measure of both axial diffusivity and radial diffusivity) suggests non-specific loss of WM integrity (Lu, Lee et al., 2014). Alterations of DT MRI parameters therefore suggest axonal pathology and loss of structural connectivity within the brain (Andica, Kamagata et al., 2020).

a. FTD presentations

DT MRI allows differentiation of FTD from other types of dementia (such as AD), or from cognitively unimpaired individuals. In several studies, when compared with AD, bvFTD patients have shown more severe damage of anterior WM regions, including the genu of the corpus callosum, inferior fronto-occipital fasciculus (IFOF), uncinate, cingulum and anterior corona radiata (Avants, Cook et al., 2010, Canu et al., 2017, Zhang, Schuff et al., 2009). In particular, uncinate fasciculus WM damage has been considered as a key predictor to distinguish bvFTD from early-onset AD clinical presentations (Canu et al., 2017). By contrast, AD patients generally did not show areas of significant WM damage relative to FTD patients (Avants et al., 2010, Zhang et al., 2009), thus suggesting that WM injury might be more prominent in bvFTD than in AD. In bvFTD presentations, the cingulum bundle and genu of the corpus callosum and superior longitudinal fasciculus (SLF) seem to be particularly involved (Mahoney et al., 2014), as well as tracts of the ventral stream in the temporal lobes, such as the inferior longitudinal fasciculus (ILF), uncinate, and IFOF. Diffusivity abnormalities have also been reported in more posterior WM regions, including the cingulum and posterior SLF (Agosta et al., 2012a, Whitwell, Avula et al., 2010, Zhang, Tartaglia et al., 2013).

PPA subtypes, on the other hand, are characterized by different spatial patterns of WM damage. nfvPPA mainly affects the left orbitofrontal and anterior temporal WM (SLF) (Agosta et al., 2012a, Galantucci, Tartaglia et al., 2011, Mahoney, Malone et al., 2013, Whitwell et al., 2010, Zhang et al., 2013). By contrast, ventral tracts connecting the

temporal lobe with occipital and orbitofrontal regions (i.e., the ILF and uncinate fasciculi) are relatively spared in nfvPPA and typically most affected in svPPA (Agosta et al., 2012a, Galantucci et al., 2011, Mahoney et al., 2013, Whitwell et al., 2010, Zhang et al., 2013). In fact, a greater involvement of tracts of the ventral stream (i.e., the uncinate and ILF) has proven to indicate an svPPA diagnosis when nfvPPA is in the differential (Agosta et al., 2015a). Moreover, in nfvPPA patients with prominent apraxia of speech, WM connections within the frontal lobe and in fronto-striatal circuits show prominent damage (Mandelli, Caverzasi et al., 2014). The frontal aslant tract, which connects Broca's area to the anterior supplementary motor regions, is particularly vulnerable in nfvPPA with apraxia of speech (Catani, Mesulam et al., 2013).

DT MRI can also provide some suggestions in order to differentiate FTLD-tau from FTLD-TDP. A more severe damage of WM integrity has been shown in FTLD-tau (Agosta, Galantucci et al., 2015b, McMillan, Irwin et al., 2013). It has also been demonstrated that svPPA-tau is associated with severe frontal WM atrophy, while WM atrophy in svPPA-TDP is restricted to the anterior temporal regions, consistent with the view that WM changes in FTLD-tau relative to FTLD-TDP are more widespread (Spinelli et al., 2017). Similarly, nfvPPA-TDP was found to lack any significant WM damage, while nfvPPA-tau WM damage followed the frontal aslant tract (Caso, Mandelli et al., 2014, Catani et al., 2013, Spinelli et al., 2017).

Longitudinal change in WM of FTD patients seems to occur mostly in areas of baseline abnormality (Elahi et al., 2017). bvFTD patients show the largest reductions in FA within bilateral paracallosal cingulum (right: -6.8%/year; left: -5.5%/year) and bilateral uncinate fasciculus (right: -4.2%/year; left: -3.1%/year) and the largest increases in mean diffusivity (MD) within bilateral uncinate fasciculus (right: 5.1%/year; left: 6.2%/year) and bilateral parahippocampal cingulum (right: 4.3%/year; left: 5.0%/year) (Mahoney, Simpson et al., 2015). In nfvPPA patients, when compared with baseline, additional WM abnormalities are observed in diverse regions: anterior thalamic radiation, anterior cingulum, uncinate fasciculus, genu of the corpus callosum and brainstem; these changes are more pronounced in the right hemisphere compared to the left one (except for the anterior thalamic radiation, which presents a bigger progression in the left hemisphere) (Lam, Halliday et al., 2014). In svPPA patients, instead, progressive longitudinal WM changes extend into the IFOF and the splenium of the corpus callosum, with no

progression in the cingulum (Lam et al., 2014). In a longitudinal analysis of healthy controls, small changes in FA were observed bilaterally in the SLF, ILF, IFOF and uncinate fasciculi; nonetheless, the scale of these changes was about two to threefold less compared to FTLD patients, thus confirming that the abnormalities found in the pathologic group reflected disease, rather than simple ageing effects (Lam et al., 2014).

b. MND

Part of the following paragraph has been published in Agosta F, Spinelli EG, Filippi M. Expert Rev Neurother. 2018 May;18(5):395-406, doi: 10.1080/14737175.2018.1463160. DT MRI studies performed in ALS patients have consistently shown a pattern of decreased FA and increased mean diffusivity (MD) in a characteristic WM region encompassing the CST and the body of the corpus callosum, as confirmed by a large multicenter study (Muller, Turner et al., 2016). Similar to GM atrophy, additional microstructural damage to extra-motor frontotemporal tracts has also been shown, especially in ALS patients with variable degree of cognitive or neuropsychiatric impairment (Agosta et al., 2016, Lillo et al., 2012, Spinelli et al., 2016, Trojsi, Corbo et al., 2013). The greatest and most widespread DT MRI alterations were found in patients with primary lateral sclerosis, encompassing both motor and extra-motor areas and correlating with the severity of cognitive deficits (Agosta, Galantucci et al., 2014b). On the contrary, the least diffuse WM damage was observed in patients with predominant LMN involvement (Prudlo, Bissbort et al., 2012, Rosenbohm, Muller et al., 2016, Spinelli et al., 2016).

The topographical distribution of WM damage, extending from motor to extra-motor tracts, has been used to classify patients according to stage of disease (Kassubek, Muller et al., 2014) in agreement with pathological studies (Brettschneider et al., 2013). In this context, longitudinal studies are fundamental to validate current views about pathological spreading in ALS *in vivo*. Most of these studies focused on alterations within the motor tracts, reporting a significant progression of CST damage in the brain (Kassubek, Muller et al., 2017, Keil, Prell et al., 2012, van der Graaff, Sage et al., 2011). These studies have also demonstrated a significant association between WM motor tract degeneration and the progression of functional disability in MND patients (Kassubek et al., 2017, Keil et al., 2012).

1.3.3. Resting-state functional MRI

Resting-state connectivity network functional MRI maps large-scale neural networks and highlights functional and dysfunctional activities. Resting state (or task-free) functional MRI (RS fMRI) allows the characterization of fluctuations of blood oxygenation level-dependent (BOLD) signal across the brain, which are consistently organized into distinct, tightly correlated functional-anatomic networks, some of which are typically disrupted in FTLD.

a. FTD presentations

RS fMRI allows distinguishing bvFTD from AD by evidencing differences in connectivity at the level of an anterior “Salience Network” (SN, altered in bvFTD) and a posterior “Default Mode Network” (DMN, typically affected in AD). bvFTD shows attenuated SN connectivity most notably in frontoinsula, cingulate, striatal, thalamic and brainstem nodes, with co-occurrent enhanced connectivity within the DMN; on the contrary, AD shows reduced DMN connectivity to posterior hippocampus, medial cingulo-parieto-occipital regions and dorsal raphe nucleus, in contrast with intensified SN connectivity (Zhou, Greicius et al., 2010). A combination of SN and DMN connectivity scores was able to classify healthy subjects, AD patients, and bvFTD patients with an accuracy greater than 90% (Zhou et al., 2010).

Several studies have explored RS functional connectivity in patients with bvFTD (Farb, Grady et al., 2013, Filippi, Agosta et al., 2013, Whitwell, Josephs et al., 2011, Zhou et al., 2010), demonstrating an altered connectivity of the SN. Briefly, the SN is activated in response to emotionally significant internal and external (interpersonal) stimuli (Seeley, Menon et al., 2007), while DMN participates in episodic memory (Buckner, Snyder et al., 2005, Zysset, Huber et al., 2002). Furthermore, bvFTD is also characterized by decreased connectivity of the ventral salience network in the basal ganglia, and divergent connectivity effects in the dorsolateral prefrontal cortex (decreased) and precuneus (enhanced) within the right attention/working memory network. The executive network also shows decreased connectivity in bvFTD compared with controls, whereas, compared to AD, bvFTD express attenuated connectivity in the dorsal salience network (Filippi et al., 2013). Low-frequency fluctuations showed in the left insula by patients

with both bvFTD and svPPA in baseline RS scores can predict changes in Frontal Behavioral Inventory scores at follow up (Day, Farb et al., 2013).

In nfvPPA, selective functional changes within the left fronto-insular speech production network (including the frontal operculum, primary and supplementary motor areas and inferior parietal lobule) have been shown to precede the onset of structural alterations (Bonakdarpour, Rogalski et al., 2017). Focal neurodegeneration within the speech production network in nfvPPA has been associated with network-specific topological functional alterations, providing evidence of a network-based degeneration also in this clinical syndrome (Seeley, Crawford et al., 2009). In svPPA, reduced functional connectivity was shown to affect selectively a semantic network centered on the left anterior temporal lobe, but also involving interconnected modality-selective regions in the sensory, motor and association cortices (Guo, Gorno-Tempini et al., 2013).

A longitudinal study assessing functional connectivity between selected brain areas in bvFTD patients during a 1.8 years period revealed a reduction in the mean connectivity between the inferior frontal gyrus and the left frontoparietal network and between the supramarginal gyrus and the right frontoparietal network, with the latter finding being also observed in AD patients (Hafkemeijer, Moller et al., 2017). The same patients also showed a decrease in functional connectivity between the paracingulate gyrus and the DMN and between the angular gyrus and the right frontoparietal network (Hafkemeijer et al., 2017). At the last follow up, when compared with AD patients, the bvFTD group presented lower connectivity between the lateral occipital cortex and the medial visual network and between the anterior cingulate gyrus and the executive control network (Hafkemeijer et al., 2017).

b. MND

Part of the following paragraph has been published in Agosta F, Spinelli EG, Filippi M. Expert Rev Neurother. 2018 May;18(5):395-406, doi: 10.1080/14737175.2018.1463160.

Several studies performed in patients with MND have shown a decreased functional connectivity of the sensorimotor network (Fekete, Zach et al., 2013, Mohammadi, Kollwe et al., 2009, Trojsi, Esposito et al., 2015), whereas others found increased connectivity (Agosta, Canu et al., 2014a, Douaud, Filippini et al., 2011), or complex regional patterns of decreased and increased functional connectivity (Zhou, Xu et al.,

2014). Altered functional connectivity has also been shown in brain networks related to cognition and behavior (especially the DMN and frontoparietal networks) (Agosta, Canu et al., 2013a, Luo, Chen et al., 2012).

Based on RS fMRI findings, it has been suggested that a widespread increase in brain functional connectivity might prevail in earlier stages of the disease as a compensatory mechanism, with subsequent decrease as pathological burden accumulates (Agosta, Spinelli et al., 2018a). Consistent with this hypothesis, increased functional connectivity was found to be higher in patients with less severe WM damage of the CST (Agosta, Valsasina et al., 2011), and associated with lower rate of disease progression (Luo et al., 2012) and preserved motor capabilities (Agosta et al., 2011). Moreover, a recent longitudinal study showed consistent decreased RS functional connectivity within the sensorimotor and thalamic networks, with co-occurrent progressively increased functional connectivity within extra-motor networks, (Menke, Proudfoot et al., 2018), which is also in line with a “disconnection” hypothesis due to the loss of compensation.

1.3.4. MRI connectomics

The term “connectomics” refers to the application of graph theoretical analysis to the study of brain connectivity, from either a structural or a functional point of view. Structural connectivity can be assessed using DT MRI, whereas RS fMRI is used to investigate functional brain connectivity.

MRI connectomics considers the brain as a graph made of nodes (the brain regions) and edges (the structural/functional connectivity between two non-contiguous regions), therefore studying its integrity assessing its network properties, which can be divided in nodal metrics and global metrics. Nodal metrics include nodal degree, indicating the number of connections of a node, and betweenness centrality (or network centrality), indicating the fraction of all shortest paths in the network that pass through a given node, thus providing a measure of the importance of that node for the efficient integration across the network. Global metrics include clustering coefficient, characteristic path length, modularity and assortativity: clustering coefficient is the average fraction in which pairs of neighboring nodes are also neighbors of each other and it is a measure of how the network is organized into subnetworks specialized in specific tasks (Mandelli, Welch et al., 2018); characteristic path length is the average of the shortest path length between all

pairs of nodes of the network and its inverse, the global efficiency, represents the measure of overall information transfer efficiency across the network (Mandelli et al., 2018); modularity describes to which extent groups of nodes in the graph are connected to the members of their own group, indicating the formation of sub-networks within the full network (van den Heuvel and Hulshoff Pol, 2010); assortativity is a measure of correlation between the degree of a node and the mean degree of its nearest neighbors (Newman, 2002): if a network shows positive assortativity, it means that its nodes are likely to be connected to other nodes with the same degree and therefore high-degree nodes (so called hubs) are connected to each other; by contrast, in a network with negative assortativity, hubs are likely not connected to each other (Agosta, Sala et al., 2013c). Assortativity can be considered as a measure of the resilience of a network, since in an assortative network the removal of one high-degree node can be overcome by the interconnectedness of the others (Newman, 2002).

The metrics mentioned above, especially the global ones, can be used to differentiate the networks on the basis of their architecture: a “regular” network, with a high clustering coefficient and a high path length, is characterized by a good local organization but a low global efficiency; on the other hand, a “random” network, with low clustering coefficient and path length, shows a high global efficiency but poor local interconnectedness. Previous studies (Achard, Salvador et al., 2006, Watts & Strogatz, 1998) revealed that the brain network is structured according to the so called “small-world” model, which combines high clustering coefficient and low path length, thus presenting both good local and global connectivity (van den Heuvel and Hulshoff Pol, 2010). As a side effect, this kind of organization causes most of the information processing inside the network to rely on few nodes, called hubs, which are both the fulcrums of local clusters and the links between distant regions and are characterized by high nodal degree and high betweenness centrality.

Pathologies that involve the hubs of the brain network can rapidly disrupt large portions of it and this is the reason why it is of great interest to study the difference in brain network organization between patients affected by neurodegenerative diseases and healthy controls.

Studying the structural and functional connectome of FTLD patients might better elucidate how this pathology spreads through the brain of these subjects, in the same way

as it has already been done in other neurodegenerative diseases, like AD (Filippi, Basaia et al., 2020).

a. FTD presentations

Functional connectomes of both bvFTD patients (Agosta et al., 2013c) and svPPA patients (Agosta, Galantucci et al., 2014c), when compared with controls, show reduced mean network degree (the mean of all the nodal degrees in the network) and clustering coefficient and higher path length and assortativity. In nfvPPA patients, a decrease in assortativity was found, along with an increase in the characteristic path length and the clustering coefficient, although these alterations seem to be limited to the speech production network (Mandelli et al., 2018). Functional global efficiency results higher in bvFTD patients than in nfvPPA ones (Reyes, Ortega-Merchan et al., 2018), although it was found to be lower in bvFTD (Agosta et al., 2013c), svPPA (Agosta et al., 2014c) and nfvPPA (Mandelli et al., 2018) patients than in controls.

Pathologic functional brain networks are also characterized by the loss of hubs and the creation of new ones: in bvFTD patients these new hubs include the right precentral gyrus, left postcentral gyrus and bilateral superior temporal gyrus (Agosta et al., 2013c), while in svPPA patients they comprehend the right inferior frontal gyrus, left precentral gyrus and supplementary motor area and bilateral superior temporal gyrus, middle frontal gyrus and thalamus (Agosta et al., 2014c); on the contrary, some regions including the right superior frontal gyrus and inferior orbitofrontal gyrus, left inferior temporal gyrus, anterior cingulate cortex and bilateral cuneus represent hubs in healthy controls but not in affected patients (Agosta et al., 2014c, Agosta et al., 2013c). nfvPPA patients, when compared with controls, show new hubs in the bilateral inferior and middle frontal gyri (showing increased betweenness centrality) and a loss of hubs in the parietal regions and supplementary motor cortex (both showing reduced nodal degree) (Mandelli et al., 2018).

bvFTD patients exhibit, in their functional connectomes, reduced betweenness centrality in both sides of the frontotemporoinular network (Sedeno, Couto et al., 2016); these patients also present decreased nodal degree in several frontal regions (including the right superior frontal gyrus, left middle orbitofrontal, superior orbitofrontal and middle frontal gyri and bilateral anterior cingulate cortex), in the left insula and caudate nucleus, superior parietal and occipital lobes and bilateral superior temporal pole (Agosta,

Galantucci et al., 2013b, Filippi, Basaia et al., 2017). On the other hand, svPPA patients show reduced nodal degree in various left temporal areas (including the amygdala, parahippocampal gyrus, fusiform gyrus, hippocampus, inferior temporal gyrus and superior temporal pole), some left fronto-occipital regions (like the anterior cingulate cortex, rectus gyrus, olfactory cortex, superior orbitofrontal cortex, cuneus and inferior occipital gyrus), the left caudate nucleus and, in the right hemisphere, the parahippocampal gyrus, middle orbitofrontal cortex, middle and inferior occipital gyri and cuneus (Agosta et al., 2014c).

Compared with healthy subjects, bvFTD patients are characterized by a focal pattern of functional connectivity alterations including frontotemporal pathways and connections to the motor cortex and basal ganglia. However, these patients show higher mean nodal strength, higher local efficiency, and shorter mean path length of the parietal lobe than AD patients (Filippi et al., 2017).

One longitudinal study demonstrated how the functional connectomic approach can help predict the brain atrophy patterns in bvFTD and svPPA patients over time (Brown, Deng et al., 2019). In that study, the baseline atrophy map of each patient was projected onto the functional connectome of a healthy subject and then three different measures (i.e., shortest path length to the disease epicenter, nodal hazard – a measure quantifying atrophy within a given region’s network neighbors –, and baseline atrophy) were used to accurately predict longitudinal atrophy in different brain regions. More precisely, the highest longitudinal atrophy was observed in those regions that were first-degree network neighbors of the disease epicenter and that, at baseline, presented higher nodal hazard and an intermediate level of atrophy (Brown et al., 2019).

b. MND

Graph analysis and connectomics were applied also to study MND. In a cross-sectional study assessing structural connectivity (Verstraete, Veldink et al., 2011), ALS patients showed reduced WM connectivity compared with healthy controls, centered around the primary but also including the frontal cortex and the pallidum, along with globally decreased network efficiency and clustering coefficient. Another study assessed WM alterations using network analysis, showing a significant impairment of motor-frontal-subcortical connections in ALS patients, as compared with healthy controls (Buchanan,

Pettit et al., 2015). Fewer studies applied network-based analyses to the assessment of functional alterations in ALS patients using RS fMRI, demonstrating complex connectivity alterations encompassing frontal, temporal and occipital regions (Geevasinga, Korgaonkar et al., 2017, Zhou, Hu et al., 2016), mirroring widespread multisystem functional rearrangements, as a possible consequence of the pathological progression of TDP-43 deposition through brain networks.

References

- Abrahams S, Goldstein LH, Suckling J, Ng V, Simmons A, Chitnis X, Atkins L, Williams SC, Leigh PN (2005) Frontotemporal white matter changes in amyotrophic lateral sclerosis. *J Neurol* 252: 321-31
- Achard S, Salvador R, Whitcher B, Suckling J, Bullmore E (2006) A resilient, low-frequency, small-world human brain functional network with highly connected association cortical hubs. *J Neurosci* 26: 63-72
- Agosta F, Canu E, Inuggi A, Chio A, Riva N, Silani V, Calvo A, Messina S, Falini A, Comi G, Filippi M (2014a) Resting state functional connectivity alterations in primary lateral sclerosis. *Neurobiol Aging* 35: 916-25
- Agosta F, Canu E, Sarro L, Comi G, Filippi M (2012a) Neuroimaging findings in frontotemporal lobar degeneration spectrum of disorders. *Cortex* 48: 389-413
- Agosta F, Canu E, Valsasina P, Riva N, Prella A, Comi G, Filippi M (2013a) Divergent brain network connectivity in amyotrophic lateral sclerosis. *Neurobiol Aging* 34: 419-27
- Agosta F, Ferraro PM, Canu E, Copetti M, Galantucci S, Magnani G, Marcone A, Valsasina P, Sodero A, Comi G, Falini A, Filippi M (2015a) Differentiation between Subtypes of Primary Progressive Aphasia by Using Cortical Thickness and Diffusion-Tensor MR Imaging Measures. *Radiology* 276: 219-27
- Agosta F, Ferraro PM, Riva N, Spinelli EG, Chio A, Canu E, Valsasina P, Lunetta C, Iannaccone S, Copetti M, Prudente E, Comi G, Falini A, Filippi M (2016) Structural brain correlates of cognitive and behavioral impairment in MND. *Hum Brain Mapp* 37: 1614-26
- Agosta F, Galantucci S, Canu E, Cappa SF, Magnani G, Franceschi M, Falini A, Comi G, Filippi M (2013b) Disruption of structural connectivity along the dorsal and ventral language pathways in patients with nonfluent and semantic variant primary progressive aphasia: a DT MRI study and a literature review. *Brain Lang* 127: 157-66
- Agosta F, Galantucci S, Magnani G, Marcone A, Martinelli D, Antonietta Volonte M, Riva N, Iannaccone S, Ferraro PM, Caso F, Chio A, Comi G, Falini A, Filippi M (2015b) MRI signatures of the frontotemporal lobar degeneration continuum. *Hum Brain Mapp* 36: 2602-14

Agosta F, Galantucci S, Riva N, Chio A, Messina S, Iannaccone S, Calvo A, Silani V, Copetti M, Falini A, Comi G, Filippi M (2014b) Intrahemispheric and interhemispheric structural network abnormalities in PLS and ALS. *Hum Brain Mapp* 35: 1710-22

Agosta F, Galantucci S, Valsasina P, Canu E, Meani A, Marcone A, Magnani G, Falini A, Comi G, Filippi M (2014c) Disrupted brain connectome in semantic variant of primary progressive aphasia. *Neurobiol Aging* 35: 2646-2655

Agosta F, Pagani E, Rocca MA, Caputo D, Perini M, Salvi F, Prella A, Filippi M (2007) Voxel-based morphometry study of brain volumetry and diffusivity in amyotrophic lateral sclerosis patients with mild disability. *Hum Brain Mapp* 28: 1430-8

Agosta F, Sala S, Valsasina P, Meani A, Canu E, Magnani G, Cappa SF, Scola E, Quatto P, Horsfield MA, Falini A, Comi G, Filippi M (2013c) Brain network connectivity assessed using graph theory in frontotemporal dementia. *Neurology* 81: 134-43

Agosta F, Spinelli EG, Filippi M (2018a) Neuroimaging in amyotrophic lateral sclerosis: current and emerging uses. *Expert Rev Neurother* 18: 395-406

Agosta F, Spinelli EG, Marjanovic IV, Stevic Z, Pagani E, Valsasina P, Salak-Djokic B, Jankovic M, Lavrnic D, Kostic VS, Filippi M (2018b) Unraveling ALS due to SOD1 mutation through the combination of brain and cervical cord MRI. *Neurology* 90: e707-e716

Agosta F, Valsasina P, Absinta M, Riva N, Sala S, Prella A, Copetti M, Comola M, Comi G, Filippi M (2011) Sensorimotor functional connectivity changes in amyotrophic lateral sclerosis. *Cereb Cortex* 21: 2291-8

Agosta F, Valsasina P, Riva N, Copetti M, Messina MJ, Prella A, Comi G, Filippi M (2012b) The cortical signature of amyotrophic lateral sclerosis. *PLoS One* 7: e42816

Alruwaili AR, Pannek K, Coulthard A, Henderson R, Kurniawan ND, McCombe P (2017) A combined tract-based spatial statistics and voxel-based morphometry study of the first MRI scan after diagnosis of amyotrophic lateral sclerosis with subgroup analysis. *J Neuroradiol*

Andica C, Kamagata K, Hatano T, Saito Y, Ogaki K, Hattori N, Aoki S (2020) MR Biomarkers of Degenerative Brain Disorders Derived From Diffusion Imaging. *J Magn Reson Imaging* 52: 1620-1636

Andreadis A (2012) Tau splicing and the intricacies of dementia. *J Cell Physiol* 227: 1220-5

Avants BB, Cook PA, Ungar L, Gee JC, Grossman M (2010) Dementia induces correlated reductions in white matter integrity and cortical thickness: a multivariate neuroimaging study with sparse canonical correlation analysis. *Neuroimage* 50: 1004-16

Baker M, Mackenzie IR, Pickering-Brown SM, Gass J, Rademakers R, Lindholm C, Snowden J, Adamson J, Sadovnick AD, Rollinson S, Cannon A, Dwosh E, Neary D, Melquist S, Richardson A, Dickson D, Berger Z, Eriksen J, Robinson T, Zehr C et al. (2006) Mutations in progranulin cause tau-negative frontotemporal dementia linked to chromosome 17. *Nature* 442: 916-9

Beck J, Rohrer JD, Campbell T, Isaacs A, Morrison KE, Goodall EF, Warrington EK, Stevens J, Revesz T, Holton J, Al-Sarraj S, King A, Scahill R, Warren JD, Fox NC, Rossor MN, Collinge J, Mead S (2008) A distinct clinical, neuropsychological and radiological phenotype is associated with progranulin gene mutations in a large UK series. *Brain* 131: 706-20

Bede P, Bokde A, Elamin M, Byrne S, McLaughlin RL, Jordan N, Hampel H, Gallagher L, Lynch C, Fagan AJ, Pender N, Hardiman O (2013) Grey matter correlates of clinical variables in amyotrophic lateral sclerosis (ALS): a neuroimaging study of ALS motor phenotype heterogeneity and cortical focality. *J Neurol Neurosurg Psychiatry* 84: 766-73

Bede P, Elamin M, Byrne S, McLaughlin RL, Kenna K, Vajda A, Pender N, Bradley DG, Hardiman O (2013) Basal ganglia involvement in amyotrophic lateral sclerosis. *Neurology* 81: 2107-15

Bensimon G, Lacomblez L, Meininger V (1994) A controlled trial of riluzole in amyotrophic lateral sclerosis. ALS/Riluzole Study Group. *N Engl J Med* 330: 585-91

Bergeron D, Gorno-Tempini ML, Rabinovici GD, Santos-Santos MA, Seeley W, Miller BL, Pijnenburg Y, Keulen MA, Groot C, van Berckel BNM, van der Flier WM, Scheltens P, Rohrer JD, Warren JD, Schott JM, Fox NC, Sanchez-Valle R, Grau-Rivera O, Gelpi E, Seelaar H et al. (2018) Prevalence of amyloid-beta pathology in distinct variants of primary progressive aphasia. *Ann Neurol* 84: 729-740

Bessi V, Bagnoli S, Nacmias B, Tedde A, Sorbi S, Bracco L (2010) Semantic dementia associated with mutation V363I in the tau gene. *J Neurol Sci* 296: 112-4

Boccardi M, Sabbatoli F, Laakso MP, Testa C, Rossi R, Beltramello A, Soininen H, Frisoni GB (2005) Frontotemporal dementia as a neural system disease. *Neurobiol Aging* 26: 37-44

Bocchetta M, Cardoso MJ, Cash DM, Ourselin S, Warren JD, Rohrer JD (2016) Patterns of regional cerebellar atrophy in genetic frontotemporal dementia. *Neuroimage Clin* 11: 287-290

Boeve BF, Boylan KB, Graff-Radford NR, DeJesus-Hernandez M, Knopman DS, Pedraza O, Vemuri P, Jones D, Lowe V, Murray ME, Dickson DW, Josephs KA, Rush BK, Machulda MM, Fields JA, Ferman TJ, Baker M, Rutherford NJ, Adamson J, Wszolek ZK et al. (2012) Characterization of frontotemporal dementia and/or amyotrophic lateral sclerosis associated with the GGGGCC repeat expansion in C9ORF72. *Brain* 135: 765-83

Boeve BF, Tremont-Lukats IW, Waclawik AJ, Murrell JR, Hermann B, Jack CR, Jr., Shiung MM, Smith GE, Nair AR, Lindor N, Koppikar V, Ghetti B (2005) Longitudinal characterization of two siblings with frontotemporal dementia and parkinsonism linked to chromosome 17 associated with the S305N tau mutation. *Brain* 128: 752-72

Bonakdarpour B, Rogalski EJ, Wang A, Sridhar J, Mesulam MM, Hurley RS (2017) Functional Connectivity is Reduced in Early-stage Primary Progressive Aphasia When Atrophy is not Prominent. *Alzheimer Dis Assoc Disord* 31: 101-106

Borghero G, Pugliatti M, Marrosu F, Marrosu MG, Murru MR, Floris G, Cannas A, Occhineri P, Cau TB, Loi D, Ticca A, Traccis S, Manera U, Canosa A, Moglia C, Calvo A, Barberis M, Brunetti M, Gibbs JR, Renton AE et al. (2016) TBK1 is associated with ALS and ALS-FTD in Sardinian patients. *Neurobiol Aging* 43: 180 e1-5

Borroni B, Bonvicini C, Alberici A, Buratti E, Agosti C, Archetti S, Papetti A, Stuani C, Di Luca M, Gennarelli M, Padovani A (2009) Mutation within TARDBP leads to frontotemporal dementia without motor neuron disease. *Hum Mutat* 30: E974-83

Bourinaris T, Houlden H (2018) C9orf72 and its Relevance in Parkinsonism and Movement Disorders: A Comprehensive Review of the Literature. *Mov Disord Clin Pract* 5: 575-585

Boxer AL, Geschwind MD, Belfor N, Gorno-Tempini ML, Schauer GF, Miller BL, Weiner MW, Rosen HJ (2006) Patterns of brain atrophy that differentiate corticobasal degeneration syndrome from progressive supranuclear palsy. *Arch Neurol* 63: 81-6

Boxer AL, Gold M, Feldman H, Boeve BF, Dickinson SL, Fillit H, Ho C, Paul R, Pearlman R, Sutherland M, Verma A, Arneric SP, Alexander BM, Dickerson BC, Dorsey ER, Grossman M, Huey ED, Irizarry MC, Marks WJ, Masellis M et al. (2020) New directions in clinical trials for frontotemporal lobar degeneration: Methods and outcome measures. *Alzheimers Dement* 16: 131-143

Boxer AL, Knopman DS, Kaufer DI, Grossman M, Onyike C, Graf-Radford N, Mendez M, Kerwin D, Lerner A, Wu CK, Koestler M, Shapira J, Sullivan K, Klepac K, Lipowski K, Ullah J, Fields S, Kramer JH, Merrilees J, Neuhaus J et al. (2013) Memantine in patients with frontotemporal lobar degeneration: a multicentre, randomised, double-blind, placebo-controlled trial. *Lancet Neurol* 12: 149-56

Boxer AL, Miller BL (2005) Clinical features of frontotemporal dementia. *Alzheimer Dis Assoc Disord* 19 Suppl 1: S3-6

Brambati SM, Rankin KP, Narvid J, Seeley WW, Dean D, Rosen HJ, Miller BL, Ashburner J, Gorno-Tempini ML (2009) Atrophy progression in semantic dementia with asymmetric temporal involvement: a tensor-based morphometry study. *Neurobiol Aging* 30: 103-11

Brettschneider J, Del Tredici K, Irwin DJ, Grossman M, Robinson JL, Toledo JB, Fang L, Van Deerlin VM, Ludolph AC, Lee VM, Braak H, Trojanowski JQ (2014) Sequential distribution of pTDP-43 pathology in behavioral variant frontotemporal dementia (bvFTD). *Acta Neuropathol* 127: 423-439

Brettschneider J, Del Tredici K, Toledo JB, Robinson JL, Irwin DJ, Grossman M, Suh E, Van Deerlin VM, Wood EM, Baek Y, Kwong L, Lee EB, Elman L, McCluskey L, Fang L, Feldengut S, Ludolph AC, Lee VM, Braak H, Trojanowski JQ (2013) Stages of pTDP-43 pathology in amyotrophic lateral sclerosis. *Ann Neurol* 74: 20-38

Brown JA, Deng J, Neuhaus J, Sible IJ, Sias AC, Lee SE, Kornak J, Marx GA, Karydas AM, Spina S, Grinberg LT, Coppola G, Geschwind DH, Kramer JH, Gorno-Tempini ML, Miller BL, Rosen HJ, Seeley WW (2019) Patient-Tailored, Connectivity-Based Forecasts of Spreading Brain Atrophy. *Neuron* 104: 856-868 e5

Buchanan CR, Pettit LD, Storkey AJ, Abrahams S, Bastin ME (2015) Reduced structural connectivity within a prefrontal-motor-subcortical network in amyotrophic lateral sclerosis. *J Magn Reson Imaging* 41: 1342-52

Buckner RL, Snyder AZ, Shannon BJ, LaRossa G, Sachs R, Fotenos AF, Sheline YI, Klunk WE, Mathis CA, Morris JC, Mintun MA (2005) Molecular, structural, and functional characterization of Alzheimer's disease: evidence for a relationship between default activity, amyloid, and memory. *J Neurosci* 25: 7709-17

Bugiani O, Murrell JR, Giaccone G, Hasegawa M, Ghigo G, Tabaton M, Morbin M, Primavera A, Carella F, Solaro C, Grisoli M, Savoiaro M, Spillantini MG, Tagliavini F, Goedert M, Ghetti B (1999) Frontotemporal dementia and corticobasal degeneration in a family with a P301S mutation in tau. *J Neuropathol Exp Neurol* 58: 667-77

Buhour MS, Doidy F, Laisney M, Pitel AL, de La Sayette V, Viader F, Eustache F, Desgranges B (2017) Pathophysiology of the behavioral variant of frontotemporal lobar degeneration: A study combining MRI and FDG-PET. *Brain Imaging Behav* 11: 240-252

Burrell JR, Kiernan MC, Vucic S, Hodges JR (2011) Motor neuron dysfunction in frontotemporal dementia. *Brain* 134: 2582-94

Cacace R, Van Cauwenberghe C, Bettens K, Gijssels I, van der Zee J, Engelborghs S, Vandenbulcke M, Van Dongen J, Baumer V, Dillen L, Mattheijssens M, Peeters K, Cruts M, Vandenberghe R, De Deyn PP, Van Broeckhoven C, Sleegers K (2013) C9orf72 G4C2 repeat expansions in Alzheimer's disease and mild cognitive impairment. *Neurobiol Aging* 34: 1712 e1-7

Canu E, Agosta F, Mandic-Stojmenovic G, Stojkovic T, Stefanova E, Inuggi A, Imperiale F, Copetti M, Kostic VS, Filippi M (2017) Multiparametric MRI to distinguish early onset Alzheimer's disease and behavioural variant of frontotemporal dementia. *Neuroimage Clin* 15: 428-438

Caroppo P, Le Ber I, Camuzat A, Clot F, Naccache L, Lamari F, De Septenville A, Bertrand A, Belliard S, Hannequin D, Colliot O, Brice A (2014) Extensive white matter involvement in patients with frontotemporal lobar degeneration: think progranulin. *JAMA Neurol* 71: 1562-6

Caso F, Mandelli ML, Henry M, Gesierich B, Bettcher BM, Ogar J, Filippi M, Comi G, Magnani G, Sidhu M, Trojanowski JQ, Huang EJ, Grinberg LT, Miller BL, Dronkers N, Seeley WW, Gorno-Tempini ML (2014) In vivo signatures of nonfluent/agrammatic primary progressive aphasia caused by FTLD pathology. *Neurology* 82: 239-47

Caso F, Villa C, Fenoglio C, Santangelo R, Agosta F, Coppi E, Falautano M, Comi G, Filippi M, Scarpini E, Magnani G, Galimberti D (2012) The progranulin (GRN)

Cys157LysfsX97 mutation is associated with nonfluent variant of primary progressive aphasia clinical phenotype. *J Alzheimers Dis* 28: 759-63

Catani M, Mesulam MM, Jakobsen E, Malik F, Martersteck A, Wieneke C, Thompson CK, Thiebaut de Schotten M, Dell'Acqua F, Weintraub S, Rogalski E (2013) A novel frontal pathway underlies verbal fluency in primary progressive aphasia. *Brain* 136: 2619-28

Cerami C, Dodich A, Greco L, Iannaccone S, Magnani G, Marcone A, Pelagallo E, Santangelo R, Cappa SF, Perani D (2017) The Role of Single-Subject Brain Metabolic Patterns in the Early Differential Diagnosis of Primary Progressive Aphasias and in Prediction of Progression to Dementia. *J Alzheimers Dis* 55: 183-197

Chan D, Fox NC, Jenkins R, Scahill RI, Crum WR, Rossor MN (2001a) Rates of global and regional cerebral atrophy in AD and frontotemporal dementia. *Neurology* 57: 1756-63

Chan D, Fox NC, Scahill RI, Crum WR, Whitwell JL, Leschziner G, Rossor AM, Stevens JM, Cipelotti L, Rossor MN (2001b) Patterns of temporal lobe atrophy in semantic dementia and Alzheimer's disease. *Ann Neurol* 49: 433-42

Chao LL, Schuff N, Clevenger EM, Mueller SG, Rosen HJ, Gorno-Tempini ML, Kramer JH, Miller BL, Weiner MW (2007) Patterns of white matter atrophy in frontotemporal lobar degeneration. *Arch Neurol* 64: 1619-24

Chen-Plotkin AS, Martinez-Lage M, Sleiman PM, Hu W, Greene R, Wood EM, Bing S, Grossman M, Schellenberg GD, Hatanpaa KJ, Weiner MF, White CL, 3rd, Brooks WS, Halliday GM, Kril JJ, Gearing M, Beach TG, Graff-Radford NR, Dickson DW, Rademakers R et al. (2011) Genetic and clinical features of progranulin-associated frontotemporal lobar degeneration. *Arch Neurol* 68: 488-97

Cheng ST, Chow PK, Song YQ, Yu EC, Chan AC, Lee TM, Lam JH (2014) Mental and physical activities delay cognitive decline in older persons with dementia. *Am J Geriatr Psychiatry* 22: 63-74

Chiang HH, Rosvall L, Brohede J, Axelman K, Bjork BF, Nennesmo I, Robins T, Graff C (2008) Progranulin mutation causes frontotemporal dementia in the Swedish Karolinska family. *Alzheimers Dement* 4: 414-20

Chio A, Borghero G, Restagno G, Mora G, Drepper C, Traynor BJ, Sendtner M, Brunetti M, Ossola I, Calvo A, Pugliatti M, Sotgiu MA, Murru MR, Marrosu MG,

Marrosu F, Marinou K, Mandrioli J, Sola P, Caponnetto C, Mancardi G et al. (2012) Clinical characteristics of patients with familial amyotrophic lateral sclerosis carrying the pathogenic GGGGCC hexanucleotide repeat expansion of C9ORF72. *Brain* 135: 784-93

Chio A, Calvo A, Moglia C, Restagno G, Ossola I, Brunetti M, Montuschi A, Cistaro A, Ticca A, Traynor BJ, Schymick JC, Mutani R, Marrosu MG, Murru MR, Borghero G (2010) Amyotrophic lateral sclerosis-frontotemporal lobar dementia in 3 families with p.Ala382Thr TARDBP mutations. *Arch Neurol* 67: 1002-9

Chio A, Moglia C, Canosa A, Manera U, D'Ovidio F, Vasta R, Grassano M, Brunetti M, Barberis M, Corrado L, D'Alfonso S, Iazzolino B, Peotta L, Sarnelli MF, Solara V, Zucchetti JP, De Marchi F, Mazzini L, Mora G, Calvo A (2020) ALS phenotype is influenced by age, sex, and genetics: A population-based study. *Neurology* 94: e802-e810

Chow TW, Hynan LS, Lipton AM (2006) MMSE scores decline at a greater rate in frontotemporal degeneration than in AD. *Dement Geriatr Cogn Disord* 22: 194-9

Cirulli ET, Lasseigne BN, Petrovski S, Sapp PC, Dion PA, Leblond CS, Couthouis J, Lu YF, Wang Q, Krueger BJ, Ren Z, Keebler J, Han Y, Levy SE, Boone BE, Wimbish JR, Waite LL, Jones AL, Carulli JP, Day-Williams AG et al. (2015) Exome sequencing in amyotrophic lateral sclerosis identifies risk genes and pathways. *Science* 347: 1436-41

Cohen-Adad J, Zhao W, Keil B, Ratai EM, Triantafyllou C, Lawson R, Dheel C, Wald LL, Rosen BR, Cudkowicz M, Atassi N (2013) 7-T MRI of the spinal cord can detect lateral corticospinal tract abnormality in amyotrophic lateral sclerosis. *Muscle Nerve* 47: 760-2

Collins JA, Montal V, Hochberg D, Quimby M, Mandelli ML, Makris N, Seeley WW, Gorno-Tempini ML, Dickerson BC (2017) Focal temporal pole atrophy and network degeneration in semantic variant primary progressive aphasia. *Brain* 140: 457-471

Cooper-Knock J, Hewitt C, Highley JR, Brockington A, Milano A, Man S, Martindale J, Hartley J, Walsh T, Gelsthorpe C, Baxter L, Forster G, Fox M, Bury J, Mok K, McDermott CJ, Traynor BJ, Kirby J, Wharton SB, Ince PG et al. (2012) Clinico-pathological features in amyotrophic lateral sclerosis with expansions in C9ORF72. *Brain* 135: 751-64

Coyle-Gilchrist IT, Dick KM, Patterson K, Vazquez Rodriguez P, Wehmann E, Wilcox A, Lansdall CJ, Dawson KE, Wiggins J, Mead S, Brayne C, Rowe JB (2016)

Prevalence, characteristics, and survival of frontotemporal lobar degeneration syndromes. *Neurology* 86: 1736-43

Cruz M, Marinho V, Fontenelle LF, Engelhardt E, Laks J (2008) Topiramate may modulate alcohol abuse but not other compulsive behaviors in frontotemporal dementia: case report. *Cogn Behav Neurol* 21: 104-6

Davies RR, Kipps CM, Mitchell J, Kril JJ, Halliday GM, Hodges JR (2006) Progression in frontotemporal dementia: identifying a benign behavioral variant by magnetic resonance imaging. *Arch Neurol* 63: 1627-31

Day GS, Farb NA, Tang-Wai DF, Masellis M, Black SE, Freedman M, Pollock BG, Chow TW (2013) Saliience network resting-state activity: prediction of frontotemporal dementia progression. *JAMA Neurol* 70: 1249-53

Dayanandan R, Van Slegtenhorst M, Mack TG, Ko L, Yen SH, Leroy K, Brion JP, Anderton BH, Hutton M, Lovestone S (1999) Mutations in tau reduce its microtubule binding properties in intact cells and affect its phosphorylation. *FEBS Lett* 446: 228-32

DeJesus-Hernandez M, Mackenzie IR, Boeve BF, Boxer AL, Baker M, Rutherford NJ, Nicholson AM, Finch NA, Flynn H, Adamson J, Kouri N, Wojtas A, Sengdy P, Hsiung GY, Karydas A, Seeley WW, Josephs KA, Coppola G, Geschwind DH, Wszolek ZK et al. (2011) Expanded GGGGCC hexanucleotide repeat in noncoding region of C9ORF72 causes chromosome 9p-linked FTD and ALS. *Neuron* 72: 245-56

Devenney E, Foxe D, Dobson-Stone C, Kwok JB, Kiernan MC, Hodges JR (2015) Clinical heterogeneity of the C9orf72 genetic mutation in frontotemporal dementia. *Neurocase* 21: 535-41

Devenney E, Hornberger M, Irish M, Mioshi E, Burrell J, Tan R, Kiernan MC, Hodges JR (2014) Frontotemporal dementia associated with the C9ORF72 mutation: a unique clinical profile. *JAMA Neurol* 71: 331-9

Diagnosis ETFo, Management of Amyotrophic Lateral S, Andersen PM, Abrahams S, Borasio GD, de Carvalho M, Chio A, Van Damme P, Hardiman O, Kollewe K, Morrison KE, Petri S, Pradat PF, Silani V, Tomik B, Wasner M, Weber M (2012) EFNS guidelines on the clinical management of amyotrophic lateral sclerosis (MALS)--revised report of an EFNS task force. *Eur J Neurol* 19: 360-75

Diehl-Schmid J, Grimmer T, Drzezga A, Bornschein S, Riemenschneider M, Forstl H, Schwaiger M, Kurz A (2007) Decline of cerebral glucose metabolism in frontotemporal dementia: a longitudinal 18F-FDG-PET-study. *Neurobiol Aging* 28: 42-50

Douaud G, Filippini N, Knight S, Talbot K, Turner MR (2011) Integration of structural and functional magnetic resonance imaging in amyotrophic lateral sclerosis. *Brain* 134: 3470-9

Drzezga A, Grimmer T, Henriksen G, Stangier I, Perneczky R, Diehl-Schmid J, Mathis CA, Klunk WE, Price J, DeKosky S, Wester HJ, Schwaiger M, Kurz A (2008) Imaging of amyloid plaques and cerebral glucose metabolism in semantic dementia and Alzheimer's disease. *Neuroimage* 39: 619-33

Dukart J, Mueller K, Horstmann A, Barthel H, Moller HE, Villringer A, Sabri O, Schroeter ML (2011) Combined evaluation of FDG-PET and MRI improves detection and differentiation of dementia. *PLoS One* 6: e18111

Dumanchin C, Camuzat A, Campion D, Verpillat P, Hannequin D, Dubois B, Saugier-veber P, Martin C, Penet C, Charbonnier F, Agid Y, Frebourg T, Brice A (1998) Segregation of a missense mutation in the microtubule-associated protein tau gene with familial frontotemporal dementia and parkinsonism. *Hum Mol Genet* 7: 1825-9

Elahi FM, Marx G, Cobigo Y, Staffaroni AM, Kornak J, Tosun D, Boxer AL, Kramer JH, Miller BL, Rosen HJ (2017) Longitudinal white matter change in frontotemporal dementia subtypes and sporadic late onset Alzheimer's disease. *Neuroimage Clin* 16: 595-603

Evans JJ, Heggs AJ, Antoun N, Hodges JR (1995) Progressive prosopagnosia associated with selective right temporal lobe atrophy. A new syndrome? *Brain* 118 (Pt 1): 1-13

Fabes J, Matthews L, Filippini N, Talbot K, Jenkinson M, Turner MR (2017) Quantitative FLAIR MRI in Amyotrophic Lateral Sclerosis. *Acad Radiol* 24: 1187-1194

Farb NA, Grady CL, Strother S, Tang-Wai DF, Masellis M, Black S, Freedman M, Pollock BG, Campbell KL, Hasher L, Chow TW (2013) Abnormal network connectivity in frontotemporal dementia: evidence for prefrontal isolation. *Cortex* 49: 1856-73

Fekete T, Zach N, Mujica-Parodi LR, Turner MR (2013) Multiple kernel learning captures a systems-level functional connectivity biomarker signature in amyotrophic lateral sclerosis. *PLoS One* 8: e85190

Ferrari R, Kapogiannis D, Huey ED, Momeni P (2011) FTD and ALS: a tale of two diseases. *Curr Alzheimer Res* 8: 273-94

Filippi M, Agosta F, Abrahams S, Fazekas F, Grosskreutz J, Kalra S, Kassubek J, Silani V, Turner MR, Masdeu JC, European Federation of Neurological S (2010) EFNS guidelines on the use of neuroimaging in the management of motor neuron diseases. *Eur J Neurol* 17: 526-e20

Filippi M, Agosta F, Scola E, Canu E, Magnani G, Marcone A, Valsasina P, Caso F, Copetti M, Comi G, Cappa SF, Falini A (2013) Functional network connectivity in the behavioral variant of frontotemporal dementia. *Cortex* 49: 2389-401

Filippi M, Basaia S, Canu E, Imperiale F, Magnani G, Falautano M, Comi G, Falini A, Agosta F (2020) Changes in functional and structural brain connectome along the Alzheimer's disease continuum. *Mol Psychiatry* 25: 230-239

Filippi M, Basaia S, Canu E, Imperiale F, Meani A, Caso F, Magnani G, Falautano M, Comi G, Falini A, Agosta F (2017) Brain network connectivity differs in early-onset neurodegenerative dementia. *Neurology* 89: 1764-1772

Flanagan EP, Baker MC, Perkerson RB, Duffy JR, Strand EA, Whitwell JL, Machulda MM, Rademakers R, Josephs KA (2015) Dominant frontotemporal dementia mutations in 140 cases of primary progressive aphasia and speech apraxia. *Dement Geriatr Cogn Disord* 39: 281-6

Folstein MF, Robins LN, Helzer JE (1983) The Mini-Mental State Examination. *Arch Gen Psychiatry* 40: 812

Forman MS (2004) Genotype-phenotype correlations in FTDP-17: does form follow function? *Exp Neurol* 187: 229-34

Forman MS, Farmer J, Johnson JK, Clark CM, Arnold SE, Coslett HB, Chatterjee A, Hurtig HI, Karlawish JH, Rosen HJ, Van Deerlin V, Lee VM, Miller BL, Trojanowski JQ, Grossman M (2006) Frontotemporal dementia: clinicopathological correlations. *Ann Neurol* 59: 952-62

Freischmidt A, Wieland T, Richter B, Ruf W, Schaeffer V, Muller K, Marroquin N, Nordin F, Hubers A, Weydt P, Pinto S, Press R, Millecamps S, Molko N, Bernard E, Desnuelle C, Soriani MH, Dorst J, Graf E, Nordstrom U et al. (2015) Haploinsufficiency of TBK1 causes familial ALS and fronto-temporal dementia. *Nat Neurosci* 18: 631-6

Gainotti G (2007) Different patterns of famous people recognition disorders in patients with right and left anterior temporal lesions: a systematic review. *Neuropsychologia* 45: 1591-607

Galantucci S, Tartaglia MC, Wilson SM, Henry ML, Filippi M, Agosta F, Dronkers NF, Henry RG, Ogar JM, Miller BL, Gorno-Tempini ML (2011) White matter damage in primary progressive aphasia: a diffusion tensor tractography study. *Brain* 134: 3011-29

Galimberti D, Reif A, Dell'osso B, Kittel-Schneider S, Leonhard C, Herr A, Palazzo C, Villa C, Fenoglio C, Serpente M, Cioffi SM, Prunas C, Paoli RA, Altamura AC, Scarpini E (2014) C9ORF72 hexanucleotide repeat expansion is a rare cause of schizophrenia. *Neurobiol Aging* 35: 1214 e7-1214 e10

Galton CJ, Patterson K, Graham K, Lambon-Ralph MA, Williams G, Antoun N, Sahakian BJ, Hodges JR (2001) Differing patterns of temporal atrophy in Alzheimer's disease and semantic dementia. *Neurology* 57: 216-25

Garibotto V, Borroni B, Agosti C, Premi E, Alberici A, Eickhoff SB, Brambati SM, Bellelli G, Gasparotti R, Perani D, Padovani A (2011) Subcortical and deep cortical atrophy in Frontotemporal Lobar Degeneration. *Neurobiol Aging* 32: 875-84

Geevasinga N, Korgaonkar MS, Menon P, Van den Bos M, Gomes L, Foster S, Kiernan MC, Vucic S (2017) Brain functional connectome abnormalities in amyotrophic lateral sclerosis are associated with disability and cortical hyperexcitability. *Eur J Neurol* 24: 1507-1517

Gelpi E, van der Zee J, Turon Estrada A, Van Broeckhoven C, Sanchez-Valle R (2014) TARDBP mutation p.Ile383Val associated with semantic dementia and complex proteinopathy. *Neuropathol Appl Neurobiol* 40: 225-30

Gendron TF, Bieniek KF, Zhang YJ, Jansen-West K, Ash PE, Caulfield T, Daugherty L, Dunmore JH, Castanedes-Casey M, Chew J, Cosio DM, van Blitterswijk M, Lee WC, Rademakers R, Boylan KB, Dickson DW, Petrucelli L (2013) Antisense transcripts of the expanded C9ORF72 hexanucleotide repeat form nuclear RNA foci and undergo repeat-associated non-ATG translation in c9FTD/ALS. *Acta Neuropathol* 126: 829-44

Gijselinck I, Van Langenhove T, van der Zee J, Sleegers K, Philtjens S, Kleinberger G, Janssens J, Bettens K, Van Cauwenberghe C, Pereson S, Engelborghs S, Sieben A, De Jonghe P, Vandenberghe R, Santens P, De Bleecker J, Maes G, Baumer V, Dillen L, Joris

G et al. (2012) A C9orf72 promoter repeat expansion in a Flanders-Belgian cohort with disorders of the frontotemporal lobar degeneration-amyotrophic lateral sclerosis spectrum: a gene identification study. *Lancet Neurol* 11: 54-65

Gijselinck I, Van Mossevelde S, van der Zee J, Sieben A, Philtjens S, Heeman B, Engelborghs S, Vandebulcke M, De Baets G, Baumer V, Cuijt I, Van den Broeck M, Peeters K, Mattheijssens M, Rousseau F, Vandenberghe R, De Jonghe P, Cras P, De Deyn PP, Martin JJ et al. (2015) Loss of TBK1 is a frequent cause of frontotemporal dementia in a Belgian cohort. *Neurology* 85: 2116-25

Gitcho MA, Bigio EH, Mishra M, Johnson N, Weintraub S, Mesulam M, Rademakers R, Chakraverty S, Cruchaga C, Morris JC, Goate AM, Cairns NJ (2009) TARDBP 3'-UTR variant in autopsy-confirmed frontotemporal lobar degeneration with TDP-43 proteinopathy. *Acta Neuropathol* 118: 633-45

Gleason CE, Ordureau A, Gourlay R, Arthur JSC, Cohen P (2011) Polyubiquitin binding to optineurin is required for optimal activation of TANK-binding kinase 1 and production of interferon beta. *J Biol Chem* 286: 35663-35674

Goedert M, Jakes R (1990) Expression of separate isoforms of human tau protein: correlation with the tau pattern in brain and effects on tubulin polymerization. *EMBO J* 9: 4225-30

Gorno-Tempini ML, Dronkers NF, Rankin KP, Ogar JM, Phengrasamy L, Rosen HJ, Johnson JK, Weiner MW, Miller BL (2004) Cognition and anatomy in three variants of primary progressive aphasia. *Ann Neurol* 55: 335-46

Gorno-Tempini ML, Hillis AE, Weintraub S, Kertesz A, Mendez M, Cappa SF, Ogar JM, Rohrer JD, Black S, Boeve BF, Manes F, Dronkers NF, Vandenberghe R, Rascovsky K, Patterson K, Miller BL, Knopman DS, Hodges JR, Mesulam MM, Grossman M (2011) Classification of primary progressive aphasia and its variants. *Neurology* 76: 1006-14

Greaves CV, Rohrer JD (2019) An update on genetic frontotemporal dementia. *J Neurol* 266: 2075-2086

Grimmer T, Diehl J, Drzezga A, Forstl H, Kurz A (2004) Region-specific decline of cerebral glucose metabolism in patients with frontotemporal dementia: a prospective 18F-FDG-PET study. *Dement Geriatr Cogn Disord* 18: 32-6

Guo CC, Gorno-Tempini ML, Gesierich B, Henry M, Trujillo A, Shany-Ur T, Jovicich J, Robinson SD, Kramer JH, Rankin KP, Miller BL, Seeley WW (2013) Anterior

temporal lobe degeneration produces widespread network-driven dysfunction. *Brain* 136: 2979-91

Hafkemeijer A, Moller C, Dopfer EG, Jiskoot LC, van den Berg-Huysmans AA, van Swieten JC, van der Flier WM, Vrenken H, Pijnenburg YA, Barkhof F, Scheltens P, van der Grond J, Rombouts SA (2017) A Longitudinal Study on Resting State Functional Connectivity in Behavioral Variant Frontotemporal Dementia and Alzheimer's Disease. *J Alzheimers Dis* 55: 521-537

Hannaford A, Pavey N, van den Bos M, Geevasinga N, Menon P, Shefner JM, Kiernan MC, Vucic S (2021) Diagnostic Utility of Gold Coast Criteria in Amyotrophic Lateral Sclerosis. *Ann Neurol* 89: 979-986

Harms M, Benitez BA, Cairns N, Cooper B, Cooper P, Mayo K, Carrell D, Faber K, Williamson J, Bird T, Diaz-Arrastia R, Foroud TM, Boeve BF, Graff-Radford NR, Mayeux R, Chakraverty S, Goate AM, Cruchaga C, Consortium N-LNFS (2013) C9orf72 hexanucleotide repeat expansions in clinical Alzheimer disease. *JAMA Neurol* 70: 736-41

Harper L, Fumagalli GG, Barkhof F, Scheltens P, O'Brien JT, Bouwman F, Burton EJ, Rohrer JD, Fox NC, Ridgway GR, Schott JM (2016) MRI visual rating scales in the diagnosis of dementia: evaluation in 184 post-mortem confirmed cases. *Brain* 139: 1211-25

Harris JM, Gall C, Thompson JC, Richardson AM, Neary D, du Plessis D, Pal P, Mann DM, Snowden JS, Jones M (2013) Sensitivity and specificity of FTDC criteria for behavioral variant frontotemporal dementia. *Neurology* 80: 1881-7

Hensman Moss DJ, Poulter M, Beck J, Hehir J, Polke JM, Campbell T, Adamson G, Mudanohwo E, McColgan P, Haworth A, Wild EJ, Sweeney MG, Houlden H, Mead S, Tabrizi SJ (2014) C9orf72 expansions are the most common genetic cause of Huntington disease phenocopies. *Neurology* 82: 292-9

Hodges JR, Davies RR, Xuereb JH, Casey B, Broe M, Bak TH, Kril JJ, Halliday GM (2004) Clinicopathological correlates in frontotemporal dementia. *Ann Neurol* 56: 399-406

Hogan DB, Jette N, Fiest KM, Roberts JI, Pearson D, Smith EE, Roach P, Kirk A, Pringsheim T, Maxwell CJ (2016) The Prevalence and Incidence of Frontotemporal Dementia: a Systematic Review. *Can J Neurol Sci* 43 Suppl 1: S96-S109

Hsiung GY, DeJesus-Hernandez M, Feldman HH, Sengdy P, Bouchard-Kerr P, Dwosh E, Butler R, Leung B, Fok A, Rutherford NJ, Baker M, Rademakers R, Mackenzie IR (2012) Clinical and pathological features of familial frontotemporal dementia caused by C9ORF72 mutation on chromosome 9p. *Brain* 135: 709-22

Huey ED, Nagy PL, Rodriguez-Murillo L, Manoochehri M, Goldman J, Lieberman J, Karayiorgou M, Mayeux R (2013) C9ORF72 repeat expansions not detected in a group of patients with schizophrenia. *Neurobiol Aging* 34: 1309 e9-10

Ikeda M, Shigenobu K, Fukuhara R, Hokoishi K, Maki N, Nebu A, Komori K, Tanabe H (2004) Efficacy of fluvoxamine as a treatment for behavioral symptoms in frontotemporal lobar degeneration patients. *Dement Geriatr Cogn Disord* 17: 117-21

Irish M, Devenney E, Wong S, Dobson-Stone C, Kwok JB, Piguet O, Hodges JR, Hornberger M (2013) Neural substrates of episodic memory dysfunction in behavioural variant frontotemporal dementia with and without C9ORF72 expansions. *Neuroimage Clin* 2: 836-43

Ishii K, Sakamoto S, Sasaki M, Kitagaki H, Yamaji S, Hashimoto M, Imamura T, Shimomura T, Hirono N, Mori E (1998) Cerebral glucose metabolism in patients with frontotemporal dementia. *J Nucl Med* 39: 1875-8

Jeong Y, Cho SS, Park JM, Kang SJ, Lee JS, Kang E, Na DL, Kim SE (2005) 18F-FDG PET findings in frontotemporal dementia: an SPM analysis of 29 patients. *J Nucl Med* 46: 233-9

Jesso S, Morlog D, Ross S, Pell MD, Pasternak SH, Mitchell DG, Kertesz A, Finger EC (2011) The effects of oxytocin on social cognition and behaviour in frontotemporal dementia. *Brain* 134: 2493-501

Josephs KA, Ahmed Z, Katsuse O, Parisi JF, Boeve BF, Knopman DS, Petersen RC, Davies P, Duara R, Graff-Radford NR, Uitti RJ, Rademakers R, Adamson J, Baker M, Hutton ML, Dickson DW (2007) Neuropathologic features of frontotemporal lobar degeneration with ubiquitin-positive inclusions with progranulin gene (PGRN) mutations. *J Neuropathol Exp Neurol* 66: 142-51

Josephs KA, Duffy JR, Strand EA, Machulda MM, Vemuri P, Senjem ML, Perkerson RB, Baker MC, Lowe V, Jack CR, Jr., Rademakers R, Whitwell JL (2014) Progranulin-associated PiB-negative logopenic primary progressive aphasia. *J Neurol* 261: 604-14

Josephs KA, Duffy JR, Strand EA, Whitwell JL, Layton KF, Parisi JE, Hauser MF, Witte RJ, Boeve BF, Knopman DS, Dickson DW, Jack CR, Jr., Petersen RC (2006) Clinicopathological and imaging correlates of progressive aphasia and apraxia of speech. *Brain* 129: 1385-98

Josephs KA, Lin WL, Ahmed Z, Stroh DA, Graff-Radford NR, Dickson DW (2008) Frontotemporal lobar degeneration with ubiquitin-positive, but TDP-43-negative inclusions. *Acta Neuropathol* 116: 159-67

Josephs KA, Whitwell JL, Dickson DW, Boeve BF, Knopman DS, Petersen RC, Parisi JE, Jack CR, Jr. (2008) Voxel-based morphometry in autopsy proven PSP and CBD. *Neurobiol Aging* 29: 280-9

Josephs KA, Whitwell JL, Knopman DS, Boeve BF, Vemuri P, Senjem ML, Parisi JE, Ivnik RJ, Dickson DW, Petersen RC, Jack CR, Jr. (2009) Two distinct subtypes of right temporal variant frontotemporal dementia. *Neurology* 73: 1443-50

Jovicic A, Paul JW, 3rd, Gitler AD (2016) Nuclear transport dysfunction: a common theme in amyotrophic lateral sclerosis and frontotemporal dementia. *J Neurochem* 138 Suppl 1: 134-44

Kaivorinne AL, Bode MK, Paavola L, Tuominen H, Kallio M, Renton AE, Traynor BJ, Moilanen V, Remes AM (2013) Clinical Characteristics of C9ORF72-Linked Frontotemporal Lobar Degeneration. *Dement Geriatr Cogn Dis Extra* 3: 251-62

Karageorgiou E, Miller BL (2014) Frontotemporal lobar degeneration: a clinical approach. *Semin Neurol* 34: 189-201

Kassubek J, Muller HP, Del Tredici K, Brettschneider J, Pinkhardt EH, Lule D, Bohm S, Braak H, Ludolph AC (2014) Diffusion tensor imaging analysis of sequential spreading of disease in amyotrophic lateral sclerosis confirms patterns of TDP-43 pathology. *Brain* 137: 1733-40

Kassubek J, Muller HP, Del Tredici K, Lule D, Gorges M, Braak H, Ludolph AC (2017) Imaging the pathoanatomy of amyotrophic lateral sclerosis in vivo: targeting a propagation-based biological marker. *J Neurol Neurosurg Psychiatry*

Katyal N, Govindarajan R (2017) Shortcomings in the Current Amyotrophic Lateral Sclerosis Trials and Potential Solutions for Improvement. *Front Neurol* 8: 521

Keil C, Prell T, Peschel T, Hartung V, Dengler R, Grosskreutz J (2012) Longitudinal diffusion tensor imaging in amyotrophic lateral sclerosis. *BMC Neurosci* 13: 141

Kelley BJ, Haidar W, Boeve BF, Baker M, Shiung M, Knopman DS, Rademakers R, Hutton M, Adamson J, Kuntz KM, Dickson DW, Parisi JE, Smith GE, Petersen RC (2010) Alzheimer disease-like phenotype associated with the c.154delA mutation in progranulin. *Arch Neurol* 67: 171-7

Kertesz A, Ang LC, Jesso S, MacKinley J, Baker M, Brown P, Shoesmith C, Rademakers R, Finger EC (2013) Psychosis and hallucinations in frontotemporal dementia with the C9ORF72 mutation: a detailed clinical cohort. *Cogn Behav Neurol* 26: 146-54

Kim G, Ahmadian SS, Peterson M, Parton Z, Memon R, Weintraub S, Rademaker A, Bigio E, Mesulam MM, Geula C (2016) Asymmetric pathology in primary progressive aphasia with progranulin mutations and TDP inclusions. *Neurology* 86: 627-36

Kim YE, Oh KW, Noh MY, Nahm M, Park J, Lim SM, Jang JH, Cho EH, Ki CS, Lee S, Kim SH (2017) Genetic and functional analysis of TBK1 variants in Korean patients with sporadic amyotrophic lateral sclerosis. *Neurobiol Aging* 50: 170 e1-170 e6

Kimura T, Takamatsu J (2013) Pilot study of pharmacological treatment for frontotemporal dementia: risk of donepezil treatment for behavioral and psychological symptoms. *Geriatr Gerontol Int* 13: 506-7

Kipps CM, Davies RR, Mitchell J, Kril JJ, Halliday GM, Hodges JR (2007) Clinical significance of lobar atrophy in frontotemporal dementia: application of an MRI visual rating scale. *Dement Geriatr Cogn Disord* 23: 334-42

Knibb JA, Woollams AM, Hodges JR, Patterson K (2009) Making sense of progressive non-fluent aphasia: an analysis of conversational speech. *Brain* 132: 2734-46

Knopman DS, Jack CR, Jr., Kramer JH, Boeve BF, Caselli RJ, Graff-Radford NR, Mendez MF, Miller BL, Mercaldo ND (2009) Brain and ventricular volumetric changes in frontotemporal lobar degeneration over 1 year. *Neurology* 72: 1843-9

Knopman DS, Roberts RO (2011) Estimating the number of persons with frontotemporal lobar degeneration in the US population. *J Mol Neurosci* 45: 330-5

Kortte KB, Rogalski EJ (2013) Behavioural interventions for enhancing life participation in behavioural variant frontotemporal dementia and primary progressive aphasia. *Int Rev Psychiatry* 25: 237-45

Krueger CE, Dean DL, Rosen HJ, Halabi C, Weiner M, Miller BL, Kramer JH (2010) Longitudinal rates of lobar atrophy in frontotemporal dementia, semantic dementia, and Alzheimer's disease. *Alzheimer Dis Assoc Disord* 24: 43-8

Kumar-Singh S, Van Broeckhoven C (2007) Frontotemporal lobar degeneration: current concepts in the light of recent advances. *Brain Pathol* 17: 104-14

Kuuluvainen L, Poyhonen M, Pasanen P, Siitonen M, Rummukainen J, Tienari PJ, Paetau A, Myllykangas L (2017) A Novel Loss-of-Function GRN Mutation p.(Tyr229*): Clinical and Neuropathological Features. *J Alzheimers Dis* 55: 1167-1174

Kwan JY, Meoded A, Danielian LE, Wu T, Floeter MK (2012) Structural imaging differences and longitudinal changes in primary lateral sclerosis and amyotrophic lateral sclerosis. *Neuroimage Clin* 2: 151-60

Lacomblez L, Bensimon G, Leigh PN, Guillet P, Meininger V (1996) Dose-ranging study of riluzole in amyotrophic lateral sclerosis. Amyotrophic Lateral Sclerosis/Riluzole Study Group II. *Lancet* 347: 1425-31

Lam BY, Halliday GM, Irish M, Hodges JR, Piguet O (2014) Longitudinal white matter changes in frontotemporal dementia subtypes. *Hum Brain Mapp* 35: 3547-57

Lattante S, Ciura S, Rouleau GA, Kabashi E (2015) Defining the genetic connection linking amyotrophic lateral sclerosis (ALS) with frontotemporal dementia (FTD). *Trends Genet* 31: 263-73

Le Ber I, Camuzat A, Hannequin D, Pasquier F, Guedj E, Rovelet-Lecrux A, Hahn-Barma V, van der Zee J, Clot F, Bakchine S, Puel M, Ghanim M, Lacomblez L, Mikol J, Deramecourt V, Lejeune P, de la Sayette V, Belliard S, Vercelletto M, Meyrignac C et al. (2008) Phenotype variability in progranulin mutation carriers: a clinical, neuropsychological, imaging and genetic study. *Brain* 131: 732-46

Lee SE, Seeley WW, Poorzand P, Rademakers R, Karydas A, Stanley CM, Miller BL, Rankin KP (2012) Clinical characterization of bvFTD due to FUS neuropathology. *Neurocase* 18: 305-17

Lehmann M, Rohrer JD, Clarkson MJ, Ridgway GR, Scahill RI, Modat M, Warren JD, Ourselin S, Barnes J, Rossor MN, Fox NC (2010) Reduced cortical thickness in the posterior cingulate gyrus is characteristic of both typical and atypical Alzheimer's disease. *J Alzheimers Dis* 20: 587-98

Lillo P, Mioshi E, Burrell JR, Kiernan MC, Hodges JR, Hornberger M (2012) Grey and white matter changes across the amyotrophic lateral sclerosis-frontotemporal dementia continuum. *PLoS One* 7: e43993

Ling SC, Polymenidou M, Cleveland DW (2013) Converging mechanisms in ALS and FTD: disrupted RNA and protein homeostasis. *Neuron* 79: 416-38

Ljubenkova PA, Boxer AL (2021) FTLD Treatment: Current Practice and Future Possibilities. *Adv Exp Med Biol* 1281: 297-310

Lu PH, Lee GJ, Shapira J, Jimenez E, Mather MJ, Thompson PM, Bartzokis G, Mendez MF (2014) Regional differences in white matter breakdown between frontotemporal dementia and early-onset Alzheimer's disease. *J Alzheimers Dis* 39: 261-9

Luo C, Chen Q, Huang R, Chen X, Chen K, Huang X, Tang H, Gong Q, Shang HF (2012) Patterns of spontaneous brain activity in amyotrophic lateral sclerosis: a resting-state fMRI study. *PLoS One* 7: e45470

Mackenzie IR, Neumann M (2016) Molecular neuropathology of frontotemporal dementia: insights into disease mechanisms from postmortem studies. *J Neurochem* 138 Suppl 1: 54-70

Mackenzie IR, Neumann M, Bigio EH, Cairns NJ, Alafuzoff I, Kril J, Kovacs GG, Ghetti B, Halliday G, Holm IE, Ince PG, Kamphorst W, Revesz T, Rozemuller AJ, Kumar-Singh S, Akiyama H, Baborie A, Spina S, Dickson DW, Trojanowski JQ et al. (2010) Nomenclature and nosology for neuropathologic subtypes of frontotemporal lobar degeneration: an update. *Acta Neuropathol* 119: 1-4

Mahoney CJ, Beck J, Rohrer JD, Lashley T, Mok K, Shakespeare T, Yeatman T, Warrington EK, Schott JM, Fox NC, Rossor MN, Hardy J, Collinge J, Revesz T, Mead S, Warren JD (2012) Frontotemporal dementia with the C9ORF72 hexanucleotide repeat expansion: clinical, neuroanatomical and neuropathological features. *Brain* 135: 736-50

Mahoney CJ, Malone IB, Ridgway GR, Buckley AH, Downey LE, Golden HL, Ryan NS, Ourselin S, Schott JM, Rossor MN, Fox NC, Warren JD (2013) White matter tract signatures of the progressive aphasia. *Neurobiol Aging* 34: 1687-99

Mahoney CJ, Ridgway GR, Malone IB, Downey LE, Beck J, Kinnunen KM, Schmitz N, Golden HL, Rohrer JD, Schott JM, Rossor MN, Ourselin S, Mead S, Fox NC, Warren

JD (2014) Profiles of white matter tract pathology in frontotemporal dementia. *Hum Brain Mapp* 35: 4163-79

Mahoney CJ, Simpson IJ, Nicholas JM, Fletcher PD, Downey LE, Golden HL, Clark CN, Schmitz N, Rohrer JD, Schott JM, Zhang H, Ourselin S, Warren JD, Fox NC (2015) Longitudinal diffusion tensor imaging in frontotemporal dementia. *Ann Neurol* 77: 33-46

Majounie E, Abramzon Y, Renton AE, Keller MF, Traynor BJ, Singleton AB (2012) Large C9orf72 repeat expansions are not a common cause of Parkinson's disease. *Neurobiol Aging* 33: 2527 e1-2

Majounie E, Renton AE, Mok K, Dopper EG, Waite A, Rollinson S, Chio A, Restagno G, Nicolaou N, Simon-Sanchez J, van Swieten JC, Abramzon Y, Johnson JO, Sendtner M, Pamphelet R, Orrell RW, Mead S, Sidle KC, Houlden H, Rohrer JD et al. (2012) Frequency of the C9orf72 hexanucleotide repeat expansion in patients with amyotrophic lateral sclerosis and frontotemporal dementia: a cross-sectional study. *Lancet Neurol* 11: 323-30

Mandelli ML, Caverzasi E, Binney RJ, Henry ML, Lobach I, Block N, Amirbekian B, Dronkers N, Miller BL, Henry RG, Gorno-Tempini ML (2014) Frontal white matter tracts sustaining speech production in primary progressive aphasia. *J Neurosci* 34: 9754-67

Mandelli ML, Welch AE, Vilaplana E, Watson C, Battistella G, Brown JA, Possin KL, Hubbard HI, Miller ZA, Henry ML, Marx GA, Santos-Santos MA, Bajorek LP, Fortea J, Boxer A, Rabinovici G, Lee S, Deleon J, Rosen HJ, Miller BL et al. (2018) Altered topology of the functional speech production network in non-fluent/agrammatic variant of PPA. *Cortex* 108: 252-264

Masuda M, Senda J, Watanabe H, Epifanio B, Tanaka Y, Imai K, Riku Y, Li Y, Nakamura R, Ito M, Ishigaki S, Atsuta N, Koike H, Katsuno M, Hattori N, Naganawa S, Sobue G (2016) Involvement of the caudate nucleus head and its networks in sporadic amyotrophic lateral sclerosis-frontotemporal dementia continuum. *Amyotroph Lateral Scler Frontotemporal Degener* 17: 571-579

McMillan CT, Irwin DJ, Avants BB, Powers J, Cook PA, Toledo JB, McCarty Wood E, Van Deerlin VM, Lee VM, Trojanowski JQ, Grossman M (2013) White matter imaging helps dissociate tau from TDP-43 in frontotemporal lobar degeneration. *J Neurol Neurosurg Psychiatry* 84: 949-55

- Mendez MF, Shapira JS, McMurtray A, Licht E (2007a) Preliminary findings: behavioral worsening on donepezil in patients with frontotemporal dementia. *Am J Geriatr Psychiatry* 15: 84-7
- Mendez MF, Shapira JS, McMurtray A, Licht E, Miller BL (2007b) Accuracy of the clinical evaluation for frontotemporal dementia. *Arch Neurol* 64: 830-5
- Menke RA, Korner S, Filippini N, Douaud G, Knight S, Talbot K, Turner MR (2014) Widespread grey matter pathology dominates the longitudinal cerebral MRI and clinical landscape of amyotrophic lateral sclerosis. *Brain* 137: 2546-55
- Menke RAL, Proudfoot M, Talbot K, Turner MR (2018) The two-year progression of structural and functional cerebral MRI in amyotrophic lateral sclerosis. *Neuroimage Clin* 17: 953-961
- Merrilees J (2007) A model for management of behavioral symptoms in frontotemporal lobar degeneration. *Alzheimer Dis Assoc Disord* 21: S64-9
- Mesulam M, Johnson N, Kreffit TA, Gass JM, Cannon AD, Adamson JL, Bigio EH, Weintraub S, Dickson DW, Hutton ML, Graff-Radford NR (2007) Progranulin mutations in primary progressive aphasia: the PPA1 and PPA3 families. *Arch Neurol* 64: 43-7
- Mesulam M, Wicklund A, Johnson N, Rogalski E, Leger GC, Rademaker A, Weintraub S, Bigio EH (2008) Alzheimer and frontotemporal pathology in subsets of primary progressive aphasia. *Ann Neurol* 63: 709-19
- Mesulam MM (1982) Slowly progressive aphasia without generalized dementia. *Ann Neurol* 11: 592-8
- Mesulam MM (2003) Primary progressive aphasia--a language-based dementia. *N Engl J Med* 349: 1535-42
- Meteyard L, Patterson K (2009) The relation between content and structure in language production: an analysis of speech errors in semantic dementia. *Brain Lang* 110: 121-34
- Milan G, Napoletano S, Pappata S, Gentile MT, Colucci-D'Amato L, Della Rocca G, Maciag A, Rossetti CP, Fucci L, Puca A, Grossi D, Postiglione A, Vitale E (2017) GRN deletion in familial frontotemporal dementia showing association with clinical variability in 3 familial cases. *Neurobiol Aging* 53: 193 e9-193 e16

Mohammadi B, Kollewe K, Samii A, Krampfl K, Dengler R, Munte TF (2009) Changes of resting state brain networks in amyotrophic lateral sclerosis. *Exp Neurol* 217: 147-53

Morbelli S, Ferrara M, Fiz F, Dessi B, Arnaldi D, Picco A, Bossert I, Buschiazzo A, Accardo J, Picori L, Girtler N, Mandich P, Pagani M, Sambuceti G, Nobili F (2016) Mapping brain morphological and functional conversion patterns in predementia late-onset bvFTD. *Eur J Nucl Med Mol Imaging* 43: 1337-47

Moreno F, Rabinovici GD, Karydas A, Miller Z, Hsu SC, Legati A, Fong J, Schonhaut D, Esselmann H, Watson C, Stephens ML, Kramer J, Wiltfang J, Seeley WW, Miller BL, Coppola G, Grinberg LT (2015) A novel mutation P112H in the TARDBP gene associated with frontotemporal lobar degeneration without motor neuron disease and abundant neuritic amyloid plaques. *Acta Neuropathol Commun* 3: 19

Muller HP, Turner MR, Grosskreutz J, Abrahams S, Bede P, Govind V, Prudlo J, Ludolph AC, Filippi M, Kassubek J, Neuroimaging Society in ALS DTISG (2016) A large-scale multicentre cerebral diffusion tensor imaging study in amyotrophic lateral sclerosis. *J Neurol Neurosurg Psychiatry* 87: 570-9

Mummery CJ, Patterson K, Price CJ, Ashburner J, Frackowiak RS, Hodges JR (2000) A voxel-based morphometry study of semantic dementia: relationship between temporal lobe atrophy and semantic memory. *Ann Neurol* 47: 36-45

Munoz DG, Ros R, Fatas M, Bermejo F, de Yébenes JG (2007) Progressive nonfluent aphasia associated with a new mutation V363I in tau gene. *Am J Alzheimers Dis Other Demen* 22: 294-9

Murray ME, DeJesus-Hernandez M, Rutherford NJ, Baker M, Duara R, Graff-Radford NR, Wszolek ZK, Ferman TJ, Josephs KA, Boylan KB, Rademakers R, Dickson DW (2011) Clinical and neuropathologic heterogeneity of c9FTD/ALS associated with hexanucleotide repeat expansion in C9ORF72. *Acta Neuropathol* 122: 673-90

Murray ME, Kouri N, Lin WL, Jack CR, Jr., Dickson DW, Vemuri P (2014) Clinicopathologic assessment and imaging of tauopathies in neurodegenerative dementias. *Alzheimers Res Ther* 6: 1

Murrell JR, Spillantini MG, Zolo P, Guazzelli M, Smith MJ, Hasegawa M, Redi F, Crowther RA, Pietrini P, Ghetti B, Goedert M (1999) Tau gene mutation G389R causes

a tauopathy with abundant pick body-like inclusions and axonal deposits. *J Neuropathol Exp Neurol* 58: 1207-26

Neary D, Snowden JS, Gustafson L, Passant U, Stuss D, Black S, Freedman M, Kertesz A, Robert PH, Albert M, Boone K, Miller BL, Cummings J, Benson DF (1998) Frontotemporal lobar degeneration: a consensus on clinical diagnostic criteria. *Neurology* 51: 1546-54

Nestor PJ, Balan K, Cheow HK, Fryer TD, Knibb JA, Xuereb JH, Hodges JR (2007) Nuclear imaging can predict pathologic diagnosis in progressive nonfluent aphasia. *Neurology* 68: 238-9

Nestor PJ, Fryer TD, Hodges JR (2006) Declarative memory impairments in Alzheimer's disease and semantic dementia. *Neuroimage* 30: 1010-20

Neumann M, Kwong LK, Truax AC, Vanmassenhove B, Kretschmar HA, Van Deerlin VM, Clark CM, Grossman M, Miller BL, Trojanowski JQ, Lee VM (2007) TDP-43-positive white matter pathology in frontotemporal lobar degeneration with ubiquitin-positive inclusions. *J Neuropathol Exp Neurol* 66: 177-83

Neumann M, Rademakers R, Roeber S, Baker M, Kretschmar HA, Mackenzie IR (2009) A new subtype of frontotemporal lobar degeneration with FUS pathology. *Brain* 132: 2922-31

Neumann M, Sampathu DM, Kwong LK, Truax AC, Micsenyi MC, Chou TT, Bruce J, Schuck T, Grossman M, Clark CM, McCluskey LF, Miller BL, Masliah E, Mackenzie IR, Feldman H, Feiden W, Kretschmar HA, Trojanowski JQ, Lee VM (2006) Ubiquitinated TDP-43 in frontotemporal lobar degeneration and amyotrophic lateral sclerosis. *Science* 314: 130-3

Newman ME (2002) Assortative mixing in networks. *Phys Rev Lett* 89: 208701

Nuytemans K, Inchausti V, Beecham GW, Wang L, Dickson DW, Trojanowski JQ, Lee VM, Mash DC, Frosch MP, Foroud TM, Honig LS, Montine TJ, Dawson TM, Martin ER, Scott WK, Vance JM (2014) Absence of C9ORF72 expanded or intermediate repeats in autopsy-confirmed Parkinson's disease. *Mov Disord* 29: 827-30

Ogar JM, Dronkers NF, Brambati SM, Miller BL, Gorno-Tempini ML (2007) Progressive nonfluent aphasia and its characteristic motor speech deficits. *Alzheimer Dis Assoc Disord* 21: S23-30

Olney NT, Spina S, Miller BL (2017) Frontotemporal Dementia. *Neurol Clin* 35: 339-374

Onyike CU, Diehl-Schmid J (2013) The epidemiology of frontotemporal dementia. *Int Rev Psychiatry* 25: 130-7

Paternico D, Premi E, Gazzina S, Cosseddu M, Alberici A, Archetti S, Cotelli MS, Micheli A, Turla M, Gasparotti R, Padovani A, Borroni B (2016) White matter hyperintensities characterize monogenic frontotemporal dementia with granulin mutations. *Neurobiol Aging* 38: 176-180

Peelle JE, Troiani V, Gee J, Moore P, McMillan C, Vesely L, Grossman M (2008) Sentence comprehension and voxel-based morphometry in progressive nonfluent aphasia, semantic dementia, and nonaphasic frontotemporal dementia. *J Neurolinguistics* 21: 418-432

Perneczky R, Diehl-Schmid J, Pohl C, Drzezga A, Kurz A (2007) Non-fluent progressive aphasia: cerebral metabolic patterns and brain reserve. *Brain Res* 1133: 178-85

Perry DC, Brown JA, Possin KL, Datta S, Trujillo A, Radke A, Karydas A, Kornak J, Sias AC, Rabinovici GD, Gorno-Tempini ML, Boxer AL, De May M, Rankin KP, Sturm VE, Lee SE, Matthews BR, Kao AW, Vessel KA, Tartaglia MC et al. (2017) Clinicopathological correlations in behavioural variant frontotemporal dementia. *Brain* 140: 3329-3345

Perry RJ, Graham A, Williams G, Rosen H, Erzinclioglu S, Weiner M, Miller B, Hodges J (2006) Patterns of frontal lobe atrophy in frontotemporal dementia: a volumetric MRI study. *Dement Geriatr Cogn Disord* 22: 278-87

Petkau TL, Leavitt BR (2014) Progranulin in neurodegenerative disease. *Trends Neurosci* 37: 388-98

Petrov D, Mansfield C, Moussy A, Hermine O (2017) ALS Clinical Trials Review: 20 Years of Failure. Are We Any Closer to Registering a New Treatment? *Front Aging Neurosci* 9: 68

Phukan J, Pender NP, Hardiman O (2007) Cognitive impairment in amyotrophic lateral sclerosis. *Lancet Neurol* 6: 994-1003

Pickering-Brown SM, Rollinson S, Du Plessis D, Morrison KE, Varma A, Richardson AM, Neary D, Snowden JS, Mann DM (2008) Frequency and clinical characteristics of

progranulin mutation carriers in the Manchester frontotemporal lobar degeneration cohort: comparison with patients with MAPT and no known mutations. *Brain* 131: 721-31

Pietroboni AM, Fumagalli GG, Ghezzi L, Fenoglio C, Cortini F, Serpente M, Cantoni C, Rotondo E, Corti P, Carecchio M, Bassi M, Bresolin N, Galbiati D, Galimberti D, Scarpini E (2011) Phenotypic heterogeneity of the GRN Asp22fs mutation in a large Italian kindred. *J Alzheimers Dis* 24: 253-9

Pijnenburg YA, Sampson EL, Harvey RJ, Fox NC, Rossor MN (2003) Vulnerability to neuroleptic side effects in frontotemporal lobar degeneration. *Int J Geriatr Psychiatry* 18: 67-72

Pires C, Coelho M, Valadas A, Barroso C, Pimentel J, Martins M, Duyckaerts C, de Mendonca A, Verdelho A, Miltenberger-Miltenyi G (2013) Phenotypic variability of familial and sporadic Progranulin p.Gln257Profs*27 mutation. *J Alzheimers Dis* 37: 335-42

Pottier C, Bieniek KF, Finch N, van de Vorst M, Baker M, Perkersen R, Brown P, Ravenscroft T, van Blitterswijk M, Nicholson AM, DeTure M, Knopman DS, Josephs KA, Parisi JE, Petersen RC, Boylan KB, Boeve BF, Graff-Radford NR, Veltman JA, Gilissen C et al. (2015) Whole-genome sequencing reveals important role for TBK1 and OPTN mutations in frontotemporal lobar degeneration without motor neuron disease. *Acta Neuropathol* 130: 77-92

Premi E, Formenti A, Gazzina S, Archetti S, Gasparotti R, Padovani A, Borroni B (2014) Effect of TMEM106B polymorphism on functional network connectivity in asymptomatic GRN mutation carriers. *JAMA Neurol* 71: 216-21

Prudlo J, Bissbort C, Glass A, Grossmann A, Hauenstein K, Benecke R, Teipel SJ (2012) White matter pathology in ALS and lower motor neuron ALS variants: a diffusion tensor imaging study using tract-based spatial statistics. *J Neurol* 259: 1848-59

Puoti G, Lerza MC, Ferretti MG, Bugiani O, Tagliavini F, Rossi G (2014) A mutation in the 5'-UTR of GRN gene associated with frontotemporal lobar degeneration: phenotypic variability and possible pathogenetic mechanisms. *J Alzheimers Dis* 42: 939-47

Rabinovici GD, Jagust WJ, Furst AJ, Ogar JM, Racine CA, Mormino EC, O'Neil JP, Lal RA, Dronkers NF, Miller BL, Gorno-Tempini ML (2008) Abeta amyloid and glucose metabolism in three variants of primary progressive aphasia. *Ann Neurol* 64: 388-401

Rankin KP, Mayo MC, Seeley WW, Lee S, Rabinovici G, Gorno-Tempini ML, Boxer AL, Weiner MW, Trojanowski JQ, DeArmond SJ, Miller BL (2011) Behavioral variant frontotemporal dementia with corticobasal degeneration pathology: phenotypic comparison to bvFTD with Pick's disease. *J Mol Neurosci* 45: 594-608

Rascovsky K, Hodges JR, Knopman D, Mendez MF, Kramer JH, Neuhaus J, van Swieten JC, Seelaar H, Dopper EG, Onyike CU, Hillis AE, Josephs KA, Boeve BF, Kertesz A, Seeley WW, Rankin KP, Johnson JK, Gorno-Tempini ML, Rosen H, Prioleau-Latham CE et al. (2011) Sensitivity of revised diagnostic criteria for the behavioural variant of frontotemporal dementia. *Brain* 134: 2456-77

Rascovsky K, Salmon DP, Lipton AM, Leverenz JB, DeCarli C, Jagust WJ, Clark CM, Mendez MF, Tang-Wai DF, Graff-Radford NR, Galasko D (2005) Rate of progression differs in frontotemporal dementia and Alzheimer disease. *Neurology* 65: 397-403

Reed LA, Grabowski TJ, Schmidt ML, Morris JC, Goate A, Solodkin A, Van Hoesen GW, Schelper RL, Talbot CJ, Wragg MA, Trojanowski JQ (1997) Autosomal dominant dementia with widespread neurofibrillary tangles. *Ann Neurol* 42: 564-72

Reed LA, Wszolek ZK, Hutton M (2001) Phenotypic correlations in FTDP-17. *Neurobiol Aging* 22: 89-107

Renton AE, Majounie E, Waite A, Simon-Sanchez J, Rollinson S, Gibbs JR, Schymick JC, Laaksovirta H, van Swieten JC, Myllykangas L, Kalimo H, Paetau A, Abramzon Y, Remes AM, Kaganovich A, Scholz SW, Duckworth J, Ding J, Harmer DW, Hernandez DG et al. (2011) A hexanucleotide repeat expansion in C9ORF72 is the cause of chromosome 9p21-linked ALS-FTD. *Neuron* 72: 257-68

Reyes P, Ortega-Merchan MP, Rueda A, Uriza F, Santamaria-Garcia H, Rojas-Serrano N, Rodriguez-Santos J, Velasco-Leon MC, Rodriguez-Parra JD, Mora-Diaz DE, Matallana D (2018) Functional Connectivity Changes in Behavioral, Semantic, and Nonfluent Variants of Frontotemporal Dementia. *Behav Neurol* 2018: 9684129

Rogalski E, Cobia D, Harrison TM, Wieneke C, Weintraub S, Mesulam MM (2011) Progression of language decline and cortical atrophy in subtypes of primary progressive aphasia. *Neurology* 76: 1804-10

- Rohrer JD, Crutch SJ, Warrington EK, Warren JD (2010) Progranulin-associated primary progressive aphasia: a distinct phenotype? *Neuropsychologia* 48: 288-97
- Rohrer JD, Rosen HJ (2013) Neuroimaging in frontotemporal dementia. *Int Rev Psychiatry* 25: 221-9
- Rohrer JD, Warren JD (2011) Phenotypic signatures of genetic frontotemporal dementia. *Curr Opin Neurol* 24: 542-9
- Rohrer JD, Warren JD, Modat M, Ridgway GR, Douiri A, Rossor MN, Ourselin S, Fox NC (2009) Patterns of cortical thinning in the language variants of frontotemporal lobar degeneration. *Neurology* 72: 1562-9
- Rosen HJ, Gorno-Tempini ML, Goldman WP, Perry RJ, Schuff N, Weiner M, Feiwell R, Kramer JH, Miller BL (2002) Patterns of brain atrophy in frontotemporal dementia and semantic dementia. *Neurology* 58: 198-208
- Rosenbohm A, Muller HP, Hubers A, Ludolph AC, Kassubek J (2016) Corticoefferent pathways in pure lower motor neuron disease: a diffusion tensor imaging study. *J Neurol* 263: 2430-2437
- Rutherford NJ, Zhang YJ, Baker M, Gass JM, Finch NA, Xu YF, Stewart H, Kelley BJ, Kuntz K, Crook RJ, Sreedharan J, Vance C, Sorenson E, Lippa C, Bigio EH, Geschwind DH, Knopman DS, Mitsumoto H, Petersen RC, Cashman NR et al. (2008) Novel mutations in TARDBP (TDP-43) in patients with familial amyotrophic lateral sclerosis. *PLoS Genet* 4: e1000193
- Santos-Santos MA, Mandelli ML, Binney RJ, Ogar J, Wilson SM, Henry ML, Hubbard HI, Meese M, Attygalle S, Rosenberg L, Pakvasa M, Trojanowski JQ, Grinberg LT, Rosen H, Boxer AL, Miller BL, Seeley WW, Gorno-Tempini ML (2016) Features of Patients With Nonfluent/Agrammatic Primary Progressive Aphasia With Underlying Progressive Supranuclear Palsy Pathology or Corticobasal Degeneration. *JAMA Neurol* 73: 733-42
- Sassi C, Capozzo R, Gibbs R, Crews C, Zecca C, Arcuti S, Copetti M, Barulli MR, Brescia V, Singleton AB, Logroscino G (2016) A Novel Splice-Acceptor Site Mutation in GRN (c.709-2 A>T) Causes Frontotemporal Dementia Spectrum in a Large Family from Southern Italy. *J Alzheimers Dis* 53: 475-85
- Schroeter ML, Laird AR, Chwiesko C, Deuschl C, Schneider E, Bzdok D, Eickhoff SB, Neumann J (2014) Conceptualizing neuropsychiatric diseases with multimodal data-

driven meta-analyses - the case of behavioral variant frontotemporal dementia. *Cortex* 57: 22-37

Schroeter ML, Raczka K, Neumann J, Yves von Cramon D (2007) Towards a nosology for frontotemporal lobar degenerations-a meta-analysis involving 267 subjects. *Neuroimage* 36: 497-510

Schuster C, Kasper E, Dyrba M, Machts J, Bittner D, Kaufmann J, Mitchell AJ, Benecke R, Teipel S, Vielhaber S, Prudlo J (2014a) Cortical thinning and its relation to cognition in amyotrophic lateral sclerosis. *Neurobiol Aging* 35: 240-6

Schuster C, Kasper E, Machts J, Bittner D, Kaufmann J, Benecke R, Teipel S, Vielhaber S, Prudlo J (2013) Focal thinning of the motor cortex mirrors clinical features of amyotrophic lateral sclerosis and their phenotypes: a neuroimaging study. *J Neurol* 260: 2856-64

Schuster C, Kasper E, Machts J, Bittner D, Kaufmann J, Benecke R, Teipel S, Vielhaber S, Prudlo J (2014b) Longitudinal course of cortical thickness decline in amyotrophic lateral sclerosis. *J Neurol* 261: 1871-80

Schymick JC, Yang Y, Andersen PM, Vonsattel JP, Greenway M, Momeni P, Elder J, Chio A, Restagno G, Robberecht W, Dahlberg C, Mukherjee O, Goate A, Graff-Radford N, Caselli RJ, Hutton M, Gass J, Cannon A, Rademakers R, Singleton AB et al. (2007) Progranulin mutations and amyotrophic lateral sclerosis or amyotrophic lateral sclerosis-frontotemporal dementia phenotypes. *J Neurol Neurosurg Psychiatry* 78: 754-6

Sedeno L, Couto B, Garcia-Cordero I, Melloni M, Baez S, Morales Sepulveda JP, Fraiman D, Huepe D, Hurtado E, Matallana D, Kuljis R, Torralva T, Chialvo D, Sigman M, Piguet O, Manes F, Ibanez A (2016) Brain Network Organization and Social Executive Performance in Frontotemporal Dementia. *J Int Neuropsychol Soc* 22: 250-62

Seelaar H, Rohrer JD, Pijnenburg YA, Fox NC, van Swieten JC (2011) Clinical, genetic and pathological heterogeneity of frontotemporal dementia: a review. *J Neurol Neurosurg Psychiatry* 82: 476-86

Seeley WW, Bauer AM, Miller BL, Gorno-Tempini ML, Kramer JH, Weiner M, Rosen HJ (2005) The natural history of temporal variant frontotemporal dementia. *Neurology* 64: 1384-90

Seeley WW, Crawford R, Rascofsky K, Kramer JH, Weiner M, Miller BL, Gorno-Tempini ML (2008) Frontal paralimbic network atrophy in very mild behavioral variant frontotemporal dementia. *Arch Neurol* 65: 249-55

Seeley WW, Crawford RK, Zhou J, Miller BL, Greicius MD (2009) Neurodegenerative diseases target large-scale human brain networks. *Neuron* 62: 42-52

Seeley WW, Menon V, Schatzberg AF, Keller J, Glover GH, Kenna H, Reiss AL, Greicius MD (2007) Dissociable intrinsic connectivity networks for salience processing and executive control. *J Neurosci* 27: 2349-56

Sha SJ, Takada LT, Rankin KP, Yokoyama JS, Rutherford NJ, Fong JC, Khan B, Karydas A, Baker MC, DeJesus-Hernandez M, Pribadi M, Coppola G, Geschwind DH, Rademakers R, Lee SE, Seeley W, Miller BL, Boxer AL (2012) Frontotemporal dementia due to C9ORF72 mutations: clinical and imaging features. *Neurology* 79: 1002-11

Shefner JM, Al-Chalabi A, Baker MR, Cui LY, de Carvalho M, Eisen A, Grosskreutz J, Hardiman O, Henderson R, Matamala JM, Mitsumoto H, Paulus W, Simon N, Swash M, Talbot K, Turner MR, Ugawa Y, van den Berg LH, Verdugo R, Vucic S et al. (2020) A proposal for new diagnostic criteria for ALS. *Clin Neurophysiol* 131: 1975-1978

Shen D, Cui L, Fang J, Cui B, Li D, Tai H (2016) Voxel-Wise Meta-Analysis of Gray Matter Changes in Amyotrophic Lateral Sclerosis. *Front Aging Neurosci* 8: 64

Shinagawa S, Nakajima S, Plitman E, Graff-Guerrero A, Mimura M, Nakayama K, Miller BL (2015) Non-pharmacological management for patients with frontotemporal dementia: a systematic review. *J Alzheimers Dis* 45: 283-93

Simon-Sanchez J, Dopper EG, Cohn-Hokke PE, Hukema RK, Nicolaou N, Seelaar H, de Graaf JR, de Koning I, van Schoor NM, Deeg DJ, Smits M, Raaphorst J, van den Berg LH, Schelhaas HJ, De Die-Smulders CE, Majoor-Krakauer D, Rozemuller AJ, Willemsen R, Pijnenburg YA, Heutink P et al. (2012) The clinical and pathological phenotype of C9ORF72 hexanucleotide repeat expansions. *Brain* 135: 723-35

Sleegers K, Brouwers N, Maurer-Stroh S, van Es MA, Van Damme P, van Vught PW, van der Zee J, Serneels S, De Pooter T, Van den Broeck M, Cruts M, Schymkowitz J, De Jonghe P, Rousseau F, van den Berg LH, Robberecht W, Van Broeckhoven C (2008) Progranulin genetic variability contributes to amyotrophic lateral sclerosis. *Neurology* 71: 253-9

Snowden JS, Neary D, Mann DM (2004) Autopsy proven sporadic frontotemporal dementia due to microvacuolar-type histology, with onset at 21 years of age. *J Neurol Neurosurg Psychiatry* 75: 1337-9

Snowden JS, Rollinson S, Thompson JC, Harris JM, Stopford CL, Richardson AM, Jones M, Gerhard A, Davidson YS, Robinson A, Gibbons L, Hu Q, DuPlessis D, Neary D, Mann DM, Pickering-Brown SM (2012) Distinct clinical and pathological characteristics of frontotemporal dementia associated with C9ORF72 mutations. *Brain* 135: 693-708

Spina S, Murrell JR, Huey ED, Wassermann EM, Pietrini P, Baraibar MA, Barbeito AG, Troncoso JC, Vidal R, Ghetti B, Grafman J (2007) Clinicopathologic features of frontotemporal dementia with progranulin sequence variation. *Neurology* 68: 820-7

Spinelli EG, Agosta F, Ferraro PM, Riva N, Lunetta C, Falzone YM, Comi G, Falini A, Filippi M (2016) Brain MR Imaging in Patients with Lower Motor Neuron-Predominant Disease. *Radiology* 280: 545-56

Spinelli EG, Mandelli ML, Miller ZA, Santos-Santos MA, Wilson SM, Agosta F, Grinberg LT, Huang EJ, Trojanowski JQ, Meyer M, Henry ML, Comi G, Rabinovici G, Rosen HJ, Filippi M, Miller BL, Seeley WW, Gorno-Tempini ML (2017) Typical and atypical pathology in primary progressive aphasia variants. *Ann Neurol* 81: 430-443

Strong MJ, Abrahams S, Goldstein LH, Woolley S, McLaughlin P, Snowden J, Mioshi E, Roberts-South A, Benatar M, HortobaGyi T, Rosenfeld J, Silani V, Ince PG, Turner MR (2017) Amyotrophic lateral sclerosis - frontotemporal spectrum disorder (ALS-FTSD): Revised diagnostic criteria. *Amyotroph Lateral Scler Frontotemporal Degener* 18: 153-174

Swinnen B, Robberecht W (2014) The phenotypic variability of amyotrophic lateral sclerosis. *Nat Rev Neurol* 10: 661-70

Tan RH, Devenney E, Dobson-Stone C, Kwok JB, Hodges JR, Kiernan MC, Halliday GM, Hornberger M (2014) Cerebellar integrity in the amyotrophic lateral sclerosis-frontotemporal dementia continuum. *PLoS One* 9: e105632

Taylor JP, Brown RH, Jr., Cleveland DW (2016) Decoding ALS: from genes to mechanism. *Nature* 539: 197-206

Taylor LJ, Brown RG, Tsermentseli S, Al-Chalabi A, Shaw CE, Ellis CM, Leigh PN, Goldstein LH (2013) Is language impairment more common than executive dysfunction in amyotrophic lateral sclerosis? *J Neurol Neurosurg Psychiatry* 84: 494-8

Theuns J, Verstraeten A, Slegers K, Wauters E, Gijssels I, Smolders S, Crosiers D, Corsmit E, Elinck E, Sharma M, Kruger R, Lesage S, Brice A, Chung SJ, Kim MJ, Kim YJ, Ross OA, Wszolek ZK, Rogaeva E, Xi Z et al. (2014) Global investigation and meta-analysis of the C9orf72 (G4C2)_n repeat in Parkinson disease. *Neurology* 83: 1906-13

Trojci F, Corbo D, Caiazzo G, Piccirillo G, Monsurro MR, Cirillo S, Esposito F, Tedeschi G (2013) Motor and extramotor neurodegeneration in amyotrophic lateral sclerosis: a 3T high angular resolution diffusion imaging (HARDI) study. *Amyotroph Lateral Scler Frontotemporal Degener* 14: 553-61

Trojci F, Esposito F, de Stefano M, Buonanno D, Conforti FL, Corbo D, Piccirillo G, Cirillo M, Monsurro MR, Montella P, Tedeschi G (2015) Functional overlap and divergence between ALS and bvFTD. *Neurobiol Aging* 36: 413-23

Tsai PC, Liu YC, Lin KP, Liu YT, Liao YC, Hsiao CT, Soong BW, Yip PK, Lee YC (2016) Mutational analysis of TBK1 in Taiwanese patients with amyotrophic lateral sclerosis. *Neurobiol Aging* 40: 191 e11-191 e16

Tsai RM, Boxer AL (2016) Therapy and clinical trials in frontotemporal dementia: past, present, and future. *J Neurochem* 138 Suppl 1: 211-21

Turner MR, Hammers A, Allsop J, Al-Chalabi A, Shaw CE, Brooks DJ, Leigh PN, Andersen PM (2007) Volumetric cortical loss in sporadic and familial amyotrophic lateral sclerosis. *Amyotroph Lateral Scler* 8: 343-7

Ulugut H, Stek S, Wagemans LEE, Jutten RJ, Keulen MA, Bouwman FH, Prins ND, Lemstra AW, Krudop W, Teunissen CE, van Berckel BNM, Ossenkoppele R, Barkhof F, van der Flier WM, Scheltens P, Pijnenburg YAL (2021) The natural history of primary progressive aphasia: beyond aphasia. *J Neurol*

van de Pol LA, Hensel A, van der Flier WM, Visser PJ, Pijnenburg YA, Barkhof F, Gertz HJ, Scheltens P (2006) Hippocampal atrophy on MRI in frontotemporal lobar degeneration and Alzheimer's disease. *J Neurol Neurosurg Psychiatry* 77: 439-42

van der Graaff MM, Sage CA, Caan MW, Akkerman EM, Lavini C, Majoie CB, Nederveen AJ, Zwinderman AH, Vos F, Brugman F, van den Berg LH, de Rijk MC, van Doorn PA, Van Hecke W, Peeters RR, Robberecht W, Sunaert S, de Visser M (2011)

Upper and extra-motoneuron involvement in early motoneuron disease: a diffusion tensor imaging study. *Brain* 134: 1211-28

van der Zee J, Gijssels I, Dillen L, Van Langenhove T, Theuns J, Engelborghs S, Philtjens S, Vandenbulcke M, Sleegers K, Sieben A, Baumer V, Maes G, Corsmit E, Borroni B, Padovani A, Archetti S, Pernecky R, Diehl-Schmid J, de Mendonca A, Miltenberger-Miltenyi G et al. (2013) A pan-European study of the C9orf72 repeat associated with FTLN: geographic prevalence, genomic instability, and intermediate repeats. *Hum Mutat* 34: 363-73

van der Zee J, Gijssels I, Van Mossevelde S, Perrone F, Dillen L, Heeman B, Baumer V, Engelborghs S, De Bleeker J, Baets J, Gelpi E, Rojas-Garcia R, Clarimon J, Lleo A, Diehl-Schmid J, Alexopoulos P, Pernecky R, Synofzik M, Just J, Schols L et al. (2017) TBK1 Mutation Spectrum in an Extended European Patient Cohort with Frontotemporal Dementia and Amyotrophic Lateral Sclerosis. *Hum Mutat* 38: 297-309

van der Zee J, Le Ber I, Maurer-Stroh S, Engelborghs S, Gijssels I, Camuzat A, Brouwers N, Vandenberghe R, Sleegers K, Hannequin D, Dermaut B, Schymkowitz J, Champion D, Santens P, Martin JJ, Lacomblez L, De Pooter T, Peeters K, Mattheijssens M, Vercelletto M et al. (2007) Mutations other than null mutations producing a pathogenic loss of progranulin in frontotemporal dementia. *Hum Mutat* 28: 416

Van Langenhove T, Piguet O, Burrell JR, Leyton C, Foxe D, Abela M, Bartley L, Kim WS, Jary E, Huang Y, Dobson-Stone C, Kwok JB, Halliday GM, Hodges JR (2017) Predicting Development of Amyotrophic Lateral Sclerosis in Frontotemporal Dementia. *J Alzheimers Dis* 58: 163-170

Van Langenhove T, van der Zee J, Gijssels I, Engelborghs S, Vandenberghe R, Vandenbulcke M, De Bleeker J, Sieben A, Versijpt J, Ivanoiu A, Deryck O, Willems C, Dillen L, Philtjens S, Maes G, Baumer V, Van Den Broeck M, Mattheijssens M, Peeters K, Martin JJ et al. (2013) Distinct clinical characteristics of C9orf72 expansion carriers compared with GRN, MAPT, and nonmutation carriers in a Flanders-Belgian FTLN cohort. *JAMA Neurol* 70: 365-73

Van Mossevelde S, Engelborghs S, van der Zee J, Van Broeckhoven C (2018) Genotype-phenotype links in frontotemporal lobar degeneration. *Nat Rev Neurol* 14: 363-378

Van Mossevelde S, van der Zee J, Cruts M, Van Broeckhoven C (2017) Relationship between C9orf72 repeat size and clinical phenotype. *Curr Opin Genet Dev* 44: 117-124

Van Mossevelde S, van der Zee J, Gijselinck I, Engelborghs S, Sieben A, Van Langenhove T, De Bleecker J, Baets J, Vandenbulcke M, Van Laere K, Ceyskens S, Van den Broeck M, Peeters K, Mattheijssens M, Cras P, Vandenberghe R, De Jonghe P, Martin JJ, De Deyn PP, Cruts M et al. (2016) Clinical features of TBK1 carriers compared with C9orf72, GRN and non-mutation carriers in a Belgian cohort. *Brain* 139: 452-67

van Rheenen W, van Blitterswijk M, Huisman MH, Vlam L, van Doormaal PT, Seelen M, Medic J, Dooijes D, de Visser M, van der Kooij AJ, Raaphorst J, Schelhaas HJ, van der Pol WL, Veldink JH, van den Berg LH (2012) Hexanucleotide repeat expansions in C9ORF72 in the spectrum of motor neuron diseases. *Neurology* 79: 878-82

Vercelletto M, Boutoleau-Bretonniere C, Volteau C, Puel M, Auriacombe S, Sarazin M, Michel BF, Couratier P, Thomas-Anterion C, Verpillat P, Gabelle A, Golfier V, Cerato E, Lacomblez L, French research network on Frontotemporal d (2011) Memantine in behavioral variant frontotemporal dementia: negative results. *J Alzheimers Dis* 23: 749-59

Verstraete E, van den Heuvel MP, Veldink JH, Blanken N, Mandl RC, Hulshoff Pol HE, van den Berg LH (2010) Motor network degeneration in amyotrophic lateral sclerosis: a structural and functional connectivity study. *PLoS One* 5: e13664

Verstraete E, Veldink JH, Mandl RC, van den Berg LH, van den Heuvel MP (2011) Impaired structural motor connectome in amyotrophic lateral sclerosis. *PLoS One* 6: e24239

Vijverberg EG, Wattjes MP, Dols A, Krudop WA, Moller C, Peters A, Kerssens CJ, Gossink F, Prins ND, Stek ML, Scheltens P, van Berckel BN, Barkhof F, Pijnenburg YA (2016) Diagnostic Accuracy of MRI and Additional [18F]FDG-PET for Behavioral Variant Frontotemporal Dementia in Patients with Late Onset Behavioral Changes. *J Alzheimers Dis* 53: 1287-97

Vinceti G, Olney N, Mandelli ML, Spina S, Hubbard HI, Santos-Santos MA, Watson C, Miller ZA, Lomen-Hoerth C, Nichelli P, Miller BL, Grinberg LT, Seeley WW, Gorno-Tempini ML (2019) Primary progressive aphasia and the FTD-MND spectrum disorders: clinical, pathological, and neuroimaging correlates. *Amyotroph Lateral Scler Frontotemporal Degener* 20: 146-158

Walhout R, Westeneng HJ, Verstraete E, Hendrikse J, Veldink JH, van den Heuvel MP, van den Berg LH (2015) Cortical thickness in ALS: towards a marker for upper motor neuron involvement. *J Neurol Neurosurg Psychiatry* 86: 288-94

Watts DJ, Strogatz SH (1998) Collective dynamics of 'small-world' networks. *Nature* 393: 440-2

Weidberg H, Elazar Z (2011) TBK1 mediates crosstalk between the innate immune response and autophagy. *Sci Signal* 4: pe39

Westeneng HJ, Verstraete E, Walhout R, Schmidt R, Hendrikse J, Veldink JH, van den Heuvel MP, van den Berg LH (2015) Subcortical structures in amyotrophic lateral sclerosis. *Neurobiol Aging* 36: 1075-82

Whitwell JL, Anderson VM, Scahill RI, Rossor MN, Fox NC (2004) Longitudinal patterns of regional change on volumetric MRI in frontotemporal lobar degeneration. *Dement Geriatr Cogn Disord* 17: 307-10

Whitwell JL, Avula R, Senjem ML, Kantarci K, Weigand SD, Samikoglu A, Edmonson HA, Vemuri P, Knopman DS, Boeve BF, Petersen RC, Josephs KA, Jack CR, Jr. (2010) Gray and white matter water diffusion in the syndromic variants of frontotemporal dementia. *Neurology* 74: 1279-87

Whitwell JL, Boeve BF, Weigand SD, Senjem ML, Gunter JL, Baker MC, DeJesus-Hernandez M, Knopman DS, Wszolek ZK, Petersen RC, Rademakers R, Jack CR, Jr., Josephs KA (2015) Brain atrophy over time in genetic and sporadic frontotemporal dementia: a study of 198 serial magnetic resonance images. *Eur J Neurol* 22: 745-52

Whitwell JL, Jack CR, Jr., Baker M, Rademakers R, Adamson J, Boeve BF, Knopman DS, Parisi JF, Petersen RC, Dickson DW, Hutton ML, Josephs KA (2007) Voxel-based morphometry in frontotemporal lobar degeneration with ubiquitin-positive inclusions with and without progranulin mutations. *Arch Neurol* 64: 371-6

Whitwell JL, Jack CR, Jr., Boeve BF, Senjem ML, Baker M, Ivnik RJ, Knopman DS, Wszolek ZK, Petersen RC, Rademakers R, Josephs KA (2009a) Atrophy patterns in IVS10+16, IVS10+3, N279K, S305N, P301L, and V337M MAPT mutations. *Neurology* 73: 1058-65

Whitwell JL, Jack CR, Jr., Boeve BF, Senjem ML, Baker M, Rademakers R, Ivnik RJ, Knopman DS, Wszolek ZK, Petersen RC, Josephs KA (2009b) Voxel-based

morphometry patterns of atrophy in FTLD with mutations in MAPT or PGRN. *Neurology* 72: 813-20

Whitwell JL, Jack CR, Jr., Parisi JE, Knopman DS, Boeve BF, Petersen RC, Dickson DW, Josephs KA (2011a) Imaging signatures of molecular pathology in behavioral variant frontotemporal dementia. *J Mol Neurosci* 45: 372-8

Whitwell JL, Jack CR, Jr., Przybelski SA, Parisi JE, Senjem ML, Boeve BF, Knopman DS, Petersen RC, Dickson DW, Josephs KA (2011b) Temporoparietal atrophy: a marker of AD pathology independent of clinical diagnosis. *Neurobiol Aging* 32: 1531-41

Whitwell JL, Josephs KA (2012) Neuroimaging in frontotemporal lobar degeneration-predicting molecular pathology. *Nat Rev Neurol* 8: 131-42

Whitwell JL, Josephs KA, Avula R, Tosakulwong N, Weigand SD, Senjem ML, Vemuri P, Jones DT, Gunter JL, Baker M, Wszolek ZK, Knopman DS, Rademakers R, Petersen RC, Boeve BF, Jack CR, Jr. (2011) Altered functional connectivity in asymptomatic MAPT subjects: a comparison to bvFTD. *Neurology* 77: 866-74

Whitwell JL, Weigand SD, Boeve BF, Senjem ML, Gunter JL, DeJesus-Hernandez M, Rutherford NJ, Baker M, Knopman DS, Wszolek ZK, Parisi JE, Dickson DW, Petersen RC, Rademakers R, Jack CR, Jr., Josephs KA (2012) Neuroimaging signatures of frontotemporal dementia genetics: C9ORF72, tau, progranulin and sporadics. *Brain* 135: 794-806

Whitwell JL, Weigand SD, Gunter JL, Boeve BF, Rademakers R, Baker M, Knopman DS, Wszolek ZK, Petersen RC, Jack CR, Jr., Josephs KA (2011) Trajectories of brain and hippocampal atrophy in FTD with mutations in MAPT or GRN. *Neurology* 77: 393-8

Wicks P, Abrahams S, Papps B, Al-Chalabi A, Shaw CE, Leigh PN, Goldstein LH (2009) SOD1 and cognitive dysfunction in familial amyotrophic lateral sclerosis. *J Neurol* 256: 234-41

Williams KL, McCann EP, Fifita JA, Zhang K, Duncan EL, Leo PJ, Marshall M, Rowe DB, Nicholson GA, Blair IP (2015) Novel TBK1 truncating mutation in a familial amyotrophic lateral sclerosis patient of Chinese origin. *Neurobiol Aging* 36: 3334 e1-3334 e5

Wilson SM, Dronkers NF, Ogar JM, Jang J, Growdon ME, Agosta F, Henry ML, Miller BL, Gorno-Tempini ML (2010) Neural correlates of syntactic processing in the nonfluent variant of primary progressive aphasia. *J Neurosci* 30: 16845-54

Wilson SM, Ogar JM, Laluz V, Growdon M, Jang J, Glenn S, Miller BL, Weiner MW, Gorno-Tempini ML (2009) Automated MRI-based classification of primary progressive aphasia variants. *Neuroimage* 47: 1558-67

Woollacott IO, Rohrer JD (2016) The clinical spectrum of sporadic and familial forms of frontotemporal dementia. *J Neurochem* 138 Suppl 1: 6-31

Woollacott IOC, Bocchetta M, Sudre CH, Ridha BH, Strand C, Courtney R, Ourselin S, Cardoso MJ, Warren JD, Rossor MN, Revesz T, Fox NC, Holton JL, Lashley T, Rohrer JD (2018) Pathological correlates of white matter hyperintensities in a case of progranulin mutation associated frontotemporal dementia. *Neurocase* 24: 166-174

Writing G, Edaravone ALSSG (2017) Safety and efficacy of edaravone in well defined patients with amyotrophic lateral sclerosis: a randomised, double-blind, placebo-controlled trial. *Lancet Neurol* 16: 505-512

Wszolek ZK, Krygowska-Wajs A, Barcikowska M (2003) [Fronto-temporal dementia and parkinsonism linked to chromosome 17 (FTDP-17): clinical criteria]. *Neurol Neurochir Pol* 37: 173-84

Yasuda M, Yokoyama K, Nakayasu T, Nishimura Y, Matsui M, Yokoyama T, Miyoshi K, Tanaka C (2000) A Japanese patient with frontotemporal dementia and parkinsonism by a tau P301S mutation. *Neurology* 55: 1224-7

Yi HA, Moore P, Grossman M (2007) Reversal of the concreteness effect for verbs in patients with semantic dementia. *Neuropsychology* 21: 9-19

Zhang Y, Schuff N, Du AT, Rosen HJ, Kramer JH, Gorno-Tempini ML, Miller BL, Weiner MW (2009) White matter damage in frontotemporal dementia and Alzheimer's disease measured by diffusion MRI. *Brain* 132: 2579-92

Zhang Y, Tartaglia MC, Schuff N, Chiang GC, Ching C, Rosen HJ, Gorno-Tempini ML, Miller BL, Weiner MW (2013) MRI signatures of brain macrostructural atrophy and microstructural degradation in frontotemporal lobar degeneration subtypes. *J Alzheimers Dis* 33: 431-44

Zhou C, Hu X, Hu J, Liang M, Yin X, Chen L, Zhang J, Wang J (2016) Altered Brain Network in Amyotrophic Lateral Sclerosis: A Resting Graph Theory-Based Network Study at Voxel-Wise Level. *Front Neurosci* 10: 204

Zhou F, Xu R, Dowd E, Zang Y, Gong H, Wang Z (2014) Alterations in regional functional coherence within the sensory-motor network in amyotrophic lateral sclerosis. *Neurosci Lett* 558: 192-6

Zhou J, Greicius MD, Gennatas ED, Growdon ME, Jang JY, Rabinovici GD, Kramer JH, Weiner M, Miller BL, Seeley WW (2010) Divergent network connectivity changes in behavioural variant frontotemporal dementia and Alzheimer's disease. *Brain* 133: 1352-67

Zysset S, Huber O, Ferstl E, von Cramon DY (2002) The anterior frontomedian cortex and evaluative judgment: an fMRI study. *Neuroimage* 15: 983-91

2. AIMS OF THE WORK

Neurodegenerative diseases are caused by a multitude of factors, many of which are still incompletely understood. The majority of these conditions appear to be associated with the accumulation of toxic proteins which form inclusions and are used to characterize the disease at the neuropathological examination (Brettschneider, Del Tredici et al., 2015, Dawson & Dawson, 2003). A “prion-like” spreading of pathologic proteins from damaged brain regions to connected neurons via a cell-to-cell transmission is an intriguing mechanistic hypothesis (Jucker & Walker, 2013). In general, there is evidence suggesting that the clinical picture of each neurodegenerative disease might depend not only on loss of neural cell bodies, but also on the damage of the anatomical pathways connecting the different regions of the brain (Chio, Pagani et al., 2014, Galantucci, Tartaglia et al., 2011, Gorno-Tempini, Dronkers et al., 2004, Seeley, Crawford et al., 2008). MRI advanced techniques, particularly diffusion tensor imaging and resting state functional imaging, allow researchers to study brain network structural and functional connectivity *in vivo*, offering a valuable tool to elucidate the expansion of pathology across brain networks and eventually provide useful biomarkers to track and even predict the progression of pathology across brain networks in these devastating neurological diseases (Agosta, Weiler et al., 2015). Although a growing body of knowledge about brain structure and function in neurodegenerative disorders has been gathered, we still have a poor understanding of their exact relationship and evolution over time. Moreover, the influence of genetic background on the vulnerability of specific brain networks to different pathological processes is yet to be clarified.

In such a complex framework, FTLD is attractive as a biological paradigm, as it may present with different clinical syndromes, each showing a selective vulnerability of specific regions (disease epicenters) and “target” networks and a progressive spreading to “off-target” connected regions (Seeley, Crawford et al., 2009), determined by heterogeneous clinical, pathological and genetic factors. On top of such heterogeneity, FTLD presentations include not only a range of purely cognitive disorders leading to behavioral or linguistic presentations of FTD, but also motor syndromes such as MND (including ALS). The overlap between ALS and FTD has been suggested not only by the presence of mixed clinical presentations, but also by common pathological underpinnings

(i.e., the FTLT-DTP pathology) and genetic determinants (e.g., the *C9orf72* mutation), challenging the traditional view of ALS as a pure motor disease. Therefore, these advances have allowed to recognize ALS and FTD as part of a complex disease continuum instead of separate nosographic entities.

In the present work, I have applied advanced MRI techniques to explore brain structural and functional changes across different presentations of the ALS/FTD continuum, with the ultimate goal of mapping spatiotemporal patterns of neurodegeneration and connectivity alterations in these conditions.

Specific aims of the project included:

Aim 1. Characterizing the relationships between brain structural/functional alterations and their impact on motor disability and cognitive impairment in MND presentations.

Aim 2. Identifying neuroanatomical markers and potential predictors of aggressive disease progression in MND.

Aim 3. Describing characteristic alterations of structural and functional brain networks in FTD syndromes (i.e., bvFTD and PPA).

Aim 4. Combining structural and functional MRI to detect brain signatures of damage related to pathological spreading across the clinical and genetic continuum of ALS/FTD presentations.

The studies reported in **Chapter 3** address Aims 1 and 2; **Chapter 4** is dedicated to Aim 3; and **Chapter 5** provides results relative to Aim 4. General findings of the present dissertations are jointly discussed in **Chapter 6**.

References

- Agosta F, Weiler M, Filippi M (2015) Propagation of pathology through brain networks in neurodegenerative diseases: from molecules to clinical phenotypes. *CNS Neurosci Ther* 21: 754-67
- Brettschneider J, Del Tredici K, Lee VM, Trojanowski JQ (2015) Spreading of pathology in neurodegenerative diseases: a focus on human studies. *Nature reviews Neuroscience* 16: 109-20
- Chio A, Pagani M, Agosta F, Calvo A, Cistaro A, Filippi M (2014) Neuroimaging in amyotrophic lateral sclerosis: insights into structural and functional changes. *Lancet Neurol* 13: 1228-40
- Dawson TM, Dawson VL (2003) Molecular pathways of neurodegeneration in Parkinson's disease. *Science* 302: 819-22
- Galantucci S, Tartaglia MC, Wilson SM, Henry ML, Filippi M, Agosta F, Dronkers NF, Henry RG, Ogar JM, Miller BL, Gorno-Tempini ML (2011) White matter damage in primary progressive aphasia: a diffusion tensor tractography study. *Brain* 134: 3011-29
- Gorno-Tempini ML, Dronkers NF, Rankin KP, Ogar JM, Phengrasamy L, Rosen HJ, Johnson JK, Weiner MW, Miller BL (2004) Cognition and anatomy in three variants of primary progressive aphasia. *Ann Neurol* 55: 335-46
- Jucker M, Walker LC (2013) Self-propagation of pathogenic protein aggregates in neurodegenerative diseases. *Nature* 501: 45-51
- Seeley WW, Crawford R, Rascovsky K, Kramer JH, Weiner M, Miller BL, Gorno-Tempini ML (2008) Frontal paralimbic network atrophy in very mild behavioral variant frontotemporal dementia. *Arch Neurol* 65: 249-55
- Seeley WW, Crawford RK, Zhou J, Miller BL, Greicius MD (2009) Neurodegenerative diseases target large-scale human brain networks. *Neuron* 62: 42-52

3. NEUROIMAGING PROGRESSION MARKERS IN MOTOR NEURON DISEASE

3.1. Survival prediction models in motor neuron disease

ORIGINAL ARTICLE

Survival prediction models in motor neuron disease

F. Agosta^a, E. G. Spinelli^a, N. Riva^b, A. Fontana^c, S. Basaia^a, E. Canu^a, V. Castelnovo^a, Y. Falzone^b, P. Carrera^d, G. Comi^b and M. Filippi^{a,b}

^aNeuroimaging Research Unit, Institute of Experimental Neurology, Division of Neuroscience, San Raffaele Scientific Institute, Vita-Salute San Raffaele University, Milan; ^bDepartment of Neurology, Institute of Experimental Neurology, Division of Neuroscience, San Raffaele Scientific Institute, Vita-Salute San Raffaele University, Milan; ^cUnit of Biostatistics, Fondazione IRCCS Casa Sollievo della Sofferenza, San Giovanni Rotondo, Foggia; and ^dUnit of Genomics for Human Disease Diagnosis, Division of Genetics and Cell Biology, Clinical Molecular Biology Laboratory, San Raffaele Scientific Institute, Milan, Italy

Keywords:

amyotrophic lateral sclerosis, atrophy, diffusion imaging, motor neuron disease, MRI, survival

Received 14 November 2018
Accepted 18 March 2019

European Journal of Neurology 2019, **26**: 1143–1152

doi:10.1111/ene.13957

Background and purpose: This study aimed to assess the predictive value of multimodal brain magnetic resonance imaging (MRI) on survival in a large cohort of patients with motor neuron disease (MND), in combination with clinical and cognitive features.

Methods: Two hundred MND patients were followed up prospectively for a median of 4.13 years. At baseline, subjects underwent neurological examination, cognitive assessment and brain MRI. Grey matter volumes of cortical and subcortical structures and diffusion tensor MRI metrics of white matter tracts were obtained. A multivariable Royston–Parmar survival model was created using clinical and cognitive variables. The increase of survival prediction accuracy provided by MRI variables was assessed.

Results: The multivariable clinical model included predominant upper or lower motor neuron presentations and diagnostic delay as significant prognostic predictors, reaching an area under the receiver operating characteristic curve (AUC) of a 4-year survival prediction of 0.79. The combined clinical and MRI model including selected grey matter fronto-temporal volumes and diffusion tensor MRI metrics of the corticospinal and extra-motor tracts reached an AUC of 0.89. Considering amyotrophic lateral sclerosis patients only, the clinical model including diagnostic delay and semantic fluency scores provided an AUC of 0.62, whereas the combined clinical and MRI model reached an AUC of 0.77.

Conclusion: Our study demonstrated that brain MRI measures of motor and extra-motor structural damage, when combined with clinical and cognitive features, are useful predictors of survival in patients with MND, particularly when a diagnosis of amyotrophic lateral sclerosis is made.

The following data have been published (Agosta, Spinelli et al., Eur J Neurol. 2019 Sep;26(9):1143-1152. doi: 10.1111/ene.13957).

INTRODUCTION

Motor neuron disease (MND) is a fatal neurodegenerative condition encompassing a wide spectrum of clinical presentations, according to the relative involvement of upper (UMN) and lower motor neurons (LMN). A key issue in MND is the heterogeneous evolution to

severe disability, tracheostomy or death. The success of new therapies critically depends on the ability to provide new drugs at the earliest possible stage with a high diagnostic certainty and capacity to stage patients in prognostic classes.

Neuroimaging provides reliable markers of MND pathological processes, mirroring the selective involvement of motor networks (i.e., the primary motor cortex [PMC], corticospinal tract [CST] and callosal motor fibers) in early stages and the progressive spread to extra-motor, mainly fronto-temporal areas that accompanies functional decline and the development of executive and behavioral deficits, configuring a wide spectrum of syndromes overlapping with frontotemporal dementia (FTD) (Agosta, Spinelli et al., 2018). Brain grey matter (GM) and white matter (WM) structural MRI alterations have been correlated with disease progression (Kassubek et al., 2017, Kwan et al., 2012) and survival (Agosta, Pagani et al., 2010, Schuster, Hardiman et al., 2017). Considering the complexity of MND, multimodal approaches and advanced statistical models are needed to elaborate accurate prognostic markers.

The aim of this study was to create a data-driven prognostic survival model based on clinical, cognitive and structural brain MRI features to be applied to MND at a single-patient level. We focused on the assessment of the additional predictive value provided by multimodal MRI measures on a relatively long-term survival endpoint (4 years) compared with the exclusive use of clinical and cognitive features.

METHODS

Participants and study design

208 MND patients (including 156 patients meeting a diagnosis of probable or definite amyotrophic lateral sclerosis [ALS] (Brooks, Miller et al., 2000), 21 with a predominant UMN [PUMN] phenotype, and 31 with a predominant LMN [PLMN] phenotype) were consecutively screened at San Raffaele Hospital in Milan between 2010 and 2016. PUMN patients did not show any LMN sign on clinical assessment or any electromyographical evidence of active denervation. Fourteen had a disease duration >3 years, and were diagnosed with primary lateral sclerosis (PLS) (Pringle, Hudson et al., 1992). PLMN patients did not show clinical signs of definite UMN involvement, such as pseudobulbar symptoms, clonus or masseter reflex, and extensor plantar response. Ten were diagnosed with progressive muscular atrophy (PMA), based on disease duration >4 years (van den

Berg-Vos, Visser et al., 2003). All patients were receiving riluzole at study entry. Sixty-one age- and sex-matched healthy controls (mean age 63.2 ± 8.4 years, 36 women) were recruited by word of mouth, based on the following criteria: normal neurological assessment; MMSE score ≥ 28 ; no family history of neurodegenerative diseases. Among ALS patients, four were excluded due to extensive cerebrovascular alterations, two due to focal brain lesions (one meningioma and one post-traumatic lesion), and one due to severe head motion artifacts at MRI. One PLMN patient was also excluded due to cerebrovascular alterations. As a result, 200 MND patients (including 149 ALS, 21 PUMN, and 30 PLMN) were included (Table 1).

All patients underwent neurological examination and brain MRI on a 3T scanner at study entry. 189 patients underwent cognitive screening including Mini Mental State Examination (MMSE) (Folstein, Folstein et al., 1975) and fluency tests (Novelli, Papagno et al., 1986). A comprehensive, multi-domain cognitive testing was available for 139 patients, allowing a diagnosis of cognitive and/or behavioral impairment (i.e., MND with cognitive impairment [MNDci], behavioral impairment [MNDbi], or a combination thereof [MNDcbi]) (Strong, Abrahams et al., 2017). Behavioral variant of FTD was diagnosed according to the established criteria (Rascovsky et al., 2011). Blood samples for the assessment of MND-related known genetic alterations were available for 183 patients. Details of clinical, cognitive, and genetic assessments are reported in the Supplementary material. Mortality events (i.e., death or tracheostomy) were recorded until December 31, 2017.

Local ethical standards committee on human experimentation approved the study protocol and all participants provided written informed consent.

MRI analysis

Full details of MRI acquisition protocol and analysis are reported in the Supplementary materials. Voxel-based morphometry (VBM) was performed to investigate grey matter (GM) volume alterations, as described previously (Filippi, Basaia et al., 2018). Subsequently, 90 regional cortical and subcortical GM volumes were obtained, based on the Automated Anatomical Labeling atlas (Tzourio-Mazoyer, Landeau et al., 2002). Diffusion tensor (DT) MRI analysis and tractography of the CST, corpus callosum (CC), cingulum, superior longitudinal (SLF), inferior longitudinal (ILF) and uncinate fasciculi

were performed, as described previously (Agosta et al., 2014b). The CC was segmented into three portions to identify the callosal fibers linking the PMC (CC-PMC), lateral premotor cortices (CC-premotor) and supplementary motor areas (CC-SMA) (Agosta et al., 2014b). For each tract, the average mean diffusivity (MD), fractional anisotropy (FA), axial diffusivity (axD), and radial diffusivity (radD) were calculated.

Statistical analysis

Normal distribution assumption of demographic, clinical, neuropsychological and MRI variables was checked by means of Q-Q plot and Shapiro-Wilks and Kolmogorov-Smirnov tests. Group comparisons of continuous and count variables (i.e., scores) were performed using one-way ANOVA and Poisson regression models with overdispersion, respectively. Group comparisons of categorical variables were performed using Fisher exact test. All models were followed by post-hoc pairwise comparisons, false-discovery rate (FDR)-corrected.

Survival from study entry was plotted using the Kaplan-Meier method. A multi-step statistical procedure was performed to: a) build a Royston-Parmar prognostic survival model based on clinical, cognitive and genetic variables (for simplicity, here defined as the multivariable clinical model); and b) to assess the additional predicting value provided by MRI variables. The prognostic ability was quantified by the concordance c-statistic (or area under the ROC curve [AUC]) from the time-dependent ROC curve estimated at 4 years, i.e. approximately the median follow-up time. The analysis was performed both in the global MND sample and in ALS patients only. Detailed steps of this procedure are reported in the Supplementary material.

Two-sided *p*-value <0.05 was considered for statistical significance. Statistical analyses were performed using SAS 9.3 (SAS Institute, Cary, NC, USA) and R software (version 3.5.1, <http://www.R-project.org>).

RESULTS

Demographic, clinical, neuropsychological and genetic data

Patient groups were comparable in terms of age, sex, and baseline ALSFRS-r score (Table 1). Table S1 summarizes neuropsychological findings. Among those undergoing a comprehensive cognitive assessment, 89 (64%) were cognitively normal, 13 (9.4%) met

a diagnosis of MNDci, 22 (15.8%) were MNDbi, 5 (3.6%) MNDcbi, and 10 (7.2%) FTD-MND.

Among the 183 patients with genetic data, 18 (9.8%) carried a *C9ORF72* repeat expansion, 7 (3.8%) a *TARDBP* mutation, 6 (3.3%) a *SOD1* mutation, 1 (0.5%) a *FUS* mutation, and 1 (0.5%) had both *C9ORF72* and *TARDBP* mutations.

MRI analysis

VBM analysis

In ALS patients, VBM showed GM atrophy of the precentral gyri and medial superior frontal gyri bilaterally, as well as the left middle temporal gyrus, insula, and middle frontal gyrus (MFG), compared with healthy controls ($p < 0.05$, FWE-corrected, Figure S1-a). ALS patients also showed GM atrophy in the left precentral gyrus compared with PLMN (Figure S1-a). Compared with healthy controls, PUMN patients showed selective atrophy of the precentral gyri, bilaterally (Figure S1-a). No other differences were found between groups. Figure S1-b shows VBM results at $p < 0.001$ uncorrected, demonstrating subtle alterations extending to widespread frontal, temporal and parietal cortical regions in ALS patients.

GM volumes

Patients and controls did not show any significant difference in GM volumes of the 90 assessed cortical and subcortical regions (data not shown).

WM tractography

Compared with controls, both ALS and PUMN patients showed WM alterations (i.e., decreased FA, increased radD or MD) in the CC-PMC, CC-SMA, CST and SLF, bilaterally (Table S2). ALS patients also showed increased radD and nearly-significant ($p = 0.06$) decreased FA in the left uncinate fasciculus, as well as increased axD in the left cingulum. PLMN patients did not show any DT MRI alterations. Compared with ALS, PUMN patients showed a more severe damage of the CC-PMC and the CC-SMA. No other significant differences were found between groups.

Survival analysis

Of the total 200 MND patients, 120 (60%) died or underwent tracheostomy by the end of the study. According to the reverse Kaplan-Meier technique, the median follow-up time was 4.13 years (IQR: 3.24–6.04). Median survival time was 2.59 years (IQR: 1.23–7.34). ALS patients showed the highest mortality (69.8%), compared with PUMN (9.5%) and PLMN (46.7%). Figure 1 displays the corresponding Kaplan-Meier survival curves.

Definition of a multivariable clinical model of survival prediction

All MND patients. Two of the 15 candidate clinical predictors were included into the multivariable model: clinical phenotype (99.91% of bootstraps) and diagnostic delay (74.25%). The most appropriate prediction model was a proportional odds model with zero internal knots. Acceleration factors (AF) estimates of the corresponding accelerated failure time (AFT) log-logistic survival model are reported in Table 2. The 4-year prognostic accuracy of the clinical model reached an AUC of 0.79 (95% CI: 0.69-0.88). The survival conditional tree analysis identified two patient groups (Figure 2-a, Table 3): specifically, 160 short (144 ALS and 16 PLMN) and 40 long survivors (5 ALS, 21 PUMN, and 14 PLMN).

ALS patients. Considering ALS patients only, diagnostic delay (79.42% of bootstraps) and semantic fluency score (70.01%) were included into the multivariable clinical model. Like the whole MND sample, the most appropriate prediction model was a Royston-Parmar proportional odds model with zero internal knots (Table 2). The AUC of survival prediction at 4 years was 0.62 (95% CI: 0.49-0.75). The survival tree analysis identified two groups of patients (Figure 2-b, Table 3).

Univariable analysis of survival prediction

Table S3 reports results of the selected univariable AFT log-logistic survival analysis, for both the global MND sample and ALS patients only.

Combination of clinical and MRI features for survival prediction

All MND patients. Table S4 displays the increase in AUC when each MRI variable was included into the multivariable model. After the exclusion of variables showing multicollinearity, the “clinical+MRI” model included clinical phenotype, diagnostic delay, GM volumes of the right IFG pars triangularis, left IFG pars opercularis, left

fusiform gyrus and right superior temporal pole, FA values of the right CST and left uncinate fasciculus, and axD values of the right uncinate fasciculus. The resulting AUC of 4-year survival prediction was 0.89 (95% IC: 0.83–0.95), compared with 0.79 provided by the clinical model (Figure 3-a, $p=0.003$). Conditional tree analysis identified three survival groups (Figure 2-c), namely 106 short (103 ALS and 3 PLMN), 46 intermediate (35 ALS and 11 PLMN), and 48 long survivors (11 ALS, 21 PLMN, and 16 PLMN). Table 3 displays predicted and observed survival times of the identified groups.

ALS patients. The “clinical+MRI” model included diagnostic delay, semantic fluency, GM volume of the right superior temporal pole, FA of the left CST, right CST and left uncinate, axD of the left ILF, and radD of the left cingulum (Table S4). This model reached an AUC of 0.77 (95% IC: 0.65–0.88), compared with 0.62 of the clinical model (Figure 3-b, $p=0.001$). Conditional tree analysis identified two survival groups (Figure 2-d, Table 3).

DISCUSSION

This study explored the comprehensive use of clinical, cognitive and multimodal MRI variables for the development of a prognostic survival model in a large MND cohort. The inclusion of quantitative measures of structural brain damage into a multivariable model based on clinical and cognitive data provided a significant increase of accuracy for survival prediction at 4-year follow-up across MND phenotypes and, specifically, in patients with a classic ALS presentation. MRI measures providing the greatest prognostic improvement included GM volumes of inferior frontal and temporal regions and DT MRI metrics of the CST and extra-motor WM tracts (namely, the uncinate, ILF, and cingulum). DT MRI measures were crucial to improve prognostic accuracy when only ALS patients were considered.

Compared with the large number of studies assessing the diagnostic value of advanced structural MRI techniques in MND, only a few focused on their prognostic implications. Cox regression analyses have identified FA of the CST (Agosta et al., 2010) and NAA/Cho ratio of the PMC (Kalra, Hanstock et al., 2006) as survival predictors. Recently, the combination of clinical features with volumetric and DT MRI data has been tested as a prognostic method to classify ALS patients as “short” and “long survivors” by means of deep learning (Schuster et al., 2017, van der Burgh, Schmidt et al., 2017),

demonstrating a significant increase in prediction accuracy (ranging 79-84%) compared with clinical characteristics alone (66-69%). This approach allows a categorical classification into *a priori*-defined survival classes, but does not estimate the expected survival time at a single-patient level. A recent large multicenter study developed a multivariable Royston-Parmar survival model using clinical and cognitive features in ALS patients, allowing the data-driven identification of survival groups, showing good reproducibility across cohorts (Westeneng, Debray et al., 2018). To our knowledge, this is the first study that aimed to develop a similar prognostic model by the combination of multimodal neuroimaging with clinical and cognitive features.

When the whole MND cohort was considered, the main clinical predictor of survival was a PUMN or PLMN presentation, which, together with diagnostic delay, yielded an AUC of 0.79 for survival prediction at 4 years. This finding was expected, as PUMN and PLMN phenotypes are known to show a more benign course (Chio, Calvo et al., 2011), and a significant proportion of patients in our cohort met the criteria of PLS (Pringle et al., 1992) or PMA (van den Berg-Vos et al., 2003), based on their already long disease duration at baseline. In fact, as demonstrated by VBM and WM tractography, these phenotypes had distinctive anatomical damage compared with ALS, with PUMN showing a relatively selective involvement of the motor system and PLMN having no significant brain alterations, consistent with previous neuroimaging studies (Agosta et al., 2014b, Muller et al., 2018b) assessing these opposite ends of the MND spectrum. Diagnostic delay is another known favorable prognostic factor (Calvo, Moglia et al., 2017, Knibb, Keren et al., 2016), as a more indolent disease course is likely reflected by a longer time to the seek of medical attention.

Although the clinical model alone obtained a good prognostic accuracy across MND phenotypes, the combined clinical and MRI model yielded a significant improvement, reaching an AUC of 0.89. The presence of CST FA among survival predictors is consistent with previous studies in ALS patients (Agosta et al., 2010, Schuster et al., 2017) and supports the translation of this measure of UMN damage to the clinical practice not only as a diagnostic, but also as a prognostic tool. Measures of GM and WM damage of extra-motor fronto-temporal regions also provided increased prognostic accuracy. This finding is consistent with the subtle alterations shown by VBM and tractography analyses in widespread fronto-temporal cortical regions and the uncinate fasciculus of patients

with ALS (i.e., the most rapidly progressive clinical phenotype), and is in line with the presence of cognitive and/or behavioral impairment in approximately one third of patients, across MND phenotypes. Our findings suggest that the involvement of extra-motor brain regions might reflect a more advanced pathological stage (Brettschneider et al., 2013), and therefore a more rapid progression to death/tracheostomy.

MRI inclusion into the multivariable model of MND patients also provided critical information for the survival tree analysis, allowing the identification of a third group of intermediate survivors. Moreover, a larger proportion of ALS patients were selected into the long-surviving group, suggesting that milder neuroanatomical damage may indicate long survivors among unfavorable clinical phenotypes. On the other hand, a significant proportion of PLMN patients was classified into the short- and intermediate-surviving groups by the combined model, suggesting that MRI might distinguish and stratify those PLMN patients with subtle CNS alterations, probably representing early ALS presentations (Muller et al., 2018b). All PUMN patients were classified into the long-surviving group both by the clinical and combined models, supporting the notion that these patients constitute a rather homogeneous clinical phenotype.

When our analysis was restricted to ALS patients, to eliminate the effect of benign clinical presentations, the clinical multivariable model provided a much less accurate 4-year survival prediction, reaching an AUC of 0.62. This clinical model included diagnostic delay and semantic fluency as significant survival predictors. The inclusion of a measure of executive impairment among prognostic factors is consistent with previous literature (Elamin, Bede et al., 2015) and current views considering MND and FTD as parts of a clinico-pathological continuum.

The contribution of MRI variables as predictive factors in ALS was even more relevant compared with the whole MND cohort, as the combined model attained an AUC of 0.77 for survival prediction at 4 years. Similar to the global MND model, MRI measures providing the best gain of accuracy in ALS were FA values of the CST and uncinate fasciculus. Temporal GM volumes showed a less relevant, although significant role, whereas additional measures of extra-motor WM tract damage (i.e., left ILF axD and cingulum radD) significantly improved survival prediction. These findings mirror the inclusion of a cognitive measure of executive impairment into the clinical model and further support our suggestion that the involvement of associative frontal and temporal

regions might indicate a more advanced disease stage or a more aggressive clinical course.

Several clinical (e.g., age at onset, disease progression rate, ALSFRS-r score, bulbar onset, FTD diagnosis, phonemic fluency, genetic alterations) (Calvo et al., 2017, Elamin et al., 2015, Westeneng et al., 2018) and some MRI features (particularly, GM alterations of the PMC) (Kalra et al., 2006, Schuster et al., 2017) that have been previously associated with ALS prognosis were not selected by our multivariable models. However, many of these variables (including age at onset, ALSFRS-r score, disease progression rate, phonemic fluency, and right precentral gyrus volume) showed a significant influence over survival in the univariable analysis. This might be partly due to the conservative statistical procedure we performed, which eliminated from the final model all variables showing multicollinearity. For instance, diagnostic delay is intrinsically related to disease progression rate and ALSFRS-r baseline score. Therefore, the model might have selected only the most relevant features. Another possible explanation is the relatively small sample size, compared with the studies that identified the above-mentioned prognostic factors from large epidemiological registries. This observation might be particularly relevant as regards the absence of additional cognitive/behavioral features and genetic status among the clinical predictors, as this information was available only for a subset of patients.

The main limitation of this study was the absence of an external validation of the multivariable prognostic model in an independent cohort. We have also mentioned the lack of full neuropsychological and genetic data in a proportion of the included subjects, as well as the need for larger samples to detect a greater number of multimodal variables to be included into the prediction model. However, this study focused on the assessment of additional prognostic value provided by MRI compared with clinical and cognitive measures alone. The fact that a significant improvement in survival prediction accuracy was obtained across MND phenotypes and, particularly, in ALS patients supports the urgent need for the translation of advanced brain MRI techniques into clinical practice for the definition of prognosis and a correct stratification of patients in the design of pharmacological trials.

Acknowledgements

Work performed by Dr Edoardo Gioele Spinelli was in partial fulfillment of the requirements for obtaining the PhD degree at Vita-Salute San Raffaele University, Milano, Italy.

References

Agosta F, Galantucci S, Riva N, Chio A, Messina S, Iannaccone S, Calvo A, Silani V, Copetti M, Falini A, Comi G, Filippi M (2014) Intrahemispheric and interhemispheric structural network abnormalities in PLS and ALS. *Hum Brain Mapp* 35: 1710-22

Agosta F, Pagani E, Petrolini M, Sormani MP, Caputo D, Perini M, Prella A, Salvi F, Filippi M (2010) MRI predictors of long-term evolution in amyotrophic lateral sclerosis. *Eur J Neurosci* 32: 1490-6

Agosta F, Spinelli EG, Filippi M (2018) Neuroimaging in amyotrophic lateral sclerosis: current and emerging uses. *Expert Rev Neurother* 18: 395-406

Brettschneider J, Del Tredici K, Toledo JB, Robinson JL, Irwin DJ, Grossman M, Suh E, Van Deerlin VM, Wood EM, Baek Y, Kwong L, Lee EB, Elman L, McCluskey L, Fang L, Feldengut S, Ludolph AC, Lee VM, Braak H, Trojanowski JQ (2013) Stages of pTDP-43 pathology in amyotrophic lateral sclerosis. *Ann Neurol* 74: 20-38

Brooks BR, Miller RG, Swash M, Munsat TL, World Federation of Neurology Research Group on Motor Neuron D (2000) El Escorial revisited: revised criteria for the diagnosis of amyotrophic lateral sclerosis. *Amyotroph Lateral Scler Other Motor Neuron Disord* 1: 293-9

Calvo A, Moglia C, Lunetta C, Marinou K, Ticozzi N, Ferrante GD, Scialo C, Soraru G, Trojsi F, Conte A, Falzone YM, Tortelli R, Russo M, Chio A, Sansone VA, Mora G, Silani V, Volanti P, Caponnetto C, Querin G et al. (2017) Factors predicting survival in ALS: a multicenter Italian study. *J Neurol* 264: 54-63

Chio A, Calvo A, Moglia C, Mazzini L, Mora G, group Ps (2011) Phenotypic heterogeneity of amyotrophic lateral sclerosis: a population based study. *J Neurol Neurosurg Psychiatry* 82: 740-6

Elamin M, Bede P, Montuschi A, Pender N, Chio A, Hardiman O (2015) Predicting prognosis in amyotrophic lateral sclerosis: a simple algorithm. *J Neurol* 262: 1447-54

Filippi M, Basaia S, Canu E, Imperiale F, Magnani G, Falautano M, Comi G, Falini A, Agosta F (2018) Changes in functional and structural brain connectome along the Alzheimer's disease continuum. *Mol Psychiatry*

Folstein MF, Folstein SE, McHugh PR (1975) "Mini-mental state". A practical method for grading the cognitive state of patients for the clinician. *J Psychiatr Res* 12: 189-98

Kalra S, Hanstock CC, Martin WR, Allen PS, Johnston WS (2006) Detection of cerebral degeneration in amyotrophic lateral sclerosis using high-field magnetic resonance spectroscopy. *Arch Neurol* 63: 1144-8

Kassubek J, Muller HP, Del Tredici K, Lule D, Gorges M, Braak H, Ludolph AC (2017) Imaging the pathoanatomy of amyotrophic lateral sclerosis in vivo: targeting a propagation-based biological marker. *J Neurol Neurosurg Psychiatry*

Knibb JA, Keren N, Kulka A, Leigh PN, Martin S, Shaw CE, Tsuda M, Al-Chalabi A (2016) A clinical tool for predicting survival in ALS. *J Neurol Neurosurg Psychiatry* 87: 1361-1367

Kwan JY, Meoded A, Danielian LE, Wu T, Floeter MK (2012) Structural imaging differences and longitudinal changes in primary lateral sclerosis and amyotrophic lateral sclerosis. *Neuroimage Clin* 2: 151-60

Muller HP, Agosta F, Riva N, Spinelli EG, Comi G, Ludolph AC, Filippi M, Kassubek J (2018) Fast progressive lower motor neuron disease is an ALS variant: A two-centre tract of interest-based MRI data analysis. *Neuroimage Clin* 17: 145-152

Novelli G, Papagno C, Capitani E, Laiacona M, Vallar G, Cappa S (1986) Tre test clinici di ricerca e produzione lessicale. Taratura su soggetti normali. *Archivio di Psicologia, Neurologia e Psichiatria* oct-dec; vol 47 (4) : 477-506.: 477-506

Pringle CE, Hudson AJ, Munoz DG, Kiernan JA, Brown WF, Ebers GC (1992) Primary lateral sclerosis. Clinical features, neuropathology and diagnostic criteria. *Brain* 115 (Pt 2): 495-520

Rascovsky K, Hodges JR, Knopman D, Mendez MF, Kramer JH, Neuhaus J, van Swieten JC, Seelaar H, Dopper EG, Onyike CU, Hillis AE, Josephs KA, Boeve BF, Kertesz A, Seeley WW, Rankin KP, Johnson JK, Gorno-Tempini ML, Rosen H, Prioleau-Latham CE et al. (2011) Sensitivity of revised diagnostic criteria for the behavioural variant of frontotemporal dementia. *Brain* 134: 2456-77

Schuster C, Hardiman O, Bede P (2017) Survival prediction in Amyotrophic lateral sclerosis based on MRI measures and clinical characteristics. *BMC Neurol* 17: 73

Strong MJ, Abrahams S, Goldstein LH, Woolley S, McLaughlin P, Snowden J, Mioshi E, Roberts-South A, Benatar M, HortobaGyi T, Rosenfeld J, Silani V, Ince PG, Turner MR (2017) Amyotrophic lateral sclerosis - frontotemporal spectrum disorder (ALS-FTSD): Revised diagnostic criteria. *Amyotroph Lateral Scler Frontotemporal Degener* 18: 153-174

Tzourio-Mazoyer N, Landeau B, Papathanassiou D, Crivello F, Etard O, Delcroix N, Mazoyer B, Joliot M (2002) Automated anatomical labeling of activations in SPM using a macroscopic anatomical parcellation of the MNI MRI single-subject brain. *Neuroimage* 15: 273-89

van den Berg-Vos RM, Visser J, Franssen H, de Visser M, de Jong JM, Kalmijn S, Wokke JH, van den Berg LH (2003) Sporadic lower motor neuron disease with adult onset: classification of subtypes. *Brain* 126: 1036-47

van der Burgh HK, Schmidt R, Westeneng HJ, de Reus MA, van den Berg LH, van den Heuvel MP (2017) Deep learning predictions of survival based on MRI in amyotrophic lateral sclerosis. *Neuroimage Clin* 13: 361-369

Westeneng HJ, Debray TPA, Visser AE, van Eijk RPA, Rooney JPK, Calvo A, Martin S, McDermott CJ, Thompson AG, Pinto S, Kobeleva X, Rosenbohm A, Stubendorff B, Sommer H, Middelkoop BM, Dekker AM, van Vugt J, van Rheenen W, Vajda A, Heverin M et al. (2018) Prognosis for patients with amyotrophic lateral sclerosis: development and validation of a personalised prediction model. *Lancet Neurol* 17: 423-433

Table 1. Demographic and clinical features of MND patients.

	ALS	PUMN	PLMN	<i>p</i> ALS vs PUMN	<i>p</i> ALS vs PLMN	<i>p</i> PUMN vs PLMN
N	149	21	30	-	-	-
Age at MRI [years]	62.1 ± 10.8	63.0 ± 8.5	60.4 ± 8.3	0.73	0.62	0.62
Age at disease onset [years]	60.5 ± 11.0	56.7 ± 9.4	55.4 ± 11.6	0.20	0.06	0.68
Sex [F/M]	80/69	12/9	10/20	0.82	0.14	0.23
Disease duration at MRI [months]	19.7 ± 18.7	75.0 ± 61.9	60.5 ± 93.4	<0.001	<0.001	0.24
Diagnostic delay [months]	12.9 ± 14.7	35.1 ± 38.3	39.7 ± 77.4	<0.001	<0.001	0.57
Site of onset [limb/bulbar/ limb+bulbar]	106/40/3	18/3/0	29/1/0	0.53	0.03	0.44
ALSFRS-r [0-48]	37.5 ± 6.4	36.5 ± 6.6	38.4 ± 6.8	0.53	0.53	0.53
ALSFRS-r rate of decline [month]	0.8 ± 0.7	0.4 ± 0.6	0.5 ± 0.6	<0.001	0.003	0.45
MRC total sum score [0-120]	100.4 ± 17.2	112.0 ± 12.0	92.5 ± 20.7	0.01	0.03	<0.001
MRC upper limbs sum score [0-35]	59.5 ± 10.1	66.0 ± 6.3	55.1 ± 13.7	0.02	0.05	0.002

MRC lower limbs sum score [0-25]	40.8 ± 11.9	46.0 ± 9.4	37.4 ± 13.9	0.17	0.20	0.09
UMN score [0-16]	10.8 ± 4.4	13.8 ± 2.0	3.3 ± 3.6	0.01	<0.001	<0.001

Numbers are means ± standard deviations. *P* values refer to ANOVA models or Fisher's test, followed by post-hoc pairwise comparisons, false-discovery rate-corrected for multiple comparisons. Abbreviations: ALS = amyotrophic lateral sclerosis; ALSFRS-r = ALS Functional Rating Scale - revised version; MND = motor neuron disease; MRC = Medical Research Council scale; PLMN = patients with a predominant lower motor neuron phenotype; PUMN = patients with a predominant upper motor neuron phenotype.

Table 2. Multivariable accelerated failure time (AFT) log-logistic survival model based on clinical features.

	All MND patients		
Feature	AF estimate	Standard error	<i>p</i>
PUMN vs ALS phenotype	2.25	0.49	<0.001
PLMN vs ALS phenotype	0.49	0.25	0.05
Diagnostic delay [§]	0.14	0.05	0.009
	ALS patients only		
	AF estimate	Standard error	<i>p</i>
Diagnostic delay [§]	0.24	0.07	0.001
Semantic fluency [§]	3.12	0.94	0.001

[§]These variables were transformed by multivariable fractional polynomial models, due to non-linear relationships with the survival endpoint. Abbreviations: AF = acceleration factor; ALS = amyotrophic lateral sclerosis; MND = motor neuron disease; PLMN = patients with a predominant lower motor neuron phenotype; PUMN = patients with a predominant upper motor neuron phenotype.

Table 3. Predicted and observed survival times of groups identified by the corresponding “clinical” and “clinical+MRI” models.

		N	Predicted survival time	Observed survival time
All MND patients				
Clinical model	Short survivors	160 (144 ALS, 16 PLMN)	1.98 (0.04)	1.78 (0.12)
	Long survivors	40 (5 ALS, 21 PUMN, 14 PLMN)	4.39 (0.30)	4.43 (0.26)
Clinical + MRI model	Short survivors	106 (103 ALS, 3 PLMN)	1.80 (0.04)	1.50 (0.12)
	Intermediate survivors	46 (35 ALS, 11 PLMN)	2.80 (0.04)	2.45 (0.21)
	Long survivors	48 (11 ALS, 21 PUMN, 16 PLMN)	4.32 (0.22)	4.43 (0.26)
ALS patients only				
Clinical model	Short survivors	86	1.69 (0.03)	1.52 (0.16)
	Long survivors	63	2.54 (0.10)	2.71 (0.18)
Clinical + MRI model	Short survivors	110	1.86 (0.04)	1.59 (0.12)
	Long survivors	39	2.91 (0.16)	3.15 (0.27)

Values are medians (standard errors). Abbreviations: ALS = amyotrophic lateral sclerosis; MND = motor neuron disease.

Figure 1. Kaplan-Meier survival curves of all MND patients (A), and (B) divided based on clinical phenotype. Results of a log-rank test between clinical phenotypes is provided in (B). Abbreviations: ALS= amyotrophic lateral sclerosis; MND= motor neuron disease; PLMN= patients with a predominant lower motor neuron phenotype; PUMN= patients with a predominant upper motor neuron phenotype.

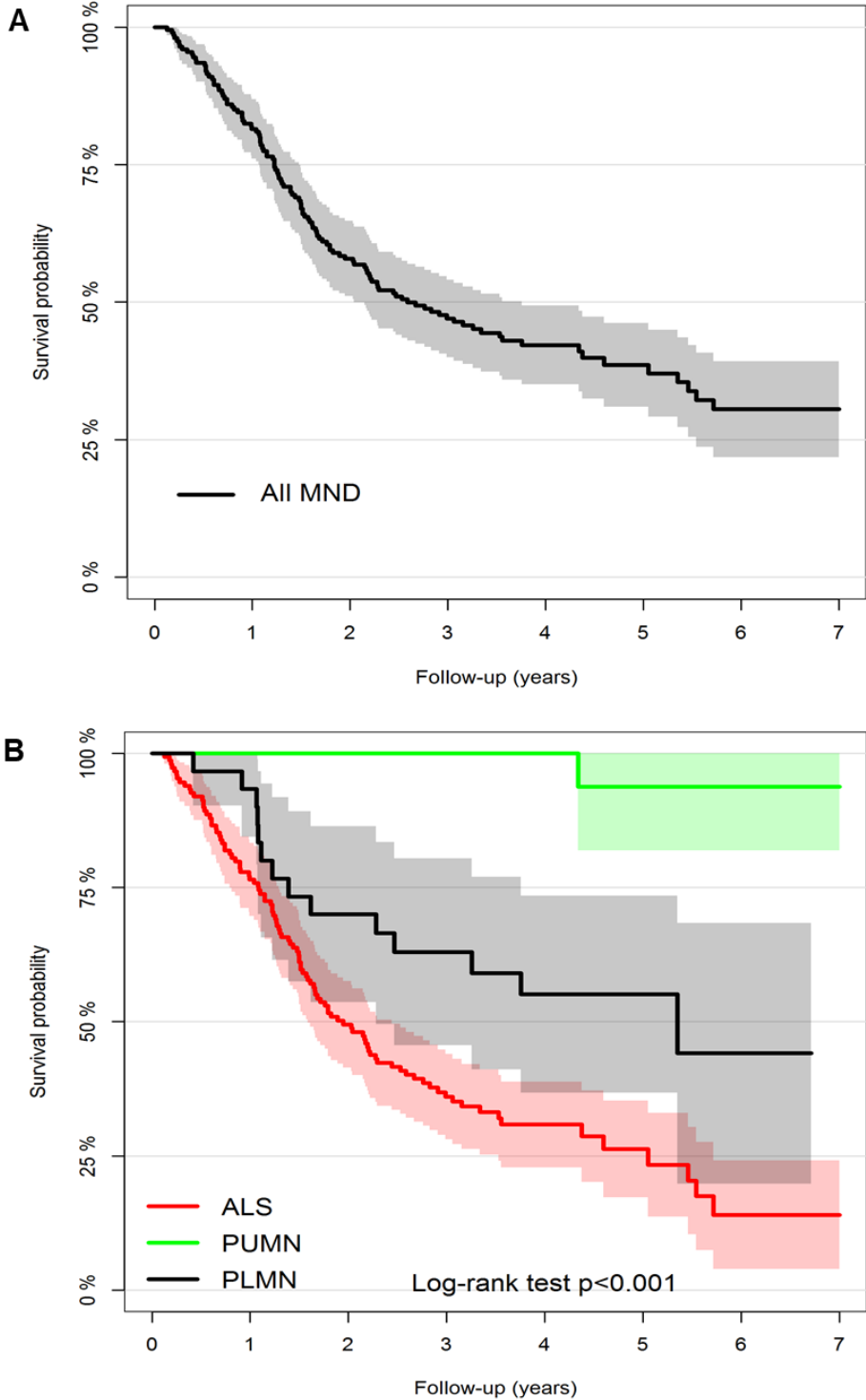


Figure 2. Top row displays Kaplan-Meier survival curves of survival group classes identified by the multivariable clinical model for (A) all MND patients, and (B) ALS patients only. Bottom row displays Kaplan-Meier survival curves of survival group classes identified by the multivariable “clinical+MRI” model for (C) all MND patients, and (D) ALS patients only. Abbreviations: ALS= amyotrophic lateral sclerosis; MND= motor neuron disease; t= estimated survival time.

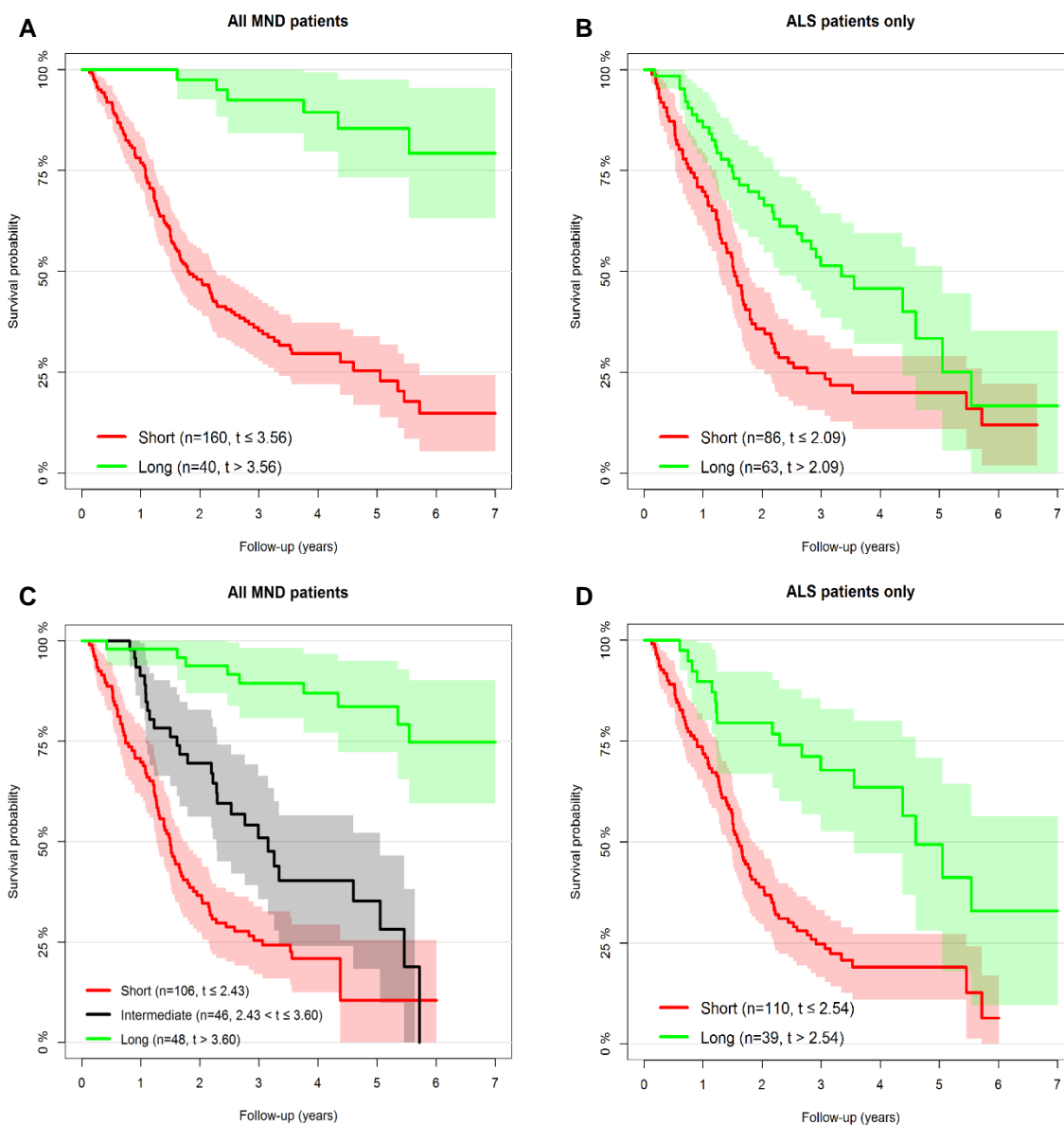
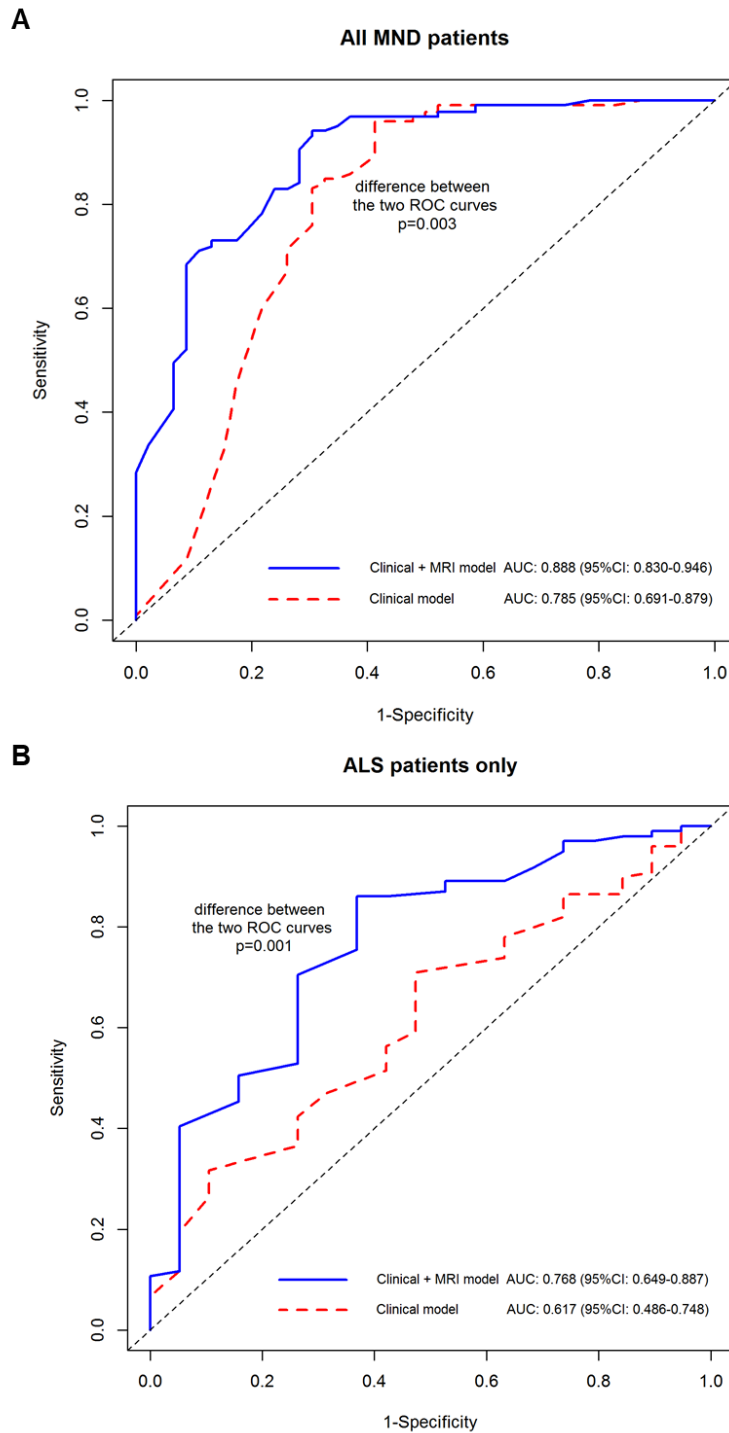


Figure 3. Plots of the two nested time-dependent ROC curves (i.e. the “clinical” model vs. the extended “clinical+MRI” model) for survival prediction at 4 years of follow-up in (A) all MND patients, and (B) ALS patients only. Abbreviations: ALS= amyotrophic lateral sclerosis; AUC= area under the curve; CI= confidence interval; MND= motor neuron disease.



Supplementary material

Clinical evaluation

Clinical evaluation was performed by experienced neurologists blinded to MRI results, recording site of disease onset and disease duration at presentation. Disease severity was assessed using the ALS Functional Rating Scale-revised (ALSFRS-r) (Cedarbaum, Stambler et al., 1999). The rate of disease progression was defined according to the following formula: $(48 - \text{ALSFRS-r score}) / \text{time from symptom onset}$. Muscular strength was assessed by manual muscle testing based on the Medical Research Council (MRC) scale, and clinical UMN involvement was graded by totaling the number of pathological UMN signs on examination (Turner, Cagnin et al., 2004).

Neuropsychological evaluation

Cognitive and behavioral assessment was performed by a trained neuropsychologist unaware of MRI results, and evaluated: global cognitive functioning with the MMSE (Folstein et al., 1975); executive functions with the Raven coloured progressive matrices (Basso, Capitani et al., 1987), digit span backward (Monaco, Costa et al., 2013), Cognitive Estimation Task (CET) (Della Sala, MacPherson et al., 2003), Wisconsin Card Sorting Test (WCST) (Laiacona, Inzaghi et al., 2000), and Weigl's Sorting test (Weigl, 1927); fluency with phonemic and semantic fluency tests (Novelli et al., 1986), fluency indices (controlling for individual variations in motor disabilities) (Abrahams, Leigh et al., 2000); verbal memory with the digit span forward (Orsini, Grossi et al., 1987) and the Rey Auditory Verbal Learning Test (RAVLT) immediate and delayed recall (Carlesimo, Caltagirone et al., 1996); and language with the oral confrontation naming subtests of BADA (Batteria per l'Analisi dei deficit Afasici) (Miceli, Laudanna et al., 1994a). Scores on neuropsychological tests were age-, sex-, and education-corrected using corresponding normative values. Mood disturbances were assessed using the Hamilton Depression Rating Scale (Hamilton, 1960). The presence of behavioral changes was determined on the basis of direct observation, patient's history, caregiver report, Frontal Behavioral Inventory (FBI) (Alberici, Geroldi et al., 2007) and ALS-FTD questionnaire (Raaphorst, Beeldman et al., 2012) administered to the patients' caregiver.

A diagnosis of cognitive and/or behavioral impairment (i.e., MND with cognitive impairment [MNDci], MND with behavioral impairment [MNDbi], or a combination thereof [MNDcbi]) was defined according to the recently revised Strong criteria (Strong et al., 2017). A diagnosis of behavioral variant of FTD was made according to the established clinical criteria (Rascovsky et al., 2011).

Genetic analysis

The presence of GGGGCC hexanucleotide expansion in the first intron of *C9ORF72* was assessed using a repeat-primed polymerase chain reaction (PCR) assay (Renton, Majounie et al., 2011). A cut-off of ≥ 30 repeats with a typical saw-tooth pattern was considered pathological. The coding sequences and intron/exon boundaries of *TARDBP*, *SOD1* and *FUS* genes were amplified by PCR using optimized protocols, looking for known pathogenic mutations (Pozzi, Valenza et al., 2017).

MRI acquisition

Using a 3.0 T scanner (Intera, Philips Medical Systems, Best, the Netherlands), the following brain MRI sequences were obtained from all subjects: T2-weighted spin echo (SE) (repetition time [TR]=3500 ms; echo time [TE]=85 ms; echo train length=15; flip angle=90°; 22 contiguous, 5-mm-thick, axial slices; matrix size=512 × 512; field of view [FOV]=230 × 184 mm²); fluid-attenuated inversion recovery (TR=11 s; TE=120 ms; flip angle=90°; 22 contiguous, 5-mm-thick, axial slices; matrix size=512 × 512; FOV=230 mm²); 3D T1-weighted fast field echo (FFE) (TR=25 ms, TE=4.6 ms, flip angle=30°, 220 contiguous axial slices with voxel size=0.89 x 0.89 x 0.8 mm, matrix size=256 x 256, FOV=230 x 182 mm²); and pulsed-gradient SE echo planar with sensitivity encoding (acceleration factor=2.5, TR=8986 ms, TE=80 ms, 55 contiguous, 2.5 mm-thick axial slices, number of acquisitions=2; acquisition matrix 96 x 96, with an in-plane pixel size of 1.87 x 1.87 mm and a FOV=240 x 240 mm²) and diffusion gradients applied in 32 noncollinear directions using a gradient scheme which is standard on this system (gradient over-plus) and optimized to reduce echo time as much as possible. The *b* factor used was 1000 s/mm². Fat saturation was performed to avoid chemical shift artifacts. All slices were positioned to run parallel to a line that joins the most inferoanterior and inferoposterior parts of the corpus callosum.

MRI analysis

Voxel-based morphometry. Voxel-based morphometry (VBM) was performed using SPM12 (<http://www.fil.ion.ucl.ac.uk/spm/>) and Diffeomorphic Anatomical Registration Exponentiated Lie Algebra (DARTEL) registration method (Ashburner, 2007), to investigate grey matter (GM) volume alterations. Briefly, (i) T1-weighted images were segmented to produce GM, WM and CSF tissue probability maps in the MNI space; (ii) the segmentation parameters obtained from the step (i) were imported in DARTEL; (iii) the rigidly aligned version of the images previously segmented (i) was generated; (iv) the DARTEL template was created and the obtained flow fields were applied to the rigidly-aligned segments to warp them to the common DARTEL space and then modulated using the Jacobian determinants. Since the DARTEL process warps to a common space that is smaller than the MNI space, we performed an additional transformation as follows: (v) the modulated images from DARTEL were normalized to the MNI template using an affine transformation estimated from the DARTEL GM template and the a priori GM probability map without resampling (<http://brainmap.wisc.edu/normalizeDARTELtoMNI>). Prior to statistical computations, images were smoothed with an 8 mm FWHM Gaussian filter. VBM group comparisons were tested using ANCOVA model adjusting for total intracranial volume, age and gender. Results were assessed at $p < 0.05$ Family-wise error (FWE)-corrected for multiple comparisons.

Grey matter volumes. To obtain quantitative measures of regional GM volumes, GM maps of patients and healthy controls were parcellated into 90 Automated Anatomical Labeling (AAL) regions of interest. Specifically, the AAL atlas was registered to the subject T1-weighted images using linear and non-linear registrations (FLIRT (Jenkinson, Bannister et al., 2002) and FNIRT (Andersson, Jenkinson et al., 2007), respectively), as implemented in the FMRIB software library (FSL, <http://www.fmrib.ox.ac.uk/fsl>). Cortical GM maps were obtained from the step (i) of VBM procedure, while maps of the basal ganglia (i.e., bilateral caudate, globus pallidus, putamen, and thalamus), hippocampus and amygdala were obtained using the FMRIB's Integrated Registration and Segmentation Tool (FIRST) in FSL (<http://www.fmrib.ox.ac.uk/fsl/first/index.html>). GM

volumes were multiplied by the normalization factor derived from SIENAx (part of FSL; <http://www.fmrib.ox.ac.uk/fsl/sienax/index.html>) to correct for subject head size.

White matter tractography. DT MRI analysis was performed using the FMRIB Diffusion Toolbox in FSL (<http://www.fmrib.ox.ac.uk/fsl/fdt/index.html>) and the JIM6 software (Version 6.0, Xinapse Systems, Northants, UK, <http://www.xinapse.com>). The diffusion-weighted data were skull-stripped using the Brain Extraction Tool implemented in FSL. Using FLIRT, the two diffusion-weighted scans were coregistered by applying the rigid transformation needed to correct for position between the two b0 images (T2-weighted, but not diffusion-weighted). The rotation component was also applied to diffusion-weighted directions. Eddy currents correction was performed using the JIM6 software (Horsfield, 1999). Then, the two acquisitions were concatenated. The DT was estimated on a voxel-by-voxel basis using DTIfit provided by the FMRIB Diffusion Toolbox. Maps of mean diffusivity (MD), fractional anisotropy (FA), axial diffusivity (axD) and radial diffusivity (radD) were obtained.

Seeds for tractography of the CST, corpus callosum, cingulum, superior longitudinal (SLF), inferior longitudinal (ILF) and uncinate fasciculi were defined in the Montreal Neurological Institute (MNI) space on the FA template provided by FSL, as previously described (Agosta, Galantucci et al., 2013b, Agosta et al., 2014b). Fiber tracking was performed in native DT MRI space using a probabilistic tractography algorithm implemented in FSL (probtrackx), which is based on Bayesian estimation of diffusion parameters (Bedpostx) (Behrens, Berg et al., 2007). Fiber tracking was initiated from all voxels within the seed masks in the diffusion space to generate 5000 streamline samples with a step length of 0.5 mm and a curvature threshold of 0.2. Using a “single-seed” approach, the reconstructions of the CC and bilateral CST, SLF and uncinate were obtained. For the ILF and cingulum, we used masks including three seeds each (anterior, middle and posterior ILF; and anterior, isthmus, and parahippocampal cingulum). In addition, using a “seed to target” approach, the corpus callosum was segmented into three portions to identify the callosal fibers linking the primary motor cortices (CC-PMC), lateral premotor cortices (CC-premotor) and supplementary motor areas (CC-SMA) (Agosta et al., 2014b). Tract maps were then normalized taking into consideration the number of voxels in the seed masks. To do so, the number of streamline samples present in the voxels of the tract maps was divided by the way-total, which corresponds to the

total number of streamline samples that were not rejected by the exclusion masks. The tract masks obtained were thresholded at a value equal to 40% of the 95th percentile of the distribution of the intensity values of the voxels included in the tract, as previously described (Galantucci et al., 2011). This normalization procedure allowed us to correct for possible differences between tracts due to the different sizes of the starting seeds. In this way, we also excluded the background noise and avoided a too restrictive thresholding when the maximum intensity value was an outlier. Group probability maps of each thresholded tract were produced to visually check their anatomical consistency across study subjects. For each tract, the average MD, FA, axD, and radD were calculated in the native space.

Survival analysis

The steps of the statistical procedure performed for the survival analysis are listed below.

i) A dataset including the candidate clinical predictors and all MRI variables (i.e., GM volumes and DT MRI metrics) was created. Candidate predictors were selected from clinical and cognitive variables (i.e., age at onset, sex, clinical phenotype, site of onset, diagnostic delay, disease duration at MRI, ALSFRS-r, disease progression rate, total MRC, UMN score, presence of a genetic alteration, cognitive diagnosis according to established criteria (Rascovsky et al., 2011, Strong et al., 2017), MMSE, phonemic and semantic fluency tests scores), based on previous reports (Calvo et al., 2017, Chio, Logroscino et al., 2009) and clinical judgement. Multivariate imputation by chained equations of missing variables was performed, assuming the “missing at random” condition (Brooks & Gelman, 1998).

ii) Multivariable fractional polynomials (Sauerbrei & Royston, 1999) were applied to transform imputed variables in the presence of non-linear relationships with the survival endpoint.

iii) A backward elimination procedure with bootstrapping was used to select predictors for the clinical model. Variables selected in more than 70% of the 40'000 resamples (Heymans, van Buuren et al., 2007) entered a multivariable Royston-Parmar model (Royston & Parmar, 2002). The model achieving the minimum Akaike information criterion (AIC) was chosen. Survival models were expressed in terms of accelerated failure time (AFT), and estimates were reported as acceleration factors (AF) of the

included parameters. As suggested by recent literature (Rooney, Byrne et al., 2013, Westeneng et al., 2018), Royston-Parmar parametric survival models were preferred over Cox regression models, since the former are more flexible in the identification of the best-fitting model and facilitate the definition of absolute risk at the individual patient level.

iv) For each patient, the multivariable clinical model was used to estimate the cumulative hazard function probability of the event occurrence (i.e., death or tracheostomy) at 4 years, which was approximately the median follow-up time. For model validation, the prognostic ability was quantified by the concordance c-statistic (or area under the ROC curve [AUC]) from the time-dependent ROC curve estimated at 4 years by inverse probability of censoring weighting estimators (KM-weights). Model's calibration (i.e., the agreement between the observed and predicted 4-year survival) was also assessed by visual inspection of the calibration plot.

v) The expected individual survival times were estimated from the multivariable clinical model, and a conditional tree analysis (Hothorn & Zeileis, 2015) was performed to identify patient subgroups with different survival times. The splitting rule was defined using Bonferroni adjustment.

vi) Univariable associations between each clinical or MRI variable of the imputed dataset and the survival outcome were assessed using the AFT survival models selected from step iii), to ensure that the resulting estimates were fully comparable with the multivariable model.

vii) The change of prognostic ability obtained by the inclusion of each MRI variable into the multivariable clinical survival model was assessed using the estimator proposed by Blanche et al. (Blanche, Dartigues et al., 2013) Finally, the whole set of MRI variables, which individually provided a statistically significant improvement in the AUC, was used to build a "clinical+MRI" model, after the exclusion of variables showing multicollinearity with other features. The resulting AUC was estimated, and the survival tree analysis was re-run applying the combined model.

Supplementary references

- Abrahams S, Leigh PN, Harvey A, Vythelingum GN, Grise D, Goldstein LH (2000) Verbal fluency and executive dysfunction in amyotrophic lateral sclerosis (ALS). *Neuropsychologia* 38: 734-47
- Agosta F, Galantucci S, Canu E, Cappa SF, Magnani G, Franceschi M, Falini A, Comi G, Filippi M (2013) Disruption of structural connectivity along the dorsal and ventral language pathways in patients with nonfluent and semantic variant primary progressive aphasia: a DT MRI study and a literature review. *Brain Lang* 127: 157-66
- Agosta F, Galantucci S, Riva N, Chio A, Messina S, Iannaccone S, Calvo A, Silani V, Copetti M, Falini A, Comi G, Filippi M (2014) Intrahemispheric and interhemispheric structural network abnormalities in PLS and ALS. *Hum Brain Mapp* 35: 1710-22
- Alberici A, Geroldi C, Cotelli M, Adorni A, Calabria M, Rossi G, Borroni B, Padovani A, Zanetti O, Kertesz A (2007) The Frontal Behavioural Inventory (Italian version) differentiates frontotemporal lobar degeneration variants from Alzheimer's disease. *Neurol Sci* 28: 80-6
- Andersson JL, Jenkinson M, Smith S (2007) Non-linear registration, aka spatial normalisation. . *Technical Report* FMRIB Centre, Oxford, United Kingdom
- Ashburner J (2007) A fast diffeomorphic image registration algorithm. *Neuroimage* 38: 95-113
- Basso A, Capitani E, Laiacona M (1987) Raven's coloured progressive matrices: normative values on 305 adult normal controls. *Funct Neurol* 2: 189-94
- Behrens TE, Berg HJ, Jbabdi S, Rushworth MF, Woolrich MW (2007) Probabilistic diffusion tractography with multiple fibre orientations: What can we gain? *Neuroimage* 34: 144-55
- Blanche P, Dartigues JF, Jacqmin-Gadda H (2013) Estimating and comparing time-dependent areas under receiver operating characteristic curves for censored event times with competing risks. *Stat Med* 32: 5381-97
- Brooks SP, Gelman A (1998) General methods for monitoring convergence of iterative simulations. *Journal of Computational and Graphical Statistics* 7(4): 434-55
- Calvo A, Moglia C, Lunetta C, Marinou K, Ticozzi N, Ferrante GD, Scialo C, Soraru G, Trojsi F, Conte A, Falzone YM, Tortelli R, Russo M, Chio A, Sansone VA, Mora G,

Silani V, Volanti P, Caponnetto C, Querin G et al. (2017) Factors predicting survival in ALS: a multicenter Italian study. *J Neurol* 264: 54-63

Carlesimo GA, Caltagirone C, Gainotti G (1996) The Mental Deterioration Battery: normative data, diagnostic reliability and qualitative analyses of cognitive impairment. The Group for the Standardization of the Mental Deterioration Battery. *European neurology* 36: 378-84

Cedarbaum JM, Stambler N, Malta E, Fuller C, Hilt D, Thurmond B, Nakanishi A (1999) The ALSFRS-R: a revised ALS functional rating scale that incorporates assessments of respiratory function. BDNF ALS Study Group (Phase III). *J Neurol Sci* 169: 13-21

Chio A, Logroscino G, Hardiman O, Swingler R, Mitchell D, Beghi E, Traynor BG, Eurlis C (2009) Prognostic factors in ALS: A critical review. *Amyotroph Lateral Scler* 10: 310-23

Della Sala S, MacPherson SE, Phillips LH, Sacco L, Spinnler H (2003) How many camels are there in Italy? Cognitive estimates standardised on the Italian population. *Neurol Sci* 24: 10-5

Folstein MF, Folstein SE, McHugh PR (1975) "Mini-mental state". A practical method for grading the cognitive state of patients for the clinician. *J Psychiatr Res* 12: 189-98

Galantucci S, Tartaglia MC, Wilson SM, Henry ML, Filippi M, Agosta F, Dronkers NF, Henry RG, Ogar JM, Miller BL, Gorno-Tempini ML (2011) White matter damage in primary progressive aphasia: a diffusion tensor tractography study. *Brain* 134: 3011-29

Hamilton M (1960) A rating scale for depression. *J Neurol Neurosurg Psychiatry* 23: 56-62

Heymans MW, van Buuren S, Knol DL, van Mechelen W, de Vet HC (2007) Variable selection under multiple imputation using the bootstrap in a prognostic study. *BMC Med Res Methodol* 7: 33

Horsfield MA (1999) Mapping eddy current induced fields for the correction of diffusion-weighted echo planar images. *Magn Reson Imaging* 17: 1335-45

Hothorn T, Zeileis A (2015) partykit: A Modular Toolkit for Recursive Partytioning in R. *Journal of Machine Learning Research* 16: 3905–3909

Jenkinson M, Bannister P, Brady M, Smith S (2002) Improved optimization for the robust and accurate linear registration and motion correction of brain images. *Neuroimage* 17: 825-41

Laiacona M, Inzaghi MG, De Tanti A, Capitani E (2000) Wisconsin card sorting test: a new global score, with Italian norms, and its relationship with the Weigl sorting test. *Neurol Sci* 21: 279-91

Miceli G, Laudanna A, Burani C, Capasso R (1994) Batteria per l'Analisi del Deficit Afasico. B.A.D.A. [B.A.D.A. A Battery for the Assessment of Aphasic Disorders]. Roma: CEPSAG

Monaco M, Costa A, Caltagirone C, Carlesimo GA (2013) Forward and backward span for verbal and visuo-spatial data: standardization and normative data from an Italian adult population. *Neurol Sci* 34: 749-54

Novelli G, Papagno C, Capitani E, Laiacona M, Vallar G, Cappa S (1986) Tre test clinici di ricerca e produzione lessicale. Taratura su soggetti normali. *Archivio di Psicologia, Neurologia e Psichiatria* oct-dec; vol 47 (4) : 477-506.: 477-506

Orsini A, Grossi D, Capitani E, Laiacona M, Papagno C, Vallar G (1987) Verbal and spatial immediate memory span: normative data from 1355 adults and 1112 children. *Ital J Neurol Sci* 8: 539-48

Pozzi L, Valenza F, Mosca L, Dal Mas A, Domi T, Romano A, Tarlarini C, Falzone YM, Tremolizzo L, Soraru G, Cerri F, Ferraro PM, Basaia S, Agosta F, Fazio R, Comola M, Comi G, Ferrari M, Quattrini A, Lunetta C et al. (2017) TBK1 mutations in Italian patients with amyotrophic lateral sclerosis: genetic and functional characterisation. *J Neurol Neurosurg Psychiatry* 88: 869-875

Raaphorst J, Beeldman E, Schmand B, Berkhout J, Linszen WH, van den Berg LH, Pijnenburg YA, Grupstra HF, Weikamp JG, Schelhaas HJ, Papma JM, van Swieten JC, de Visser M, de Haan RJ (2012) The ALS-FTD-Q: a new screening tool for behavioral disturbances in ALS. *Neurology* 79: 1377-83

Rascovsky K, Hodges JR, Knopman D, Mendez MF, Kramer JH, Neuhaus J, van Swieten JC, Seelaar H, Dopper EG, Onyike CU, Hillis AE, Josephs KA, Boeve BF, Kertesz A, Seeley WW, Rankin KP, Johnson JK, Gorno-Tempini ML, Rosen H, Prioleau-Latham CE et al. (2011) Sensitivity of revised diagnostic criteria for the behavioural variant of frontotemporal dementia. *Brain* 134: 2456-77

Renton AE, Majounie E, Waite A, Simon-Sanchez J, Rollinson S, Gibbs JR, Schymick JC, Laaksovirta H, van Swieten JC, Myllykangas L, Kalimo H, Paetau A, Abramzon Y, Remes AM, Kaganovich A, Scholz SW, Duckworth J, Ding J, Harmer DW, Hernandez DG et al. (2011) A hexanucleotide repeat expansion in C9ORF72 is the cause of chromosome 9p21-linked ALS-FTD. *Neuron* 72: 257-68

Rooney J, Byrne S, Heverin M, Corr B, Elamin M, Staines A, Goldacre B, Hardiman O (2013) Survival analysis of irish amyotrophic lateral sclerosis patients diagnosed from 1995-2010. *PLoS One* 8: e74733

Royston P, Parmar MK (2002) Flexible parametric proportional-hazards and proportional-odds models for censored survival data, with application to prognostic modelling and estimation of treatment effects. *Stat Med* 21: 2175-97

Sauerbrei W, Royston P (1999) Building multivariable prognostic and diagnostic models: transformation of the predictors by using fractional polynomials. *J R Stat Soc Series A Stats Soc* 162: 71–94

Strong MJ, Abrahams S, Goldstein LH, Woolley S, McLaughlin P, Snowden J, Mioshi E, Roberts-South A, Benatar M, HortobaGyi T, Rosenfeld J, Silani V, Ince PG, Turner MR (2017) Amyotrophic lateral sclerosis - frontotemporal spectrum disorder (ALS-FTSD): Revised diagnostic criteria. *Amyotroph Lateral Scler Frontotemporal Degener* 18: 153-174

Turner MR, Cagnin A, Turkheimer FE, Miller CC, Shaw CE, Brooks DJ, Leigh PN, Banati RB (2004) Evidence of widespread cerebral microglial activation in amyotrophic lateral sclerosis: an [11C](R)-PK11195 positron emission tomography study. *Neurobiol Dis* 15: 601-9

Weigl E (1927) On the psychology of so-called processes of abstraction. . *Zeitschrift für Psychologie* 103: 245-300

Westeneng HJ, Debray TPA, Visser AE, van Eijk RPA, Rooney JPK, Calvo A, Martin S, McDermott CJ, Thompson AG, Pinto S, Kobeleva X, Rosenbohm A, Stubendorff B, Sommer H, Middelkoop BM, Dekker AM, van Vugt J, van Rheenen W, Vajda A, Heverin M et al. (2018) Prognosis for patients with amyotrophic lateral sclerosis: development and validation of a personalised prediction model. *Lancet Neurol* 17: 423-433

Table S1. Neuropsychological and behavioral features of MND patients.

	ALS	PUMN	PLMN	<i>p</i> ALS vs PUMN	<i>p</i> ALS vs PLMN	<i>p</i> PUMN vs PLMN
Education [years]	10.7 ± 4.2	10.7 ± 4.5	10.9 ± 4.7	0.99	0.99	0.99
MMSE (cut-off 24)	28.4 ± 1.9	29.0 ± 1.3	28.3 ± 1.9	0.46	0.99	0.53
<i>Reasoning and Executive functions</i>						
Raven's colored progressive matrices (cut-off 18)	28.5 ± 5.1	30.8 ± 2.8	27.7 ± 7.7	0.03	0.66	0.13
Digit span backward (cut-off 3.29)	4.0 ± 1.0	4.5 ± 1.2	4.2 ± 0.9	0.16	0.35	0.35
CET (cut-off 18)	14.7 ± 4.0	14.6 ± 2.8	13.8 ± 4.2	0.91	0.87	0.87
WCST global score (cut-off 90.5)	59.6 ± 39.6	42.1 ± 40.5	70.6 ± 41.9	0.22	0.30	0.16
Weigl's Sorting test (cut-off 4.5)	11.5 ± 3.2	12.6 ± 2.2	11.3 ± 3.7	0.46	0.81	0.46
<i>Fluency</i>						
Phonemic fluency (cut-off 17)	29.0 ± 10.9	26.1 ± 8.3	29.6 ± 10.6	0.43	0.78	0.43
Semantic fluency (cut-off 25)	37.8 ± 10.2	38.8 ± 8.1	38.1 ± 9.7	0.87	0.87	0.87
Phonemic fluency index	7.6 ± 5.7	7.2 ± 5.7	6.6 ± 3.5	0.98	0.98	0.98
Semantic fluency index	5.4 ± 4.1	4.6 ± 1.5	4.4 ± 1.3	0.98	0.98	0.98
<i>Verbal Memory</i>						
Digit span forward (cut-off 3.75)	5.3 ± 1.0	6.1 ± 1.4	5.7 ± 0.9	0.02	0.21	0.25
RAVLT, immediate recall (cut-off 28.53)	41.8 ± 12.3	40.3 ± 9.2	40.5 ± 11.2	0.97	0.97	0.97
RAVLT, delayed recall (cut-off 4.69)	8.5 ± 3.5	7.5 ± 3.0	7.1 ± 3.2	0.42	0.28	0.72
<i>Language</i>						
Oral noun confrontation naming subtest of BADA (cut-off 28)	28.9 ± 1.6	29.3 ± 0.7	29.1 ± 1.2	0.61	0.61	0.73
Oral verb confrontation naming subtest of BADA (cut-off 26)	26.2 ± 2.5	26.9 ± 1.2	25.8 ± 2.5	0.42	0.44	0.42

<i>Behavioral disturbances</i>						
FBI	4.1 ± 5.6	3.0 ± 3.4	3.9 ± 5.5	0.90	0.90	0.90
ALS-FTD questionnaire (cut-off 22)	13.8 ± 12.4	13.7 ± 15.2	8.8 ± 8.6	0.99	0.58	0.58
<i>Depression</i>						
HDRS (cut-off 14)	5.9 ± 4.4	9.4 ± 5.6	4.1 ± 2.6	0.01	0.10	0.003
<i>Cognitive diagnosis</i>						
MNDcu/ci/bi/cbi/FTD-MND	66/8/16/2/10	9/0/4/3/0	14/5/2/0/0	-	-	-

Values are means ± standard deviations. *P* values refer to ANOVA models, false-discovery rate-corrected for multiple comparisons. ALS = amyotrophic lateral sclerosis; BADA = Batteria per l'Analisi dei deficit Afasici; CET = Cognitive Estimation Test; FBI = Frontal behavioral inventory; FTD = frontotemporal dementia; HDRS = Hamilton Depression Rating Scale; LMN = lower motor neuron; MMSE = Mini Mental State Examination; MND = motor neuron disease; MNDbi = MND patients with behavioral impairment; MNDcbi = MND patients with cognitive and behavioral impairment; MNDci = MND patients with cognitive impairment; MNDcu = MND patients cognitively unimpaired; PLMN = patients with a predominant lower motor neuron phenotype; PUMN = patients with a predominant upper motor neuron phenotype; RAVLT = Rey Auditory Verbal Learning Test; WCST = Wisconsin Card Sorting Test.

Table S2. DT MRI metrics of WM tracts in MND patients and healthy controls.

		HC	ALS	PUMN	PLMN	<i>p</i> HC vs ALS	<i>p</i> HC vs PUMN	<i>p</i> HC vs PLMN	<i>p</i> ALS vs PUMN	<i>p</i> ALS vs PLMN	<i>p</i> PUMN vs PLMN
FA											
CST	L	0.53 ± 0.03	0.51 ± 0.04	0.50 ± 0.04	0.53 ± 0.03	< 0.001	0.005	0.65	0.78	< 0.001	0.01
	R	0.53 ± 0.04	0.50 ± 0.04	0.50 ± 0.03	0.53 ± 0.03	< 0.001	0.001	0.72	0.40	< 0.001	0.001
CC		0.52 ± 0.02	0.51 ± 0.03	0.50 ± 0.02	0.52 ± 0.03	0.22	0.06	0.99	0.19	0.28	0.13
CC-PMC		0.47 ± 0.03	0.44 ± 0.04	0.42 ± 0.02	0.46 ± 0.03	< 0.001	< 0.001	0.44	0.02	0.002	< 0.001
CC-premotor		0.43 ± 0.03	0.42 ± 0.04	0.43 ± 0.04	0.43 ± 0.03	0.24	0.96	0.96	0.72	0.59	0.74
CC-SMA		0.50 ± 0.03	0.47 ± 0.04	0.45 ± 0.04	0.50 ± 0.04	< 0.001	< 0.001	0.94	0.02	0.001	< 0.001
Cingulum	L	0.37 ± 0.02	0.37 ± 0.03	0.36 ± 0.03	0.38 ± 0.04	0.95	0.52	0.39	0.35	0.14	0.14
	R	0.36 ± 0.02	0.36 ± 0.03	0.36 ± 0.03	0.37 ± 0.03	0.75	0.71	0.71	0.33	0.33	0.33
ILF	L	0.43 ± 0.03	0.43 ± 0.03	0.42 ± 0.02	0.43 ± 0.03	0.55	0.41	0.55	0.63	0.77	0.63
	R	0.43 ± 0.03	0.43 ± 0.03	0.43 ± 0.02	0.44 ± 0.03	0.52	0.52	0.52	0.39	0.78	0.39
SLF	L	0.45 ± 0.02	0.43 ± 0.03	0.43 ± 0.02	0.44 ± 0.03	0.01	0.01	0.39	0.77	0.54	0.54
	R	0.44 ± 0.03	0.42 ± 0.03	0.42 ± 0.02	0.44 ± 0.04	0.06	0.06	0.97	0.50	0.12	0.12
Uncinate	L	0.39 ± 0.03	0.38 ± 0.04	0.37 ± 0.03	0.39 ± 0.04	0.06	0.11	0.74	0.70	0.28	0.28
	R	0.40 ± 0.03	0.39 ± 0.04	0.39 ± 0.02	0.40 ± 0.04	0.62	0.62	0.69	0.83	0.47	0.47
MD [$\times 10^{-3} \text{ mm}^2 \text{ s}^{-1}$]											
CST	L	0.79 ± 0.06	0.83 ± 0.13	0.83 ± 0.10	0.78 ± 0.04	0.05	0.18	0.90	0.94	0.19	0.25
	R	0.81 ± 0.10	0.84 ± 0.12	0.84 ± 0.07	0.79 ± 0.05	0.08	0.32	0.65	0.87	0.07	0.21
CC		0.89 ± 0.05	0.92 ± 0.08	0.92 ± 0.06	0.90 ± 0.07	0.06	0.10	0.68	0.72	0.33	0.33
CC-PMC		0.87 ± 0.06	0.90 ± 0.07	0.94 ± 0.06	0.88 ± 0.05	0.005	< 0.001	0.65	0.008	0.07	0.001
CC-premotor		0.87 ± 0.06	0.88 ± 0.07	0.87 ± 0.05	0.86 ± 0.06	0.76	0.76	0.76	0.67	0.67	0.67
CC-SMA		0.83 ± 0.04	0.86 ± 0.09	0.89 ± 0.07	0.82 ± 0.04	0.005	0.004	0.84	0.16	0.03	0.01
Cingulum	L	0.87 ± 0.04	0.89 ± 0.06	0.89 ± 0.05	0.87 ± 0.06	0.10	0.57	0.82	0.64	0.19	0.53
	R	0.86 ± 0.04	0.87 ± 0.05	0.89 ± 0.05	0.87 ± 0.06	0.19	0.08	0.90	0.26	0.38	0.25

ILF	L	0.82 ± 0.04	0.83 ± 0.05	0.82 ± 0.03	0.83 ± 0.05	0.15	0.70	0.23	0.66	0.95	0.66
	R	0.84 ± 0.04	0.84 ± 0.05	0.84 ± 0.03	0.84 ± 0.06	0.98	0.98	0.98	0.94	0.94	0.94
SLF	L	0.77 ± 0.04	0.78 ± 0.05	0.79 ± 0.03	0.77 ± 0.05	0.04	0.04	0.53	0.39	0.39	0.39
	R	0.78 ± 0.03	0.80 ± 0.05	0.80 ± 0.03	0.78 ± 0.05	0.02	0.05	0.99	0.63	0.10	0.10
Uncinate	L	0.85 ± 0.05	0.88 ± 0.09	0.87 ± 0.04	0.86 ± 0.06	0.09	0.66	0.66	0.74	0.74	0.81
	R	0.85 ± 0.05	0.86 ± 0.06	0.85 ± 0.03	0.85 ± 0.06	0.68	0.94	0.94	0.84	0.84	0.84
axD [x10⁻³ mm² s⁻¹]											
CST	L	1.28 ± 0.08	1.31 ± 0.14	1.32 ± 0.12	1.29 ± 0.07	0.36	0.38	0.89	0.85	0.59	0.59
	R	1.32 ± 0.11	1.33 ± 0.14	1.32 ± 0.08	1.31 ± 0.07	0.82	0.82	0.82	0.73	0.73	0.73
CC		1.45 ± 0.07	1.48 ± 0.10	1.48 ± 0.08	1.45 ± 0.09	0.07	0.24	0.70	0.99	0.56	0.56
CC-PMC		1.33 ± 0.06	1.34 ± 0.06	1.38 ± 0.07	1.33 ± 0.05	0.41	0.02	0.91	0.04	0.46	0.04
CC-premotor		1.30 ± 0.07	1.31 ± 0.07	1.31 ± 0.07	1.29 ± 0.06	0.73	0.73	0.73	0.99	0.56	0.56
CC-SMA		1.33 ± 0.05	1.34 ± 0.09	1.36 ± 0.07	1.32 ± 0.05	0.41	0.34	0.72	0.36	0.35	0.34
Cingulum	L	1.21 ± 0.05	1.23 ± 0.06	1.22 ± 0.04	1.22 ± 0.05	0.05	0.66	0.66	0.46	0.46	0.89
	R	1.19 ± 0.04	1.21 ± 0.05	1.22 ± 0.05	1.20 ± 0.05	0.20	0.15	0.60	0.41	0.55	0.41
ILF	L	1.23 ± 0.04	1.24 ± 0.06	1.22 ± 0.04	1.24 ± 0.06	0.10	0.41	0.34	0.22	0.88	0.26
	R	1.24 ± 0.04	1.26 ± 0.06	1.24 ± 0.04	1.25 ± 0.06	0.57	0.82	0.82	0.68	0.68	0.68
SLF	L	1.15 ± 0.04	1.16 ± 0.04	1.17 ± 0.04	1.15 ± 0.05	0.23	0.17	0.87	0.36	0.36	0.36
	R	1.16 ± 0.03	1.17 ± 0.05	1.18 ± 0.03	1.16 ± 0.04	0.11	0.14	0.88	0.67	0.17	0.17
Uncinate	L	1.23 ± 0.05	1.25 ± 0.09	1.23 ± 0.04	1.24 ± 0.06	0.55	0.97	0.97	0.64	0.64	0.87
	R	1.23 ± 0.05	1.24 ± 0.06	1.24 ± 0.04	1.24 ± 0.06	0.89	0.89	0.89	0.84	0.84	0.84
radD [x10⁻³ mm² s⁻¹]											
CST	L	0.54 ± 0.05	0.58 ± 0.13	0.59 ± 0.09	0.53 ± 0.04	0.02	0.13	0.79	0.99	0.07	0.13
	R	0.55 ± 0.10	0.60 ± 0.12	0.60 ± 0.07	0.54 ± 0.05	0.01	0.12	0.60	0.96	0.01	0.07
CC		0.61 ± 0.05	0.64 ± 0.08	0.65 ± 0.06	0.62 ± 0.07	0.06	0.06	0.67	0.57	0.31	0.31
CC-PMC		0.64 ± 0.07	0.68 ± 0.08	0.72 ± 0.06	0.65 ± 0.06	<0.001	<0.001	0.62	0.01	0.03	<0.001
CC-premotor		0.65 ± 0.06	0.67 ± 0.07	0.66 ± 0.06	0.65 ± 0.07	0.60	0.94	0.94	0.77	0.77	0.77
CC-SMA		0.57 ± 0.05	0.62 ± 0.10	0.66 ± 0.07	0.57 ± 0.05	<0.001	<0.001	0.92	0.12	0.01	0.005
Cingulum	L	0.70 ± 0.05	0.72 ± 0.07	0.72 ± 0.05	0.70 ± 0.06	0.10	0.37	0.59	0.85	0.17	0.35

	R	0.70 ± 0.04	0.71 ± 0.06	0.73 ± 0.06	0.70 ± 0.06	0.26	0.10	0.91	0.27	0.37	0.25
ILF	L	0.62 ± 0.04	0.63 ± 0.05	0.63 ± 0.03	0.63 ± 0.05	0.25	0.38	0.25	0.86	0.86	0.86
	R	0.63 ± 0.05	0.63 ± 0.06	0.63 ± 0.03	0.63 ± 0.06	0.98	0.98	0.98	0.92	0.92	0.92
SLF	L	0.58 ± 0.04	0.60 ± 0.05	0.60 ± 0.03	0.59 ± 0.06	0.04	0.04	0.44	0.49	0.44	0.44
	R	0.59 ± 0.04	0.61 ± 0.05	0.62 ± 0.03	0.59 ± 0.06	0.02	0.05	0.96	0.64	0.12	0.12
Uncinate	L	0.66 ± 0.06	0.70 ± 0.10	0.68 ± 0.05	0.67 ± 0.07	0.04	0.51	0.60	0.68	0.63	0.68
	R	0.66 ± 0.06	0.67 ± 0.07	0.66 ± 0.03	0.66 ± 0.07	0.75	0.94	0.94	0.72	0.72	0.72

Values are means ± standard deviations. *p* values refer to ANOVA models, false-discovery rate-corrected for multiple comparisons. Abbreviations: ALS = amyotrophic lateral sclerosis; axD = axial diffusivity; CC = corpus callosum; CC-PMC = callosal fibers connecting the primary motor cortices; CC-premotor = callosal fibers connecting the premotor cortices; CC-SMA = callosal fibers linking the supplementary motor areas; CST = corticospinal tract; DT MRI = diffusion tensor magnetic resonance imaging; FA = fractional anisotropy; HC = healthy controls; ILF = inferior longitudinal fasciculus; L = left; MND = motor neuron disease; MD = mean diffusivity; PLMN = patients with a predominant lower motor neuron phenotype; PUMN = patients with a predominant upper motor neuron phenotype; R = right; radD = radial diffusivity; SLF = superior longitudinal fasciculus; WM = white matter.

Table S3. Univariable accelerated failure time (AFT) log-logistic survival analysis using clinical and MRI features in all MND and ALS patients only.

Feature	All MND patients			ALS patients only		
	AF estimate	Standard error	<i>p</i>	AF estimate	Standard error	<i>p</i>
<i>Clinical and cognitive variables</i>						
Age at onset	-3.11	0.85	<0.001	-2.01	0.81	0.01
Gender (M vs F)	0.11	0.19	0.57	0.04	0.19	0.80
PUMN vs ALS phenotype	2.50	0.50	<0.001	-	-	-
PLMN vs ALS phenotype	0.71	0.25	0.004	-	-	-
Presence of genetic alterations	-0.44	0.24	0.07	-0.16	0.24	0.49
Bulbar vs limb onset	-0.32	0.24	0.18	-0.18	0.22	0.40
Bulbar+limb vs limb onset	-0.17	0.69	0.81	0.19	0.61	0.76
Diagnostic delay	0.22	0.06	<0.001	0.20	0.07	0.003
Disease duration at MRI	0.16	0.05	<0.001	0.19	0.10	0.06
ALSFRS-R score	3.37	1.50	0.03	1.81	1.52	0.23
Disease progression rate	0.02	0.01	0.01	-0.02	0.01	<0.001
Total MRC score	1.47	0.51	0.004	0.71	0.54	0.19
UMN score	0.06	0.20	0.77	0.06	0.22	0.78
MMSE	1.18	0.52	0.02	1.04	0.52	0.05
Phonemic fluency	0.15	0.10	0.15	0.23	0.09	0.02
Semantic fluency	2.84	1.07	0.008	2.86	1.01	0.005
MNDci vs MNDcu	-0.26	0.37	0.48	-0.43	0.39	0.27
MNDbi vs MNDcu	-0.11	0.34	0.74	-0.23	0.33	0.49
MNDcbi vs MNDcu	0.35	0.75	0.64	-1.27	0.68	0.06
FTD-MND vs MNDcu	-0.27	0.38	0.49	0.01	0.34	0.98
<i>GM volumes*</i>						
Precentral_L	0.00010	0.00007	0.13	1.10	0.61	0.07
Precentral_R	0.00015	0.00007	0.03	1.80	0.64	0.01
Frontal_Sup_L	0.00001	0.00006	0.79	0.15	0.51	0.76
Frontal_Sup_R	0.00010	0.00006	0.95	0.13	0.51	0.80
Frontal_Sup_Orb_L	0.00011	0.00016	0.50	0.19	1.50	0.90
Frontal_Sup_Orb_R	0.00021	0.00017	0.21	2.90	1.62	0.07
Frontal_Mid_L	0.00010	0.00004	0.01	0.93	0.35	0.01
Frontal_Mid_R	0.00006	0.00004	0.08	0.71	0.34	0.04
Frontal_Mid_Orb_L	0.00020	0.00018	0.26	2.04	1.70	0.23
Frontal_Mid_Orb_R	0.00013	0.00014	0.36	1.61	1.33	0.23
Frontal_Inf_Oper_L	0.00005	0.00014	0.71	1.82	1.46	0.21
Frontal_Inf_Oper_R	0.00018	0.00011	0.10	1.84	1.03	0.07
Frontal_Inf_Tri_L	0.00009	0.00006	0.14	0.96	0.60	0.11

Frontal_Inf_Tri_R	0.00013	0.00007	0.07	1.23	0.68	0.07
Frontal_Inf_Orb_L	-0.00003	0.00010	0.77	-0.42	0.94	0.65
Frontal_Inf_Orb_R	0.00007	0.00011	0.54	0.10	1.03	0.92
Rolandic_Oper_L	-0.00001	0.00017	0.95	-0.34	1.52	0.83
Rolandic_Oper_R	-0.00014	0.00011	0.21	-1.26	0.98	0.20
Supp_Motor_Area_L	-0.00001	0.00007	0.85	0.83	0.69	0.23
Supp_Motor_Area_R	0.00002	0.00008	0.80	0.61	0.75	0.42
Olfactory_L	0.00027	0.00050	0.59	0.06	0.46	0.89
Olfactory_R	0.00057	0.00048	0.24	0.31	0.45	0.50
Frontal_Sup_Medial_L	0.00009	0.00006	0.16	0.41	0.56	0.46
Frontal_Sup_Medial_R	0.00004	0.00008	0.62	0.30	0.75	0.70
Frontal_Mid_Orb_L1	0.00026	0.00017	0.12	0.18	0.16	0.25
Frontal_Mid_Orb_R1	0.00015	0.00014	0.28	1.68	1.29	0.19
Rectus_L	0.00039	0.00017	0.03	2.70	1.63	0.10
Rectus_R	0.00033	0.00019	0.09	2.39	1.81	0.19
Insula_L	0.00001	0.00009	0.88	-0.43	0.82	0.60
Insula_R	0.00005	0.00009	0.60	0.03	0.82	0.98
Cingulum_Ant_L	0.00009	0.00010	0.39	1.23	0.93	0.19
Cingulum_Ant_R	0.00020	0.00011	0.06	1.74	1.01	0.09
Cingulum_Mid_L	0.00008	0.00008	0.34	1.00	0.77	0.19
Cingulum_Mid_R	0.00013	0.00008	0.09	1.31	0.72	0.07
Cingulum_Post_L	0.00051	0.00034	0.14	0.29	0.35	0.41
Cingulum_Post_R	0.00036	0.00056	0.51	-0.16	0.59	0.79
Hippocampus_L	0.00014	0.00018	0.43	1.20	1.65	0.47
Hippocampus_R	0.00021	0.00019	0.28	1.43	1.79	0.42
ParaHippocampal_L	0.00014	0.00017	0.39	1.59	1.70	0.35
ParaHippocampal_R	0.00019	0.00016	0.22	2.60	1.55	0.09
Amygdala_L	0.00011	0.00060	0.86	0.02	0.56	0.98
Amygdala_R	0.00007	0.00063	0.91	0.07	0.62	0.91
Calcarine_L	0.00001	0.00007	0.84	-0.05	0.66	0.94
Calcarine_R	0.00005	0.00010	0.64	0.42	0.97	0.67
Cuneus_L	0.00001	0.00010	0.96	0.24	0.91	0.79
Cuneus_R	0.00012	0.00012	0.31	0.86	1.08	0.42
Lingual_L	0.00011	0.00009	0.24	0.60	0.90	0.51
Lingual_R	0.00015	0.00010	0.15	0.95	0.96	0.32
Occipital_Sup_L	0.79339	1.48802	0.59	1.05	1.34	0.43
Occipital_Sup_R	0.00015	0.00012	0.20	2.30	1.13	0.06
Occipital_Mid_L	0.00008	0.00005	0.11	0.78	0.51	0.13
Occipital_Mid_R	0.00005	0.00007	0.48	0.56	0.64	0.38
Occipital_Inf_L	0.00012	0.00017	0.47	0.70	1.63	0.67
Occipital_Inf_R	0.00009	0.00014	0.50	0.26	1.35	0.85
Fusiform_L	0.00004	0.00008	0.66	0.77	0.78	0.32
Fusiform_R	0.00013	0.00008	0.09	1.87	0.73	0.01
Postcentral_L	0.00004	0.00006	0.55	0.58	0.59	0.33
Postcentral_R	0.00001	0.00005	0.96	0.32	0.46	0.49
Parietal_Sup_L	0.00011	0.00007	0.13	0.72	0.69	0.30

Parietal_Sup_R	0.00007	0.00008	0.39	0.81	0.75	0.28
Parietal_Inf_L	-0.00003	0.00006	0.61	-0.36	0.52	0.49
Parietal_Inf_R	0.00011	0.00008	0.16	0.54	0.77	0.49
SupraMarginal_L	-0.00007	0.00011	0.52	-1.03	1.09	0.35
SupraMarginal_R	0.00007	0.00007	0.32	-0.23	0.68	0.73
Angular_L	0.00009	0.00010	0.35	0.76	0.91	0.40
Angular_R	0.00009	0.00008	0.21	0.92	0.73	0.21
Precuneus_L	0.00003	0.00006	0.61	-0.02	0.55	0.97
Precuneus_R	0.00007	0.00007	0.28	0.44	0.62	0.48
Paracentral_Lobule_L	0.00032	0.00014	0.03	0.28	0.14	0.04
Paracentral_Lobule_R	0.00014	0.00023	0.55	0.10	0.22	0.64
Caudate_L	0.00001	0.00015	0.95	0.48	1.38	0.73
Caudate_R	0.00009	0.00018	0.61	0.61	1.60	0.70
Putamen_L	0.00022	0.00017	0.18	1.48	1.62	0.36
Putamen_R	0.00024	0.00017	0.16	2.13	1.66	0.20
Pallidum_L	0.00008	0.00050	0.87	0.46	0.48	0.34
Pallidum_R	0.00042	0.00053	0.43	0.21	0.53	0.70
Thalamus_L	0.00024	0.00018	0.18	2.68	1.65	0.10
Thalamus_R	0.00023	0.00018	0.20	3.25	1.65	0.05
Heschl_L	0.00030	0.00045	0.51	0.26	0.42	0.54
Heschl_R	-0.00025	0.00038	0.51	-0.23	0.34	0.51
Temporal_Sup_L	0.00007	0.00007	0.35	0.31	0.62	0.62
Temporal_Sup_R	0.00004	0.00006	0.48	0.21	0.52	0.68
Temporal_Pole_Sup_L	0.00003	0.00011	0.80	0.23	1.01	0.82
Temporal_Pole_Sup_R	-0.00009	0.00013	0.47	-0.40	1.19	0.74
Temporal_Mid_L	0.00006	0.00004	0.13	0.55	0.35	0.12
Temporal_Mid_R	0.00003	0.00004	0.54	0.53	0.38	0.17
Temporal_Pole_Mid_L	0.00011	0.00013	0.42	21.78	8.13	0.01
Temporal_Pole_Mid_R	-0.00005	0.00012	0.66	0.73	1.16	0.53
Temporal_Inf_L	0.00003	0.00006	0.58	0.36	0.54	0.50
Temporal_Inf_R	0.00010	0.00005	0.95	-0.06	0.50	0.91
<i>DT MRI metrics of WM tracts</i>						
CC FA	-0.60	3.48	0.86	2.33	3.28	0.48
CC MD	-1.80	1.23	0.14	-1.36	1.18	0.25
CC axD	-2.01	1.01	0.05	-1.29	0.98	0.19
CC radD	-1.25	1.29	0.33	-1.13	1.23	0.36
CC-PMC FA	-1.86	2.45	0.45	-0.06	2.42	0.98
CC-PMC MD	1.34	1.43	0.35	-0.60	1.38	0.67
CC-PMC axD	0.59	1.50	0.69	-1.35	1.43	0.35
CC-PMC radD	1.39	1.25	0.27	-0.16	1.22	0.90
CC-premotor FA	2.26	2.69	0.40	1.41	2.65	0.60
CC-premotor MD	-2.46	1.52	0.11	-2.68	1.45	0.06
CC-premotor axD	-2.89	1.47	0.05	-3.50	1.36	0.01
CC-premotor radD	-1.78	1.39	0.20	-1.81	1.35	0.18
CC-SMA FA	-0.36	2.14	0.87	0.68	2.15	0.75
CC-SMA MD	0.97	1.30	0.46	0.15	1.06	0.89

CC-SMA axD	1.04	1.41	0.46	-0.03	1.09	0.98
CC-SMA radD	0.68	1.11	0.54	0.12	0.97	0.91
CST L FA	5.11	2.34	0.03	5.45	2.20	0.01
CST L MD	-1.13	0.75	0.13	-0.99	0.67	0.14
CST L axD	-0.66	0.73	0.37	-0.59	0.65	0.37
CST L radD	-1.36	0.73	0.06	-1.21	0.66	0.07
CST R FA	5.46	2.38	0.02	5.99	2.25	0.01
CST R MD	-1.47	0.83	0.08	-1.04	0.76	0.17
CST R axD	-0.95	0.77	0.22	-0.53	0.70	0.45
CST R radD	-1.63	0.82	0.05	-1.28	0.75	0.09
Cingulum L FA	-0.90	2.74	0.74	0.02	2.70	0.99
Cingulum L MD	-3.30	1.63	0.04	-2.76	1.56	0.08
Cingulum L axD	-4.90	1.65	0.003	-3.74	1.56	0.02
Cingulum L radD	-2.16	1.45	0.14	-1.94	1.40	0.17
Cingulum R FA	-2.61	2.96	0.38	-0.80	2.97	0.79
Cingulum R MD	-1.78	1.84	0.33	-4.03	1.79	0.02
Cingulum R axD	-3.89	1.86	0.04	-5.71	1.77	0.001
Cingulum R radD	-0.73	1.62	0.66	-2.59	1.60	0.10
ILF L FA	-0.99	3.22	0.76	2.18	3.10	0.48
ILF L MD	-2.74	2.16	0.20	-1.86	2.08	0.37
ILF L axD	-2.36	1.73	0.17	-0.57	1.66	0.73
ILF L radD	-1.98	2.06	0.34	-2.07	1.97	0.30
ILF R FA	-4.16	3.13	0.18	2.33	3.00	0.44
ILF R MD	-2.43	1.82	0.18	-2.16	1.76	0.22
ILF R axD	-3.17	1.54	0.04	-2.54	1.48	0.09
ILF R radD	-1.41	1.80	0.43	-1.37	1.73	0.43
SLF L FA	2.61	3.17	0.41	4.63	3.03	0.13
SLF L MD	-3.18	2.10	0.13	-4.65	2.06	0.02
SLF L axD	-3.58	2.15	0.10	-4.49	2.14	0.04
SLF L radD	-2.58	1.91	0.18	-4.06	1.86	0.03
SLF R FA	2.44	3.01	0.42	3.80	2.96	0.20
SLF R MD	-2.98	2.01	0.14	-4.19	1.96	0.03
SLF R axD	-3.71	2.15	0.08	-4.63	2.05	0.02
SLF R radD	-2.40	1.80	0.18	-3.51	1.76	0.05
Uncinate L FA	5.08	2.62	0.05	4.06	2.61	0.12
Uncinate L MD	-2.51	1.24	0.04	-1.87	1.17	0.11
Uncinate L axD	-2.32	1.35	0.09	-1.79	1.25	0.15
Uncinate L radD	-2.26	1.13	0.04	-1.69	1.07	0.11
Uncinate R FA	0.26	2.62	0.92	-0.27	2.54	0.92
Uncinate R MD	-2.02	1.53	0.19	-1.99	1.44	0.17
Uncinate R axD	-2.90	1.57	0.07	-3.02	1.47	0.04
Uncinate R radD	-1.37	1.38	0.32	-1.27	1.30	0.33

*GM volumes are indicated by the respective AAL label. Abbreviations: AF = acceleration factor; ALS = amyotrophic lateral sclerosis; axD = axial diffusivity; CC = corpus callosum; CC-PMC = callosal fibers connecting the primary motor cortices; CC-

premotor = callosal fibers connecting the premotor cortices; CC-SMA = callosal fibers linking the supplementary motor areas; CST = corticospinal tract; DT MRI = diffusion tensor magnetic resonance imaging; FA = fractional anisotropy; GM = grey matter; ILF= inferior longitudinal fasciculus; L = left; MND = motor neuron disease; MD = mean diffusivity; PLMN = patients with a predominant lower motor neuron phenotype; PUMN= patients with a predominant upper motor neuron phenotype; R = right; radD = radial diffusivity; SLF = superior longitudinal fasciculus; WM = white matter.

Table S4. Comparisons of area under the ROC curve (AUC) for 4-year survival prediction before and after the inclusion of each MRI feature to the clinical survival model in all MND and ALS patients only.

	All MND patients		ALS patients only	
	Clinical model AUC (95% CI): 0.785 (0.691 - 0.879)		Clinical model AUC (95% CI): 0.617 (0.486 - 0.748)	
MRI feature	Clinical + MRI AUC (95% CI)	<i>p</i>	Clinical + MRI AUC (95% CI)	<i>p</i>
<i>GM volumes*</i>				
Precentral_L	0.819 (0.737 - 0.901)	0.07	0.642 (0.513 - 0.770)	0.10
Precentral_R	0.816 (0.733 - 0.900)	0.26	0.628 (0.498 - 0.758)	0.74
Frontal_Sup_L	0.801 (0.714 - 0.887)	0.15	0.617 (0.483 - 0.750)	0.99
Frontal_Sup_R	0.785 (0.691 - 0.879)	0.97	0.621 (0.490 - 0.752)	0.80
Frontal_Sup_Orb_L	0.788 (0.696 - 0.881)	0.74	0.631 (0.497 - 0.766)	0.28
Frontal_Sup_Orb_R	0.826 (0.749 - 0.904)	0.09	0.622 (0.492 - 0.752)	0.39
Frontal_Mid_L	0.828 (0.752 - 0.904)	0.07	0.644 (0.519 - 0.769)	0.28
Frontal_Mid_R	0.820 (0.736 - 0.904)	0.05	0.627 (0.496 - 0.759)	0.62
Frontal_Mid_Orb_L	0.803 (0.715 - 0.891)	0.36	0.617 (0.487 - 0.747)	1.00
Frontal_Mid_Orb_R	0.815 (0.733 - 0.897)	0.10	0.639 (0.514 - 0.765)	0.23
Frontal_Inf_Oper_L	0.827 (0.749 - 0.905)	0.03	0.645 (0.518 - 0.771)	0.14
Frontal_Inf_Oper_R	0.819 (0.741 - 0.898)	0.17	0.636 (0.509 - 0.763)	0.43
Frontal_Inf_Tri_L	0.807 (0.721 - 0.893)	0.30	0.630 (0.500 - 0.760)	0.65
Frontal_Inf_Tri_R	0.834 (0.762 - 0.906)	0.03	0.657 (0.538 - 0.776)	0.11
Frontal_Inf_Orb_L	0.787 (0.693 - 0.880)	0.90	0.623 (0.491 - 0.755)	0.80
Frontal_Inf_Orb_R	0.785 (0.695 - 0.876)	0.96	0.626 (0.495 - 0.756)	0.20
Rolandic_Oper_L	0.779 (0.683 - 0.876)	0.59	0.605 (0.466 - 0.744)	0.68
Rolandic_Oper_R	0.808 (0.724 - 0.893)	0.28	0.640 (0.505 - 0.774)	0.51
Supp_Motor_Area_L	0.791 (0.702 - 0.880)	0.69	0.625 (0.498 - 0.753)	0.47
Supp_Motor_Area_R	0.789 (0.699 - 0.879)	0.66	0.621 (0.490 - 0.752)	0.58
Olfactory_L	0.778 (0.682 - 0.875)	0.64	0.617 (0.486 - 0.748)	1.00
Olfactory_R	0.798 (0.707 - 0.888)	0.49	0.631 (0.497 - 0.766)	0.45
Frontal_Sup_Medial_L	0.802 (0.714 - 0.889)	0.36	0.619 (0.488 - 0.750)	0.80
Frontal_Sup_Medial_R	0.783 (0.689 - 0.878)	0.79	0.621 (0.493 - 0.750)	0.70
Frontal_Mid_Orb_L1	0.810 (0.726 - 0.894)	0.23	0.614 (0.483 - 0.745)	0.37
Frontal_Mid_Orb_R1	0.800 (0.713 - 0.886)	0.46	0.615 (0.484 - 0.746)	0.33
Rectus_L	0.793 (0.704 - 0.882)	0.72	0.615 (0.484 - 0.746)	0.59
Rectus_R	0.793 (0.702 - 0.884)	0.74	0.614 (0.484 - 0.745)	0.71
Insula_L	0.779 (0.684 - 0.874)	0.52	0.586 (0.442 - 0.731)	0.38
Insula_R	0.788 (0.695 - 0.881)	0.35	0.598 (0.462 - 0.734)	0.32
Cingulum_Ant_L	0.793 (0.701 - 0.886)	0.56	0.619 (0.488 - 0.750)	0.90
Cingulum_Ant_R	0.813 (0.725 - 0.900)	0.19	0.636 (0.508 - 0.763)	0.60
Cingulum_Mid_L	0.783 (0.690 - 0.876)	0.90	0.607 (0.479 - 0.736)	0.44
Cingulum_Mid_R	0.789 (0.698 - 0.880)	0.86	0.610 (0.483 - 0.737)	0.78

Cingulum_Post_L	0.791 (0.706 - 0.877)	0.75	0.614 (0.484 - 0.745)	0.75
Cingulum_Post_R	0.788 (0.696 - 0.881)	0.49	0.626 (0.495 - 0.756)	0.45
Hippocampus_L	0.799 (0.712 - 0.886)	0.34	0.619 (0.488 - 0.75)	0.59
Hippocampus_R	0.793 (0.704 - 0.882)	0.63	0.616 (0.485 - 0.747)	0.72
ParaHippocampal_L	0.804 (0.717 - 0.892)	0.26	0.614 (0.482 - 0.746)	0.68
ParaHippocampal_R	0.813 (0.731 - 0.895)	0.20	0.639 (0.508 - 0.769)	0.51
Amygdala_L	0.792 (0.702 - 0.883)	0.26	0.633 (0.500 - 0.766)	0.57
Amygdala_R	0.787 (0.694 - 0.880)	0.57	0.629 (0.502 - 0.756)	0.14
Calcarine_L	0.783 (0.689 - 0.878)	0.10	0.625 (0.501 - 0.750)	0.31
Calcarine_R	0.792 (0.698 - 0.885)	0.42	0.624 (0.490 - 0.758)	0.49
Cuneus_L	0.792 (0.703 - 0.882)	0.46	0.614 (0.483 - 0.745)	0.58
Cuneus_R	0.797 (0.707 - 0.887)	0.37	0.617 (0.484 - 0.750)	0.99
Lingual_L	0.786 (0.694 - 0.878)	0.93	0.612 (0.477 - 0.747)	0.71
Lingual_R	0.797 (0.709 - 0.885)	0.50	0.622 (0.487 - 0.756)	0.77
Occipital_Sup_L	0.799 (0.710 - 0.888)	0.15	0.630 (0.503 - 0.756)	0.34
Occipital_Sup_R	0.805 (0.722 - 0.888)	0.48	0.633 (0.506 - 0.760)	0.71
Occipital_Mid_L	0.794 (0.703 - 0.885)	0.73	0.638 (0.501 - 0.775)	0.44
Occipital_Mid_R	0.798 (0.708 - 0.888)	0.41	0.625 (0.493 - 0.758)	0.66
Occipital_Inf_L	0.791 (0.700 - 0.882)	0.63	0.617 (0.486 - 0.748)	0.93
Occipital_Inf_R	0.796 (0.705 - 0.887)	0.43	0.618 (0.487 - 0.749)	0.86
Fusiform_L	0.818 (0.735 - 0.901)	0.04	0.627 (0.494 - 0.761)	0.39
Fusiform_R	0.808 (0.725 - 0.890)	0.29	0.638 (0.508 - 0.768)	0.32
Postcentral_L	0.799 (0.711 - 0.887)	0.12	0.617 (0.486 - 0.748)	1.00
Postcentral_R	0.783 (0.690 - 0.877)	0.89	0.627 (0.498 - 0.755)	0.27
Parietal_Sup_L	0.764 (0.664 - 0.864)	0.44	0.613 (0.481 - 0.744)	0.40
Parietal_Sup_R	0.787 (0.697 - 0.877)	0.85	0.607 (0.478 - 0.737)	0.20
Parietal_Inf_L	0.801 (0.716 - 0.886)	0.42	0.650 (0.522 - 0.779)	0.18
Parietal_Inf_R	0.794 (0.704 - 0.885)	0.49	0.640 (0.507 - 0.773)	0.22
SupraMarginal_L	0.805 (0.722 - 0.889)	0.37	0.638 (0.512 - 0.763)	0.57
SupraMarginal_R	0.787 (0.693 - 0.881)	0.77	0.603 (0.467 - 0.739)	0.69
Angular_L	0.792 (0.701 - 0.883)	0.57	0.639 (0.513 - 0.766)	0.33
Angular_R	0.806 (0.721 - 0.892)	0.12	0.645 (0.514 - 0.777)	0.42
Precuneus_L	0.786 (0.692 - 0.880)	0.51	0.660 (0.533 - 0.788)	0.06
Precuneus_R	0.793 (0.703 - 0.883)	0.34	0.621 (0.491 - 0.752)	0.56
Paracentral_Lobule_L	0.798 (0.711 - 0.885)	0.63	0.616 (0.484 - 0.747)	0.96
Paracentral_Lobule_R	0.777 (0.682 - 0.872)	0.46	0.618 (0.487 - 0.749)	0.86
Caudate_L	0.795 (0.706 - 0.884)	0.29	0.634 (0.503 - 0.765)	0.16
Caudate_R	0.804 (0.718 - 0.890)	0.28	0.616 (0.485 - 0.748)	0.95
Putamen_L	0.794 (0.706 - 0.882)	0.69	0.619 (0.487 - 0.751)	0.72
Putamen_R	0.796 (0.709 - 0.883)	0.64	0.613 (0.483 - 0.744)	0.73
Pallidum_L	0.789 (0.698 - 0.880)	0.81	0.622 (0.491 - 0.753)	0.72
Pallidum_R	0.799 (0.710 - 0.888)	0.36	0.618 (0.487 - 0.749)	0.85
Thalamus_L	0.792 (0.704 - 0.879)	0.78	0.608 (0.477 - 0.738)	0.65
Thalamus_R	0.789 (0.703 - 0.875)	0.85	0.593 (0.464 - 0.722)	0.31
Heschl_L	0.799 (0.712 - 0.887)	0.21	0.609 (0.474 - 0.745)	0.64
Heschl_R	0.794 (0.704 - 0.884)	0.52	0.631 (0.497 - 0.765)	0.47

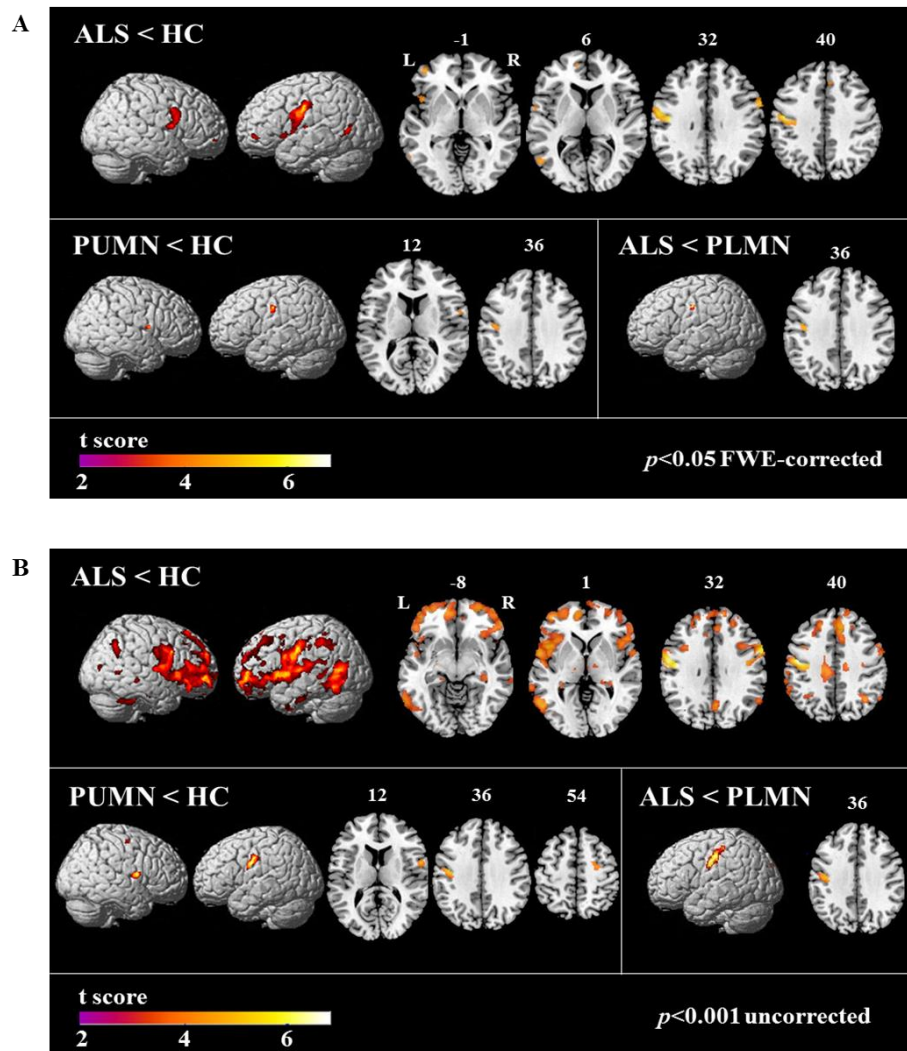
Temporal_Sup_L	0.785 (0.691 - 0.879)	1.00	0.621 (0.490 - 0.753)	0.70
Temporal_Sup_R	0.797 (0.710 - 0.885)	0.25	0.615 (0.479 - 0.750)	0.86
Temporal_Pole_Sup_L	0.777 (0.680 - 0.874)	0.44	0.641 (0.516 - 0.767)	0.08
Temporal_Pole_Sup_R	0.804 (0.718 - 0.889)	0.04	0.639 (0.512 - 0.766)	0.02
Temporal_Mid_L	0.805 (0.719 - 0.892)	0.36	0.629 (0.499 - 0.759)	0.58
Temporal_Mid_R	0.795 (0.706 - 0.885)	0.48	0.618 (0.485 - 0.751)	0.95
Temporal_Pole_Mid_L	0.778 (0.680 - 0.877)	0.72	0.612 (0.474 - 0.750)	0.91
Temporal_Pole_Mid_R	0.775 (0.678 - 0.873)	0.53	0.618 (0.487 - 0.750)	0.82
Temporal_Inf_L	0.784 (0.692 - 0.877)	0.94	0.626 (0.494 - 0.758)	0.25
Temporal_Inf_R	0.794 (0.704 - 0.884)	0.31	0.647 (0.526 - 0.769)	0.15
<i>DT MRI metrics of WM tracts</i>				
CC FA	0.805 (0.719 - 0.891)	0.13	0.598 (0.466 - 0.730)	0.15
CC MD	0.817 (0.737 - 0.898)	0.06	0.608 (0.471 - 0.745)	0.46
CC axD	0.810 (0.728 - 0.893)	0.12	0.619 (0.488 - 0.751)	0.67
CC radD	0.819 (0.737 - 0.900)	0.06	0.595 (0.456 - 0.734)	0.20
CC-PMC FA	0.785 (0.691 - 0.880)	0.94	0.594 (0.458 - 0.731)	0.20
CC-PMC MD	0.785 (0.691 - 0.879)	0.86	0.613 (0.479 - 0.747)	0.57
CC-PMC axD	0.792 (0.702 - 0.882)	0.53	0.614 (0.484 - 0.744)	0.57
CC-PMC radD	0.782 (0.688 - 0.876)	0.69	0.607 (0.473 - 0.742)	0.47
CC-premotor FA	0.795 (0.706 - 0.883)	0.39	0.601 (0.466 - 0.737)	0.54
CC-premotor MD	0.818 (0.738 - 0.898)	0.11	0.634 (0.508 - 0.760)	0.10
CC-premotor axD	0.817 (0.738 - 0.897)	0.10	0.647 (0.533 - 0.762)	0.24
CC-premotor radD	0.812 (0.729 - 0.896)	0.16	0.620 (0.490 - 0.751)	0.30
CC-SMA FA	0.794 (0.705 - 0.882)	0.46	0.600 (0.461 - 0.739)	0.49
CC-SMA MD	0.778 (0.682 - 0.874)	0.48	0.599 (0.465 - 0.733)	0.36
CC-SMA axD	0.782 (0.689 - 0.876)	0.83	0.612 (0.482 - 0.742)	0.63
CC-SMA radD	0.787 (0.694 - 0.879)	0.81	0.605 (0.472 - 0.738)	0.57
CST L FA	0.827 (0.747 - 0.906)	0.19	0.691 (0.571 - 0.811)	0.02
CST L MD	0.785 (0.694 - 0.876)	0.98	0.624 (0.495 - 0.753)	0.39
CST L axD	0.777 (0.683 - 0.871)	0.41	0.615 (0.484 - 0.746)	0.55
CST L radD	0.792 (0.705 - 0.879)	0.67	0.633 (0.507 - 0.758)	0.26
CST R FA	0.849 (0.780 - 0.917)	0.03	0.700 (0.583 - 0.816)	0.01
CST R MD	0.809 (0.727 - 0.891)	0.22	0.616 (0.485 - 0.748)	0.67
CST R axD	0.797 (0.711 - 0.884)	0.49	0.619 (0.485 - 0.753)	0.84
CST R radD	0.826 (0.750 - 0.902)	0.07	0.633 (0.508 - 0.759)	0.02
Cingulum L FA	0.785 (0.691 - 0.879)	1.00	0.600 (0.462 - 0.738)	0.47
Cingulum L MD	0.797 (0.713 - 0.881)	0.64	0.619 (0.495 - 0.744)	0.86
Cingulum L axD	0.781 (0.693 - 0.870)	0.89	0.592 (0.468 - 0.716)	0.37
Cingulum L radD	0.805 (0.722 - 0.888)	0.40	0.620 (0.489 - 0.751)	0.05
Cingulum R FA	0.797 (0.708 - 0.886)	0.28	0.611 (0.475 - 0.748)	0.85
Cingulum R MD	0.816 (0.736 - 0.896)	0.16	0.627 (0.502 - 0.752)	0.53
Cingulum R axD	0.827 (0.751 - 0.903)	0.10	0.654 (0.537 - 0.772)	0.24
Cingulum R radD	0.804 (0.719 - 0.889)	0.34	0.619 (0.490 - 0.748)	0.78
ILF L FA	0.806 (0.720 - 0.891)	0.15	0.630 (0.500 - 0.760)	0.15
ILF L MD	0.764 (0.664 - 0.865)	0.41	0.636 (0.506 - 0.766)	0.06
ILF L axD	0.746 (0.639 - 0.853)	0.08	0.662 (0.534 - 0.791)	0.01

ILF L radD	0.785 (0.692 - 0.878)	0.99	0.623 (0.493 - 0.753)	0.20
ILF R FA	0.784 (0.692 - 0.876)	0.99	0.584 (0.450 - 0.718)	0.22
ILF R MD	0.813 (0.731 - 0.895)	0.10	0.636 (0.509 - 0.763)	0.20
ILF R axD	0.810 (0.727 - 0.892)	0.17	0.640 (0.520 - 0.760)	0.29
ILF R radD	0.811 (0.728 - 0.895)	0.09	0.629 (0.500 - 0.759)	0.08
SLF L FA	0.808 (0.722 - 0.894)	0.29	0.619 (0.488 - 0.750)	0.71
SLF L MD	0.808 (0.726 - 0.890)	0.35	0.628 (0.501 - 0.754)	0.50
SLF L axD	0.806 (0.721 - 0.891)	0.38	0.633 (0.511 - 0.755)	0.30
SLF L radD	0.804 (0.720 - 0.889)	0.41	0.623 (0.495 - 0.752)	0.66
SLF R FA	0.821 (0.741 - 0.901)	0.09	0.616 (0.486 - 0.747)	0.90
SLF R MD	0.814 (0.734 - 0.895)	0.17	0.629 (0.507 - 0.752)	0.40
SLF R axD	0.806 (0.720 - 0.892)	0.29	0.636 (0.517 - 0.754)	0.36
SLF R radD	0.816 (0.735 - 0.896)	0.16	0.631 (0.509 - 0.754)	0.31
Uncinate L FA	0.851 (0.778 - 0.925)	0.03	0.682 (0.552 - 0.812)	0.03
Uncinate L MD	0.803 (0.716 - 0.889)	0.56	0.614 (0.485 - 0.743)	0.87
Uncinate L axD	0.771 (0.676 - 0.866)	0.58	0.606 (0.479 - 0.733)	0.35
Uncinate L radD	0.813 (0.728 - 0.898)	0.39	0.622 (0.492 - 0.751)	0.80
Uncinate R FA	0.798 (0.709 - 0.886)	0.09	0.591 (0.452 - 0.730)	0.41
Uncinate R MD	0.821 (0.739 - 0.903)	0.03	0.617 (0.488 - 0.747)	0.89
Uncinate R axD	0.821 (0.739 - 0.903)	0.03	0.643 (0.521 - 0.765)	0.28
Uncinate R radD	0.817 (0.734 - 0.900)	0.04	0.609 (0.474 - 0.744)	0.42

*GM volumes are indicated by the respective AAL label. Abbreviations: ALS = amyotrophic lateral sclerosis; axD = axial diffusivity; CC = corpus callosum; CC-PMC= callosal fibers connecting the primary motor cortices; CC-premotor = callosal fibers connecting the premotor cortices; CC-SMA = callosal fibers linking the supplementary motor areas; CST = corticospinal tract; DT MRI = diffusion tensor magnetic resonance imaging; FA = fractional anisotropy; GM = grey matter; ILF = inferior longitudinal fasciculus; L = left; MND = motor neuron disease; MD = mean diffusivity; R = right; radD = radial diffusivity; SLF = superior longitudinal fasciculus; WM = white matter.

Supplementary figure legend

Figure S1. Voxel-based morphometry analysis in patients with MND, thresholded at (A) $p < 0.05$ with family-wise error (FWE) correction for multiple comparisons and (B) $p < 0.001$ uncorrected. Patterns of cortical atrophy in classic ALS patients (top row of each panel) and PUMN patients (bottom row of each panel, left) relative to healthy controls are shown. Clusters of significant GM atrophy in ALS compared with PLMN patients are also shown (bottom row of each panel, right). Results are overlaid on axial sections or a three-dimensional rendering of a standard Montreal Neurologic Institute (MNI) brain. Slice labels refer to MNI coordinates. Abbreviations: ALS = amyotrophic lateral sclerosis; HC = healthy controls; MND = motor neuron disease; PLMN = patients with a predominant lower motor neuron phenotype; PUMN = patients with a predominant upper motor neuron phenotype.



3.2. Brain MRI shows white matter sparing in Kennedy's disease and slow-progressing lower motor neuron disease


HUMAN BRAIN MAPPING

Received: 4 February 2019 | Revised: 11 March 2019 | Accepted: 15 March 2019
DOI: 10.1002/hbm.24583

RESEARCH ARTICLE

WILEY

Brain MRI shows white matter sparing in Kennedy's disease and slow-progressing lower motor neuron disease

Edoardo G. Spinelli^{1,2} | Federica Agosta¹ | Pilar M. Ferraro¹ | Giorgia Querin³ | Nilo Riva² | Cinzia Bertolin³ | Iliara Martinelli³ | Christian Lunetta⁴ | Andrea Fontana⁵ | Gianni Sorarù³ | Massimo Filippi^{1,2} 

¹Neuroimaging Research Unit, Institute of Experimental Neurology, Division of Neuroscience, San Raffaele Scientific Institute, Vita-Salute San Raffaele University, Milan, Italy

²Department of Neurology, Institute of Experimental Neurology, Division of Neuroscience, San Raffaele Scientific Institute, Vita-Salute San Raffaele University, Milan, Italy

³Department of Neurosciences, Neuromuscular Center, University of Padova, Padova, Italy

⁴NeuroMuscular Omnicares, Fondazione Serena Onlus, Milan, Italy

⁵Biostatistics Unit, Fondazione IRCCS Casa Sollievo della Sofferenza, Unit of Biostatistics, Foggia, Italy

Correspondence

Massimo Filippi, Neuroimaging Research Unit, Institute of Experimental Neurology, Division of Neuroscience, San Raffaele Scientific Institute, Vita-Salute San Raffaele University, Via Olgettina, 60, Milan 20132, Italy.
Email: filippi.massimo@hsr.it

Funding information

Ministero della Salute, Grant/Award Number: #RF-2010-2313220 and #RF-2011-02351193

Abstract

The extent of central nervous system involvement in Kennedy's disease (KD) relative to other motor neuron disease (MND) phenotypes still needs to be clarified. In this study, we investigated cortical and white matter (WM) MRI alterations in 25 patients with KD, compared with 24 healthy subjects, 25 patients with sporadic amyotrophic lateral sclerosis (ALS), and 35 cases with lower motor neuron-predominant disease (LMND). LMND patients were clinically differentiated into 24 fast and 11 slow progressors. Whole-brain cortical thickness, WM tract-based spatial statistics and corticospinal tract (CST) tractography analyses were performed. No significant difference in terms of cortical thickness was found between groups. ALS patients showed widespread decreased fractional anisotropy and increased mean (MD) and radial diffusivity (radD) in the CST, corpus callosum and fronto-temporal extra-motor tracts, compared with healthy controls and other patient groups. CST tractography showed significant alterations of DT MRI metrics in ALS and LMND-fast patients whereas KD and LMND-slow patients were comparable with healthy controls. Our study demonstrated the absence of WM abnormalities in patients with KD and LMND-slow, in contrast with diffuse WM damage in ALS and focal CST degeneration in LMND-fast, supporting the use of DT MRI measures as powerful tools to differentiate fast- and slow-progressing MND syndromes, including KD.

KEYWORDS

amyotrophic lateral sclerosis, corticospinal tract, diffusion tensor MRI, Kennedy's disease, lower motor neuron disease

The following data have been published (Spinelli et al., Hum Brain Mapp. 2019 Jul;40(10):3102-3112. doi: 10.1002/hbm.24583).

INTRODUCTION

Kennedy's disease (KD) is an X-linked neurodegenerative disease of the motor neurons caused by a CAG repeat expansion within the first exon of the androgen receptor

gene (La Spada, Wilson et al., 1991, Lee, Shin et al., 2005). The clinical picture is dominated by lower motor neuron (LMN) signs, including progressive muscle wasting, fasciculations and reduced deep tendon reflexes (Grunseich, Rinaldi et al., 2014). Amongst motor neuron diseases (MND), KD shows slow disease progression and normal or minimally reduced life expectancy (Chahin, Klein et al., 2008). However, the mean diagnostic delay of this condition is 5.5 years (Finsterer, 2010, Rhodes, Freeman et al., 2009), as KD patients are often initially misdiagnosed as amyotrophic lateral sclerosis (ALS). Therefore, the identification of non-invasive biomarkers differentiating KD from classic MND phenotypes is of crucial prognostic relevance.

Only a few previous magnetic resonance imaging (MRI) studies investigated central nervous system (CNS) involvement in KD patients, showing white matter (WM) alterations mainly involving the corticospinal tracts (CST) and frontal subcortical areas, as well as subtle atrophy in frontal grey matter (GM) regions (Garaci, Toschi et al., 2015, Kassubek, Juengling et al., 2007, Pieper, Konrad et al., 2013, Unrath, Muller et al., 2010). However, previous studies have focused on structural alterations in KD relative to healthy controls, while the extent of CNS involvement relative to other MND phenotypes still needs further clarification. Particularly, WM alterations have been suggested to help in differentiating LMN-predominant disease (LMND) with faster and slower progression, as the former might represent early ALS cases (Muller et al., 2018b). Evaluating where KD cases fall within this wide range of CNS alterations has clear clinical implications.

Therefore, the aim of this multiparametric MRI study was to investigate cerebral damage in a sizeable sample of KD patients relative to healthy controls and MND patients with classic ALS and LMND.

METHODS

This prospective study was approved by the Local Ethical Committee on human studies and written informed consent from all subjects (or their legal representatives) was obtained prior to their enrollment.

Subjects

All patients were consecutively recruited from three tertiary referral MND clinics in Northern Italy between October 2009 and April 2016. Twenty-five patients with

genetically confirmed KD were included (Table 1). Two additional sets of 25 patients with sporadic possible, probable or definite ALS (Brooks et al., 2000) showing signs of both UMN and LMN involvement and 35 patients with a clinical diagnosis of sporadic LMND (Chio et al., 2011, van den Berg-Vos et al., 2003) were enrolled to match KD patients for disease severity, as assessed using the revised version of ALS Functional Rating Scale (ALSFRS-r) (Table 1). The diagnosis of LMND was based on the presence of pure LMN findings in two or more regions (bulbar, cervical, thoracic, lumbosacral) at the clinical evaluation, including evidence of LMN involvement on neurological examination (weakness and muscular atrophy, absent tendon reflexes), electrophysiological evidence of LMN involvement on standardized needle EMG, and no motor nerve conduction block. Patients with LMND were divided into fast and slow progressors, using a disease duration of 4 years as the timepoint to discriminate the two subtypes, as previously suggested (Rosenbohm et al., 2016, van den Berg-Vos et al., 2003). As a result, 24 LMND-fast and 11 LMND-slow patients were identified. All patients underwent a comprehensive evaluation including neurological examination, neuropsychological and behavioral evaluations, and MRI scan. Experienced neurologists blinded to the MRI results performed the clinical assessment. Disease duration was recorded. The rate of disease progression was calculated as 48 minus the ALS Functional Rating Score divided by time in months from symptom onset, as previously described (Cicarelli, Behrens et al., 2006). In KD patients, functional capacity was evaluated using the 6-minute walk test, and body mass index (BMI) was calculated as follows: weight (kg)/height² (m²).

Comprehensive neuropsychological and behavioral evaluations were performed by a trained neuropsychologist unaware of the MRI results, assessing: global cognitive functioning with the Mini-Mental State Examination (MMSE) {Folstein, 1975 #253}; reasoning and executive functions with the Raven coloured progressive matrices (Basso et al., 1987), phonemic and semantic fluency tests (Novelli et al., 1986), digit span backward (Monaco et al., 2013), Cognitive Estimation Task (Della Sala et al., 2003), Wisconsin Card Sorting Test (WCST) (Laiacina et al., 2000), and Weigl's Sorting test (Weigl, 1927); verbal memory with the digit span forward (Orsini et al., 1987) and the Rey Auditory Verbal Learning Test (RAVLT) immediate and delayed recall (Carlesimo et al., 1996); and language with the oral noun confrontation naming subtest of BADA

(Batteria per l'Analisi dei Deficit Afasici) (Miceli et al., 1994a). Depressive symptoms were assessed using the Hamilton Depression Rating Scale (Hamilton, 1960). Behavioral disturbances were determined based on direct observation and patient's history, caregiver report, the Frontal Behavioral Inventory (Alberici et al., 2007) and the ALS-FTD questionnaire (Raaphorst et al., 2012), which were administered to the patients' caregiver. Patient cognitive and behavioral profiles were classified according to the revised Strong criteria for cognitive impairment in ALS (Strong et al., 2017).

Twenty-four age-matched healthy controls were recruited among spouses of patients and by word of mouth (Table 1). Healthy controls were included if neurological examination was normal and MMSE was ≥ 28 . Exclusion criteria of the present study were: dementia or frontotemporal lobar degeneration (FTLD)-related disorders; significant medical illnesses or substance abuse that could interfere with cognitive functioning; any (other) major systemic, psychiatric, or neurological illness; and other causes of focal or diffuse brain damage, including lacunae and extensive cerebrovascular disorder at MRI. ALS and LMND patients were also excluded if they had a family history of MND.

MRI acquisition

For the MRI scan, the heads of the subjects were positioned carefully with restraining foam pads to reduce head motion, and ear plugs were used to reduce scanner noise. A strap was also positioned around the head to provide additional stabilization. Using a 3.0 T scanner (Intera, Philips Medical Systems, Best, the Netherlands), the following brain MRI sequences were obtained from all subjects: T2-weighted spin echo (SE) (repetition time [TR]=3500 ms; echo time [TE]=85 ms; echo train length=15; flip angle=90°; 22 contiguous, 5-mm-thick, axial slices; matrix size=512×512; field of view [FOV]=230×184 mm²); fluid-attenuated inversion recovery (TR=11 s; TE=120 ms; flip angle=90°; 22 contiguous, 5-mm-thick, axial slices; matrix size=512×512; FOV=230 mm²); 3D T1-weighted fast field echo (FFE) (TR=25 ms, TE=4.6 ms, flip angle=30°, 220 contiguous axial slices with voxel size=0.89×0.89×0.8 mm, matrix size=256×256, FOV=230×182 mm²); and pulsed-gradient SE echo planar with sensitivity encoding (acceleration factor=2.5, TR=8986 ms, TE=80 ms, 55 contiguous, 2.5 mm-thick axial slices, number of acquisitions=2; acquisition matrix 96×96, with an in-plane pixel size of

1.89×1.89 mm and a FOV=240 mm²) diffusion gradients applied in 32 non-collinear directions using a gradient scheme which is standard on this system (gradient over-plus) and optimized to reduce echo time as much as possible. The *b* factor used was 1000 s/mm². Fat saturation was performed to avoid chemical shift artifacts. All slices were positioned to run parallel to a line that joins the most inferoanterior and inferoposterior parts of the corpus callosum.

MRI analysis

Cortical thickness measurement. Cortical reconstruction and estimation of cortical thickness were performed on the 3D T1-weighted FFE images using the FreeSurfer image analysis suite, version 5.3 (<http://surfer.nmr.mgh.harvard.edu/>), by a single observer blinded to patients' identity. After registration to Talairach space and intensity normalization, the process involved an automatic skull stripping, which removes extra-cerebral structures, cerebellum and brainstem, by using a hybrid method combining watershed algorithms and deformable surface models. Images were then carefully checked for skull stripping errors. After this step, images were segmented into GM, WM, and cerebrospinal fluid (CSF), cerebral hemispheres were separated, and subcortical structures divided from cortical components. The WM/GM boundary was tessellated, and the surface was deformed following intensity gradients to optimally place WM/GM and GM/CSF borders, thus obtaining the WM and pial surfaces (Dale, Fischl et al., 1999). The results of this segmentation procedure were inspected visually, and if necessary, edited manually by adding control points. Afterwards, surface inflation and registration to a spherical atlas were performed (Dale et al., 1999). Finally, cortical thickness was estimated as the average shortest distance between the WM boundary and the pial surface.

Diffusion Tensor (DT) MRI analysis. DT MRI analysis was performed using the FMRIB software library (FSL) tools (<http://www.fmrib.ox.ac.uk/fsl/fdt/index.html>) and the JIM5 software (Xinapse Systems, Northants, UK, <http://www.xinapse.com>), as previously described (Agosta et al., 2013b, Agosta et al., 2014b). The diffusion-weighted data underwent a careful quality check for head motion and were subsequently skull-stripped using the Brain Extraction Tool implemented in FSL. Using FMRIB's Linear Image Registration Tool (FLIRT), the two diffusion-weighted scans were coregistered by

applying the rigid transformation needed to correct for position between the two b0 images (T2-weighted, but not diffusion-weighted). The rotation component was also applied to diffusion-weighted directions. Eddy currents correction was performed using JIM5 (Horsfield, 1999). The DT was estimated on a voxel-by-voxel basis using DTIfit provided by the FMRIB Diffusion Toolbox. Maps of fractional anisotropy (FA), mean diffusivity (MD), axial diffusivity (axD) and radial diffusivity (radD) were obtained.

First, a whole-brain DT MRI analysis was performed using tract-based spatial statistics (TBSS) version 1.2 (<http://www.fmrib.ox.ac.uk/fsl/tbss/index.html>). Secondly, fiber tracking of the CST bilaterally was performed. For TBSS analysis, FA volumes were aligned to a target image using the following procedure: (i) the FA template in standard space (provided by FSL) was selected as the target image, (ii) the nonlinear transformation that mapped each subject's FA to the target image was computed using the FMRIB's Nonlinear Image Registration Tool, and (iii) the same transformation was used to align each subject's FA to the standard space. A mean FA image was then created by averaging the aligned individual FA images and thinned to create a FA skeleton representing WM tracts common to all subjects. The FA skeleton was thresholded at a value of 0.2 to exclude voxels with low FA values, which are likely to include GM or CSF. Individual FA, MD, axD and radD data were projected onto this common skeleton. Seeds for tractography of the CST were drawn at the top of bulbar pyramids in the Montreal Neurological Institute (MNI) space on the FA template provided by FSL and included four axial slices, as previously described (Agosta et al., 2013b, Agosta et al., 2014b). Fiber tracking was performed in the native DT MRI space using a probabilistic tractography algorithm implemented in FSL (probtrackx), which is based on Bayesian estimation of diffusion parameters (Bedpostx) (Behrens et al., 2007). Fiber tracking was initiated from all voxels within the seed masks in the diffusion space to generate 5000 streamline samples with a step length of 0.5 mm and a curvature threshold of 0.2. Using a "single-seed" approach, the reconstruction of the CST was obtained, bilaterally. Tract maps were then normalized taking into consideration the number of voxels in the seed masks. To do so, the number of streamline samples present in the voxels of the tract maps was divided by the way-total, which corresponds to the total number of streamline samples that were not rejected by the exclusion masks. The tract maps obtained were thresholded at a value equal to 40% of the 95th percentile of the distribution of the

intensity values of the voxels included in the tract, as previously described (Galantucci et al., 2011). This normalization procedure allowed us to correct for possible differences between tracts due to the different sizes of the starting seeds. In this way, we also excluded the background noise and avoided a too restrictive thresholding when the maximum intensity value was an outlier. Group probability maps of each thresholded tract (i.e., left and right CST) were produced to visually check their anatomical consistency across study subjects (see Supporting Figure). For each subject, the average FA, MD, axD, and radD of the CST were calculated in the native space.

Statistical analysis

Group comparisons of demographic, clinical, cognitive and CST tractography data were performed using analysis of covariance (ANCOVA) models followed by post-hoc pairwise comparisons, adjusting for subjects' age and sex and controlling the False Discovery Rate (FDR) at level 0.05, using Benjamini-Hochberg step-up procedure. For the analysis of CST tractography data, p values from ANCOVA F-tests were also bootstrapped, as described by Westfall et al. (Westfall & Young, 1993). Briefly, the bootstrap procedure consisted of the following steps: a) a full ANCOVA model (which included the intercept and age, sex and subject group as covariates) was fitted and the observed F-values were obtained; b) a null model (including the intercept with age and sex as covariates) was fitted using those observations previously considered in the full model and residuals were retrieved; c) such residuals were centered and rescaled by leverage values; d) subsequently, a new dependent variable for bootstrapping was built as the sum of the fitted values of the null model and the resampled residuals estimated from the same null model; e) finally, a new "bootstrapped" full ANCOVA model was fitted using the calculated dependent variable and an F-sample was obtained. The last two steps were repeated 1000 times. The bootstrapped p value was determined as the proportion of resampled F-values that are greater than the observed F-values. Two-sided p values <0.05 were considered for statistical significance.

A vertex-by-vertex analysis was used to assess differences of cortical thickness between groups using a general linear model in FreeSurfer. Statistical maps were thresholded at $p < 0.05$, using the FDR correction for multiple comparisons, adjusting for age and sex. Regarding the TBSS analysis, DT MRI voxelwise statistics were performed

using a permutation-based inference tool for nonparametric statistical thresholding (“randomise”, part of FSL) (Nichols & Holmes, 2002). FA, MD, axD, and radD values within the skeleton were compared between groups using permutation-based two-sample t tests, adjusting for age and sex. The number of permutations was set at 5000. Statistical maps were thresholded at $p < 0.05$, family-wise error (FWE) corrected for multiple comparisons at the cluster level using the threshold-free cluster enhancement (TFCE) option (Smith & Nichols, 2009).

RESULTS

Demographic, clinical and cognitive features

Patient groups were well-matched in terms of disease severity ($p=0.67$) (Table 1). As expected, KD patients were younger than classic ALS patients ($p=0.05$). KD and LMND-slow patients had longer disease duration ($p < 0.001$) and slower disease progression ($p < 0.001$) relative to classic ALS and LMND-fast cases (Table 1).

The neuropsychological features of KD, ALS, and LMND patients are shown in Table 2. According to the revised Strong criteria (Strong et al., 2017), 36% of KD, 43% of ALS, 39% of LMND-fast, and 30% of LMND-slow patients had some degree of cognitive or behavioral impairment. Among KD patients, 20% showed isolated behavioral impairment (MND-bi) and 16% had a combined cognitive and behavioral impairment (MND-cbi). Among ALS patients, cognitive impairment (MND-ci) was found in 29% of patients, and MND-bi in 14% of cases. Among LMND-fast cases, 28% showed MND-ci, and 11% had MND-bi. Among LMND-slow, 20% of patients had MND-ci and 10% showed MND-bi. When cognitive scores were compared between groups, we found significant greater executive impairment shown by global WCST scores in ALS relative to KD patients (Table 2, $p=0.04$). No significant differences in other cognitive measures were found between groups.

MRI findings

Cortical thickness. Vertex-wise analysis did not show any significant difference between groups in terms of cortical thickness (using FDR correction).

TBSS. Compared with healthy controls, the voxel-wise analysis showed no significant alterations of DT MRI metrics in KD, LMND-fast and LMND-slow patients. Conversely,

ALS patients showed a widespread pattern of increased MD and radD and decreased FA including the whole CST, genu, mid-body and splenium of the corpus callosum, anterior limb of the internal capsule, superior longitudinal fasciculus (SLF), temporal portions of the inferior longitudinal fasciculus (ILF), and thalamic radiations bilaterally compared with healthy controls ($p < 0.05$ FWE, Figure 1). Compared with KD patients, ALS patients had a pattern of FA reduction and MD and radD increase similar to that shown relative to controls ($p < 0.05$ FWE, Figure 2). A widespread pattern of FA decrease and MD and radD increase encompassing the CST, corpus callosum, frontal, and parietal WM projections was also shown when ALS patients were compared with LMND-fast patients ($p < 0.05$ FWE, Figure 3A). A similar pattern of FA decrease and radD increase, although more centered upon the CST, corpus callosum, and the SLF, was found when ALS patients were compared with the smallest group of LMND-slow patients ($p < 0.05$ FWE, Figure 3B). The voxel-wise analysis did not show any significant difference in terms of DT MRI metrics when comparing KD, LMND-fast, and LMND-slow patients, even pooling the last two groups into one LMND group.

CST tractography. Compared with healthy controls, tractography analysis showed no alterations of DT MRI metrics of the CST in KD and LMND-slow patients (Table 3, Figure 4). By contrast, both ALS and LMND-fast patients showed increased MD and radD values of the right CST compared with healthy controls (Table 3, Figure 4). No significant difference in FA and axD values of the CST was detected between groups.

DISCUSSION

To date, this is the largest multiparametric MRI study performed in patients with KD, as well as the first assessing a direct comparison with other MND presentations, including LMND. In the present cohort, no significant structural alterations of the cerebral cortex and WM regions were demonstrated in KD patients compared with healthy controls. By contrast, classic ALS patients showed an extensive degeneration of both motor and extra-motor WM regions compared with healthy controls and all other MND phenotypes, including KD. To a lesser degree, also the other relatively fast-progressing MND group (i.e., LMND-fast) showed relevant damage of the CST, whereas LMND-slow cases had no structural alterations compared with healthy controls and KD patients.

The distributed involvement of motor and extra-motor WM regions in our ALS cohort is largely consistent with previous literature (Agosta et al., 2014b, Chio et al., 2014, Spinelli et al., 2016). The absence of significant WM alterations in KD patients is also in line with previous observations in slow-progressing MND phenotypes with predominant LMN involvement (Muller et al., 2018b, Spinelli et al., 2016) and confirms the role of DT MRI metrics as promising markers of upper motor neuron (UMN) damage. Of note, the presence of CST alterations in both the ALS and LMND-fast groups suggests that DT MRI is highly sensitive to UMN degeneration below the clinical threshold of detection, possibly even indicating those LMND cases which might represent early ALS presentations (Muller et al., 2018b). It is noteworthy that some prior MRI studies have reported WM changes in KD, mainly encompassing frontal regions, as well as the limbic system and CST (Kassubek et al., 2007, Unrath et al., 2010). One possible explanation for the discrepancy among results might be the shorter disease duration of patients here included (i.e., approximately 12 years compared with 22-24 years of other cohorts). Relative to previous MRI studies (Kassubek et al., 2007, Unrath et al., 2010), KD patients in our cohort were indeed in an earlier phase of the disease, and this might contribute to explain the lack of significant WM damage. The only study assessing DT MRI of KD patients with a disease duration similar to the present cohort actually could not detect significant WM alterations when applying correction for multiple comparisons (Pieper et al., 2013), as we did. Accordingly, one previous MRI study has reported a significant correlation between longer disease duration and WM damage encompassing the corpus callosum, association fibers and midbrain in KD (Garaci et al., 2015), suggesting that WM alterations might be a late phenomenon in the disease course.

In the present study, we could not detect significant GM atrophy in any of the included MND groups, compared with healthy controls. The absence of GM atrophy in KD accompanies the lack of WM microstructural damage in our cohort. This finding is in contrast with one previous voxel-based morphometry study reporting GM atrophy in frontal cortical regions of KD patients (Kassubek et al., 2007), but this difference likely derives from the different MRI technique here applied and the shorter disease duration of our cohort, as mentioned above. The present results showing no significant GM atrophy in LMND patients replicate previous findings from a smaller cohort (Spinelli et al., 2016), whereas the absence of GM reductions in ALS patients (using FDR correction and

adjusting for age) differs from previous studies (Agosta et al., 2016, Chio et al., 2014, Spinelli et al., 2016). However, ALS patients of this cohort were selected to match KD patients for disease severity, as measured by ALSFRS-R scale. Therefore, only patients with a relatively mild disease were included, and the lack of detectable GM alterations using a conservative statistical threshold likely mirrors the level of functional impairment of these patients.

We found mild, non-classifiable cognitive impairment in 16% of cognitively impaired KD patients, in keeping with previous studies describing subtle frontal lobe dysfunction and subclinical frontotemporal cognitive alterations during the course of the disease (Kasper, Wegrzyn et al., 2014b, Soukup, Sperfeld et al., 2009). Of note, behavioral changes were the most common symptoms in our KD cohort, being present in 36% of patients, including all those with cognitive impairment. To our knowledge, very few studies have investigated cognition and behavior in KD. One of these reports described the case of a patient showing altered social conduct, forgetfulness, and a personality disorder, suggesting that behavioral alterations might be part of the disease clinical picture (Mirowska-Guzel, Seniow et al., 2009). More recently, a larger study reported significant impairment of social cognition in KD patients, particularly in tasks assessing empathy (Di Rosa, Soraru et al., 2015). Our findings strengthen the importance of these reports, suggesting that behavioral alterations should be assessed in KD patients. Our results are also in line with previous observations of various degree of cognitive and behavioral alterations across other MND phenotypes, including LMND (Phukan, Elamin et al., 2012, Raaphorst, de Visser et al., 2011, Spinelli et al., 2016). However, the absence of significant differences from healthy controls indicated by structural MRI analysis in KD and LMND-slow patients of the present study suggests that neuroanatomical correlates of cognitive and behavioral impairment in these slow-progressing MND presentations should be sought in either functional rearrangements or very subtle structural alterations, not detectable using the techniques here applied.

The present study is not without limitations. First, this is a structural MRI study investigating GM and WM changes, while brain functional alterations have not been addressed. In fact, previous studies have reported reduced prefrontal activation during executive tasks in LMND (Raaphorst, van Tol et al., 2014), suggesting that functional MRI can provide additional insights into neuroanatomical alterations occurring during

the disease course. Another limitation deals with the cross-sectional nature of the study. In this context, longitudinal studies are warranted in order to explore the progressive evolution of brain damage in KD.

In conclusion, the results of this multiparametric study - which is the first investigating the extent of CNS involvement in KD relative to other MND phenotypes -, support the importance of a comprehensive cognitive and behavioral assessment even in rare LMN-predominant presentations, as well as the role of DT MRI as a promising diagnostic tool to be applied in the clinical setting to distinguish slow and fast-progressing MND.

Acknowledgements

The present work was performed by Dr Edoardo Gioele Spinelli in partial fulfillment of the requirements for obtaining the PhD degree at Vita-Salute San Raffaele University, Milano, Italy.

References

Agosta F, Ferraro PM, Riva N, Spinelli EG, Chio A, Canu E, Valsasina P, Lunetta C, Iannaccone S, Copetti M, Prudente E, Comi G, Falini A, Filippi M (2016) Structural brain correlates of cognitive and behavioral impairment in MND. *Hum Brain Mapp* 37: 1614-26

Agosta F, Galantucci S, Canu E, Cappa SF, Magnani G, Franceschi M, Falini A, Comi G, Filippi M (2013) Disruption of structural connectivity along the dorsal and ventral language pathways in patients with nonfluent and semantic variant primary progressive aphasia: a DT MRI study and a literature review. *Brain Lang* 127: 157-66

Agosta F, Galantucci S, Riva N, Chio A, Messina S, Iannaccone S, Calvo A, Silani V, Copetti M, Falini A, Comi G, Filippi M (2014) Intrahemispheric and interhemispheric structural network abnormalities in PLS and ALS. *Hum Brain Mapp* 35: 1710-22

Alberici A, Geroldi C, Cotelli M, Adorni A, Calabria M, Rossi G, Borroni B, Padovani A, Zanetti O, Kertesz A (2007) The Frontal Behavioural Inventory (Italian version) differentiates frontotemporal lobar degeneration variants from Alzheimer's disease. *Neurol Sci* 28: 80-6

Basso A, Capitani E, Laiacona M (1987) Raven's coloured progressive matrices: normative values on 305 adult normal controls. *Funct Neurol* 2: 189-94

Behrens TE, Berg HJ, Jbabdi S, Rushworth MF, Woolrich MW (2007) Probabilistic diffusion tractography with multiple fibre orientations: What can we gain? *Neuroimage* 34: 144-55

Brooks BR, Miller RG, Swash M, Munsat TL, World Federation of Neurology Research Group on Motor Neuron D (2000) El Escorial revisited: revised criteria for the diagnosis of amyotrophic lateral sclerosis. *Amyotroph Lateral Scler Other Motor Neuron Disord* 1: 293-9

Carlesimo GA, Caltagirone C, Gainotti G (1996) The Mental Deterioration Battery: normative data, diagnostic reliability and qualitative analyses of cognitive impairment. The Group for the Standardization of the Mental Deterioration Battery. *European neurology* 36: 378-84

Chahin N, Klein C, Mandrekar J, Sorenson E (2008) Natural history of spinal-bulbar muscular atrophy. *Neurology* 70: 1967-71

Chio A, Calvo A, Moglia C, Mazzini L, Mora G, group Ps (2011) Phenotypic heterogeneity of amyotrophic lateral sclerosis: a population based study. *J Neurol Neurosurg Psychiatry* 82: 740-6

Chio A, Pagani M, Agosta F, Calvo A, Cistaro A, Filippi M (2014) Neuroimaging in amyotrophic lateral sclerosis: insights into structural and functional changes. *Lancet Neurol* 13: 1228-40

Ciccarelli O, Behrens TE, Altmann DR, Orrell RW, Howard RS, Johansen-Berg H, Miller DH, Matthews PM, Thompson AJ (2006) Probabilistic diffusion tractography: a potential tool to assess the rate of disease progression in amyotrophic lateral sclerosis. *Brain* 129: 1859-71

Dale AM, Fischl B, Sereno MI (1999) Cortical surface-based analysis. I. Segmentation and surface reconstruction. *Neuroimage* 9: 179-94

Della Sala S, MacPherson SE, Phillips LH, Sacco L, Spinnler H (2003) How many camels are there in Italy? Cognitive estimates standardised on the Italian population. *Neurol Sci* 24: 10-5

Di Rosa E, Soraru G, Kleinbub JR, Calvo V, Vallesi A, Querin G, Marcato S, Grasso I, Palmieri A (2015) Theory of mind, empathy and neuropsychological functioning in X-linked spinal and bulbar muscular atrophy: a controlled study of 20 patients. *J Neurol* 262: 394-401

Finsterer J (2010) Perspectives of Kennedy's disease. *J Neurol Sci* 298: 1-10

Folstein MF, Folstein SE, McHugh PR (1975) "Mini-mental state". A practical method for grading the cognitive state of patients for the clinician. *J Psychiatr Res* 12: 189-98

Galantucci S, Tartaglia MC, Wilson SM, Henry ML, Filippi M, Agosta F, Dronkers NF, Henry RG, Ogar JM, Miller BL, Gorno-Tempini ML (2011) White matter damage in primary progressive aphasia: a diffusion tensor tractography study. *Brain* 134: 3011-29

Garaci F, Toschi N, Lanzafame S, Marfia GA, Marziali S, Meschini A, Di Giuliano F, Simonetti G, Guerrisi M, Massa R, Floris R (2015) Brain MR diffusion tensor imaging in Kennedy's disease. *Neuroradiol J* 28: 126-32

Grunseich C, Rinaldi C, Fischbeck KH (2014) Spinal and bulbar muscular atrophy: pathogenesis and clinical management. *Oral Dis* 20: 6-9

Hamilton M (1960) A rating scale for depression. *J Neurol Neurosurg Psychiatry* 23: 56-62

Horsfield MA (1999) Mapping eddy current induced fields for the correction of diffusion-weighted echo planar images. *Magn Reson Imaging* 17: 1335-45

Kasper E, Wegrzyn M, Marx I, Korp C, Kress W, Benecke R, Teipel SJ, Prudlo J (2014) Minor cognitive disturbances in X-linked spinal and bulbar muscular atrophy, Kennedy's disease. *Amyotroph Lateral Scler Frontotemporal Degener* 15: 15-20

Kassubek J, Juengling FD, Sperfeld AD (2007) Widespread white matter changes in Kennedy disease: a voxel based morphometry study. *J Neurol Neurosurg Psychiatry* 78: 1209-12

La Spada AR, Wilson EM, Lubahn DB, Harding AE, Fischbeck KH (1991) Androgen receptor gene mutations in X-linked spinal and bulbar muscular atrophy. *Nature* 352: 77-9

Laiacona M, Inzaghi MG, De Tanti A, Capitani E (2000) Wisconsin card sorting test: a new global score, with Italian norms, and its relationship with the Weigl sorting test. *Neurol Sci* 21: 279-91

Lee JH, Shin JH, Park KP, Kim IJ, Kim CM, Lim JG, Choi YC, Kim DS (2005) Phenotypic variability in Kennedy's disease: implication of the early diagnostic features. *Acta Neurol Scand* 112: 57-63

Miceli G, Laudanna A, Burani C, Capasso R (1994) Batteria per l'Analisi del Deficit Afasico. B.A.D.A. [B.A.D.A. A Battery for the Assessment of Aphasic Disorders]. Roma: CEPSAG

Mirowska-Guzel D, Seniow J, Sulek A, Lesniak M, Czlonkowska A (2009) Are cognitive and behavioural deficits a part of the clinical picture in Kennedy's disease? A case study. *Neurocase* 15: 332-7

Monaco M, Costa A, Caltagirone C, Carlesimo GA (2013) Forward and backward span for verbal and visuo-spatial data: standardization and normative data from an Italian adult population. *Neurol Sci* 34: 749-54

Muller HP, Agosta F, Riva N, Spinelli EG, Comi G, Ludolph AC, Filippi M, Kassubek J (2018) Fast progressive lower motor neuron disease is an ALS variant: A two-centre tract of interest-based MRI data analysis. *Neuroimage Clin* 17: 145-152

Nichols TE, Holmes AP (2002) Nonparametric permutation tests for functional neuroimaging: a primer with examples. *Hum Brain Mapp* 15: 1-25

Novelli G, Papagno C, Capitani E, Laiacona M, Vallar G, Cappa S (1986) Tre test clinici di ricerca e produzione lessicale. Taratura su soggetti normali. *Archivio di Psicologia, Neurologia e Psichiatria* oct-dec; vol 47 (4) : 477-506.: 477-506

Orsini A, Grossi D, Capitani E, Laiacona M, Papagno C, Vallar G (1987) Verbal and spatial immediate memory span: normative data from 1355 adults and 1112 children. *Ital J Neurol Sci* 8: 539-48

Phukan J, Elamin M, Bede P, Jordan N, Gallagher L, Byrne S, Lynch C, Pender N, Hardiman O (2012) The syndrome of cognitive impairment in amyotrophic lateral sclerosis: a population-based study. *J Neurol Neurosurg Psychiatry* 83: 102-8

Pieper CC, Konrad C, Sommer J, Teismann I, Schiffbauer H (2013) Structural changes of central white matter tracts in Kennedy's disease - a diffusion tensor imaging and voxel-based morphometry study. *Acta Neurol Scand* 127: 323-8

Raaphorst J, Beeldman E, Schmand B, Berkhout J, Linssen WH, van den Berg LH, Pijnenburg YA, Grupstra HF, Weikamp JG, Schelhaas HJ, Papma JM, van Swieten JC, de Visser M, de Haan RJ (2012) The ALS-FTD-Q: a new screening tool for behavioral disturbances in ALS. *Neurology* 79: 1377-83

Raaphorst J, de Visser M, van Tol MJ, Linssen WH, van der Kooij AJ, de Haan RJ, van den Berg LH, Schmand B (2011) Cognitive dysfunction in lower motor neuron disease: executive and memory deficits in progressive muscular atrophy. *J Neurol Neurosurg Psychiatry* 82: 170-5

Raaphorst J, van Tol MJ, Groot PF, Altena E, van der Werf YD, Majoie CB, van der Kooij AJ, van den Berg LH, Schmand B, de Visser M, Veltman DJ (2014) Prefrontal involvement related to cognitive impairment in progressive muscular atrophy. *Neurology* 83: 818-25

Rhodes LE, Freeman BK, Auh S, Kokkinis AD, La Pean A, Chen C, Lehky TJ, Shrader JA, Levy EW, Harris-Love M, Di Prospero NA, Fischbeck KH (2009) Clinical features of spinal and bulbar muscular atrophy. *Brain* 132: 3242-51

Rosenbohm A, Muller HP, Hubers A, Ludolph AC, Kassubek J (2016) Corticoefferent pathways in pure lower motor neuron disease: a diffusion tensor imaging study. *J Neurol* 263: 2430-2437

Smith SM, Nichols TE (2009) Threshold-free cluster enhancement: addressing problems of smoothing, threshold dependence and localisation in cluster inference. *Neuroimage* 44: 83-98

Soukup GR, Sperfeld AD, Uttner I, Karitzky J, Ludolph AC, Kassubek J, Schreiber H (2009) Frontotemporal cognitive function in X-linked spinal and bulbar muscular atrophy (SBMA): a controlled neuropsychological study of 20 patients. *J Neurol* 256: 1869-75

Spinelli EG, Agosta F, Ferraro PM, Riva N, Lunetta C, Falzone YM, Comi G, Falini A, Filippi M (2016) Brain MR Imaging in Patients with Lower Motor Neuron-Predominant Disease. *Radiology* 280: 545-56

Strong MJ, Abrahams S, Goldstein LH, Woolley S, McLaughlin P, Snowden J, Mioshi E, Roberts-South A, Benatar M, HortobaGyi T, Rosenfeld J, Silani V, Ince PG, Turner MR (2017) Amyotrophic lateral sclerosis - frontotemporal spectrum disorder (ALS-FTSD): Revised diagnostic criteria. *Amyotroph Lateral Scler Frontotemporal Degener* 18: 153-174

Unrath A, Muller HP, Riecker A, Ludolph AC, Sperfeld AD, Kassubek J (2010) Whole brain-based analysis of regional white matter tract alterations in rare motor neuron diseases by diffusion tensor imaging. *Hum Brain Mapp* 31: 1727-40

van den Berg-Vos RM, Visser J, Franssen H, de Visser M, de Jong JM, Kalmijn S, Wokke JH, van den Berg LH (2003) Sporadic lower motor neuron disease with adult onset: classification of subtypes. *Brain* 126: 1036-47

Weigl E (1927) On the psychology of so-called processes of abstraction. . *Zeitschrift für Psychologie* 103: 245-300

Westfall PH, Young SS (1993) Resampling-Based Multiple Testing: Examples and Methods for p-Value Adjustment

Table 1. Demographic and clinical findings of healthy controls, KD, ALS and LMND patients.

	Healthy controls	KD	ALS	LMND-fast	LMND-slow	<i>p</i>*
Number	24	25	25	24	11	
Age [years]	58.5 ± 5.7	57.0 ± 6.5 ^c	61.5 ± 9.7 ^b	60.8 ± 8.5	56.4 ± 7.9	0.11
Sex [W/M]	10/14 ^b	0/25 ^{a,c,d,e}	10/15 ^b	8/16 ^b	4/7 ^b	0.007
Education [years]	14.7 ± 4.6 ^{b,c,d}	11.0 ± 3.2 ^a	10.3 ± 3.8 ^a	10.8 ± 5.3 ^a	12.8 ± 3.1	0.003
Disease duration [months]	-	144.6 ± 63.9 ^{c,d}	21.8 ± 21.0 ^{b,e}	17.5 ± 9.3 ^{b,e}	146.8 ± 123 ^{c,d}	<0.001
ALSFRS-R [0-48]	-	41.3 ± 3.6	39.7 ± 6.1	39.1 ± 6.1	38.8 ± 7.9	0.67
Disease progression rate [ALSFRS-R rate of decline per month]	-	0.05 ± 0.02 ^{c,d}	0.68 ± 0.72 ^{b,e}	0.66 ± 0.61 ^{b,e}	0.09 ± 0.10 ^{c,d}	<0.001
6MWT [meters]	-	330.7 ± 98.8	-	-	-	-
BMI [kg/m ²]	-	26.5 ± 3.0	-	-	-	-
Number of CAG repeats	-	45.1 ± 5.5	-	-	-	-

Values are means \pm standard deviations. **P* values refer to Pearson Chi-Square or ANOVA models, followed by post-hoc pairwise comparisons. a = $p < 0.05$ vs HC; b = $p < 0.05$ vs KD; c = $p < 0.05$ vs classic ALS; d = $p < 0.05$ vs LMND-fast; e = $p < 0.05$ vs LMND-slow at posthoc pairwise comparisons. 6MWT= six-minute walk test; ALS= amyotrophic lateral sclerosis; ALSFRS-R= ALS Functional rating scale-revised; BMI= body mass index; LMND= lower motor neuron-predominant disease; KD= Kennedy's disease; M= men; W=women.

Table 2. Neuropsychological and behavioral features of KD, classic ALS and LMND patients.

	KD	ALS	LMND-fast	LMND-slow	p*
<i>General Cognition</i>					
MMSE (normal ≥ 24)	29.1 \pm 1.3	27.8 \pm 2.5	28.1 \pm 2.6	28.7 \pm 1.2	0.36
<i>Reasoning and Executive functions</i>					
Raven's coloured progressive matrices (normal ≥ 18)	31.5 \pm 3.5	28.3 \pm 5.9	27.3 \pm 7.9	30.3 \pm 6.5	0.61
Phonemic fluency (normal ≥ 17)	32.5 \pm 9.3	27.3 \pm 8.5	30.5 \pm 13.0	30.8 \pm 9.9	0.55
Semantic fluency (normal ≥ 25)	45.5 \pm 9.1	39.5 \pm 11.6	38.6 \pm 11.3	41.2 \pm 10.5	0.40
Digit span backward (normal ≥ 3.29)	4.7 \pm 1.0	4.3 \pm 1.4	4.1 \pm 0.8	4.3 \pm 1.0	0.71
CET (normal ≤ 18)	12.9 \pm 2.8	12.4 \pm 3.0	14.7 \pm 5.0	13.2 \pm 3.7	0.47
WCST (normal ≤ 90.5)	37.9 \pm 33.6 ^a	96.6 \pm 43.8 ^b	68.6 \pm 43.5	62.1 \pm 38.1	0.04
Weigl's Sorting test (normal ≥ 4.50)	12.3 \pm 2.6	10.6 \pm 4.3	13.0 \pm 5.7	11.7 \pm 3.9	0.60
<i>Verbal Memory</i>					
Digit span forward (normal ≥ 3.75)	5.8 \pm 0.9	5.8 \pm 1.3	5.5 \pm 0.9	6.1 \pm 0.6	0.51
RAVLT, immediate recall (normal ≥ 28.53)	43.4 \pm 10.0	38.6 \pm 12.5	39.9 \pm 12.0	46.3 \pm 10.7	0.56
RAVLT, delayed recall (normal ≥ 4.69)	8.8 \pm 2.9	8.6 \pm 3.8	7.0 \pm 3.1	8.4 \pm 3.7	0.28
<i>Language</i>					
Oral noun confrontation naming subtest of BADA (normal ≥ 28)	29.6 \pm 1.0	28.8 \pm 1.6	29.4 \pm 0.9	29.4 \pm 1.0	0.23
<i>Behavioral disturbances</i>					
FBI	7.5 \pm 5.0	3.3 \pm 6.5	2.7 \pm 3.7	3.8 \pm 6.9	0.31
ALS-FTD questionnaire (normal ≤ 22)	16.7 \pm 13.7	2.5 \pm 5.0	11.1 \pm 17.4	12.5 \pm 27.0	0.49
<i>Depression</i>					

HDRS (normal ≤ 9)	3.7 \pm 2.3	3.9 \pm 3.9	3.9 \pm 2.4	4.4 \pm 3.1	0.79
-------------------------	---------------	---------------	---------------	---------------	------

Values are means \pm standard deviations. **P* values refer to ANCOVA models adjusted for subjects' age and sex, followed by post-hoc pairwise comparisons. a = $p < 0.05$ vs classic ALS; b = $p < 0.05$ vs KD; ALS= Amyotrophic lateral sclerosis; ALS-FTD= Amyotrophic lateral sclerosis-frontotemporal dementia; CET=Cognitive Estimation Test; FBI= Frontal behavioral inventory; HC= healthy controls; HDRS=Hamilton Depression Rating Scale; LMND= lower motor neuron-predominant disease; KD= Kennedy's disease; MMSE= Mini Mental State Examination; RAVLT=Rey Auditory Verbal Learning Test; WCST=Wisconsin Card Sorting Test.

Table 3. DT MRI metrics of corticospinal tracts in healthy controls and patients with KD, classic ALS and LMND.

		HC	KD	ALS	LMND-fast	LMND-slow	<i>p</i> *	<i>Bp</i> [§]
FA	L	0.53 ± 0.03	0.53 ± 0.03	0.51 ± 0.04	0.53 ± 0.03	0.53 ± 0.02	0.13	0.12
	R	0.53 ± 0.02	0.53 ± 0.03	0.52 ± 0.04	0.53 ± 0.03	0.53 ± 0.02	0.18	0.18
MD [x10 ⁻³ mm ² s ⁻¹]	L	0.77 ± 0.04	0.77 ± 0.06	0.82 ± 0.08	0.79 ± 0.05	0.77 ± 0.04	0.11	0.11
	R	0.77 ± 0.04 ^{a,b}	0.78 ± 0.05	0.82 ± 0.07 ^c	0.81 ± 0.05 ^c	0.79 ± 0.05	0.04	0.04
axD [x10 ⁻³ mm ² s ⁻¹]	L	1.25 ± 0.07	1.27 ± 0.08	1.31 ± 0.10	1.29 ± 0.08	1.27 ± 0.05	0.31	0.32
	R	1.28 ± 0.07	1.27 ± 0.05	1.32 ± 0.09	1.32 ± 0.07	1.29 ± 0.06	0.20	0.21
radD [x10 ⁻³ mm ² s ⁻¹]	L	0.52 ± 0.05	0.52 ± 0.06	0.57 ± 0.08	0.54 ± 0.04	0.52 ± 0.04	0.10	0.08
	R	0.52 ± 0.04 ^a	0.53 ± 0.06	0.57 ± 0.07 ^b	0.55 ± 0.05 ^b	0.53 ± 0.05	0.03	0.02

Values are means ± standard deviations. **p* values refer to the between-group variance (F-values) from False Discovery Rate-corrected ANCOVA models adjusted for subjects' age and sex, followed by post-hoc pairwise comparisons: a = *p*<0.05 vs ALS; b = *p*<0.05 vs LMND-fast; c = *p*<0.05 vs HC; [§]*Bp*: bootstrapped *p* values (i.e. the proportion of resampled F-values that are greater than the observed F-values) after 1000 resamples, according to Westfall et al {Westfall, 1993 #266}. axD= axial diffusivity; ALS= Amyotrophic lateral sclerosis; FA= fractional anisotropy; HC= healthy controls; LMND= lower motor neuron-predominant disease; MD= mean diffusivity; KD= Kennedy's disease; radD= radial diffusivity.

Figure 1. TBSS results of comparison between classic ALS patients and healthy controls. Axial and coronal T1-weighted images of the Montreal Neurologic Institute standard brain show tract-based spatial statistics (TBSS) results in patients with classic ALS compared with healthy control subjects. Voxel-wise group differences in fractional anisotropy (red), mean diffusivity (blue), and radial diffusivity (purple) are shown. Results were overlaid on white-matter skeleton images (green; $p < 0.05$, corrected for multiple comparisons). Abbreviations: ALS = amyotrophic lateral sclerosis; L = left; R = right.

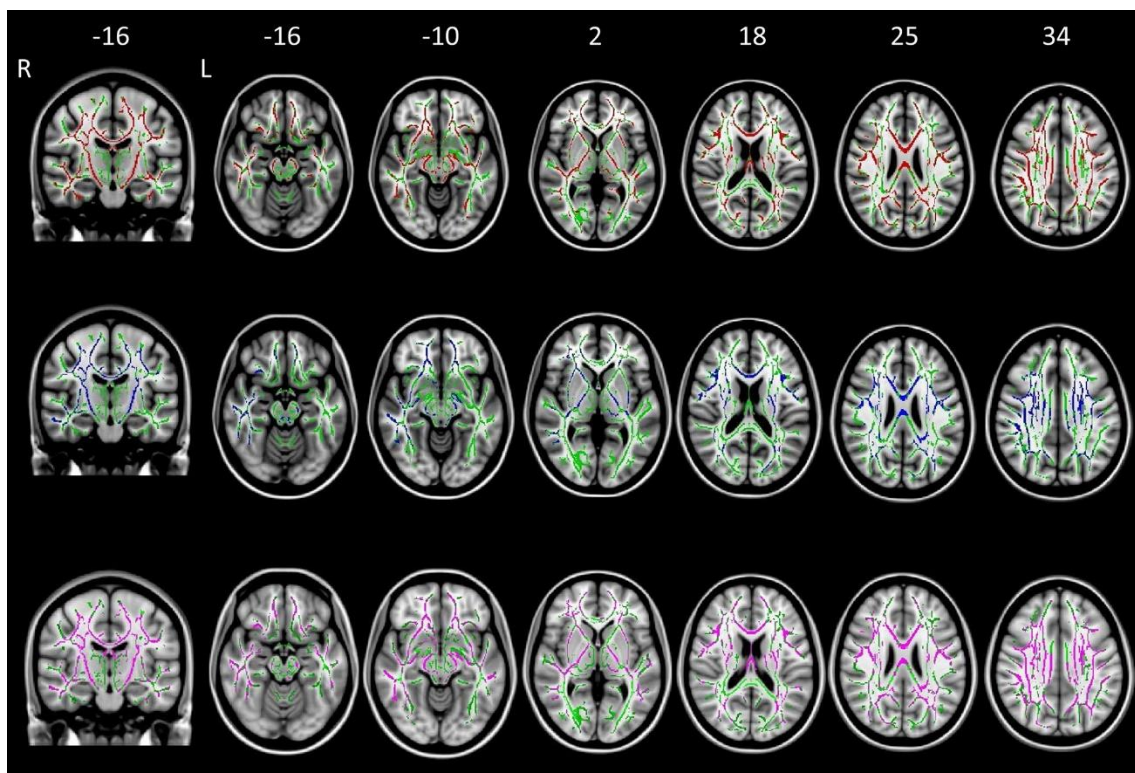


Figure 2. TBSS results of comparison between classic ALS and KD patients. Axial and coronal T1-weighted images of the Montreal Neurologic Institute standard brain show tract-based spatial statistics results in patients with classic ALS compared with KD subjects. Voxel-wise group differences in fractional anisotropy (red), mean diffusivity (blue), axial diffusivity (orange) and radial diffusivity (purple) are shown. Results were overlaid on white-matter skeleton images (green; $p < 0.05$, corrected for multiple comparisons). Abbreviations: ALS = amyotrophic lateral sclerosis; L = left; KD = Kennedy's disease; R = right.

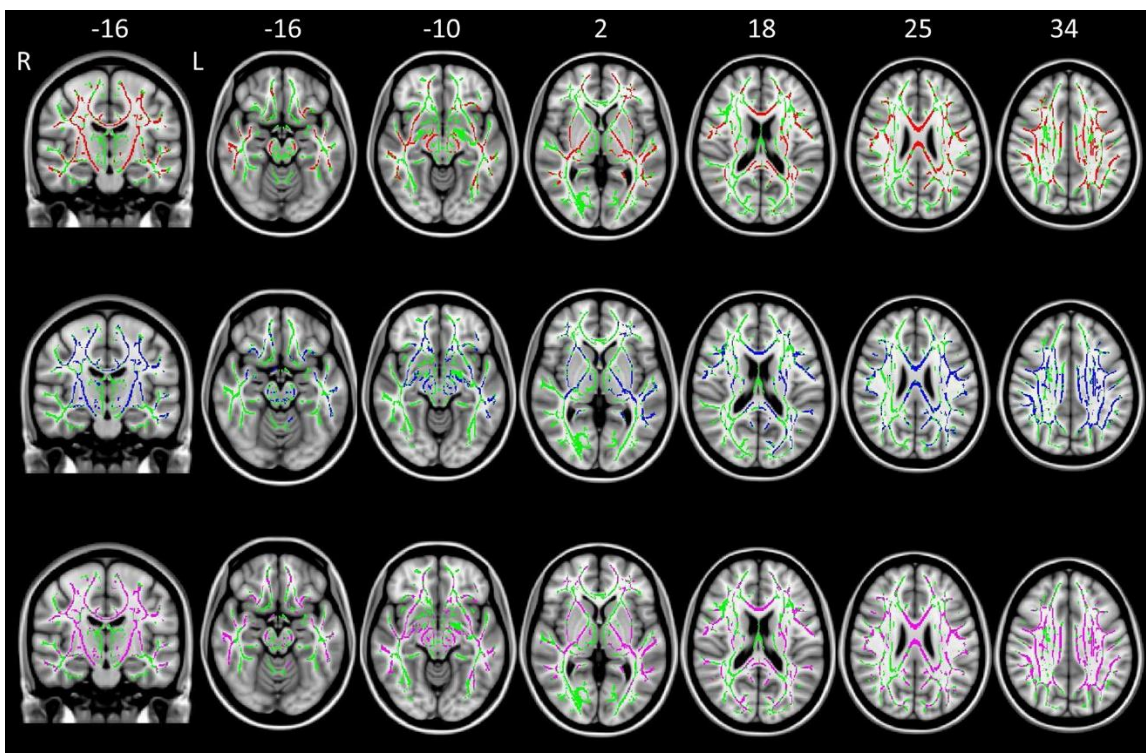
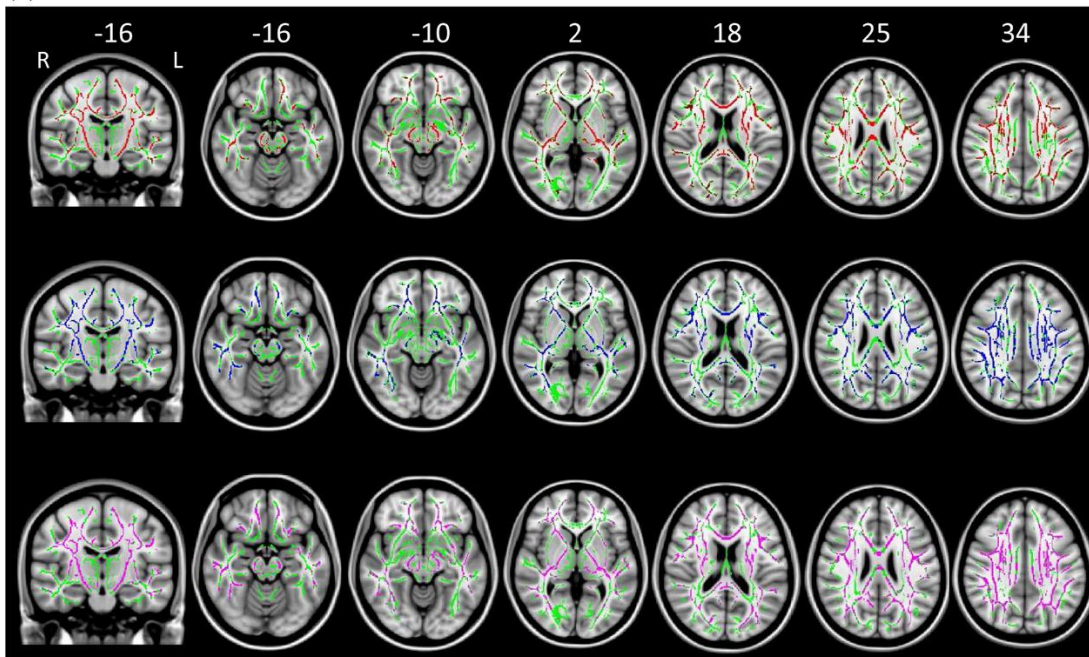


Figure 3. TBSS results of comparison between classic ALS and LMND (fast and slow) patients. Axial and coronal T1-weighted images of the Montreal Neurologic Institute standard brain show tract-based spatial statistics results in patients with classic ALS compared with (A) LMND-fast and (B) LMND-slow patients. Voxel-wise group differences in fractional anisotropy (red), mean diffusivity (blue), and radial diffusivity (purple) are shown. Results were overlaid on white-matter skeleton images (green; $p < 0.05$, corrected for multiple comparisons). Abbreviations: ALS = amyotrophic lateral sclerosis; L = left; LMND = lower motor neuron disease; R = right.

(a)



(b)

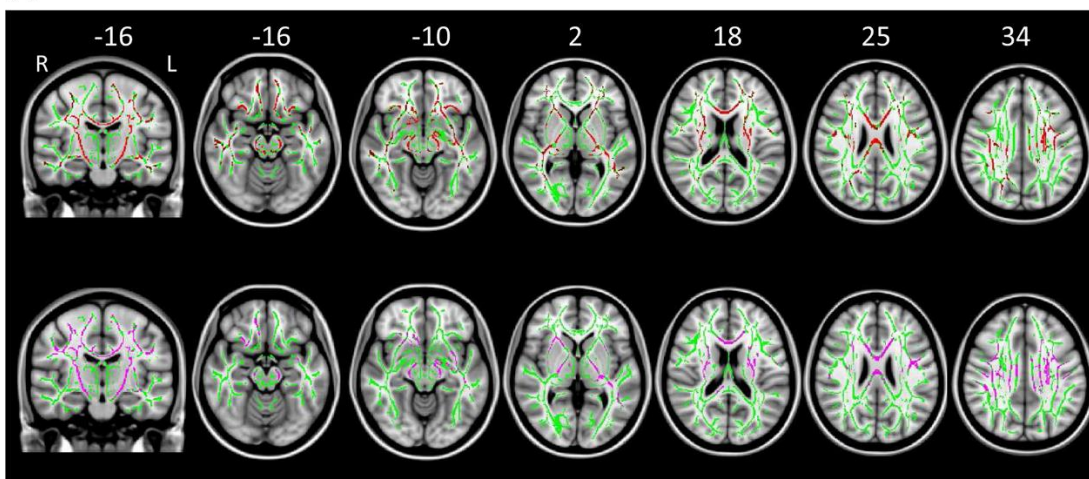
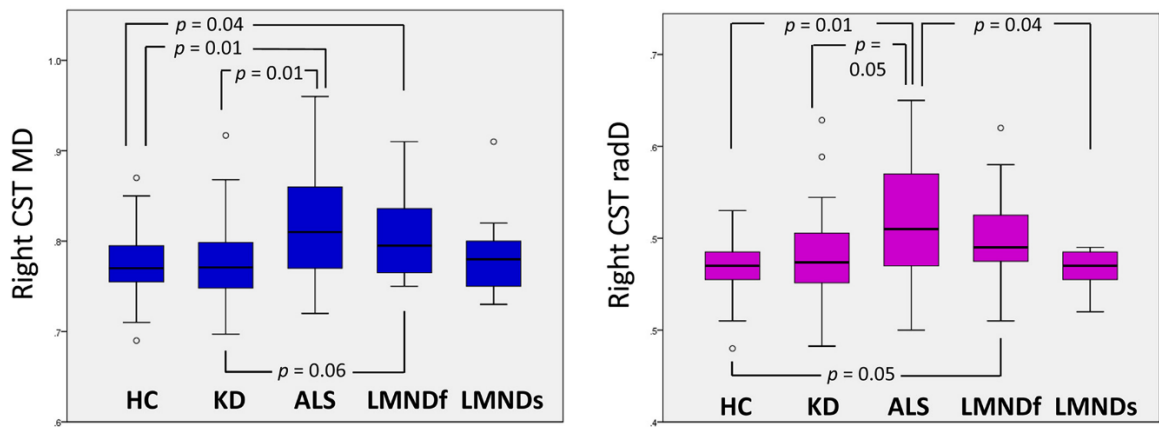


Figure 4. DT MRI metrics of the CST in healthy controls, classic ALS and LMND patients. Mean diffusivity and radial diffusivity values of the corticospinal tracts of healthy controls and patient groups are plotted. Abbreviations: ALS = amyotrophic lateral sclerosis; CST = corticospinal tract; L = left; LMNDf = fast-progressing lower motor neuron disease; LMNDs = slow-progressing lower motor neuron disease; MD = mean diffusivity; KD = Kennedy’s disease; R = right; radD = radial diffusivity.



Supporting Figure legend

Probabilistic maps of the corticospinal tracts. A) Reconstruction of the corticospinal tracts (red) in a patient with ALS, superimposed on the single subject's FA map. A coronal view (left) and an axial view of the seeds placed in the bulbar pyramids (middle) are provided. B) Probabilistic maps of the corticospinal tracts from all subjects included in the study. The tracts are overlaid on a 3D rendering of the Montreal Neurological Institute standard brain. Only voxels detected in at least 10% of the subjects are shown. Abbreviations: ALS = amyotrophic lateral sclerosis; FA = fractional anisotropy.



3.3. Structural MRI outcomes and predictors of disease progression in amyotrophic lateral sclerosis

NeuroImage: Clinical 27 (2020) 102315



Structural MRI outcomes and predictors of disease progression in amyotrophic lateral sclerosis



Edoardo G. Spinelli^{a,c,g}, Nilo Riva^b, Paola M.V. Rancoita^e, Paride Schito^c, Alberto Doretti^f, Barbara Poletti^f, Clelia Di Serio^e, Vincenzo Silani^{f,h}, Massimo Filippi^{a,c,d,g}, Federica Agosta^{a,g,*}

^a Neuroimaging Research Unit, Institute of Experimental Neurology, Division of Neuroscience, IRCCS San Raffaele Scientific Institute, Milan, Italy

^b Neurorehabilitation Unit, IRCCS San Raffaele Scientific Institute, Milan, Italy

^c Neurology Unit, IRCCS San Raffaele Scientific Institute, Milan, Italy

^d Neurophysiology Unit, IRCCS San Raffaele Scientific Institute, Milan, Italy

^e University Centre for Statistics in the Biomedical Sciences (CUSBS), Vita-Salute San Raffaele University, Milan, Italy

^f Department of Neurology and Laboratory of Neuroscience, IRCCS Istituto Auxologico Italiano, Milan, Italy

^g Vita-Salute San Raffaele University, Milan, Italy

^h "Dino Ferrari" Center, Department of Pathophysiology and Transplantation, Università degli Studi di Milano, Milan, Italy

ARTICLE INFO

Keywords:
Amyotrophic lateral sclerosis
Structural MRI
Prognosis
Cortical thickness
Diffusion tensor MRI

ABSTRACT

Background and aims: Considering the great heterogeneity of amyotrophic lateral sclerosis (ALS), the identification of accurate prognostic predictors is fundamental for both the clinical practice and the design of treatment trials. This study aimed to explore the progression of clinical and structural brain changes in patients with ALS, and to assess magnetic resonance imaging (MRI) measures of brain damage as predictors of subsequent functional decline.

Methods: 50 ALS patients underwent clinical evaluations and 3 T MRI scans at regular intervals for a maximum of 2 years (total MRI scans = 164). MRI measures of cortical thickness, as well as diffusion tensor (DT) metrics of microstructural damage along white matter (WM) tracts were obtained. Voxel-wise regression models and longitudinal mixed-effects models were used to test the relationship between clinical decline and baseline and longitudinal MRI features.

Results: The rate of decline of the ALS Functional Rating Scale revised (ALSF_{RS}-r) was significantly associated with the rate of fractional anisotropy (FA) decrease in the body of the corpus callosum (CC). Corticospinal tract (CST) and CC-body alterations had a faster progression in patients with higher baseline ALSF_{RS}-r scores and greater CC-body disruption at baseline. Lower FA of the cerebral peduncle was associated with faster subsequent clinical progression.

Conclusions: In this longitudinal study, we identified a significant association between measures of WM damage of the motor tracts and functional decline in ALS patients. Our data suggest that a multiparametric approach including DT MRI measures of brain damage would provide an optimal method for an accurate stratification of ALS patients into prognostic classes.

The following data have been published (Spinelli et al., Neuroimage Clin. 2020;27:102315. doi: 10.1016/j.nicl.2020.102315).

INTRODUCTION

Amyotrophic lateral sclerosis (ALS) is a rapidly progressive, fatal neurodegenerative condition causing prominent motor impairment (Calvo et al., 2017). Considering the great heterogeneity of ALS clinical course, the identification of accurate biomarkers of progression and prognostic predictors is important for both the clinical practice and the design of treatment trials (Kiernan, Vucic et al., 2011). Advanced magnetic resonance imaging (MRI) has recently emerged as a promising candidate to allow an objective

assessment of central nervous system (CNS) damage in ALS patients *in vivo*, showing the progressive involvement of both motor and extra-motor networks (Agosta et al., 2018). However, relatively few longitudinal MRI studies have been published (Agosta et al., 2009, Bede & Hardiman, 2018, de Albuquerque, Branco et al., 2017, Kassubek, Muller et al., 2018, Keil et al., 2012, Kwan et al., 2012, Menke et al., 2018, van der Graaff et al., 2011), mirroring the difficulties in enrolling enough patients who could undergo an appropriate number of follow-up scans. Moreover, only few of these studies included a multiparametric approach (Bede & Hardiman, 2018, de Albuquerque et al., 2017, Menke et al., 2018), and results regarding the pattern and the respective degree of grey matter (GM) and white matter (WM) degeneration over time are inconsistent. Finally, the relationship between structural alterations and the co-occurrent and subsequent evolution of functional impairment is far from being clarified (Menke, Agosta et al., 2017).

The aim of the present study was to determine which measures of GM cortical thickness and WM diffusivity provided by structural and diffusion tensor (DT) MRI were most sensitive to the progression of neurodegeneration and clinical impairment in a cohort of non-demented ALS patients who were enrolled soon after their diagnosis and followed-up at a regular interval for up to 2 years. We also assessed the potential use of these metrics as predictors of subsequent functional decline.

METHODS

Participants and study design

Fifty patients with sporadic possible (n=10), probable laboratory-supported (n=22), probable (n=9) or definite (n=9) ALS according to El Escorial revised criteria (Brooks et al., 2000) were prospectively recruited at two tertiary referral MND clinics in Milan between October 2009 and October 2015 within the framework of a longitudinal project, including only individuals within the first year after clinical diagnosis (**Table 1**). Patients received a comprehensive evaluation including clinical and MRI assessments at study entry and every 3 months for the first year; clinical evaluations were also performed every 6 months for the subsequent year. All patients underwent at least two MRI scans at the scheduled timepoints (**Figure 1**, average number of scans= 3.28 ± 1.55). A significant proportion developed respiratory problems that did not allow the acquisition of further MRI data, and several patients could not undergo clinical follow-up visits, due to severe

motor disability. In these latter cases, the development of clinical milestones of progression was assessed by phone interview to caregivers. At baseline, a screening cognitive assessment including Mini Mental State Examination (Folstein et al., 1975) and fluency tests (Novelli et al., 1986) was obtained from all patients, who were non-demented according to frontotemporal dementia criteria (Rascovsky et al., 2011) at any timepoint. When necessary, Rascovsky criteria (Rascovsky et al., 2011) were applied retrospectively, based on patients' charts. The main demographic, clinical and cognitive features of included ALS patients are shown in **Table 1**. Forty-seven age- and sex-matched healthy controls were recruited by word of mouth, based on the following criteria: normal neurological assessment; MMSE score ≥ 28 ; no family history of neurodegenerative diseases. Healthy controls performed clinical, cognitive and MRI assessments at baseline. Exclusion criteria for all subjects were: medical illnesses or substance abuse that could interfere with cognitive functioning; any (other) major systemic, psychiatric, or neurological diseases; other causes of brain damage, including lacunae and extensive cerebrovascular disorders at MRI.

The study was approved by the institutional ethics committees of the IRCCS San Raffaele Scientific Institute and IRCCS Istituto Auxologico Italiano in Milan and all participants (or their caregivers) provided written informed consent prior to study inclusion.

Clinical evaluation

At study entry and each follow-up visit, an experienced neurologist blinded to MRI results performed clinical assessments, recording site of disease onset and disease duration at presentation. Disease severity was assessed using the ALS Functional Rating Scale-revised (ALSFRS-r) (Cedarbaum et al., 1999). The baseline rate of disease progression was defined according to the following formula: $(48 - \text{ALSFRS-r score}) / \text{time between symptom onset and first visit}$. Muscular strength was assessed by manual muscle testing based on the Medical Research Council (MRC) scale, and clinical upper motor neuron (UMN) involvement was graded by totaling the number of pathological UMN signs on examination (Turner et al., 2004). Events of mortality (i.e., death or tracheostomy) were recorded either at the moment of clinical evaluations or by phone interview to caregivers until March 30, 2019.

MRI acquisition

Baseline and follow-up brain MRI scans were acquired on the same 3T Philips Medical System Intera machine. The following brain MRI sequences were obtained from all subjects: T2-weighted spin echo (SE) (repetition time [TR]=3500 ms; echo time [TE]=85 ms; echo train length=15; flip angle=90°; 22 contiguous, 5-mm-thick, axial slices; matrix size=512×512; field of view [FOV]=230×184 mm²); fluid-attenuated inversion recovery (TR=11 s; TE=120 ms; flip angle=90°; 22 contiguous, 5-mm-thick, axial slices; matrix size=512×512; FOV=230 mm²); 3D T1-weighted fast field echo (FFE) (TR=25 ms, TE=4.6 ms, flip angle=30°, 220 contiguous axial slices with voxel size=0.89×0.89×0.8 mm, matrix size=256×256, FOV=230×182 mm²); and pulsed-gradient SE echo planar with sensitivity encoding (acceleration factor=2.5, TR=8986 ms, TE=80 ms, 55 contiguous, 2.5 mm-thick axial slices, number of acquisitions=2; acquisition matrix 96×96, with an in-plane pixel size of 1.89×1.89 mm and a FOV=240 mm²) diffusion gradients applied in 32 non-collinear directions using a gradient scheme which is standard on this system (gradient over-plus) and optimized to reduce echo time as much as possible. The *b* factor used was 1000 s/mm². Fat saturation was performed to avoid chemical shift artifacts. All slices were positioned to run parallel to a line that joins the most inferoanterior and inferoposterior parts of the corpus callosum.

MRI analysis

Cortical thickness measurement

Cortical reconstruction and estimation of cortical thickness were performed on the 3D T1-weighted images using the FreeSurfer image analysis suite, version 5.3 (<http://surfer.nmr.mgh.harvard.edu/>) (Fischl & Dale, 2000). After registration to Talairach space and intensity normalization, the process involved an automatic skull stripping, which removes extra-cerebral structures, cerebellum and brainstem, by using a hybrid method combining watershed algorithms and deformable surface models. Images were carefully checked for skull stripping errors. Then, images were segmented into GM, WM, and cerebrospinal fluid (CSF), cerebral hemispheres were separated, and subcortical structures divided from cortical components. The WM/GM boundary was tessellated and

the surface was deformed following intensity gradients to optimally place WM/GM and GM/CSF borders, thus obtaining the WM and pial surfaces (Dale et al., 1999). Afterwards, surface inflation and registration to a spherical atlas were performed (Dale et al., 1999). Finally, cortical thickness was estimated as the average shortest distance between the WM boundary and the pial surface.

To evaluate longitudinal cortical changes in ALS patients, the serial 3D T1-weighted images of each subject were processed with the Freesurfer longitudinal stream (Reuter, Schmansky et al., 2012). Specifically, an unbiased within-subject template space and image was created from the available scans using a robust, inverse consistent registration. Several processing steps (including skull stripping, Talairach transforms, atlas registration, as well as spherical surface maps) were then initialized on the available scans, with common information from the within-subject template. This allowed to create surface maps of all the available timepoints (Reuter et al., 2012). Individual surface maps were registered to a common average surface and then smoothed using a Gaussian kernel of 10 mm full width half-maximum.

Diffusion Tensor (DT) MRI analysis

DT MRI analysis was performed using the FMRIB software library (FSL) tools (<http://www.fmrib.ox.ac.uk/fsl/fdt/index.html>) and the JIM software (Xinapse Systems, Northants, UK, <http://www.xinapse.com>), as previously described {Agosta, 2013 #84; Agosta, 2014 #170}. The diffusion-weighted data underwent a careful quality check for head motion and were subsequently skull-stripped using the Brain Extraction Tool implemented in FSL. Using FMRIB's Linear Image Registration Tool (FLIRT), the two diffusion-weighted scans were coregistered by applying the rigid transformation needed to correct for position between the two b0 images (T2-weighted, but not diffusion-weighted). The rotation component was also applied to diffusion-weighted directions. Eddy currents correction was performed using the JIM software (Horsfield, 1999). The DT was estimated on a voxel-by-voxel basis using DTIfit provided by the FMRIB Diffusion Toolbox. Maps of fractional anisotropy (FA), mean diffusivity (MD), axial diffusivity (axD) and radial diffusivity (radD) were obtained.

First, a whole-brain DT MRI analysis was performed using tract-based spatial statistics (TBSS) version 1.2 (<http://www.fmrib.ox.ac.uk/fsl/tbss/index.html>). FA

volumes of all timepoints acquired from all subjects were aligned to a target image using the following procedure: (i) the FA template in standard space (provided by FSL) was selected as the target image, (ii) the nonlinear transformation that mapped each subject's FA to the target image was computed using the FMRIB's Nonlinear Image Registration Tool, and (iii) the same transformation was used to align each subject's FA to the standard space. A mean FA image was then created by averaging the aligned individual FA images and thinned to create a FA skeleton representing WM tracts common to all subjects. The FA skeleton was thresholded at a value of 0.2 to exclude voxels with low FA values, which are likely to include GM or CSF. Individual FA, MD, axD and radD data were projected onto this common skeleton. For the longitudinal analysis, skeletonised maps of each DT-derived metric of all available timepoints obtained from each ALS patient were fitted to a linear model using the Fitter tool in JIM7 (Horsfield, 1999) (www.xinapse.com): the model included a constant value, and time from baseline was set as independent variable; the obtained slope was retained for the statistical analysis.

Subsequently, based on the results of the whole-brain analysis, a region-of-interest (ROI) analysis was performed to assess the degeneration of motor WM tracts in greater detail. Masks of the body of the corpus callosum (CC-body) and four sub-regions of the corticospinal tract (CST) – i.e., the bulbo-pontine CST, cerebral peduncle, posterior limb of the internal capsule, and superior corona radiata – were obtained from the Johns Hopkins University (JHU) white-matter tractography atlas (Hua, Zhang et al., 2008) and transformed onto the aligned, skeletonized TBSS data, in order to extract mean DT MRI metrics for each selected ROI at all timepoints. For CST data, the mean values of corresponding ROIs of the two hemispheres were averaged to obtain a single value.

Statistical analysis

Baseline MRI data

A cross-sectional vertex-by-vertex analysis using FreeSurfer, version 5.3 (<http://surfer.nmr.mgh.harvard.edu/>), was performed to assess differences of cortical thickness between ALS patients and healthy controls at baseline, adjusting for age and sex. The t-statistic was thresholded at $p < 0.05$, FDR-corrected for multiple comparisons.

DT MRI voxel-wise statistics were performed to compare FA, MD, axD and radD data between ALS patients and controls using a permutation-based inference tool for

nonparametric statistical thresholding (“randomize”, permutations=5000) in FSL (<https://fsl.fmrib.ox.ac.uk/fsl/fslwiki/Randomise/>), adjusting for age and sex. Statistical maps were thresholded at $p < 0.05$, family-wise error (FWE) corrected for multiple comparisons at the cluster level using the threshold-free cluster enhancement option.

DT MRI parameters of the selected WM ROIs at baseline were compared between ALS patients and healthy controls using a Multivariate Analysis of Covariance (MANCOVA) test followed by post-hoc pairwise comparisons, adjusting for sex and age and applying Bonferroni correction for multiple comparisons. SPSS Statistics 22.0 was used.

Longitudinal MRI data

Longitudinal changes of cortical thickness occurring in ALS patients were assessed using Linear Mixed Effects Models in FreeSurfer v5.3 (Bernal-Rusiel, Reuter et al., 2013) adjusting for age, sex, and ALSFRS-r score at baseline as fixed-effects covariates (without variable selection). Random effects were defined on the intercept. The t-statistic was thresholded at $p < 0.05$, FDR-corrected.

One-sample t-tests using the “randomize” voxel-wise statistical tool in FSL (permutations=5000) were performed to assess the evolution of FA, MD, axD and radD slopes, adjusting for age, sex and baseline ALSFRS-r score. Statistical maps were thresholded at $p < 0.05$, FWE-corrected.

Mixed effects models were used to model the evolution over time (from baseline) of mean DT MRI metrics within each selected WM ROI. For each DT MRI measure, both a linear (LME) and a nonlinear mixed-effects (NLME) model were estimated to investigate which could better fit the longitudinal trend. Final models were obtained with a backward procedure of variable selection on the fixed-effects covariates. The best model (among the two final ones) was chosen as the one with the lowest Akaike Information Criteria (AIC). Outliers which have been observed for both starting models were excluded from the analysis of that MRI parameter. Due to the shape of the trajectories, the NLME model was defined as either a decreasing or an increasing exponential function with horizontal left asymptote. In case of the decreasing trend (used for FA), the equation of the model (Model 1) was:

$$MRI\ measure = Asym (1 - \exp (time - xdec10 + \ln (0.1))),$$

while in case of an increasing function (used for diffusivity measures) this was (Model 2):

$$MRI\ measure = Asym (1 + \exp (time - xinc10 + \ln (0.1))),$$

where *Asym* was the horizontal left asymptote (representing the “starting value”), while *xdec10* or *xinc10* describe the time to a 10% decrease or increase for MRI measure, respectively, with respect to the asymptote. In both LME and NLME models, we assessed the effect of fixed-effects covariates (sex, age at onset, ALSFRS-r score at baseline and the value of the selected MRI parameter at baseline) on the change of each MRI parameter over time (i.e., the slope in the LME model or the 10% increase/decrease relative to the horizontal left asymptote in the NLME model) was influenced by sex, age at onset, ALSFRS-r score at baseline and the value of the selected MRI parameter at baseline. Moreover, we evaluated whether the starting value of the MRI measure (i.e., the intercept in the LME model and the asymptote in the NLME model) was affected by sex, age at baseline and ALSFRS-r score at baseline. The random effects were set on the parameter representing the starting value (namely, the intercept for the LME model and the intercept of the asymptote in the NLME model), in order to account for the heterogeneity of values of the MRI measure among patients at baseline. For all DT MRI measures the best model resulted to be the appropriate NLME model (see **Appendix**). This analysis was performed using the nlme R package with R version 3.5.0 (<http://www.R-project.org/>).

2.5.3. Clinico-anatomical correlations

In ALS patients, voxel-wise regression models were run to test the association between the rate of decline of ALSFRS-r and the slopes of DT MRI measures within the WM skeleton obtained from TBSS, using the “randomize” voxel-wise statistical tool in FSL (permutations=5000). Statistical maps were thresholded at $p < 0.05$, FWE-corrected.

In addition, a nonlinear mixed-effects model with a logistic shape was used to test the relationship between sex, age at onset and the value of FA of each selected WM ROIs at baseline and the subsequent rate of ALSFRS-r decline, using the following equation:

$$ALSFRS - r\ score = \frac{Asym}{1 + \exp \left[\frac{xmid - time}{scale} \right]}$$

where *Asym* represented the left horizontal asymptote (i.e., the “starting value” of ALSFRS-r), while the right horizontal asymptote (i.e., the “final value”) was set to 0, as the value of ALSFRS-r at the eventual time-point corresponding to the occurrence of tracheostomy/death was imputed as equivalent to this score; *xmid* represented the follow-up time (*time*) at which the ALSFRS-r score was midway between the asymptotes (thus indicating of a faster/slower progression rate); whereas *scale* was a scaling factor, which was set equal for all patients. We assessed whether the progression of the ALSFRS-r score over time (i.e., *xmid*) depended on the following fixed-effects covariates: sex, age at onset and the value of FA of the selected WM ROIs at baseline. The random effects were set on the intercept of *xmid* in order to account for the heterogeneity among patients in the rate of disease progression. We also evaluated whether the starting value of the ALSFRS-r score (*Asym*) depended on the following fixed-effects covariates: sex, age at baseline and disease duration at baseline. The final model was obtained by using a backward selection procedure on the fixed-effects covariates. The observations which were outliers for the starting model were eliminated from the analysis. This analysis was performed using the nlme R package with R version 3.5.0 (<http://www.R-project.org/>).

Sample size calculation

A minimum sample size was calculated for assessing a change at 6 months of either FA values of the bulbo-spinal CST (for this analysis, considered as representative for the whole CST) or ALSFRS-r, using data from the literature for identifying the target differences (Bede & Hardiman, 2018, Cardenas-Blanco, Machts et al., 2016, Kassubek et al., 2018). A sample of 28 patients was calculated as sufficient for showing a mean difference of bulbo-spinal CST FA values between 6 months and the baseline of -0.004 with standard deviation (SD) of 0.007, by considering 80% power and 5% significant level. By assuming a (conservative) moderate correlation between ALSFRS-r values at the baseline and at 6 months (i.e., between 0.5 and 0.7), a sample size between 15 and 23 was computed as sufficient for showing a decrease from 40 (with SD=5) to 36 (with SD=7), by considering 80% power and 5% significant level. For comparison, **Figure 1** reports the numbers of available timepoints of the present cohort.

RESULTS

Clinical evaluation

Table 1 reports the main demographic, clinical and cognitive data of participants. Forty-one ALS patients (i.e., 82%) met the survival endpoint (i.e., death or tracheostomy) at the time of censoring. All patients with a diagnosis of possible ALS at baseline had converted to a higher level of diagnostic certainty by the end of the available follow-up.

Baseline MRI findings

Cortical thickness. In ALS patients, no significant cortical thinning was detected relative to healthy controls at baseline.

WM voxel-wise analysis. On the baseline TBSS analysis, ALS patients showed extensively decreased FA relative to controls along the CST, bilaterally, and in the CC-body (**Figure 2-a**, $p < 0.05$ FWE-corrected). Decreased FA was also found in the superior longitudinal fasciculi and frontal subcortical WM, bilaterally. No significant alterations of MD, axD, or radD were found.

WM ROI analysis. At baseline, the DT-derived measures showing significant alterations at a regional level in ALS patients were the mean FA values of CC-body ($p = 0.008$) and all CST ROIs ($p = 0.008$ for bulbo-pontine, $p < 0.001$ for other subregions), as well as MD values of the upper CST (superior corona radiata, $p = 0.008$; PLIC, $p = 0.048$) (**Table 2**). Other diffusivity metrics did not differ significantly from healthy controls.

Longitudinal MRI changes

Cortical thickness. In ALS patients, no significant cortical thinning over the 1-year MRI follow-up was detected.

WM voxel-wise analysis. A significant evolution of microstructural WM damage was found, in terms of decreased FA and increased MD, axD and radD (**Figure 2-b**, $p < 0.05$ FWE-corrected). MD and radD, which did not show significant alterations at baseline, increased over time not only along the CSTs and the CC-body, but also in the genu of the CC, bilateral superior longitudinal fasciculi and anterior corona radiata, and left inferior longitudinal fasciculus. FA decreased significantly in the same areas, except for the CSTs. The longitudinal increase of axD involved only a restricted area including the genu of the CC, the PLIC and the superior-anterior corona radiata of the right hemisphere.

WM ROI analysis. The evolution over time of mean FA, MD and radD values within each selected ROI (i.e., body-CC and 4 CST subregions) was modelled using both a linear and a nonlinear mixed-effects (NLME) model. For all DT MRI measures, the best model resulted to be the nonlinear one. **Figure 3, Supplementary figure 1 and Supplementary figure 2** show the progression of such values for each subject over time, together with the corresponding estimated model. Considering the modest size and localization of axD increase in the voxel-wise analysis, we did not model the longitudinal evolution of this measure within the ROIs. The estimated models are reported in the **Appendix**. Damage to the CC-body and CST subregions consistently showed faster progression in ALS patients with higher ALSFRS-r at baseline (FA of the CC-body, MD of the bulbo-pontine CST, FA/MD/radD of the cerebral peduncle and PLIC). Greater WM damage at baseline was also associated with faster subsequent decline of FA/MD/radD of the CC-body, and FA of the PLIC, although an opposite association was found for radD of the PLIC. Female sex was mostly associated with faster WM deterioration (MD of the CC-body, FA/radD of the bulbo-pontine CST, FA of the PLIC, FA/MD/radD of the superior corona radiata), although male patients showed faster progression of radD of the PLIC. Younger age at onset was associated with faster decline of FA/MD/radD of the CC-body, FA of the cerebral peduncle, and MD/radD of the PLIC, whereas an opposite association was shown for FA of the bulbo-pontine CST and MD of the superior corona radiata.

Relationship between structural brain changes and clinical progression in ALS patients

Voxel-wise regression models showed a significant association between the slopes of ALSFRS-r progression and FA decrease within WM fibers of the CC-body (**Figure 2-c**).

The progression of the ALSFRS-r score over time, as assessed using the nonlinear mixed-effects model, was found to occur faster in ALS patients with lower baseline FA of the cerebral peduncle ($p=0.047$), indicating this DT MRI measure as a predictor of more rapid subsequent functional decline. The starting value of ALSFRS-r showed, as expected, an inverse association with disease duration ($p=0.049$; **Figure 4, Table 3**). Other demographic (i.e., age at onset, sex) and MRI measures were not significantly related with ALSFRS-r progression over time.

DISCUSSION

In this longitudinal study, a whole-brain voxel-wise approach with no *a priori* assumptions was adopted to identify which MRI measures were the most sensitive to early and progressive brain damage in ALS patients enrolled within one year from clinical diagnosis, who showed consequently mild disease severity at baseline (mean ALSFRS-r = 41.5 ± 5.1). We found consistent alterations of MRI measures of WM microstructural integrity that were mostly restricted to the CC-body and CST at baseline and later progressed to involve widespread anterior frontal, temporal and parietal tracts over a one-year follow-up time in ALS patients. DT MRI metrics showed progressive worsening over time that was influenced by several demographic, clinical and MRI features. FA decrease in the CC-body was found to correlate with the progression of ALSFRS-r, whereas baseline FA values of the cerebral peduncle predicted a more rapid subsequent clinical course. By contrast, no significant cortical thinning was detected either at baseline or over time.

Results from previous longitudinal MRI studies in ALS are conflicting as regards the relative impact of pathology progression over cortical GM and WM disruption. In fact, some have suggested a key role of GM atrophy over time (Bede & Hardiman, 2018, Kwan et al., 2012, Menke et al., 2018), whereas others found no significant longitudinal cortical changes (de Albuquerque et al., 2017, Schuster et al., 2014b, Verstraete, Veldink et al., 2014). Progression of WM damage demonstrated by DT MRI has been reported more consistently (Bede & Hardiman, 2018, de Albuquerque et al., 2017, Kassubek et al., 2018, Keil et al., 2012, Menke et al., 2018, Steinbach, Loewe et al., 2015), although a minority of studies could not detect such longitudinal evolution (Agosta et al., 2009, Kwan et al., 2012), and some variability regarding the entity and the pattern of such progression likely derive from the heterogeneous disease course and great variability across studies in sample sizes, follow-up intervals and functional impairment at baseline.

In our study, no cross-sectional or longitudinal cortical thinning was detected at a statistical threshold corrected for multiple comparisons, after adjusting for age and sex. The lack of GM alterations in ALS patients even at baseline contrasts with previous results from our (Spinelli et al., 2016) and other research groups (Kwan et al., 2012, Verstraete et al., 2010), but is likely due to the shorter disease duration and milder disability of the present sample, as well as to the use of different statistical approaches.

By contrast, the identification of the known signature of FA decrease relative to healthy controls at baseline, encompassing the CST in its entirety and the motor callosal fibers (i.e., the CC-body), was expected and consistent with previous reports from several research groups (Agosta et al., 2014b, Bede & Hardiman, 2018, Kassubek et al., 2018, Schuster, Elamin et al., 2016) and a recent large multicenter study pooling DT MRI data of ALS patients from eight sites (Muller et al., 2016). The cross-sectional, ROI-based analysis confirmed such difference when averaged values within each motor tract ROI (i.e., four CST subregions and CC-body) were considered. In particular, FA was the earliest DT-derived measure to be altered, whereas diffusivity metrics were relatively spared at baseline, with the exception of MD of the superior corona radiata and PLIC. This is in keeping with previous studies showing most widespread baseline alterations of FA in ALS cohorts (Agosta et al., 2014; Bede and Hardiman, 2018; de Albuquerque et al., 2017), possibly consistent with early axonal degeneration. On the other hand, a longitudinal analysis that considered all available timepoints within a one-year follow-up demonstrated progression of FA, MD and radD alterations in widespread WM regions, involving not only motor tracts, but also extra-motor fronto-temporo-parietal WM. This is in line with the pattern described by previous reports (Bede & Hardiman, 2018, Menke et al., 2018) and mirrors the pathological staging described by Brettschneider et al. (Brettschneider et al., 2013), although a strict correspondence is difficult to draw, as this staging is based on TDP-43 depositions in the cortical GM. When our longitudinal analysis focused on the ROIs of the motor tracts, FA decrease and MD/radD increase in ALS patients showed a non-linear evolution over time with a complex dependence on demographic, clinical and MRI features, as further discussed below. Taken together, our results suggest that advanced structural MRI techniques assessing WM integrity might have greater sensitivity to early damage and subsequent evolution of ALS pathology, compared with those evaluating GM.

The longitudinal analysis of WM alterations within the selected ROIs has provided some intriguing suggestions regarding the pattern and timing of DT MRI alterations in ALS patients. Particularly, the association of a more rapid WM disruption within these regions with higher baseline ALSFRS-r values and, for the CC-body, greater baseline MRI alterations suggests, on the one hand, that WM microstructural rearrangements occur early in ALS disease course, even before the development of a

severe functional impairment; on the other hand, that once WM degeneration of the callosal fibers has started, this does not tend towards reaching a plateau, but rather to a greater rate of deterioration, at least in the early phases covered by the 1-year timeframe of the present MRI study. The relationship of WM longitudinal damage with other demographic features (i.e., sex and age) is more difficult to interpret, as our results showed diverging consequences of the same factors across different WM subregions (although female sex was most consistently associated with faster WM disruption). The complex influence of these factors over DT MRI metrics has been explored only recently in different contexts (i.e., healthy aging and pathological conditions, including ALS) (Bede, Elamin et al., 2014, O'Dwyer, Lamberton et al., 2012, Rathee, Rallabandi et al., 2016). In the present study, given the absence of longitudinal data of healthy controls, it is impossible to discriminate between the “normal” influence of demographic features over WM integrity and their interaction with disease status, although demographic factors have been indicated as fundamental prognostic factors (Calvo et al., 2017, Chio et al., 2020) and previous neuroimaging evidence suggests significant sexual dimorphism in the evolution of ALS pathology (Bede et al., 2014).

This study has also identified significant associations between measures of WM damage of the motor tracts and functional decline in ALS patients. FA decrease of the CC-body correlated with the decline of ALSFRS-r (**Figure 2-c**), suggesting that functional decline in ALS might at least partially derive from an interhemispheric disconnection between contralateral motor networks. This is in line with previous studies showing a significant association between WM motor tract degeneration and worsening disability (Kassubek et al., 2018, Keil et al., 2012, Menke et al., 2018), and supports these measures as possible additional quantitative outcomes – more specifically related to CNS damage compared with ALSFRS-r – when following disease evolution. Moreover, we demonstrated that decreased FA of the cerebral peduncle is an independent predictor of a faster subsequent ALSFRS-r decline (**Figure 4, Table 3**). The cerebral peduncle has already been indicated as a key region to discriminate ALS patients from controls based on DT MRI, even more than other CST subregions (Schuster et al., 2016). Moreover, the process of tract reconstruction in the cerebral peduncle might be less affected by the presence of crossing fibers, when compared to other CST subregions (Mandelli, Berger et al., 2014), possibly making this measure more closely related to the underlying WM

pathology. Therefore, it is not surprising that greater damage to this region might also have a prognostic, as well as diagnostic role in ALS. This finding integrates previous studies specifically assessing DT MRI measures of the CST for a prediction of survival (Agosta, Spinelli et al., 2019, Schuster et al., 2017, van der Burgh et al., 2017), and strongly suggests that a multimodal approach including such measures would provide an optimal method for an accurate prognostic stratification of ALS patients.

Compared with previous studies adopting a similar multiparametric MRI approach (Bede & Hardiman, 2018, de Albuquerque et al., 2017, Menke et al., 2018), we were able to enroll a well-sized sample of patients who underwent at least 2 MRI scans over the follow up, strengthening our claim that the lack of significant GM alterations is not due to an insufficient sample. A limitation of this longitudinal study is the relatively high attrition rate, as only 18/50 patients could undergo the last, 12-month MRI scan. However, this was expected given the aggressive course of ALS; moreover, the specific statistical design that we used was meant to take into account missing values and differences in follow-up time. Another limitation was the unavailability of longitudinal data of healthy controls, although this did not affect the main focus of our study, which was on identifying the structural MRI alterations that were most sensitive to ALS clinical progression and could contribute to predict a faster functional deterioration.

Despite these limitations, our data allow to conclude that DT MRI metrics are sensitive to brain damage in the first stages of ALS and can provide useful information to monitor disease progression and aid in the prognostic stratification of patients. Larger samples will be needed to further explore these suggestions in specific subpopulations (e.g., according to site of onset, different cognitive status, etc.).

Acknowledgements

The present work was performed by Dr Edoardo Gioele Spinelli in partial fulfillment of the requirements for obtaining the PhD degree at Vita-Salute San Raffaele University, Milano, Italy.

References

Agosta F, Galantucci S, Canu E, Cappa SF, Magnani G, Franceschi M, Falini A, Comi G, Filippi M (2013) Disruption of structural connectivity along the dorsal and ventral language pathways in patients with nonfluent and semantic variant primary progressive aphasia: a DT MRI study and a literature review. *Brain Lang* 127: 157-66

Agosta F, Galantucci S, Riva N, Chio A, Messina S, Iannaccone S, Calvo A, Silani V, Copetti M, Falini A, Comi G, Filippi M (2014) Intrahemispheric and interhemispheric structural network abnormalities in PLS and ALS. *Hum Brain Mapp* 35: 1710-22

Agosta F, Rocca MA, Valsasina P, Sala S, Caputo D, Perini M, Salvi F, Prella A, Filippi M (2009) A longitudinal diffusion tensor MRI study of the cervical cord and brain in amyotrophic lateral sclerosis patients. *J Neurol Neurosurg Psychiatry* 80: 53-5

Agosta F, Spinelli EG, Filippi M (2018) Neuroimaging in amyotrophic lateral sclerosis: current and emerging uses. *Expert Rev Neurother* 18: 395-406

Agosta F, Spinelli EG, Riva N, Fontana A, Basaia S, Canu E, Castelnovo V, Falzone Y, Carrera P, Comi G, Filippi M (2019) Survival prediction models in motor neuron disease. *Eur J Neurol* 26: 1143-1152

Bede P, Elamin M, Byrne S, Hardiman O (2014) Sexual dimorphism in ALS: exploring gender-specific neuroimaging signatures. *Amyotroph Lateral Scler Frontotemporal Degener* 15: 235-43

Bede P, Hardiman O (2018) Longitudinal structural changes in ALS: a three time-point imaging study of white and gray matter degeneration. *Amyotroph Lateral Scler Frontotemporal Degener* 19: 232-241

Bernal-Rusiel JL, Reuter M, Greve DN, Fischl B, Sabuncu MR, Alzheimer's Disease Neuroimaging I (2013) Spatiotemporal linear mixed effects modeling for the mass-univariate analysis of longitudinal neuroimage data. *Neuroimage* 81: 358-370

Brettschneider J, Del Tredici K, Toledo JB, Robinson JL, Irwin DJ, Grossman M, Suh E, Van Deerlin VM, Wood EM, Baek Y, Kwong L, Lee EB, Elman L, McCluskey L,

Fang L, Feldengut S, Ludolph AC, Lee VM, Braak H, Trojanowski JQ (2013) Stages of pTDP-43 pathology in amyotrophic lateral sclerosis. *Ann Neurol* 74: 20-38

Brooks BR, Miller RG, Swash M, Munsat TL, World Federation of Neurology Research Group on Motor Neuron D (2000) El Escorial revisited: revised criteria for the diagnosis of amyotrophic lateral sclerosis. *Amyotroph Lateral Scler Other Motor Neuron Disord* 1: 293-9

Calvo A, Moglia C, Lunetta C, Marinou K, Ticozzi N, Ferrante GD, Scialo C, Soraru G, Trojsi F, Conte A, Falzone YM, Tortelli R, Russo M, Chio A, Sansone VA, Mora G, Silani V, Volanti P, Caponnetto C, Querin G et al. (2017) Factors predicting survival in ALS: a multicenter Italian study. *J Neurol* 264: 54-63

Cardenas-Blanco A, Machts J, Acosta-Cabronero J, Kaufmann J, Abdulla S, Kollwe K, Petri S, Schreiber S, Heinze HJ, Dengler R, Vielhaber S, Nestor PJ (2016) Structural and diffusion imaging versus clinical assessment to monitor amyotrophic lateral sclerosis. *Neuroimage Clin* 11: 408-414

Cedarbaum JM, Stambler N, Malta E, Fuller C, Hilt D, Thurmond B, Nakanishi A (1999) The ALSFRS-R: a revised ALS functional rating scale that incorporates assessments of respiratory function. BDNF ALS Study Group (Phase III). *J Neurol Sci* 169: 13-21

Chio A, Moglia C, Canosa A, Manera U, D'Ovidio F, Vasta R, Grassano M, Brunetti M, Barberis M, Corrado L, D'Alfonso S, Iazzolino B, Peotta L, Sarnelli MF, Solara V, Zucchetti JP, De Marchi F, Mazzini L, Mora G, Calvo A (2020) ALS phenotype is influenced by age, sex, and genetics: A population-based study. *Neurology* 94: e802-e810

Dale AM, Fischl B, Sereno MI (1999) Cortical surface-based analysis. I. Segmentation and surface reconstruction. *Neuroimage* 9: 179-94

de Albuquerque M, Branco LM, Rezende TJ, de Andrade HM, Nucci A, Franca MC, Jr. (2017) Longitudinal evaluation of cerebral and spinal cord damage in Amyotrophic Lateral Sclerosis. *Neuroimage Clin* 14: 269-276

Fischl B, Dale AM (2000) Measuring the thickness of the human cerebral cortex from magnetic resonance images. *Proc Natl Acad Sci U S A* 97: 11050-5

Folstein MF, Folstein SE, McHugh PR (1975) "Mini-mental state". A practical method for grading the cognitive state of patients for the clinician. *J Psychiatr Res* 12: 189-98

Horsfield MA (1999) Mapping eddy current induced fields for the correction of diffusion-weighted echo planar images. *Magn Reson Imaging* 17: 1335-45

Hua K, Zhang J, Wakana S, Jiang H, Li X, Reich DS, Calabresi PA, Pekar JJ, van Zijl PC, Mori S (2008) Tract probability maps in stereotaxic spaces: analyses of white matter anatomy and tract-specific quantification. *Neuroimage* 39: 336-47

Kassubek J, Muller HP, Del Tredici K, Lule D, Gorges M, Braak H, Ludolph AC (2018) Imaging the pathoanatomy of amyotrophic lateral sclerosis in vivo: targeting a propagation-based biological marker. *J Neurol Neurosurg Psychiatry* 89: 374-381

Keil C, Prell T, Peschel T, Hartung V, Dengler R, Grosskreutz J (2012) Longitudinal diffusion tensor imaging in amyotrophic lateral sclerosis. *BMC Neurosci* 13: 141

Kiernan MC, Vucic S, Cheah BC, Turner MR, Eisen A, Hardiman O, Burrell JR, Zoing MC (2011) Amyotrophic lateral sclerosis. *Lancet* 377: 942-55

Kwan JY, Meoded A, Danielian LE, Wu T, Floeter MK (2012) Structural imaging differences and longitudinal changes in primary lateral sclerosis and amyotrophic lateral sclerosis. *Neuroimage Clin* 2: 151-60

Mandelli ML, Berger MS, Bucci M, Berman JI, Amirbekian B, Henry RG (2014) Quantifying accuracy and precision of diffusion MR tractography of the corticospinal tract in brain tumors. *J Neurosurg* 121: 349-58

Menke RA, Agosta F, Grosskreutz J, Filippi M, Turner MR (2017) Neuroimaging Endpoints in Amyotrophic Lateral Sclerosis. *Neurotherapeutics* 14: 11-23

Menke RAL, Proudfoot M, Talbot K, Turner MR (2018) The two-year progression of structural and functional cerebral MRI in amyotrophic lateral sclerosis. *Neuroimage Clin* 17: 953-961

Muller HP, Turner MR, Grosskreutz J, Abrahams S, Bede P, Govind V, Prudlo J, Ludolph AC, Filippi M, Kassubek J, Neuroimaging Society in ALS DTISG (2016) A large-scale multicentre cerebral diffusion tensor imaging study in amyotrophic lateral sclerosis. *J Neurol Neurosurg Psychiatry* 87: 570-9

Novelli G, Papagno C, Capitani E, Laiacona M, Vallar G, Cappa S (1986) Tre test clinici di ricerca e produzione lessicale. Taratura su soggetti normali. *Archivio di Psicologia, Neurologia e Psichiatria* oct-dec; vol 47 (4) : 477-506.: 477-506

O'Dwyer L, Lambertson F, Bokde AL, Ewers M, Faluyi YO, Tanner C, Mazoyer B, O'Neill D, Bartley M, Collins R, Coughlan T, Prvulovic D, Hampel H (2012) Sexual

dimorphism in healthy aging and mild cognitive impairment: a DTI study. *PLoS One* 7: e37021

Rascovsky K, Hodges JR, Knopman D, Mendez MF, Kramer JH, Neuhaus J, van Swieten JC, Seelaar H, Dopper EG, Onyike CU, Hillis AE, Josephs KA, Boeve BF, Kertesz A, Seeley WW, Rankin KP, Johnson JK, Gorno-Tempini ML, Rosen H, Prigleau-Latham CE et al. (2011) Sensitivity of revised diagnostic criteria for the behavioural variant of frontotemporal dementia. *Brain* 134: 2456-77

Rathee R, Rallabandi VP, Roy PK (2016) Age-Related Differences in White Matter Integrity in Healthy Human Brain: Evidence from Structural MRI and Diffusion Tensor Imaging. *Magn Reson Insights* 9: 9-20

Reuter M, Schmansky NJ, Rosas HD, Fischl B (2012) Within-subject template estimation for unbiased longitudinal image analysis. *Neuroimage* 61: 1402-18

Schuster C, Elamin M, Hardiman O, Bede P (2016) The segmental diffusivity profile of amyotrophic lateral sclerosis associated white matter degeneration. *Eur J Neurol* 23: 1361-71

Schuster C, Hardiman O, Bede P (2017) Survival prediction in Amyotrophic lateral sclerosis based on MRI measures and clinical characteristics. *BMC Neurol* 17: 73

Schuster C, Kasper E, Machts J, Bittner D, Kaufmann J, Benecke R, Teipel S, Vielhaber S, Prudlo J (2014) Longitudinal course of cortical thickness decline in amyotrophic lateral sclerosis. *J Neurol* 261: 1871-80

Spinelli EG, Agosta F, Ferraro PM, Riva N, Lunetta C, Falzone YM, Comi G, Falini A, Filippi M (2016) Brain MR Imaging in Patients with Lower Motor Neuron-Predominant Disease. *Radiology* 280: 545-56

Steinbach R, Loewe K, Kaufmann J, Machts J, Kollwe K, Petri S, Dengler R, Heinze HJ, Vielhaber S, Schoenfeld MA, Stoppel CM (2015) Structural hallmarks of amyotrophic lateral sclerosis progression revealed by probabilistic fiber tractography. *J Neurol* 262: 2257-70

Turner MR, Cagnin A, Turkheimer FE, Miller CC, Shaw CE, Brooks DJ, Leigh PN, Banati RB (2004) Evidence of widespread cerebral microglial activation in amyotrophic lateral sclerosis: an [11C](R)-PK11195 positron emission tomography study. *Neurobiol Dis* 15: 601-9

van der Burgh HK, Schmidt R, Westeneng HJ, de Reus MA, van den Berg LH, van den Heuvel MP (2017) Deep learning predictions of survival based on MRI in amyotrophic lateral sclerosis. *Neuroimage Clin* 13: 361-369

van der Graaff MM, Sage CA, Caan MW, Akkerman EM, Lavini C, Majoie CB, Nederveen AJ, Zwinderman AH, Vos F, Brugman F, van den Berg LH, de Rijk MC, van Doorn PA, Van Hecke W, Peeters RR, Robberecht W, Sunaert S, de Visser M (2011) Upper and extra-motoneuron involvement in early motoneuron disease: a diffusion tensor imaging study. *Brain* 134: 1211-28

Verstraete E, van den Heuvel MP, Veldink JH, Blanken N, Mandl RC, Hulshoff Pol HE, van den Berg LH (2010) Motor network degeneration in amyotrophic lateral sclerosis: a structural and functional connectivity study. *PLoS One* 5: e13664

Verstraete E, Veldink JH, van den Berg LH, van den Heuvel MP (2014) Structural brain network imaging shows expanding disconnection of the motor system in amyotrophic lateral sclerosis. *Hum Brain Mapp* 35: 1351-61

Table 1. Demographic, clinical and cognitive characteristics at study entry in ALS patients and healthy controls (HC).

	ALS (n=50)	HC (n=47)	p
Sex, males (%)	35 (70%)	28 (60%)	0.30
Age at baseline (years)	59.8 ± 11.5	60.8 ± 8.1	0.66
Disease duration (months)	16.2 ± 10.3	-	-
ALSFRS-r at baseline [0-48]	41.5 ± 5.1	-	-
ALSFRS-r progression rate (decrease/month)	0.5 ± 0.4	-	-
Site of symptom onset (limb/bulbar)	40/10	-	-
El Escorial diagnosis at baseline (possible/probable lab-supported/probable/definite)	10/22/9/9	-	-
El Escorial diagnosis at last visit (possible/probable lab-supported/probable/definite)	0/4/28/18	-	-
Total MRC sum score [0-120]	108.0 ± 11.2	-	-
UMN score [0-16]	9.2 ± 4.6	-	-
MMSE (% of correct/administrable items)	96.7 ± 3.2	-	-
Phonemic fluency [normal range >17] (Novelli et al., 1986)	29.7 ± 9.4	-	-
Index PF	6.5 ± 2.9	-	-
Semantic fluency [normal range >25] (Novelli et al., 1986)	39.2 ± 9.2	-	-
Index SF	5.2 ± 3.6	-	-
Deceased or tracheotomized at censoring (%)	41 (82%)	-	-
Survival from onset (months)	46.2 ± 18.1	-	-
Survival from baseline visit (months)	30.6 ± 15.8	-	-

Values are reported as mean ± standard deviation or absolute and percentage frequency (%) for continuous and categorical variables, respectively. Differences between ALS patients and healthy controls were assessed using Mann-Whitney (for age), or Fisher test (for sex). **Abbreviations:** ALS= amyotrophic lateral sclerosis; ALSFRS-r= ALS functional rating scale, revised version; HC= healthy controls; MMSE= Mini Mental State Examination; MRC= Medical Research Council scale for muscular strength; PF= phonemic fluency; SF= semantic fluency; UMN= upper motor neuron.

Table 2. Mean DT MRI measures of the selected WM regions of interest (ROIs) in ALS patients and healthy controls (HC).

Variable	HC	ALS patients	<i>p</i>
FA CC-body	0.684 ± 0.04	0.664 ± 0.037	0.008
FA Bulbo-pontine CST	0.618 ± 0.035	0.599 ± 0.033	0.008
FA Cerebral peduncle	0.712 ± 0.023	0.69 ± 0.025	<0.001
FA Posterior internal capsule	0.69 ± 0.024	0.671 ± 0.025	<0.001
FA Superior corona radiata	0.49 ± 0.028	0.471 ± 0.022	<0.001
MD CC-body	0.84 ± 0.059	0.847 ± 0.057	0.600
MD Bulbo-pontine CST	0.685 ± 0.042	0.695 ± 0.03	0.212
MD Cerebral peduncle	0.718 ± 0.031	0.722 ± 0.032	0.639
MD Posterior internal capsule	0.704 ± 0.022	0.714 ± 0.024	0.048
MD Superior corona radiata	0.719 ± 0.028	0.736 ± 0.030	0.008
axD CC-body	1.641 ± 0.067	1.618 ± 0.067	0.06
axD Bulbo-pontine CST	1.21 ± 0.067	1.204 ± 0.067	0.553
axD Cerebral peduncle	1.425 ± 0.071	1.406 ± 0.055	0.082
axD Posterior internal capsule	1.374 ± 0.055	1.366 ± 0.044	0.293
axD Superior corona radiata	1.143 ± 0.047	1.151 ± 0.048	0.542
radD CC-body	0.449 ± 0.083	0.461 ± 0.063	0.428
radD Bulbo-pontine CST	0.432 ± 0.083	0.44 ± 0.03	0.610
radD Cerebral peduncle	0.367 ± 0.058	0.38 ± 0.031	0.206
radD Posterior internal capsule	0.377 ± 0.059	0.389 ± 0.027	0.255
radD Superior corona radiata	0.518 ± 0.08	0.529 ± 0.027	0.484

Values are reported as mean ± standard deviation. Differences between ALS patients and healthy controls were assessed using a Multivariate Analysis of Covariance (MANCOVA) test, adjusting for sex and age and applying Bonferroni correction. **Abbreviations:** ALS= amyotrophic lateral sclerosis; axD= axial diffusivity; CC= corpus callosum; CST= corticospinal tract; FA= fractional anisotropy; MD= mean diffusivity; HC= healthy controls; radD= radial diffusivity.

Table 3. Nonlinear mixed-effects model analyzing the longitudinal evolution of ALSFRS-r from baseline in ALS patients.

Parameter	Coefficient	SE	<i>p</i> value
<i>xmid (i.e., 50% decrease of ALSFRS-r)</i>			
Intercept	-43.833	28.454	0.013
Baseline FA of Cerebral peduncle	83.085	41.435	0.047
<i>Asym (i.e., starting value of ALSFRS-r)</i>			
Intercept	44.200	0.803	<0.001
Disease duration at baseline	-0.078	0.039	0.049
<i>Scale</i>	3.098	0.224	<0.001

Positive values of the estimated coefficients, in the submodel of the parameter *xmid*, indicate that 50% decrease of ALSFRS-r is reached later as the corresponding variable increases; whereas, in the submodel of the parameter *Asym*, positive values indicate that the starting value of ALSFRS-r is higher as the corresponding variable increases. **Abbreviations:** ALS= amyotrophic lateral sclerosis; ALSFRS-r= ALS Functional Rating Scale, revised version; CST= corticospinal tract; FA= fractional anisotropy; SE= standard error.

Figure 1. Flow-chart describing design of the study and follow-up of ALS patients.

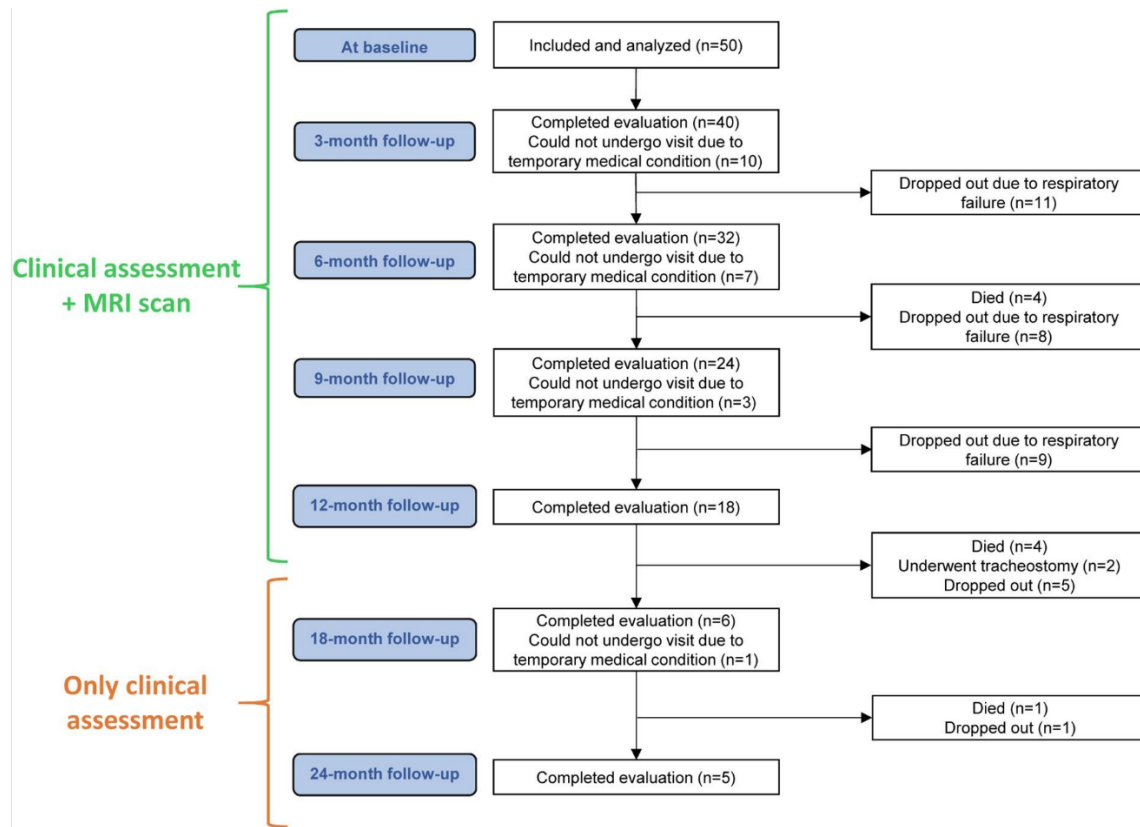


Figure 2. Results of white matter (WM) voxel-wise analysis: A) cross-sectional results of TBSS analysis comparing ALS patients with healthy controls at baseline; B) regions of significant decrease/increase of DT MRI metrics over time, as measured in terms of slopes of FA (red), MD (blue), axD (orange), or radD (violet) change; and C) regions of significant correlation between ALSFRS-r and FA decline over follow-up time. All results are superimposed on the WM skeleton of TBSS (light green) and on the Montreal Neurological Institute (MNI) template, thresholded at $p < 0.05$ FWE-corrected, and adjusted for age and sex. Results displayed in B) and C) are also adjusted for baseline ALSFRS-r values. **Abbreviations:** ALS= amyotrophic lateral sclerosis; ALSFRS-r= ALS Functional Rating Scale, revised version, axD= axial diffusivity; CST= corticospinal tract; DT= diffusion tensor; MD= mean diffusivity; radD= radial diffusivity; TBSS= Tract-based Spatial Statistics; WM= white matter.

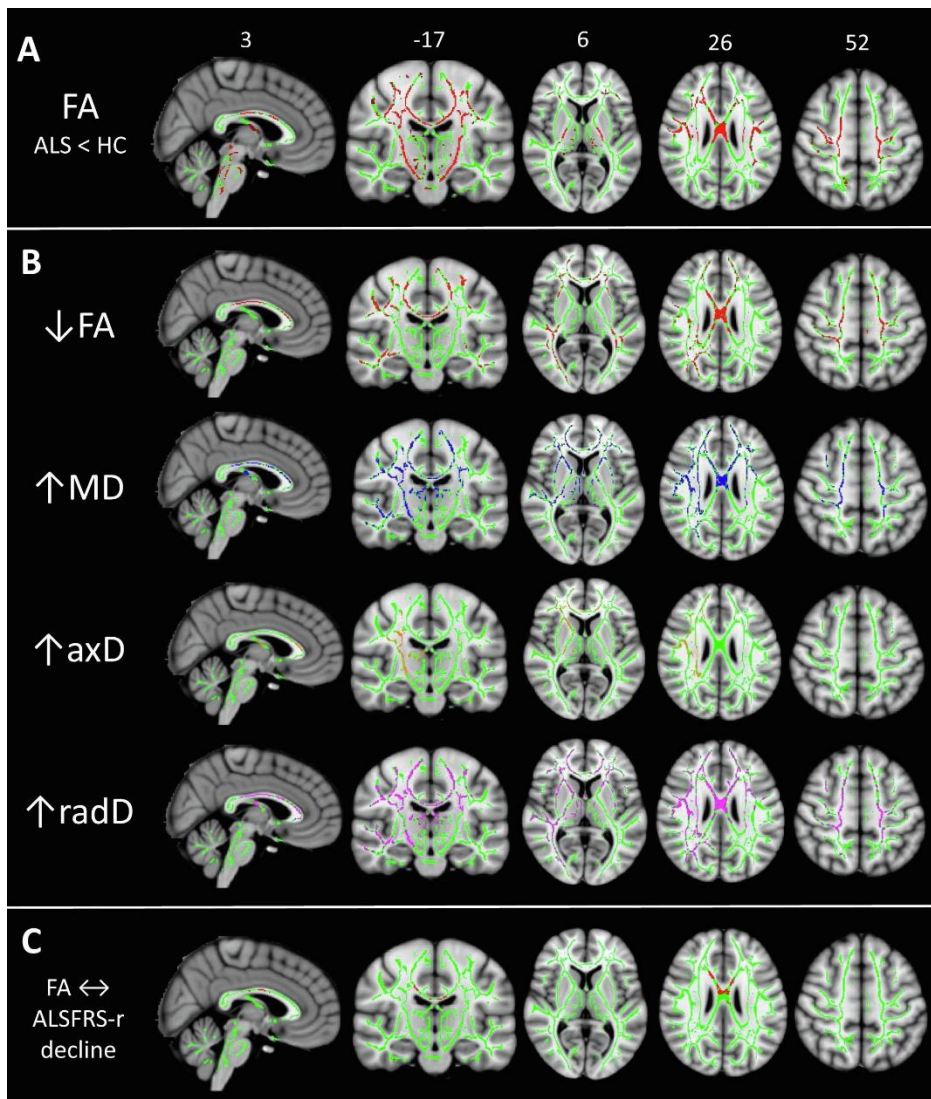


Figure 3. Regions of interest (ROIs) selected from the Johns Hopkins University (JHU) white-matter tractography atlas, superimposed on the Montreal Neurological Institute (MNI) template (in the top left corner), and plots showing the longitudinal evolution of FA for each selected ROI over follow-up time from baseline, together with the corresponding nonlinear mixed-effects model. Individual FA values are represented in grey for male patients and in orange for female patients, whereas the curves represent the estimated models by varying the values of some covariates in the model. When not specified, the covariates were set equal to the median value. **Abbreviations:** CC= corpus callosum; CST= corticospinal tract; DT= diffusion tensor; FA= fractional anisotropy; ROI= region of interest; WM= white matter.

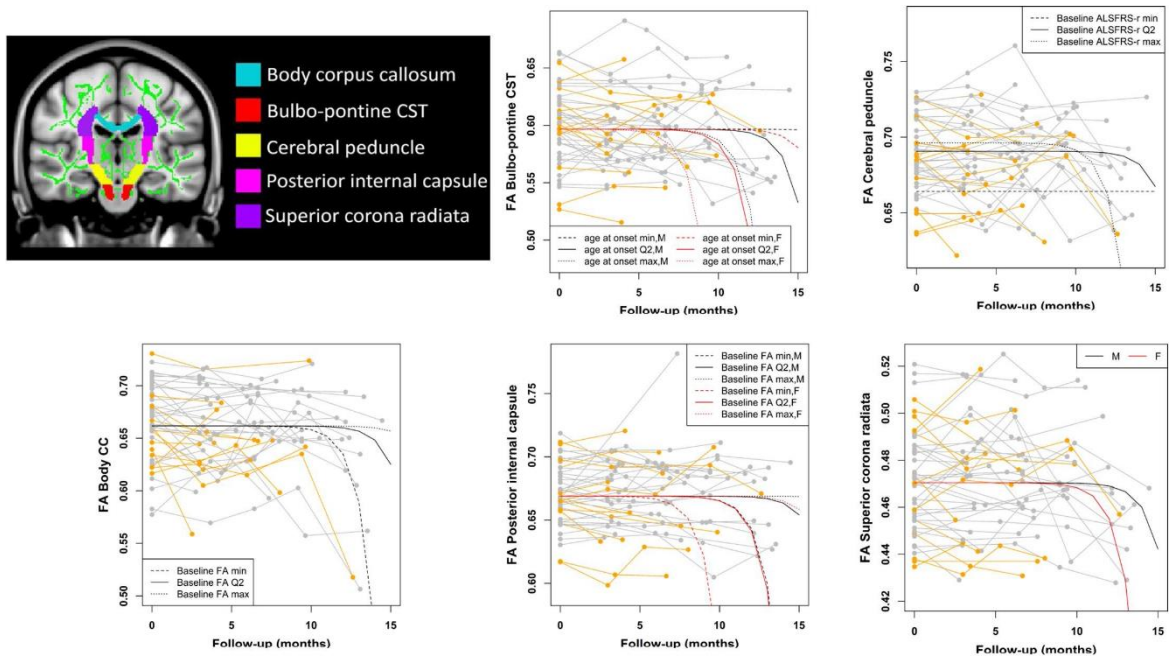
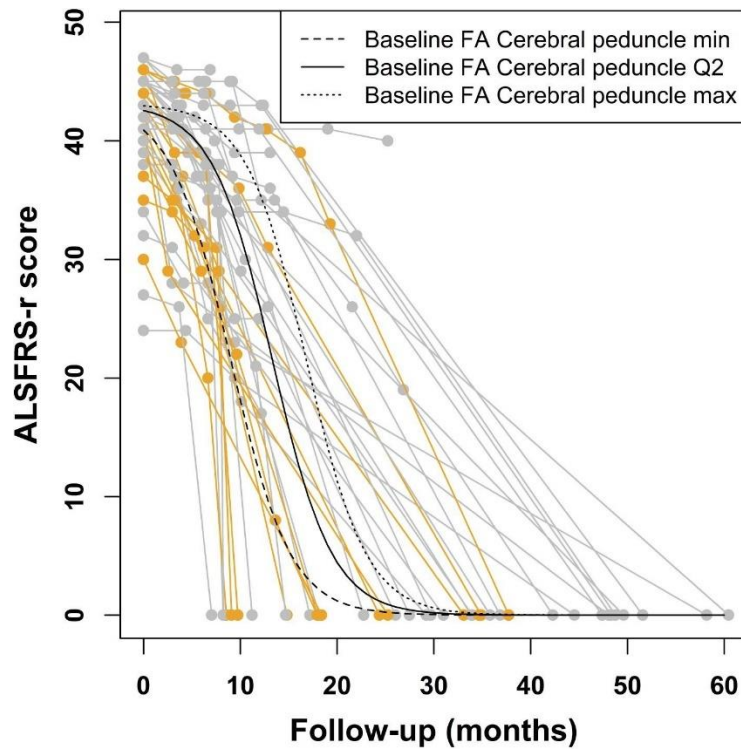


Figure 4. Nonlinear mixed-effects model describing the ALSFRS-r evolution over follow-up time from baseline. Individual scores are represented in grey for male patients and in orange for female patients, whereas the curves represent the estimated model by varying the baseline FA of the cerebral peduncle. **Abbreviations:** *ALSFRS-r*= *ALS Functional Rating Scale, revised version*; *CST*= *corticospinal tract*; *FA*= *fractional anisotropy*; *Q2*= *median*.



APPENDIX - Longitudinal models of DT MRI metrics

For all DT MRI measures the best model resulted to be the appropriate NLME model. The final NLME models for all the analyzed DT MRI measures are reported below. SE denotes the standard error in all the tables.

NLME model (Model 1): FA CC-body

Parameter	Coefficient	SE	P-value
<i>Asym</i>	0.662	0.005	<0.001
<i>xdec10</i>			
Intercept	2.091	11.734	0.859
Baseline FA value	30.650	8.240	<0.001
Baseline ALSFRS-r score	-0.383	0.163	0.021
Age at onset	0.157	0.039	<0.001

NLME model (Model 2): MD CC-body

Parameter	Coefficient	SE	P-value
<i>Asym</i>	0.853	0.008	<0.001
<i>xinc10</i>			
Intercept	92.688	9.994	<0.001
Baseline MD value	-121.127	13.123	<0.001
Age at onset	0.598	0.070	<0.001
Female sex	-7.012	1.217	<0.001

NLME model (Model 2): radD CC-body

Parameter	Coefficient	SE	P-value
<i>Asym</i>	0.467	0.009	<0.001
<i>xinc10</i>			
Intercept	9.833	1.028	<0.001
Baseline L23 value	-14.866	3.420	<0.001
Age at onset	0.187	0.032	<0.001

NLME model (Model 1): FA Bulbo-pontine CST

Parameter	Coefficient	SE	P-value
<i>Asym</i>	0.597	0.005	<0.001
<i>xdec10</i>			
Intercept	23.490	2.964	<0.001
Age at onset	-0.140	0.045	0.003
Female sex	-3.397	0.791	<0.001

NLME model (Model 2): MD Bulbo-pontine CST

Parameter	Coefficient	SE	P-value
<i>Asym</i>	0.696	0.004	<0.001
<i>xinc10</i>			
Intercept	40.579	10.321	<0.001
Baseline ALSFRS-r score	-0.585	0.226	0.011

NLME model (Model 2): radD Bulbo-pontine CST

Parameter	Coefficient	SE	P-value
<i>Asym</i>	0.445	0.004	<0.001
<i>xinc10</i>			
Intercept	14.774	0.558	<0.001
Female sex	-1.835	0.895	0.043

NLME model (Model 1): FA Cerebral peduncle

Parameter	Coefficient	SE	P-value
<i>Asym</i>			
Intercept	0.631	0.027	<0.001

Baseline ALSFRS-r score	0.001	0.001	0.031
<i>xdec10</i>			
Intercept	49.468	7.306	<0.001
Baseline ALSFRS-r score	-0.843	0.162	<0.001
Age at onset	0.047	0.019	0.016

NLME model (Model 2): MD Cerebral peduncle

Parameter	Coefficient	SE	P-value
<i>Asym</i>	0.723	0.004	<0.001
<i>xinc10</i>			
Intercept	52.241	12.076	<0.001
Baseline ALSFRS-r score	-0.838	0.261	0.002

NLME model (Model 2): radD Cerebral peduncle

Parameter	Coefficient	SE	P-value
<i>Asym</i>	0.383	0.004	<0.001
<i>xinc10</i>			
Intercept	45.671	8.294	<0.001
Baseline ALSFRS-r score	-0.716	0.18	<0.001

NLME model (Model 1): FA Posterior limb of the internal capsule

Parameter	Coefficient	SE	P-value
<i>Asym</i>	0.669	0.004	<0.001
<i>xdec10</i>			
Intercept	-12.211	17.88	0.496
Baseline FA value	68.817	30.584	0.027

Baseline ALSFRS-r score	-0.402	0.187	0.035
Female sex	-3.608	1.502	0.018

NLME model (Model 2): MD Posterior limb of the internal capsule

Parameter	Coefficient	SE	P-value
<i>Asym</i>	0.719	0.003	<0.001
<i>xinc10</i>			
Intercept	168.606	46.352	<0.001
Baseline ALSFRS-r score	-3.654	1.027	<0.001
Age at onset	0.285	0.077	<0.001

NLME model (Model 2): radD Posterior limb of the internal capsule

Parameter	Coefficient	SE	P-value
<i>Asym</i>	0.393	0.004	<0.001
<i>xinc10</i>			
Intercept	98.738	35.801	0.007
Baseline radD value	66.505	29.219	0.025
Baseline ALSFRS-r score	-2.575	0.858	0.004
Age at onset	0.124	0.055	0.028
Female sex	2.751	0.952	0.005

NLME model (Model 1): FA Superior corona radiata

Parameter	Coefficient	SE	P-value
<i>Asym</i>	0.470	0.003	<0.001
<i>xdec10</i>			
Intercept	15.510	0.475	<0.001

Female sex	-2.391	0.571	<0.001
------------	--------	-------	--------

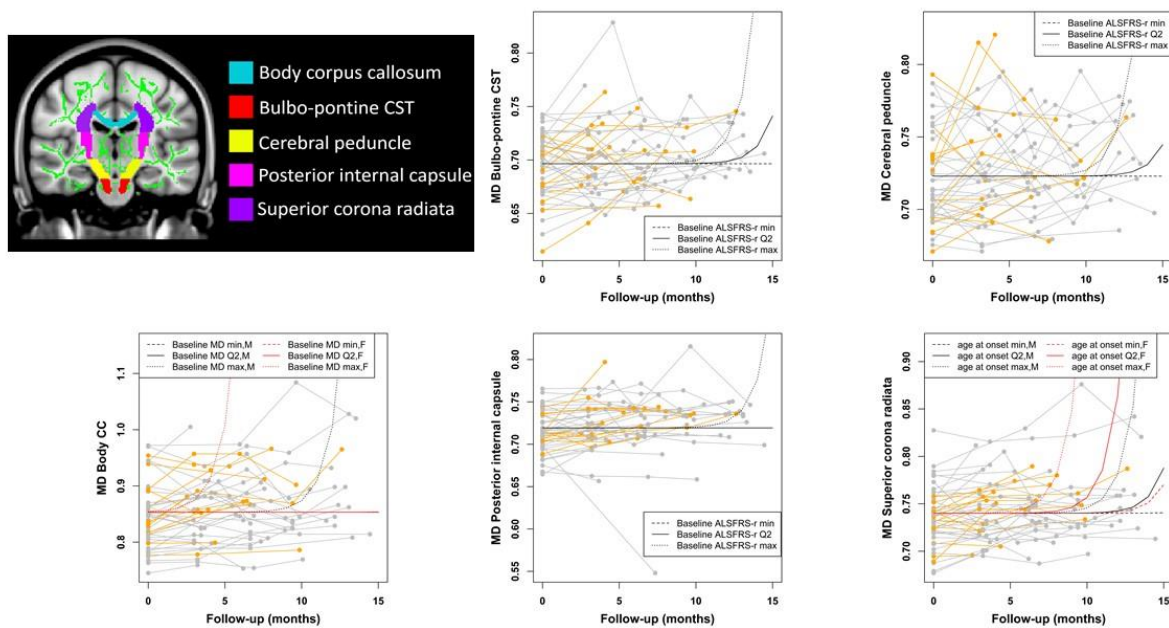
NLME model (Model 2): MD Superior corona radiata

Parameter	Coefficient	SE	P-value
<i>Asym</i>	0.740	0.004	<0.001
<i>xinc10</i>			
Intercept	23.355	2.349	<0.001
Age at onset	-0.130	0.036	<0.001
Female sex	-3.953	0.707	<0.001

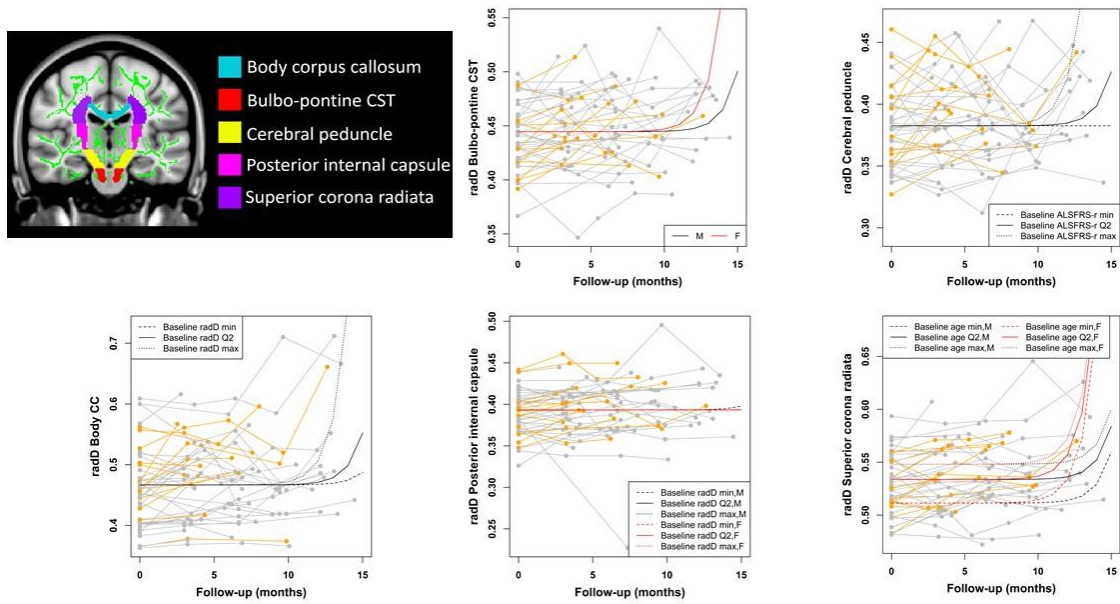
NLME model (Model 2): radD Superior corona radiata

Parameter	Coefficient	SE	P-value
<i>Asym</i>			
Intercept	0.493	0.020	<0.001
Age at baseline	0.001	0.000	0.044
<i>xinc10</i>			
Intercept	15.059	0.408	<0.001
Female sex	-2.223	0.531	0.001

Supplementary figure 1. Regions of interest (ROIs) selected from the Johns Hopkins University (JHU) white-matter tractography atlas, superimposed on the Montreal Neurological Institute (MNI) template (in the top left corner), and plots showing the longitudinal evolution of MD for each selected ROI over follow-up time from baseline, together with the corresponding nonlinear mixed-effects model. Individual MD values are represented in grey for male patients and in orange for female patients, whereas the curves represent the estimated models by varying the values of some covariates in the model. When not specified, the covariates were set equal to the median value. **Abbreviations:** CC= corpus callosum; CST= corticospinal tract; DT= diffusion tensor; MD = mean diffusivity; ROI= region of interest; WM= white matter.



Supplementary figure 2. Regions of interest (ROIs) selected from the Johns Hopkins University (JHU) white-matter tractography atlas, superimposed on the Montreal Neurological Institute (MNI) template (in the top left corner), and plots showing the longitudinal evolution of radD for each selected ROI over follow-up time from baseline, together with the corresponding nonlinear mixed-effects model. Individual radD values are represented in grey for male patients and in orange for female patients, whereas the curves represent the estimated models by varying the values of some covariates in the model. When not specified, the covariates were set equal to the median value. **Abbreviations:** CC= corpus callosum; CST= corticospinal tract; DT= diffusion tensor; radD = radial diffusivity; ROI= region of interest; WM= white matter.



3.4. Structural and functional brain connectome in motor neuron diseases: a multicenter MRI study

ARTICLE OPEN ACCESS

Structural and functional brain connectome in motor neuron diseases

A multicenter MRI study

Silvia Basaia, PhD, Federica Agosta, MD, PhD, Camilla Cividini, MSc, Francesca Trojsi, MD, PhD, Nilo Riva, MD, PhD, Edoardo G. Spinelli, MD, Cristina Moglia, MD, PhD, Cinzia Femiano, MD, Veronica Castelnuovo, MSc, Elisa Canu, PhD, Yuri Falzone, MD, Maria Rosaria Monsurro, MD, Andrea Falini, MD, Adriano Chiò, MD, Gioacchino Tedeschi, MD, and Massimo Filippi, MD

Correspondence
Prof. Filippi
filippi.massimo@hsr.it

Neurology® 2020;95:e2552-e2564. doi:10.1212/WNL.0000000000010731

Abstract

Objective

To investigate structural and functional neural organization in amyotrophic lateral sclerosis (ALS), primary lateral sclerosis (PLS), and progressive muscular atrophy (PMA).

Methods

A total of 173 patients with sporadic ALS, 38 patients with PLS, 28 patients with PMA, and 79 healthy controls were recruited from 3 Italian centers. Participants underwent clinical, neuropsychological, and brain MRI evaluations. Using graph analysis and connectomics, global and lobar topologic network properties and regional structural and functional brain connectivity were assessed. The association between structural and functional network organization and clinical and cognitive data was investigated.

Results

Compared with healthy controls, patients with ALS and patients with PLS showed altered structural global network properties, as well as local topologic alterations and decreased structural connectivity in sensorimotor, basal ganglia, frontal, and parietal areas. Patients with PMA showed preserved global structure. Patient groups did not show significant alterations of functional network topologic properties relative to controls. Increased local functional connectivity was observed in patients with ALS in the precentral, middle, and superior frontal areas, and in patients with PLS in the sensorimotor, basal ganglia, and temporal networks. In patients with ALS and patients with PLS, structural connectivity alterations correlated with motor impairment, whereas functional connectivity disruption was closely related to executive dysfunction and behavioral disturbances.

Conclusions

This multicenter study showed widespread motor and extramotor network degeneration in ALS and PLS, suggesting that graph analysis and connectomics might represent a powerful approach to detect upper motor neuron degeneration, extramotor brain changes, and network reorganization associated with the disease. Network-based advanced MRI provides an objective in vivo assessment of motor neuron diseases, delivering potential prognostic markers.

The following data have been published (Basaia et al., Neurology. 2020 Nov 3;95(18):e2552-e2564. doi: 10.1212/WNL.0000000000010731).

INTRODUCTION

Motor neuron diseases (MND) are progressive neurodegenerative conditions characterized by the breakdown of the motor system. The involvement of the upper motor neurons (UMN) and/or lower motor neurons (LMN) defines different clinical phenotypes, including amyotrophic lateral sclerosis (ALS), primary lateral sclerosis (PLS) and progressive muscular atrophy (PMA) (Norris, Shepherd et al., 1993). Compared with ALS, PLS and PMA patients are characterized by a slower rate of progression and a more benign prognosis (Chio et al., 2011).

Validation of noninvasive biomarkers to characterize different MND phenotypes is a challenge of growing importance in order to recognize subjects known to be at risk of more rapid progression (i.e., conversion to the ALS phenotype) prior to the appearance of clinically apparent disease. Brain magnetic resonance imaging (MRI) has shown to be promising, over the last decades, to detect *in vivo* structural and functional brain abnormalities and to monitor degeneration within the central nervous system of MND patients (Basaia, Filippi et al., 2019). To date, it is of great relevance to evaluate whether MRI biomarkers are suitable and reliable in a multicenter context.

In ALS patients, many diffusion tensor (DT) MRI studies have consistently identified structural alterations in a “signature” white matter (WM) region involving the corticospinal tract (CST) and the middle and posterior parts of the corpus callosum (Muller et al., 2016). DT MRI has proven useful in distinguishing MND variants (Agosta et al., 2014b, Rosenbohm et al., 2016, Spinelli et al., 2016), as PLS patients showed more widespread DT MRI damage compared to ALS (Agosta et al., 2014b), whereas the least diffuse WM damage was observed in patients with predominant LMN involvement (Rosenbohm et al., 2016, Spinelli et al., 2016).

In ALS, resting-state functional MRI (RS fMRI) studies reported inconsistent results, showing either decreased or increased functional connectivity in the premotor, motor and subcortical regions (Agosta et al., 2014a, Menke, Proudfoot et al., 2016). To date, other MND phenotypes are yet to be explored using RS fMRI, as only one study reported increased functional connectivity within the sensorimotor, frontal, and left frontoparietal networks of PLS patients (Agosta et al., 2014a), and no studies assessed brain functional underpinnings of PMA.

In the last decade, neuroimaging research has zeroed in on the study of changes in structural and functional connectivity at a whole-brain-system level, rather than on alterations in single brain regions (Bullmore & Sporns, 2009), applying the ‘graph theory’ analysis (Tijms, Wink et al., 2013). It has been widely demonstrated that this approach is a powerful tool to measure structural and functional reorganization in neurodegenerative diseases (van den Heuvel & Sporns, 2019), including ALS (Geevasinga et al., 2017, Verstraete et al., 2014). To date, no studies used graph analysis and connectomics to investigate structural and functional networks in different phenotypes of MND. In addition, previous network-based studies involved single-center cohorts, thus limiting the generalizability of findings.

Considering this background, the aim of the present study was to investigate structural and functional neural organization in ALS, PLS and PMA patients using graph analysis and connectomics. One of the main novelties of our study was the use of data from different centers, neuroimaging protocols and scanners, in order to reach both reliability and reproducibility of results.

METHODS

The present work is a prospective and multicenter study. Subjects were recruited and clinically evaluated at three Italian ALS centers (San Raffaele Scientific Institute, Milan; Azienda Ospedaliera Città della Salute e della Scienza, Turin; and Università degli Studi della Campania “Luigi Vanvitelli”, Naples) from 2009 to 2017 in the framework of a large, observational study. MRI scans were obtained from all participants using two 3T scanners: Philips Medical Systems Intera machine (for Milan and Turin patients) and GE Signa HDxt machine (for Naples patients). All MRI data were analyzed at the Neuroimaging Research Unit, Division of Neuroscience, San Raffaele Scientific Institute and Vita-Salute San Raffaele University, Milan, Italy.

Participants

239 sporadic MND patients (173 cases with classic ALS, 38 with PLS, and 28 with PMA) were consecutively recruited from those routinely evaluated at the three clinical centers (Table 1). Classic ALS patients (131 from Milan/Turin and 42 from Naples) met a diagnosis of probable or definite ALS according to the revised El Escorial criteria

(Brooks et al., 2000). Thirty-eight patients (all from the Milan/Turin dataset) were diagnosed as PLS according to Pringle's criteria at the last available clinical follow up (Pringle et al., 1992). Twenty-eight patients had PMA (all from the Milan/Turin dataset) (van den Berg-Vos et al., 2003). All patients were receiving riluzole at study entry. Seventy-nine age- and sex-matched healthy controls (61 from Milan/Turin and 18 from Naples) were recruited by word of mouth (Table 1), based on the following criteria: normal neurological assessment; mini mental state examination (MMSE) score ≥ 28 ; no family history of neurodegenerative diseases. Exclusion criteria for all subjects (i.e., patients and healthy controls) were: medical illnesses or substance abuse that could interfere with cognitive functioning; any (other) major systemic, psychiatric, or neurological diseases; other causes of brain damage, including lacunae and extensive cerebrovascular disorders at MRI.

Disease severity was assessed using the ALS Functional Rating Scale-revised (ALSFRS-r) (Cedarbaum et al., 1999). The baseline rate of disease progression was defined according to the following formula: $(48 - \text{ALSFRS-r score}) / \text{time between symptom onset and first visit}$. Muscular strength was assessed by manual muscle testing based on the Medical Research Council (MRC) scale, and clinical upper motor neuron (UMN) involvement was graded by totaling the number of pathological UMN signs on examination (Turner et al., 2004). For the UMN score, we also considered the presence of non-definite UMN signs such as reduced, but still evocable reflexes in muscles with LMN signs, which were detected in few PMA individuals.

Standard Protocol Approvals, Registrations, and Patient Consents

Local ethical standards committee on human experimentation approved the study protocol and all participants provided written informed consent (Ethical committee numbers: RF-2011-02351193 and ConnectALS).

Neuropsychological assessment

Neuropsychological assessments were performed by experienced neuropsychologists unaware of the MRI results (Additional Table 1). The following cognitive functions were evaluated: global cognitive functioning with the MMSE (Folstein et al., 1975); long and short term verbal memory with the Rey Auditory Verbal Learning Test (Carlesimo et al.,

1996) and the digit span forward (Orsini et al., 1987), respectively; executive functions with the digit span backward (Monaco et al., 2013), the Stroop interference test (Barbarotto, Laiacona et al., 1998), the Cognitive Estimation Task (Della Sala et al., 2003), the Weigl's Sorting test (Tognoni, 1987), the Wisconsin Card Sorting Test (Laiacona et al., 2000) or the Modified Card Sorting Test (Caffarra, Vezzadini et al., 2004), and the Raven's coloured progressive matrices (Basso et al., 1987); fluency with the phonemic and semantic fluency tests (Carlesimo et al., 1996, Novelli, 1986, Tognoni, 1987) and the relative fluency indices (controlling for individual motor disabilities) (Abrahams et al., 2000); language with the Italian battery for the assessment of aphasic disorders (Miceli, neuropsicologia et al., 1994b). Mood was evaluated with the Hamilton depression rating scale (Hamilton, 1960) or Beck Depression Inventory (Beck, Ward et al., 1961). The presence of behavioral disturbances was assessed with the Frontal Behavioral Inventory (Alberici et al., 2007) and the Amyotrophic Lateral Sclerosis-Frontotemporal Dementia-Questionnaire (ALS-FTD-Q) (Raaphorst et al., 2012) administered to patients' caregivers. Healthy controls underwent the entire assessment except for the Stroop interference test, the Cognitive Estimation Task and the Weigl's Sorting test.

MRI analysis

Using two 3T MR scanners, T1-weighted, T2-weighted, fluid-attenuated inversion recovery, DT MRI and RS fMRI sequences were obtained from all participants (, Additional Table 2 for MRI sequence parameters). An experienced observer, blinded to participants' identity and diagnosis, performed MRI analysis. Grey matter (GM) was parcellated into 220 similarly-sized brain regions, which included cerebral cortex and basal ganglia but excluded the cerebellum (Figure 1-Ia) (Filippi, Basaia et al., 2017). DT MRI and RS fMRI pre-processing and construction of brain structural and functional connectome have been described previously (Filippi, Basaia et al., 2020) (Figure 1-Ia and Ib).

Global brain and lobar network analysis

Global and mean lobar structural and functional network characteristics were explored using the Brain Connectivity Matlab toolbox (<http://www.brain-connectivity->

toolbox.net). Network metrics, including nodal strength, characteristic path length, local efficiency and clustering coefficient were assessed to characterize the topological organization of global brain and lobar networks in patients and healthy controls (Figure 1-II). (Sporns & Zwi, 2004) In order to investigate the network characteristics in different areas of the brain, the 220 regions of interest (ROIs) from both hemispheres were grouped into six anatomical macro-areas (hereafter referred to as brain lobes): temporal, parietal, occipital, fronto-insular, basal ganglia, and sensorimotor areas (Filippi et al., 2017). Structural network properties were generated according to fractional anisotropy (FA) values, while analysis of brain network function was based on functional connectivity strength values (z-transformed Pearson's correlation coefficients). Global and lobar metrics were compared between groups using age-, sex- and MR scanner-adjusted ANOVA models, followed by post-hoc pairwise comparisons, Bonferroni-corrected for multiple comparisons ($p < 0.05$, SPSS Statistics 22.0). In addition, to evaluate the effect of the full-blown dementia patients into the results, the analyses were performed also without the eight ALS-FTD patients. Furthermore, the comparison between ALS and controls subjects, recruited only from Milan/Turin centers, was performed in order to assess the reproducibility of the findings when MRI were obtained using a single MR scanner.

Connectivity analysis

Network Based Statistics (NBS) (Zalesky, Fornito et al., 2010a) were performed to assess regional FA and functional connectivity strength network data in patients and controls at the level of significance $p < 0.05$ (Figure 1-III). The largest (or principal) connected component and the smaller clusters of altered connections, which were not included in the principal component, were studied (Galantucci, Agosta et al., 2017, Zalesky et al., 2010a). A corrected p value in the direct comparison between ALS patients and healthy controls (both provided by Milan/Turin and Naples centers) was calculated for each component using an age-, sex-, and MR scanner-adjusted permutation analysis (10000 permutations). Regarding the other comparisons, only MND patients and controls from Milan/Turin centers were included in the age- and sex-adjusted permutation analysis. In line with previous global and lobar network analysis, NBS was performed

also excluding ALS-FTD patients and ALS/controls subjects recruited at the Naples center.

Correlation analysis

To assess the relationship between structural and functional brain network properties and clinical and neuropsychological variables, correlation analysis was performed in each patient group. Partial correlations between MRI measures (exhibiting significant differences between patients and controls), clinical variables and cognitive data were estimated using Pearson's correlation coefficient (R), at the level of significance $p < 0.05$ (Figure 1-IV). Correlation analyses were adjusted for age, sex (in PLS patients) and age, sex, and MR scanner (in ALS patients). Relationship with neuropsychological data were also adjusted for education and ALSFRS-r. Correlation analyses at global/lobar and regional level were also controlled for multiple comparisons, applying respectively Bonferroni and false discovery rate (FDR) adjustment.

Data availability

The dataset used and analyzed during the current study will be made available by the corresponding author upon request to qualified researchers (i.e., affiliated to a university or research institution/hospital).

RESULTS

A summary of structural and functional altered metrics at global, lobar and regional levels in the different MND phenotypes has been reported in Table 2.

ALS vs healthy controls

Compared to healthy controls, ALS patients showed altered structural global network properties (lower mean local efficiency) (Additional Table 3). ALS patients showed a reduced mean structural local efficiency in the sensorimotor, basal ganglia and frontal networks and longer path length in basal ganglia, frontal and temporal networks relative to healthy controls (Figure 2; Additional Table 4). They showed also reduced mean nodal strength in frontal and temporal regions relative to controls (Figure 2; Additional Table 4). ALS patients had preserved global and lobar functional nodal properties compared to

controls (Additional Tables 3 and 4). NBS showed structural changes in ALS patients relative to controls: decreased FA in the sensorimotor networks, including precentral and postcentral gyri, supplementary motor area and basal ganglia, and among the connections of the medial and lateral prefrontal cortex (Figure 3A). ALS patients showed also increased functional connectivity compared to controls involving precentral gyrus, middle and superior frontal gyri (Figure 3B). The listed results were confirmed excluding from the analysis ALS-FTD patients (Additional Table 5 and Figure 1) or ALS and healthy controls acquired at the Naples center (Additional Table 6 and Figure 2).

PLS vs healthy controls

Compared to healthy controls, PLS patients showed altered structural global network properties (lower mean local efficiency and clustering coefficient, longer mean path length) (Additional Table 3). PLS patients showed a reduced mean structural local efficiency and clustering coefficient and longer path length in the sensorimotor, basal ganglia, frontal and parietal areas relative to healthy controls (Figure 2; Additional Table 4). PLS patients had a relatively preserved global and lobar functional nodal properties compared to controls (Figure 2; Additional Tables 3 and 4). Using NBS, widespread structural changes were observed in PLS patients relative to controls: decreased FA within the sensorimotor networks, including precentral and postcentral gyri, supplementary motor area and basal ganglia, and among connections within temporal and occipito-parietal areas (Figure 3A). NBS analysis showed that PLS patients had higher functional connectivity in the sensorimotor, basal ganglia and temporal networks relative to controls (Figure 3B). PLS structural and functional damage mimics the one observed in classical ALS (Figure 4).

PMA vs healthy controls

PMA patients did not show differences in structural and functional graph and connectivity properties at both global and regional level (Figures 2 and 3; Additional Tables 3 and 4).

ALS vs PLS

ALS and PLS patients did not show differences in structural and functional graph properties at global level (Additional Table 3). PLS patients demonstrated altered local structural, but not functional, alterations in sensorimotor network relative to ALS group (longer path length) (Figure 2; Additional Table 4). NBS did not show differences between ALS and PLS patients (Figure 3). These findings were confirmed excluding ALS-FTD patients from the analysis (Additional Table 5 and Figure 1).

ALS vs PMA

ALS and PMA patients did not show differences in structural and functional graph properties at both global and lobar level (Figure 2; Additional Tables 3 and 4). However, ALS patients showed decreased FA relative to PMA cases within the sensorimotor network including precentral and postcentral gyri and frontal network (Figure 3A). NBS did not show functional connectivity differences between ALS and PMA patients (Figure 3B). The presented results have been validated excluding ALS-FTD patients from the analysis (Additional Table 5 and Figure 1).

PLS vs PMA

PLS and PMA patients did not show differences in structural and functional graph properties at global level (Additional Table 3). PLS patients demonstrated altered local structural, but not functional, alterations in sensorimotor and frontal networks relative to PMA group (lower mean local efficiency and clustering coefficient and longer mean path length) (Figure 2; Additional Table 4). In the NBS analysis, PLS patients showed decreased FA relative to PMA cases in the connections within and among sensorimotor network basal ganglia, frontal and parieto-occipital areas (Figure 3A). NBS did not show functional connectivity differences between PLS and PMA patients (Figure 3B).

Correlation analysis

In ALS patients, graph analysis structural brain changes mostly correlated with clinical disease severity (Figure 5A). Indeed, a longer path length was related to disease progression rate (Δdp) both at the global ($R= 0.25$, $p= 0.01$) and lobar levels, particularly within sensorimotor ($R= 0.23$, $p= 0.01$), basal ganglia ($R= 0.22$, $p= 0.02$) and frontal-insular ($R= 0.22$, $p= 0.02$) networks. Moreover, structural local efficiency in parietal

network correlated negatively with Δdp ($R = -0.20$, $p = 0.03$) and positively with ALSFRS-r score ($R = 0.29$, $p < 0.001$). Regarding regional analysis, in ALS patients, a decreased FA of the connections within temporal network correlated with a worse performance in global cognition ($R = 0.36$, $p = 0.03$), while a higher disruption within the sensorimotor areas correlated with longer disease duration (R ranging from -0.51 to -0.28 , $p < 0.05$) and greater disease severity (R ranging from -0.34 to 0.30 , $p < 0.05$). In ALS patients, functional connectivity changes within basal ganglia network and connections between basal ganglia and premotor areas correlated with disease progression (R ranging from -0.60 to 0.24 , $p < 0.05$). Moreover, higher functional connectivity, within extra-motor areas (temporo-frontal network), correlated with worse performance at executive ($R = 0.37$, $p = 0.01$) and behavioral tests ($R = 0.50$, $p = 0.04$). In PLS patients, disrupted structural connections within motor and premotor areas correlated with lower ALSFRS-r scores ($R = 0.56$, $p = 0.02$) (Figure 5B). On the other hand, functional connectivity alterations were more related to cognitive performance. Particularly, functional clustering coefficient correlated with executive dysfunctions within basal ganglia network ($R = -0.65$, $p = 0.04$). Moreover, higher functional connectivity of the connections among temporal and frontal areas correlated with a worse performance at behavioral test (R ranging from 0.65 to 0.72 , $p < 0.05$). Correlations were not assessed in the PMA group since no significant structural and functional differences were found in the previous analyses relative to controls.

DISCUSSION

Using graph analysis and connectomics to explore structural and functional brain networks, the present multicenter study showed that clinical variants within the MND spectrum result in different patterns of brain network changes. ALS patients showed altered structural global and lobar network properties and regional connectivity, with a specific involvement of sensorimotor, basal ganglia, frontal and temporal areas. On the same line, the structural damage in the PLS group was found in the sensorimotor network, together with a more widespread damage in extra-motor regions, such as the parietal lobe. On the contrary, PMA patients showed preserved structural and functional connectomes. Finally, in both ALS and PLS groups, alterations in structural connectivity correlated with measures of motor impairment, while functional connectivity disruptions were mostly

related to executive dysfunctions and behavioral disturbances. These results proved to be independent of the presence of full-blown dementia, being confirmed also excluding eight ALS-FTD patients from the analyses.

To date, several MRI studies have highlighted structural (Muller et al., 2016, Spinelli et al., 2016) and/or functional (Agosta et al., 2014a, Menke et al., 2016) ‘signatures’ of different phenotypes within the MND spectrum. However, while DT MRI studies have described consistent results, the literature of functional studies have reported inconsistent findings. Moreover, the above-mentioned studies have zeroed in on the study of structural and functional alterations at a voxel or regional level, rather than on alterations at brain-system level (Bullmore & Sporns, 2009). In order to overcome this limitation, the present study has applied advanced network-based neuroimaging techniques, aiming to provide information about how networks are embedded and interact in the brain of different phenotypes within the MND spectrum, deepening previous findings of standard MRI techniques. Whereas whole-brain approaches might detect alterations at voxel or regional level, connectome analysis considers the relationships between degenerating connections and is able to provide connectivity information about the integrated nature of brain (Crossley, Mechelli et al., 2014). Another advantage of this new approach is that it may help in bridging the gap between different types of data, such as anatomical and functional connectivity. In fact, the use of a common parcellating system and the same statistical approach allows a straightforward comparison between the two types of information.

Up to date, graph analysis and connectomics have already been applied to characterize structural and functional damage in ALS patients. Particularly, our findings are consistent with previous DT MRI studies that reported the presence of an impaired subnetwork including bilateral primary motor regions, supplementary motor areas and basal ganglia (Buchanan et al., 2015). Furthermore, our study highlights that affected extra-motor regions are structurally connected to the sensorimotor network, known to be the “epicenter” of the degenerative process of the disease (Brettschneider et al., 2013). This hypothesis is consistent with the pattern of progression of TDP-43 pathological burden described by Brettschneider et al. (Brettschneider et al., 2013) in *post mortem* tissue, and supports a network-based degeneration model in ALS (Seeley, Crawford et al., 2009), although longitudinal MRI studies are needed to validate this hypothesis.

On the other hand, very few RS fMRI studies applied network-based analyses on ALS patients, demonstrating complex connectivity alterations encompassing frontal, temporal, occipital and subcortical regions (Geevasinga et al., 2017, Zhou et al., 2016). In our study, we found increased functional connectivity in sensorimotor, basal ganglia and frontal areas in ALS patients. Our results are mostly consistent with previous studies, although showing more focal functional rearrangements, possibly due to differences in disease stage and methodology (as in our study only functional edges with existing structural connections were considered). Although our study confirms previous findings, our strength is the application of advanced neuroimaging techniques in an unprecedented number of ALS patients due to the fact that is a multicenter study. In light of this, the great number of patients have a strong impact on the statistical power of the analysis and influenced the quality and reliability of our results. Of note, this is the first study that applied graph theory in patients with PLS and PMA. Particularly, PLS patients showed widespread structural and functional alterations encompassing both motor and extra-motor areas with a pattern resembling classic ALS patients (Figure 4), in line with previous studies (Agosta et al., 2014b, Muller, Agosta et al., 2018a). By contrast, PMA patients did not show any structural or functional damage relative to healthy controls. These findings are in line with previous studies that could not demonstrate central nervous system damage in PMA patients (Rosenbohm et al., 2016, Spinelli et al., 2016), even using a technique that is highly sensitive to local disruptions in the brain networks. Therefore, here we have demonstrated the high sensitivity of graph-based analysis to detect different disease related disconnection patterns and its potential use to facilitate clinical diagnosis and offer new insights into syndromes' clinical diversity.

Noteworthy, ALS and PLS patients are characterized by more widespread structural than functional damage relative to healthy controls (Figure 3). The presence of functionally unaffected, but structurally impaired nodes and connections in both groups suggests that structural alterations may be earlier in the course of the disease compared with functional network abnormalities. In keeping with the network-based hypothesis (Jucker & Walker, 2013), pathological alterations physically spread along neuroanatomical connections in the brain; therefore, it is reasonable to speculate that functional connectivity alterations may follow the structural disruption of the brain network. These findings are also in line with those recently observed in other

neurodegenerative diseases (Filippi et al., 2020). However, it should also be considered that this cross-sectional study cannot fully address the temporal sequence or causal relationships between structural and functional abnormalities, and different techniques (i.e., DT MRI and RS fMRI) may intrinsically show different sensitivities to underlying biological processes.

In the present study, the regional (i.e., NBS) analysis showed greater sensitivity for the detection of structural and, particularly, functional damage of brain networks, compared with the evaluation of single network properties. Moreover, the results of the global/lobar structural analysis provided some apparent inconsistencies across different network measures. For example, although structural nodal strength did not show significant alterations in the sensorimotor regions of MND patients compared with healthy controls, all other graph theoretical measures (i.e., local efficiency, clustering coefficient and path length) did. Given the inter-dependence of these measures, and the fact that nevertheless nodal strength was on average lower than healthy controls in all MND groups, we argue that nodal strength might simply be less sensitive than other measures to the structural disruption of the sensorimotor network in our cohort. This might differ in other anatomical areas with different topological organization, such as the temporal regions (which are also affected in MND), where nodal strength and path length were significantly altered in ALS patients, in contrast with the sparing of other network properties. Therefore, our results support the utility of graph theoretical measures used in combination, rather than as single measures, also considering the current impossibility of establishing a clear-cut neuropathological substrate for each of these.

Concerning the correlation analysis, our findings suggest that the presence of structural damage in ALS patients in motor, premotor and parietal regions, key elements for the correct programming and processing/execution of the movement, is specifically related to clinical measures of motor impairment, rate of progression and disease duration. Particularly, the rate of progression was more closely related to global and lobar alterations, while measures of disease severity and duration were associated with regional connectivity disruption, although correlation coefficients were generally moderate in size (0.2 to 0.4). By contrast, the (possibly, maladaptive) increase of functional connectivity in frontal and temporal regions was related to executive dysfunctions and behavioral impairment, as previously shown (Agosta et al., 2014a). PLS patients showed a similar

pattern of correlations, although with a lower number of significant findings, partly due to the small sample size. Nevertheless, a strong relationship between functional connectivity in extra-motor areas and behavioral impairment was found, to point out that the cognitive profile in PLS patients traced the one in ALS patients, with more prominent deficits in the behavioral domain.

One of the most important caveats of previous studies is the single-center origin of imaging data that limits the generalizability of findings. In light of this, one of the main novelties of our study was including data from different centers, neuroimaging protocols and scanners. Although MRI protocols were not harmonized between the two acquisition centers, the obtained results proved to be solid (as shown by the single-center sub-analysis) and the approach was easily reproducible despite protocol differences. On the other hand, this study is not without limitations. First, the PLS and PMA groups were relatively small, affecting the statistical power of the results. In particular, the absence of differences between PMA patients and healthy controls might partially depend on the relatively small sample size. However, PMA also showed significant structural sparing compared with both ALS and PLS patients, consistent with previous studies performed using different techniques (Rosenbohm et al., 2016, Spinelli et al., 2016), as well as with the common notion of PMA as a predominant lower motor neuron disease. Second, cognitive test scores were not available for all patients. However, we selected tests for which patient samples were sufficiently represented. Third, healthy controls showed higher education than ALS and PLS patients, although the analyses involving neuropsychological data were adjusted for education. Fourth, we chose arbitrarily to parcellate the brain into 220 similarly sized regions based on the Automated Anatomical Labeling (AAL) atlas, excluding the cerebellum. Technically, network science applied to the human brain has yet to reach consensus regarding the best way to divide the brain into its most relevant anatomical units (Zalesky, Fornito et al., 2010b) as well as to threshold connectivity matrices (van den Heuvel, de Lange et al., 2017). The definition of an optimal framework has not yet been reached in the neuroscience community, and the field of network data analysis remains an area of active methodological development. However, it is generally acknowledged that similarly sized regions of interest avoid larger regions to have higher connectivity because of their larger surface. The exclusion of the cerebellum was motivated by the fact that the AAL atlas is rather inaccurate to segment

this anatomical region, and other, unbiased *ad-hoc* methods should be preferred in future studies. Fifth, although RS-fMRI data were carefully registered to and masked with GM maps to avoid a regional atrophy influence, a possible partial volume effect on our results cannot be excluded. Finally, this is a cross-sectional study. Longitudinal studies are needed to evaluate structural and functional changes along with the disease progression over time and are warranted in order to confirm the role of MRI network-based analysis for a differential diagnosis and prognosis of MND in a clinical context, as well to support the hypothesis of a single continuum from ALS to FTD.

In conclusion, this study showed a considerable motor and extra-motor network degeneration in ALS patients and an even more widespread damage in PLS patients, suggesting that graph analysis and connectomics might represent a powerful approach to detect overlapping and specific regions of damage in different MND phenotypes. Importantly, these techniques have proven robust and suitable to manage the multicenter setting variability. Network-based advanced MRI analyses hold the promise to provide an objective in vivo assessment of MND-related pathological changes, delivering potential prognostic markers.

Acknowledgements

Work performed by Dr Edoardo Gioele Spinelli was in partial fulfillment of the requirements for obtaining the PhD degree at Vita-Salute San Raffaele University, Milano, Italy.

References

- Abrahams S, Leigh PN, Harvey A, Vythelingum GN, Grise D, Goldstein LH (2000) Verbal fluency and executive dysfunction in amyotrophic lateral sclerosis (ALS). *Neuropsychologia* 38: 734-47
- Agosta F, Canu E, Inuggi A, Chio A, Riva N, Silani V, Calvo A, Messina S, Falini A, Comi G, Filippi M (2014a) Resting state functional connectivity alterations in primary lateral sclerosis. *Neurobiology of aging* 35: 916-25
- Agosta F, Galantucci S, Riva N, Chio A, Messina S, Iannaccone S, Calvo A, Silani V, Copetti M, Falini A, Comi G, Filippi M (2014b) Intrahemispheric and interhemispheric structural network abnormalities in PLS and ALS. *Human brain mapping* 35: 1710-22
- Alberici A, Geroldi C, Cotelli M, Adorni A, Calabria M, Rossi G, Borroni B, Padovani A, Zanetti O, Kertesz A (2007) The Frontal Behavioural Inventory (Italian version) differentiates frontotemporal lobar degeneration variants from Alzheimer's disease. *Neurological sciences : official journal of the Italian Neurological Society and of the Italian Society of Clinical Neurophysiology* 28: 80-6
- Barbarotto R, Laiacona M, Frosio R, Vecchio M, Farinato A, Capitani E (1998) A normative study on visual reaction times and two Stroop colour-word tests. *Italian journal of neurological sciences* 19: 161-70
- Basaia S, Filippi M, Spinelli EG, Agosta F (2019) White Matter Microstructure Breakdown in the Motor Neuron Disease Spectrum: Recent Advances Using Diffusion Magnetic Resonance Imaging. *Frontiers in neurology* 10: 193
- Basso A, Capitani E, Laiacona M (1987) Raven's coloured progressive matrices: normative values on 305 adult normal controls. *Functional neurology* 2: 189-94
- Beck AT, Ward CH, Mendelson M, Mock J, Erbaugh J (1961) An inventory for measuring depression. *Arch Gen Psychiatry* 4: 561-71

Brettschneider J, Del Tredici K, Toledo JB, Robinson JL, Irwin DJ, Grossman M, Suh E, Van Deerlin VM, Wood EM, Baek Y, Kwong L, Lee EB, Elman L, McCluskey L, Fang L, Feldengut S, Ludolph AC, Lee VM, Braak H, Trojanowski JQ (2013) Stages of pTDP-43 pathology in amyotrophic lateral sclerosis. *Annals of neurology* 74: 20-38

Brooks BR, Miller RG, Swash M, Munsat TL, World Federation of Neurology Research Group on Motor Neuron D (2000) El Escorial revisited: revised criteria for the diagnosis of amyotrophic lateral sclerosis. *Amyotrophic lateral sclerosis and other motor neuron disorders : official publication of the World Federation of Neurology, Research Group on Motor Neuron Diseases* 1: 293-9

Buchanan CR, Pettit LD, Storkey AJ, Abrahams S, Bastin ME (2015) Reduced structural connectivity within a prefrontal-motor-subcortical network in amyotrophic lateral sclerosis. *Journal of magnetic resonance imaging : JMRI* 41: 1342-52

Bullmore E, Sporns O (2009) Complex brain networks: graph theoretical analysis of structural and functional systems. *Nature reviews Neuroscience* 10: 186-98

Caffarra P, Vezzadini G, Dieci F, Zonato F, Venneri A (2004) Modified Card Sorting Test: normative data. *Journal of clinical and experimental neuropsychology* 26: 246-50

Carlesimo GA, Caltagirone C, Gainotti G (1996) The Mental Deterioration Battery: normative data, diagnostic reliability and qualitative analyses of cognitive impairment. The Group for the Standardization of the Mental Deterioration Battery. *European neurology* 36: 378-84

Cedarbaum JM, Stambler N, Malta E, Fuller C, Hilt D, Thurmond B, Nakanishi A (1999) The ALSFRS-R: a revised ALS functional rating scale that incorporates assessments of respiratory function. BDNF ALS Study Group (Phase III). *Journal of the neurological sciences* 169: 13-21

Chio A, Calvo A, Moglia C, Mazzini L, Mora G, group Ps (2011) Phenotypic heterogeneity of amyotrophic lateral sclerosis: a population based study. *Journal of neurology, neurosurgery, and psychiatry* 82: 740-6

Crossley NA, Mechelli A, Scott J, Carletti F, Fox PT, McGuire P, Bullmore ET (2014) The hubs of the human connectome are generally implicated in the anatomy of brain disorders. *Brain* 137: 2382-95

Della Sala S, MacPherson SE, Phillips LH, Sacco L, Spinnler H (2003) How many camels are there in Italy? Cognitive estimates standardised on the Italian population.

Neurological sciences : official journal of the Italian Neurological Society and of the Italian Society of Clinical Neurophysiology 24: 10-5

Filippi M, Basaia S, Canu E, Imperiale F, Magnani G, Falautano M, Comi G, Falini A, Agosta F (2020) Changes in functional and structural brain connectome along the Alzheimer's disease continuum. *Molecular psychiatry* 25: 230-239

Filippi M, Basaia S, Canu E, Imperiale F, Meani A, Caso F, Magnani G, Falautano M, Comi G, Falini A, Agosta F (2017) Brain network connectivity differs in early-onset neurodegenerative dementia. *Neurology* 89: 1764-1772

Folstein MF, Folstein SE, McHugh PR (1975) "Mini-mental state". A practical method for grading the cognitive state of patients for the clinician. *Journal of psychiatric research* 12: 189-98

Galantucci S, Agosta F, Stefanova E, Basaia S, van den Heuvel MP, Stojkovic T, Canu E, Stankovic I, Spica V, Copetti M, Gagliardi D, Kostic VS, Filippi M (2017) Structural Brain Connectome and Cognitive Impairment in Parkinson Disease. *Radiology* 283: 515-525

Geevasinga N, Korgaonkar MS, Menon P, Van den Bos M, Gomes L, Foster S, Kiernan MC, Vucic S (2017) Brain functional connectome abnormalities in amyotrophic lateral sclerosis are associated with disability and cortical hyperexcitability. *European journal of neurology* 24: 1507-1517

Hamilton M (1960) A rating scale for depression. *Journal of neurology, neurosurgery, and psychiatry* 23: 56-62

Jucker M, Walker LC (2013) Self-propagation of pathogenic protein aggregates in neurodegenerative diseases. *Nature* 501: 45-51

Laiacina M, Inzaghi MG, De Tanti A, Capitani E (2000) Wisconsin card sorting test: a new global score, with Italian norms, and its relationship with the Weigl sorting test. *Neurological sciences : official journal of the Italian Neurological Society and of the Italian Society of Clinical Neurophysiology* 21: 279-91

Menke RA, Proudfoot M, Wu J, Andersen PM, Talbot K, Benatar M, Turner MR (2016) Increased functional connectivity common to symptomatic amyotrophic lateral sclerosis and those at genetic risk. *Journal of neurology, neurosurgery, and psychiatry* 87: 580-8

Miceli G, neuropsicologia UcdSCSd, psicologia CndrId (1994) *Batteria per l'analisi dei deficit afasici B.A.D.A.* Servizio di neuropsicologia, Università cattolica del S. Cuore,

Monaco M, Costa A, Caltagirone C, Carlesimo GA (2013) Forward and backward span for verbal and visuo-spatial data: standardization and normative data from an Italian adult population. *Neurological sciences : official journal of the Italian Neurological Society and of the Italian Society of Clinical Neurophysiology* 34: 749-54

Muller HP, Agosta F, Gorges M, Kassubek R, Spinelli EG, Riva N, Ludolph AC, Filippi M, Kassubek J (2018) Cortico-efferent tract involvement in primary lateral sclerosis and amyotrophic lateral sclerosis: A two-centre tract of interest-based DTI analysis. *NeuroImage Clinical* 20: 1062-1069

Muller HP, Turner MR, Grosskreutz J, Abrahams S, Bede P, Govind V, Prudlo J, Ludolph AC, Filippi M, Kassubek J, Neuroimaging Society in ALS DTISG (2016) A large-scale multicentre cerebral diffusion tensor imaging study in amyotrophic lateral sclerosis. *Journal of neurology, neurosurgery, and psychiatry* 87: 570-9

Norris F, Shepherd R, Denys E, U K, Mukai E, Elias L, Holden D, Norris H (1993) Onset, natural history and outcome in idiopathic adult motor neuron disease. *Journal of the neurological sciences* 118: 48-55

Novelli G, Laiacona M, Papagno C, Vallar G, Capitani E, Cappa SF (1986) Three clinical tests to research and rate the lexical performance of normal subjects. *Arch Psicol Neurol Psichiatr* 47: 477-506

Orsini A, Grossi D, Capitani E, Laiacona M, Papagno C, Vallar G (1987) Verbal and spatial immediate memory span: normative data from 1355 adults and 1112 children. *Italian journal of neurological sciences* 8: 539-48

Pringle CE, Hudson AJ, Munoz DG, Kiernan JA, Brown WF, Ebers GC (1992) Primary lateral sclerosis. Clinical features, neuropathology and diagnostic criteria. *Brain : a journal of neurology* 115 (Pt 2): 495-520

Raaphorst J, Beeldman E, Schmand B, Berkhout J, Linssen WH, van den Berg LH, Pijnenburg YA, Grupstra HF, Weikamp JG, Schelhaas HJ, Papma JM, van Swieten JC, de Visser M, de Haan RJ (2012) The ALS-FTD-Q: a new screening tool for behavioral disturbances in ALS. *Neurology* 79: 1377-83

Rosenbohm A, Muller HP, Hubers A, Ludolph AC, Kassubek J (2016) Corticoefferent pathways in pure lower motor neuron disease: a diffusion tensor imaging study. *Journal of neurology* 263: 2430-2437

Seeley WW, Crawford RK, Zhou J, Miller BL, Greicius MD (2009) Neurodegenerative diseases target large-scale human brain networks. *Neuron* 62: 42-52

Spinelli EG, Agosta F, Ferraro PM, Riva N, Lunetta C, Falzone YM, Comi G, Falini A, Filippi M (2016) Brain MR Imaging in Patients with Lower Motor Neuron-Predominant Disease. *Radiology* 280: 545-56

Sporns O, Zwi JD (2004) The small world of the cerebral cortex. *Neuroinformatics* 2: 145-62

Tijms BM, Wink AM, de Haan W, van der Flier WM, Stam CJ, Scheltens P, Barkhof F (2013) Alzheimer's disease: connecting findings from graph theoretical studies of brain networks. *Neurobiology of aging* 34: 2023-36

Tognoni HSaG (1987) *Standardizzazione e Taratura Italiana di Test Neuropsicologici*.

Turner MR, Cagnin A, Turkheimer FE, Miller CC, Shaw CE, Brooks DJ, Leigh PN, Banati RB (2004) Evidence of widespread cerebral microglial activation in amyotrophic lateral sclerosis: an [11C](R)-PK11195 positron emission tomography study. *Neurobiology of disease* 15: 601-9

van den Berg-Vos RM, Visser J, Franssen H, de Visser M, de Jong JM, Kalmijn S, Wokke JH, van den Berg LH (2003) Sporadic lower motor neuron disease with adult onset: classification of subtypes. *Brain : a journal of neurology* 126: 1036-47

van den Heuvel MP, de Lange SC, Zalesky A, Seguin C, Yeo BTT, Schmidt R (2017) Proportional thresholding in resting-state fMRI functional connectivity networks and consequences for patient-control connectome studies: Issues and recommendations. *NeuroImage* 152: 437-449

van den Heuvel MP, Sporns O (2019) A cross-disorder connectome landscape of brain dysconnectivity. *Nature reviews Neuroscience* 20: 435-446

Verstraete E, Veldink JH, van den Berg LH, van den Heuvel MP (2014) Structural brain network imaging shows expanding disconnection of the motor system in amyotrophic lateral sclerosis. *Human brain mapping* 35: 1351-61

Zalesky A, Fornito A, Bullmore ET (2010a) Network-based statistic: identifying differences in brain networks. *NeuroImage* 53: 1197-207

Zalesky A, Fornito A, Harding IH, Cocchi L, Yucel M, Pantelis C, Bullmore ET (2010b) Whole-brain anatomical networks: does the choice of nodes matter? *NeuroImage* 50: 970-83

Zhou C, Hu X, Hu J, Liang M, Yin X, Chen L, Zhang J, Wang J (2016) Altered Brain Network in Amyotrophic Lateral Sclerosis: A Resting Graph Theory-Based Network Study at Voxel-Wise Level. *Frontiers in neuroscience* 10: 204

Table 1. Demographic and clinical features of ALS, PLS and PMA patients and matched healthy controls.

	HC	ALS	PLS	PMA	P ALS vs HC	P PLS vs HC	P PMA vs HC	P ALS vs PLS	P ALS vs PMA	P PLS vs PMA
N	79	173	38	28						
Age [years]	61.84 ± 8.82 (42.00 - 81.81)	61.56 ± 10.64 (28.47 - 86.12)	63.20 ± 7.89 (43.87 - 80.26)	58.44 ± 8.99 (39.62 - 73.91)	1.00	1.00	0.69	1.00	0.71	0.31
Sex [women/men]	46/33	72/101	20/18	8/20	0.02	0.69	0.01	0.28	0.22	0.08
Education [years]	12.87 ± 4.38 (5 - 24)	10.41 ± 4.42 (3 - 24)	10.40 ± 4.43 (2 - 18)	10.82 ± 4.81 (5 - 24)	<0.001	0.03	0.23	1.00	1.00	1.00
Onset [limb/bulbar]	-	128/45	33/5	27/1	-	-	-	0.10	0.01	0.23
Disease duration [months]	-	18.97 ± 17.66 (2 - 136)	79.32 ± 60.46 (8 - 247)	69.14 ± 98.61 (4 - 457)	-	-	-	<0.001	<0.001	1.00
ALSFRS-r [0-48]	-	37.92 ± 6.95 (11 - 47)	37.16 ± 5.72 (22 - 44)	40.14 ± 6.00 (25 - 48)	-	-	-	1.00	0.31	0.22
UMN score	-	9.82 ± 4.75 (0 - 16)	13.67 ± 2.11 (10 - 16)	2.14 ± 1.70 (0 - 5)	-	-	-	0.001	<0.001	<0.001
MRC global score	-	96.04 ± 23.86 (5 - 148)	112.86 ± 10.43 (80 - 121)	96.25 ± 17.73 (51 - 119)	-	-	-	0.004	1.00	0.04

Disease progression rate	-	0.78 ± 0.70 (0.04 - 4.11)	0.31 ± 0.49 (0.03 - 2.89)	0.33 ± 0.42 (0 - 2.00)	-	-	-	<0.001	0.002	1.00
---------------------------------	---	------------------------------	------------------------------	---------------------------	---	---	---	------------------	--------------	------

Values are numbers or means ± standard deviations (range). Disease duration was defined as months from onset to date of MRI scan. P values refer to ANOVA models, followed by post-hoc pairwise comparisons (Bonferroni-corrected for multiple comparisons), or Chi-squared test. Abbreviations: ALS= Amyotrophic lateral sclerosis; ALSFRS-r= Amyotrophic lateral sclerosis functional rating scale revised; HC= healthy controls; MRC= Medical Research Council; N= Number; PLS= Primary lateral sclerosis; PMA= Progressive muscular atrophy; UMN= Upper motor neuron.

Table 2. Summary of altered structural and functional metrics in the different MND variants.

ALS	STRUCTURAL CONNECTIVITY (FA)																																				
	GLOBAL BRAIN ANALYSIS	Whole brain																																			
	LOBAR NETWORK ANALYSIS	Fronto-Insular					Temporal					Parietal					Occipital					Basal Ganglia					Sensorimotor										
	CONNECTIVITY ANALYSIS	FI	T	P	O	BG	S	FI	T	P	O	BG	S	FI	T	P	O	BG	S	FI	T	P	O	BG	S	FI	T	P	O	BG	S	FI	T	P	O	BG	S
	FUNCTIONAL CONNECTIVITY																																				
	GLOBAL BRAIN ANALYSIS	Whole brain																																			
	LOBAR NETWORK ANALYSIS	Fronto-Insular					Temporal					Parietal					Occipital					Basal Ganglia					Sensorimotor										

ANALYSIS																																				
LOBAR NETWORK ANALYSIS	Fronto-Insular					Temporal					Parietal					Occipital					Basal Ganglia					Sensorimotor										
CONNECTIVITY ANALYSIS	FI	T	P	O	BG	S	FI	T	P	O	BG	S	FI	T	P	O	BG	S	FI	T	P	O	BG	S	FI	T	P	O	BG	S	FI	T	P	O	BG	S

Three shades of green color were used to define the severity of damage in terms of percentage of altered metrics (global and lobar analyses) and percentage of altered connections between two lobes (connectivity analysis). The three shades of green depicted the following ranks: 1-25% (light green), 26-50% (medium green) and 51-75% (dark green). White background represents the absence of alterations. Abbreviations: ALS= Amyotrophic Lateral Sclerosis; BG= basal ganglia; FA= fractional anisotropy; FI= fronto-insular; O= occipital; P= parietal; PLS= Primary Lateral Sclerosis; S= sensorimotor; T= temporal.

Figure 1. MRI processing pipeline. (IA) Grey matter was parcellated in 220 similarly-sized brain regions, which included cerebral cortex and basal ganglia but excluded the cerebellum. (IB) Diagram reported diffusion-tensor MRI and resting-state functional MRI pre-processing steps and construction of brain structural and functional connectomes. Structural and functional matrices were the input for three distinctive analyses: (II) Global and lobar graph analysis; (III) Connectivity analysis; and (IV) Correlation analysis. Abbreviations: AAL= automated anatomical labeling; FA= fractional anisotropy; MRI= magnetic resonance imaging.

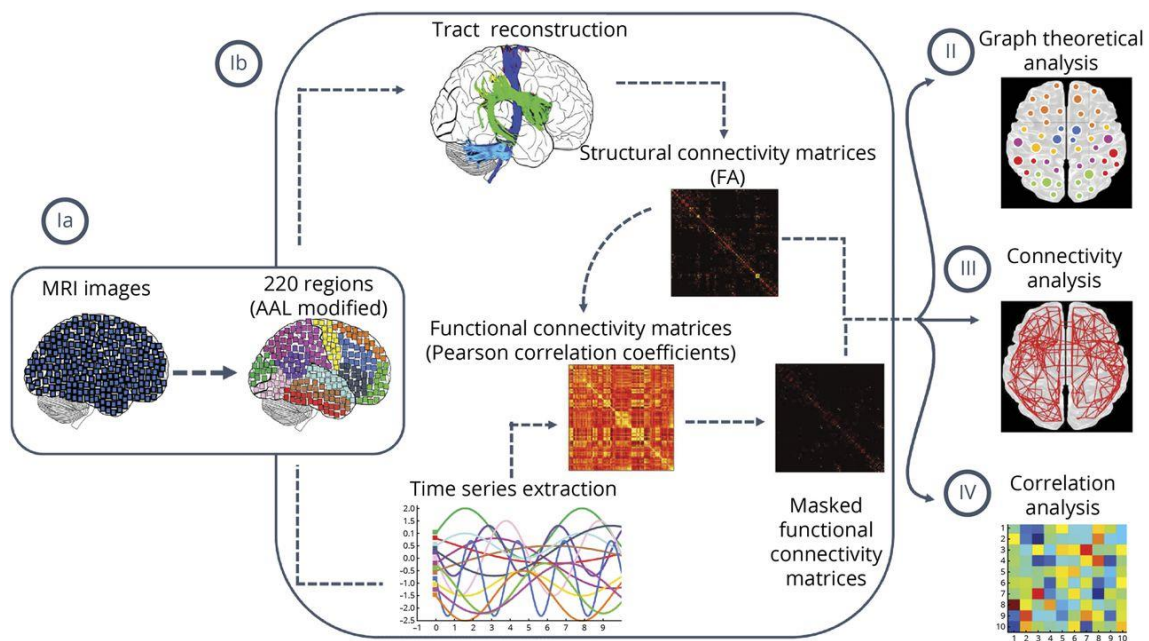


Figure 2. Graph analysis properties of brain lobar networks in ALS, PLS and PMA patients and healthy controls. Box plot of structural nodal strength, path length, local efficiency and clustering coefficient of each brain lobe are shown for patient groups and matched healthy controls. The red horizontal line in each box plot represents the median, the two lines just above and below the median represent the 25th and 75th percentiles, whiskers represent the minimum and maximum values, and all the dots outside the confidence interval are considered as outliers. * $p < 0.05$. All the comparisons were adjusted for age, sex and MR scanner. Abbreviations: ALS= Amyotrophic Lateral Sclerosis; HC= healthy controls; PLS= Primary Lateral Sclerosis; PMA= Progressive Muscular Atrophy.

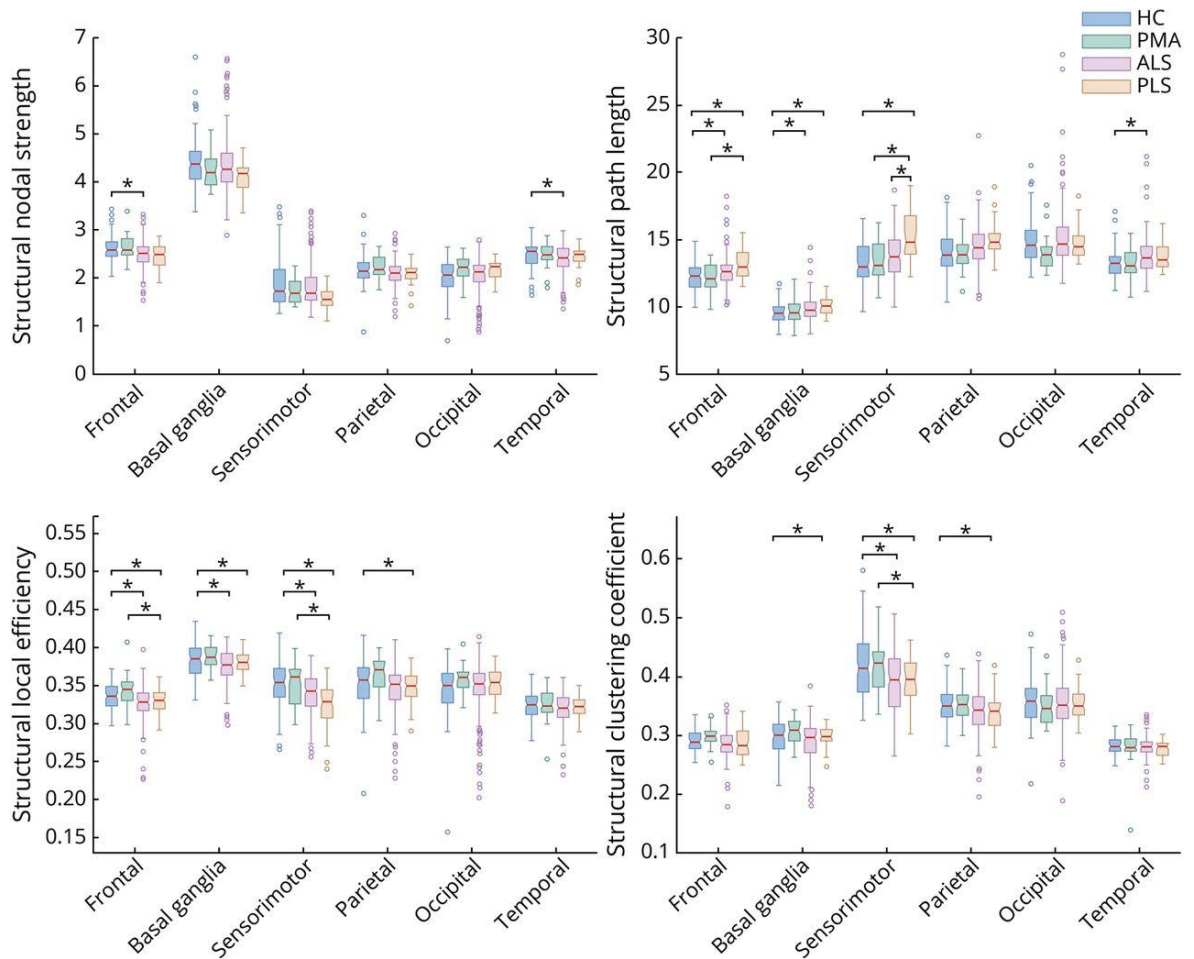


Figure 3. Subnetworks showing altered structural and functional connectivity in ALS, PLS and PMA patients relative to healthy controls and between patient groups. Altered structural (A) and functional (B) connections are represented in magenta and orange, respectively. All the comparisons were adjusted for age, sex and MR scanner. Six shades of blue color were used to define the belonging of each node to different lobes starting with light blue (frontal lobe) to dark blue (posterior lobe, i.e. occipital). Abbreviations: A= anterior; ALS= Amyotrophic Lateral Sclerosis; FA= fractional anisotropy; HC= healthy controls; L= left; P= posterior; PLS= Primary Lateral Sclerosis; PMA= Progressive Muscular Atrophy; R= right.

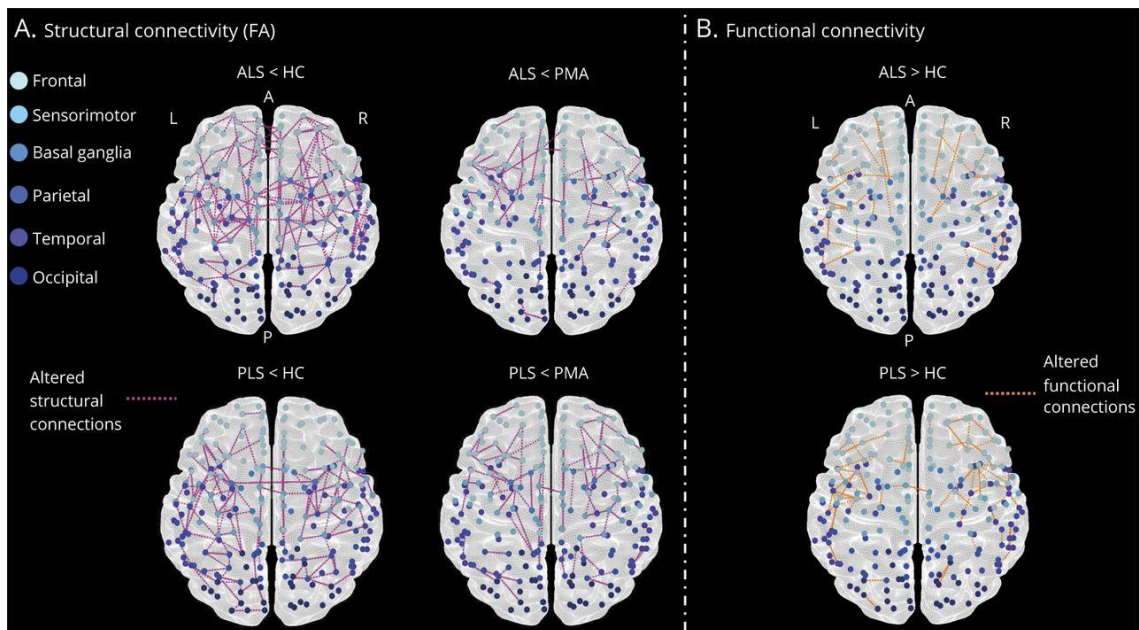


Figure 4. Subnetworks showing overlapping affected connections. Overlapping affected connections in ALS and PLS patients in structural and functional MRI (A) and overlapping structural and functional affected connections within the two groups (B) are represented in red. Six shades of blue color were used to define the belonging of each node to different lobes starting with light blue (frontal lobe) to dark blue (posterior lobe, i.e. occipital). Abbreviations: A= anterior; ALS= Amyotrophic Lateral Sclerosis; FA= fractional anisotropy; HC= healthy controls; L= left; P = posterior; PLS= Primary Lateral Sclerosis; R= right.

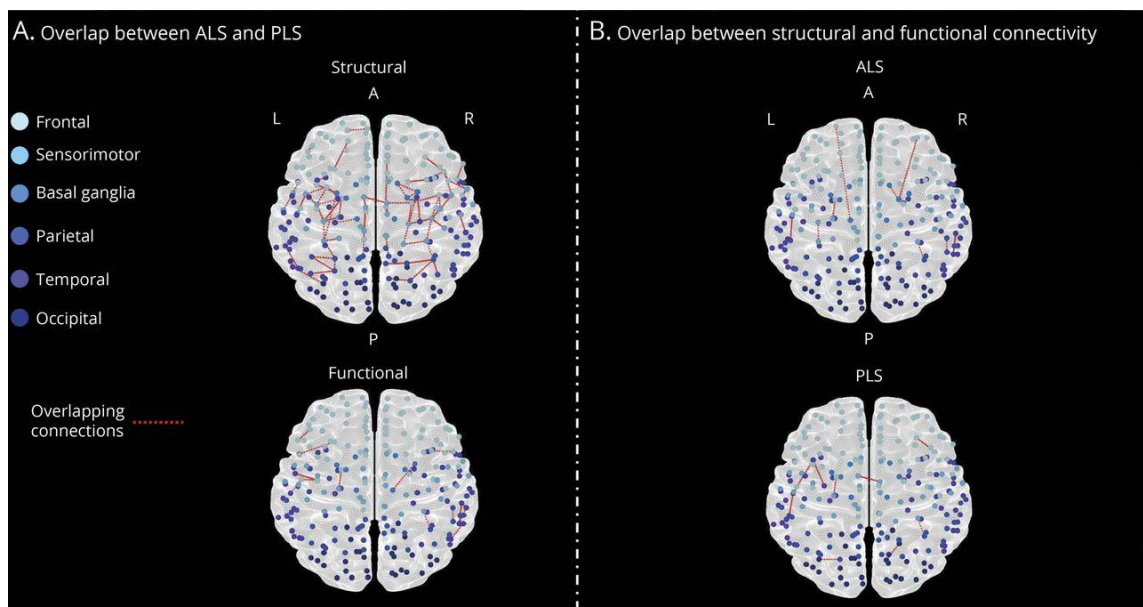
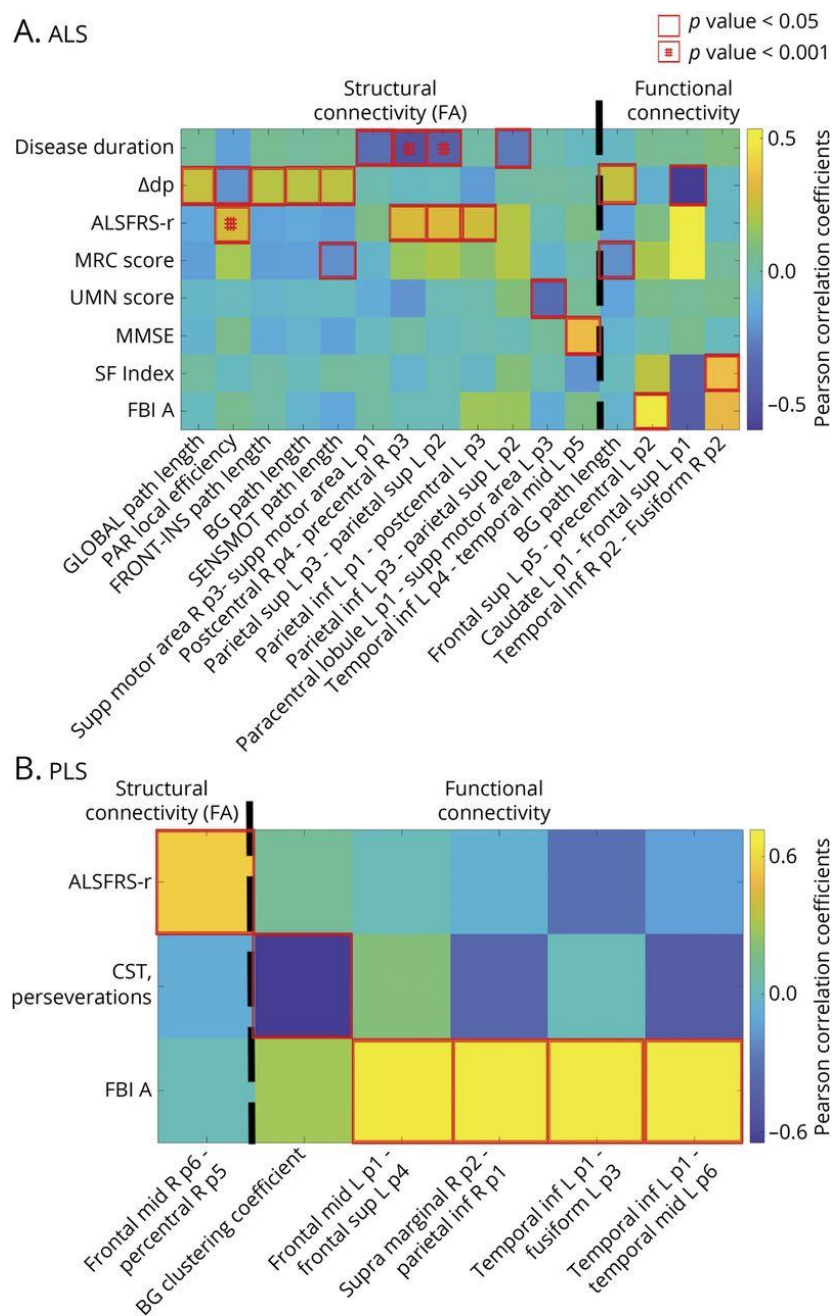


Figure 5. Characterization of the relationship between structural and functional MRI metrics and clinical/cognitive data in ALS and PLS patients. Each row shows structural and functional brain proprieties and each column clinical and cognitive scores in ALS (A) and PLS (B) patients. Color scale represents Pearson's correlation coefficient. Red square alone or with a hash indicate statistical significance, respectively, at a threshold of $p < 0.05$ and $p < 0.001$.



Abbreviations: Δ dp= disease progression rate; ALS= Amyotrophic Lateral Sclerosis; ALSFRS-r= Amyotrophic Lateral Sclerosis functional rating scale revised; BG= basal ganglia; CST= Card Sorting Test; FA= fractional anisotropy; FBI= Frontal Behavioral Inventory; FRONT-INS= fronto-insular; Inf= inferior; L= left; Mid= middle; MMSE= Mini-Mental state examination; MRC= Medical Research Council; p=part; PAR= parietal; PLS= Primary Lateral Sclerosis; R= right; SENSMOT= sensorimotor; SF= semantic fluency; Sup= superior; Supp= supplementary; UMN= upper motor neuron.

Additional Table 1. Neuropsychological features of ALS, PLS and PMA patients and matched healthy controls.

	HC	ALS	PLS	PMA	P ALS vs HC	P PLS vs HC	P PMA vs HC	P ALS vs PLS	P ALS vs PMA	P PLS vs PMA
Global cognition										
MMSE*	n 41 0.98 ± 0.03 (0.87 - 1.00)	n 129 0.94 ± 0.07 (0.67 - 1.00)	n 31 0.97 ± 0.04 (0.83 - 1.00)	n 21 0.95 ± 0.05 (0.83 - 1.00)	0.03	1.00	0.35	0.03	1.00	0.32
Memory										
Digit span forward	n 40 5.95 ± 0.96 (4.00 - 9.00)	n 101 5.17 ± 0.95 (3.00 - 9.00)	n 31 5.77 ± 1.41 (3.00 - 9.00)	n 20 5.65 ± 0.81 (4.00 - 7.00)	<0.001	1.00	0.59	0.003	0.38	0.95
RAVLT immediate	n 40 46.08 ± 9.43 (26.00 - 62.00)	n 102 39.69 ± 12.04 (11.00 - 64.00)	n 31 39.77 ± 9.94 (23.00 - 55.00)	n 19 43.00 ± 11.26 (14.00 - 60.00)	0.50	0.66	1.00	1.00	0.98	0.92
RAVLT delayed	n 40 9.23 ± 3.25 (3.00 - 15.00)	n 102 8.19 ± 3.35 (0.00 - 15.00)	n 31 7.81 ± 3.25 (0.00 - 14.00)	n 19 7.47 ± 3.44 (0.00 - 13.00)	1.00	1.00	0.68	1.00	0.38	1.00
Executive function										
CPM	n 37 30.43 ± 3.79 (22.00 - 36.00)	n 99 27.53 ± 5.16 (14.00 - 36.00)	n 32 29.03 ± 3.89 (21.00 - 35.00)	n 20 28.30 ± 7.41 (6.00 - 36.00)	0.06	1.00	0.94	0.36	1.00	1.00
Digit span backward	n 33 4.45 ± 1.09 (2.00 - 7.00)	n 97 3.52 ± 1.17 (0.00 - 6.00)	n 30 4.33 ± 1.16 (2.00 - 6.00)	n 20 4.15 ± 0.88 (3.00 - 6.00)	0.001	1.00	1.00	0.001	0.07	1.00
Stroop interference (seconds)	-	n 65 42.31 ± 34.26 (6.00 - 196.00)	n 22 42.47 ± 24.81 (10.00 - 98.00)	n 19 43.30 ± 20.47 (12.00 - 93.00)	-	-	-	1.00	1.00	1.00
CET	-	n 90 14.34 ± 4.08 (6.00 - 25.00)	n 27 14.63 ± 2.88 (10.00 - 22.00)	n 18 13.06 ± 3.75 (6.00 - 20.00)	-	-	-	1.00	0.70	0.79
Test di Weigl	-	n 86 10.85 ± 3.36	n 26 13.04 ± 2.11	n 17 11.53 ± 4.02	-	-	-	0.002	1.00	0.20

		(1.00 - 15.00)	(7.00 - 15.00)	(0.00 - 15.00)						
CST, perseverations**	n 33 0.11 ± 0.15 (0.00 - 0.83)	n 85 0.17 ± 0.13 (0.01 - 0.73)	n 24 0.12 ± 0.10 (0.02 - 0.30)	n 17 0.18 ± 0.19 (0.03 - 0.80)	0.56	1.00	0.79	0.38	1.00	0.92
Language										
BADA (noun)	n 22 29.73 ± 0.63 (28.00 - 30.00)	n 99 28.78 ± 2.12 (13.00 - 30.00)	n 31 29.39 ± 0.72 (28.00 - 30.00)	n 19 29.21 ± 1.08 (27.00 - 30.00)	0.16	1.00	1.00	0.33	1.00	1.00
BADA (action)	n 22 27.68 ± 0.57 (26.00 - 28.00)	n 99 26.63 ± 2.22 (17.00 - 28.00)	n 30 26.57 ± 1.48 (23.00 - 28.00)	n 19 26.32 ± 2.52 (20.00 - 28.00)	0.11	0.25	0.04	1.00	0.98	1.00
Fluency										
Index PF***	n 29 4.82 ± 2.17 (2.60 - 12.05)	n 102 8.07 ± 7.99 (1.81 - 59.00)	n 27 7.23 ± 4.61 (3.41 - 27.19)	n 21 6.47 ± 3.88 (1.90 - 18.80)	0.44	1.00	1.00	1.00	1.00	1.00
Index SF***	n 29 4.20 ± 1.62 (2.49 - 10.90)	n 101 5.57 ± 3.51 (2.20 - 23.00)	n 27 4.88 ± 1.61 (2.61 - 8.70)	n 19 4.03 ± 1.02 (2.76 - 5.89)	0.07	1.00	1.00	0.21	0.44	1.00
Mood & Behavior										
BDI	n 25 5.00 ± 4.42 (0.00 - 15.00)	-	-	-	-	-	-	-	-	-
HDRS	-	n 80 7.33 ± 5.00 (0.00 - 23.00)	n 28 7.29 ± 5.32 (1.00 - 24.00)	n 15 4.60 ± 2.50 (0.00 - 8.00)	-	-	-	1.00	0.24	0.40
FBI A	-	n 67 4.31 ± 5.07 (0.00 - 25.00)	n 22 1.77 ± 3.84 (0.00 - 16.00)	n 8 2.25 ± 2.96 (0.00 - 8.00)	-	-	-	0.13	1.00	1.00
FBI B	-	n 67 1.49 ± 1.93 (0.00 - 8.00)	n 22 0.86 ± 1.88 (0.00 - 8.00)	n 8 1.38 ± 2.33 (0.00 - 6.00)	-	-	-	0.62	1.00	0.92
FBI total	-	n 73 5.74 ± 6.41 (0.00 - 32.00)	n 24 2.79 ± 5.28 (0.00 - 24.00)	n 11 3.64 ± 4.82 (0.00 - 14.00)	-	-	-	0.15	1.00	1.00
ALS-FTD-Q	-	n 62	n 5	n 5	-	-	-	1.00	0.28	1.00

		11.79 ± 8.88 (0.00 - 35.00)	14.80 ± 17.85 (0.00 - 44.00)	20.00 ± 18.83 (5.00 - 50.00)						
--	--	--------------------------------	---------------------------------	---------------------------------	--	--	--	--	--	--

Values are numbers or means ± standard deviations (range). Differences between patient groups and healthy controls were assessed using one-way ANOVA (statistical contrasts) corrected for age, sex and education. Comparisons among patients were also corrected for ALSFRS-r. *= Ratio between the number of correct items and the maximum number of administered items; **= Perseverations are reported as the ratio between perseveration absolute number and the maximum number of cards provided during the test; ***= Verbal fluency indices were obtained as following: time for generation condition - time for control condition (reading or writing generated words)/total number of items generated. Abbreviations: ALS= Amyotrophic lateral sclerosis; ALS-FTD-Q= ALS-FTD questionnaire; BADA= Battery for aphasic deficit analysis; BDI= Beck Depression Inventory; CET= Cognitive estimation test; CPM= Colored progressive matrices; CST= Card sorting tests; FBI= Frontal Behavioral Inventory; HDRS= Hamilton Depression Rating Scale; HC= Healthy controls; MMSE= Mini-Mental state examination; PF= Phonemic fluency; PLS= Primary lateral sclerosis; PMA= Progressive muscular atrophy; RAVLT= Rey auditory verbal learning test; SF= Semantic fluency.

Additional Table 2. MRI acquisition parameters.

Milan/Turin	Philips Medical System Intera 3T scan				
	T2-weighted SE	FLAIR	3D T1-weighted FFE	Pulsed-gradient SE echo planar with sensitivity encoding	T2*-weighted single-shot EPI sequence (resting state fMRI)
Repetition time (msec)	3500	11000	25	8986	3000
Echo time (msec)	85	120	4.6	80	35
Flip angle	90°	90°	30°	-	90°
Section thickness (mm)	5	5	-	2.5	4
No. of sections	22	22	220	55	30 for 220 volumes
Matrix	512x512	512x512	256x256	96x96	128x128
Field of view (mm²)	230x184	230x230	230x182	240x240	240x240
Diffusion gradient directions	-	-	-	32	-
b value sec/mm²	-	-	-	1000	-
Naples	GE Signa HDxt scan				
	T2-weighted FSE	FLAIR	T1-weighted sagittal images	Gradient echo planar imaging	T2*-weighted echo planar sequence (resting state fMRI)
Repetition time (msec)	3444	9052	7000	13000	1508
Echo time (msec)	128	122.4	2848	83.6	32
Flip angle	-	-	8°	-	90°
Section thickness (mm)	4	4	-	-	4
No. of sections	32	32	-	50	29 for 240 volumes
Matrix	512x512	512x512	256x256	128x128	64x64

Field of view (mm²)	240x240	240x240	260x260	320x320	256x256
Diffusion gradient directions	-	-	-	32	-
<i>b</i> value sec/mm²	-	-	-	1000	-

Abbreviations: FFE= fast field echo; FLAIR= fluid-attenuated inversion recovery; FSE= fast spin echo; MRI= magnetic resonance imaging; msec= millisecond; mm= millimeter; No= number; SE=spin echo; sec=second.

Additional Table 3. Global graph analysis properties of structural and functional brain networks in ALS, PLS and PMA patients and matched healthy controls.

		HC	ALS	PLS	PMA	P ALS vs HC	P PLS vs HC	P PMA vs HC	P ALS vs PLS	P ALS vs PMA	P PLS vs PMA
Nodal strength	Structural (FA)	2.42 ± 0.24 (1.83 - 3.18)	2.34 ± 0.25 (1.49 - 3.16)	2.30 ± 0.17 (1.82 - 2.64)	2.42 ± 0.20 (2.12 - 2.91)	0.05	0.21	1.00	1.00	1.00	1.00
	Functional	2.58 ± 0.44 (1.75 - 4.01)	2.58 ± 0.52 (1.46 - 4.95)	2.62 ± 0.53 (1.65 - 4.30)	2.60 ± 0.37 (1.82 - 3.31)	1.00	1.00	0.74	1.00	1.00	1.00
Path length	Structural (FA)	13.13 ± 1.05 (10.74 - 15.54)	13.54 ± 1.32 (10.89 - 20.59)	13.88 ± 1.02 (12.33 - 16.64)	12.98 ± 1.02 (10.57 - 14.86)	0.06	0.01	1.00	0.71	0.63	0.08
	Functional	12.67 ± 2.45 (7.70 - 21.93)	12.67 ± 2.63 (5.45 - 23.31)	12.44 ± 2.59 (7.62 - 21.43)	12.09 ± 1.64 (9.40 - 16.27)	1.00	1.00	1.00	1.00	1.00	1.00
Local efficiency	Structural (FA)	0.34 ± 0.02 (0.29 - 0.37)	0.33 ± 0.02 (0.25 - 0.39)	0.33 ± 0.01 (0.29 - 0.36)	0.35 ± 0.02 (0.31 - 0.39)	0.02	0.003	1.00	0.71	0.89	0.12
	Functional	0.26 ± 0.05 (0.17 - 0.42)	0.26 ± 0.06 (0.13 - 0.50)	0.26 ± 0.07 (0.16 - 0.48)	0.26 ± 0.04 (0.16 - 0.33)	1.00	1.00	0.45	1.00	0.59	0.97
Clustering coefficient	Structural (FA)	0.32 ± 0.02 (0.28 - 0.36)	0.32 ± 0.02 (0.20 - 0.37)	0.32 ± 0.01 (0.28 - 0.35)	0.32 ± 0.02 (0.29 - 0.37)	0.11	0.01	1.00	0.45	1.00	0.71
	Functional	0.17 ± 0.03 (0.11 - 0.26)	0.17 ± 0.04 (0.10 - 0.33)	0.17 ± 0.04 (0.12 - 0.30)	0.17 ± 0.03 (0.10 - 0.21)	1.00	1.00	0.24	1.00	0.18	0.60

Values are numbers or means ± standard deviations (range). P values refer to age-, sex- and center-adjusted ANOVA models, followed by post-hoc pairwise comparisons (Bonferroni-corrected for multiple comparisons). Abbreviations: ALS= Amyotrophic lateral sclerosis; FA= fractional anisotropy; HC= healthy controls; PLS= Primary lateral sclerosis; PMA= Progressive muscular atrophy.

Additional Table 4. Lobar graph analysis properties of structural and functional brain networks in ALS, PLS and PMA patients and matched healthy controls.

Regions	Graph analysis properties		HC	ALS	PLS	PMA	P ALS vs HC	P PLS vs HC	P PMA vs HC	P ALS vs PLS	P ALS vs PMA	P PLS vs PMA
			79	173	38	28						
Fronto-insular	Nodal strength	Structural (FA)	2.61 ± 0.28 (2.03 - 3.43)	2.50 ± 0.30 (1.54 - 3.33)	2.45 ± 0.23 (1.90 - 2.87)	2.62 ± 0.26 (2.17 - 3.38)	0.01	0.13	1.00	1.00	0.25	0.51
		Functional	2.80 ± 0.51 (1.70 - 4.26)	2.73 ± 0.59 (1.54 - 5.35)	2.71 ± 0.63 (1.72 - 4.75)	2.71 ± 0.42 (1.92 - 3.71)	1.00	1.00	0.57	1.00	1.00	1.00
	Path length	Structural (FA)	12.30 ± 1.05 (9.97 - 14.87)	12.70 ± 1.23 (10.12 - 18.18)	13.17 ± 1.07 (11.53 - 15.52)	12.20 ± 1.02 (9.79 - 13.87)	0.045	0.003	1.00	0.40	0.41	0.03
		Functional	11.80 ± 2.09 (7.57 - 19.53)	11.95 ± 2.30 (5.33 - 19.63)	12.05 ± 2.65 (7.07 - 20.96)	11.55 ± 1.61 (8.42 - 15.63)	1.00	0.61	1.00	1.00	1.00	1.00
	Local efficiency	Structural (FA)	0.34 ± 0.02 (0.30 - 0.37)	0.33 ± 0.02 (0.23 - 0.40)	0.33 ± 0.02 (0.29 - 0.36)	0.34 ± 0.02 (0.30 - 0.41)	0.01	0.02	1.00	1.00	0.07	0.049
		Functional	0.27 ± 0.06 (0.15 - 0.46)	0.27 ± 0.07 (0.12 - 0.55)	0.26 ± 0.07 (0.16 - 0.48)	0.26 ± 0.05 (0.15 - 0.39)	1.00	1.00	1.00	1.00	1.00	1.00
	Clustering coefficient	Structural (FA)	0.29 ± 0.02 (0.25 - 0.34)	0.29 ± 0.02 (0.18 - 0.35)	0.29 ± 0.02 (0.26 - 0.33)	0.30 ± 0.02 (0.25 - 0.33)	0.71	0.62	1.00	1.00	0.94	0.62
		Functional	0.17 ± 0.03 (0.10 - 0.29)	0.17 ± 0.04 (0.09 - 0.36)	0.16 ± 0.04 (0.11 - 0.28)	0.16 ± 0.03 (0.10 - 0.23)	1.00	1.00	0.63	1.00	1.00	1.00
Temporal	Nodal strength	Structural (FA)	2.49 ± 0.26 (1.65 - 3.04)	2.39 ± 0.31 (1.36 - 2.99)	2.45 ± 0.20 (1.86 - 2.81)	2.48 ± 0.25 (1.80 - 2.89)	0.02	0.30	0.22	1.00	1.00	1.00
		Functional	2.65 ± 0.54 (1.33 - 4.29)	2.65 ± 0.65 (1.27 - 5.27)	2.84 ± 0.56 (1.71 - 4.38)	2.73 ± 0.45 (1.83 - 3.62)	1.00	1.00	0.47	1.00	0.64	0.61
	Path length	Structural (FA)	13.29 ± 1.06	13.77 ± 1.42	13.73 ± 0.85	13.24 ± 1.03 (10.73 - 15.47)	0.02	0.07	1.00	1.00	1.00	1.00

			(11.24 - 17.05)	(11.16 - 21.19)	(12.40 - 16.20)							
		Functional	13.08 ± 2.61 (7.70 - 23.80)	13.13 ± 2.91 (5.66 - 25.69)	12.47 ± 2.32 (7.79 - 19.42)	12.37 ± 1.63 (10.02 - 17.05)	1.00	1.00	1.00	1.00	1.00	1.00
	Local Efficiency	Structural (FA)	0.32 ± 0.02 (0.28 - 0.37)	0.32 ± 0.02 (0.23 - 0.36)	0.32 ± 0.01 (0.29 - 0.35)	0.32 ± 0.02 (0.25 - 0.36)	0.24	0.28	0.66	1.00	1.00	1.00
		Functional	0.29 ± 0.07 (0.13 - 0.50)	0.29 ± 0.08 (0.10 - 0.62)	0.32 ± 0.08 (0.14 - 0.56)	0.30 ± 0.06 (0.17 - 0.42)	1.00	1.00	0.33	1.00	0.54	0.35
	Clustering coefficient	Structural (FA)	0.28 ± 0.01 (0.25 - 0.32)	0.28 ± 0.02 (0.21 - 0.34)	0.28 ± 0.01 (0.25 - 0.30)	0.28 ± 0.03 (0.14 - 0.32)	1.00	1.00	0.93	1.00	1.00	1.00
		Functional	0.18 ± 0.04 (0.08 - 0.28)	0.18 ± 0.05 (0.08 - 0.37)	0.20 ± 0.05 (0.10 - 0.34)	0.18 ± 0.04 (0.08 - 0.25)	1.00	1.00	0.12	1.00	0.10	0.14
Parietal	Nodal strength	Structural (FA)	2.16 ± 0.31 (0.87 - 3.29)	2.11 ± 0.27 (1.19 - 2.93)	2.09 ± 0.20 (1.41 - 2.50)	2.23 ± 0.23 (1.75 - 2.66)	0.69	0.93	1.00	1.00	0.82	0.79
		Functional	2.43 ± 0.47 (1.05 - 3.75)	2.46 ± 0.51 (1.31 - 4.80)	2.57 ± 0.56 (1.76 - 3.76)	2.46 ± 0.34 (1.67 - 2.95)	1.00	1.00	1.00	1.00	0.90	0.99
	Path length	Structural (FA)	14.06 ± 1.54 (10.38 - 18.14)	14.46 ± 1.54 (10.58 - 22.75)	14.98 ± 1.23 (12.73 - 18.94)	13.94 ± 1.18 (11.10 - 16.52)	0.24	0.07	1.00	1.00	0.42	0.10
		Functional	12.96 ± 2.70 (7.85 - 24.04)	12.97 ± 3.44 (5.76 - 36.07)	12.38 ± 2.71 (7.89 - 22.14)	12.36 ± 1.92 (9.48 - 16.70)	1.00	1.00	1.00	1.00	1.00	1.00
	Local efficiency	Structural (FA)	0.35 ± 0.03 (0.21 - 0.42)	0.35 ± 0.03 (0.23 - 0.41)	0.35 ± 0.02 (0.29 - 0.39)	0.36 ± 0.02 (0.30 - 0.40)	0.20	0.01	1.00	0.36	1.00	0.10
		Functional	0.23 ± 0.06 (0.08 - 0.41)	0.23 ± 0.07 (0.10 - 0.45)	0.24 ± 0.08 (0.11 - 0.38)	0.22 ± 0.05 (0.10 - 0.30)	1.00	1.00	0.30	1.00	0.13	0.48
	Clustering coefficient	Structural (FA)	0.35 ± 0.03 (0.28 - 0.44)	0.34 ± 0.04 (0.19 - 0.44)	0.34 ± 0.03 (0.28 - 0.42)	0.35 ± 0.03 (0.30 - 0.41)	0.67	0.02	1.00	0.20	1.00	0.83
		Functional	0.16 ± 0.04 (0.07 - 0.30)	0.17 ± 0.05 (0.07 - 0.31)	0.18 ± 0.05 (0.09 - 0.27)	0.16 ± 0.04 (0.07 - 0.24)	1.00	1.00	0.24	1.00	0.07	0.36
Occipital	Nodal strength	Structural (FA)	2.03 ± 0.34 (0.69 - 2.64)	2.02 ± 0.41 (0.87 - 2.79)	2.16 ± 0.20 (1.71 - 2.49)	2.20 ± 0.23 (1.59 - 2.62)	1.00	1.00	1.00	1.00	1.00	1.00
		Functional	2.79 ± 0.87	2.79 ± 0.97	2.94 ± 0.85	2.99 ± 0.79	1.00	1.00	1.00	1.00	1.00	1.00

			(1.21 - 4.97)	(0.62 - 5.75)	(1.47 - 5.26)	(1.91 - 4.97)						
	Path length	Structural (FA)	14.89 ± 1.72 (12.20 - 20.48)	15.17 ± 2.34 (11.71 - 28.71)	14.66 ± 1.14 (13.18 - 18.19)	14.01 ± 1.18 (12.33 - 17.55)	1.00	1.00	1.00	1.00	1.00	1.00
		Functional	13.28 ± 3.30 (7.62 - 26.83)	13.17 ± 3.58 (6.03 - 28.63)	12.43 ± 2.61 (7.43 - 21.60)	12.29 ± 1.95 (9.31 - 16.84)	1.00	1.00	1.00	1.00	1.00	1.00
	Local efficiency	Structural (FA)	0.35 ± 0.03 (0.16 - 0.40)	0.34 ± 0.04 (0.20 - 0.41)	0.35 ± 0.02 (0.31 - 0.39)	0.36 ± 0.02 (0.32 - 0.40)	1.00	1.00	1.00	1.00	1.00	1.00
		Functional	0.30 ± 0.12 (0.06 - 0.61)	0.30 ± 0.13 (0.02 - 0.63)	0.34 ± 0.12 (0.15 - 0.74)	0.32 ± 0.11 (0.13 - 0.54)	1.00	1.00	1.00	1.00	1.00	1.00
	Clustering coefficient	Structural (FA)	0.36 ± 0.04 (0.22 - 0.47)	0.36 ± 0.04 (0.19 - 0.51)	0.35 ± 0.03 (0.30 - 0.43)	0.35 ± 0.03 (0.31 - 0.44)	1.00	1.00	1.00	1.00	1.00	1.00
		Functional	0.20 ± 0.07 (0.06 - 0.41)	0.20 ± 0.08 (0.01 - 0.44)	0.22 ± 0.08 (0.11 - 0.46)	0.21 ± 0.06 (0.10 - 0.32)	1.00	1.00	1.00	1.00	1.00	1.00
Basal ganglia	Nodal strength	Structural (FA)	4.43 ± 0.54 (3.38 - 6.59)	4.40 ± 0.67 (2.88 - 6.56)	4.12 ± 0.31 (3.36 - 4.71)	4.24 ± 0.36 (3.74 - 5.07)	1.00	1.00	1.00	1.00	1.00	1.00
		Functional	2.65 ± 0.75 (1.49 - 5.23)	2.82 ± 0.87 (1.34 - 6.27)	2.61 ± 0.67 (1.48 - 4.55)	2.75 ± 0.60 (1.70 - 3.78)	0.91	1.00	1.00	0.37	1.00	1.00
	Path length	Structural (FA)	9.57 ± 0.74 (7.94 - 11.70)	9.88 ± 0.95 (8.01 - 14.43)	10.09 ± 0.63 (8.93 - 11.53)	9.59 ± 0.78 (7.87 - 11.38)	0.04	0.03	1.00	1.00	0.97	0.32
		Functional	10.86 ± 2.21 (5.97 - 16.65)	10.86 ± 2.69 (4.15 - 26.50)	10.91 ± 2.41 (7.13 - 19.02)	10.34 ± 1.58 (7.93 - 13.62)	1.00	1.00	1.00	1.00	1.00	1.00
	Local efficiency	Structural (FA)	0.38 ± 0.02 (0.33 - 0.43)	0.38 ± 0.02 (0.30 - 0.41)	0.38 ± 0.01 (0.35 - 0.41)	0.39 ± 0.02 (0.36 - 0.42)	0.004	0.03	1.00	1.00	1.00	1.00
		Functional	0.18 ± 0.06 (0.06 - 0.36)	0.20 ± 0.07 (0.04 - 0.47)	0.18 ± 0.05 (0.08 - 0.32)	0.20 ± 0.06 (0.11 - 0.33)	0.10	1.00	1.00	0.24	1.00	1.00
	Clustering coefficient	Structural (FA)	0.29 ± 0.03 (0.22 - 0.36)	0.29 ± 0.04 (0.18 - 0.39)	0.30 ± 0.02 (0.25 - 0.33)	0.31 ± 0.02 (0.26 - 0.34)	0.05	0.03	1.00	1.00	1.00	0.56
		Functional	0.12 ± 0.04 (0.04 - 0.23)	0.14 ± 0.05 (0.03 - 0.32)	0.13 ± 0.03 (0.05 - 0.21)	0.14 ± 0.05 (0.06 - 0.25)	0.12	1.00	1.00	0.67	1.00	1.00
Sensorimotor	Nodal strength	Structural (FA)	1.90 ± 0.54 (1.26 - 3.49)	1.85 ± 0.48 (1.18 - 3.38)	1.55 ± 0.22 (1.11 - 2.04)	1.74 ± 0.26 (1.40 - 2.25)	0.51	0.09	1.00	1.00	1.00	0.20

		Functional	1.86 ± 0.66 (0.93 - 4.68)	1.95 ± 0.63 (0.61 - 4.41)	1.79 ± 0.61 (0.99 - 3.59)	1.84 ± 0.50 (1.04 - 2.64)	1.00	1.00	1.00	1.00	1.00	1.00
	Path length	Structural (FA)	13.27 ± 1.64 (9.67 - 16.53)	13.75 ± 1.71 (10.00 - 18.64)	15.15 ± 1.72 (12.25 - 19.02)	13.42 ± 1.39 (10.68 - 16.27)	0.10	<0.001	1.00	0.004	0.21	<0.001
		Functional	13.99 ± 5.05 (8.50 - 51.35)	13.47 ± 3.01 (4.72 - 21.53)	14.06 ± 3.74 (7.98 - 26.98)	13.01 ± 2.36 (9.50 - 20.04)	1.00	1.00	1.00	1.00	1.00	1.00
	Local efficiency	Structural (FA)	0.35 ± 0.03 (0.27 - 0.42)	0.34 ± 0.03 (0.26 - 0.39)	0.32 ± 0.03 (0.24 - 0.37)	0.35 ± 0.03 (0.30 - 0.40)	0.01	<0.001	1.00	0.05	0.42	0.004
		Functional	0.16 ± 0.09 (0.05 - 0.56)	0.17 ± 0.08 (0.02 - 0.46)	0.14 ± 0.06 (0.04 - 0.36)	0.15 ± 0.06 (0.05 - 0.32)	1.00	1.00	1.00	1.00	1.00	1.00
	Clustering coefficient	Structural (FA)	0.42 ± 0.05 (0.33 - 0.58)	0.39 ± 0.05 (0.27 - 0.51)	0.39 ± 0.04 (0.30 - 0.46)	0.42 ± 0.04 (0.34 - 0.52)	<0.001	<0.001	0.67	0.15	0.82	0.03
		Functional	0.12 ± 0.06 (0.04 - 0.34)	0.12 ± 0.05 (0.02 - 0.30)	0.11 ± 0.05 (0.03 - 0.25)	0.11 ± 0.04 (0.04 - 0.27)	1.00	1.00	1.00	1.00	1.00	1.00

Values are reported as mean ± standard deviation (range). Differences between patient groups and healthy controls were assessed using one-way ANOVA (statistical contrasts) corrected for age, sex and center. P-values were adjusted for multiple comparisons at significance level 0.05 using Bonferroni post-hoc test. Abbreviations: ALS= Amyotrophic lateral sclerosis; FA= Fractional anisotropy; HC= Healthy controls; PLS= Primary lateral sclerosis; PMA= Progressive muscular atrophy.

Additional Table 5. Global and lobar graph analysis properties of structural and functional brain networks in ALS (without ALS-FTD patients), PLS and PMA patients and matched healthy controls.

Regions	Graph analysis properties		HC	ALS	PLS	PMA	P ALS vs HC	P PLS vs HC	P PMA vs HC	P ALS vs PLS	P ALS vs PMA	P PLS vs PMA
			79	165	38	28						
Global	Nodal strength	Structural (FA)	2.42 ± 0.24 (1.83 - 3.18)	2.34 ± 0.26 (1.49 - 3.16)	2.30 ± 0.17 (1.82 - 2.64)	2.42 ± 0.20 (2.12 - 2.91)	0.06	0.17	1.00	1.00	1.00	1.00
		Functional	2.58 ± 0.44 (1.75 - 4.01)	2.58 ± 0.52 (1.46 - 4.95)	2.62 ± 0.53 (1.65 - 4.30)	2.60 ± 0.37 (1.82 - 3.31)	1.00	1.00	0.70	1.00	0.98	1.00
	Path length	Structural (FA)	13.13 ± 1.05 (10.74 - 15.54)	13.53 ± 1.33 (10.89 - 20.59)	13.88 ± 1.02 (12.33 - 16.64)	12.98 ± 1.02 (10.57 - 14.86)	0.07	0.01	1.00	0.59	0.77	0.08
		Functional	12.67 ± 2.45 (7.70 - 21.93)	12.66 ± 2.67 (5.45 - 23.31)	12.44 ± 2.59 (7.62 - 21.43)	12.09 ± 1.64 (9.40 - 16.27)	1.00	1.00	1.00	1.00	1.00	1.00
	Local efficiency	Structural (FA)	0.34 ± 0.02 (0.29 - 0.37)	0.33 ± 0.02 (0.25 - 0.39)	0.33 ± 0.01 (0.29 - 0.36)	0.35 ± 0.02 (0.31 - 0.39)	0.03	0.002	1.00	0.50	1.00	0.12
		Functional	0.26 ± 0.05 (0.17 - 0.42)	0.26 ± 0.06 (0.13 - 0.50)	0.26 ± 0.07 (0.16 - 0.48)	0.26 ± 0.04 (0.16 - 0.33)	1.00	1.00	0.42	1.00	0.52	0.99
	Clustering coefficient	Structural (FA)	0.32 ± 0.02 (0.28 - 0.36)	0.32 ± 0.02 (0.20 - 0.37)	0.32 ± 0.01 (0.28 - 0.35)	0.32 ± 0.02 (0.29 - 0.37)	0.20	0.01	1.00	0.26	1.00	0.73
		Functional	0.17 ± 0.03 (0.11 - 0.26)	0.17 ± 0.04 (0.10 - 0.33)	0.17 ± 0.04 (0.12 - 0.30)	0.17 ± 0.03 (0.10 - 0.21)	1.00	1.00	0.23	1.00	0.16	0.63
Fronto-insular	Nodal strength	Structural (FA)	2.61 ± 0.28 (2.03 - 3.43)	2.11 ± 0.28 (1.19 - 2.93)	2.45 ± 0.23 (1.90 - 2.87)	2.62 ± 0.26 (2.17 - 3.38)	0.01	0.10	1.00	1.00	0.38	0.51
		Functional	2.80 ± 0.51 (1.70 - 4.26)	2.74 ± 0.59 (1.54 - 5.35)	2.71 ± 0.63 (1.72 - 4.75)	2.71 ± 0.42 (1.92 - 3.71)	1.00	1.00	0.54	1.00	1.00	1.00
	Path length	Structural (FA)	12.30 ± 1.05 (9.97 - 14.87)	14.45 ± 1.57	13.17 ± 1.07	12.20 ± 1.02 (9.79 - 13.87)	0.06	0.002	1.00	0.28	0.34	0.03

				(10.58 - 22.75)	(11.53 - 15.52)							
		Functional	11.80 ± 2.09 (7.57 - 19.53)	11.94 ± 2.32 (5.33 - 19.63)	12.05 ± 2.65 (7.07 - 20.96)	11.55 ± 1.61 (8.42 - 15.63)	1.00	0.56	1.00	1.00	1.00	1.00
	Local efficiency	Structural (FA)	0.34 ± 0.02 (0.30 - 0.37)	0.35 ± 0.03 (0.23 - 0.41)	0.33 ± 0.02 (0.29 - 0.36)	0.34 ± 0.02 (0.30 - 0.41)	0.01	0.01	1.00	1.00	0.13	0.046
		Functional	0.27 ± 0.06 (0.15 - 0.46)	0.27 ± 0.07 (0.12 - 0.55)	0.26 ± 0.07 (0.16 - 0.48)	0.26 ± 0.05 (0.15 - 0.39)	1.00	1.00	1.00	1.00	1.00	1.00
	Clustering coefficient	Structural (FA)	0.29 ± 0.02 (0.25 - 0.34)	0.34 ± 0.04 (0.20 - 0.44)	0.29 ± 0.02 (0.26 - 0.33)	0.30 ± 0.02 (0.25 - 0.33)	1.00	0.53	1.00	1.00	1.00	0.64
		Functional	0.17 ± 0.03 (0.10 - 0.29)	0.17 ± 0.04 (0.09 - 0.36)	0.16 ± 0.04 (0.11 - 0.28)	0.16 ± 0.03 (0.10 - 0.23)	1.00	1.00	0.62	1.00	1.00	1.00
Temporal	Nodal strength	Structural (FA)	2.49 ± 0.26 (1.65 - 3.04)	2.39 ± 0.32 (1.36 - 2.99)	2.45 ± 0.20 (1.86 - 2.81)	2.48 ± 0.25 (1.80 - 2.89)	0.02	0.25	0.17	1.00	1.00	1.00
		Functional	2.65 ± 0.54 (1.33 - 4.29)	2.65 ± 0.66 (1.27 - 5.27)	2.84 ± 0.56 (1.71 - 4.38)	2.73 ± 0.45 (1.83 - 3.62)	1.00	1.00	0.42	1.00	0.51	0.63
	Path length	Structural (FA)	13.29 ± 1.06 (11.24 - 17.05)	13.77 ± 1.44 (11.16 - 21.19)	13.73 ± 0.85 (12.40 - 16.20)	13.24 ± 1.03 (10.73 - 15.47)	0.02	0.06	1.00	1.00	1.00	1.00
		Functional	13.08 ± 2.61 (7.70 - 23.80)	13.11 ± 2.94 (5.67 - 25.69)	12.47 ± 2.32 (7.79 - 19.42)	12.37 ± 1.63 (10.02 - 17.05)	1.00	1.00	1.00	1.00	1.00	1.00
	Local Efficiency	Structural (FA)	0.32 ± 0.02 (0.28 - 0.37)	0.32 ± 0.02 (0.23 - 0.36)	0.32 ± 0.01 (0.29 - 0.35)	0.32 ± 0.02 (0.25 - 0.36)	0.22	0.23	0.53	1.00	1.00	1.00
		Functional	0.29 ± 0.07 (0.13 - 0.50)	0.29 ± 0.09 (0.10 - 0.62)	0.32 ± 0.08 (0.14 - 0.56)	0.30 ± 0.06 (0.17 - 0.42)	1.00	1.00	0.27	1.00	0.42	0.34
	Clustering coefficient	Structural (FA)	0.28 ± 0.01 (0.25 - 0.32)	0.28 ± 0.02 (0.21 - 0.34)	0.28 ± 0.01 (0.25 - 0.30)	0.28 ± 0.03 (0.14 - 0.32)	1.00	1.00	0.84	1.00	1.00	1.00
		Functional	0.18 ± 0.04 (0.08 - 0.28)	0.18 ± 0.05 (0.08 - 0.37)	0.20 ± 0.05 (0.10 - 0.34)	0.18 ± 0.04 (0.08 - 0.25)	1.00	1.00	0.09	1.00	0.07	0.13
Parietal	Nodal strength	Structural (FA)	2.16 ± 0.31 (0.87 - 3.29)	2.11 ± 0.28 (1.19 - 2.93)	2.09 ± 0.20 (1.41 - 2.50)	2.23 ± 0.23 (1.75 - 2.66)	0.68	0.84	1.00	1.00	0.94	0.82
		Functional	2.43 ± 0.47	2.45 ± 0.52	2.57 ± 0.56	2.46 ± 0.34	1.00	1.00	1.00	1.00	1.00	1.00

			(1.05 - 3.75)	(1.31 - 4.80)	(1.76 - 3.76)	(1.67 - 2.95)						
	Path length	Structural (FA)	14.06 ± 1.54 (10.38 - 18.14)	14.45 ± 1.57 (10.58 - 22.75)	14.98 ± 1.23 (12.73 - 18.94)	13.94 ± 1.18 (11.10 - 16.52)	0.21	0.06	1.00	1.00	0.44	0.11
		Functional	12.96 ± 2.70 (7.85 - 24.04)	13.02 ± 3.50 (5.76 - 36.07)	12.38 ± 2.71 (7.89 - 22.14)	12.36 ± 1.92 (9.48 - 16.70)	1.00	1.00	1.00	1.00	1.00	1.00
	Local efficiency	Structural (FA)	0.35 ± 0.03 (0.21 - 0.42)	0.35 ± 0.03 (0.23 - 0.41)	0.35 ± 0.02 (0.29 - 0.39)	0.36 ± 0.02 (0.30 - 0.40)	0.24	0.01	1.00	0.27	1.00	0.10
		Functional	0.23 ± 0.06 (0.08 - 0.41)	0.23 ± 0.07 (0.10 - 0.45)	0.24 ± 0.08 (0.11 - 0.38)	0.22 ± 0.05 (0.10 - 0.30)	1.00	1.00	0.31	1.00	0.15	0.50
	Clustering coefficient	Structural (FA)	0.35 ± 0.03 (0.28 - 0.44)	0.34 ± 0.04 (0.20 - 0.44)	0.34 ± 0.03 (0.28 - 0.42)	0.35 ± 0.03 (0.30 - 0.41)	1.00	0.01	1.00	0.10	1.00	0.83
		Functional	0.16 ± 0.04 (0.07 - 0.30)	0.17 ± 0.05 (0.076 - 0.31)	0.18 ± 0.05 (0.09 - 0.27)	0.16 ± 0.04 (0.07 - 0.24)	1.00	1.00	0.25	1.00	0.08	0.37
Occipital	Nodal strength	Structural (FA)	2.03 ± 0.34 (0.69 - 2.64)	2.02 ± 0.42 (0.87 - 2.79)	2.16 ± 0.20 (1.71 - 2.49)	2.20 ± 0.23 (1.59 - 2.62)	1.00	1.00	1.00	1.00	1.00	1.00
		Functional	2.79 ± 0.87 (1.21 - 4.97)	2.78 ± 0.99 (0.62 - 5.65)	2.94 ± 0.85 (1.47 - 5.26)	2.99 ± 0.79 (1.91 - 4.97)	1.00	1.00	1.00	1.00	1.00	1.00
	Path length	Structural (FA)	14.89 ± 1.72 (12.20 - 20.48)	15.18 ± 2.39 (11.71 - 28.71)	14.66 ± 1.14 (13.18 - 18.19)	14.01 ± 1.18 (12.33 - 17.55)	1.00	1.00	1.00	1.00	1.00	1.00
		Functional	13.28 ± 3.30 (7.62 - 26.83)	13.19 ± 3.65 (6.03 - 28.63)	12.43 ± 2.61 (7.43 - 21.60)	12.29 ± 1.95 (9.31 - 16.84)	1.00	1.00	1.00	1.00	1.00	1.00
	Local efficiency	Structural (FA)	0.35 ± 0.03 (0.16 - 0.40)	0.34 ± 0.04 (0.20 - 0.41)	0.35 ± 0.02 (0.31 - 0.39)	0.36 ± 0.02 (0.32 - 0.40)	1.00	1.00	1.00	1.00	1.00	1.00
		Functional	0.30 ± 0.12 (0.06 - 0.61)	0.30 ± 0.13 (0.02 - 0.63)	0.34 ± 0.12 (0.15 - 0.74)	0.32 ± 0.11 (0.13 - 0.54)	1.00	1.00	1.00	1.00	1.00	1.00
	Clustering coefficient	Structural (FA)	0.36 ± 0.04 (0.22 - 0.47)	0.36 ± 0.05 (0.19 - 0.51)	0.35 ± 0.03 (0.30 - 0.43)	0.35 ± 0.03 (0.31 - 0.44)	1.00	1.00	1.00	1.00	1.00	1.00
		Functional	0.20 ± 0.07 (0.06 - 0.41)	0.20 ± 0.08 (0.01 - 0.44)	0.22 ± 0.08 (0.11 - 0.46)	0.21 ± 0.06 (0.10 - 0.32)	1.00	1.00	0.94	1.00	0.88	1.00
		Structural (FA)	4.43 ± 0.54	4.42 ± 0.68	4.12 ± 0.31	4.24 ± 0.36	1.00	1.00	1.00	1.00	1.00	1.00

Basal ganglia	Nodal strength		(3.38 - 6.59)	(2.88 - 6.56)	(3.36 - 4.71)	(3.74 - 5.07)						
		Functional	2.65 ± 0.75 (1.49 - 5.23)	2.83 ± 0.88 (1.34 - 6.27)	2.61 ± 0.67 (1.48 - 4.55)	2.75 ± 0.60 (1.70 - 3.78)	0.69	1.00	1.00	0.28	1.00	1.00
	Path length	Structural (FA)	9.57 ± 0.74 (7.94 - 11.70)	9.88 ± 0.96 (8.01 - 14.43)	10.09 ± 0.63 (8.93 - 11.53)	9.59 ± 0.78 (7.87 - 11.38)	0.04	0.02	1.00	1.00	1.00	0.31
		Functional	10.86 ± 2.21 (5.97 - 16.65)	10.85 ± 2.71 (4.14 - 26.50)	10.91 ± 2.41 (7.13 - 19.02)	10.34 ± 1.58 (7.93 - 13.62)	1.00	1.00	1.00	1.00	1.00	1.00
	Local efficiency	Structural (FA)	0.38 ± 0.02 (0.33 - 0.43)	0.38 ± 0.02 (0.30 - 0.41)	0.38 ± 0.01 (0.35 - 0.41)	0.39 ± 0.02 (0.36 - 0.42)	0.01	0.02	1.00	1.00	1.00	1.00
		Functional	0.18 ± 0.06 (0.06 - 0.36)	0.20 ± 0.07 (0.09 - 0.47)	0.18 ± 0.05 (0.08 - 0.32)	0.20 ± 0.06 (0.11 - 0.33)	0.06	1.00	1.00	0.15	1.00	1.00
	Clustering coefficient	Structural (FA)	0.29 ± 0.03 (0.22 - 0.36)	0.29 ± 0.04 (0.18 - 0.39)	0.30 ± 0.02 (0.25 - 0.33)	0.31 ± 0.02 (0.26 - 0.34)	0.08	0.03	1.00	1.00	1.00	0.62
		Functional	0.12 ± 0.04 (0.04 - 0.23)	0.14 ± 0.05 (0.05 - 0.32)	0.13 ± 0.03 (0.05 - 0.21)	0.14 ± 0.05 (0.06 - 0.25)	0.08	1.00	1.00	0.48	1.00	1.00
Sensorimotor	Nodal strength	Structural (FA)	1.90 ± 0.54 (1.26 - 3.49)	1.86 ± 0.49 (1.18 - 3.38)	1.55 ± 0.22 (1.11 - 2.04)	1.74 ± 0.26 (1.40 - 2.25)	0.44	0.08	1.00	1.00	1.00	0.20
		Functional	1.86 ± 0.66 (0.93 - 4.68)	1.95 ± 0.64 (0.61 - 4.41)	1.79 ± 0.61 (0.99 - 3.59)	1.84 ± 0.50 (1.04 - 2.64)	1.00	1.00	1.00	1.00	1.00	1.00
	Path length	Structural (FA)	13.27 ± 1.64 (9.67 - 16.53)	13.71 ± 1.71 (9.99 - 18.64)	15.15 ± 1.72 (12.25 - 19.02)	13.42 ± 1.39 (10.68 - 16.27)	0.11	<0.001	1.00	0.003	0.26	<0.001
		Functional	13.99 ± 5.05 (8.50 - 51.35)	13.42 ± 3.00 (4.71 - 21.53)	14.06 ± 3.74 (7.98 - 26.98)	13.01 ± 2.36 (9.50 - 20.04)	1.00	1.00	1.00	1.00	1.00	1.00
	Local efficiency	Structural (FA)	0.35 ± 0.03 (0.27 - 0.42)	0.34 ± 0.03 (0.26 - 0.39)	0.32 ± 0.03 (0.24 - 0.37)	0.35 ± 0.03 (0.30 - 0.40)	0.001	<0.001	1.00	0.05	0.48	0.01
		Functional	0.16 ± 0.09 (0.05 - 0.56)	0.17 ± 0.08 (0.02 - 0.46)	0.14 ± 0.06 (0.04 - 0.36)	0.15 ± 0.06 (0.05 - 0.32)	1.00	1.00	1.00	1.00	1.00	1.00
	Clustering coefficient	Structural (FA)	0.42 ± 0.05 (0.33 - 0.58)	0.39 ± 0.05 (0.27 - 0.51)	0.39 ± 0.04 (0.30 - 0.46)	0.42 ± 0.04 (0.34 - 0.52)	<0.001	<0.001	0.63	0.09	1.00	0.03
		Functional	0.12 ± 0.06 (0.04 - 0.34)	0.12 ± 0.05 (0.02 - 0.30)	0.11 ± 0.05 (0.03 - 0.25)	0.11 ± 0.04 (0.04 - 0.27)	1.00	1.00	1.00	1.00	1.00	1.00

Values are reported as mean \pm standard deviation (range). Differences between patient groups and healthy controls were assessed using one-way ANOVA (statistical contrasts) corrected for age, sex and center. P-values were adjusted for multiple comparisons at significance level 0.05 using Bonferroni post-hoc test. Abbreviations: ALS= Amyotrophic lateral sclerosis; FA= Fractional anisotropy; FTD= Fronto-temporal dementia; HC= Healthy controls; PLS= Primary lateral sclerosis; PMA= Progressive muscular atrophy.

Additional Table 6. Global and lobar graph analysis properties of structural and functional brain networks in ALS, PLS and PMA patients and matched healthy controls acquired with Philips Medical Systems Intera machine in San Raffaele Scientific Institute, Milan.

Regions	Graph analysis properties		HC	ALS	PLS	PMA	P ALS vs HC	P PLS vs HC	P PMA vs HC	P ALS vs PLS	P ALS vs PMA	P PLS vs PMA
			61	131	38	28						
Global	Nodal strength	Structural (FA)	2.37 ± 0.19 (1.83 - 2.91)	2.33 ± 0.16 (1.96 - 2.91)	2.30 ± 0.17 (1.82 - 2.64)	2.42 ± 0.20 (2.12 - 2.91)	0.81	0.29	1.00	1.00	1.00	0.40
		Functional	2.64 ± 0.43 (1.84 - 4.01)	2.67 ± 0.49 (1.70 - 4.95)	2.62 ± 0.53 (1.65 - 4.30)	2.60 ± 0.37 (1.82 - 3.31)	1.00	1.00	1.00	1.00	0.89	1.00
	Path length	Structural (FA)	13.24 ± 0.98 (11.11 - 15.54)	13.47 ± 0.94 (11.11 - 15.54)	13.88 ± 1.02 (12.33 - 16.64)	12.98 ± 1.02 (10.57 - 14.86)	0.60	0.01	1.00	0.14	0.44	0.01
		Functional	12.10 ± 2.14 (7.70 - 19.68)	11.98 ± 2.09 (5.45 - 19.04)	12.44 ± 2.59 (7.62 - 21.43)	12.09 ± 1.64 (9.40 - 16.27)	1.00	1.00	1.00	1.00	1.00	1.00
	Local efficiency	Structural (FA)	0.34 ± 0.02 (0.30 - 0.37)	0.34 ± 0.01 (0.30 - 0.39)	0.33 ± 0.01 (0.29 - 0.36)	0.35 ± 0.02 (0.31 - 0.39)	0.63	0.01	1.00	0.17	1.00	0.04
		Functional	0.26 ± 0.05 (0.19 - 0.42)	0.27 ± 0.06 (0.16 - 0.50)	0.26 ± 0.07 (0.16 - 0.48)	0.26 ± 0.04 (0.16 - 0.33)	1.00	1.00	0.91	1.00	0.44	0.99
	Clustering coefficient	Structural (FA)	0.33 ± 0.02 (0.29 - 0.36)	0.32 ± 0.02 (0.28 - 0.37)	0.32 ± 0.01 (0.28 - 0.35)	0.32 ± 0.02 (0.29 - 0.37)	0.12	0.003	1.00	0.26	1.00	0.47
		Functional	0.17 ± 0.03 (0.13 - 0.26)	0.18 ± 0.03 (0.11 - 0.33)	0.17 ± 0.04 (0.12 - 0.30)	0.17 ± 0.03 (0.10 - 0.21)	1.00	1.00	0.45	1.00	0.15	0.64
Fronto-insular	Nodal strength	Structural (FA)	2.53 ± 0.21 (2.03 - 3.06)	2.48 ± 0.22 (1.85 - 3.23)	2.45 ± 0.23 (1.90 - 2.87)	2.62 ± 0.26 (2.17 - 3.38)	0.53	0.40	1.00	1.00	0.19	0.15
		Functional	2.81 ± 0.52 (1.70 - 4.26)	2.74 ± 0.59 (1.54 - 5.34)	2.71 ± 0.63 (1.72 - 4.75)	2.71 ± 0.42 (1.92 - 3.71)	1.00	1.00	0.49	1.00	1.00	1.00
		Structural (FA)	12.51 ± 0.97	12.71 ± 0.92	13.17 ± 1.07	12.20 ± 1.02	0.93	0.01	1.00	0.06	0.33	0.003

	Path length		(10.45 - 14.88)	(10.48 - 15.23)	(11.53 - 15.52)	(9.79 - 13.87)						
		Functional	11.43 ± 1.93 (7.57 - 16.32)	11.53 ± 2.13 (5.33 - 19.63)	12.05 ± 2.65 (7.07 - 20.96)	11.55 ± 1.61 (8.42 - 15.63)	1.00	0.79	1.00	1.00	1.00	1.00
	Local efficiency	Structural (FA)	0.34 ± 0.02 (0.30 - 0.37)	0.33 ± 0.02 (0.28 - 0.40)	0.33 ± 0.02 (0.29 - 0.36)	0.34 ± 0.02 (0.30 - 0.41)	0.58	0.10	1.00	1.00	0.09	0.02
		Functional	0.27 ± 0.06 (0.15 - 0.46)	0.26 ± 0.07 (0.12 - 0.55)	0.26 ± 0.07 (0.16 - 0.48)	0.26 ± 0.05 (0.15 - 0.39)	1.00	1.00	1.00	1.00	1.00	1.00
	Clustering coefficient	Structural (FA)	0.30 ± 0.01 (0.27 - 0.34)	0.29 ± 0.02 (0.25 - 0.35)	0.29 ± 0.02 (0.26 - 0.33)	0.30 ± 0.02 (0.25 - 0.33)	1.00	0.95	1.00	1.00	1.00	0.43
		Functional	0.17 ± 0.04 (0.10 - 0.29)	0.17 ± 0.04 (0.09 - 0.36)	0.16 ± 0.04 (0.11 - 0.28)	0.16 ± 0.03 (0.10 - 0.23)	1.00	1.00	0.54	1.00	1.00	1.00
Temporal	Nodal strength	Structural (FA)	2.52 ± 0.22 (1.72 - 3.04)	2.47 ± 0.20 (2.01 - 2.94)	2.45 ± 0.20 (1.86 - 2.81)	2.48 ± 0.25 (1.80 - 2.89)	0.36	0.55	0.30	1.00	1.00	1.00
		Functional	2.79 ± 0.46 (2.10 - 4.29)	2.84 ± 0.59 (1.65 - 5.27)	2.84 ± 0.56 (1.71 - 4.38)	2.73 ± 0.45 (1.83 - 3.62)	1.00	1.00	1.00	1.00	0.57	0.74
	Path length	Structural (FA)	13.26 ± 0.94 (11.24 - 16.46)	13.51 ± 0.90 (11.16 - 15.58)	13.73 ± 0.85 (12.40 - 16.20)	13.24 ± 1.03 (10.73 - 15.47)	0.38	0.08	1.00	1.00	1.00	0.62
		Functional	12.34 ± 2.09 (7.70 - 16.90)	12.23 ± 2.10 (5.67 - 19.03)	12.47 ± 2.32 (7.79 - 19.42)	12.37 ± 1.63 (10.02 - 17.05)	1.00	1.00	1.00	1.00	1.00	1.00
	Local Efficiency	Structural (FA)	0.33 ± 0.02 (0.28 - 0.37)	0.32 ± 0.02 (0.29 - 0.36)	0.32 ± 0.01 (0.29 - 0.35)	0.32 ± 0.02 (0.25 - 0.36)	1.00	0.60	1.00	1.00	1.00	1.00
		Functional	0.31 ± 0.06 (0.21 - 0.50)	0.31 ± 0.08 (0.16 - 0.62)	0.32 ± 0.08 (0.14 - 0.56)	0.30 ± 0.06 (0.17 - 0.42)	1.00	1.00	0.91	1.00	0.44	0.44
	Clustering coefficient	Structural (FA)	0.28 ± 0.01 (0.25 - 0.32)	0.28 ± 0.01 (0.25 - 0.31)	0.28 ± 0.01 (0.25 - 0.30)	0.28 ± 0.03 (0.14 - 0.32)	1.00	0.81	0.53	1.00	0.87	1.00
		Functional	0.19 ± 0.03 (0.13 - 0.28)	0.20 ± 0.05 (0.11 - 0.37)	0.20 ± 0.05 (0.10 - 0.34)	0.18 ± 0.04 (0.08 - 0.25)	1.00	1.00	0.32	1.00	0.11	0.20
Parietal	Nodal strength	Structural (FA)	2.15 ± 0.21 (1.73 - 2.68)	2.12 ± 0.19 (1.61 - 2.80)	2.09 ± 0.20 (1.41 - 2.50)	2.23 ± 0.23 (1.75 - 2.66)	1.00	0.65	1.00	1.00	0.25	0.16

		Functional	2.52 ± 0.42 (1.69 - 3.75)	2.56 ± 0.56 (1.62 - 4.80)	2.57 ± 0.56 (1.76 - 3.76)	2.46 ± 0.34 (1.67 - 2.95)	1.00	1.00	1.00	1.00	1.00	1.00
	Path length	Structural (FA)	14.35 ± 1.32 (11.68 - 17.75)	14.60 ± 1.10 (11.76 - 17.10)	14.98 ± 1.23 (12.73 - 18.94)	13.94 ± 1.18 (11.10 - 16.52)	0.89	0.05	1.00	0.51	0.22	0.02
		Functional	12.26 ± 2.20 (7.85 - 18.69)	12.06 ± 2.15 (5.76 - 18.86)	12.38 ± 2.71 (7.89 - 22.14)	12.36 ± 1.92 (9.48 - 16.70)	1.00	1.00	1.00	1.00	1.00	1.00
	Local efficiency	Structural (FA)	0.36 ± 0.02 (0.32 - 0.40)	0.36 ± 0.02 (0.29 - 0.41)	0.35 ± 0.02 (0.29 - 0.39)	0.36 ± 0.02 (0.30 - 0.40)	0.42	0.01	1.00	0.14	0.79	0.02
		Functional	0.24 ± 0.05 (0.13 - 0.41)	0.25 ± 0.06 (0.12 - 0.45)	0.24 ± 0.08 (0.11 - 0.38)	0.22 ± 0.05 (0.10 - 0.30)	1.00	1.00	0.48	1.00	0.18	0.60
	Clustering coefficient	Structural (FA)	0.36 ± 0.03 (0.30 - 0.44)	0.35 ± 0.03 (0.27 - 0.44)	0.34 ± 0.03 (0.28 - 0.42)	0.35 ± 0.03 (0.30 - 0.41)	0.67	0.01	1.00	0.18	1.00	0.69
		Functional	0.17 ± 0.04 (0.09 - 0.30)	0.18 ± 0.04 (0.09 - 0.31)	0.18 ± 0.05 (0.09 - 0.27)	0.16 ± 0.04 (0.07 - 0.24)	1.00	1.00	0.40	1.00	0.11	0.48
Occipital	Nodal strength	Structural (FA)	2.14 ± 0.22 (1.69 - 2.64)	2.19 ± 0.20 (1.65 - 2.79)	2.16 ± 0.20 (1.71 - 2.49)	2.20 ± 0.23 (1.59 - 2.62)	0.76	1.00	1.00	1.00	1.00	1.00
		Functional	3.00 ± 0.83 (1.72 - 4.79)	3.10 ± 0.82 (1.57 - 5.75)	2.94 ± 0.85 (1.47 - 5.26)	2.99 ± 0.79 (1.91 - 4.97)	1.00	1.00	1.00	1.00	1.00	1.00
	Path length	Structural (FA)	14.32 ± 1.09 (12.20 - 17.10)	14.44 ± 1.19 (11.71 - 18.23)	14.66 ± 1.14 (13.18 - 18.19)	14.01 ± 1.18 (12.33 - 17.55)	1.00	0.83	1.00	1.00	1.00	0.66
		Functional	12.10 ± 1.99 (7.62 - 16.81)	11.89 ± 1.89 (6.03 - 17.88)	12.43 ± 2.61 (7.43 - 21.60)	12.29 ± 1.95 (9.31 - 16.84)	1.00	1.00	1.00	1.00	1.00	1.00
	Local efficiency	Structural (FA)	0.35 ± 0.02 (0.31 - 0.40)	0.36 ± 0.02 (0.32 - 0.41)	0.35 ± 0.02 (0.31 - 0.39)	0.36 ± 0.02 (0.32 - 0.40)	1.00	1.00	1.00	0.38	1.00	1.00
		Functional	0.33 ± 0.11 (0.13 - 0.61)	0.35 ± 0.10 (0.16 - 0.63)	0.34 ± 0.12 (0.15 - 0.74)	0.32 ± 0.11 (0.13 - 0.54)	1.00	1.00	1.00	1.00	0.81	1.00
	Clustering coefficient	Structural (FA)	0.36 ± 0.03 (0.30 - 0.42)	0.35 ± 0.03 (0.29 - 0.44)	0.35 ± 0.03 (0.30 - 0.43)	0.35 ± 0.03 (0.31 - 0.44)	1.00	1.00	1.00	1.00	1.00	1.00
		Functional	0.22 ± 0.07	0.23 ± 0.07 (0.11 - 0.44)	0.22 ± 0.08 (0.11 - 0.46)	0.21 ± 0.06 (0.10 - 0.32)	1.00	1.00	1.00	1.00	0.69	1.00

			(0.09 - 0.41)									
Basal ganglia	Nodal strength	Structural (FA)	4.24 ± 0.34 (3.38 - 5.00)	4.15 ± 0.35 (3.20 - 4.87)	4.12 ± 0.31 (3.36 - 4.71)	4.24 ± 0.36 (3.74 - 5.07)	0.47	0.61	1.00	1.00	1.00	1.00
		Functional	2.73 ± 0.81 1.49 - 5.23	2.88 ± 0.91 (1.34 - 0.25)	2.61 ± 0.67 (1.48 - 4.55)	2.75 ± 0.60 (1.70 - 3.78)	1.00	1.00	1.00	0.48	1.00	1.00
	Path length	Structural (FA)	9.66 ± 0.73 (8.21 - 11.70)	9.88 ± 0.75 (8.03 - 11.85)	10.09 ± 0.63 (8.93 - 11.53)	9.59 ± 0.78 (7.87 - 11.38)	0.27	0.03	1.00	0.83	0.84	0.13
		Functional	10.39 ± 2.05 (5.97 - 15.16)	10.38 ± 2.59 (4.15 - 26.50)	10.91 ± 2.41 (7.13 - 19.02)	10.34 ± 1.58 (7.93 - 13.62)	1.00	1.00	1.00	1.00	1.00	1.00
	Local efficiency	Structural (FA)	0.39 ± 0.02 (0.35 - 0.43)	0.38 ± 0.02 (0.34 - 0.41)	0.38 ± 0.01 (0.35 - 0.41)	0.39 ± 0.02 (0.36 - 0.42)	0.02	0.03	1.00	1.00	1.00	1.00
		Functional	0.19 ± 0.06 (0.07 - 0.36)	0.21 ± 0.07 (0.04 - 0.47)	0.18 ± 0.05 (0.08 - 0.32)	0.20 ± 0.06 (0.11 - 0.33)	0.45	1.00	1.00	0.33	1.00	1.00
	Clustering coefficient	Structural (FA)	0.31 ± 0.02 (0.26 - 0.36)	0.30 ± 0.02 (0.26 - 0.39)	0.30 ± 0.02 (0.25 - 0.33)	0.31 ± 0.02 (0.26 - 0.34)	0.51	0.08	1.00	1.00	1.00	0.60
		Functional	0.13 ± 0.04 (0.05 - 0.23)	0.14 ± 0.05 (0.03 - 0.31)	0.13 ± 0.03 (0.05 - 0.21)	0.14 ± 0.05 (0.06 - 0.25)	0.28	1.00	1.00	0.70	1.00	1.00
Sensorimotor	Nodal strength	Structural (FA)	1.65 ± 0.23 (1.26 - 2.25)	1.63 ± 0.20 (1.18 - 2.24)	1.55 ± 0.22 (1.11 - 2.04)	1.74 ± 0.26 (1.40 - 2.25)	1.00	0.10	1.00	0.27	0.68	0.03
		Functional	1.69 ± 0.50 (0.93 - 3.36)	1.82 ± 0.55 (0.6 - 3.91)	1.79 ± 0.61 (0.99 - 3.59)	1.84 ± 0.50 (1.04 - 2.64)	1.00	1.00	1.00	1.00	1.00	1.00
	Path length	Structural (FA)	13.34 ± 1.33 (11.18 - 16.53)	14.19 ± 1.44 (10.82 - 17.53)	15.15 ± 1.72 (12.25 - 19.02)	13.42 ± 1.39 (10.68 - 16.27)	0.69	<0.001	1.00	0.002	0.27	<0.001
		Functional	13.92 ± 5.50 (8.50 - 51.35)	13.19 ± 2.97 (4.71 - 21.40)	14.06 ± 3.74 (7.98 - 26.98)	13.01 ± 2.36 (9.50 - 20.04)	1.00	1.00	1.00	1.00	1.00	1.00
	Local efficiency	Structural (FA)	0.35 ± 0.03 (0.27 - 0.40)	0.34 ± 0.03 (0.26 - 0.39)	0.32 ± 0.03 (0.24 - 0.37)	0.35 ± 0.03 (0.30 - 0.40)	0.27	<0.001	1.00	0.03	0.71	0.01
		Functional	0.14 ± 0.06 (0.05 - 0.41)	0.15 ± 0.06 (0.02 - 0.41)	0.14 ± 0.06 (0.04 - 0.36)	0.15 ± 0.06 (0.05 - 0.32)	1.00	1.00	1.00	1.00	1.00	1.00
		Structural (FA)	0.44 ± 0.04	0.41 ± 0.04	0.39 ± 0.04	0.42 ± 0.04	<0.001	<0.001	0.91	0.22	0.87	0.04

	Clustering coefficient		(0.36 - 0.58)	(0.34 - 0.51)	(0.30 - 0.46)	(0.34 - 0.52)						
		Functional	0.11 ± 0.05 0.04 - 0.32)	0.12 ± 0.05 (0.02 - 0.30)	0.11 ± 0.05 (0.03 - 0.25)	0.11 ± 0.04 (0.04 - 0.27)	1.00	1.00	1.00	1.00	1.00	1.00

Values are reported as mean ± standard deviation (range). Differences between patient groups and healthy controls were assessed using one-way ANOVA (statistical contrasts) corrected for age and sex. P-values were adjusted for multiple comparisons at significance level 0.05 using Bonferroni post-hoc test. Abbreviations: ALS= Amyotrophic lateral sclerosis; FA= Fractional anisotropy; HC= Healthy controls; PLS= Primary lateral sclerosis; PMA= Progressive muscular atrophy.

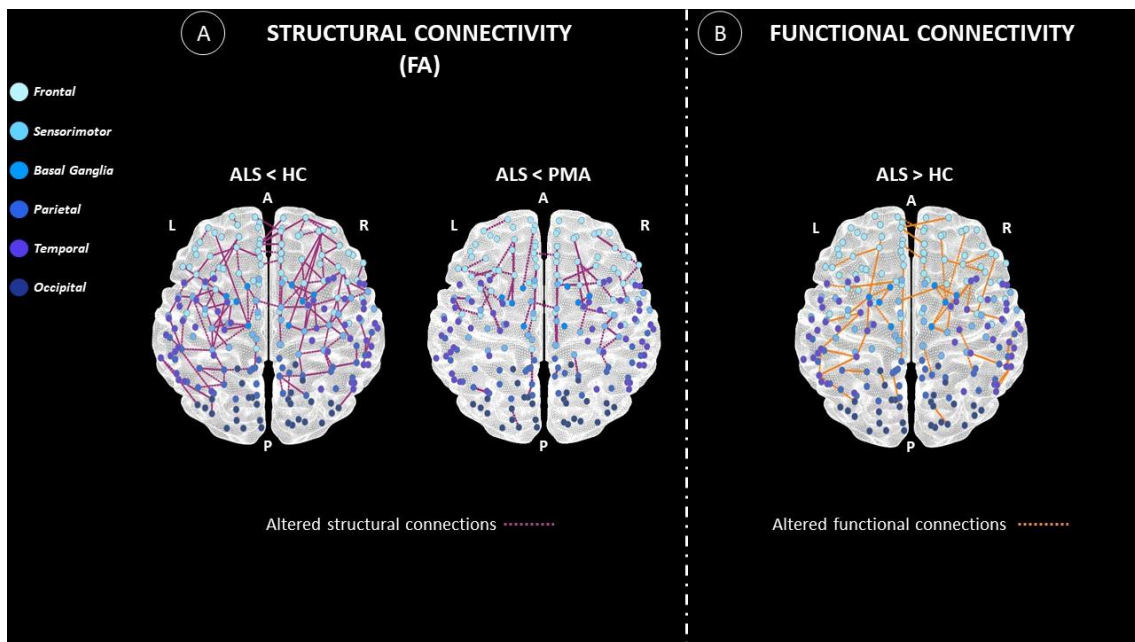
Additional Table 7. Brain nodes of the network.

N	Node	Lobe	N	Node	Lobe	N	Node	Lobe
1	Precentral_L_p1	SENSMOT	75	Insula_L_p2	FRONT-INS	149	Parietal_Inf_L_p1	PAR
2	Precentral_L_p2	SENSMOT	76	Insula_L_p3	FRONT-INS	150	Parietal_Inf_L_p2	PAR
3	Precentral_L_p3	SENSMOT	77	Insula_R_p1	FRONT-INS	151	Parietal_Inf_L_p3	PAR
4	Precentral_L_p4	SENSMOT	78	Insula_R_p2	FRONT-INS	152	Parietal_Inf_R_p1	PAR
5	Precentral_L_p5	SENSMOT	79	Cingulum_Ant_L_p1	FRONT-INS	153	Parietal_Inf_R_p2	PAR
6	Precentral_R_p1	SENSMOT	80	Cingulum_Ant_L_p2	FRONT-INS	154	SupraMarginal_L_p1	PAR
7	Precentral_R_p2	SENSMOT	81	Cingulum_Ant_R_p1	FRONT-INS	155	SupraMarginal_L_p2	PAR
8	Precentral_R_p3	SENSMOT	82	Cingulum_Ant_R_p2	FRONT-INS	156	SupraMarginal_R_p1	PAR
9	Precentral_R_p4	SENSMOT	83	Cingulum_Mid_L_p1	FRONT-INS	157	SupraMarginal_R_p2	PAR
10	Precentral_R_p5	SENSMOT	84	Cingulum_Mid_L_p2	FRONT-INS	158	SupraMarginal_R_p3	PAR
11	Frontal_Sup_L_p1	FRONT-INS	85	Cingulum_Mid_L_p3	FRONT-INS	159	Angular_L_p1	PAR
12	Frontal_Sup_L_p2	FRONT-INS	86	Cingulum_Mid_R_p1	FRONT-INS	160	Angular_L_p2	PAR
13	Frontal_Sup_L_p3	FRONT-INS	87	Cingulum_Mid_R_p2	FRONT-INS	161	Angular_R_p1	PAR
14	Frontal_Sup_L_p4	FRONT-INS	88	Cingulum_Mid_R_p3	FRONT-INS	162	Angular_R_p2	PAR
15	Frontal_Sup_L_p5	FRONT-INS	89	Cingulum_Post_L_p1	PAR	163	Precuneus_L_p1	PAR
16	Frontal_Sup_R_p1	FRONT-INS	90	Cingulum_Post_R_p1	PAR	164	Precuneus_L_p2	PAR
17	Frontal_Sup_R_p2	FRONT-INS	91	Hippocampus_L_p1	TEMP	165	Precuneus_L_p3	PAR
18	Frontal_Sup_R_p3	FRONT-INS	92	Hippocampus_R_p1	TEMP	166	Precuneus_L_p4	PAR
19	Frontal_Sup_R_p4	FRONT-INS	93	ParaHippocampal_L_p1	TEMP	167	Precuneus_L_p5	PAR
20	Frontal_Sup_R_p5	FRONT-INS	94	ParaHippocampal_R_p1	TEMP	168	Precuneus_R_p1	PAR
21	Frontal_Sup_Orb_L_p1	FRONT-INS	95	ParaHippocampal_R_p2	TEMP	169	Precuneus_R_p2	PAR
22	Frontal_Sup_Orb_R_p1	FRONT-INS	96	Amygdala_L_p1	TEMP	170	Precuneus_R_p3	PAR
23	Frontal_Mid_L_p1	FRONT-INS	97	Amygdala_R_p1	TEMP	171	Precuneus_R_p4	PAR
24	Frontal_Mid_L_p2	FRONT-INS	98	Calcarine_L_p1	OCC	172	Paracentral_Lobule_L_p1	SENSMOT
25	Frontal_Mid_L_p3	FRONT-INS	99	Calcarine_L_p2	OCC	173	Paracentral_Lobule_L_p2	SENSMOT
26	Frontal_Mid_L_p4	FRONT-INS	100	Calcarine_L_p3	OCC	174	Paracentral_Lobule_R_p1	SENSMOT
27	Frontal_Mid_L_p5	FRONT-INS	101	Calcarine_R_p1	OCC	175	Caudate_L_p1	BG
28	Frontal_Mid_L_p6	FRONT-INS	102	Calcarine_R_p2	OCC	176	Caudate_R_p1	BG
29	Frontal_Mid_L_p7	FRONT-INS	103	Calcarine_R_p3	OCC	177	Putamen_L_p1	BG
30	Frontal_Mid_R_p1	FRONT-INS	104	Cuneus_L_p1	OCC	178	Putamen_R_p1	BG
31	Frontal_Mid_R_p2	FRONT-INS	105	Cuneus_L_p2	OCC	179	Pallidum_L_p1	BG
32	Frontal_Mid_R_p3	FRONT-INS	106	Cuneus_R_p1	OCC	180	Pallidum_R_p1	BG
33	Frontal_Mid_R_p4	FRONT-INS	107	Cuneus_R_p2	OCC	181	Thalamus_L_p1	BG
34	Frontal_Mid_R_p5	FRONT-INS	108	Lingual_L_p1	OCC	182	Thalamus_R_p1	BG
35	Frontal_Mid_R_p6	FRONT-INS	109	Lingual_L_p2	OCC	183	Heschl_L_p1	TEMP
36	Frontal_Mid_R_p7	FRONT-INS	110	Lingual_L_p3	OCC	184	Heschl_R_p1	TEMP
37	Frontal_Mid_Orb_L_p1	FRONT-INS	111	Lingual_R_p1	OCC	185	Temporal_Sup_L_p1	TEMP
38	Frontal_Mid_Orb_R_p1	FRONT-INS	112	Lingual_R_p2	OCC	186	Temporal_Sup_L_p2	TEMP
39	Frontal_Inf_Oper_L_p1	FRONT-INS	113	Lingual_R_p3	OCC	187	Temporal_Sup_L_p3	TEMP
40	Frontal_Inf_Oper_R_p1	FRONT-INS	114	Occipital_Sup_L_p1	OCC	188	Temporal_Sup_R_p1	TEMP
41	Frontal_Inf_Oper_R_p2	FRONT-INS	115	Occipital_Sup_L_p2	OCC	189	Temporal_Sup_R_p2	TEMP
42	Frontal_Inf_Tri_L_p1	FRONT-INS	116	Occipital_Sup_R_p1	OCC	190	Temporal_Sup_R_p3	TEMP
43	Frontal_Inf_Tri_L_p2	FRONT-INS	117	Occipital_Sup_R_p2	OCC	191	Temporal_Sup_R_p4	TEMP
44	Frontal_Inf_Tri_L_p3	FRONT-INS	118	Occipital_Mid_L_p1	OCC	192	Temporal_Pole_Sup_L_p1	TEMP
45	Frontal_Inf_Tri_R_p1	FRONT-INS	119	Occipital_Mid_L_p2	OCC	193	Temporal_Pole_Sup_L_p2	TEMP
46	Frontal_Inf_Tri_R_p2	FRONT-INS	120	Occipital_Mid_L_p3	OCC	194	Temporal_Pole_Sup_R_p1	TEMP
47	Frontal_Inf_Tri_R_p3	FRONT-INS	121	Occipital_Mid_L_p4	OCC	195	Temporal_Pole_Sup_R_p2	TEMP
48	Frontal_Inf_Orb_L_p1	FRONT-INS	122	Occipital_Mid_R_p1	OCC	196	Temporal_Mid_L_p1	TEMP
49	Frontal_Inf_Orb_L_p2	FRONT-INS	123	Occipital_Mid_R_p2	OCC	197	Temporal_Mid_L_p2	TEMP
50	Frontal_Inf_Orb_R_p1	FRONT-INS	124	Occipital_Mid_R_p3	OCC	198	Temporal_Mid_L_p3	TEMP
51	Frontal_Inf_Orb_R_p2	FRONT-INS	125	Occipital_Inf_L_p1	OCC	199	Temporal_Mid_L_p4	TEMP
52	Rolandic_Oper_L_p1	FRONT-INS	126	Occipital_Inf_R_p1	OCC	200	Temporal_Mid_L_p5	TEMP
53	Rolandic_Oper_R_p1	FRONT-INS	127	Fusiform_L_p1	TEMP	201	Temporal_Mid_L_p6	TEMP
54	Rolandic_Oper_R_p2	FRONT-INS	128	Fusiform_L_p2	TEMP	202	Temporal_Mid_L_p7	TEMP
55	Supp_Motor_Area_L_p1	SENSMOT	129	Fusiform_L_p3	TEMP	203	Temporal_Mid_R_p1	TEMP
56	Supp_Motor_Area_L_p2	SENSMOT	130	Fusiform_R_p1	TEMP	204	Temporal_Mid_R_p2	TEMP
57	Supp_Motor_Area_L_p3	SENSMOT	131	Fusiform_R_p2	TEMP	205	Temporal_Mid_R_p3	TEMP
58	Supp_Motor_Area_R_p1	SENSMOT	132	Fusiform_R_p3	TEMP	206	Temporal_Mid_R_p4	TEMP
59	Supp_Motor_Area_R_p2	SENSMOT	133	Postcentral_L_p1	SENSMOT	207	Temporal_Mid_R_p5	TEMP
60	Supp_Motor_Area_R_p3	SENSMOT	134	Postcentral_L_p2	SENSMOT	208	Temporal_Mid_R_p6	TEMP
61	Olfactory_L_p1	FRONT-INS	135	Postcentral_L_p3	SENSMOT	209	Temporal_Pole_Mid_L_p1	TEMP
62	Olfactory_R_p1	FRONT-INS	136	Postcentral_L_p4	SENSMOT	210	Temporal_Pole_Mid_R_p1	TEMP

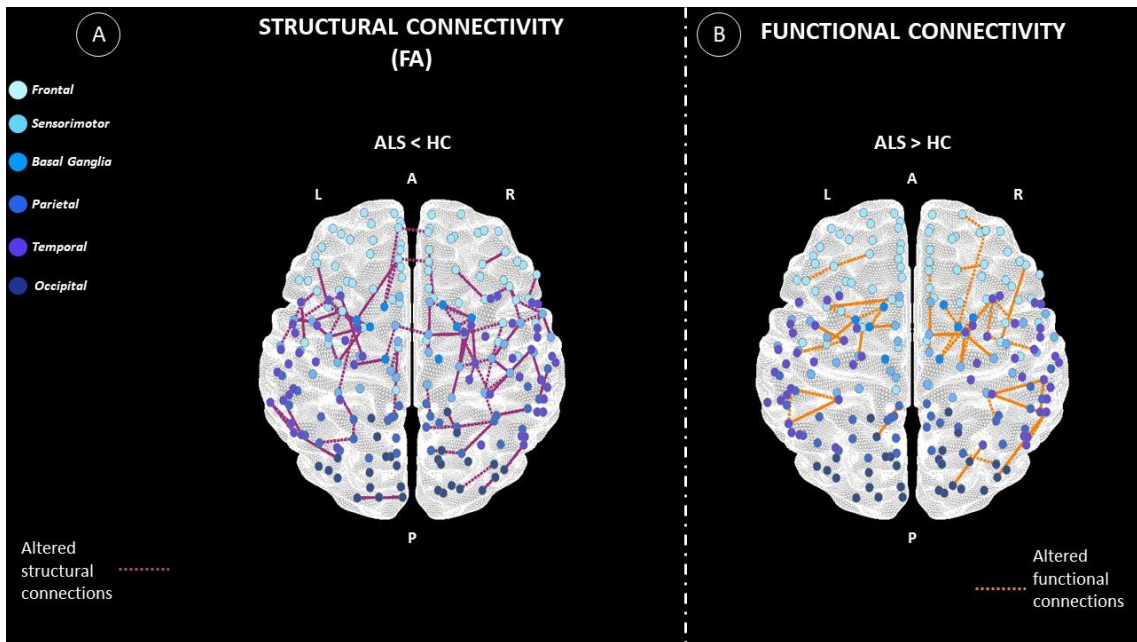
63	Frontal_Sup_Medial_L_p1	FRONT-INS	137	Postcentral_L_p5	SENSMOT	211	Temporal_Pole_Mid_R_p2	TEMP
64	Frontal_Sup_Medial_L_p2	FRONT-INS	138	Postcentral_R_p1	SENSMOT	212	Temporal_Inf_L_p1	TEMP
65	Frontal_Sup_Medial_L_p3	FRONT-INS	139	Postcentral_R_p2	SENSMOT	213	Temporal_Inf_L_p2	TEMP
66	Frontal_Sup_Medial_L_p4	FRONT-INS	140	Postcentral_R_p3	SENSMOT	214	Temporal_Inf_L_p3	TEMP
67	Frontal_Sup_Medial_R_p1	FRONT-INS	141	Postcentral_R_p4	SENSMOT	215	Temporal_Inf_L_p4	TEMP
68	Frontal_Sup_Medial_R_p2	FRONT-INS	142	Postcentral_R_p5	SENSMOT	216	Temporal_Inf_R_p1	TEMP
69	Frontal_Sup_Medial_R_p3	FRONT-INS	143	Parietal_Sup_L_p1	PAR	217	Temporal_Inf_R_p2	TEMP
70	Frontal_Mid_Orb_L_p2	FRONT-INS	144	Parietal_Sup_L_p2	PAR	218	Temporal_Inf_R_p3	TEMP
71	Frontal_Mid_Orb_R_p2	FRONT-INS	145	Parietal_Sup_L_p3	PAR	219	Temporal_Inf_R_p4	TEMP
72	Rectus_L_p1	FRONT-INS	146	Parietal_Sup_R_p1	PAR	220	Temporal_Inf_R_p5	TEMP
73	Rectus_R_p1	FRONT-INS	147	Parietal_Sup_R_p2	PAR			
74	Insula_L_p1	FRONT-INS	148	Parietal_Sup_R_p3	PAR			

Abbreviations: Ant= anterior; BG= basal ganglia; FRONT-INS= fronto-insular; Inf= inferior; L= left; Mid= middle; N= region number; Oper= operculum; OCC= occipital; Orb= orbital; p= part; PAR= parietal; Post= posterior; R= right; SENSMOT= sensorimotor; Sup= superior; Supp= supplementary; TEMP= temporal; Tri= triangularis.

Additional Figure 1. Subnetworks showing altered structural and functional connectivity in ALS (excluding ALS-FTD patients), PLS and PMA patients and healthy controls. Altered structural (A) and functional (B) connections are represented in magenta and orange, respectively. ALS patients and healthy controls comparison was adjusted for age, sex, and MR scanner. All the other comparisons were adjusted for age and sex. Six shades of blue color were used to define the belonging of each node to different lobes starting with light blue (frontal lobe) to dark blue (posterior lobe, i.e. occipital). Abbreviations: A= anterior; ALS= Amyotrophic Lateral Sclerosis; FA= fractional anisotropy; FTD= frontotemporal dementia; HC= healthy controls; L= left; P = posterior; PMA= Progressive muscular atrophy; R= right.



Additional Figure 2. Subnetworks showing affected connections between groups acquired in Milan. Altered structural (A) and functional (B) connections are represented in magenta and orange, respectively. All the comparisons were adjusted for age and sex. Six shades of blue color were used to define the belonging of each node to different lobes starting with light blue (frontal lobe) to dark blue (posterior lobe, i.e. occipital). Abbreviations: A= anterior; ALS= Amyotrophic Lateral Sclerosis; FA= fractional anisotropy; HC= healthy controls; L= left; P = posterior; R= right.



4. TRACKING NEURODEGENERATION IN FRONTOTEMPORAL DEMENTIA VARIANTS

4.1. Speech production differences in English and Italian speakers with non-fluent variant PPA

ARTICLE

Speech production differences in English and Italian speakers with nonfluent variant PPA

Elisa Canu, PhD, Federica Agosta, MD, PhD, Giovanni Battistella, PhD, Edoardo G. Spinelli, MD, Jessica DeLeon, MD, Ariane E. Welch, MSLP, Maria Luisa Mandelli, PhD, H. Isabel Hubbard, PhD, Andrea Moro, PhD, Giuseppe Magnani, MD, Stefano F. Cappa, MD, Bruce L. Miller, MD, Massimo Filippi, MD, and Maria Luisa Gorno-Tempini, MD, PhD

Correspondence
Dr. Canu
canu.elisa@hsr.it

Neurology® 2020;94:e1062-e1072. doi:10.1212/WNL.0000000000008879

Abstract

Objective

To understand whether the clinical phenotype of nonfluent/agrammatic primary progressive aphasia (nfvPPA) could present differences depending on the patient's native language.

Methods

In this cross-sectional study, we analyzed connected speech samples in monolingual English (nfvPPA-E) and Italian speakers (nfvPPA-I) who were diagnosed with nfvPPA and matched for age, sex, and Mini-Mental State Examination scores. Patients also received a comprehensive neuropsychological battery. All patients and 2 groups of age-matched healthy controls underwent an MRI scan with 3D T1-weighted sequences. Connected speech measures and the other cognitive features were compared between patient groups. MRI variables, in terms of gray matter volume, were compared between each patient group and the corresponding controls.

Results

Compared to nfvPPA-E, nfvPPA-I had fewer years of education and shorter reported disease duration. The 2 groups showed similar regional atrophy compatible with clinical diagnosis. Patients did not differ in nonlanguage domains, comprising executive scores. Connected speech sample analysis showed that nfvPPA-E had significantly more distortions than nfvPPA-I, while nfvPPA-I showed reduced scores in some measures of syntactic complexity. On language measures, Italian speakers performed more poorly on syntactic comprehension.

Conclusions

nfvPPA-E showed greater motor speech impairment than nfvPPA-I despite higher level of education and comparable disease severity and atrophy changes. The data also suggest greater grammatical impairment in nfvPPA-I. This study illustrates the need to take into account the possible effect of the individual's spoken language on the phenotype and clinical presentation of primary progressive aphasia variants.

The following data have been published (Canu et al., Neurology. 2020 Mar 10;94(10):e1062-e1072. doi: 10.1212/WNL.0000000000008879).

INTRODUCTION

Current diagnostic guidelines for primary progressive aphasia (PPA) recognize three variants: non-fluent/agrammatic PPA (nfvPPA), semantic PPA (svPPA), and logopenic PPA (lvPPA) (Gorno-Tempini, Hillis et al., 2011). These variants differ in terms of the impacted language domains (Gorno-Tempini et al., 2011), distribution of atrophy (Gorno-Tempini, Dronkers et al., 2004) and pathological substrates (Spinelli, Mandelli et al., 2017). Education, bilingualism, rural dwelling, and intrinsic aspects of native language can influence language symptoms in neurodegenerative diseases (Alladi & Hachinski, 2018). The world languages show an enormous amount of variation, although this variation is restricted by a set of universal principles which are presently under investigation (Christiansen MH, 2009, Moro, 2015, Rizzi, 2009). Phonology and orthography differences between English and Italian can affect reading deficits, as previously shown in dyslexia (Lindgren, De Renzi et al., 1985) and in few cases of semantic aphasia (Cappa, Nespors et al., 1997, Folegatti, Pia et al., 2015, Rozzini L, 1997). Similarly, we speculate that articulatory and morpho-syntactic differences between languages could impact speech production deficits in nfvPPA. For instance, English is a Germanic language mainly characterized by frequent consonant clusters (Haspelmath M, 2005) while Italian is a Romance language, with prevalent consonant-vowel syllable structure and few consonant-clusters (Nespor, 1994). On the other hand, Italian is a highly synthetic language, characterized by the extensive use of inflectional and derivational morphology (Nespor, 1994). Since PPA diagnostic criteria (Gorno-Tempini et al., 2011) were mostly defined by observations in native English speakers, difference in phenotypic presentation based on intrinsic language features could lead to possible misdiagnosis.

In this study, we compared connected speech samples in monolingual English and Italian speakers with a diagnosis of nfvPPA and compared patterns of speech and language errors between the two patient groups. Neuroanatomical differences were also analyzed. We hypothesized that, despite a similar brain cortical damage, English-speaking nfvPPA patients might show higher number of distortions and motor speech errors, while Italian patients might show more morpho-syntactic difficulties.

METHODS

Participants

Thirty-eight patients with nfvPPA (18 Italian native speakers and 20 English native speakers) were studied. Italian patients (nfvPPA-I) were prospectively recruited at the Department of Neurology of the San Raffaele Hospital in Milan, Italy. English nfvPPA patients (nfvPPA-E) were selected from 44 nfvPPA cases recruited at the Memory and Aging Center at University of California, San Francisco (UCSF) to be age-, sex- and Mini Mental State Examination (MMSE)-matched with nfvPPA-I cases. We matched study groups for severity using MMSE, the only objective measure that was available at both sites. We also report disease duration but did not match for it since identification of first symptom, especially subtle linguistic impairment, is highly subjective and can be affected by education level, cultural and social context in each country (Alladi & Hachinski, 2018). Other inclusion criteria at both sites were: clinical diagnosis of imaging-supported sporadic nfvPPA (Gorno-Tempini et al., 2011); right-handedness; monolingual Italian or English current and native speakers; availability of an audiotaped picture description from the Western Aphasia Battery (Kertesz, 1982); not mute: sufficiently intelligible speech such that the intended target could be determined for the majority of words. In addition, subjects were excluded if they had: significant medical illnesses or substance abuse that could interfere with cognitive functioning; any other systemic, psychiatric, or neurological illnesses; other causes of focal or diffuse brain damage, including cerebrovascular disorders at routine MRI.

Patients received a comprehensive evaluation including structured history and neurological examination, neuropsychological testing, extensive battery of language tests, and MRI. Clinical diagnosis was based on history, neurological evaluation and review of neuroimaging findings (i.e., conventional MRI, CT, and/or PET scans). When available, a non-AD pathology was suggested by cerebrospinal fluid (CSF) biomarkers or amyloid PET. Fifty-one right-handed, monolingual Italian (N=38) and English (N=31) speakers, age- and sex-matched healthy controls were recruited at both centres among spouses of patients and by word of mouth. Healthy controls underwent a multidimensional assessment, including neurological and neuropsychological evaluation, and were included only if results were in the normal range.

Standard protocol approvals and patient consents

Local ethical standards committee on human experimentation approved the study protocol and all participants (or their caregivers) provided written informed consent prior to study inclusion.

Neuropsychological assessment

At each centre, nfvPPA patients underwent a comprehensive neuropsychological evaluation as previously described for Italian (Agosta, Ferraro et al., 2015, Canu, Agosta et al., 2018) and English (Kramer, Jurik et al., 2003, Spinelli et al., 2017) languages (Table 1).

The evaluation of language included the examination of: confrontation naming with subtests from CaGi battery (nfvPPA-I) and the 15-item version of the Boston Naming Test (nfvPPA-E); object knowledge with the Pyramids and Palm Trees Test; single-word comprehension with word-picture matching tests from CaGi battery (nfvPPA-I) and a subtest of the Western Aphasia Battery (WAB, nfvPPA-E); visual and auditory comprehension of syntactically complex sentences with the Token test, the subtests from the BADA battery (nfvPPA-I) and the syntax comprehension test (nfvPPA-E); repetition with the subtest of Aachen Aphasia Test (nfvPPA-I) and a subtest of the WAB (nfvPPA-E). To evaluate connected speech production, patient speech samples were recorded while they described the image of the picnic picture subtest of the WAB.

Quantitative analysis of speech samples

The speech sample was the picnic picture description component of the Western Aphasia Battery (Kertesz, 1982). Patients were instructed as follows: *'take a look at this picture, tell me what you see, and try to talk in sentences'*. Speech samples were audio-recorded using the software "Audacity" (<http://audacity.sourceforge.net>) and analysed according to a previously described quantitative procedure. (Wilson, Henry et al., 2010) We investigated four different aspects of the speech samples: (i) speech rate and speech sound errors; (ii) other disruptions to fluency; (iii) lexical content and (iv) syntactic structure and complexity. Specifically, the following measures were recorded:

(i) *Speech rate and speech sound errors*. Total duration of the sample; duration of pauses; duration of the sample without pauses; total number of words; speech production rate (total number of words/duration of the sample without pauses); distortions;

phonological paraphasias and neologisms; motor speech rate [(number of distortions/number of words)*100].

(ii) *Other disruptions to fluency*. False starts; filled pauses; repaired sequences; incomplete sequences.

(iii) *Lexical content*. Open class words; closed class words; verbs; nouns; open class proportion (open class words/closed class words); and verb proportion (verbs/verbs+nouns).

(iv) *Syntactic structure and complexity*. Number of utterances (i.e., a sequence of words not interrupted by a pause lasting more than two seconds, whose boundaries could be identified on the basis of prosodic cues. An utterance could then correspond to a word, a phrase, a part of a phrase or a sentence); number of sentences (i.e., a syntactic structure including at least a subject and a verb); number of words in sentences; mean length of sentence (number of words in sentences/number of sentences); proportion of sentences (number of sentences/number of utterances); number of embeddings; morphosyntactic errors; syntax production rate (number of words in sentences/number of words); morphosyntactic error rate (number of morphosyntactic errors/number of words in sentences); and semantic errors.

MRI acquisition

In both centres, all subjects underwent a brain MRI scan with 3D T1 sequences.

NfvPPA-I. Brain MRI scans were obtained using a 3.0 T scanner (Intera, Philips Medical Systems, Best, the Netherlands). The following sequence was acquired: 3D T1-weighted fast field echo (TR=25 ms, TE=4.6 ms, flip angle=30°, 220 contiguous axial slices with voxel size=0.89 x 0.89 x 0.8 mm, matrix size=256 × 256, FOV=230 × 182 mm²).

NfvPPA-E. Brain MRI scans were obtained using 1.5 T (Siemens, Magnetom VISION), 3.0 T (Siemens, Trio), or 4.0 T Bruker/Siemens scanners. The following sequences were acquired: 1) 1.5 T scanner: T1-weighted volumetric Magnetization Prepared Rapid Acquisition Gradient Echo (MPRAGE; TR=10 ms, TE=4 ms, flip angle=15°, 154 contiguous coronal slices with voxel size=1 x 1 x 1.5 mm); 2) 3.0 T scanner: T1-weighted volumetric MPRAGE (TR=23 ms, TE=2.98 ms, flip angle=9°, 160 contiguous sagittal slices with voxel size=1 x 1 x 1 mm, FOV=256 × 256 mm²); 3) 4.0 T

scanner: T1-weighted volumetric MPRAGE (TR=2330 ms, TE=3 ms, flip angle=7°, 157 continuous sagittal slices with voxel size= $1 \times 1 \times 1 \text{ mm}^3$).

MRI analysis

Whole-brain and regions of interest (ROIs) analyses were conducted to investigate potential differences between nfvPPA-E and nfvPPA-I versus controls and versus each other. For the neuroimaging portion of the study, one NfvPPA-E and four healthy participants in the Italian cohort failed the quality check and were excluded from the analyses.

Voxel-Based Morphometry (VBM) analysis. Structural MRI data were pre-processed using the Computational Anatomy Toolbox (CAT12; <http://dbm.neuro.uni-jena.de/cat>) in Statistical Parametric Mapping software (SPM12; <http://www.fil.ion.ucl.ac.uk/spm/software/spm12>) using Matlab version R2017b. CAT12 classifies T1-weighted data as gray matter (GM), white matter (WM), and cerebrospinal fluid (CSF) using an improved segmentation approach compared to the traditional unified segmentation (Ashburner & Friston, 2005), based on an Adaptive Maximum A Posterior (AMAP) technique without the need for a priori information on the tissue probabilities. This means that the Tissue Probability Maps (TPM) are only used for spatial normalization, initial skull-stripping, and as initial segmentation estimate. The subsequent AMAP estimation is adaptive in the sense that local variations of the parameters (i.e., means and variance) are modelled as slowly varying spatial functions (Rajapakse, Giedd et al., 1997). This accounts not only for intensity inhomogeneities, but also for other local intensity variations. In addition, the segmentation approach uses a Partial Volume Estimation (PVE) with a simplified mixed model of a maximum of two tissue types (Tohka, Zijdenbos et al., 2004). GM probability maps were non-linearly normalized to the Montreal Neurological Institute (MNI) space using DARTEL (Ashburner, 2007), modulated by the Jacobian determinant of the deformations derived from the spatial normalization, and smoothed with an isotropic Gaussian kernel of 8 mm full width at half maximum (FWHM).

Region of interest analysis. For each participant, mean GM volumes in left-lateralized ROIs were extracted. ROIs were obtained from the Juelich and Harvard-Oxford atlases (<http://fsl.fmrib.ox.ac.uk/fsl/fsl4.0/fslview/atlas-descriptions.html>) and were chosen

independently from the VBM results and based on previous evidence: *pars opercularis* and *pars triangularis* of the inferior frontal gyrus, premotor cortex, anterior insula, pre-supplementary motor area (pre-SMA), SMA, striatum, angular and supramarginal gyri, and finally the posterior cingulate cortex (PCC) as a control region.

Statistical analysis

Demographic, clinical and cognitive data. Participant characteristics were compared between groups using t-test models or Fisher's exact test. In order to make the cognitive data comparable between groups, we transformed raw performance scores of the neuropsychological assessment in Z-scores by using normative data of age-, sex- and education-matched populations of healthy Italian and English controls. The measures extracted from the speech samples were compared between groups as raw scores accounting for patients' years of education.

MRI data. VBM analysis. Inferential statistic was performed on the smoothed-modulated GM tissue probability maps using a voxel-by-voxel 2x2 ANOVA with 2 levels per factor (Factor 1 = Site - levels = UCSF, Milan; Factor 2: Group - levels = nfvPPA, healthy controls) including age, sex, whole brain total GM volume, and MRI scanner type (3.0T Philips; 1.5T and 3.0T Siemens; 4.0T Bruker/Siemens) as covariates. Each group of patients was compared against the matched healthy controls and a Group x Site interaction was performed in order to investigate differences between US and Italian patient groups. The statistical threshold was applied at $p < 0.05$ after family-wise error (FWE) correction for multiple comparisons over the whole brain and $k > 100$ for cluster extent.

ROI analysis. A 2x2 ANOVA factorial design (the same as for VBM) was run for each ROI accounting for age, sex, whole brain total GM volume, and scanner type as covariates using Matlab (Statistics and Machine Learning Toolbox). The same contrasts as for VBM were performed. The statistical threshold was set at $p < 0.05$ uncorrected and Bonferroni corrected for multiple comparisons over the number of tests performed (i.e. 10, one per each ROI. This set the corrected p-value to 0.005 [0.05/10]).

Data availability statement

The dataset used and analyzed during the current study is available from the corresponding author upon request to qualified researchers (i.e., affiliated to a university or research institution/hospital).

RESULTS

Demographic, clinical and cognitive data

Table 1 shows demographic, clinical and cognitive data. Patient groups were matched for age, sex, and performances at the test assessing global cognition (MMSE), memory and executive functions (Table 1). E-sample had longer disease duration, while I-sample had less years of education and performed worse in tests assessing syntactic comprehension (Table 1). The remaining language features were similar between groups.

Table 2 shows the quantitative features of connected speech production. The nfvPPA-E patients showed higher number of distortions and greater motor speech rate, while the nfvPPA-I presented with a higher number of phonological paraphasias and utterances, and reduced mean length of sentences (Table 2). Concerning distortions, nfvPPA-E produced a total of 187 distortions. Among those that were ascribable to recognizable words (N=158), 140 (89%) were consonant (singleton or cluster) distortions, the remaining were vowel distortions. NfvPPA-I produced a total of 10 distortions, among those that were ascribable to recognizable words (N=6), all were consonant (singleton or cluster) distortions.

MRI

VBM analysis. Table 3 and Figure 1 show the reduced GM volume in each group of patients compared to controls. In both groups, patients showed atrophy at the left hemisphere in the opercularis portion of the inferior frontal gyrus, pre-SMA, precentral gyrus, thalamus, insula, and hippocampus. Atrophy extended also to the left caudate nucleus in nfvPPA-I and to the left postcentral gyrus in the nfvPPA-E. We did not find a Group x Site significant interaction, thus no differences between patient groups were observed.

ROI analysis. Table 4 and Figure 2 show the ROI volume reduction in patients compared with controls. In both groups, patients showed reduced GM volumes of the left pars opercularis of the inferior frontal gyrus, premotor cortex, anterior insula, pre-SMA,

angular gyrus, and striatum. Additionally, nfvPPA-E patients showed an involvement of the left supramarginal gyrus that was near to be significant also in the nfvPPA-I group. The remaining ROI volumes, including PCC, were similar to those of healthy controls. No Group x Site interaction was observed.

DISCUSSION

We compared two cohorts of nfvPPA patients who were native speakers of Italian or English with the aim of assessing the presence of language-specific phenotypic differences. During connected speech samples, nfvPPA-E cases showed higher number of distortions. NfvPPA-I had reduced mean length of sentences and showed greater difficulty in syntax comprehension. These findings occur in patients with similar cognitive impairment, disease severity and brain atrophy, and while controlling for differences in education level. These results highlight the need of taking into consideration linguistic and cultural differences when evaluating patients with neurodegenerative disorders and suggest that PPA diagnostic criteria defined by symptoms of English-speaking patients might be less effective for diagnosing individuals speaking other languages.

NfvPPA-E produced more phonetic distortions, in terms of absolute numbers and in proportion of total number of produced words, compared to nfvPPA-I. This greater impairment is compatible with the hypothesis that frequent consonant clusters typical of the English language might create a greater motoric challenge for a degenerating motor speech planning system. On the other hand, the prevalence of consonant-vowel sequences in Italian words might influence the greater number of phonological paraphasias in nfvPPA-I patients. This issue is relevant for PPA differential diagnosis in Italian patients because, in the English description of the disorder (Wilson et al., 2010), phonological paraphasias are considered more common in the logopenic variant.

We observed that, compared to English cases, nfvPPA-I patients showed reduced complexity of speech production by limiting the number of words in sentences, even after controlling for educational level. A similar argument as described above can apply and we speculate that this difference might reflect difficulties related to the higher demands of the highly synthetic Italian language compared to English. As we will discuss below,

the lower education level of the Italian cohort, although controlled for in the analyses, could be a confounding factor of this result.

The idea that language-specific features affect the clinical phenotypes of the same disorder in different languages has been previously reported. In developmental dyslexia, the Italian relatively transparent alphabetic system leads to better reading scores in Italian cases compared to English and French dyslexics, despite a similar pattern of altered brain activations (Paulesu, Demonet et al., 2001). Similarly, the same system influences the manifestation of reading errors in acquired language disorders, (Cappa et al., 1997, Folegatti et al., 2015) such as semantic variant of PPA (svPPA) with anterior temporal atrophy (Rozzini L, 1997). In svPPA, the more phonologically opaque alphabetic structure of English is reflected in the regularization errors that English patients make when reading atypically spelled words [e.g. ‘choir’ for ‘quire’ (kwarə)] (Haspelmath M, 2005). On the other hand, in Italian the only irregularity in converting written words to utterances mainly regard stress assignment. (Nespor, 1994) Word stress predominantly falls on the heavy penultimate syllable; words without a heavy penultimate syllable are phonological unpredictable and, thus, necessitate to be lexically/semantically marked (Cappa et al., 1997, Folegatti et al., 2015). Therefore, the typical errors that Italian svPPA patients make when reading aloud are stress assignment errors (e.g., ‘tavòlo’ for ‘tàvolo’). Gogi aphasia is another example of a unique presentation of a lexical/semantic reading disorders in Japanese speakers who make errors only in the non-phonetic kanji script (Imura, 1943, Jibiki & Yamaguchi, 1993).

In the present study, nfvPPA-I patients had less years of education and shorter reported disease duration (despite similar disease severity) compared to nfvPPA-E. Level of education is one of the main determinants of the so-called ‘cognitive reserve’, influencing disease duration and severity. While this difference can certainly impact the results of the analyses, our main finding is that the group with lower education (the Italian group) showed milder, and in some case absent, motor speech impairment. Our study cannot provide evidence regarding the nature of cognitive reserve in our two experimental groups since patients were explicitly matched for age and general disease severity (MMSE). An effect of education on cognition and disease progression can be hypothesized since the Italian native speakers group reached similar disease severity to the US group in shorter amount of time. However, we cannot exclude a bias in the highly subjective estimation

of symptom onset nor that lower performances on syntactic production in nfvPPA-I cases is due to their lower education.

The current diagnostic criteria for PPA (Gorno-Tempini et al., 2011) are mainly based on deficits seen in the English-speaking patients. As a result, the criteria may not entirely capture the speech and language changes that occur in non-English native speakers. Specifically, nfvPPA diagnosis can be considered whether one of the two core features, among agrammatism in language production and presence of motor speech deficits (apraxia of speech and dysarthria), is satisfied (Gorno-Tempini et al., 2011). Although a diagnosis of nfvPPA was still possible, most of the Italian cases presented in this study satisfied only one of these core features (agrammatism) despite similar pattern of brain atrophy. These results suggest the necessity to define or refine specific linguistic features (and criteria) that pertain to the patient's native and spoken language. Our results suggest that similar patterns of brain atrophy might be associated with different symptomatology depending on the patients native language. Therefore, applying current PPA sub-variants diagnostic criteria to patients speaking languages with different features from English might lead to misdiagnosis or at least diagnostic confusion. For example, orthographic semantic errors, rather than anomia, might be the first sign of semantic variant PPA in a pictographic language such as Chinese, while grammatical errors might be more common in lvPPA patients speaking languages with complex morphosyntactic structures such as French or Italian. Our paper is the first attempt at highlighting these differences and we hope will inspire collaborative international research that will lead to language-specific testing and diagnostic tools.

As mentioned above, the limitations of our study relate to the fact that we cannot completely exclude that difference in dementia severity, undetected anatomical involvement and education level could play a role in our results. Finally, the lack of healthy control data for speech production is a limitation for a deep interpretation of our findings.

To conclude, this study reveals the relevance of native language on the phenotype and clinical presentation of PPA and the need to consider cultural and language-specific effects during the diagnostic process.

Acknowledgements

Work performed by Dr Edoardo Gioele Spinelli was in partial fulfillment of the requirements for obtaining the PhD degree at Vita-Salute San Raffaele University, Milano, Italy.

References

- Agosta F, Ferraro PM, Canu E, Copetti M, Galantucci S, Magnani G, Marcone A, Valsasina P, Sodero A, Comi G, Falini A, Filippi M (2015) Differentiation between Subtypes of Primary Progressive Aphasia by Using Cortical Thickness and Diffusion-Tensor MR Imaging Measures. *Radiology* 276: 219-27
- Alladi S, Hachinski V (2018) World dementia: One approach does not fit all. *Neurology* 91: 264-270
- Ashburner J (2007) A fast diffeomorphic image registration algorithm. *NeuroImage* 38: 95-113
- Ashburner J, Friston KJ (2005) Unified segmentation. *Neuroimage* 26: 839-51
- Canu E, Agosta F, Imperiale F, Fontana A, Caso F, Spinelli EG, Magnani G, Falini A, Comi G, Filippi M (2018) Added value of multimodal MRI to the clinical diagnosis of primary progressive aphasia variants. *Cortex; a journal devoted to the study of the nervous system and behavior* 113: 58-66
- Cappa SF, Nespors M, Ielasi W, Miozzo A (1997) The representation of stress: evidence from an aphasic patient. *Cognition* 65: 1-13
- Christiansen MH CC, and Edelman S (2009) *Language universals*. Oxford University Press,
- Folegatti A, Pia L, Berti A, Cubelli R (2015) Stress Assignment Errors in Surface Dyslexia: Evidence from Two Italian Patients with a Selective Deficit of the Orthographic Input Lexicon. *Behavioural neurology* 2015: 769013
- Gorno-Tempini ML, Dronkers NF, Rankin KP, Ogar JM, Phengrasamy L, Rosen HJ, Johnson JK, Weiner MW, Miller BL (2004) Cognition and anatomy in three variants of primary progressive aphasia. *Ann Neurol* 55: 335-46
- Gorno-Tempini ML, Hillis AE, Weintraub S, Kertesz A, Mendez M, Cappa SF, Ogar JM, Rohrer JD, Black S, Boeve BF, Manes F, Dronkers NF, Vandenberghe R, Rascovsky

- K, Patterson K, Miller BL, Knopman DS, Hodges JR, Mesulam MM, Grossman M (2011) Classification of primary progressive aphasia and its variants. *Neurology* 76: 1006-14
- Haspelmath M DM, Gil D, Comrie B (2005) *The World Atlas of Language Structures*. Oxford University Press, Oxford
- Imura T (1943) Aphasia: Characteristic symptoms in Japanese. *Psychiatria et Neurologia Japonica* 47: 196-218
- Jibiki I, Yamaguchi N (1993) The Gogi (word-meaning) syndrome with impaired kanji processing: alexia with agraphia. *Brain and language* 45: 61-9
- Kertesz A (1982) *Western Aphasia Battery*. Grune & Stratton, New York
- Kramer JH, Jurik J, Sha SJ, Rankin KP, Rosen HJ, Johnson JK, Miller BL (2003) Distinctive neuropsychological patterns in frontotemporal dementia, semantic dementia, and Alzheimer disease. *Cognitive and behavioral neurology : official journal of the Society for Behavioral and Cognitive Neurology* 16: 211-8
- Lindgren SD, De Renzi E, Richman LC (1985) Cross-national comparisons of developmental dyslexia in Italy and the United States. *Child development* 56: 1404-17
- Moro A (2015) *The boundaries of Babel*. MIT Press, Cambridge, Massachusetts
- Nespor M (1994) *Le strutture del linguaggio: fonologia*. il Mulino, Bologna
- Paulesu E, Demonet JF, Fazio F, McCrory E, Chanoine V, Brunswick N, Cappa SF, Cossu G, Habib M, Frith CD, Frith U (2001) Dyslexia: cultural diversity and biological unity. *Science* 291: 2165-7
- Rajapakse JC, Giedd JN, Rapoport JL (1997) Statistical approach to segmentation of single-channel cerebral MR images. *IEEE transactions on medical imaging* 16: 176-86
- Rizzi L (2009) The discovery of language invariance and variation, and its relevance for the cognitive sciences. *Behavioral and Brain Sciences* 32: 467-468
- Rozzini L BA, Lussignoli G, Cappa S, Trabucchi M (1997) Surface dyslexia in an Italian patient with semantic dementia. *Neurocase* 3: 307-312
- Spinelli EG, Mandelli ML, Miller ZA, Santos-Santos MA, Wilson SM, Agosta F, Grinberg LT, Huang EJ, Trojanowski JQ, Meyer M, Henry ML, Comi G, Rabinovici G, Rosen HJ, Filippi M, Miller BL, Seeley WW, Gorno-Tempini ML (2017) Typical and atypical pathology in primary progressive aphasia variants. *Ann Neurol* 81: 430-443
- Tohka J, Zijdenbos A, Evans A (2004) Fast and robust parameter estimation for statistical partial volume models in brain MRI. *NeuroImage* 23: 84-97

Wilson SM, Henry ML, Besbris M, Ogar JM, Dronkers NF, Jarrold W, Miller BL, Gorno-Tempini ML (2010) Connected speech production in three variants of primary progressive aphasia. *Brain* 133: 2069-88

Table 1. Demographic, clinical and language features of PPA patients and healthy controls.

	nvPPA-E	nvPPA-I	p nvPPA-E vs nvPPA-I	CI (95%)
N	20	18	-	
Age	68.94 ± 6.27	69.18 ± 7.68	0.916	-4.42/4.90
Sex, females	15 (75%)	12 (67%)	0.724	
Disease duration [years]	3.85 ± 1.57	2.35 ± 1.06	0.002*	-2.38/-0.62
Education [years]	16.10 ± 3.16	9.17 ± 5.27	<0.001*	-9.87/-4.00
MMSE	25.90 ± 2.97	24.44 ± 3.97	0.214	-3.80/0.89
CSF, Aβ42*	-	753.82 ± 177.78	-	
CSF, T-tau*	-	285.27 ± 184.20	-	
CSF, p-tau*	-	42.32 ± 10.54	-	
Amyloid PET positive (%)	0 (0%)	-	-	
Memory				
RAVLT, immediate	-2.00 ± 2.27	-1.82 ± 1.74	0.789	-1.20/1.56
RAVLT, delayed	-1.09 ± 1.93	-0.84 ± 1.72	0.686	-1.00/1.51
Complex figure, recall	-0.63 ± 1.49	-0.53 ± 1.36	0.834	-0.87/1.07
Executive functions				
Digit span, backward	-1.79 ± 1.28	-1.69 ± 1.76	0.872	-1.13/1.32
Phonemic fluency	-2.38 ± 0.68	-2.00 ± 0.71	0.109	-0.09/0.85
Semantic fluency	-2.27 ± 1.21	-1.76 ± 1.37	0.250	-0.37/1.37
Language				
Confrontation Naming	-1.58 ± 1.78	-3.37 ± 5.16	0.190	-4.53/0.96
Single word comprehension	-1.50 ± 2.25	-0.22 ± 1.29	0.050	0.01/2.54
Object knowledge	-1.08 ± 1.82	-0.14 ± 1.24	0.110	-0.23/2.11
Repetition	-10.11 ± 9.08	-7.05 ± 9.11	0.307	-2.94/9.06
Syntactic comprehension, auditory	-0.35 ± 1.15	-16.13 ± 17.52	0.003*	-25.12/-6.43
Syntactic comprehension, visual	-2.90 ± 4.05	-10.26 ± 13.08	0.04*	-14.64/-0.09

Values denotes means±standard deviations (or frequencies). CI denotes confidence intervals of differences. Cognitive scores are expressed as Z-scores based on normative

values. P values refer to t-test models or Fisher's exact test. *denotes significance at $p < 0.05$.

Abbreviations: CI=confidence intervals; MMSE=Mini Mental State Examination; nfv=nonfluent variant; PPA-E/I=primary progressive aphasia-English/Italian; RAVLT=Rey Auditory Verbal Learning Test. *Data available for 11 (61%) nfvPPA-I. CSF cut off= $A\beta_{42} > 500$ ng/L (values below are considered abnormal); T-tau= 0-450 ng/L and p-tau= 0-61 ng/L (values above are considered abnormal).

Table 2. Quantitative features of connected speech production.

	nfvPPA-E	nfvPPA-I	P nfvPPA-E vs nfvPPA-I	CI (95%)
N	20	18		
Speech rate and speech sound errors				
Total duration	153.13 ± 82.68	124.22 ± 51.74	0.457	-38.56/83.89
Duration of pauses	69.18 ± 42.62	62.97 ± 45.17	0.188	-12.69/62.21
Duration of the sample without pauses	75.79 ± 86.29	61.25 ± 26.65	0.886	-59.53/51.61
Total number of words	99.15 ± 119.74	75.11 ± 30.04	0.681	-90.04/59.45
Speech production rate	1.55 ± 0.62	1.33 ± 0.42	0.740	-0.38/0.54
Distortions	9.84 ± 9.01	0.56 ± 1.69	0.001*	5.01/16.34
Phonological paraphasias and neologisms	0.84 ± 1.34	8.89 ± 10.23	0.028*	-13.27/-0.80
Motor speech rate	19.75 ± 21.41	0.95 ± 2.89	<0.001*	11.73-37.85
Other disruptions to fluency				
False starts	1.95 ± 2.30	4.67 ± 8.42	0.169	-8.94/-1.63
Filled pauses	7.32 ± 7.10	4.72 ± 6.98	0.901	-5.63/-6.34
Repaired sequences	3.45 ± 4.41	7.50 ± 9.81	0.188	-10.77/2.20
Incomplete sequences	0.50 ± 1.05	0.33 ± 0.49	0.674	-0.85/0.56
Lexical content				
Open class words	37.10 ± 34.38	30.28 ± 11.23	0.676	-26.41/17.34
Closed class words	62.05 ± 85.79	46.17 ± 24.99	0.717	-64.24/44.66
Verbs	14.05 ± 16.89	10.22 ± 6.93	0.755	-12.76/9.33
Nouns	31.95 ± 38.72	20.44 ± 9.59	0.975	-24.65/23.90

Open class proportion	0.45 ± 0.16	0.43 ± 0.11	0.596	-0.09/0.15
Verb proportion	0.29 ± 0.11	0.33 ± 0.21	0.582	-0.19/0.11
Syntactic structure and complexity				
Number of utterances	15.20 ± 11.71	26.56 ± 9.05	0.004*	-22.84/-4.71
Number of sentences	10.40 ± 12.71	8.50 ± 5.57	0.467	-11.27/5.28
Number of words in sentences	84.60 ± 122.51	40.44 ± 30.61	0.954	-77.61/73.33
Mean length of sentences	7.05 ± 2.34	4.37 ± 1.59	0.032*	0.17/3.57
Proportion of sentences	0.63 ± 0.36	0.34 ± 0.24	0.211	-0.10/0.42
Embeddings	1.90 ± 3.58	1.44 ± 1.69	0.329	-3.46/1.19
Morphosyntactic errors	4.30 ± 4.51	3.78 ± 3.44	0.095	-0.51/6.08
Syntax production rate	0.69 ± 0.34	0.47 ± 0.31	0.527	-0.19/0.36
Morphosyntactic error rate	0.19 ± 0.29	0.28 ± 0.79	0.487	-0.32/0.67
Semantic errors	0.95 ± 1.32	2.17 ± 2.26	0.591	-1.93/1.12

Values denotes means ± standard deviations. CI denotes confidence intervals of differences. P values refer to univariate general linear models which account for education. *denotes significance at $p < 0.05$. Speech production rate=total number of words/duration of the sample without pauses; motor speech rate=(number of distortions/number of words)*100; open class proportion=open class words/closed class words; verb proportion=verbs/verbs+nouns; mean length of sentence=number of words in sentences/number of sentences; proportion of sentences=number of sentences/number of utterances; syntax production rate=number of words in sentences/number of words; morphosyntactic error rate=number of morphosyntactic errors/number of words in sentences.

Abbreviations: CI=Confidence intervals; nfv=nonfluent variant; PPA-E/I=primary progressive aphasia-English/Italian.

Table 3. Voxel-based Morphometry. Montreal Neurological Institute (MNI) coordinates of the significant clusters showing gray matter loss in each group of nfvPPA patients compared with healthy controls. Results are shown at $p < 0.001$ family-wise error (FWE) corrected at peak level over the whole brain and $k > 100$ for cluster extent accounting for age, sex, scanner, and whole brain total gray matter volume. Color map represents T scores.

	Hemisphere	Coordinates			T-score
		x	y	z	
<i>NfvPPA-E vs healthy controls</i>					
<i>opIFG</i>	Left	-53	8	20	4.6
Precentral gyrus	Left	-43	7	31	4.6
Postcentral gyrus	Left	-50	11	35	4.8
Insula	Left	-36	11	8	4.8
Pre-SMA	Left	-6	15	51	4.8
Thalamus	Left	-13	-16	12	3.5
Hippocampus	Left	-38	-24	-14	5.6
<i>NfvPPA-I vs healthy controls</i>					
<i>opIFG</i>	Left	-55	9	17	5.3
Precentral gyrus	Left	-39	1	42	5
Insula	Left	-40	9	5	5.7
Pre-SMA	Left	0	24	51	4
Thalamus	Left	-16	-12	15	7.8
Caudate nucleus	Left	-12	11	11	4.7
Hippocampus	Left	-36	-28	-9	4.4

Abbreviations. *opIFG*=pars opercularis of the inferior frontal gyrus; NfvPPA-E/I=nonfluent variant of primary progressive aphasia-English/Italians; SMA=supplementary motor area.

Table 4. Gray matter volumes in left-lateralized *a-priori* defined regions of interest in healthy controls and in nfvPPA patients for each of the study sites.

	HC-E	nfvPPA-E	<i>p value-E</i>	<u>CI (95%)</u>	HC-I	nfvPPA-I	<i>p value-I</i>	<u>CI (95%)</u>
AG	0.39 ± 0.05	0.35 ± 0.04	0.02	0.003/0.05	0.34 ± 0.04	0.31 ± 0.05	0.03	0.002/0.04
Premotor	0.27 ± 0.03	0.24 ± 0.03	0.04	0.001/0.04	0.21 ± 0.04	0.17 ± 0.02	0.01	0.01/0.03
<i>opIFG</i>	0.36 ± 0.05	0.31 ± 0.05	0.004*	0.01/0.07	0.34 ± 0.04	0.28 ± 0.04	<0.001*	0.03/0.07
<i>triIFG</i>	0.35 ± 0.04	0.32 ± 0.05	0.05	-0.001/0.04	0.31 ± 0.04	0.28 ± 0.04	0.08	-0.002/0.04
AI	0.51 ± 0.04	0.47 ± 0.06	0.04	0.001/0.04	0.49 ± 0.05	0.43 ± 0.05	0.002*	0.01/0.06
PCC	0.34 ± 0.05	0.32 ± 0.04	0.86	-0.02/0.02	0.31 ± 0.04	0.29 ± 0.04	0.68	-0.02/0.02
Pre-SMA	0.32 ± 0.04	0.28 ± 0.03	0.001*	0.01/0.05	0.29 ± 0.04	0.24 ± 0.04	0.001*	0.01/ 0.05
SMA	0.29 ± 0.04	0.27 ± 0.03	0.40	-0.01/0.02	0.26 ± 0.04	0.24 ± 0.04	0.67	-0.01/0.02
SMG	0.36 ± 0.04	0.32 ± 0.04	0.03	0.002/0.04	0.32 ± 0.05	0.28 ± 0.05	0.07	-0.001/0.04
Striatum	0.35 ± 0.04	0.31 ± 0.03	0.001*	0.01/0.04	0.30 ± 0.03	0.26 ± 0.05	0.01	0.01/0.05

Values of tissue probability denote means ± standard deviations. CI denotes confidence intervals of differences. P values refer to t-test models accounting for age, sex, scanner, and whole brain total gray matter volume. *P values<0.005 denote significance between groups at each site Bonferroni corrected for multiple comparisons (uncorrected p-value/number of regions - 0.05/10). Abbreviations: AG=Angular Gyrus; AI=anterior insula; CI=Confidence intervals; HC-E/I=healthy controls-English/Italians; nfvPPA-E/I=nonfluent variant of primary progressive aphasia-English/Italians; *op/triIFG*=pars opercularis/triangularis of the inferior frontal gyrus; PCC=posterior cingulate cortex; SMA=supplementary Motor Area; SMG=supramarginal gyrus.

Figure 1. Gray matter atrophy detected by voxel-based morphometry in *nvPPA patients compared with healthy controls.* Brain regions showing gray matter loss in each group of *nvPPA* patients compared with healthy controls. Results are overlaid on a three-dimensional rendering of the Montreal Neurological Institute standard brain at $p < 0.05$ after family-wise error (FWE) correction for multiple comparisons over the whole brain and $k > 100$ for cluster extent accounting for age, sex, scanner, and whole brain total gray matter volume. Color map represents T scores. Abbreviations. *nvPPA-E/I*=nonfluent variant of primary progressive aphasia-English/Italians.

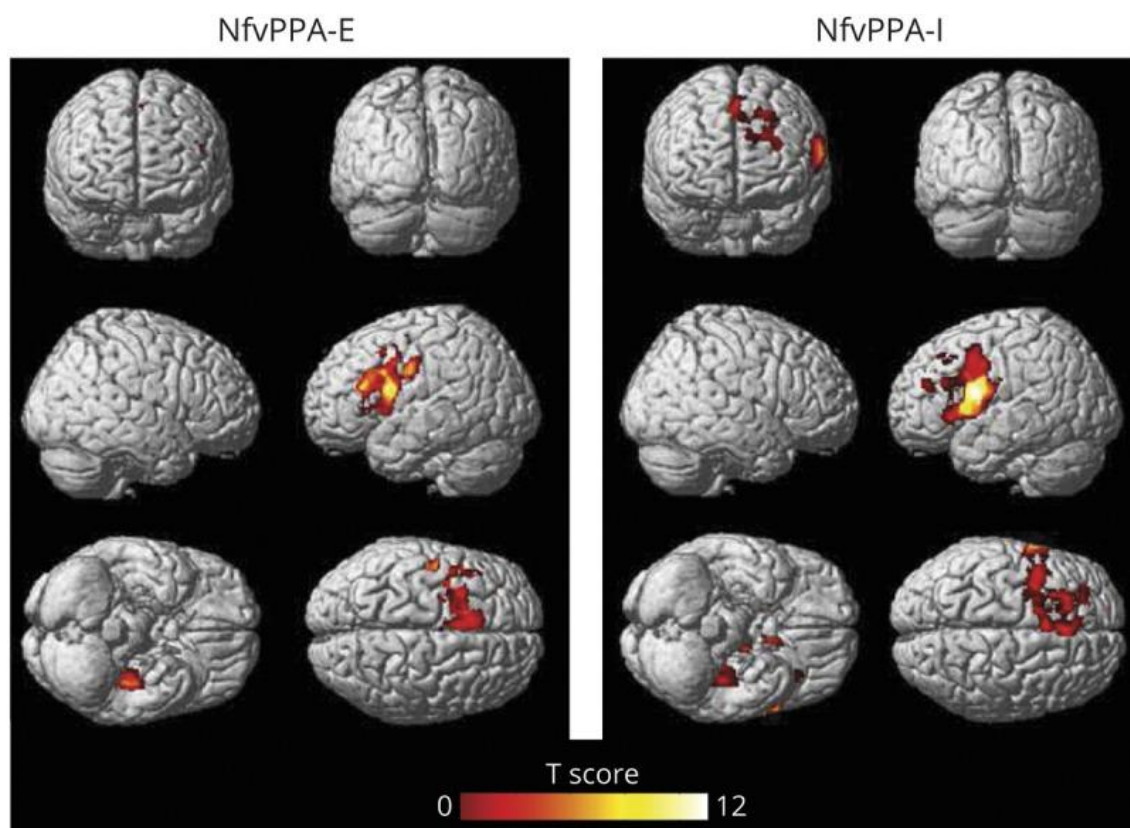
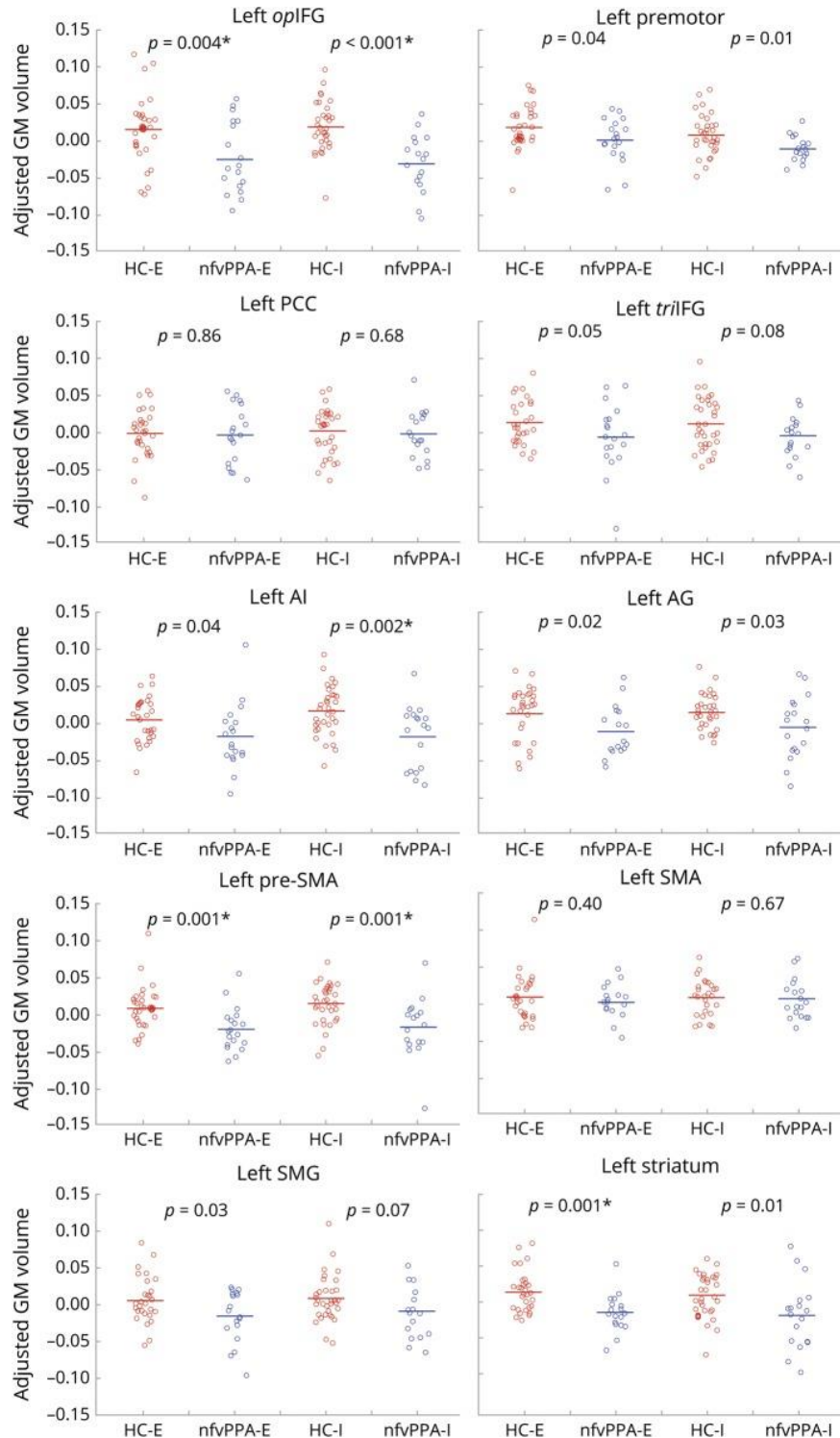


Figure 2. Plots of gray matter volumes of regions of interest in nfvPPA patients and healthy controls. Plots of gray matter volumes in *a-priori* defined regions of interest in healthy controls (in red) vs nfvPPA patients (in blue) for each of the study sites. Gray matter volume values represent the residuals of a general linear model (GLM) taking into account age, sex, scanner, and whole brain total gray matter volume.



*P values < 0.005 denote significance between groups at each site Bonferroni corrected for multiple comparisons (uncorrected p-value/number of regions - 0.05/10), accounting for age, sex, scanner, and whole brain total gray matter volume. Abbreviations. AG=angular gyrus; AI=anterior insula; GM=gray matter; HC-E/I=healthy controls-English/Italians; nfvPPA-E/I=nonfluent variant of primary progressive aphasia-English/Italians; *op/tri*IFG=pars opercularis/triangularis of the inferior frontal gyrus; PCC=posterior cingulate cortex; SMA=supplementary motor area; SMG=supramarginal gyrus.

4.2. Functional connectivity rearrangements propagating from disease epicenters in frontotemporal lobar degeneration variants

ABSTRACT

Introduction. Stepwise functional connectivity (SFC) is a graph-theory-based neuroimaging method, which detects whole-brain functional couplings of a selected region of interest, at increasing link-step distances. This study assessed SFC rearrangements in frontotemporal lobar degeneration (FTLD) presentations.

Methods. Patients with behavioral variant of frontotemporal dementia (bvFTD, n=64), non-fluent (nfvPPA, n=34) or semantic variant of primary progressive aphasia (svPPA, n=36) and 94 healthy controls underwent 3T MRI. The peaks of atrophy of each variant (identified in an independent cohort of path-proven cases) were used as seed regions for the subsequent SFC analyses. SFC rearrangements were compared between patient groups and controls. Correlations between SFC architecture in controls and atrophy patterns in FTLD patients were tested.

Results. Selected seeds were the left anterior insula for bvFTD, left supplementary motor area for nfvPPA, and left inferior temporal gyrus (ITG) for svPPA. Compared with controls, bvFTD and nfvPPA patients showed widespread decreased SFC in bilateral cortical regions with direct/intermediate connections, and increased SFC either in circumscribed regions close to the respective seed region or in more distant cortical and posterior cerebellar areas. Across all link-steps, svPPA showed SFC decrease mostly localized in the temporal lobes, with co-occurrent SFC increase in cerebellar regions at intermediate link-steps. Average functional link-step distance from the left ITG in healthy controls was found to correlate with regional grey matter volume in svPPA patients ($r=0.29$, $p=0.03$).

Conclusions. This was the first study exploring SFC in FTLD, opening promising perspectives to understand the physiopathological underpinnings of these presentations and model disease evolution.

INTRODUCTION

Frontotemporal lobar degeneration (FTLD) is an umbrella term encompassing a wide spectrum of heterogeneous neurodegenerative syndromes, characterized by progressive changes in behavior, language and executive functions associated with degeneration of the frontal and temporal brain lobes. The three main clinical syndromes included in the FTLD spectrum are: i) the behavioral variant of frontotemporal dementia (bvFTD); ii) the nonfluent variant of primary progressive aphasia (nfvPPA); and iii) the semantic variant of primary progressive aphasia (svPPA) (Gorno-Tempini, Hillis et al., 2011, Rascovsky, Hodges et al., 2011). Similar to other neurodegenerative diseases, FTLD presentations are being increasingly conceptualized as “disconnection syndromes” (Warren, Rohrer et al., 2012, Zuo, Ehmke et al., 2012), due to the extensive damage to both structural and functional connections. Such alterations are thought to cause the loss of an efficient balance between local (short-range) and global (long-range) connectivity, which is critical for an effective integration of information from different regions and appropriate motor/cognitive performance (van den Heuvel & Sporns, 2013). In recent years, graph-theory analyses and MRI connectomic approaches have allowed a systematic assessment of the combination of structural and functional connectivity alterations in several neurodegenerative conditions, demonstrating characteristic spatial patterns of neurodegeneration following large-scale connectivity networks also in the wide range of FTLD disorders (Agosta, Galantucci et al., 2014, Agosta, Sala et al., 2013, Battistella, Henry et al., 2019, Filippi, Basaia et al., 2017, Mandelli, Welch et al., 2018, Reyes, Ortega-Merchan et al., 2018), supporting a trans-neuronal spread model of pathological protein deposits in these diseases. However, the majority of previous neuroimaging studies have assessed connectivity abnormalities on a whole-brain scale, without discerning between direct and indirect connections. Stepwise functional connectivity (SFC), on the other hand, assesses functional connectivity modifications at different link-step distances from a seed region of interest (e.g., the region with most severe neurodegeneration in a particular disease, or “disease epicenter”) (Costumero, d'Oleire Uquillas et al., 2020, Sepulcre, Sabuncu et al., 2012), thus helping to discriminate between alterations of one-step (direct) and longer-distance (indirect) connections. This novel framework for *in vivo* neuroimaging analyses has great potential for the study of

neurodegenerative disorders, which are characterized by a progressive deposition of misfolded proteins in the brain.

To our best knowledge, SFC has never been applied to the assessment of FTLD. The main aim of this study was to propose this technique as a new approach for the assessment of brain network disruption in patients affected by FTLD. In detail, we focused on exploring how the different step-distance functional connections of disease epicenters were altered in each of FTLD most important clinical variants (i.e., bvFTD, nfvPPA and svPPA). We have also explored the relationship between whole-brain SFC architecture of healthy controls and the distribution of atrophy in each FTLD variant, in order to test SFC as a determinant of pathological progression in this disease.

MATERIALS AND SUBJECTS

Participants

Milan cohort. A total of 176 patients with a suspected diagnosis of disorders of the FTLD spectrum were referred between October 2009 and April 2021 to the Neurology Unit of San Raffaele Hospital in Milan to perform a complete neurological work-up, as well as a neuropsychological evaluation and an MRI scan on a 3 Tesla scanner, including both structural and resting-state functional MRI (RS fMRI) sequences. Following this multidisciplinary evaluation, 157 patients received a clinical diagnosis of FTD according to either bvFTD (Rascovsky et al., 2011), nfvPPA or svPPA (Gorno-Tempini et al., 2011) clinical criteria, and were therefore evaluated for inclusion in the present study. In order to mitigate sources of sample heterogeneity, after screening for known pathogenic mutations on the *C9orf72*, *GRN*, *MAPT*, *FUS*, *TARDBP*, *TBK1*, *TREM2*, *OPTN* or *VCP* genes (see below for methodological details), 17 genetic patients (i.e., 6 *C9orf72*, 9 *GRN*, 1 *MAPT* and 1 *TREM2*) were identified and excluded from the present study. Six FTLD patients (i.e., 1 bvFTD, 4 nfvPPA, 1 svPPA), who demonstrated a high cerebrovascular burden or motion artifacts on MRI, were not included in the study. As a result of this screening process, the final cohort included 134 sporadic FTLD patients, divided into 64 bvFTD, 34 nfvPPA, and 36 svPPA patients.

Ninety-six healthy controls, comparable for age and sex with the patient groups, were recruited among spouses of patients and by word of mouth. The controls were included if the following criteria were satisfied: normal neurological assessment; Mini-Mental

State Examination (MMSE) (Folstein, Folstein et al., 1975) score ≥ 28 ; no family history of neurodegenerative diseases. Exclusion criteria for all subjects were: significant medical illnesses or substance abuse that could interfere with cognitive functioning; any (other) major systemic, psychiatric, or neurological illnesses; and other causes of focal or diffuse brain damage, including lacunae and extensive cerebrovascular disorders at routine MRI. **Table 1** summarizes the main demographic and clinical features of patients and age-matched healthy controls of the cohort recruited in Milan.

In addition to FTLD patients and age-matched healthy controls (HC-old), 50 young healthy controls (HC-young, i.e., age range between 20 and 30 years, 23 females) were also recruited at San Raffaele Hospital. These subjects would represent a “reference” healthy connectome for correlation analyses between SFC maps and regional atrophy in FTLD patients, eliminating the influence of age-related connectome alterations.

Mayo Clinic cohort. In order to identify the “disease epicenters” to be used as seeds of an SFC analysis performed on the main study cohort (i.e., Milan cohort), T1-weighted MRI scans obtained from an independent group of subjects were also used in the context of the present study. This population had been recruited at the Mayo Clinic in Rochester (MN, United States of America) between April 2007 and September 2020, and comprised 43 patients (i.e., 11 bvFTD, 14 nvPPA and 18 svPPA) with a confirmed diagnosis of FTLD, based on either *post-mortem* pathological demonstration (n=17, including 14 nvPPA and 3 bvFTD) or a negative amyloid PET scan (n=26, including 18 svPPA and 8 bvFTD). Similar to the Milan cohort, FTLD patients did not present any known genetic mutation. Fifteen age- and sex-matched healthy controls were also selected. Healthy subjects fulfilled the same inclusion/exclusion criteria as in the Milan cohort. **Table 2** summarizes the demographic characteristics of the Mayo Clinic cohort.

Local ethical standards committees on human experimentation approved the study protocols and all participants provided written informed consent.

Clinical evaluation

Clinical evaluation at San Raffaele Hospital was performed by experienced neurologists blinded to the genetic and MRI results, recording disease duration at presentation. The global disease severity was assessed using the Clinical Dementia Rating (CDR) scale

(Morris, 1993) and its variant specifically designed for FTD (CDR-FTD) (Knopman, Kramer et al., 2008).

Neuropsychological assessment

Participants of the Milan cohort underwent a comprehensive neuropsychological assessment performed by an experienced neuropsychologist unaware of the MRI results. The following cognitive functions were evaluated (**Table 3**): global cognitive functioning with the MMSE (Folstein et al., 1975) and the Frontal Assessment Battery (Appollonio, Leone et al., 2005); long and short term verbal memory with the Rey Auditory Verbal Learning Test (Carlesimo, Caltagirone et al., 1996) and the digit span forward (Orsini, Fragassi et al., 1987), respectively; visuospatial short term working memory with the Corsi Block-Tapping Test (Orsini et al., 1987); attentive and executive functions with the digit span backward (Monaco, Costa et al., 2013), the Wisconsin Card Sorting Test (Laiacona, Inzaghi et al., 2000), the Modified Card Sorting Test (Caffarra, Vezzadini et al., 2004) the Raven's colored progressive matrices (Basso, Capitani et al., 1987) and the attentive matrices test (Spinnler & Tognoni, 1987); fluency with the phonemic and semantic fluency tests (Novelli, Papagno et al., 1986); visuospatial abilities with the Rey Figure copy (Caffarra, Vezzadini et al., 2002); language with the Token test (De Renzi & Vignolo, 1962); mood with the Beck Depression Inventory (Beck, Ward et al., 1961) and the presence of behavioral disturbances with the Frontal Behavioral Inventory (Alberici, Geroldi et al., 2007); the severity of neuropsychiatric symptoms was also assessed and graded according to the Neuropsychiatric Inventory (NPI) questionnaire (Kaufer, Cummings et al., 2000).

PPA participants also underwent a comprehensive speech evaluation that included the examination of the following: object knowledge with the Pyramids and Palm Trees Test (Klein & Buchanan, 2009); single-word comprehension with the word picture matching test of the CaGi (Catricala, Della Rosa et al., 2013); confrontation naming with the subtests of CaGi and Aachener Aphasie Test (Huber, Poeck et al., 1984); written language with the reading and writing subtests of Aachener Aphasie Test (Huber et al., 1984); grammatical comprehension of syntactically complex sentences with the Token Test (De Renzi & Vignolo, 1962); and repetition with the subtest of Aachener Aphasie Test (Huber et al., 1984).

Genetic testing

Blood samples were collected from all recruited patients. The presence of GGGGCC hexanucleotide expansion in the first intron of *C9orf72* was assessed using a repeat-primed polymerase chain reaction (PCR) assay (Renton, Majounie et al., 2011). A cut-off of ≥ 30 repeats combined with a typical saw-tooth pattern was considered pathological. In addition, the coding sequences and intron/exon boundaries of *GRN*, *MAPT*, *TARDBP*, *FUS*, *TBK1*, *TREM2*, *OPTN* and *VCP* genes were amplified by PCR using optimized protocols, looking for known pathogenic mutations (Pozzi, Valenza et al., 2017). All subjects presenting a pathological mutation were excluded from the study.

MRI acquisition

Milan sample. All patients and healthy controls of the main (i.e., Milan) cohort underwent brain MRI on a 3 T scanner (Philips Medical Systems, Best, the Netherlands) at San Raffaele Hospital. The original scanner (for brevity, Scanner 1) was substituted with an upgraded model from the same manufacturer in 2016 (below defined as Scanner 2).

Using Scanner 1, the following brain MRI sequences were obtained: a 3D T1-weighted fast field echo (FFE) sequence (TR=25 ms, TE=4.6 ms, flip angle=30°, 220 axial slices with voxel size=0.89x0.89x0.8 mm, matrix size=256x256, FOV=230x182 mm²); and a T2*-weighted single-shot echoplanar images (EPI) for RS fMRI (TR/TE 3000/35 ms, flip angle 90°, FOV 240 mm², matrix 128 x 128, 200 sets of 30, 4-mm thick axial slices).

Using Scanner 2, the following brain MRI sequences were obtained: a 3D T1-weighted turbo field echo (TFE) (TR=7 ms, TE=3.2 ms, TI=1000 ms, 204 sagittal slices with voxel size=1x1x1 mm, matrix=256x256, FOV=256x256 mm²); and a T2*-weighted single-shot EPI for RS fMRI (TR/TE 1567/35 ms, flip angle 70°, FOV 240 mm², pixel size = 2.5x2.5 mm, 320 sets of 48, 3-mm thick axial slices).

For acquisitions on both scanners, all slices were positioned to run parallel to a line that joins the most inferoanterior and inferoposterior parts of the corpus callosum. During RS fMRI scanning, subjects were instructed to remain motionless, to keep their eyes closed, and not to think about anything in particular.

Mayo Clinic sample. Patients and healthy controls of the Mayo Clinic cohort also underwent a 3 T brain MRI including including a 3D T1-weighted magnetization prepared rapid gradient echo (MPRAGE) sequence (TR/TE/T1 = 2300/3/900 ms; flip angle 8°, FOV 260 mm²; 256 × 256 in-plane matrix with a phase field of view of 0.94, slice thickness of 1.2 mm, in-plane resolution 1). All MRI scans were acquired on one of two Prisma scanners (Siemens Healthcare, Erlangen, Germany).

MRI analysis

The MRI analysis was performed at the Neuroimaging Research Unit of San Raffaele Hospital in Milan by experienced observers, blinded to subjects' identity.

Voxel-based morphometry (VBM)

First, we aimed to identify the disease epicenters of each FTLD variant, to be used as seeds for a subsequent SFC analysis. To this purpose, we investigated grey matter (GM) volumetric alterations in an independent (i.e., Mayo Clinic) patient cohort. In this population, a voxel-based morphometry (VBM) analysis was performed using SPM12 (<http://www.fil.ion.ucl.ac.uk/spm/>) and the Diffeomorphic Anatomical Registration Exponentiated Lie Algebra (DARTEL) registration method (Ashburner, 2007).

Briefly, (i) T1-weighted images were segmented to produce GM, WM and CSF tissue probability maps in the MNI space; (ii) the segmentation parameters obtained from the step (i) were imported in DARTEL; (iii) the rigidly aligned version of the images previously segmented (i) was generated; (iv) the DARTEL template was created and the obtained flow fields were applied to the rigidly-aligned segments to warp them to the common DARTEL space and then modulated using the Jacobian determinants. Since the DARTEL process warps to a common space that is smaller than the MNI space, we performed an additional transformation as follows: (v) the modulated images from DARTEL were normalized to the MNI template using an affine transformation estimated from the DARTEL GM template and the a priori GM probability map without resampling (<http://brainmap.wisc.edu/normalizeDARTELtoMNI>). Prior to statistical computations, images were smoothed with an 8 mm FWHM Gaussian filter.

VBM group comparisons were then tested using ANOVA models between each group of FTLD and healthy controls of the Mayo Clinic cohort. Such comparison allowed the

identification of the atrophy peaks for each clinical variant, i.e., the local maximum of the t-statistics across significant clusters. Using the MarsBaR region of interest toolbox for SPM12 (<http://marsbar.sourceforge.net>), a spherical, 10-mm radius, region of interest (ROI) was created around each subgroup's most significant atrophy peak (i.e., the disease epicenter of each FTL variant).

RS fMRI pre-processing

RS fMRI data processing was performed with the Data Processing Assistant for Resting-State toolbox (DPARSFA, <http://rfmri.org/DPARSA>) (Chao-Gan & Yu-Feng, 2010), based on Statistical Parametric Mapping (SPM12, <http://www.fil.ion.ucl.ac.uk/spm>), and the RS fMRI Data Analysis Toolkit (<http://www.restfmri.net>) (Song, Dong et al., 2011). Preprocessing included the following steps:

- 1) removal of first four volumes of each raw RS fMRI dataset to allow for T1 equilibration;
- 2) slice timing correction for interleaved acquisitions (the middle slice was used as the reference point);
- 3) head motion correction using a six-parameter (rigid body) linear transformation with a two-pass procedure (registered to the first image and then registered to the mean of the images after the first realignment);
- 4) spatial normalization to the Montreal Neurological Institute (MNI) atlas template with voxel size was set at $5 \times 5 \times 5 \text{ mm}^3$ for computational efficiency;
- 5) removal of spurious variance through linear regression: including 24 parameters from the head motion correction step (6 head motion parameters, 6 head motion parameters one time point before, and the 12 corresponding squared items) (Friston, Williams et al., 1996), scrubbing with regression (signal spike regression as well as 1 back and 2 forward neighbors) (Yan, Cheung et al., 2013) at time points with a frame-wise displacement (FD) $>0.5\text{mm}$, linear and quadratic trends, global signal, white matter signal, and the cerebrospinal fluid signal;
- 6) spatial smoothing with a 4 mm FWHM Gaussian Kernel;
- 7) band-pass temporal filtering (0.01-0.08 Hz) to reduce the effect of low frequency drift and high frequency noise (Lowe, Mock et al., 1998).

Functional connectome reconstruction

Association matrices were computed by calculating the Pearson correlation between each voxel time course and every other voxel time course within a mask covering cortical and subcortical grey matter. To perform this analysis, the preprocessed resting state images of each subject were previously converted to an N-by-M matrix, where N was the image voxels in MNI space, and M was the 200 acquisition time points. From this step, a 11705x11705 matrix of Pearson correlation coefficients (r-values) was obtained for each individual. Fisher z transformation was applied to r-values. Then, all correlations that did not reach a false discovery rate (FDR) correction threshold of $p < 0.05$ were excluded from further analyses.

SFC analysis

In SFC analysis, the degree of stepwise connectivity of a voxel j for a given step distance l and a seed area i (A_{ji}^l) is computed from the count of all paths that (1) connect voxel j and any voxel in seed area i , and (2) have an exact length of l . Each SFC matrix A_l of size m-by-m can be recursively represented as per following equation:

$$A_l(i, j) = \begin{cases} A(i, j) & [i \neq j, l = 1] \\ \sum_{k=1}^m \left(\frac{A_{l-1}(i, k) - \min(A_{l-1})}{\max(A_{l-1}) - \min(A_{l-1})} \right) \left(\frac{A(k, j) - \min(A)}{\max(A) - \min(A)} \right) & [i \neq j, l \geq 2] \end{cases}$$

Here, A_l is the functional connectivity matrix with a step distance of l , and A is the correlation matrix after Fisher transformation. Matrices were then normalized between 0 and 1, keeping the final distribution of values intact while making them comparable across step distances. In this sense, a larger SFC degree under the step distance l indicates stronger paths connecting two voxels via link one, while a smaller degree indicates weaker connectivity paths.

For each disease subgroup of the Milan cohort, an SFC analysis was performed using as seed region the specific seed ROI previously identified in the Mayo Clinic population (see the Results section). For each group of healthy controls (i.e., HC-old and HC-young), three different SFC models were created, one for each ROI. Given the lack of directionality information provided by RS fMRI data, in SFC we did not include any

restrictions about recurrent pathways crossing the seed regions multiple times. Therefore, we explored a wide range of link-step distances, from 1 to 20, to characterize the progression of the derived maps. However, as we found that the SFC patterns are topographically dissimilar between consecutive maps from steps one to three and become stable for link-step distances above four, we only included maps from one to four steps in our results. All maps across different link-step distances from one to four (i.e., SFC maps 1 to 4) were used in the characterization of connectivity alterations between HC-old and FTLD participants.

In addition to this, a combined version of all SFC 1 to 4 maps into one single map from non-disrupted connectivity pathways of HC-young (combined SFC map) was employed to investigate the relationships between standard neuroimaging patterns and volumetric measures of FTLD participants. To build the SFC combined map, we established, for each pair of voxels, at which step the relative degree of stepwise connectivity (across the four-step distances) was maximized. Thus, we obtained an SFC combined map for each subject whose values ranged from 1 to 4. As a final step, all resulting SFC maps were projected onto the cerebral hemispheres of the Population-Average Landmark and Surface-based (PALS) surface (PALS-B12) provided with Caret software (Van Essen, 2005) using the “enclosing voxel algorithm” and “multifiducial mapping” settings. Finally, the combined SFC map was converted from the voxel-level spatial resolution to the 90 regions of the Automated Anatomical Labeling (AAL) atlas parcellation, in order to allow correlations with GM volumetric measures of FTLD patients.

Regional grey matter (GM) volumetric measures

To obtain quantitative measures of regional atrophy in FTLD patients of the Milan cohort, GM maps of these subjects were also parcellated into the 90 AAL regions of interest. Specifically, cortical GM maps were obtained using the segmentation step (i) of VBM, while maps of the basal ganglia, hippocampus and amygdala were obtained using the FMRIB's Integrated Registration and Segmentation Tool (FIRST) in FSL (<http://www.fmrib.ox.ac.uk/fsl/first/index.html>). The AAL atlas was then registered to the subject T1-weighted images, masked using the GM maps, by means of linear (FLIRT) (Jenkinson, Bannister et al., 2002) and non-linear (FNIRT) (Andersson, Jenkinson et al., 2007) registrations in FSL. GM volumes were obtained and multiplied by the

normalization factor derived from SIENAx (part of FSL; <http://www.fmrib.ox.ac.uk/fsl/sienax/index.html>) to correct for individual head size.

Statistical analysis

Clinical and cognitive data. Normal distribution assumption was checked by means of Q-Q plot and Shapiro-Wilks and Kolmogorov-Smirnov tests. Demographic, clinical and neuropsychological data were compared between groups using age-, sex- and education-adjusted ANOVA models, followed by post-hoc pairwise comparisons, Bonferroni-corrected for multiple comparisons. The threshold of statistical significance was set at $p < 0.05$. The SPSS Statistics 26.0 software was used.

MRI data. For the assessment of GM atrophy patterns in the Mayo Clinic cohort, VBM group comparisons were tested using ANOVA model adjusting for total intracranial volume, age, and sex. Results were assessed at $p < 0.05$ Family-wise error (FWE)-corrected for multiple comparisons.

For the assessment of stepwise functional connectivity in the Milan cohort, voxel-wise analyses were performed using general linear models as implemented in SPM12. Whole-brain two-sample t-test comparisons between healthy controls and each patient group were performed for each of the four steps, including age, sex and scanner type as covariates. A threshold-free cluster enhancement method, combined with nonparametric permutation testing (5000 permutations) as implemented in the Computational Anatomy Toolbox 12 (CAT12, <http://www.neuro.uni-jena.de/cat/>) was used to detect statistically significant differences at $p < 0.05$, family-wise error (FWE) corrected.

Correlation analysis. For each region of the AAL-90 atlas, correlations between the combined SFC maps obtained in HC-young subjects for each seed ROI and average GM volumes of FTLD patients of the Milan sample were tested using the Spearman's correlation coefficient (SPSS Statistics 26.0).

RESULTS

Clinical and sociodemographic features

All groups were comparable in terms of age at MRI, sex, and scanner type (*Table 1*), although healthy controls (HC-old) were significantly more educated than each patient group. FTLD subgroups were also comparable among them in terms of education, CDR-

FTD, and MMSE scores. Patients with nfvPPA had a significantly shorter disease duration at MRI, as well as milder CDR and CDR-sb scores, compared with bvFTD and svPPA.

After adjusting for age, sex, and education levels, statistically significant differences were observed between each FTLD group and HC-old regarding several measures assessing memory, attention, language, fluency and executive functions (**Table 3**). Patients with bvFTD also showed significant impairment of visuospatial abilities, as well as worse performance at the card sorting test compared with healthy controls and svPPA patients. As expected per clinical criteria, svPPA patients showed significant impairment of confrontation naming, single-word comprehension, and semantic knowledge language, compared with nfvPPA.

Identification of disease epicenters

First, we aimed to identify the disease epicenters of each FTLD variant, to be used as seeds for a subsequent SFC analysis. To this purpose, we investigated GM volumetric alterations in an independent (i.e., Mayo Clinic) patient cohort (see **Table 2**). **Figure 1A** and **Table 4** report the results of VBM analysis in these subjects. Compared with age- and sex-matched healthy controls:

- bvFTD patients showed atrophy of the insular cortex bilaterally, left precentral, middle and superior frontal gyri, and right cingulate cortex;
- nfvPPA patients showed prevalent atrophy of the left hemisphere, involving in particular the SMA, precentral gyrus, inferior frontal gyrus, and paracentral lobule, as well as the right middle frontal gyrus;
- svPPA patients presented a severe atrophy pattern, although more circumscribed to the anterior and inferior temporal regions, bilaterally with a prevalence in the left hemisphere.

The most significant atrophy peak of each disease subgroup was used to create a variant-specific seed ROI, namely: the left anterior insula (MNI coordinates = -40; 20; 3) for bvFTD, the left supplementary motor area (SMA, MNI coordinates = -8; 12; 58) for nfvPPA and the anterior portion of the left inferior temporal gyrus (ITG, MNI coordinates = -46; -4; -42) for svPPA (**Table 4, Figure 1B**).

Seed-specific functional networks

The variant-specific ROIs were used to create three different SFC models in the HC-young group. This allowed us to assess the functional connections, at different link-step distances, of the disease epicenters in healthy brains (*Figure 2*).

Left anterior insula. The ROI placed in the left anterior insula showed strong direct connections (step 1, yellow-red regions in *Figure 2A*) with other insular, anterior cingulate, inferior frontal and middle frontal regions, supplementary motor areas and temporo-parietal junction, bilaterally, although with a prevalence in the left hemisphere. Strong direct connections were also found with the caudate nuclei, bilaterally, and the right posterior cerebellar cortex. Moving to longer step-distances (steps 2-4), this seed ROI showed progressively stronger functional connections with more posterior brain regions, including posterior frontal (precentral gyrus), parietal (superior parietal cortex, postcentral gyrus and precuneus), occipital (cuneus and pericalcarine cortex), posterior cingulate and superior temporal cortical regions, bilaterally, although with a left-sided predominance; strong long-distance connections were also detected with posterior cerebellar regions, bilaterally.

Left SMA. The ROI placed in the left SMA showed strong direct connections (step 1, yellow-red regions in *Figure 2B*) with the surrounding voxels of the same cortical region, as well as the contralateral SMA; strong direct connections were also found with the inferior frontal gyrus pars opercularis, caudal and rostral middle frontal gyri, superior temporal pole, anterior insula, anterior cingulate, superior parietal and supramarginal cortex, as well as caudate nuclei and posterior cerebellar regions, bilaterally. On longer step-distances (steps 2-4), the left SMA showed strong functional connections with parietal (postcentral gyrus and precuneus), occipital (cuneus and pericalcarine cortex) and posterior cingulate cortices, bilaterally, although with a left-sided predominance, as well as with bilateral infero-posterior cerebellar lobules.

Left ITG. The ROI placed in the left ITG presented strong direct functional connections (step 1, yellow-red regions in *Figure 2C*) with the temporal pole, superior temporal gyrus, inferior parietal lobule, inferior frontal gyrus pars triangularis and superior medial frontal regions, anterior cingulate cortex, fusiform gyrus, precuneus, and medial posterior cerebellar lobules, bilaterally with a symmetrical pattern. At longer step-distances (steps 2-4), the left ITG showed strong functional connections, bilaterally,

mostly with parietal regions (superior parietal cortex, postcentral gyrus and precuneus), occipital regions (lingual gyrus, cuneus and pericalcarine cortex) and the posterior cingulate cortex.

SFC alterations in FTLD variants

The variant-specific ROIs were also used as seed regions to create an SFC model for each disease subgroup. Each one of these models was then compared with the one created from the same ROI in the HC-old group, in order to assess the differences in functional connectivity of each disease epicenter between patients and age-matched healthy controls (*Tables 5, 6 and 7*).

bvFTD. At one link-step distance, the seed ROI placed in the left anterior insula of bvFTD patients, compared with HC-old subjects, showed reduced functional connectivity (step 1, yellow-red regions in *Figure 3*) with bilateral posterior insular, frontal (SMA, paracentral lobule, middle frontal gyrus, inferior frontal gyrus pars opercularis), parietal (supramarginal gyrus, precuneus), superior temporal and (mostly anterior) cingulate cortical regions, as well as the most posterior part of the right middle temporal gyrus, and the right cerebellar crus I and II and lobules VI, VIIIa and VIIIb. On the other hand, the same region showed increased direct functional connections (step 1, blue-green regions in *Figure 3*) with its surrounding anterior insular cortical area, the contralateral homologous anterior insular cortex in the right hemisphere, bilateral parietal (inferior parietal lobule), occipital (cuneus, pericalcarine cortex), frontal (superior and inferior frontal gyrus pars triangularis), and temporal (inferior and middle temporal, fusiform) regions, as well as the caudate nuclei (bilaterally, with a prevalence in the left hemisphere) and left cerebellar regions including crus II, lobules VI and VIIb. When considering longer link-step distances (steps 2-4), the left anterior insula of bvFTD patients showed decreased functional connectivity with the same widespread frontal, temporal and parietal cortical regions as in step 1, with the additional involvement of precentral and postcentral gyri and the most part of the insular cortex, bilaterally. Increased indirect functional connectivity was found with diffuse parietal and occipital cortical regions (partly, similar to step 1), with the additional involvement of the orbitofrontal cortex, bilaterally, the right middle frontal gyrus, left putamen and all lobules of the posterior cerebellar lobes, bilaterally. At intermediate link-step distances, increased connectivity within the anterior

insula was absent (step 2) or localized to a small region in the left hemisphere (steps 3-4).

nfvPPA. At one link-step distance, the ROI placed in the left SMA of *nfvPPA* patients, compared with HC-old, showed reduced functional connectivity (step 1, yellow-red regions in **Figure 4**) with the inferior frontal gyrus (pars opercularis and pars triangularis), lateral precentral gyrus, anterior insula, paracentral gyrus, and rostral anterior cingulate cortex, bilaterally, and the right supramarginal gyrus. Patients with *nfvPPA* also showed increased direct functional connectivity of the left SMA (step 1, blue-green regions in **Figure 4**) with the surrounding superior frontal regions, as well as the homologous contralateral regions, the left lateral middle frontal, and the right superior frontal, lingual, fusiform and parahippocampal gyri. At intermediate link-steps (steps 2-4), the pattern of decreased functional connectivity involved the same regions as in step 1, with the additional involvement of the whole precentral, postcentral, anterior cingulate and insular cortex, bilaterally. On the contrary, the left SMA of *nfvPPA* showed increased indirect functional connectivity (steps 2-4) with more diffuse superior frontal, and inferior temporal regions, bilaterally. Across all link-steps, *nfvPPA* patients also showed increased connectivity of the left SMA with cerebellar crus I (mostly, on the right side) and posterior cerebellar lobules (in particular, lobule VI), bilaterally.

svPPA. At one link-step distance, the ROI placed in the left ITG of *svPPA* patients, compared with HC-old, showed reduced functional connectivity (step 1, yellow-red regions in **Figure 5**) with regions of the right hemisphere, including the anterior portions of the superior, middle and inferior temporal gyri, insula, and inferior parietal lobule. No areas of increased functional connectivity were identified in *svPPA* patients, compared with controls. When considering intermediate link-steps (steps 2-4), *svPPA* patients showed decreased connectivity of the left ITG with the bilateral anterior temporal and insular regions, which remained stable at increasing steps. Regions with increased indirect functional connectivity of the left ITG in *svPPA* patients (blue-green regions in **Figure 5**) were found in the left lingual gyrus, cerebellar vermis and bilateral posterior cerebellar lobes (in particular, crus I, crus II, lobules V and VI).

Correlations between atrophy and SFC measures

When we assessed the relationship between the combined SFC maps obtained in HC-young subjects and GM volumes of FTLD patients, for each region of the AAL atlas, a significant correlation was found between average functional link-step distance from the left ITG and mean GM volume in svPPA patients (*Figure 6*, $r=0.29$, $p=0.03$). No significant correlations were found between functional link-step distance from the left anterior insula and the regional mean GM volumes in bvFTD patients ($r=0.10$, $p=0.35$), nor between link-step distance from the left SMA and GM volumes in nvPPA patients ($r=0.08$, $p=0.47$).

DISCUSSION

In the present study, we explored the pattern of rearrangements of functional connectivity at increasing topological distance from the disease epicenters of FTLD clinical variants, using up-to-date neuroimaging techniques. SFC analysis is a graph-theory-based neuroimaging method that detects functional couplings of a selected ROI with other brain regions, at increasing levels of link-step distances. Selecting the peaks of atrophy of an independent cohort of patients with high confidence of FTLD pathology as the seed ROIs for a subsequent whole-brain SFC analyses, we showed for all patient groups extensive reductions of functional connectivity in brain regions with direct and intermediate connections with the respective seed regions. In addition to this, FTLD patients also showed more localized increases of functional connectivity involving either short-range direct connections (i.e., 1 step-link distance) or more distant indirect connections (i.e., 2-4 step-link distance). In the case of svPPA, we also demonstrated a relationship between SFC architecture of the healthy brain from the disease epicenter and the regional distribution of atrophy in patients. These findings open fundamental insights supporting the notion of FTLD variants as “disconnection syndromes”, providing also promising perspectives to understand the physiopathological underpinnings of these complex clinical presentations.

Patients with bvFTD present with a combination of behavioral and cognitive – mostly executive – symptoms that result from prominent atrophy in frontal, insular, anterior cingulate and striatal brain regions (Landin-Romero, Kumfor et al., 2017, Perry, Brown et al., 2017, Rascovsky et al., 2011). These regions form a “salience network” in healthy subjects, detectable using RS fMRI (Seeley, Menon et al., 2007), which is the primary

network targeted in bvFTD (Seeley, Crawford et al., 2008). On the other hand, nfvPPA and svPPA are characterized by specific language deficits associated with prominent neurodegeneration in the fronto-insular or anterior temporal brain regions, respectively (Gorno-Tempini et al., 2011, Spinelli, Mandelli et al., 2017). In nfvPPA patients, grey matter atrophy is accompanied by a corresponding functional disruption within the left fronto-insular “speech production network” (involving the frontal operculum, primary and supplementary motor areas and inferior parietal lobule) (Bonakdarpour, Hurley et al., 2019, Seeley, Crawford et al., 2009), whereas alterations of functional connectivity in svPPA patients have been shown to affect a “semantic network” centered on the left anterior temporal lobe, but also involving widespread interconnected modality-selective regions in the visual, sensory and association cortices (Guo, Gorno-Tempini et al., 2013).

In our study, the patterns of grey matter atrophy and, more specifically, the location of atrophy peaks for each FTLD variant were consistent with several previous structural neuroimaging studies (Bejanin, Tammewar et al., 2020, Perry et al., 2017, Rohrer & Warren, 2011, Spinelli et al., 2017, Whitwell, Jack et al., 2011). In particular, the identification of the insula, the left SMA and the left anterior temporal lobe as the brain regions with the greatest accumulation of neurodegeneration for bvFTD, nfvPPA and svPPA, respectively, matches the findings reported in a recent MRI volumetric study performed across all three FTLD variants (Bejanin et al., 2020). The average patterns of grey matter atrophy also broadly mirror current imaging supporting criteria for the diagnosis of each FTLD presentation (Gorno-Tempini et al., 2011, Rascovsky et al., 2011), consistent with an accurate selection of our sample, in combination with the defining clinical and cognitive features. Based on such highly-replicated observations, we have therefore identified our atrophy peaks as the “disease epicenters” of each variant, using the same approach previously adopted by other studies performed in FTLD (Zhou, Gennatas et al., 2012), Alzheimer’s disease (Mutlu, Landeau et al., 2017), and Parkinson’s disease (Zheng, Zhang et al., 2019). However, to our knowledge, this was the first study to ever use disease epicenters as seed regions for an SFC analysis in the context of FTLD. This approach combines structural data with RS fMRI in a revolutionary way, which does not simply describe alterations of functional connectivity on a whole-brain scale, but also discriminates whether are one-step (direct) or longer-distance (indirect) connections to be affected.

Across FTLD variants, significant decrease of functional connectivity was observed in widespread brain regions that were directly connected with the corresponding seed region. In detail, regarding bvFTD patients and the seed in the anterior insula, these regions included the anterior/middle cingulate cortices, superior and middle frontal gyri, the precuneus, the supramarginal gyrus and the posterior insula. The substantial decrease of functional connectivity between the anterior insula and the anterior cingulate cortex that we observed in bvFTD patients is consistent with previous observations of primary damage of the salience network in this clinical presentation, as the anterior cingulate and insular cortices are important hubs of this functional network (Ducharme, Price et al., 2018, Filippi, Agosta et al., 2013, Seeley et al., 2008). Similarly, decreased connectivity of the anterior insula with widespread frontal regions, including the middle frontal gyrus and supplementary motor regions, is in line with the view that fronto-insular disconnection may cause executive, attentional and goal-oriented motor planning deficits (Benarroch, 2019, Menon & Uddin, 2010), as recently suggested in other neurodegenerative diseases such as Parkinson's disease (Fathy, Hepp et al., 2020). Decreased functional connectivity of the anterior insula with a key posterior associative region such as the precuneus, which is a central component of the default mode network, is also in line with the known presence of alterations within this network in bvFTD (Seeley et al., 2007, Zhou, Greicius et al., 2010). In fact, a within-network hyperconnectivity of the default mode network is thought to be a direct consequence of disconnection of posterior brain regions from the frontal hubs (Zhou et al., 2010). Similarly, decreased direct functional connectivity with the posterior insula and the closely related parietal somatosensory association cortex (involved in the cortical elaboration of interoceptive and nociceptive stimuli) (Aguilar-Rivera, Kim et al., 2020) might be due to the loss of integration from the anterior insular regions, which are involved instead in emotional salience and cognitive control and present different cytoarchitecture features and structural connections (Benarroch, 2019, Cloutman, Binney et al., 2012). At increasing link-step distances from the anterior insula, the pattern of decreased functional connectivity observed in bvFTD patients became even more widespread, with more consistent damage to frontal, insular and cingulate regions and involvement of the sensorimotor regions, supporting the hypothesis that the failure of functional integrity observed in bvFTD (Agosta et al., 2013, Filippi et al., 2017, Reyes et

al., 2018) might result from widespread downstream propagation effects of atrophy from the disease epicenter.

Also when examining the results obtained in nfvPPA and svPPA patients, we demonstrated predominantly reduced functional connectivity of the respective seed regions with directly connected cortical regions, including the inferior frontal opercular regions in nfvPPA, and the contralateral anterior temporal lobe in the case of svPPA patients. Similar to what we have observed in bvFTD – although to a lesser extent – we found further evolution of patterns of decreased connectivity at increasing step-link distances from the respective seed regions, involving more diffuse fronto-opercular regions in nfvPPA and the bilateral anterior temporal regions in svPPA (as, in this case, SFC disruption patterns apparently “bounced back” to the disease epicenters, likely through returning intercommissural fibers). Therefore, also in the case of PPA variants, we can delineate patterns of functional decoupling of disease epicenters with brain regions showing direct or intermediate connections through the frontal aslant tract and the dorsal frontoparietal language pathway for nfvPPA (Bonakdarpour et al., 2019, Mandelli, Caverzasi et al., 2014, Mandelli et al., 2018) or the interhemispheric fibers of the anterior commissure mediating integration of multimodal semantic knowledge in the case of svPPA patients (Catani & Thiebaut de Schotten, 2008, Collins, Montal et al., 2017), consistent with previous evidence in the neuroimaging field (Bonakdarpour et al., 2019, Collins et al., 2017, Mandelli et al., 2018).

In bvFTD and nfvPPA patients, the SFC analysis was also able to detect increased connectivity of the respective disease epicenters with regions at one-link steps, either with maximal physical proximity in the surrounding grey matter regions, or within the homologous contralateral cortices. Moreover, bvFTD also showed increased direct connectivity with widespread long-range connected regions. Namely, bvFTD showed increased functional connectivity of the seed region in the left anterior insula with the surrounding voxels, the contralateral anterior insula (through trans-callosal fibers), the caudate nuclei (through insulo-striatal fibers) (Ghaziri, Tucholka et al., 2018), the orbitofrontal and parieto-occipital cortices (interconnected by the inferior fronto-occipital fasciculus, which receives fiber contributions from the anterior insula) (Nomi, Schettini et al., 2018), the inferior temporal cortices (connected with the insula through the uncinate fasciculus) (Nomi et al., 2018) and the ipsilateral posterior cerebellum (through cerebro-

cerebellar circuits) (Strick, Dum et al., 2009); whereas nvPPA showed increased connectivity of the left SMA with the surrounding and – to a lesser extent – homologous contralateral cortical regions. Such pattern of both short-range (common to bvFTD and nvPPA) and long-range increased direct connectivity (here observed mostly for bvFTD) might be compatible, on the one hand, with a loss of local interneuronal and, at the same time, with a more complex and widespread mechanism of functional rearrangements. This was not the first RS fMRI study showing increased local connectivity within the prefrontal and parieto-occipital cortices of FTD patients (Farb, Grady et al., 2013, Seeley et al., 2007, Zhou et al., 2010). However, SFC analysis allowed us to draw a more complex picture of the interaction between three phenomena, namely: i) the widespread patterns of long-range decreased connectivity within regions of the salience network, across both direct and indirect connections; ii) short-range increased connectivity, mostly evident when assessing direct connections; and iii) long-range increased connectivity, progressively apparent from direct to intermediate connections. Based on our observations in bvFTD patients, we speculate that the relationship between – at least – the former two phenomena might be more compatible with a maladaptive process, whereas the long-range increased connectivity might also play a role to partially compensate for the neurodegenerative process, although we could not provide within the cross-sectional design of our study unconfutable evidence pointing toward this suggestion. To our knowledge, this was also the first study suggesting a similar interplay between locally increased direct connectivity and longer-range functional disconnection in the context of nvPPA, although our findings in this group need further replication in larger cohorts.

Increased functional connectivity was also found in regions at intermediate link-step distances for all three FTLD variants. Of note, a consistent increased connectivity with the posterior cerebellar cortical regions (in particular, the crus regions and lobule VI) was found across bvFTD, nvPPA and svPPA patients, compared with controls. This finding is consistent with the physiological role of these cognitive/affective regions of the posterior cerebellum (particularly involved in the modulation of emotions and social behavior) (Stoodley & Schmahmann, 2010), as well as with the few previous fMRI reports reporting disrupted functional connectivity of cerebellar regions in FTLD presentations (Farb et al., 2013, Meijboom, Steketee et al., 2017). Although the role in

cognition and the topological organization of the cerebellar cortex has started being elucidated only in the last years (Stoodley & Schmahmann, 2010), this is an exciting area of developing research to provide greater understanding of pathophysiology of the FTL spectrum of disorders.

A secondary aim of the present study was to test the relationship between healthy-brain SFC architecture, assessed using each of the identified disease epicenters, and the distribution of atrophy in the relative FTL variant. We were able to provide evidence of a significant – although weak – correlation between SFC architecture propagating from the left ITG and the distribution of atrophy in svPPA patients. This finding is consistent with recent evidence of a striking resemblance between the large-scale functional network propagating from the left temporal pole and atrophy patterns in an independent sample of svPPA patients (Collins et al., 2017), in line with the hypothesis that pathological propagation in FTL might be due to a transsynaptic or transneuronal spreading mediated by the extremely complex, highly structured topology of neural architecture constituting brain networks (Fornito, Zalesky et al., 2015, Seeley et al., 2009), as recently shown also for Alzheimer's (Filippi, Basaia et al., 2020) and Parkinson's disease (Filippi, Basaia et al., 2021). However, we could not replicate this finding in bvFTD and nvPPA patients. We hypothesize that the more severe and, overall, discretely localized pattern of atrophy, together with the relatively longer disease duration characterizing svPPA patients, might have driven, in this variant only, the significance of such correlation, which would need larger samples and a longitudinal study design to be definitively demonstrated also in other FTL variants.

Our study was not without limitations. First, as already acknowledged, our cross-sectional design did not allow to draw strong conclusions regarding the evolution of observed increased/decreased connectivity, its maladaptive or compensatory role, or its relationship with disease worsening and atrophy distribution. Moreover, we needed to establish an intermediate size of 10-mm radius for seed ROIs, consistently used for the three variants, to make a balance between region specificity and matrix dimensions of functional MRI data. This technical constraint did not allow to discriminate SFC rearrangements between dorsal and ventral anterior insular regions, which are known to harbour different structural connections with surrounding brain regions (Benarroch, 2019, Cloutman et al., 2012).

Nonetheless, we fulfilled the main aim of our study, which was to propose SFC analysis as a new approach for the assessment of brain network disruption in patients affected by FTLN disorders, both through direct and indirect connections. Our findings revealed novel insights regarding the topology of functional disconnection across FTLN syndromes, holding the promise to be used in order to model disease progression in future longitudinal studies.

Acknowledgements

The present work was performed by Dr Edoardo Gioele Spinelli in partial fulfillment of the requirements for obtaining the PhD degree at Vita-Salute San Raffaele University, Milano, Italy.

References

Agosta F, Galantucci S, Valsasina P, Canu E, Meani A, Marcone A, Magnani G, Falini A, Comi G, Filippi M (2014) Disrupted brain connectome in semantic variant of primary progressive aphasia. *Neurobiol Aging* 35: 2646-2655

Agosta F, Sala S, Valsasina P, Meani A, Canu E, Magnani G, Cappa SF, Scola E, Quatto P, Horsfield MA, Falini A, Comi G, Filippi M (2013) Brain network connectivity assessed using graph theory in frontotemporal dementia. *Neurology* 81: 134-43

Aguilar-Rivera M, Kim S, Coleman TP, Maldonado PE, Torrealba F (2020) Interoceptive insular cortex participates in sensory processing of gastrointestinal malaise and associated behaviors. *Sci Rep* 10: 21642

Alberici A, Geroldi C, Cotelli M, Adorni A, Calabria M, Rossi G, Borroni B, Padovani A, Zanetti O, Kertesz A (2007) The Frontal Behavioural Inventory (Italian version) differentiates frontotemporal lobar degeneration variants from Alzheimer's disease. *Neurol Sci* 28: 80-6

Andersson J, Jenkinson M, Smith S (2007) FMRIB technical report TR07JA2. FMRIB Analysis Group of the University of Oxford

Appollonio I, Leone M, Isella V, Piamarta F, Consoli T, Villa ML, Forapani E, Russo A, Nichelli P (2005) The Frontal Assessment Battery (FAB): normative values in an Italian population sample. *Neurol Sci* 26: 108-16

Ashburner J (2007) A fast diffeomorphic image registration algorithm. *Neuroimage* 38: 95-113

Basso A, Capitani E, Laiacona M (1987) Raven's coloured progressive matrices: normative values on 305 adult normal controls. *Funct Neurol* 2: 189-94

Battistella G, Henry M, Gesierich B, Wilson SM, Borghesani V, Shwe W, Miller Z, Deleon J, Miller BL, Jovicich J, Papinutto N, Dronkers NF, Seeley WW, Mandelli ML,

Gorno-Tempini ML (2019) Differential intrinsic functional connectivity changes in semantic variant primary progressive aphasia. *Neuroimage Clin* 22: 101797

Beck AT, Ward CH, Mendelson M, Mock J, Erbaugh J (1961) An inventory for measuring depression. *Arch Gen Psychiatry* 4: 561-71

Bejanin A, Tammewar G, Marx G, Cobigo Y, Iaccarino L, Kornak J, Staffaroni AM, Dickerson BC, Boeve BF, Knopman DS, Gorno-Tempini M, Miller BL, Jagust WJ, Boxer AL, Rosen HJ, Rabinovici GD (2020) Longitudinal structural and metabolic changes in frontotemporal dementia. *Neurology* 95: e140-e154

Benarroch EE (2019) Insular cortex: Functional complexity and clinical correlations. *Neurology* 93: 932-938

Bonakdarpour B, Hurley RS, Wang AR, Ferreira HR, Basu A, Chatrathi A, Guillaume K, Rogalski EJ, Mesulam MM (2019) Perturbations of language network connectivity in primary progressive aphasia. *Cortex* 121: 468-480

Caffarra P, Vezzadini G, Dieci F, Zonato F, Venneri A (2002) Rey-Osterrieth complex figure: normative values in an Italian population sample. *Neurol Sci* 22: 443-7

Caffarra P, Vezzadini G, Dieci F, Zonato F, Venneri A (2004) Modified Card Sorting Test: normative data. *J Clin Exp Neuropsychol* 26: 246-50

Carlesimo GA, Caltagirone C, Gainotti G (1996) The Mental Deterioration Battery: normative data, diagnostic reliability and qualitative analyses of cognitive impairment. The Group for the Standardization of the Mental Deterioration Battery. *Eur Neurol* 36: 378-84

Catani M, Thiebaut de Schotten M (2008) A diffusion tensor imaging tractography atlas for virtual in vivo dissections. *Cortex* 44: 1105-32

Catricala E, Della Rosa PA, Ginex V, Mussetti Z, Plebani V, Cappa SF (2013) An Italian battery for the assessment of semantic memory disorders. *Neurol Sci* 34: 985-93

Chao-Gan Y, Yu-Feng Z (2010) DPARSF: A MATLAB Toolbox for "Pipeline" Data Analysis of Resting-State fMRI. *Front Syst Neurosci* 4: 13

Cloutman LL, Binney RJ, Drakesmith M, Parker GJ, Lambon Ralph MA (2012) The variation of function across the human insula mirrors its patterns of structural connectivity: evidence from in vivo probabilistic tractography. *Neuroimage* 59: 3514-21

Collins JA, Montal V, Hochberg D, Quimby M, Mandelli ML, Makris N, Seeley WW, Gorno-Tempini ML, Dickerson BC (2017) Focal temporal pole atrophy and network degeneration in semantic variant primary progressive aphasia. *Brain* 140: 457-471

Costumero V, d'Oleire Uquillas F, Diez I, Andorra M, Basaia S, Bueicheku E, Ortiz-Teran L, Belloch V, Escudero J, Avila C, Sepulcre J (2020) Distance disintegration delineates the brain connectivity failure of Alzheimer's disease. *Neurobiol Aging* 88: 51-60

De Renzi E, Vignolo LA (1962) The token test: A sensitive test to detect receptive disturbances in aphasics. *Brain* 85: 665-78

Ducharme S, Price BH, Dickerson BC (2018) Apathy: a neurocircuitry model based on frontotemporal dementia. *J Neurol Neurosurg Psychiatry* 89: 389-396

Farb NA, Grady CL, Strother S, Tang-Wai DF, Masellis M, Black S, Freedman M, Pollock BG, Campbell KL, Hasher L, Chow TW (2013) Abnormal network connectivity in frontotemporal dementia: evidence for prefrontal isolation. *Cortex* 49: 1856-73

Fathy YY, Hepp DH, de Jong FJ, Geurts JGG, Foncke EMJ, Berendse HW, van de Berg WDJ, Schoonheim MM (2020) Anterior insular network disconnection and cognitive impairment in Parkinson's disease. *Neuroimage Clin* 28: 102364

Filippi M, Agosta F, Scola E, Canu E, Magnani G, Marcone A, Valsasina P, Caso F, Copetti M, Comi G, Cappa SF, Falini A (2013) Functional network connectivity in the behavioral variant of frontotemporal dementia. *Cortex* 49: 2389-401

Filippi M, Basaia S, Canu E, Imperiale F, Magnani G, Falautano M, Comi G, Falini A, Agosta F (2020) Changes in functional and structural brain connectome along the Alzheimer's disease continuum. *Mol Psychiatry* 25: 230-239

Filippi M, Basaia S, Canu E, Imperiale F, Meani A, Caso F, Magnani G, Falautano M, Comi G, Falini A, Agosta F (2017) Brain network connectivity differs in early-onset neurodegenerative dementia. *Neurology* 89: 1764-1772

Filippi M, Basaia S, Sarasso E, Stojkovic T, Stankovic I, Fontana A, Tomic A, Piramide N, Stefanova E, Markovic V, Kostic VS, Agosta F (2021) Longitudinal brain connectivity changes and clinical evolution in Parkinson's disease. *Mol Psychiatry* 26: 5429-5440

Folstein MF, Folstein SE, McHugh PR (1975) "Mini-mental state". A practical method for grading the cognitive state of patients for the clinician. *J Psychiatr Res* 12: 189-98

Fornito A, Zalesky A, Breakspear M (2015) The connectomics of brain disorders. *Nat Rev Neurosci* 16: 159-72

Friston KJ, Williams S, Howard R, Frackowiak RS, Turner R (1996) Movement-related effects in fMRI time-series. *Magn Reson Med* 35: 346-55

Ghaziri J, Tucholka A, Girard G, Boucher O, Houde JC, Descoteaux M, Obaid S, Gilbert G, Rouleau I, Nguyen DK (2018) Subcortical structural connectivity of insular subregions. *Sci Rep* 8: 8596

Gorno-Tempini ML, Hillis AE, Weintraub S, Kertesz A, Mendez M, Cappa SF, Ogar JM, Rohrer JD, Black S, Boeve BF, Manes F, Dronkers NF, Vandenberghe R, Rascovsky K, Patterson K, Miller BL, Knopman DS, Hodges JR, Mesulam MM, Grossman M (2011) Classification of primary progressive aphasia and its variants. *Neurology* 76: 1006-14

Guo CC, Gorno-Tempini ML, Gesierich B, Henry M, Trujillo A, Shany-Ur T, Jovicich J, Robinson SD, Kramer JH, Rankin KP, Miller BL, Seeley WW (2013) Anterior temporal lobe degeneration produces widespread network-driven dysfunction. *Brain* 136: 2979-91

Huber W, Poeck K, Willmes K (1984) The Aachen Aphasia Test. *Adv Neurol* 42: 291-303

Jenkinson M, Bannister P, Brady M, Smith S (2002) Improved optimization for the robust and accurate linear registration and motion correction of brain images. *Neuroimage* 17: 825-41

Kaufer DI, Cummings JL, Ketchel P, Smith V, MacMillan A, Shelley T, Lopez OL, DeKosky ST (2000) Validation of the NPI-Q, a brief clinical form of the Neuropsychiatric Inventory. *J Neuropsychiatry Clin Neurosci* 12: 233-9

Klein LA, Buchanan JA (2009) Psychometric properties of the Pyramids and Palm Trees Test. *J Clin Exp Neuropsychol* 31: 803-8

Knopman DS, Kramer JH, Boeve BF, Caselli RJ, Graff-Radford NR, Mendez MF, Miller BL, Mercaldo N (2008) Development of methodology for conducting clinical trials in frontotemporal lobar degeneration. *Brain* 131: 2957-68

Laiacona M, Inzaghi MG, De Tanti A, Capitani E (2000) Wisconsin card sorting test: a new global score, with Italian norms, and its relationship with the Weigl sorting test. *Neurol Sci* 21: 279-91

Landin-Romero R, Kumfor F, Leyton CE, Irish M, Hodges JR, Piguet O (2017) Disease-specific patterns of cortical and subcortical degeneration in a longitudinal study of Alzheimer's disease and behavioural-variant frontotemporal dementia. *Neuroimage* 151: 72-80

Lowe MJ, Mock BJ, Sorenson JA (1998) Functional connectivity in single and multislice echoplanar imaging using resting-state fluctuations. *Neuroimage* 7: 119-32

Mandelli ML, Caverzasi E, Binney RJ, Henry ML, Lobach I, Block N, Amirbekian B, Dronkers N, Miller BL, Henry RG, Gorno-Tempini ML (2014) Frontal white matter tracts sustaining speech production in primary progressive aphasia. *J Neurosci* 34: 9754-67

Mandelli ML, Welch AE, Vilaplana E, Watson C, Battistella G, Brown JA, Possin KL, Hubbard HI, Miller ZA, Henry ML, Marx GA, Santos-Santos MA, Bajorek LP, Fortea J, Boxer A, Rabinovici G, Lee S, Deleon J, Rosen HJ, Miller BL et al. (2018) Altered topology of the functional speech production network in non-fluent/agrammatic variant of PPA. *Cortex* 108: 252-264

Meijboom R, Steketee RME, de Koning I, Osse RJ, Jiskoot LC, de Jong FJ, van der Lugt A, van Swieten JC, Smits M (2017) Functional connectivity and microstructural white matter changes in phenocopy frontotemporal dementia. *Eur Radiol* 27: 1352-1360

Menon V, Uddin LQ (2010) Saliency, switching, attention and control: a network model of insula function. *Brain Struct Funct* 214: 655-67

Monaco M, Costa A, Caltagirone C, Carlesimo GA (2013) Forward and backward span for verbal and visuo-spatial data: standardization and normative data from an Italian adult population. *Neurol Sci* 34: 749-54

Morris JC (1993) The Clinical Dementia Rating (CDR): current version and scoring rules. *Neurology* 43: 2412-4

Mutlu J, Landeau B, Gaubert M, de La Sayette V, Desgranges B, Chetelat G (2017) Distinct influence of specific versus global connectivity on the different Alzheimer's disease biomarkers. *Brain* 140: 3317-3328

Nomi JS, Schettini E, Broce I, Dick AS, Uddin LQ (2018) Structural Connections of Functionally Defined Human Insular Subdivisions. *Cereb Cortex* 28: 3445-3456

Novelli G, Papagno C, Capitani E, Laiacona M, Vallar G, Cappa SF (1986) Tre test clinici di ricerca e produzione lessicale. Taratura su soggetti normali. *Archivio di Psicologia, Neurologia e Psichiatria* 47: 477-506

Orsini A, Fragassi NA, Chiacchio L, Falanga AM, Cocchiaro C, Grossi D (1987) Verbal and spatial memory span in patients with extrapyramidal diseases. *Percept Mot Skills* 65: 555-8

Perry DC, Brown JA, Possin KL, Datta S, Trujillo A, Radke A, Karydas A, Kornak J, Sias AC, Rabinovici GD, Gorno-Tempini ML, Boxer AL, De May M, Rankin KP, Sturm VE, Lee SE, Matthews BR, Kao AW, Vessel KA, Tartaglia MC et al. (2017) Clinicopathological correlations in behavioural variant frontotemporal dementia. *Brain* 140: 3329-3345

Pozzi L, Valenza F, Mosca L, Dal Mas A, Domi T, Romano A, Tarlarini C, Falzone YM, Tremolizzo L, Soraru G, Cerri F, Ferraro PM, Basaia S, Agosta F, Fazio R, Comola M, Comi G, Ferrari M, Quattrini A, Lunetta C et al. (2017) TBK1 mutations in Italian patients with amyotrophic lateral sclerosis: genetic and functional characterisation. *J Neurol Neurosurg Psychiatry* 88: 869-875

Rascovsky K, Hodges JR, Knopman D, Mendez MF, Kramer JH, Neuhaus J, van Swieten JC, Seelaar H, Dopper EG, Onyike CU, Hillis AE, Josephs KA, Boeve BF, Kertesz A, Seeley WW, Rankin KP, Johnson JK, Gorno-Tempini ML, Rosen H, Prioleau-Latham CE et al. (2011) Sensitivity of revised diagnostic criteria for the behavioural variant of frontotemporal dementia. *Brain* 134: 2456-77

Renton AE, Majounie E, Waite A, Simon-Sanchez J, Rollinson S, Gibbs JR, Schymick JC, Laaksovirta H, van Swieten JC, Myllykangas L, Kalimo H, Paetau A, Abramzon Y, Remes AM, Kaganovich A, Scholz SW, Duckworth J, Ding J, Harmer DW, Hernandez DG et al. (2011) A hexanucleotide repeat expansion in C9ORF72 is the cause of chromosome 9p21-linked ALS-FTD. *Neuron* 72: 257-68

Reyes P, Ortega-Merchan MP, Rueda A, Uriza F, Santamaria-Garcia H, Rojas-Serrano N, Rodriguez-Santos J, Velasco-Leon MC, Rodriguez-Parra JD, Mora-Diaz DE, Matallana D (2018) Functional Connectivity Changes in Behavioral, Semantic, and Nonfluent Variants of Frontotemporal Dementia. *Behav Neurol* 2018: 9684129

Rohrer JD, Warren JD (2011) Phenotypic signatures of genetic frontotemporal dementia. *Curr Opin Neurol* 24: 542-9

Seeley WW, Crawford R, Rascovsky K, Kramer JH, Weiner M, Miller BL, Gorno-Tempini ML (2008) Frontal paralimbic network atrophy in very mild behavioral variant frontotemporal dementia. *Arch Neurol* 65: 249-55

- Seeley WW, Crawford RK, Zhou J, Miller BL, Greicius MD (2009) Neurodegenerative diseases target large-scale human brain networks. *Neuron* 62: 42-52
- Seeley WW, Menon V, Schatzberg AF, Keller J, Glover GH, Kenna H, Reiss AL, Greicius MD (2007) Dissociable intrinsic connectivity networks for salience processing and executive control. *J Neurosci* 27: 2349-56
- Sepulcre J, Sabuncu MR, Yeo TB, Liu H, Johnson KA (2012) Stepwise connectivity of the modal cortex reveals the multimodal organization of the human brain. *J Neurosci* 32: 10649-61
- Song XW, Dong ZY, Long XY, Li SF, Zuo XN, Zhu CZ, He Y, Yan CG, Zang YF (2011) REST: a toolkit for resting-state functional magnetic resonance imaging data processing. *PLoS One* 6: e25031
- Spinelli EG, Mandelli ML, Miller ZA, Santos-Santos MA, Wilson SM, Agosta F, Grinberg LT, Huang EJ, Trojanowski JQ, Meyer M, Henry ML, Comi G, Rabinovici G, Rosen HJ, Filippi M, Miller BL, Seeley WW, Gorno-Tempini ML (2017) Typical and atypical pathology in primary progressive aphasia variants. *Ann Neurol* 81: 430-443
- Spinnler H, Tognoni G (1987) Standardizzazione e taratura italiana di test neuropsicologici. Vol. Supplementum N. 8. In Milano: Masson Italia Periodici
- Stoodley CJ, Schmahmann JD (2010) Evidence for topographic organization in the cerebellum of motor control versus cognitive and affective processing. *Cortex* 46: 831-44
- Strick PL, Dum RP, Fiez JA (2009) Cerebellum and nonmotor function. *Annu Rev Neurosci* 32: 413-34
- van den Heuvel MP, Sporns O (2013) Network hubs in the human brain. *Trends Cogn Sci* 17: 683-96
- Van Essen DC (2005) A Population-Average, Landmark- and Surface-based (PALS) atlas of human cerebral cortex. *Neuroimage* 28: 635-62
- Warren JD, Rohrer JD, Hardy J (2012) Disintegrating brain networks: from syndromes to molecular nexopathies. *Neuron* 73: 1060-2
- Whitwell JL, Jack CR, Jr., Parisi JE, Knopman DS, Boeve BF, Petersen RC, Dickson DW, Josephs KA (2011) Imaging signatures of molecular pathology in behavioral variant frontotemporal dementia. *J Mol Neurosci* 45: 372-8

Yan CG, Cheung B, Kelly C, Colcombe S, Craddock RC, Di Martino A, Li Q, Zuo XN, Castellanos FX, Milham MP (2013) A comprehensive assessment of regional variation in the impact of head micromovements on functional connectomics. *Neuroimage* 76: 183-201

Zheng YQ, Zhang Y, Yau Y, Zeighami Y, Larcher K, Masic B, Dagher A (2019) Local vulnerability and global connectivity jointly shape neurodegenerative disease propagation. *PLoS Biol* 17: e3000495

Zhou J, Gennatas ED, Kramer JH, Miller BL, Seeley WW (2012) Predicting regional neurodegeneration from the healthy brain functional connectome. *Neuron* 73: 1216-27

Zhou J, Greicius MD, Gennatas ED, Growdon ME, Jang JY, Rabinovici GD, Kramer JH, Weiner M, Miller BL, Seeley WW (2010) Divergent network connectivity changes in behavioural variant frontotemporal dementia and Alzheimer's disease. *Brain* 133: 1352-67

Zuo XN, Ehmke R, Mennes M, Imperati D, Castellanos FX, Sporns O, Milham MP (2012) Network centrality in the human functional connectome. *Cereb Cortex* 22: 1862-75

Table 1. Demographic and main clinical characteristics of the Milan cohort.

	HC-old	bvFTD	nfvPPA	svPPA	p
N	94	64	34	36	
Age at MRI (years)	65.35 ± 6.39 (51.22- 79.34)	65.92 ± 7.91 (45.51- 79.76)	69.01 ± 8.3 (53.83- 83.35)	66.94 ± 8.34 (48.46- 81.63)	0.11
Sex (M/F)	36/58	38/26	12/22	18/18	0.09
Education (years)	12.51 ± 4.35 (5-24) #	9.65 ± 3.53 (3-17)	10.06 ± 5.8 (3-22)	11.83 ± 4.68 (3-18)	0.001
Disease duration (years)	-	3.62 ± 2.25 (0.57-12.06)	2.55 ± 1.48 (0.13-6.17) #*	4.03 ± 2.07 (0.94-10.82)	0.01
CDR	-	1.12 ± 1.17 (0 – 3)	0.50 ± 0.11 (0 – 2) #	0.74 ± 0.63 (0 – 2)	0.03
CDR-FTD	-	8.34 ± 5.68 (2 – 18)	5.38 ± 3.29 (2 – 11.5)	5.86 ± 4.35 (1.5 – 13.5)	0.29
CDR-sb	-	5.54 ± 3.75 (1 – 14)	2.76 ± 2.44 (0 – 9) #	3.44 ± 3.19 (0.5 – 10.5)	0.04
MMSE	29.03 ± 1.96 (27 – 30)	23.47 ± 5.67 [6 – 30] §	23.77 ± 5.69 [5 – 30] §	21.73 ± 6.83 [5 – 30] §	<0.001
Scanner type (1/2)	44/50	35/29	18/16	14/22	0.44

Values are reported as means ± standard deviations (min – max). The threshold of statistical significance was set at $p < 0.05$. p values refer to ANOVA models followed by post-hoc, Bonferroni-corrected comparisons or Pearson's chi square, as appropriate. Abbreviations: bvFTD = behavioral variant Frontotemporal Dementia; CDR = Clinical Dementia Rating; CDR-FTD = Clinical Dementia Rating for Frontotemporal Dementia; CDR-sb = Clinical Dementia Rating sum of boxes; HC = Healthy Controls; MMSE = Mini-Mental State Examination; nfvPPA = nonfluent/agrammatic variant Primary Progressive Aphasia; NPI = Neuropsychiatric Inventory; svPPA = semantic variant Primary Progressive Aphasia.

§ = statistically significant difference with HC

= statistically significant difference with bvFTD

* = statistically significant difference with svPPA

Table 2. Demographic and main clinical characteristics of the Mayo Clinic cohort.

	HC	bvFTD	nfvPPA	svPPA	p
N	15	11	14	18	
Age at MRI (years)	61.07±7.75 (51-77)	60.57±9.59 (47.2-75.6)	66.95±7.81 (48.4-77)	62.49±7.77 (44.6-72.8)	0.13
Sex (M/F)	5/10	4/7	9/5	10/8	0.91

Values are reported as means ± standard deviations (min – max). The threshold of statistical significance was set at $p < 0.05$. p values refer to Kruskal-Wallis t-tests followed by post-hoc comparisons or Pearson’s chi square, as appropriate. Abbreviations: bvFTD = behavioral variant Frontotemporal Dementia; HC = Healthy Controls; nfvPPA = nonfluent/agrammatic variant Primary Progressive Aphasia; svPPA = semantic variant Primary Progressive Aphasia.

Table 3. Neuropsychological features of the Milan cohort.

	HC	bvFTD	nfvPPA	svPPA
N	94	64	34	36
Global cognition				
MMSE	29.03±1.96 (16-30)	23.47±5.67* (6-30)	23.94±5.67* (5-30)	21.73±6.83* (5-30)
FAB	-	11±4.23 (1-17)	9.7±4.99 (0-16)	12.68±4.63 (0-17)
Memory				
Digit span forward	5.86±1.29 (0-9)	4.85±1.14* (3-7)	4.03±0.93* (2-6)	4.94±1.46* (0-7)
RAVLT delayed	9.42±2.92 (3-14)	2.96±3.18*§ (0-11)	6.61±3.77* (0-12)	3±3.66*§ (0-11)
Corsi block-tapping	5.13±1.17 (2-7)	3.84±1.45 (0-7)	5.46±7.45 (2-40)	4.42±1.23 (2-7)
Attention and executive functions				
Attentive matrices	50.32±8.04 (23-60)	39.47±11.81* (10-60)	34.96±14.24* (1-58)	40.97±13.49* (12-59)
CPM	30.79±4.75 (11-35)	21.61±8.13* (0-35)	22.44±7.63* (6-34)	24.24±7.91* (7-36)
Digit span backward	4.56±1.24 (2-8)	3.44-1.1* (0-5)	2.5±1.25* (0-4)	3.33±1.44* (0-6)
Card sorting test perseverations	4.18±3.79 (0-16)	17.25±14.57* # (0-46)	9.71±10.16 (0-42)	6.33±6.07 (0-21)
Visuospatial abilities				
Rey Figure copy	30.3±5.5 (4-36)	22.84±10.32* (0-36)	22.67±9.18 (0-35)	29.09±5.25 (16-35)
Language				
AAT (repetition)	-	-	127.83±24.62	142.43±11.24

			(49-148)	(120-180)
Token test	33.68±2.92 (15-36)	27.47±6.87*	24.74±6.34* (13-35)	22.33±9.54* (4-36)
CaGi confrontation naming	-	-	43.12±6.73# (22-48)	19.44±12.95 § (0-47)
CaGi single-word comprehension	-	-	47.55±1.53# (41-48)	38.35±9.07 § (18-48)
Pyramid-palm tree	-	-	46.8±5.66# (29-52)	36.35±6.85 § (25-50)
Fluency				
Phonemic Fluency	36.85±10 (7-56)	15.02±11.29* (0-39)	8.62±7.38* (0-25)	15.25±11.1* (0-31)
Semantic Fluency	43.65±10.31 (12-66)	21.6±10.56*# (0-48)	19.9±11.3*# (0-48)	11.45±8.1* (0-28)
Mood & Behavior				
NPI	-	28.46±19.35 (3-74)	16.25±18.82 (1-71)	16.23±12.05 (0-44)
BDI	6.86±3.6 (0-12)	-	-	-
FBI total	-	21.23±11.26 (6-46)	14.5±10.37 (5-36)	18±10.7 (6-38)

Values are means ± standard deviations [range]. P values refer to ANOVA models, corrected for age, sex and education, followed by post-hoc pairwise comparisons, Bonferroni-corrected for multiple comparisons. The threshold of statistical significance was set at $p < 0.05$.

Abbreviations: AAT = Aachener Aphasia Test; BDI = Beck Depression Inventory; bvFTD = behavioral variant Frontotemporal Dementia; CPM = Colored Progressive Matrices; CST = Card Sorting Tests; FAB = Frontal Assessment Battery; FBI = Frontal Behavioral Inventory; HC = Healthy Controls; MMSE = Mini-Mental State Examination;

nfvPPA = nonfluent/agrammatic variant Primary Progressive Aphasia; RAVLT = Rey Auditory Verbal Learning Test; svPPA= semantic variant Primary Progressive Aphasia.

* = statistically significant difference with HC

= statistically significant difference with svPPA

§ = statistically significant difference with nfvPPA

Table 4. Montreal Neurological Institute (MNI) coordinates of the significant clusters of VBM analysis, showing regions of GM loss in each group of FTLD patients compared with healthy controls of the Mayo Clinic cohort. Clusters presented in table survived a $p < 0.05$ FWE-corrected at cluster level, accounting for age and sex. Abbreviations: bvFTD = behavioral variant Frontotemporal Dementia; L= left hemisphere; nfvPPA = nonfluent/agrammatic variant Primary Progressive Aphasia; R= right hemisphere; svPPA= semantic variant Primary Progressive Aphasia.

bvFTD < HC						
Anatomic regions	Side	Cluster size	MNI coordinates			T values
			x	y	z	
Insula	L	1402	-40	20	3	6.35
Supplementary motor area	L	228	-2	16	54	6.24
Precentral gyrus	L	877	-42	9	36	6.10
Superior frontal cortex	L	467	-20	39	33	6.02
Middle frontal cortex	L	435	-24	14	54	6.01
Insula	R	359	38	15	6	5.80
Supero-medial frontal cortex	L	116	-10	30	32	5.40
Supero-medial frontal cortex	L	60	-4	36	45	5.35
Anterior cingulate cortex	R	22	12	30	30	5.12
nfvPPA < HC						
Anatomic regions	Side	Cluster size	MNI coordinates			T values
			x	y	z	
Supplementary motor area	L	60	-8	12	58	6.08
Middle frontal cortex	R	152	39	-3	60	5.84
Precentral gyrus	L	375	-45	0	45	5.71
Precentral gyrus	L	38	-40	-3	56	5.48
Inferior frontal gyrus – pars triangularis	L	47	-36	14	24	5.30
svPPA < HC						
Anatomic regions	Side	Cluster size	MNI coordinates			T values
			x	y	z	
Inferior temporal cortex	L	19264	-46	-4	-42	11.93
Inferior temporal cortex	R	1650	34	2	-40	6.86
Inferior temporal cortex	R	31	56	-21	-27	5.29
Paracentral lobule	L	63	-15	-21	72	5.29

Table 5. Brain regions showing significant functional connectivity differences between bvFTD patients and controls. L= left; R= right. Colors refer to legend of **Figure 3**.

bvFTD patients vs healthy controls				
<i>Left insula</i>	<i>Step 1</i>	<i>Step 2</i>	<i>Step 3</i>	<i>Step 4</i>
↓ [yellow - red]	L & R superior frontal (posterior), paracentral, caudal anterior cingulate, posterior cingulate, supramarginal, superior temporal, inferior insula, rostral middle frontal, postcentral, superior parietal (posterior), precuneus (anterior, L>R), R middle temporal	L & R insula, precentral, postcentral, superior temporal, supramarginal, opercularis, triangularis, rostral middle frontal, superior frontal, posterior cingulate gyrus, paracentral lobule, rostral anterior cingulate, caudal anterior cingulate, orbitalis, lateral orbitofrontal cortex	L & R insula, precentral, postcentral, superior temporal, opercularis, triangularis, superior frontal, paracentral, caudal anterior cingulate, posterior cingulate, rostral anterior cingulate, precuneus. R supramarginal, rostral middle frontal cortex, orbitalis	L & R insula, precentral, postcentral, superior temporal, superior frontal, superior parietal, rostral anterior cingulate, caudal anterior cingulate, posterior cingulate, paracentral, opercularis, triangularis. L supramarginal, caudal middle frontal cortex
↑ [blue - green]	L & R ant-sup insula, middle temporal, inferior temporal, superior frontal (anterior), triangularis, superior parietal lobule (posterior), inferior parietal lobule, medial orbitofrontal cortex, fusiform, precuneus (posterior), cuneus, lingual, pericalcarine cortex, entorhinal cortex, parahippocampal, opercularis. L lateral occipital cortex, triangularis. R isthmus cingulate	L & R inferior parietal lobule, cuneus, pericalcarine cortex, lingual, fusiform, parahippocampal, medial orbitofrontal cortex, lateral occipital cortex, precuneus (posterior), inferior temporal, middle temporal, isthmus cingulate R caudal middle frontal,	L & R middle temporal, inferior temporal, fusiform, inferior parietal lobule, medial orbitofrontal cortex, parahippocampal, lingual, lateral occipital cortex, superior parietal lobule R caudal middle frontal, superior frontal (anterior), pericalcarine cortex L ant-sup insula	L & R middle temporal, inferior temporal, inferior parietal lobule, medial orbitofrontal cortex, parahippocampal, fusiform, lingual R superior parietal lobule (posterior), caudal middle frontal, superior frontal (anterior), pericalcarine cortex L ant-sup insula
Subcortical differences	↑ L & R caudate, ↑ L cerebellum (crus II, lobule VIIB, lobule V, lobule VI) ↓ R cerebellum (lobule VI, lobule VIIIA, lobule VIIIB, crus I, crus II, crus IIB)	↑ L & R cerebellum (lobule V, VI, IX) ↑ L cerebellum (crus I, VIIB) ↑ R cerebellum (crus II)	↑ L & R cerebellum (lobule IX, crus II, lobule VIIIA). ↑ L cerebellum (lobule VIIB), putamen	↑ L & R cerebellum (crus I, crus II, lobule V, lobule VI, lobule VIIb, lobule VIIIB, lobule IX). L putamen

Table 6. Brain regions showing significant functional connectivity differences between nfvPPA patients and controls. L= left; R= right. Colors refer to legend of **Figure 4**.

nfvPPA patients vs healthy controls				
<i>Left Supplementary motor area</i>	<i>Step 1</i>	<i>Step 2</i>	<i>Step 3</i>	<i>Step 4</i>
↓ [yellow – red]	L & R opercularis, triangularis, precentral gyrus, insula, paracentral gyrus, rostral anterior cingulate gyrus, superior temporal gyrus (L>R) R supramarginal gyrus	L & R insula, superior temporal gyrus (R>L), posterior cingulate gyrus, caudal anterior cingulate gyrus, rostral cingulate gyrus, paracentral gyrus, precentral gyrus, postcentral gyrus, opercularis, triangularis, rostral middle frontal gyrus. R supramarginal gyrus	L & R insula, precentral gyrus, postcentral gyrus, opercularis, supramarginal cortex, superior temporal gyrus, posterior cingulate gyrus, caudal anterior cingulate gyrus, paracentral gyrus (R>L) L triangularis	L & R insula, precentral gyrus, postcentral gyrus, opercularis, posterior cingulate gyrus, paracentral gyrus, caudal anterior cingulate gyrus, superior parietal gyrus. L superior temporal gyrus. R supramarginal gyrus
↑ [blue – green]	L & R superior frontal gyrus, lingual gyrus. L caudal middle frontal gyrus, R parahippocampal, fusiform	L & R superior frontal gyrus (L>R), medial orbitofrontal gyrus (L>R), fusiform gyrus, parahippocampal gyrus. L entorhinal cortex. R middle temporal gyrus, inferior temporal gyrus	L & R superior frontal gyrus, medial orbitofrontal cortex (L>R), parahippocampal gyrus, fusiform gyrus, lateral orbitofrontal gyrus (L>>R), entorhinal cortex (L>R). R middle temporal gyrus, inferior temporal gyrus	L & R superior frontal gyrus, parahippocampal gyrus. L rostral middle frontal gyrus, fusiform gyrus, entorhinal cortex
Subcortical differences	↑ L & R cerebellum (crus I) ↑ R cerebellum (lobule V, VI, IX)	↑ L & R cerebellum (lobule VI) ↑ R cerebellum (crus I)	↑ L & R cerebellum (lobules VI) ↑ R cerebellum (crus I)	↑ L & R cerebellum (lobule VI) ↑ R cerebellum (crus I)

Table 7. Brain regions showing significant functional connectivity differences between svPPA patients and controls. L= left; R= right. Colors refer to legend of **Figure 5**.

svPPA patients vs healthy controls				
<i>Left Inferior temporal</i>	<i>Step 1</i>	<i>Step 2</i>	<i>Step 3</i>	<i>Step 4</i>
↓ [yellow - red]	R superior temporal gyrus, middle temporal gyrus, inferior temporal gyrus, insula, inferior parietal lobule, inferior frontal pars orbitalis	L & R superior temporal gyrus, insula, pars orbitalis, inferior temporal gyrus (R>L). L transverse temporal gyrus. R entorhinal cortex.	L & R insula, superior temporal gyrus. L transverse temporal gyrus. R middle temporal gyrus, entorhinal cortex.	L & R insula, superior temporal gyrus (R>L). L transverse temporal gyrus. R entorhinal cortex.
↑ [blue - green]	No alterations	L lingual gyrus.	L lingual gyrus.	L lingual gyrus.
Subcortical differences	No alterations	↑ L & R cerebellum (lobule VI, crus I)	↑ L & R cerebellum (lobule V, lobule IX, vermis) ↑ R cerebellum (lobule VI, lobule VIIIA, crus II)	↑ L & R cerebellum (lobules V-VI) ↑ R cerebellum (crus I, crus II, lobule VIIB)

Figure 1. (A) Results of voxel-based morphometry analysis showing regions of significant GM atrophy in FTLD patients of the Mayo Clinic cohort when compared with healthy controls. Significant clusters are overlaid on the axial sections of the Montreal Neurological Institute (MNI) standard brain. Analyses were corrected for age, sex, and total intracranial volume. Statistical threshold for significance was $p < 0.05$, FWE-corrected for multiple comparisons. (B) 10-mm radius spheres overlaid on the MNI standard brain show the identified peaks of atrophy. Abbreviations: bvFTD = behavioral variant Frontotemporal Dementia; ITG= inferior temporal gyrus; L= left hemisphere; nfvPPA = nonfluent/agrammatic variant Primary Progressive Aphasia; R= right hemisphere; SMA= supplementary motor area; svPPA= semantic variant Primary Progressive Aphasia.

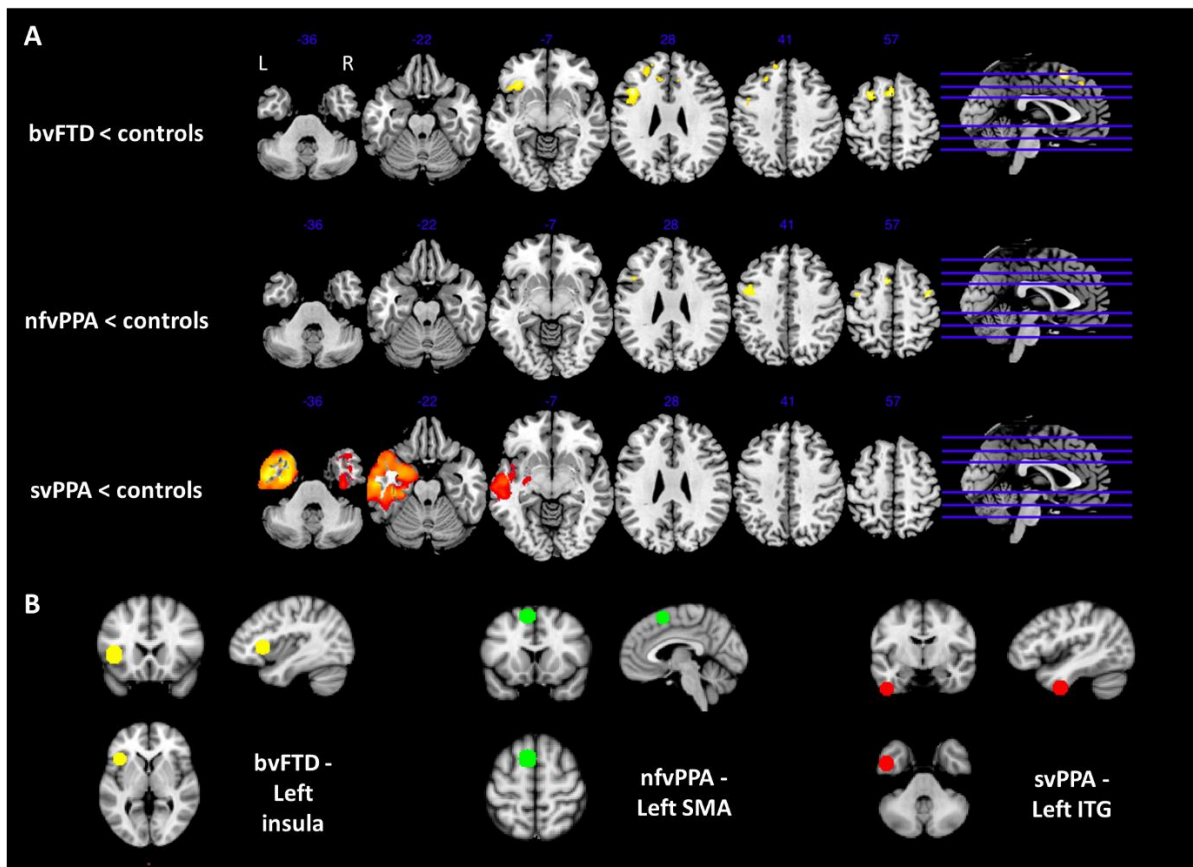


Figure 2. Average stepwise functional connectivity maps in young healthy controls (HC-young) using each seed ROI. Results are depicted in surface space. Red-yellow indicates high strength of connectivity; blue-violet indicates low strength of connectivity.

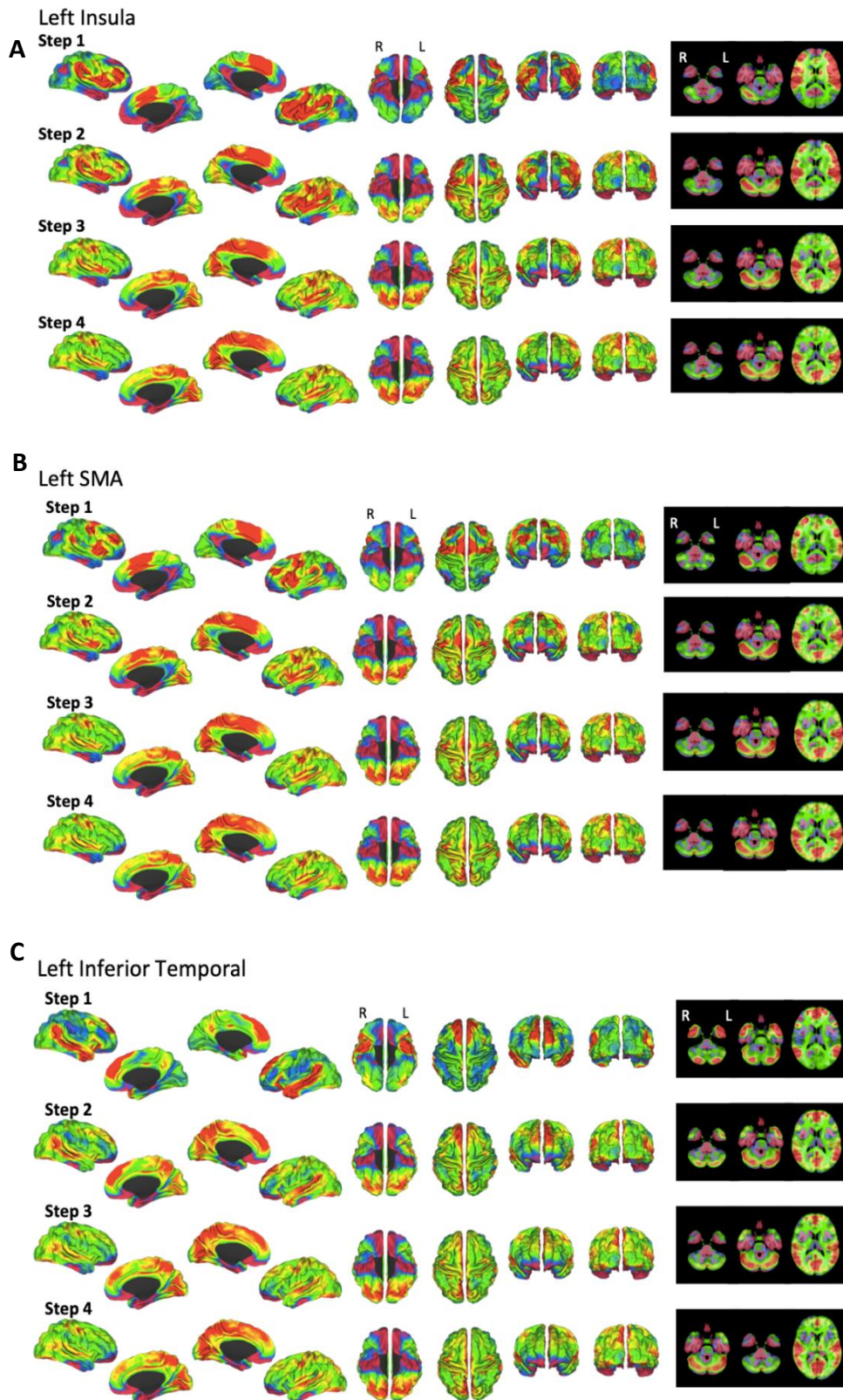


Figure 3. Cortical and subcortical differences between bvFTD patients and age-matched healthy controls (HC-old) in stepwise functional connectivity of the left anterior insula (red-yellow = lower functional connectivity, blue-green = higher functional connectivity).

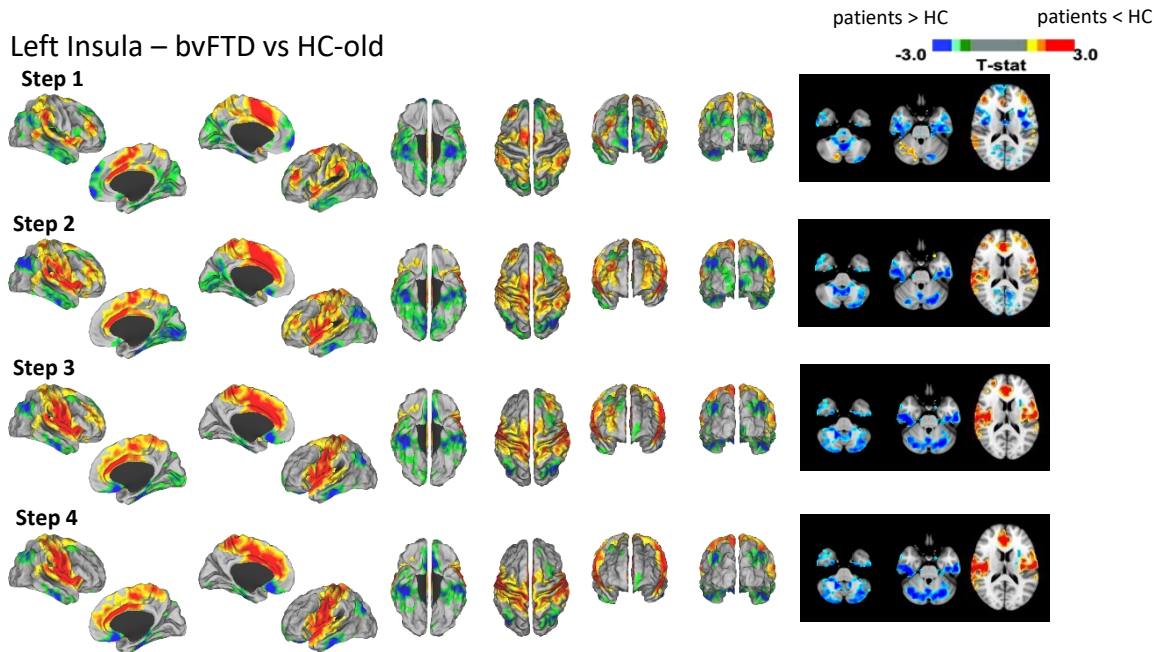


Figure 4. Cortical and subcortical differences between nfvPPA patients and age-matched healthy controls (HC-old) in stepwise functional connectivity of the left supplementary motor area (red-yellow = lower functional connectivity, blue-green = higher functional connectivity).

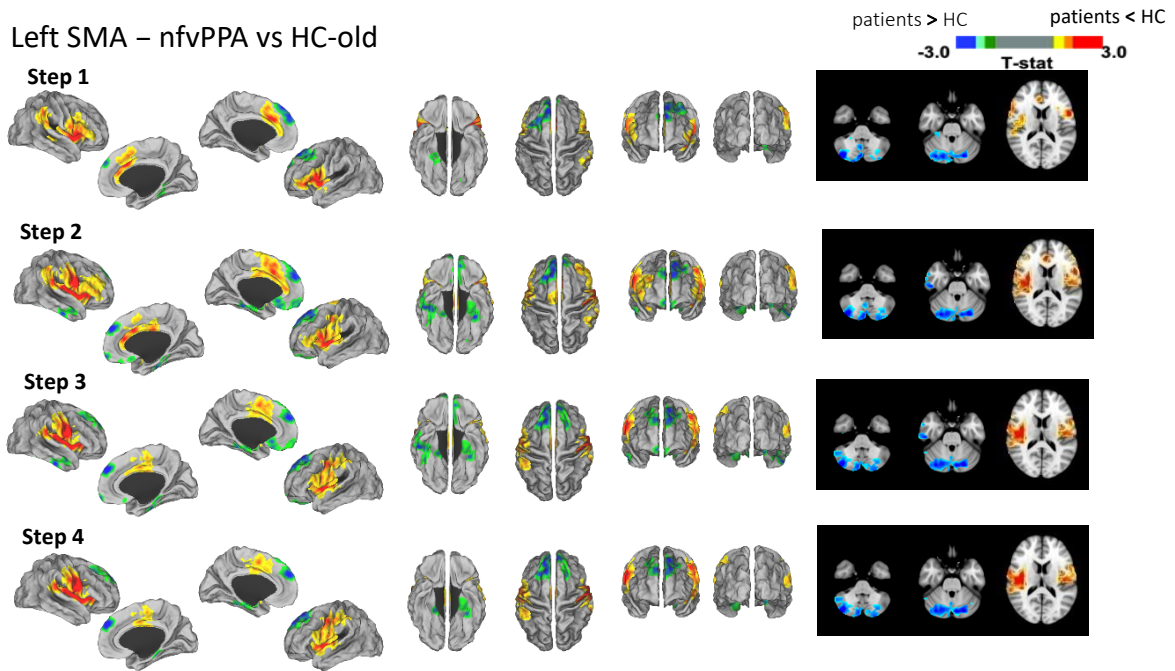


Figure 5. Cortical and subcortical differences between svPPA patients and healthy controls in stepwise functional connectivity of the left inferior temporal gyrus (red-yellow = lower functional connectivity, blue-green = higher functional connectivity).

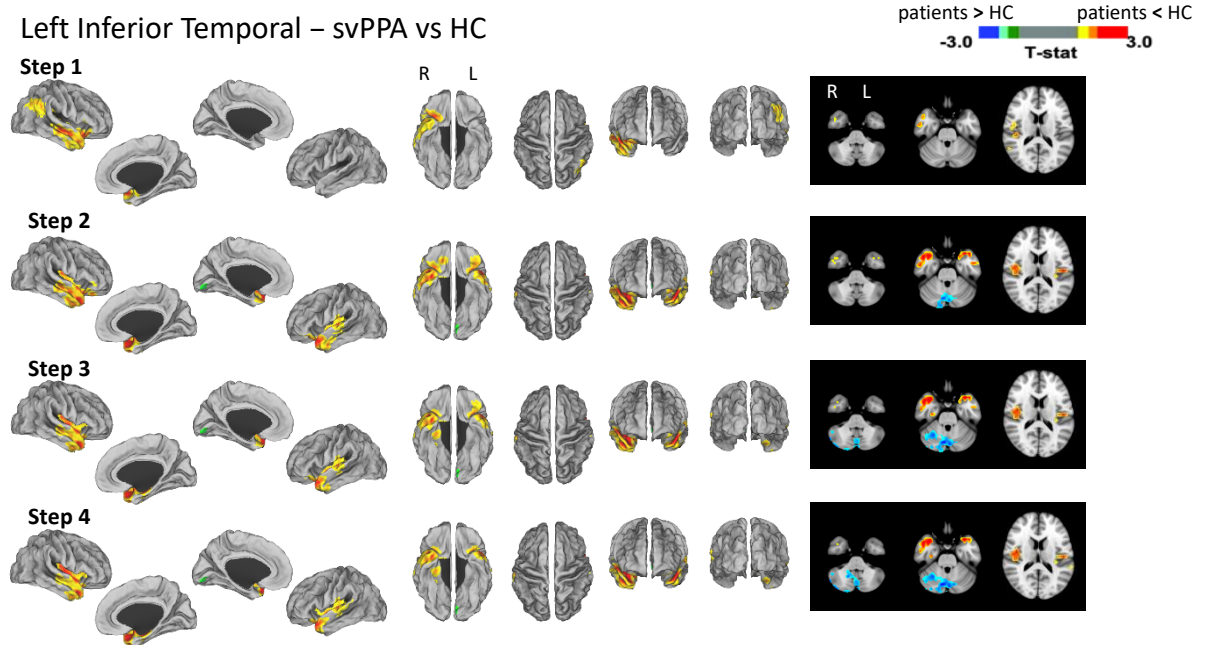
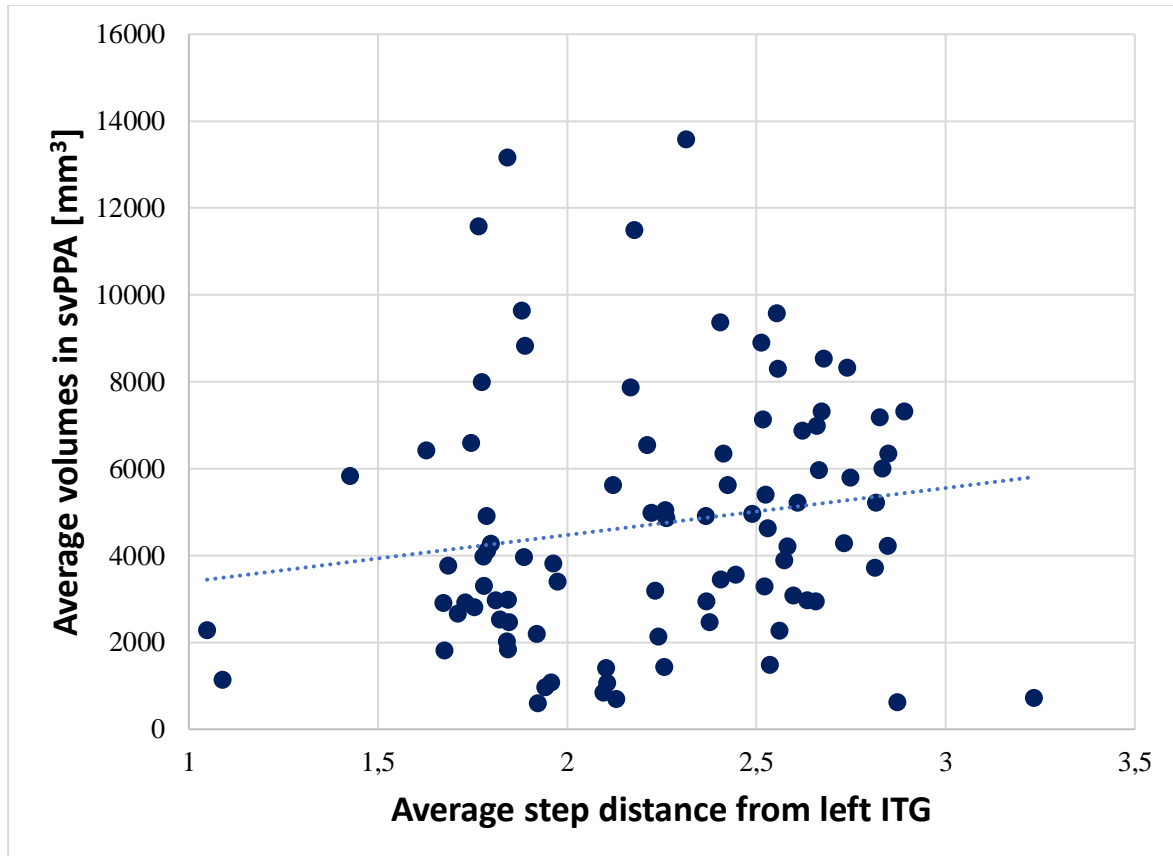


Figure 6. Correlation analysis between average step distance from the left ITG in HC-young subjects and average volume in svPPA patients for each of the 90 GM regions of the AAL atlas. Abbreviations: GM=grey matter; HC= healthy controls; ITG= inferior temporal gyrus; svPPA= semantic variant of primary progressive aphasia.



5. NEURODEGENERATION PATTERNS ACROSS THE ALS/FTD CONTINUUM

5.1. Structural MRI signatures in genetic presentations of the frontotemporal dementia/motor neuron disease spectrum

RESEARCH ARTICLE OPEN ACCESS

Structural MRI Signatures in Genetic Presentations of the Frontotemporal Dementia/Motor Neuron Disease Spectrum

Edoardo Gioele Spinelli, MD, Alma Ghirelli, MD, Silvia Basaia, PhD, Camilla Cividini, MSc, Nilo Riva, MD, PhD, Elisa Canu, PhD, Veronica Castelnovo, MSc, Teuta Dorni, PhD, Giuseppe Magnani, MD, Francesca Caso, MD, PhD, Paola Caroppo, MD, PhD, Sara Prioni, MSc, Giacomina Rossi, PhD, Lucio Tremolizzo, MD, Ildebrando Appollonio, MD, Vincenzo Silani, MD, Paola Carrera, BSc, Massimo Filippi, MD, and Federica Agosta, MD, PhD

Correspondence
Dr. Agosta
agosta.federica@hsr.it

Neurology® 2021;97:e1594-e1607. doi:10.1212/WNL.00000000000012702

Abstract

Background and Objectives

To assess cortical, subcortical, and cerebellar gray matter (GM) atrophy using MRI in patients with disorders of the frontotemporal lobar degeneration (FTLD) spectrum with known genetic mutations.

Methods

Sixty-six patients carrying FTLD-related mutations were enrolled, including 44 with pure motor neuron disease (MND) and 22 with frontotemporal dementia (FTD). Sixty-one patients with sporadic FTLD (sFTLD) matched for age, sex, and disease severity with genetic FTLD (gFTLD) were also included, as well as 52 healthy controls. A whole-brain voxel-based morphometry (VBM) analysis was performed. GM volumes of subcortical and cerebellar structures were obtained.

Results

Compared with controls, GM atrophy on VBM was greater and more diffuse in genetic FTD, followed by sporadic FTD and genetic MND cases, whereas patients with sporadic MND (sMND) showed focal motor cortical atrophy. Patients carrying *C9orf72* and *GRN* mutations showed the most widespread cortical volume loss, in contrast with GM sparing in *SOD1* and *TARDBP*. Globally, patients with gFTLD showed greater atrophy of parietal cortices and thalami compared with sFTLD. In volumetric analysis, patients with gFTLD showed volume loss compared with sFTLD in the caudate nuclei and thalami, in particular comparing C9-MND with sMND cases. In the cerebellum, patients with gFTLD showed greater atrophy of the right lobule VIIb than sFTLD. Thalamic volumes of patients with gFTLD with a *C9orf72* mutation showed an inverse correlation with Frontal Behavioral Inventory scores.

Discussion

Measures of deep GM and cerebellar structural involvement may be useful markers of gFTLD, particularly *C9orf72*-related disorders, regardless of the clinical presentation within the FTLD spectrum.

The following data have been published (Spinelli et al., Neurology. 2021 Oct 19;97(16):e1594-e1607. doi: 10.1212/WNL.00000000000012702).

INTRODUCTION

The successful identification of new therapies for frontotemporal lobar degeneration (FTLD) critically depends on the ability to identify useful markers mirroring specific biological processes within this heterogeneous spectrum of clinical syndromes. Cases due to genetic mutations represent up to 30% of FTLD presentations (Ferrari, Manzoni et al., 2019), and provide an ideal model for studying these processes, as the underlying pathology can be inferred (even in the absence of post-mortem confirmation), facilitating the design of therapeutic trials targeting specific molecular mechanisms. Neuroimaging has demonstrated to provide in vivo, non-invasive measures of neurodegeneration in FTLD phenotypes (Filippi & Agosta, 2018). Distinctive patterns of atrophy on structural MRI contribute to establishing the correct diagnosis of behavioral variant of frontotemporal dementia (bvFTD) and primary progressive aphasia (PPA) (Gorno-Tempini, Hillis et al., 2011, Rascovsky, Hodges et al., 2011), help to distinguish FTLD patients from those with different pathologies (Elahi & Miller, 2017) and even provide hints about the underlying genetic and pathological substrate of each patient (Cash, Bocchetta et al., 2018). Only recently, the role of pathological burden within grey matter (GM) structures other than the brain cortex has been investigated, suggesting a distinctive degeneration of deep GM and cerebellar structures in genetic FTLD (gFTLD) presentations (Bocchetta, Cardoso et al., 2016, Bocchetta, Iglesias et al., 2020, Whitwell & Josephs, 2012), including motor neuron disease (MND) (Bede, Omer et al., 2018). However, most previous studies were mainly focused on pure cognitive phenotypes (Bocchetta et al., 2016, Bocchetta et al., 2020, Whitwell, Boeve et al., 2015), and an extensive characterization of subcortical and cerebellar damage across genetic forms of the FTD/MND spectrum (including *C9orf72*-related disorders) is still in progress.

The aim of this study was to explore the neuroanatomical structural correlates of genetic heterogeneity in a cohort of patients affected by the wide spectrum of FTLD disorders, including MND. More specifically, we assessed with a systematic approach the patterns of atrophy of cortical, subcortical and cerebellar structures using up-to-date MRI volumetric techniques, to identify neuroimaging measures associated with specific genetic alterations.

METHODS

Participants

A total of 658 patients with a suspected diagnosis of FTLD-related disorders were prospectively enrolled in four referral clinics in Lombardy, Italy and referred to San Raffaele Hospital in Milan between October 2007 and July 2019 to perform MRI on a 3T scanner, as part of their diagnostic work-up. Of these, 362 patients gave consent to be screened for known pathogenic mutations and evaluated for inclusion in the present multicenter, case-control study. Patients who underwent genetic screening had received a clinical diagnosis of FTD (n=110) according to either bvFTD (Rascovsky et al., 2011) or PPA (Gorno-Tempini et al., 2011) clinical criteria, or MND variants (n=252), including ALS (Brooks, Miller et al., 2000), progressive muscular atrophy (PMA) (van den Berg-Vos, Visser et al., 2003) and primary lateral sclerosis (PLS) (Pringle, Hudson et al., 1992). Sixty-six mutation carriers were identified, of which 22 presented with a clinical variant of FTD (i.e., bvFTD, n=12; bvFTD-ALS, n=5; nfvPPA, n=3; svPPA, n=1; and right-predominant variant of svPPA, n=1) and 44 with a pure MND phenotype (i.e., ALS, n=35; PMA, n= 6; and PLS, n=3). Patients fulfilling both bvFTD (Rascovsky et al., 2011) and ALS criteria (Brooks et al., 2000) were considered as FTD for the subsequent MRI analyses, considering that greater atrophy was expected compared with pure MND. Figure 1A outlines the screening process of gFTLD, whereas Table 1 and eTables 1 and 4 summarize the demographic and clinical features of included subjects. Among patients who proved negative for known pathogenic mutations (i.e., sporadic FTLD [sFTLD]), we selected 61 subjects to be matched with gFTLD cases for age, sex, and MR scanner type, with comparable clinical diagnoses and disease severity assessed by FTLD-Clinical Dementia Rating (CDR-FTLD) scale (Knopman, Kramer et al., 2008) for FTD and ALS Functional Rating Scale Revised (ALSFRS-r) (Cedarbaum, Stambler et al., 1999) for MND patients. Therefore, 16 sporadic FTD (sFTD, including bvFTD, n=12; nfvPPA, n=2; and svPPA, n=2) and 45 sporadic pure MND (sMND) patients (i.e., ALS, n=37; PMA, n=5; PLS, n=3) were included (Table 1). All patients underwent neurological examination, multi-domain cognitive testing and brain MRI at study entry. Fifteen sFTD patients (i.e., all but one with svPPA) and 10 gFTD patients also underwent lumbar puncture to exclude cerebrospinal fluid biomarker profile suggestive of Alzheimer's disease pathology, as part of their diagnostic work-up (Table 1). No patient showed a p-tau/A β ₄₂ ratio >0.13, considered as pathological (Santangelo, Dell'Edera et al., 2019).

Fifty-two healthy controls comparable for age, sex, and MR scanner type with patient groups were recruited by word of mouth among subjects unrelated to the patient population. Controls were included if the following criteria were satisfied: normal neurological assessment; Mini-Mental Status Examination (MMSE) score ≥ 28 ; no family history of neurodegenerative diseases.

Exclusion criteria for all subjects were: medical illnesses or substance abuse that could interfere with cognitive functioning; any (other) major systemic, psychiatric, or neurological illnesses; and other causes of focal or diffuse brain damage, including lacunae and extensive cerebrovascular disorders at routine MRI.

Standard Protocol Approvals, Registrations, and Patient Consents

Local ethical standards committee on human experimentation approved the study protocol and all participants provided written informed consent.

Genetic analysis

Blood samples were collected from all patients and genomic DNA was obtained and processed in each of the recruiting centers. The presence of GGGGCC hexanucleotide expansion in the first intron of the *C9orf72* gene was assessed using fluorescent amplicon-length analysis and a repeat-primed polymerase chain reaction (PCR) assay. A cut-off of ≥ 30 repeats combined with a typical saw-tooth pattern was considered pathological. In addition, *GRN*, *MAPT*, *TARDBP*, *SOD1*, *FUS*, *TBK1*, *TREM2*, *OPTN* and *VCP* genes were analyzed by Next Generation Sequencing (NGS) and their mutations were confirmed by standard Sanger sequencing. All MND patients were systematically tested for *C9orf72*, *TARDBP*, and *SOD1* mutations, and additional testing of *FUS* and *TBK1* was performed in the presence of positive family history of MND/dementia. Similarly, all FTD patients were tested for *C9orf72*, *TARDBP*, *MAPT*, and *GRN* mutations, with additional testing of *FUS*, *TBK1*, *TREM2*, *OPTN* and *VCP* in the presence of positive family history.

Clinical and neuropsychological evaluations

Clinical evaluation was performed by experienced neurologists blinded to MRI results. For patients presenting with FTD variants, disease severity was assessed using the CDR-

FTLD (Knopman et al., 2008). For MND patients, site of disease onset, disease severity using the ALSFRS-r (Cedarbaum et al., 1999) and manual muscle testing of strength based on the Medical Research Council (MRC) scale were recorded. The rate of disease progression was defined according to the formula: $[48 - \text{ALSFRS-r score}] / \text{time from symptom onset}$.

Neuropsychological assessment was performed by experienced neuropsychologists unaware of MRI results. A comprehensive multi-domain cognitive and behavioral battery was administered, as previously described (Spinelli, Agosta et al., 2019). Based on available cognitive measures, a diagnosis according to the revised Strong criteria for cognitive/behavioral impairment in MND (Strong, Abrahams et al., 2017) could be made for 30 sMND and 29 gMND patients.

MRI acquisition

All patients and healthy controls underwent brain MRI on a 3T scanner (Philips Medical Systems, Best, the Netherlands) at San Raffaele Hospital between 2007 and 2019. The original scanner (for brevity, Scanner 1) was substituted with an upgraded model from the same manufacturer in 2016 (Scanner 2).

Using Scanner 1, a 3D T1-weighted fast field echo (FFE) sequence was acquired (TR=25 ms, TE=4.6 ms, flip angle=30°, 220 axial slices with voxel size=0.89x0.89x0.8 mm, matrix size=256x256, FOV=230x182 mm²). Using Scanner 2, a 3D T1-weighted turbo field echo (TFE) with comparable resolution was acquired (TR=7 ms, TE=3.2 ms, TI=1000 ms, 204 sagittal slices with voxel size=1x1x1 mm, matrix=256x256, FOV=256x256 mm²).

MRI analysis

Voxel-based morphometry

Voxel-based morphometry (VBM) was performed using SPM12 (<http://www.fil.ion.ucl.ac.uk/spm/>) and Diffeomorphic Anatomical Registration Exponentiated Lie Algebra (DARTEL) registration method (Ashburner, 2007), to investigate GM volume alterations at a whole-brain level. Details of the VBM pipeline have been described previously (Filippi, Basaia et al., 2020).

Volumetric analysis

Volumes of the deep GM structures (i.e., bilateral caudate, globus pallidus, putamen, and thalamus), hippocampus and amygdala were obtained using the FMRIB's Integrated Registration and Segmentation Tool (FIRST) in FSL (<http://www.fmrib.ox.ac.uk/fsl/first/index.html>). Local GM volumes of the cerebellar lobules and vermis were calculated automatically using an atlas propagation and label fusion strategy based on the SUIT atlas (Diedrichsen, Balsters et al., 2009, Diedrichsen, Maderwald et al., 2011). GM volumes were multiplied by the normalization factor derived from SIENAx (<http://www.fmrib.ox.ac.uk/fsl/sienax/index.html>) to correct for subject head size.

Statistical analysis

Normal distribution assumption was checked by means of Q-Q plot and Shapiro-Wilks and Kolmogorov-Smirnov tests. Clinical, neuropsychological and MRI volumetric measures were compared between groups using age-, sex- and MR scanner-adjusted ANOVA models, followed by post-hoc pairwise comparisons, Bonferroni-corrected for multiple comparisons. The threshold of significance was set at $p < 0.05$. The SPSS Statistics 22.0 software was used.

VBM group comparisons were tested using ANOVA models in SPM12, adjusting for total intracranial volume, age, sex and MR scanner type. Results were assessed at $p < 0.05$, Family-wise error (FWE)-corrected for multiple comparisons.

Correlations between clinical, cognitive and MRI volumetric features of FTLN patients (i.e., gFTLN and sFTLN, separately) were tested by means of partial correlation analyses adjusted for age, sex and education. Subsequently, the same analysis was performed subdividing the gFTLN group according to the *C9orf72* status. The threshold of statistical significance was set at $p < 0.05$, Bonferroni-corrected for multiple comparisons. The SPSS Statistics 22.0 software was used.

Data Availability Statement

The dataset used and analyzed during the current study is available from the corresponding author on reasonable request.

RESULTS

Genetic findings

The 66 FTLN mutation carriers (Figure 1A) showed pathogenic alterations of the following genes: *C9orf72* (n=33); *TARDBP* (n=10); *GRN* (n=8); *SOD1* (n=7); *FUS* (n=2); *TBK1* (n=2); *TREM2* (n=1); one patient showed both a *C9orf72* expansion and a mutation of the *GRN* gene; and one had both a *C9orf72* and a *TARDBP* mutation.

Clinical diagnosis according to genotype

eTables 1 and 4 report the clinical diagnoses of gFTLD patients, according to the identified mutation(s). We found that each mutation was specifically associated with either an FTD (as for *GRN*, *MAPT*, and *TREM2*) or an MND presentation (as for *TARDBP*, *SOD1*, *TBK1*, and *FUS*), with the notable exception of patients with a *C9orf72* mutation, 22 of which presented with MND (C9-MND) and 11 with FTD (C9-FTD). Patients carrying a double mutation (i.e., the C9orf72+GRN and C9orf72+TARDBP cases) presented, respectively, with FTD and MND.

Clinical and sociodemographic features

Sociodemographic and clinical characteristics of groups defined by clinical diagnosis and genetic status are reported in Table 1. Groups were comparable in terms of sex, education, age at MRI and disease duration at MRI, and specific measures of disease severity for FTD or MND.

When assessing the most sizeable gFTLD subgroups, according to underlying mutation (i.e. C9-MND, C9-FTD, SOD1, TARDBP and GRN), a faster disease progression rate was found in TARDBP patients as compared to sMND, C9-MND and SOD1 (eTable 1).

Neuropsychological features

eTable 2 reports the neuropsychological test scores of groups defined by clinical diagnosis and genetic status. Both sFTD and gFTD patients showed significant impairment of memory, executive, and linguistic functions. Notably, only gFTD patients had significant visuospatial impairment, compared with healthy controls. Overall, neuropsychological features of MND groups were comparable with healthy controls,

although 9 sMND and 10 gMND met criteria for mild cognitive and/or behavioral impairment. When comparing gMND and gFTD with the relative sporadic groups, no significant differences were detected.

eTables 3 and 4 report detailed neuropsychological features according to the underlying mutation. Of note, *GRN* mutation carriers showed the greatest visuospatial impairment, although this was not statistically significant compared with other groups.

GM atrophy

For both VBM and volumetric analyses, characteristic patterns of GM atrophy in gFTLD were investigated using three different levels of comparison, following a systematic scheme that would allow an unbiased reading and interpretation of results (Figure 1B). First, three broad groups were compared: gFTLD, sFTLD and healthy controls (*Level 1*). As a second step, FTLD patients were subdivided according to genetic status and phenotypic manifestation, so that sMND, sFTD, gMND and gFTD patients were considered separately (*Level 2*). Finally, for sufficiently sized genotypic groups, a further subdivision according to specific mutations was considered (*Level 3*). Considering the clinical rationale of the study, aiming at describing variability of atrophy according to the genetic background, and the expected greater atrophy in FTD compared with MND, comparisons between sporadic/genetic patients and healthy controls were performed separately for MND and FTD presentations for Levels 2 and 3.

Voxel-based morphometry (VBM)

Level 1 (gFTLD vs sFTLD vs controls)

Compared with healthy controls, both sFTLD and gFTLD patients showed significant GM volume loss of the prefrontal, anterior cingulate, insular and anterior temporal cortical regions, hippocampi, caudate nuclei and cerebellar crus II, bilaterally (Figure 2A-B, eTable 5); in addition to this, gFTLD showed a more widespread pattern of atrophy, also including the angular gyri, posterior temporal and posterior cingulate cortices, and the thalami (Figure 2B). When compared directly with sFTLD, gFTLD patients showed greater GM atrophy of the left angular gyrus (Figure 2C). No regions showing significant greater atrophy in sFTLD compared with gFTLD patients were found.

Level 2 (gMND vs sMND vs controls; gFTD vs sFTD vs controls)

Compared with healthy controls, sMND patients showed selective atrophy of the left precentral cortex (Figure 3A, eTable 6); gMND patients showed atrophy of the left hippocampus, angular gyrus, occipital cortex, and Rolandic operculum, left crus II, cerebellar vermis VIIIa, and lobule VIIb, bilaterally (Figure 3B). Compared with sMND, gMND patients showed greater atrophy of the left superior frontal and angular gyri (Figure 3E).

Compared with controls, sFTD patients showed widespread atrophy of the prefrontal, insular, anterior temporal and anterior cingulate cortical regions, caudate nuclei, and cerebellar crus I, bilaterally (Figure 3C); gFTD patients showed atrophy of similar regions, with the additional involvement of the thalami, posterior cingulate, fusiform and angular gyri bilaterally, left middle temporal gyrus, and right primary sensory cortex (Figure 3D). Compared with sFTD, gFTD patients showed greater GM atrophy of the thalami and superior parietal lobules, bilaterally, left angular gyrus and right posterior cingulate cortex (Figure 3F).

No regions showing significant greater atrophy in sporadic MND/FTD compared with genetic MND/FTD patients were found.

Level 3 (C9-MND vs SOD1 vs TARDBP vs sMND vs controls; C9-FTD vs GRN vs sFTD vs controls)

Compared with healthy controls, C9-MND patients showed atrophy of the left precentral and postcentral gyri, left supplementary motor area, right angular gyrus, and right occipital cortex, as well as the left thalamus and cerebellar vermis lobule V and lobule VIIb, bilaterally (Figure 4A, eTable 7); MND patients with other mutations (i.e., *SOD1* and *TARDBP* mutation carriers) did not show significant GM atrophy. Compared with sMND patients, C9-MND patients showed greater atrophy of the inferior frontal gyri, bilaterally, left postcentral gyrus, and right posterior thalamus (Figure 4D). No other statistically significant differences between MND groups were found.

C9-FTD patients showed widespread bilateral atrophy of the prefrontal, insular and cingulate cortices, angular gyri, caudate nuclei, thalami and cerebellar left crus II and vermis lobule IX (Figure 4B); GRN patients showed atrophy of the prefrontal, insular, and anterior cingulate cortices, hippocampi, bilaterally, left angular and fusiform gyri,

caudate nuclei, thalami, and cerebellar crus II, bilaterally (Figure 4C). Although no statistically significant differences between FTD groups were found, it is worth noting that thalamic involvement in C9-FTD was more widespread, involving both anterior and posterior regions, if visually compared with the selective damage of anterior thalamic regions observed in GRN cases.

Volumetric GM analysis

Level 1 (gFTLD vs sFTLD vs controls)

Compared with healthy controls, sFTLD patients showed decreased volume of the right thalamus, left putamen, left amygdala, and left hippocampus; gFTLD patients showed volumetric reduction of the caudate nuclei and thalami, bilaterally, left putamen, left hippocampus, right cerebellar crus II and right cerebellar lobule VIIb (eFigure 1 and eTable 8). Compared with sFTLD, gFTLD patients showed volumetric reduction of the thalami, bilaterally, right caudate, and right cerebellar lobule VIIb.

Level 2 (gMND vs sMND vs controls; gFTD vs sFTD vs controls)

Compared with healthy controls, sMND did not show any significant volumetric reduction of the considered GM structures, whereas gMND patients showed decreased thalamic volumes, bilaterally, and greater atrophy of the right cerebellar crus II and right lobule VIIb (Figure 5, eTable 9). Compared with sMND, gMND showed volumetric reduction of the left caudate and left thalamus, and a trend toward greater atrophy of the right crus II ($p=0.07$).

Compared with controls, sFTD patients showed decreased volume of the caudate nuclei, thalami, hippocampi, putamina and pallidi, bilaterally, and left amygdala; gFTD showed similar widespread volume loss of the caudate nuclei, thalami, hippocampi, putamina and pallidi, bilaterally, as well as a trend toward greater atrophy of the right cerebellar lobule VIIb ($p=0.067$) (Figure 5, eTable 9). No significant differences between sFTD and gFTD were found.

Level 3 (C9-MND vs SOD1 vs TARDBP vs sMND vs controls; C9-FTD vs GRN vs sFTD vs controls)

Compared with healthy controls, C9-MND patients showed significant volumetric reduction of the caudate nuclei, thalami, cerebellar lobules VIIb, bilaterally, and right crus II (eFigure 2, eTables 10-11). Compared with sMND, C9-MND patients showed significant volumetric reduction of the thalami, bilaterally, and left caudate, and a trend toward greater atrophy of the right cerebellar lobule VIIb ($p=0.07$).

Compared with healthy controls, C9-FTD patients showed volumetric reduction of the caudate nuclei and thalami, bilaterally; GRN patients showed volumetric reduction of the caudate nuclei, thalami and hippocampi, bilaterally, and left putamen (eFigure 2, eTables 10-11). Compared with sFTD, no statistically significant differences of MRI volumetric measures of C9-FTD and GRN patients were found.

Correlations between clinical, cognitive and MRI volumes of FTLN patients

Thalamic volumes of gFTLD patients showed an inverse correlation with Frontal Behavioral Inventory total scores (left: $r=-0.473$, $p=0.031$; right: $r=-0.638$, $p=0.002$). After subdividing gFTLD according to *C9orf72* status (i.e., C9-FTLD and non-C9 gFTLD), this correlation remained significant only for C9-FTLD (left: $r=-0.579$, $p=0.024$; right: $r=-0.613$, $p=0.025$) (Figure 6).

No other statistically significant correlations between clinical/cognitive and MRI volumetric features of FTLN patients were found.

DISCUSSION

The present study provides a comprehensive report of clinical and GM structural MRI findings in a cohort of patients affected by disorders of the FTLN spectrum with known genetic mutations. Genetically determined FTLN patients (i.e., both FTD and MND presentations) consistently showed greater GM disruption, compared with sporadic cases who were matched for clinical presentation and degree of functional and cognitive impairment. In particular, the involvement of parietal cortices, thalami and cerebellar regions was observed consistently in gFTLD cases, in contrast with sFTD showing atrophy mostly affecting fronto-temporo-insular regions and basal ganglia, and sMND displaying focal damage of motor cortical regions. We have described distinctive patterns of atrophy that associate with each specific mutation, identifying the reduction of thalamic volumes as mostly indicative of *C9orf72*-mutated cases, in particular for patients

presenting with MND. The results provide interesting insights into the pathophysiology of gFTLD and suggest possible neuroimaging markers of underlying pathology that may help to disentangle the heterogeneity of disorders of the FTLN spectrum.

First of all, some important observations can be drawn regarding the relationship between clinical phenotype and the underlying genetic background in the present sample. Our cohort of gFTLD included a prevalent proportion of MND cases, compared with previous studies which were mostly focused on FTD (Bocchetta et al., 2016, Bocchetta et al., 2020, Whitwell et al., 2015). Only studies assessing *C9orf72* mutation carriers (Floeter, Danielian et al., 2018, Mahoney, Beck et al., 2012a) had a larger representation of MND, consistent with the known association of this mutation with both cognitive and motor FTLN presentations. In fact, in our cohort, *C9orf72* was the only mutation that was observed both in FTD and MND cases, and all patients presenting with a mixed FTD-ALS phenotype carried this genetic alteration. The composition of our cohort also allowed the identification of relatively sizeable groups of less common MND-related mutation carriers, whose neuroanatomical damage has been rarely described, such as *SOD1* (Agosta, Spinelli et al., 2018, Turner, Hammers et al., 2007) or *TARDBP* (Borroni, Bonvicini et al., 2009, Gelpi, van der Zee et al., 2014). In addition, we highlighted that not only ALS, but also other MND phenotypes (i.e., PLS and PMA) can be associated with *C9orf72*, *TARDBP* or *SOD1* mutations. PLS/PMA cases with a *C9orf72* expansion have been rarely described (van Rheenen, van Blitterswijk et al., 2012), whereas an association with *SOD1* or *TARDBP* mutations is practically anecdotic (van Blitterswijk, Vlam et al., 2012). Therefore, our findings suggest that the common notion of PLS and PMA as sporadic MND presentations should be at least reconsidered (van Blitterswijk et al., 2012).

The sporadic groups of our sample were selected to be matched with gFTLD cases for clinical presentation and disease severity. Consistently, gMND and gFTD were comparable with the respective sporadic groups in terms of the main clinical and cognitive measures. A notable exception was provided by *TARDBP* mutation carriers, whose disease progression rate was faster than other MND groups, although with a high interindividual variability consistent with previous reports (Corcia, Valdmanis et al., 2012). Although we did not detect significant differences in neuropsychological measures between genetic FTD/MND patients and the respective sporadic groups, gFTD (in

particular, *GRN* mutation carriers) had the most severe impairment of visuospatial skills, suggesting a more rapid evolution to multidomain cognitive impairment, similar to previous reports in *GRN* mutation carriers (Beck, Rohrer et al., 2008).

The most consistent result provided by VBM was a more severe and widespread GM atrophy in gFTLD patients, compared with sFTLD. We revealed a characteristic involvement of the inferior parietal, posterior cingulate, thalamic and posterior cerebellar regions in gFTD and gMND patients, that the respective sporadic groups lacked. GM atrophy was generally greater and more diffuse in gFTD cases, followed by sFTD and gMND cases, whereas sMND showed very focal, subtle atrophy of the motor cortex (which was shared by gMND). The presence of diffuse neuroanatomical damage in gFTLD compared with sFTLD, extending to posterior cortical and subcortical regions despite a comparable disease severity and duration, supports the notion that an “unfavorable” genetic background might accelerate neurodegeneration in neuronal populations that are relatively distant from those classically involved in FTLTLD (Agosta, Ferraro et al., 2017, Schonecker, Neuhofer et al., 2018).

When we assessed patients defined on the specific underlying mutation, a greater damage of the inferior parietal cortices (namely, the angular gyrus) and the thalami was shared by C9-MND, C9-FTD and *GRN* mutation carriers, compared with sporadic cases. The greater involvement of the inferior parietal regions is consistent with previous reports in *C9orf72* (Bertrand, Wen et al., 2018, Bocchetta, Todd et al., 2021, Boeve, Boylan et al., 2012, Mahoney et al., 2012a) and *GRN* mutation carriers (Beck et al., 2008, Whitwell et al., 2015), even from the presymptomatic stages (Bertrand et al., 2018, Bocchetta et al., 2021). *GRN* patients showed a left-sided prevalence of parietal cortical damage, consistent with the relatively large proportion (3/8) of PPA presentations in our cohort and the known asymmetrical atrophy of this group (Beck et al., 2008, Whitwell et al., 2015), although the overall average pattern of GM atrophy was relatively symmetrical. Of note, characteristic posterior thalamic and cerebellar atrophy was found in *C9orf72* mutation carriers with either FTD or MND presentations, in contrast with the involvement of anterior thalamic regions in *GRN* mutation carriers. Our findings are in line with previous studies highlighting the specific involvement of the pulvinar and posterior cerebellar regions in FTD cases with a *C9orf72* expansion, and expanding the validity of these findings to pure MND cases (Bocchetta et al., 2016, Bocchetta et al., 2020, Whitwell

et al., 2015). By contrast, we were not able to detect significant atrophy in the cortical regions of TARDBP and SOD1 patients, although these groups were similarly sized when compared with C9-MND. To our knowledge, there are no published reports of MRI volumetric findings in a cohort of TARDBP patients, due to the rarity of this mutation. Although our findings need to be confirmed in larger samples, these suggest a substantial absence of GM involvement in MND patients carrying a *TARDBP* mutation, in contrast with the few case reports demonstrating frontotemporal atrophy in *TARDBP*-related FTD cases (Borroni et al., 2009, Gelpi et al., 2014). The absence of brain GM atrophy in our SOD1 group is in line with studies suggesting a different distribution of the non-TDP-43 pathology associated with this mutation (Agosta et al., 2018, Turner et al., 2007), that prevalently involves the lower motor neurons in the spinal cord (Cudkowicz, McKenna-Yasek et al., 1998).

Intrigued by the results that we obtained at the whole-brain level, we then focused on the involvement of deep GM and cerebellar structures, in order to identify quantitative volumetric markers that could provide relevant group-specific measures of neurodegeneration in gFTLD. In this case, the difference in severity of atrophy between MND and FTD patients was even more relevant compared with the VBM analysis, since both sFTD and gFTD showed a similarly widespread severe involvement of basal ganglia, thalami and hippocampi, in contrast with a general preservation of these structures in sMND and gMND. The only notable exception was the significant bilateral thalamic atrophy identified in gMND, that emerged particularly when only C9-MND were considered, as a distinctive feature compared with sMND cases. In fact, our findings strengthen previous evidence that thalamic atrophy in FTLT is highly indicative of a genetic underlying cause, mostly pointing toward a *C9orf72* expansion (Bocchetta et al., 2020, Irish, Devenney et al., 2013, Mahoney et al., 2012a, Mahoney, Downey et al., 2012b). We have also shown distinctive atrophy of the caudate nucleus in C9-MND cases, consistent with previous MRI studies demonstrating typical basal ganglia involvement in *C9orf72*-related MND (Bede et al., 2018) and subtle functional rearrangements in the thalami and basal ganglia of *C9orf72* mutation carriers, even in presymptomatic phases (De Vocht, Blommaert et al., 2020, Lee, Sias et al., 2017). We have also found an inverse correlation between thalamic volumes and behavioral impairment in gFTLD patients, which was mostly driven by *C9orf72* mutation carriers. This suggests a significant

influence of such characteristic neuroanatomical damage over the progression of neurobehavioral impairment in *C9orf72*-related FTLD, consistent with the involvement of the thalami in cognition and complex behavior (Wolff & Vann, 2019). Therefore, our results strongly point towards the use of measures of deep GM involvement as useful markers of *C9orf72*-related disorders, regardless of the clinical presentation within the FTLD spectrum.

The analysis of cerebellar volumes showed a substantial preservation of these regions in sFTLD, in contrast with atrophy of the lobule VIIb and crus II detected in gFTLD. Particularly, the single cerebellar structure showing greater damage in gFTLD compared with sFTLD was the right lobule VIIb. When looking at single genetic alterations, we identified gMND and, particularly, C9-MND as the subjects driving these results, which are consistent with recent studies indicating the involvement of the cognitive/affective regions of the posterior cerebellum (particularly, lobule VII and crus regions, involved in the modulation of emotions and social behaviors) as indicative of the presence of a *C9orf72* mutation (Bocchetta et al., 2020), possibly as a consequence of the close structural and functional connections with the thalami through cerebello-thalamo-cortical networks (Lee et al., 2017, Stoodley & Schmahmann, 2010). Similar alterations have been demonstrated in presymptomatic *C9orf72* mutation carriers (Bertrand et al., 2018, Bocchetta et al., 2021, Montembeault, Sayah et al., 2020), correlating with cognitive inhibition deficits (Montembeault et al., 2020). Although the role in cognition and the topological organization of the cerebellar cortex has started being elucidated only in recent years (Stoodley & Schmahmann, 2010), this is an exciting area of developing research for biomarkers of disease pathology in the FTLD spectrum (including MND), that might be combined with other more established measures of cortical damage.

This study is not without limitations. First, in order to include the largest possible number of gFTLD cases, we included subjects acquired using two different MRI scanners. For this reason, we corrected all analyses for scanner type. Moreover, we lacked neuropathological post-mortem diagnosis of the sporadic cases. This might have partially influenced the results when comparing sFTD patients with gFTD who, in our cohort, were almost exclusively due to mutations leading to FTLD-TDP pathology. Finally, we did not involve presymptomatic mutation carriers, that would be needed to understand how early the volumetric changes that we detected can be observed in the course of the disease.

Future longitudinal studies involving these subjects will be fundamental to understand the potential clinical relevance of these measures for early identification of patients close to symptom onset and as outcome measures in clinical trials targeting specific FTLD-related molecular mechanisms.

In conclusion, this study encompassed the entire FTLD spectrum, providing an accurate overview of clinical, neuropsychological and MRI volumetric findings in patients with a genetically determined FTD/MND clinical phenotype. We have described also mutations that have been rarely reported previously in the neuroimaging literature and identified specific imaging measures of FTLD genotypes, which proved especially useful when it comes to *C9orf72*-associated presentations. Our results strongly suggest that neuroimaging can provide useful volumetric measures applicable to future clinical trials targeting these genetic mutations.

Acknowledgements

The present work was performed by Dr Edoardo Gioele Spinelli in partial fulfillment of the requirements for obtaining the PhD degree at Vita-Salute San Raffaele University, Milano, Italy.

References

Agosta F, Ferraro PM, Riva N, Spinelli EG, Domi T, Carrera P, Copetti M, Falzone Y, Ferrari M, Lunetta C, Comi G, Falini A, Quattrini A, Filippi M (2017) Structural and functional brain signatures of C9orf72 in motor neuron disease. *Neurobiol Aging* 57: 206-219

Agosta F, Spinelli EG, Marjanovic IV, Stevic Z, Pagani E, Valsasina P, Salak-Djokic B, Jankovic M, Lavrnjic D, Kostic VS, Filippi M (2018) Unraveling ALS due to SOD1 mutation through the combination of brain and cervical cord MRI. *Neurology* 90: e707-e716

Ashburner J (2007) A fast diffeomorphic image registration algorithm. *Neuroimage* 38: 95-113

Beck J, Rohrer JD, Campbell T, Isaacs A, Morrison KE, Goodall EF, Warrington EK, Stevens J, Revesz T, Holton J, Al-Sarraj S, King A, Scahill R, Warren JD, Fox NC, Rossor MN, Collinge J, Mead S (2008) A distinct clinical, neuropsychological and radiological phenotype is associated with progranulin gene mutations in a large UK series. *Brain : a journal of neurology* 131: 706-20

Bede P, Omer T, Finegan E, Chipika RH, Iyer PM, Doherty MA, Vajda A, Pender N, McLaughlin RL, Hutchinson S, Hardiman O (2018) Connectivity-based characterisation of subcortical grey matter pathology in frontotemporal dementia and ALS: a multimodal neuroimaging study. *Brain Imaging Behav* 12: 1696-1707

Bertrand A, Wen J, Rinaldi D, Houot M, Sayah S, Camuzat A, Fournier C, Fontanella S, Routier A, Couratier P, Pasquier F, Habert MO, Hannequin D, Martinaud O, Caroppo P, Levy R, Dubois B, Brice A, Durrleman S, Colliot O et al. (2018) Early Cognitive, Structural, and Microstructural Changes in Presymptomatic C9orf72 Carriers Younger Than 40 Years. *JAMA Neurol* 75: 236-245

Bocchetta M, Cardoso MJ, Cash DM, Ourselin S, Warren JD, Rohrer JD (2016) Patterns of regional cerebellar atrophy in genetic frontotemporal dementia. *Neuroimage Clin* 11: 287-290

Bocchetta M, Iglesias JE, Neason M, Cash DM, Warren JD, Rohrer JD (2020) Thalamic nuclei in frontotemporal dementia: Mediodorsal nucleus involvement is universal but pulvinar atrophy is unique to C9orf72. *Hum Brain Mapp* 41: 1006-1016

Bocchetta M, Todd EG, Peakman G, Cash DM, Convery RS, Russell LL, Thomas DL, Eugenio Iglesias J, van Swieten JC, Jiskoot LC, Seelaar H, Borroni B, Galimberti D, Sanchez-Valle R, Laforce R, Moreno F, Synofzik M, Graff C, Masellis M, Carmela Tartaglia M et al. (2021) Differential early subcortical involvement in genetic FTD within the GENFI cohort. *Neuroimage Clin* 30: 102646

Boeve BF, Boylan KB, Graff-Radford NR, DeJesus-Hernandez M, Knopman DS, Pedraza O, Vemuri P, Jones D, Lowe V, Murray ME, Dickson DW, Josephs KA, Rush BK, Machulda MM, Fields JA, Ferman TJ, Baker M, Rutherford NJ, Adamson J, Wszolek ZK et al. (2012) Characterization of frontotemporal dementia and/or amyotrophic lateral sclerosis associated with the GGGGCC repeat expansion in C9ORF72. *Brain : a journal of neurology* 135: 765-83

Borroni B, Bonvicini C, Alberici A, Buratti E, Agosti C, Archetti S, Papetti A, Stuardi C, Di Luca M, Gennarelli M, Padovani A (2009) Mutation within TARDBP leads to frontotemporal dementia without motor neuron disease. *Hum Mutat* 30: E974-83

Brooks BR, Miller RG, Swash M, Munsat TL, World Federation of Neurology Research Group on Motor Neuron D (2000) El Escorial revisited: revised criteria for the diagnosis of amyotrophic lateral sclerosis. *Amyotroph Lateral Scler Other Motor Neuron Disord* 1: 293-9

Cash DM, Bocchetta M, Thomas DL, Dick KM, van Swieten JC, Borroni B, Galimberti D, Masellis M, Tartaglia MC, Rowe JB, Graff C, Tagliavini F, Frisoni GB, Laforce R, Jr., Finger E, de Mendonca A, Sorbi S, Rossor MN, Ourselin S, Rohrer JD et al. (2018) Patterns of gray matter atrophy in genetic frontotemporal dementia: results from the GENFI study. *Neurobiol Aging* 62: 191-196

Cedarbaum JM, Stambler N, Malta E, Fuller C, Hilt D, Thurmond B, Nakanishi A (1999) The ALSFRS-R: a revised ALS functional rating scale that incorporates

assessments of respiratory function. BDNF ALS Study Group (Phase III). *J Neurol Sci* 169: 13-21

Corcia P, Valdmanis P, Millicamps S, Lionnet C, Blasco H, Mouzat K, Daoud H, Belzil V, Morales R, Pageot N, Danel-Brunaud V, Vandenberghe N, Pradat PF, Couratier P, Salachas F, Lumbroso S, Rouleau GA, Meisinger V, Camu W (2012) Phenotype and genotype analysis in amyotrophic lateral sclerosis with TARDBP gene mutations. *Neurology* 78: 1519-26

Cudkovicz ME, McKenna-Yasek D, Chen C, Hedley-Whyte ET, Brown RH, Jr. (1998) Limited corticospinal tract involvement in amyotrophic lateral sclerosis subjects with the A4V mutation in the copper/zinc superoxide dismutase gene. *Ann Neurol* 43: 703-10

De Vocht J, Blommaert J, Devrome M, Radwan A, Van Weehaeghe D, De Schaepdryver M, Ceccarini J, Rezaei A, Schramm G, van Aalst J, Chio A, Pagani M, Stam D, Van Esch H, Lamaire N, Verhaegen M, Mertens N, Poesen K, van den Berg LH, van Es MA et al. (2020) Use of Multimodal Imaging and Clinical Biomarkers in Presymptomatic Carriers of C9orf72 Repeat Expansion. *JAMA Neurol* 77: 1008-1017

Diedrichsen J, Balsters JH, Flavell J, Cussans E, Ramnani N (2009) A probabilistic MR atlas of the human cerebellum. *Neuroimage* 46: 39-46

Diedrichsen J, Maderwald S, Kuper M, Thurling M, Rabe K, Gizewski ER, Ladd ME, Timmann D (2011) Imaging the deep cerebellar nuclei: a probabilistic atlas and normalization procedure. *Neuroimage* 54: 1786-94

Elahi FM, Miller BL (2017) A clinicopathological approach to the diagnosis of dementia. *Nat Rev Neurol* 13: 457-476

Ferrari R, Manzoni C, Hardy J (2019) Genetics and molecular mechanisms of frontotemporal lobar degeneration: an update and future avenues. *Neurobiol Aging* 78: 98-110

Filippi M, Agosta F (2018) MRI of non-Alzheimer's dementia: current and emerging knowledge. *Curr Opin Neurol* 31: 405-414

Filippi M, Basaia S, Canu E, Imperiale F, Magnani G, Falautano M, Comi G, Falini A, Agosta F (2020) Changes in functional and structural brain connectome along the Alzheimer's disease continuum. *Mol Psychiatry* 25: 230-239

Floeter MK, Danielian LE, Braun LE, Wu T (2018) Longitudinal diffusion imaging across the C9orf72 clinical spectrum. *J Neurol Neurosurg Psychiatry* 89: 53-60

Gelpi E, van der Zee J, Turon Estrada A, Van Broeckhoven C, Sanchez-Valle R (2014) TARDBP mutation p.Ile383Val associated with semantic dementia and complex proteinopathy. *Neuropathol Appl Neurobiol* 40: 225-30

Gorno-Tempini ML, Hillis AE, Weintraub S, Kertesz A, Mendez M, Cappa SF, Ogar JM, Rohrer JD, Black S, Boeve BF, Manes F, Dronkers NF, Vandenberghe R, Rascovsky K, Patterson K, Miller BL, Knopman DS, Hodges JR, Mesulam MM, Grossman M (2011) Classification of primary progressive aphasia and its variants. *Neurology* 76: 1006-14

Irish M, Devenney E, Wong S, Dobson-Stone C, Kwok JB, Piguet O, Hodges JR, Hornberger M (2013) Neural substrates of episodic memory dysfunction in behavioural variant frontotemporal dementia with and without C9ORF72 expansions. *Neuroimage Clin* 2: 836-43

Knopman DS, Kramer JH, Boeve BF, Caselli RJ, Graff-Radford NR, Mendez MF, Miller BL, Mercaldo N (2008) Development of methodology for conducting clinical trials in frontotemporal lobar degeneration. *Brain : a journal of neurology* 131: 2957-68

Lee SE, Sias AC, Mandelli ML, Brown JA, Brown AB, Khazenzon AM, Vidovszky AA, Zanto TP, Karydas AM, Pribadi M, Dokuru D, Coppola G, Geschwind DH, Rademakers R, Gorno-Tempini ML, Rosen HJ, Miller BL, Seeley WW (2017) Network degeneration and dysfunction in presymptomatic C9ORF72 expansion carriers. *Neuroimage Clin* 14: 286-297

Mahoney CJ, Beck J, Rohrer JD, Lashley T, Mok K, Shakespeare T, Yeatman T, Warrington EK, Schott JM, Fox NC, Rossor MN, Hardy J, Collinge J, Revesz T, Mead S, Warren JD (2012a) Frontotemporal dementia with the C9ORF72 hexanucleotide repeat expansion: clinical, neuroanatomical and neuropathological features. *Brain : a journal of neurology* 135: 736-50

Mahoney CJ, Downey LE, Ridgway GR, Beck J, Clegg S, Blair M, Finnegan S, Leung KK, Yeatman T, Golden H, Mead S, Rohrer JD, Fox NC, Warren JD (2012b) Longitudinal neuroimaging and neuropsychological profiles of frontotemporal dementia with C9ORF72 expansions. *Alzheimers Res Ther* 4: 41

Montembeault M, Sayah S, Rinaldi D, Le Toullec B, Bertrand A, Funkiewiez A, Saracino D, Camuzat A, Couratier P, Chouly M, Hannequin D, Aubier-Girard C, Pasquier

F, Delbeuck X, Colliot O, Batrancourt B, Azuar C, Levy R, Dubois B, Le Ber I et al. (2020) Cognitive inhibition impairments in presymptomatic C9orf72 carriers. *J Neurol Neurosurg Psychiatry* 91: 366-372

Pringle CE, Hudson AJ, Munoz DG, Kiernan JA, Brown WF, Ebers GC (1992) Primary lateral sclerosis. Clinical features, neuropathology and diagnostic criteria. *Brain : a journal of neurology* 115 (Pt 2): 495-520

Rascovsky K, Hodges JR, Knopman D, Mendez MF, Kramer JH, Neuhaus J, van Swieten JC, Seelaar H, Dopper EG, Onyike CU, Hillis AE, Josephs KA, Boeve BF, Kertesz A, Seeley WW, Rankin KP, Johnson JK, Gorno-Tempini ML, Rosen H, Prioleau-Latham CE et al. (2011) Sensitivity of revised diagnostic criteria for the behavioural variant of frontotemporal dementia. *Brain* 134: 2456-77

Santangelo R, Dell'Edera A, Sala A, Cecchetti G, Masserini F, Caso F, Pinto P, Leocani L, Falautano M, Passerini G, Martinelli V, Comi G, Perani D, Magnani G (2019) The CSF p-tau181/Abeta42 Ratio Offers a Good Accuracy "In Vivo" in the Differential Diagnosis of Alzheimer's Dementia. *Curr Alzheimer Res* 16: 587-595

Schonecker S, Neuhofer C, Otto M, Ludolph A, Kassubek J, Landwehrmeyer B, Anderl-Straub S, Semler E, Diehl-Schmid J, Prix C, Vollmar C, Fortea J, Deutsches F-K, Huppertz HJ, Arzberger T, Edbauer D, Feddersen B, Dieterich M, Schroeter ML, Volk AE et al. (2018) Atrophy in the Thalamus But Not Cerebellum Is Specific for C9orf72 FTD and ALS Patients - An Atlas-Based Volumetric MRI Study. *Front Aging Neurosci* 10: 45

Spinelli EG, Agosta F, Ferraro PM, Querin G, Riva N, Bertolin C, Martinelli I, Lunetta C, Fontana A, Soraru G, Filippi M (2019) Brain MRI shows white matter sparing in Kennedy's disease and slow-progressing lower motor neuron disease. *Hum Brain Mapp* 40: 3102-3112

Stoodley CJ, Schmahmann JD (2010) Evidence for topographic organization in the cerebellum of motor control versus cognitive and affective processing. *Cortex* 46: 831-44

Strong MJ, Abrahams S, Goldstein LH, Woolley S, McLaughlin P, Snowden J, Mioshi E, Roberts-South A, Benatar M, HortobaGyi T, Rosenfeld J, Silani V, Ince PG, Turner MR (2017) Amyotrophic lateral sclerosis - frontotemporal spectrum disorder (ALS-

FTSD): Revised diagnostic criteria. *Amyotroph Lateral Scler Frontotemporal Degener* 18: 153-174

Turner MR, Hammers A, Allsop J, Al-Chalabi A, Shaw CE, Brooks DJ, Leigh PN, Andersen PM (2007) Volumetric cortical loss in sporadic and familial amyotrophic lateral sclerosis. *Amyotroph Lateral Scler* 8: 343-7

van Blitterswijk M, Vlam L, van Es MA, van der Pol WL, Hennekam EA, Dooijes D, Schelhaas HJ, van der Kooi AJ, de Visser M, Veldink JH, van den Berg LH (2012) Genetic overlap between apparently sporadic motor neuron diseases. *PLoS One* 7: e48983

van den Berg-Vos RM, Visser J, Franssen H, de Visser M, de Jong JM, Kalmijn S, Wokke JH, van den Berg LH (2003) Sporadic lower motor neuron disease with adult onset: classification of subtypes. *Brain : a journal of neurology* 126: 1036-47

van Rheenen W, van Blitterswijk M, Huisman MH, Vlam L, van Doormaal PT, Seelen M, Medic J, Dooijes D, de Visser M, van der Kooi AJ, Raaphorst J, Schelhaas HJ, van der Pol WL, Veldink JH, van den Berg LH (2012) Hexanucleotide repeat expansions in C9ORF72 in the spectrum of motor neuron diseases. *Neurology* 79: 878-82

Whitwell JL, Boeve BF, Weigand SD, Senjem ML, Gunter JL, Baker MC, DeJesus-Hernandez M, Knopman DS, Wszolek ZK, Petersen RC, Rademakers R, Jack CR, Jr., Josephs KA (2015) Brain atrophy over time in genetic and sporadic frontotemporal dementia: a study of 198 serial magnetic resonance images. *Eur J Neurol* 22: 745-52

Whitwell JL, Josephs KA (2012) Neuroimaging in frontotemporal lobar degeneration-predicting molecular pathology. *Nat Rev Neurol* 8: 131-42

Wolff M, Vann SD (2019) The Cognitive Thalamus as a Gateway to Mental Representations. *J Neurosci* 39: 3-14

Table 1. Main socio-demographic and clinical characteristics of healthy controls and FTLD patients classified by clinical presentation and genetic status.

	HC	sMND	gMND	sFTD	gFTD	p
Number	52	45	44	16	22	
Diagnosis	-	37 ALS, 5 PMA, 3 PLS	35 ALS, 6 PMA, 3 PLS	12 bvFTD, 2 nvPPA, 2 svPPA	12 bvFTD, 5 bvFTD/ALS, 1 svPPA, 3 nvPPA, 1 R-SD	-
Sex (M/F)	26/26	23/22	22/22	9/7	11/11	0.99
Genetic mutation	-	-	22 C9orf72, 10 TARDBP, 7 SOD1, 2 TBK1, 2 FUS, 1 C9orf72 + TARDBP	-	11 C9orf72, 8 GRN, 1 MAPT, 1 TREM2, 1 C9orf72 + GRN	-
Family history (+/-)	0/52	3/42	18/26 ^{a,b,c}	2/14	13/9 ^{a,b,c}	<0.001
Education (years)	12.75 ± 3.70 (5 – 20)	12.07 ± 4.10 (5 – 24)	10.84 ± 3.23 (5-20)	10.36 ± 3.81 (5 – 17)	11.11 ± 4.19 (5 – 21)	0.13
Age at MRI (years)	59.2 ± 6.6 (44.7 – 72.7)	58.03 ± 9.7 (36 – 71)	57.25 ± 10.01 (31 – 75)	61.4 ± 5.7 (46 – 71)	60.26 ± 4.78 (49 – 67)	0.34
Disease duration (months)	-	29.6 ± 42.9 (4 – 277)	25.70 ± 26.57 (4 – 112)	30 ± 10.4 (22 – 48)	29.35 ± 30.35 (9 – 119)	0.96
CDR	-	-	-	1.23 ± 0.97 (0 - 3)	1.18 ± 0.93 (0-3)	0.61
CDR-FTLD	-	-	-	10.20 ± 6.70 (1 – 23)	7.25 ± 6.96 (0.5 – 20)	0.37
CDR-sb	-	-	-	7.53 ± 5.3 (1 – 17)	6.14 ± 4.55 (1 – 15)	0.38
MMSE (%) [#]	0.98 ± 0.03 (0.90-1)	0.97 ± 0.03 (0.90-1)	0.96 ± 0.05 (0.71-1)	0.77 ± 0.2 (0.2-0.93) ^{a,b,d}	0.78 ± 0.2 (0.33-0.97) ^{a,b,d}	0.003
FBI total (0-72)	-	1.95 ± 1.83 (0-6)	2.82 ± 3.13 (0-13)	28.00 ± 11.6 (15-45) ^{b,d}	17.33 ± 13.09 (0-35) ^{b,d}	<0.001
ALSFRS-r (0-48)	-	37.36 ± 6.2 (23 – 47)	36.71 ± 7.22 (20 – 46)	-	35.2 ± 5.6 (26 – 41)*	0.76

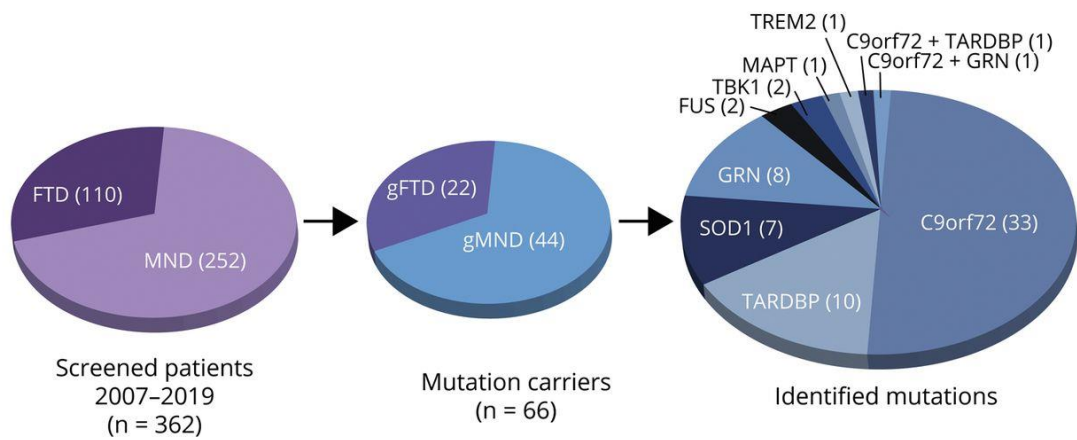
MRC sum score (0-120)	-	97.08 ± 20.63 (34 - 120)	95.25 ± 20.96 (41 - 120)	-	90.4 ± 12.58 (78 - 110)*	0.77
Disease progression rate	-	0.64 ± 0.6 (0.07 - 2.4)	0.91 ± 0.84 (0.22 - 4)	-	1.18 ± 0.6 (0.75 - 2.2)*	0.11
Onset bulb/limb/ bulb+limb	-	8/36/1	4/40/0	-	2/3/0*	-
CSF β-amyloid 42 (pg/mL)	-	-	-	732.18 ± 241.23 (447-1101)	785 ± 325.9 (452-1470)	0.68
CSF total tau (pg/mL)	-	-	-	193.73 ± 67.08 (121-350)	286.3 ± 177.24 (72-751)	0.13
CSF phosphorylated tau (pg/mL)	-	-	-	31.49 ± 12.51 (15-57)	38.7 ± 16.62 (20-64)	0.28

Values are reported as means ± standard deviations (range). P values refer to ANOVA models, Bonferroni-corrected for multiple comparisons. # = ratio between correct and administered items, considering patient's motor disability; * = bvFTD/ALS cases; - = not applicable; a= statistically significant difference with HC; b= statistically significant difference with sMND; c= statistically significant difference with sFTD; d= statistically significant difference with gMND. Abbreviations: ALSFRS-r= Amyotrophic Lateral Sclerosis Functional Rating Scale, revised version; bvFTD: behavioral variant frontotemporal dementia; CDR= Clinical Dementia Rating scale; CDR-sb= Clinical Dementia Rating scale, sum of boxes; CSF= cerebrospinal fluid; FBI= frontal behavioral assessment; gMND= genetic motor neuron disease; gFTD= genetic frontotemporal dementia; HC= healthy controls; MND= motor neuron disease; nfvPPA= non-fluent variant primary progressive aphasia; sFTD= sporadic frontotemporal dementia; sMND= sporadic motor neuron disease; R-SD= right-sided semantic dementia; svPPA= semantic variant primary progressive aphasia.

Figure legends

Figure 1. Sample selection and study design. (A) A total of 362 patients with disorders of the FTL spectrum referred between 2007 and 2019 were screened for known pathogenic mutations. Sixty-six mutation carriers were identified. Detected mutations are reported in the last pie chart. **(B)** Diagram showing the hierarchical organization of the three-level statistical analysis. *Abbreviations: FTD= frontotemporal dementia; gFTD= genetic frontotemporal dementia; gMND= genetic motor neuron disease; MND= motor neuron disease.*

A



B

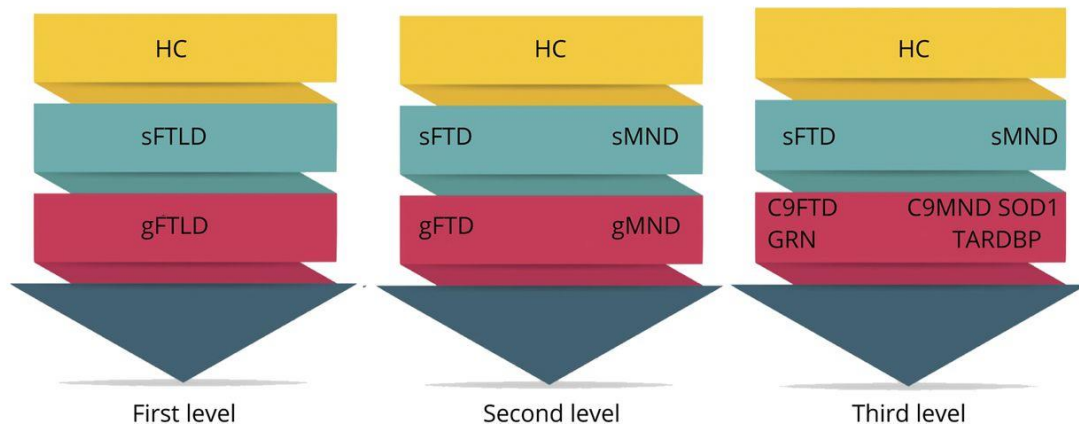


Figure 2. Patterns of GM atrophy in genetic and sporadic FTLD patients. Results of voxel-based morphometry analysis showing regions of significant GM atrophy in sFTLD and gFTLD patients when compared with HC (A-B) and between each other (C). Significant clusters are overlaid on the axial sections of the Montreal Neurological Institute standard brain. Analyses were corrected for age, sex, and total intracranial volume. Statistical threshold for significance was $p < 0.05$, FWE-corrected for multiple comparisons. *Abbreviations: FTLD= frontotemporal lobar degeneration; GM= grey matter; g= genetic; HC= healthy controls; s= sporadic.*

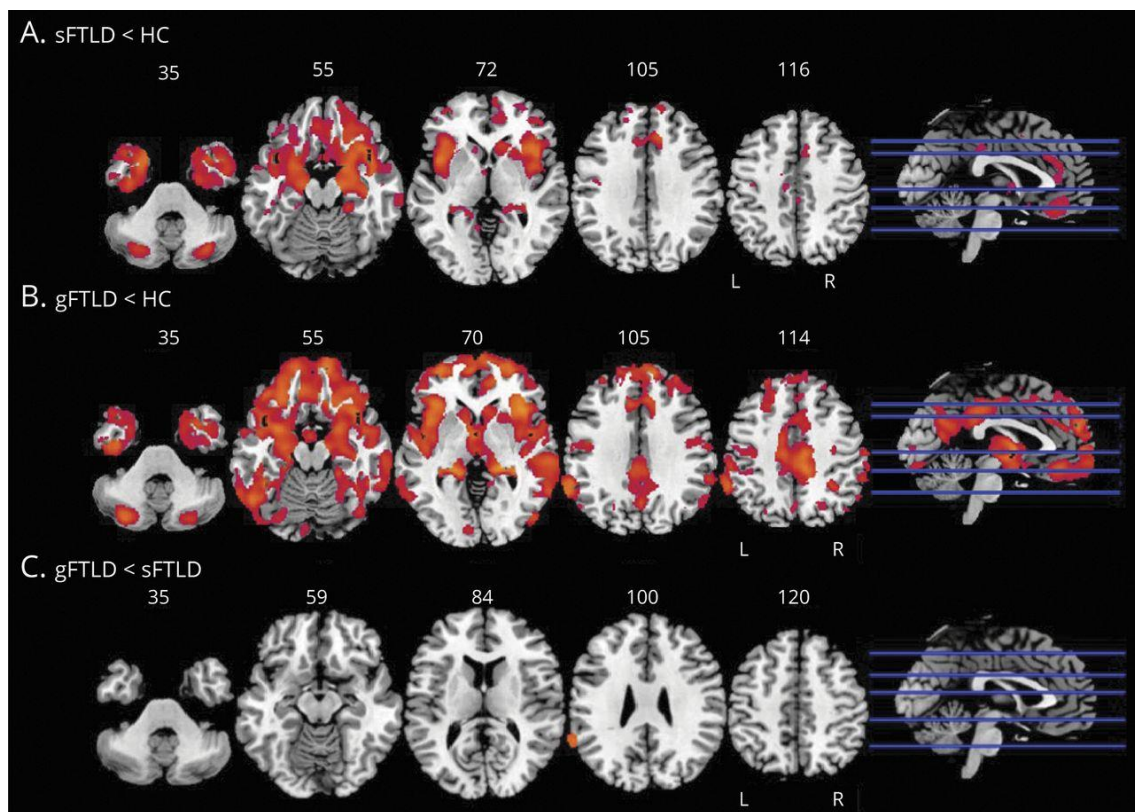


Figure 3. Patterns of GM atrophy in FTLD patients according to genetic status and clinical presentation. Results of voxel-based morphometry analysis showing regions of significant GM atrophy in sporadic and genetic FTD/MND patients when compared with HC (A-D) and between each other (E-F). Significant clusters are overlaid on the axial sections of the Montreal Neurological Institute standard brain. Analyses were corrected for age, sex, and total intracranial volume. Statistical threshold for significance was $p < 0.05$, FWE-corrected for multiple comparisons. *Abbreviations: FTD= frontotemporal dementia; g= genetic; GM= grey matter; HC= healthy controls; MND= motor neuron disease; s= sporadic.*

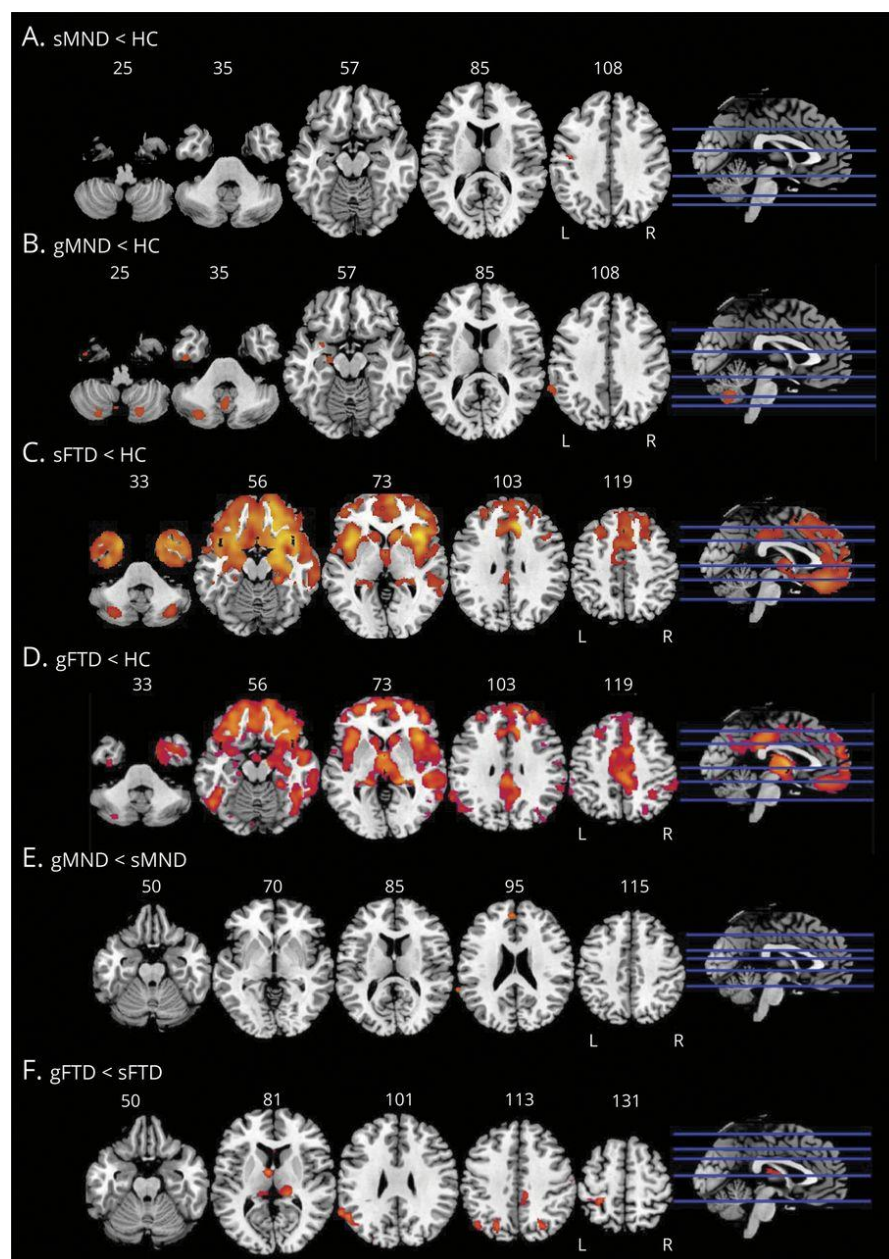


Figure 4. GM volumes of subcortical and cerebellar structures in FTLD patients according to genetic status and clinical presentation. Comparisons between groups were made using age-, sex- and MR scanner-adjusted ANOVA models, followed by post-hoc pairwise comparisons, Bonferroni-corrected for multiple comparisons. *Symbols: * = $p < 0.05$ compared with HC; # = $p < 0.05$ compared with sMND . Abbreviations: FTD= frontotemporal dementia; g= genetic; GM= grey matter; HC= healthy controls; MND= motor neuron disease; s= sporadic.*

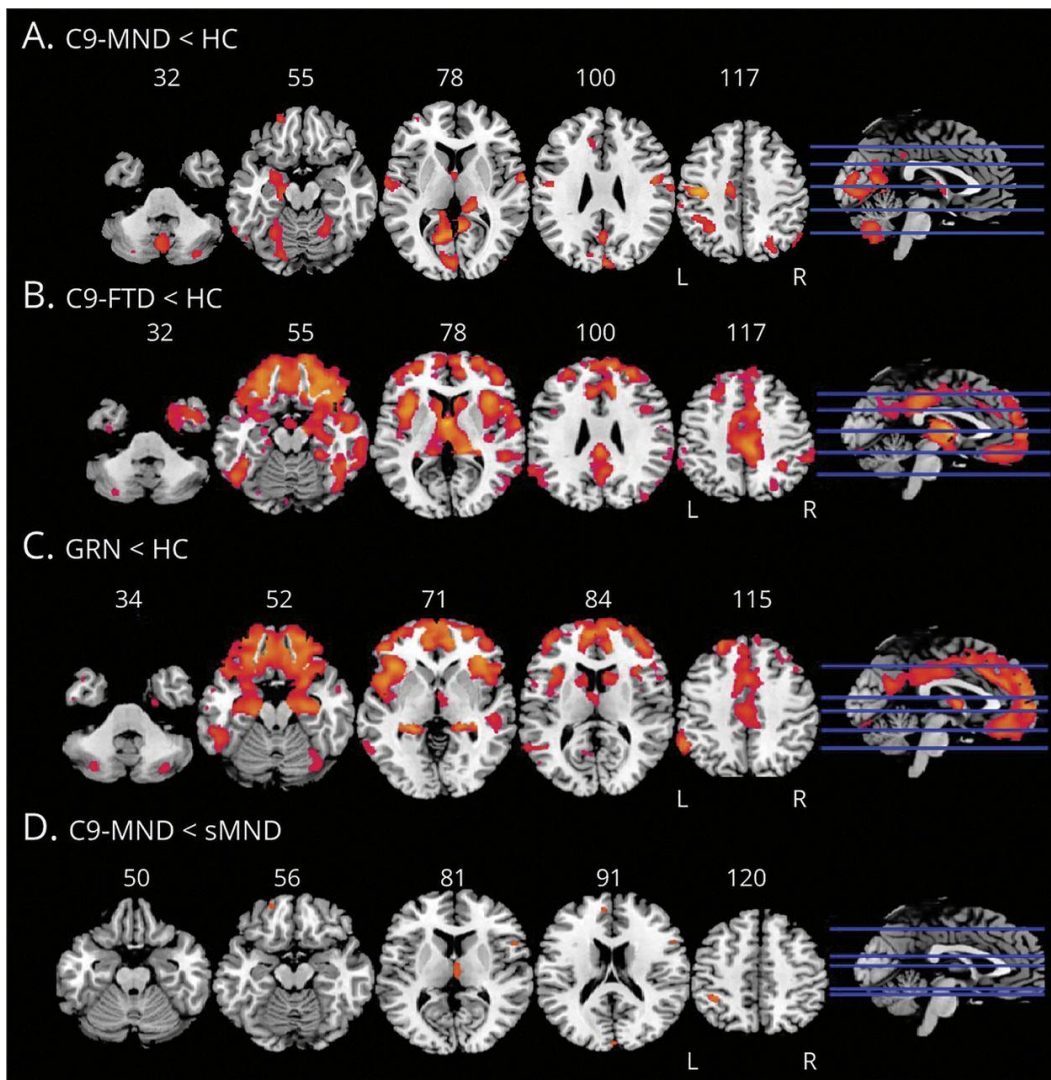


Figure 5. Patterns of GM atrophy in FTL D patients according to genetic mutation.

Results of voxel-based morphometry analysis showing regions of significant GM atrophy in FTL D genetic subgroups when compared with HC, sporadic patients and between each other. Significant clusters are overlaid on the axial sections of the Montreal Neurological Institute standard brain. Analyses were corrected for age, sex, and total intracranial volume. Statistical threshold for significance was $p < 0.05$, FWE-corrected for multiple comparisons. *Abbreviations: C9-FTD= frontotemporal dementia patients carrying a C9orf72 mutation; C9-MND= motor neuron disease patients carrying a C9orf72 mutation; FTD= frontotemporal dementia; GM= grey matter; HC= healthy controls; MND= motor neuron disease; s= sporadic.*

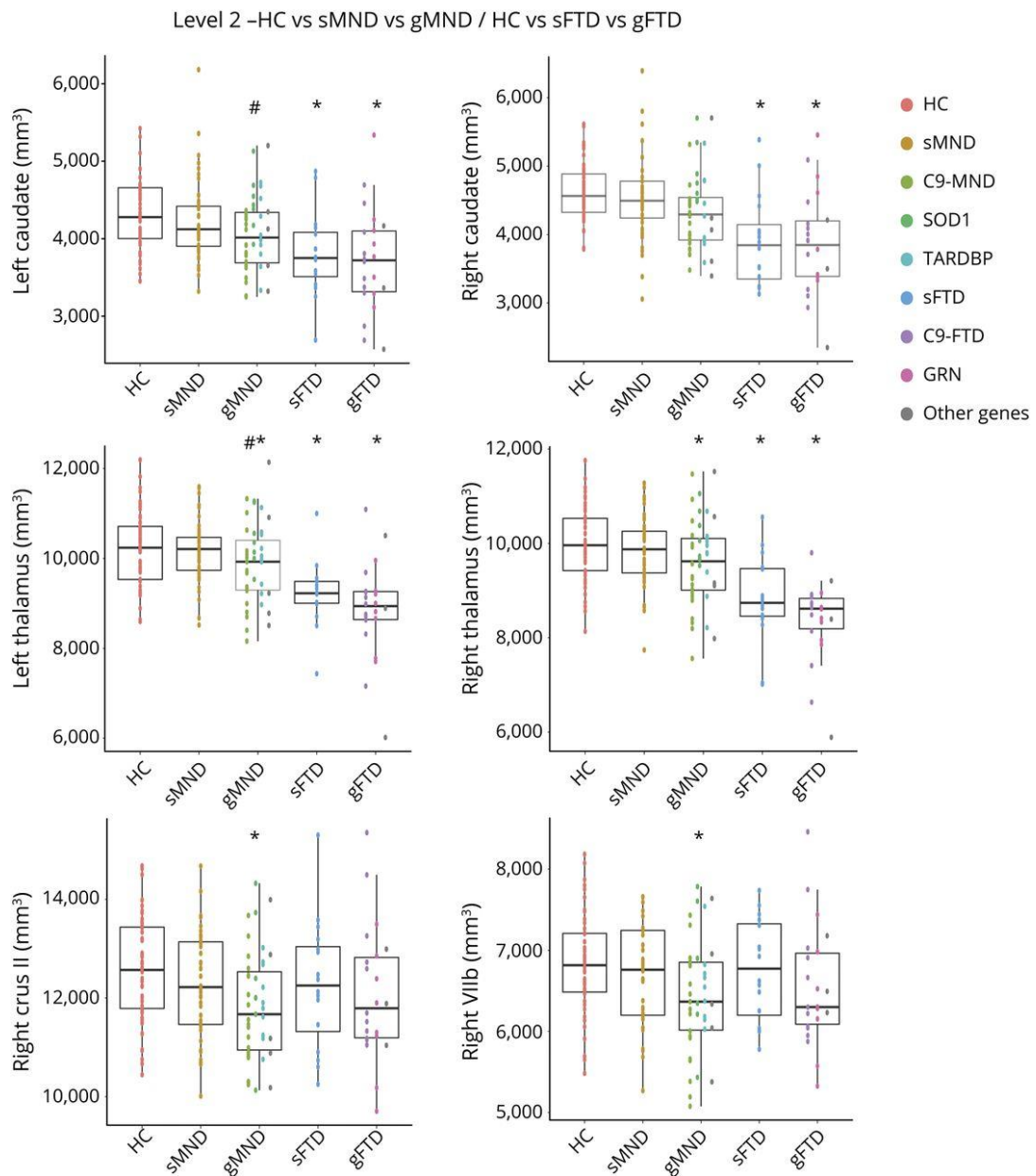
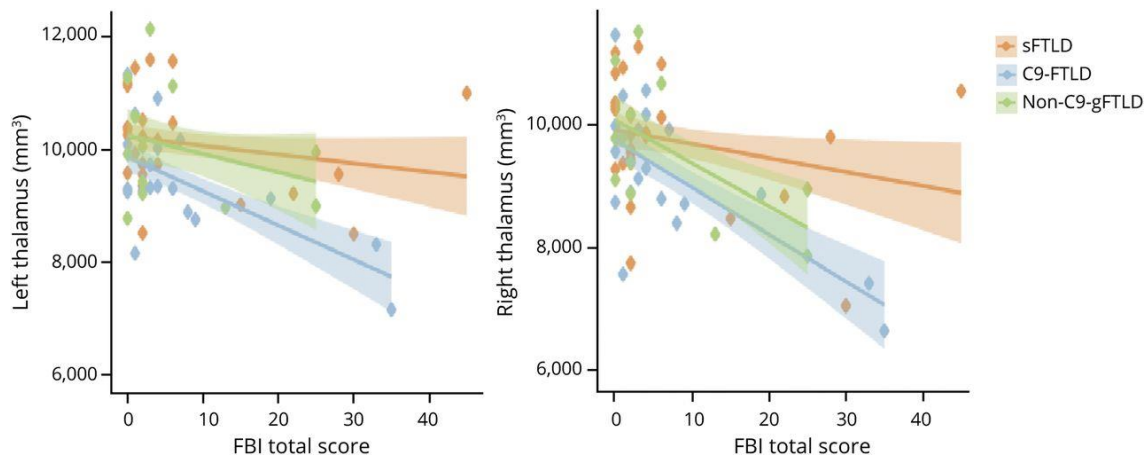


Figure 6. Relationship between thalamic volume and FBI total scores in FTLD patients. Plots showing significant inverse correlation only in the C9-FTLD group (left thalamus: $r=-0.579$, $p=0.024$; right thalamus: $r=-0.613$, $p=0.025$). Orange dots represent plotted values of sFTLD patients ($n=26$, based on availability of FBI scores), blue dots represent C9-FTLD patients ($n=19$), and green dots represent gFTLD patients with mutations other than *C9orf72* ($n=12$). Partial correlation analyses were Bonferroni-corrected for multiple comparisons, adjusted for age, sex and education. *Abbreviations:* C9-FTLD= frontotemporal lobar degeneration patients carrying a *C9orf72* mutation; FBI= frontal behavioral inventory; FTLD= frontotemporal lobar degeneration; g= genetic; s= sporadic.



eTable 1. Main socio-demographic and clinical characteristics of healthy controls and FTLD patients classified by clinical presentation and genotype. Individual features of genetic FTLD patients with uncommon or double mutations are reported in **eTable 4**.

	HC	sMND	C9-MND	SOD1	TARDBP	sFTD	C9-FTD	GRN	p
Number	52	45	22	7	10	16	11	8	-
Diagnosis	-	37 ALS, 3 PLS, 5 PMA	18 ALS, 1 PLS, 3 PMA	6 ALS, 1 PLS	6 ALS, 1 PLS, 3 PMA	12 bvFTD, 2 nfvPPA, 2 svPPA	5 bvFTD, 5bvFTD/ALS, 1 svPPA	5 bvFTD, 3 nfvPPA	-
Sex (M/F)	26/26	23/22	12/10	2/5	5/5	9/7	6/5	4/4	0.973
Family history (+/-)	0/52	3/42	10/12 ^{a,b}	1/6	4/6 ^a	2/14	7/4 ^{a,c}	4/4	0.001
Education (years)	12.75 ± 3.70 [5 – 20]	12.07 ± 4.10 [5 – 24]	11.05 ± 3.47 [5 – 20]	11 ± 2.60	9.67 ± 2.89 [8 – 13]	10.36 ± 3.81 [5 – 17]	12.10 ± 4.60 [5 – 21]	8.83 ± 3.43 [5 – 13]	0.180
Age at MRI (years)	59.2 ± 6.6 [44.7 – 72.7]	58 ± 9.7 [36 – 71]	55.8 ± 9.2 [42.7 – 71.7]	55 ± 8.2 [39.8 – 62.9]	61.4 ± 6.6 [48.3 – 71]	61.4 ± 5.7 [46 – 71]	60.6 ± 3.9 [54.9 – 67.2]	62.1 ± 4.1 [53.7 – 65.3]	0.161
Disease duration (months)	-	29.6 ± 42.9 [4 – 277]	19.8 ± 21.9 [4 – 122]	61.1 ± 30.9 [7 – 93]	17.7 ± 19.4 [5 – 67]	30 ± 10.4 [22 – 48]	31.9 ± 39.6 [9 – 112]	30 ± 8.5 [24 – 36]	0.187
CDR	-	-	-	-	-	1.23 ± 0.97 [0 – 3]	0.67 ± 0.29 [0.5 – 1.00]	1.67 ± 1.03 [0 – 3]	0.340
CDR-FTLD	-	-	-	-	-	10.20 ± 6.70 [1 – 23]	5.50 ± 4.24 [2.5 – 8.5] (2)	7.83 ± 7.91 [0.5 – 20.00]	0.556
CDR-sb	-	-	-	-	-	7.53 ± 5.30 [1.00 – 17.00]	5.33 ± 2.75 [2.50 – 8.00]	7.83 ± 5.35 [1.00 – 15.00]	0.472
ALSFRS-r [0-48]	-	37.36 ± 6.2 [23 – 47]	37.1 ± 6.6 [25 – 46]	40.8 ± 6.7 [28 – 46]	33.5 ± 9 [20 – 44]	-	35.2 ± 5.6 [26 – 41]*	-	0.276
MRC sum score	-	97.08 ± 20.63 [34 – 120]	95.80 ± 23.80 [41 – 121]	109.25 ± 9.39 [97 – 118]	84.83 ± 18.75 [50 – 103]	-	90.40 ± 12.58 [78 – 110]*	-	0.421
Disease progression rate	-	0.64 ± 0.60 [0.07 – 2.40]	0.7 0 ± 0.39 [0.07 – 1.3]	0.18 ± 0.13 [0.02 – 0.30]	1.80 ± 1.23 ^{b,c,d} [0.18 – 4.00]	-	1.18 ± 0.60 [0.75 – 2.20]*	-	< 0.001
Onset bulb/limb/ bulb+limb	-	8/33/1	2/20/0	0/7/0	2/8/0	-	2/3/0*	-	-

Values are reported as means \pm standard deviations [range]. P values refer to ANOVA models, Bonferroni-corrected for multiple comparisons. * = bvFTD/ALS cases. Abbreviations: HC= healthy controls; sMND= sporadic motor neuron disease; sFTD= sporadic frontotemporal dementia; C9-MND= motor neuron disease with *C9orf72* mutation; C9-FTD= frontotemporal dementia with *C9orf72* mutation; SOD1= motor neuron disease due to *SOD1* mutation; TDP43= motor neuron disease due to *TARDBP* mutation; GRN= frontotemporal dementia due to *GRN* mutation. Symbols: - = not applicable; a= statistically significant difference with HC; b= statistically significant difference with sMND; c= statistically significant difference with C9-MND; d= statistically significant difference with SOD1; e= statistically significant difference with sFTD.

eTable 2. Neuropsychological features of healthy controls and FTLN patients classified by clinical presentation and genetic status.

	HC	sMND	gMND	sFTD	gFTD
Global cognition	52	45	44	16	22
MMSE*	0.98 ± 0.03 [0.90-1]	0.97 ± 0.03 ^{b,c} [0.90-1]	0.96 ± 0.05 ^{b,c} [0.71-1]	0.77 ± 0.20 ^a [0.20-0.93]	0.78 ± 0.20 ^a [0.33-0.97]
Memory					
Digit span forward	6.23 ± 1.09 [4-9]	5.52 ± 0.94 [4-7]	5.41 ± 0.87 [3-7]	4.89 ± 1.62 [2-7]	4.29 ± 1.36 ^a [0-6]
RAVLT delayed	9.94 ± 2.84 [3-15]	10.11 ± 3.42 ^{b,c} [1-15]	8.06 ± 3.17 ^{b,c} [3-14]	2.56 ± 2.70 ^a [0-7]	4.14 ± 2.91 ^a [0-9]
RAVLT recognition	14.29 ± 0.86 [14-15]	14.35 ± 0.78 ^{b,c} [13-15]	14.15 ± 1.03 ^{b,c} [12-15]	9.29 ± 4.92 ^a [0-15]	11.30 ± 4.11 ^a [3-15]
Executive functions					
CPM	31.50 ± 3.09 [22-36]	29.12 ± 5.28 ^b [16-36]	29.38 ± 4.88 ^b [16-35]	20.00 ± 9.85 ^a [3-32]	23.13 ± 8.41 ^a [7-35]
Digit span backward	4.85 ± 1.23 [3-8]	4.54 ± 1.42 [2-9]	4.25 ± 1.41 [0-8]	3.00 ± 1.41 [0-4]	3.21 ± 1.58 [0-6]
Visuospatial abilities					
Rey Figure copy	31.38 ± 2.67 [28-36]	20.08 ± 9.16 [10-33]	-	28.50 ± 7.66 [14.5-36]	14.88 ± 10.09 ^a [0-25.5]
Language					
BADA (noun)	29.88 ± 0.35 [29-30]	29.48 ± 0.95 [27-30]	29.08 ± 1.09 [27-30]	-	27.80 ± 2.59 [25-30]
BADA (action)	27.88 ± 0.35 [27-28]	27.43 ± 0.79 ^c [26-28]	25.93 ± 2.51 ^c [18-28]	-	22.80 ± 3.70 ^a [18-27]
Token test	33.63 ± 2.03 [30-36]	29.61 ± 2.58 [27-33.5]	-	24.28 ± 10.31 ^a [7-36]	22.00 ± 14.14 [12-32]
Fluency					
Phonemic Fluency	37.31 ± 8.40 [18-55]	32.34 ± 10.72 ^{b,c} [16-65]	28.40 ± 9.69 ^{a,c} [10-55]	17.89 ± 10.43 ^a [6-30]	10.13 ± 5.60 ^a [0-22]
Index PF**	5.00 ± 1.92 [2.60-12.05]	5.57 ± 2.29 ^c [1.90-10.82]	6.75 ± 2.50 ^c [2.72-12.14]	-	-
Semantic Fluency	47.47 ± 9.45 [28-70]	40.86 ± 7.89 ^{a,b,c} [27-54]	39.09 ± 8.39 ^{a,b,c} [19-53]	19.22 ± 6.46 ^a [10-28]	21.71 ± 9.04 ^a [1-33]
Index SF**	3.71 ± 0.94 [2.49-6.97]	4.10 ± 1.22 [2.20-8.04]	4.92 ± 1.64 [3.00-8.70]	-	-
Mood & Behavior					

BDI	6.80 ± 6.10 [0-21]	10.82 ± 3.63 [6-20]	6.57 ± 3.69 [1-13]	-	-
FBI total score	-	1.95 ± 1.83 ^{b,c} [0-6]	2.82 ± 3.126 ^{b,c} [0-13]	28.00 ± 11.6 [15-45]	17.33 ± 13.09 [0-35]
ALS-FTD-Q	-	6.00 ± 5.01 ^c [2-17]	11.11 ± 11.20 [0-43]	-	30.50 ± 4.44 [26-36]
Cognitive diagnosis					
MND-cu/ci/bi/cbi/NA	-	21/1/6/2/15	19/3/4/3/15	-	-

Values are numbers or means ± standard deviations [range]. P values refer to univariate GLM analysis, followed by Bonferroni t-test for multiple comparisons corrected for age, sex and education. Comparisons among MND patients were also corrected for ALSFRS-r. *= Ratio between the number of correct items and the maximum number of administered items; **= Verbal fluency indices were obtained as following: time for generation condition - time for control condition (reading or writing generated words)/total number of items generated. Abbreviations: ALS= Amyotrophic lateral sclerosis; ALS-FTD-Q= ALS-FTD questionnaire; BADA= Battery for aphasic deficit analysis; BDI= Beck Depression Inventory; FTD= frontotemporal dementia; CDR= Clinical dementia rating scale; CET= Cognitive estimation test; CPM= Colored progressive matrices; CST= Card sorting tests; FBI= Frontal Behavioral Inventory; HDRS= Hamilton Depression Rating Scale; HC= Healthy controls; MMSE= Mini-Mental state examination; MNDcu= motor neuron disease cognitively unimpaired; MNDci= MND with cognitive impairment; MNDbi= MND with behavioral impairment; MNDcbi= MND with cognitive and behavioral impairment; NA= not available; PF= Phonemic fluency; PLS= Primary lateral sclerosis; RAVLT= Rey auditory verbal learning test; SB= Sum of boxes; SF= Semantic fluency; TMT= Trail making test.

-= not applicable.

a= statistically significant difference with HC.

b= statistically significant difference with sFTD.

c= statistically significant difference with gFTD.

eTable 3. Neuropsychological features of healthy controls and FTLN patients classified by clinical presentation and genotype. Individual features of genetic FTLN patients with uncommon or double mutations are reported in **Table e-4**.

	HC	sMND	C9-MND	SOD1	TARDBP	sFTD	C9-FTD	GRN
Global cognition	52	45	22	7	10	16	11	8
MMSE*	0.98 ± 0.03 [0.90-1]	0.97 ± 0.03 ^{b,d} [0.90-1]	0.96 ± 0.03 ^{b,d} [0.90-1]	0.98 ± 0.02 ^{b,d} [0.97-1]	0.95 ± 0.09 ^{b,d} [0.71-1]	0.77 ± 0.20 ^a [0.20-0.93]	0.88 ± 0.09 ^d [0.63-0.97]	0.65 ± 0.20 ^a [0.33-0.87]
Memory								
Digit span forward	6.23 ± 1.09 [4-9]	5.52 ± 0.94 [4-7]	5.60 ± 0.63 [4-6]	5.00 ± 0.71 [4-6]	5.44 ± 1.24 [3-7]	4.89 ± 1.62 [2-7]	4.56 ± 0.92 [3-6]	3.60 ± 2.19 [0-6]
RAVLT delayed	9.94 ± 2.84 [3-15]	10.11 ± 3.42 ^{b,d} [1-15]	8.60 ± 3.25 ^b [4-14]	10.25 ± 3.30 [6-14]	7.22 ± 2.64 [4-13]	2.56 ± 2.70 ^a [0-7]	6.00 ± 1.85 [4-9]	1.25 ± 1.50 ^a [0-3]
RAVLT recognition	14.29 ± 0.86 [14-15]	14.35 ± 0.78 ^{b,d} [13-15]	14.15 ± 1.07 ^{b,d} [12-15]	14.67 ± 0.58 ^{b,d} [14-15]	14.22 ± 0.97 ^{b,d} [13-15]	9.29 ± 4.92# [0-15]	13.50 ± 2.35 ^{b,d} [9-15]	6.33 ± 3.06# [3-9]
Executive functions								
CPM	31.50 ± 3.09 [22-36]	29.12 ± 5.28 ^d [16-36]	29.36 ± 4.94 [17-35]	30.00 ± 3.67 [24-33]	28.29 ± 6.32 [16-34]	20.00 ± 9.85 ^a [3-32]	26.00 ± 6.48 [19-35]	18.00 ± 9.35 ^a [7-28]
Digit span backward	4.85 ± 1.23 [3-8]	4.54 ± 1.42 [2-9]	4.50 ± 1.63 [0-8]	3.75 ± 0.50 [3-4]	4.33 ± 1.23 [3-6]	3.00 ± 1.41 [0-4]	3.56 ± 1.59 [0-6]	2.00 ± 1.73 [0-3]
Visuospatial abilities								
Rey Figure copy	31.38 ± 2.67 [28-36]	20.08 ± 9.16 [10-33]	-	-	-	28.50 ± 7.66 [14.5-36]	23.88 ± 2.30 [22.25-25.50]	13.83 ± 7.65 [8.00-22.5]
Language								
BADA (noun)	29.88 ± 0.35 [29-30]	29.48 ± 0.95 [27-30]	29.00 ± 1.11 [27-30]	29.67 ± 0.58 [29-30]	29.00 ± 1.41 [27-30]	-	27.80 ± 2.59 [25-30]	-
BADA (action)	27.88 ± 0.35 [27-28]	27.43 ± 0.79 ^c [26-28]	26.29 ± 2.16 [22-28]	27.00 ± 1.73 [25-28]	25.86 ± 1.86 [23-28]	-	22.80 ± 3.70 ^a [18-27]	-
Token test	33.63 ± 2.03 [30-36]	29.61 ± 2.58 [27-33.5]	-	-	-	24.28 ± 10.31 ^a [7-36]	-	32.00 ± 0.00 [32-32]
Fluency								
Phonemic Fluency	37.31 ± 8.40 [18-55]	32.34 ± 10.72 ^{b,c,d} [16-65]	27.35 ± 8.51 ^c [10-45]	31.83 ± 11.27 [15-44]	29.89 ± 11.10 ^c [19-55]	17.89 ± 10.43 ^a [6-30]	12.10 ± 5.72 ^a [4-22]	6.50 ± 4.66 ^a [0-11]

Index PF**	5.00 ± 1.92 [2.60- 12.05]	5.57 ± 2.29 ^c [1.90- 10.82]	6.76 ± 1.85 ^c [3.27- 9.19]	6.25 ± 3.94 ^c [4.00- 12.14]	6.23 ± 2.35 ^c [2.72- 9.43]	-	-	-
Semantic Fluency	47.47 ± 9.45 [28-70]	40.86 ± 7.89 ^{b,c,d} [27-54]	38.88 ± 7.27 ^b [26-53]	45.17 ± 7.25 ^{b,c,d} [35-53]	37.67 ± 10.22 ^{b,d} [19-50]	19.22 ± 6.46 ^a [10-28]	26.70 ± 4.47 ^a [18-33]	16.20 ± 8.59 ^a [7-28]
Index SF**	3.71 ± 0.94 [2.49- 6.97]	4.10 ± 1.22 [2.20- 8.04]	5.13 ± 1.65 [3.10- 7.89]	3.84 ± 0.51 [3.13- 4.36]	4.71 ± 1.62 [3.00- 8.08]	-	-	-
Mood & Behavior								
BDI	6.80 ± 6.10 [0-21]	10.82 ± 3.63 [6-20]	7.00 ± 5.16 [1-13]	6.00 ± 6.00 [3-12]	6.00 ± 3.40 [3-7]	-	-	-
FBI total	-	1.95 ± 1.83 ^{b,c,d} [0-6]	2-64 ± 2.46 ^b [0-7]	-	3.71 ± 4.50 ^b [0-13]	28.00 ± 11.6 [15-45]	16.33 ± 15.23 [0-35]	25.00 ± 2.40 [22-27]
ALS-FTD-Q	-	6.00 ± 5.01 [2-17]	13.44 ± 13.69 [0-43]	1.00 ± 0.00 [1-1]	9.83 ± 10.07 [1-28]	-	30.50 ± 4.44 [26-36]	-

Values are numbers or means ± standard deviations [range]. P values refer to univariate GLM analysis, followed by Bonferroni t-test for multiple comparisons corrected for age, sex and education. Comparisons among MND patients were also corrected for ALSFRS-r. *= Ratio between the number of correct items and the maximum number of administered items; **= Verbal fluency indices were obtained as following: time for generation condition - time for control condition (reading or writing generated words)/total number of items generated. Abbreviations: ALS= Amyotrophic lateral sclerosis; ALS-FTD-Q= ALS-FTD questionnaire; BADA= Battery for aphasic deficit analysis; BDI= Beck Depression Inventory; FTD= frontotemporal dementia; CDR= Clinical dementia rating scale; CET= Cognitive estimation test; CPM= Colored progressive matrices; CST= Card sorting tests; FBI= Frontal Behavioral Inventory; HDRS= Hamilton Depression Rating Scale; HC= Healthy controls; MMSE= Mini-Mental state examination; PF= Phonemic fluency; PLS= Primary lateral sclerosis; RAVLT= Rey auditory verbal learning test; SB= Sum of boxes; SF= Semantic fluency; TMT= Trail making test.

-= not applicable

a= statistically significant difference with HC

b= statistically significant difference with sFTD

c= statistically significant difference with C9-FTD

d=statistically significant difference with GRN

eTable 4. Main sociodemographic, clinical and neuropsychological features of FTL D patients affected by uncommon or double mutations.

	Subject 1	Subject 2	Subject 3	Subject 4	Subject 5	Subject 6	Subject 7	Subject 8
Mutation	TBK1	TBK1	FUS	FUS	TREM2	MAPT	C9 + TDP43	C9 + GRN
Diagnosis	ALS	ALS	ALS	ALS	bvFTD	Right-SD	ALS	bvFTD
Sex (M/F)	M	M	F	M	F	F	F	M
Education (years)	-	8	13	-	13	-	-	13
Age at MRI (years)	75	67	31	74	49	53	47	60
Disease duration (months)	14	22	10	8	24	-	29	12
CDR	-	-	-	-	-	0.5	-	0.5
CDR-sb	-	-	-	-	-	2	-	2.5
ALSFRS-r [0-48]	-	39	36	35	-	-	-	-
MRC sum score	-	108	98	78	-	-	-	-
Disease progression rate	-	0.41	1.2	1.63	-	-	-	-
Onset bulb/limb	limb	limb	limb	limb	-	-	limb	-
Global cognition								
MMSE*	0.93	1.00	-	1.00	0.40	-	1.00	0.90
FAB	-	-	-	-	2	-	-	-
Memory								
Digit span forward	6	-	-	5	4	-	4	5
RAVLT delayed	3	-	-	5	0	-	7	5
RAVLT recognition	12	-	-	-	13	-	14	-
Corsi block-tapping	5	-	-	-	2	-	5	-
Executive functions								
CPM	34	-	-	26	9	-	33	29
Digit span backward	5	-	-	3	3	-	2	4

CST, perseverations**	-	-	-	-	0.26	-	0.14	0.45
Visuospatial abilities								
Rey Figure copy	-	-	-	-	0	-	-	-
Language								
BADA (noun)	-	-	-	29	-	-	29	-
BADA (action)	18	-	-	24	-	-	28	-
Token test	-	-	-	-	12	-	-	-
Fluency								
Phonemic Fluency	-	16	-	18	6	-	35	9
Index PF***	-	10.4	-	11.8	-	-	4.6	-
Semantic Fluency	-	31	-	28	1	-	38	20
Index SF***	-	5.29	-	8.70	-	-	4.08	-
Mood & Behavior								
BDI	-	-	-	-	-	-	-	-
FBI total	0	-	-	3	-	-	4	8
ALS-FTD-Q	3	11	-	-	-	-	16	-

Values are numbers. *= Ratio between the number of correct items and the maximum number of administered items; **= Perseverations are reported as the ratio between perseveration absolute number and the maximum number of cards provided during the test; ***= Verbal fluency indices were obtained as following: time for generation condition - time for control condition (reading or writing generated words)/total number of items generated. -= not applicable. Abbreviations: ALS= Amyotrophic lateral sclerosis; ALS-FTD-Q= ALS-FTD questionnaire; BADA= Battery for aphasic deficit analysis; BDI= Beck Depression Inventory; bvFTD= behavioral variant frontotemporal dementia; CDR= Clinical dementia rating scale; CET= Cognitive estimation test; CPM= Colored progressive matrices; CST= Card sorting tests; FBI= Frontal Behavioral Inventory; HDRS= Hamilton Depression Rating Scale; HC= Healthy controls; MMSE= Mini-Mental state examination; NA=not available; PF= Phonemic fluency; PLS= Primary lateral sclerosis; RAVLT= Rey auditory verbal learning test; right-SD= right-sided semantic dementia; SB= Sum of boxes; SF= Semantic fluency; TMT= Trail making test

eTable 5**VBM results – Level 1 (sFTLD vs gFTLD vs HC)**Regions presented in table survived a $p < 0.05$ FWE-corrected at cluster level.

sFTLD < HC						
Anatomic regions (BA)	Side	Cluster size	MNI coordinates			T values
			x	y	z	
Inferior frontal gyrus – orbital part (47)	R	48934	27	10	-22	7.71
Cerebellum –Crus I	R	521	32	-72	-38	6.13
Anterior prefrontal cortex (10)	R	1027	39	46	10	6.01
Anterior prefrontal cortex (10)	L	190	-34	51	2	5.88
Cerebellum – Crus I	L	473	-26	-74	-36	5.75
Dorsolateral prefrontal cortex (9)	L	256	-15	48	38	5.63
Dorsolateral prefrontal cortex (9)	R	438	12	56	30	5.63
Premotor cortex (6)	L	156	-42	-10	36	5.28
Thalamus (50)	L	58	-2	-2	2	5.13
Inferior frontal gyrus (44)	R	129	44	21	18	4.94
Dorsal posterior cingulate cortex (31)	R	119	0	-28	39	4.92
Frontal eye fields (8)	R	39	46	20	38	4.91
Premotor cortex (6)	L	141	-8	6	52	4.91
Secondary visual cortex (18)	L	31	-18	-78	-14	4.91
gFTLD < HC						
Anatomic regions (BA)	Side	Cluster size	MNI coordinates			T values
			x	y	z	
Inferior frontal gyrus (47)	R	111322	38	26	-4	7.89
Cerebellum –Crus II	L	1441	-30	-76	-40	6.48
Angular gyrus (39)	R	1178	38	-62	54	5.73
Cerebellum –Crus II	R	1000	27	-80	-38	5.44
Primary visual cortex (17)	L	237	-8	-90	2	5.28
Superior parietal lobule (7)	L	146	-21	-69	36	5.28
Dorsolateral prefrontal cortex (46)	L	118	-52	28	21	5.17
Angular gyrus (39)	R	124	44	-70	38	4.96

Middle temporal gyrus (21)	L	49	-60	-15	-20	4.93
Inferior frontal gyrus (44)	L	52	-39	9	24	4.89
gFTLD < sFTLD						
Anatomic regions (BA)	Side	Cluster size	MNI coordinates			T values
			x	y	z	
Angular gyrus (39)	L	395	-63	-51	30	5.08

eTable 6**VBM results – Level 2 (sMND vs gMND vs sFTD vs gFTD vs HC)**Regions presented in table survived a $p < 0.05$ FWE-corrected at cluster level.

sMND < HC						
Anatomic regions (BA)	Side	Cluster size	MNI coordinates			T values
			x	y	z	
Precentral cortex (4)	L	38	-42	-7	37	5.45
gMND < HC						
Anatomic regions (BA)	Side	Cluster size	MNI coordinates			T values
			x	y	z	
Secondary visual cortex (18)	L	224	-10	-68	-8	5.31
Cerebellum - Vermis VIIIa		418	2	-60	-33	5.29
Hippocampus (54)	L	112	-21	-15	-12	5.20
Cerebellum – Lobule VIIb	R	332	21	-70	-48	5.19
Inferior temporal gyrus (20)	L	229	-40	-8	-42	5.13
Cerebellum – Crus II	L	231	-28	-75	-39	5.06
Angular gyrus (39)	L	42	-69	-44	20	4.97
Angular gyrus (39)	L	299	-66	-51	28	4.95
Cerebellum – Lobule VIIb	L	183	-26	-70	-48	4.95
Dorsal entorhinal cortex (34)	L	38	-30	3	-16	4.81
Associative visual cortex (19)	R	45	50	-82	-4	4.80
Superior temporal gyrus (22)	L	45	-48	-3	-4	4.77
Rolandic operculum (4)	L	20	-41	-8	14	4.60
sFTD < HC						
Anatomic regions (BA)	Side	Cluster size	MNI coordinates			T values
			x	y	z	
Inferior frontal gyrus – orbital part (47)	R	99854	27	10	-22	9.14
Cerebellum – Crus I	R	376	34	-70	-39	5.74
Cerebellum – Crus I	L	410	-30	-74	-36	5.43
Ventral posterior cingulate cortex (23)	L	42	-8	-48	22	4.63
gFTD < HC						
Anatomic regions (BA)	Side	Cluster size	MNI coordinates			T values
			x	y	z	
Thalamus (50)	L	88130	-2	-3	4	7.87

Fusiform (37)	L	2439	-50	-60	-18	6.48
Angular gyrus (39)	R	705	39	-57	54	5.75
Angular gyrus (39)	L	1431	-63	-56	33	5.66
Middle temporal gyrus (21)	L	108	-57	-38	-20	5.31
Angular gyrus (39)	R	654	36	-69	36	5.27
Fusiform (37)	R	293	26	-57	-12	5.24
Associative visual cortex (19)	L	108	-28	-72	-12	5.16
Primary sensory (1)	R	158	60	-15	39	5.09
sMND > gMND						
Anatomic regions (BA)	Side	Cluster size	MNI coordinates			T values
			x	y	z	
Dorsolateral prefrontal cortex (9)	L	73	-4	50	22	5.14
Angular gyrus (39)	L	54	-66	-44	22	4.84
sFTD > gFTD						
Anatomic regions (BA)	Side	Cluster size	MNI coordinates			T values
			x	y	z	
Thalamus (50)	L	457	-6	-4	10	3.84
Superior parietal lobule (7)	R	377	27	-64	48	3.80
Angular gyrus (39)	L	846	-54	-58	28	3.78
Thalamus (50)	R	452	16	-30	8	3.64
Superior parietal lobule (7)	L	201	-22	-69	39	3.60
Superior parietal lobule (5)	L	189	-28	-39	58	3.55
Dorsal posterior cingulate cortex (31)	R	185	9	-33	40	3.47
Associative visual cortex (19)	L	35	-28	-87	33	3.28

eTable 7**VBM results – Level 3 (C9-MND vs C9-FTD vs GRN vs TARDBP vs SOD1 vs sMND vs sFTD vs HC)**Regions presented in table survived a $p < 0.05$ FWE-corrected at cluster level.

C9-MND < HC						
Anatomic regions (BA)	Side	Cluster size	MNI coordinates			T values
			x	y	z	
Primary motor cortex (4)	L	1766	-39	-16	44	6.76
Ventral posterior cingulate cortex (23)	L	10464	-12	-62	9	6.71
Associative visual cortex (19)	R	330	48	-82	-9	5.92
Primary Auditory (41)	R	1195	63	-4	8	5.89
Cerebellum – Lobule V	L	1202	-4	-66	-48	5.61
Putamen (49)	L	926	-26	-4	-10	5.60
Ventral anterior cingulate cortex (24)	L	368	-15	-15	39	5.58
Superior parietal lobule (7)	L	986	-36	-45	50	5.50
Cerebellum – Lobule VIIIb	L	418	-15	-50	-52	5.48
Orbitofrontal area (11)	L	137	-21	54	-21	5.46
Angular gyrus (39)	R	516	42	-57	52	5.34
C9-FTD < HC						
Anatomic regions (BA)	Side	Cluster size	MNI coordinates			T values
			x	y	z	
Insula (13)	R	182058	50	4	-2	8.40
Cerebellum – Crus II	L	669	-32	-78	-36	5.98
Cerebellum – Lobule IX	R	467	2	-46	-45	5.47
Primary Motor (4)	R	197	32	-27	50	5.40
Angular gyrus (39)	L	52	-36	-72	44	5.04
GRN < HC						
Anatomic regions (BA)	Side	Cluster size	MNI coordinates			T values
			x	y	z	
Anterior prefrontal cortex (10)	R	62052	22	51	-14	7.51
Thalamus (50)	L	1344	0	-2	4	6.49
Angular gyrus (39)	L	2524	-57	-52	42	6.45
Fusiform (37)	L	776	-51	-46	-21	5.72
Caudate (48)	R	595	8	14	14	5.65
Superior temporal gyrus (22)	R	1293	51	-24	-6	5.49
Middle temporal gyrus (21)	L	345	-63	-22	-9	5.45
Inferior temporal gyrus (20)	L	79	-48	-8	-34	5.06
Premotor cortex (6)	L	49	-50	-8	24	5.05

Cerebellum – Crus II	R	197	32	-75	-39	5.00
C9-MND < sMND						
Anatomic regions (BA)	Side	Cluster size	MNI coordinates			T values
			x	y	z	
Superior parietal lobule (7)	L	107	-39	-44	48	5.25
Orbitofrontal area (11)	L	56	-21	54	-21	5.06
Inferior frontal gyrus (44)	R	97	54	15	14	5.02
Visual association (18)	R	45	2	-93	18	4.94
Thalamus (50)	R	171	3	-15	9	4.83

eTable 8. Subcortical, hippocampal and cerebellar grey matter volumes in healthy controls and FTLN patients classified by genetic status.

	HC	sFTLD	gFTLD	p HC vs sFTLD	p HC vs gFTLD	p sFTLD vs gFTLD
Left Caudate	4307.65 ± 447.97 (3452.28 - 5421.81)	4118.96 ± 557.54 (2690.60 - 6181.46)	3930.99 ± 559.67 (2571.00 - 5337.44)	0.283	< 0.001	0.071
Right Caudate	4612.60 ± 407.24 (3787.15 - 5613.63)	4362.45 ± 676.53 (3056.91 - 6392.30)	4175.41 ± 660.32 (2348.50 - 5703.71)	0.077	< 0.001	0.049
Left Putamen	6129.14 ± 544.38 (4696.78 - 7348.50)	5731.35 ± 936.31 (3853.59 - 9961.50)	5633.20 ± 817.77 (3280.95 - 7692.93)	0.037	0.002	1.000
Right Putamen	5999.96 ± 577.73 (4791.13 - 7405.07)	5640.19 ± 699.89 (3255.61 - 7125.57)	5635.21 ± 1113.31 (3192.21 - 11772.49)	0.049	0.037	1.000
Left Pallidum	2327.81 ± 302.04 (1672.99 - 3306.62)	2320.30 ± 445.65 (1087.44 - 3926.37)	2254.02 ± 363.61 (1509.96 - 3302.99)	1.000	1.000	0.836
Right Pallidum	2324.39 ± 328.51 (1816.68 - 3383.09)	2273.42 ± 395.80 (1577.88 - 3789.68)	2231.27 ± 330.08 (1323.85 - 3200.47)	1.000	0.593	1.000
Left Thalamus	10214.62 ± 817.16 (8596.19 - 12191.74)	9897.77 ± 796.94 (7433.40 - 11596.03)	9522.75 ± 1054.81 (6014.01 - 12139.69)	0.056	< 0.001	0.018
Right Thalamus	9992.55 ± 791.78 (8135.10 - 11756.69)	9567.91 ± 923.86 (7014.78 - 11278.02)	9188.95 ± 1057.02 (5887.97 - 11523.94)	0.006	< 0.001	0.021
Left Hippocampus	4940.79 ± 605.41 (3280.98 - 6015.97)	4539.48 ± 701.38 (3032.31 - 6805.9)	4576.63 ± 694.89 (2694.10 - 5657.84)	0.003	0.004	1.000
Right Hippocampus	4875.9 ± 676.59 (2575.05 - 6227.41)	4618.66 ± 728.06 (2300.78 - 6025.76)	4593.01 ± 689.18 (2898.13 - 5714.81)	0.120	0.056	1.000
Left Amygdala	1828.65 ± 269.39 (1257.58 - 2485.23)	1711.40 ± 245.19 (1205.88 - 2216.55)	1753.83 ± 274.82 (1188.39 - 2397.40)	0.015	0.191	0.847
Right Amygdala	1718.00 ± 324.25 (846.45 - 2275.43)	1681.02 ± 368.41 (970.30 - 3246.56)	1769.00 ± 277.34 (921.83 - 2486.86)	1.000	1.000	0.301
Left I-IV	4224.53 ± 466.39 (2175.12 - 5128.73)	4139.88 ± 476.42 (1433.91 - 5055.45)	4200.69 ± 415.61 (3215.17 - 5236.53)	1.000	1.000	1.000
Right I-IV	4835.00 ± 454.31 (2810.96 - 5719.95)	4741.481 ± 509.26 (2121.52 - 5746.22)	4820.72 ± 472.62 (3734.50 - 5966.44)	1.000	1.000	1.000
Left V	5519.82 ± 637.48 (2396.54 - 6857.00)	5368.79 ± 667.27 (1432.51 - 6560.12)	5580.97 ± 614.52 (4456.44 - 7287.30)	0.984	1.000	0.277
Right V	5394.18 ± 556.73 (2686.64 - 6359.12)	5239.75 ± 625.25 (1769.33 - 6547.83)	5418.98 ± 571.60 (4283.85 - 6997.50)	0.778	1.000	0.372
Left VI	12238.89 ± 1483.53 (4570.48 - 15128.63)	11892.84 ± 1547.33 (3111.00 - 14900.48)	12111.77 ± 1357.43 (546.34 - 15681.68)	1.000	1.000	1.000
Vermis VI	2508.21 ± 288.01 (1194.72 - 3089.37)	2471.27 ± 276.14 (1102.69 - 2955.84)	2473.84 ± 250.00 (2052.09 - 3043.57)	1.000	1.000	1.000
Right VI	10669.18 ± 1141.67 (5130.54 - 12436.81)	10485.02 ± 1341.10 (3143.14 - 13816.95)	10717.70 ± 1189.72 (8126.65 - 13323.82)	1.000	1.000	1.000
Left Crus I	17988.07 ± 2144.14 (6579.83 - 21373.06)	17492.53 ± 2131.84 (5667.16 - 20753.11)	17675.63 ± 1789.84 (14215.09 - 22365.30)	1.000	1.000	1.000
Vermis Crus I	27.38 ± 5.92 (16.01 - 40.41)	27.57 ± 5.28 (15.37 - 37.62)	28.65 ± 5.97 (15.60 - 42.93)	1.000	0.998	0.669

Right Crus I	17517.67 ± 1713.27 (9367.11 - 19876.71)	17271.61 ± 2239.97 (6294.67 - 20454.22)	17201.69 ± 1785.86 (13659.18 - 20709.32)	1.000	0.786	1.000
Left Crus II	13395.10 ± 1337.00 (9208.45 - 16246.67)	13215.49 ± 1269.50 (8863.41 - 15346.39)	12909.04 ± 1299.24 (10549.02 - 17237.69)	1.000	0.203	0.307
Vermis Crus II	543.66 ± 55.28 (391.92 - 638.49)	533.44 ± (45.55 - 403.90)	528.32 ± 65.05 (376.50 - 656.91)	1.000	0.582	1.000
Right Crus II	12608.73 ± 1116.27 (10445.79 - 14676.75)	12274.16 ± 1146.49 (10011.94 - 15300.30)	11897.10 ± 1166.38 (9704.90 - 15349.60)	0.845	0.005	0.103
Left VIIb	6777.29 ± 640.83 (5336.57 - 8326.35)	6638.53 ± 647.11 (5367.83 - 7935.25)	6461.75 ± 725.244 (5205.39 - 8710.30)	1.000	0.071	0.185
Vermis VIIb	240.72 ± 36.27 (133.80 - 345.67)	224.84 ± 28.41 (117.40 - 271.23)	227.83 ± 36.40 (166.60 - 322.00)	0.186	0.222	1.000
Right VIIb	6836.78 ± 608.77 (5483.39 - 8184.08)	6708.94 ± 615.19 (5269.95 - 7736.57)	6460.69 ± 689.35 (5075.90 - 8459.36)	1.000	0.008	0.038
Left VIIa	7059.44 ± 699.10 (4501.80 - 8682.68)	6938.96 ± 695.65 (4976.76 - 8751.78)	6791.95 ± 752.10 (5492.15 - 8847.86)	1.000	0.241	0.374
Vermis VIIa	1547.16 ± 188.00 (792.14 - 1925.24)	1471.89 ± 162.91 (890.25 - 1800.20)	1505.47 ± 182.37 (1228.62 - 1998.04)	0.169	0.768	1.000
Right VIIa	6483.28 ± 688.87 (3506.01 - 7656.93)	6425.38 ± 651.41 (4092.09 - 7720.46)	6214.36 ± 638.84 (4962.37 - 7939.34)	1.000	0.131	0.113
Left VIIIb	5661.24 ± 580.55 (3111.71 - 6628.33)	5581.13 ± 573.98 (3802.80 - 6705.26)	5521.39 ± 593.23 (4418.25 - 7263.622)	1.000	0.868	1.000
Vermis VIIIb	776.80 ± 81.73 (428.63 - 940.87)	764.04 ± 83.20 (470.98 - 950.26)	758.36 ± 98.67 (562.38 - 1031.06)	1.000	1.000	1.000
Right VIIIb	5400.34 ± 502.96 (3105.79 - 6132.71)	5317.03 ± 503.58 (3352.78 - 6144.61)	5288.62 ± 541.36 (4194.78 - 6498.71)	1.000	0.915	1.000
Left IX	4369.81 ± 486.42 (2600.20 - 5269.52)	4305.42 ± 442.06 (3284.17 - 5259.16)	4269.57 ± 492.66 (3289.08 - 5390.65)	1.000	1.000	1.000
Vermis IX	915.68 ± 115.59 (504.41 - 1202.48)	891.38 ± 106.01 (651.56 - 1136.25)	894.93 ± 121.37 (709.83 - 1178.14)	1.000	1.000	1.000
Right IX	4571.85 ± 525.48 (2627.43 - 5465.87)	4458.41 ± 440.48 (3595.61 - 5440.52)	4483.68 ± 507.82 (3509.57 - 5598.73)	1.000	1.000	1.000
Left X	918.90 ± 100.54 (472.44 - 1122.37)	917.86 ± 100.41 (725.94 - 1166.27)	916.96 ± 94.21 (750.58 - 1179.11)	1.000	1.000	1.000
Vermis X	489.09 ± 68.21 (320.88 - 655.32)	518.39 ± 86.18 (338.21 - 714.89)	522.31 ± 84.94 (369.31 - 870.97)	0.121	0.056	1.000
Right X	902.45 ± 103.20 (468.89 - 1140.85)	903.74 ± 114.62 (422.07 - 1104.78)	913.36 ± 89.30 (734.38 - 1114.11)	1.000	1.000	1.000

Values (mm³) are reported as means ± standard deviations [range]. P values refer to age-, sex- and MR scanner-adjusted ANOVA models, followed by post-hoc pairwise comparisons, Bonferroni-corrected for multiple comparisons. Abbreviations: HC= healthy control; sFTLD= sporadic frontotemporal lobar degeneration; gFTLD= genetic frontotemporal lobar degeneration.

eTable 9. Subcortical, hippocampal and cerebellar grey matter volumes in healthy controls and FTLD patients classified by clinical presentation and genetic status.

	HC	sMND	gMND	p HC vs sMND	p HC vs gMND	p sMND vs gMND	sFTD	gFTD	p HC vs sFTD	p HC vs gFTD	p sFTD vs gFTD
Left Caudate	4307.65 ± 447.97 (3452.28 - 5421.81)	4233.82 ± 73.16 (4089.36 - 4378.28)	4016.33 ± 472.36 (3248.37 - 5200.69)	0.893	0.163	0.010	3795.91 ± 122.70 (3553.64 - 4038.18)	3708.04 ± 732.45 (2571.00 - 5337.44)	<0.001	<0.001	1.000
Right Caudate	4612.60 ± 407.24 (3787.15 - 5613.63)	4527.55 ± 80.50 (4368.60 - 4686.50)	4273.52 ± 584.39 (3104.00 - 5703.71)	1.000	0.102	0.132	3898.10 ± 1345.00 (3631.53 - 4164.66)	3921.66 ± 813.04 (2348.50 - 5454.66)	<0.001	<0.001	1.000
Left Putamen	6129.14 ± 544.38 (4696.78 - 7348.50)	5802.01 ± 114.70 (5575.51 - 6028.50)	5752.66 ± 701.28 (4345.15 - 7372.00)	1.000	0.066	0.592	5532.64 ± 192.36 (5152.79 - 5912.48)	5300.53 ± 1054.18 (3280.95 - 7692.93)	0.020	<0.001	1.000
Right Putamen	5999.96 ± 577.73 (4791.13 - 7405.07)	5810.34 ± 121.69 (5570.05 - 6050.63)	5694.41 ± 678.09 (3764.58 - 6876.74)	1.000	0.280	1.000	5161.65 ± 204.08 (4758.67 - 5564.64)	5460.58 ± 1908.05 (3192.21 - 11772.49)	0.030	0.043	1.000
Left Pallidum	2327.81 ± 302.04 (1672.99 - 3306.62)	2392.86 ± 54.57 (2285.11 - 2500.60)	2122.66 ± 358.56 (1547.20 - 3302.99)	0.090	1.000	0.250	2116.23 ± 91.51 (1935.53 - 2296.93)	2122.66 ± 358.55 (1509.96 - 2914.51)	0.024	0.044	1.000
Right Pallidum	2324.39 ± 328.51 (1816.68 - 3383.09)	2334.04 ± 51.22 (2232.89 - 2435.18)	2245.68 ± 337.74 (1323.86 - 3200.47)	0.306	1.000	0.416	2102.96 ± 85.90 (1933.33 - 2272.58)	2180.27 ± 319.74 (1680.55 - 3092.89)	0.010	0.017	1.000
Left Thalamus	10214.62 ± 817.16 (8596.19 - 12191.74)	10140.60 ± 113.560 (9916.29 - 10364.91)	9777.35 ± 872.32 (8157.97 - 12139.69)	1.000	0.017	0.032	9214.83 ± 190.51 (8838.65 - 9591.00)	8770.36 ± 1211.83 (6014.01 - 11089.68)	0.001	<0.001	0.390
Right Thalamus	9992.55 ± 791.78	9841.19 ± 118.24	9500.30 ± 907.43	1.000	0.008	0.090	8799.30 ± 198.29	8263.01 ± 937.46	<0.001	<0.001	0.172

	(8135.10 - 11756.69)	(9607.72 - 10074.67)	(7560.34 - 11523.94)				(8407.76 - 9190.85)	(5887.97 - 9801.73)			
Left Hippocampus	4940.79 ± 605.41 (3280.98 - 6015.97)	4674.49 ± 92.94 (4490.96 - 4858.02)	4694.09 ± 552.20 (3179.22 - 5628.55)	0.371	0.471	1.000	4159.78 ± 155.87 (3852.00 - 4467.56)	4225.12 ± 941.33 (2694.10 - 5657.84)	<0.001	<0.001	1.000
Right Hippocampus	4875.9 ± 676.59 (2575.05 - 6227.41)	4778.28 ± 97.83 (4585.09 - 4971.46)	4768.97 ± 535.46 (3773.09 - 5714.81)	1.000	1.000	1.000	4169.75 ± 164.07 (3845.77 - 4493.73)	4078.00 ± 840.62 (2898.13 - 5437.71)	0.004	0.001	1.000
Left Amygdala	1828.65 ± 269.39 (1257.58 - 2485.23)	1754.91 ± 38.35 (1679.19 - 1830.64)	1782.55 ± 263.47 (1197.67 - 2397.40)	0.112	1.121	1.000	1589.02 ± 64.32 (1462.02 - 1716.02)	1687.90 ± 302.71 (1188.39 - 2199.88)	0.037	0.573	0.628
Right Amygdala	1718.00 ± 324.25 (846.45 - 2275.43)	1756.29 ± 47.13 (1663.22 - 1849.36)	1785.39 ± 231.80 (1224.26 - 2169.62)	1.000	1.000	1.000	1469.34 ± 79.05 (1313.26 - 1625.42)	1709.81 ± 383.55 (921.83 - 2486.86)	0.148	1.000	0.088
Left I-IV	4224.53 ± 466.39 (2175.12 - 5128.73)	4101.63 ± 516.97 (1433.90 - 4798.41)	4144.58 ± 363.87 (3215.16 - 4896.71)	0.441	0.817	1.000	4235.49 ± 351.72 (3794.45 - 5055.45)	4333.21 ± 522.62 (3411.94 - 5236.53)	1.000	1.000	1.000
Right I-IV	4835.00 ± 454.31 (2810.96 - 5719.95)	4675.49 ± 520.08 (2121.51 - 5374.03)	4742.41 ± 429.74 (3734.50 - 5612.77)	0.341	0.986	1.000	4906.44 ± 455.01 (4279.04 - 5746.21)	5003.22 ± 536.88 (4223.44 - 5966.43)	1.000	1.000	1.000
Left V	5519.82 ± 637.48 (2396.54 - 6857.00)	5302.20 ± 716.17 (1432.51 - 6035.71)	5526.54 ± 548.20 (4456.44 - 6681.43)	0.150	1.000	0.242	5535.25 ± 507.60 (4827.28 - 6560.12)	5716.89 ± 783.83 (4837.93 - 7287.29)	1.000	1.000	1.000
Right V	5394.18 ± 556.73 (2686.64 - 6359.12)	5164.01 ± 646.51 (1769.32 - 5863.51)	5362.17 ± 527.23 (4283.84 - 6690.80)	0.091	0.278	1.000	5429.06 ± 541.44 (4730.82 - 6547.82)	5564.97 ± 688.05 (4840.21 - 6997.49)	1.000	1.000	1.000
Left VI	12238.89 ± 1483.53 (4570.48 - 15128.63)	11677.95 ± 1636.25 (3110.99 - 13296.96)	11998.54 ± 1246.71 (9546.33 - 14262.05)	0.224	1.000	0.901	12430.06 ± 1177.61 (11010.10 - 14900.47)	12387.28 ± 1660.76 (9821.44 - 15681.68)	1.000	1.000	1.000

Vermis VI	2508.21 ± 288.01 (1194.72 - 3089.37)	2450.65 ± 294.26 (1102.68 - 2795.82)	2456.74 ± 239.37 (2052.08 - 2920.22)	1.000	1.000	1.000	2522.81 ± 224.72 (2195.92 - 2955.83)	2515.12 ± 286.28 (2138.37 - 3043.56)	1.000	1.000	1.000
Right VI	10669.18 ± 1141.67 (5130.54 - 12436.81)	10291.03 ± 1373.58 (3143.14 - 12226.63)	10702.29 ± 1123.85 (8126.65 - 13323.82)	0.178	1.000	0.265	10969.97 ± 1156.69 (9613.10 - 13816.94)	10754.24 ± 1423.97 (8706.82 - 13159.07)	0.829	1.000	1.000
Left Crus I	17988.07 ± 2144.14 (6579.83 - 21373.06)	17384.04 ± 2295.39 (5667.15 - 20296.89)	17482.33 ± 1677.59 (14215.08 - 20808.86)	0.639	0.809	1.000	17763.73 ± 1689.76 (13774.84 - 20753.11)	18212.34 ± 2075.34 (15136.47 - 22365.30)	1.000	1.000	1.000
Vermis Crus I	27.38 ± 5.92 (16.01 - 40.41)	27.63 ± 4.86 (15.37 - 37.62)	28.913 ± 6.32 (15.60 - 42.93)	1.000	1.000	0.973	27.40 ± 6.37 (16.06 - 35.40)	28.32 ± 4.96 (21.26 - 41.28)	1.000	0.383	1.000
Right Crus I	17517.67 ± 1713.27 (9367.11 - 19876.71)	17350.72 ± 2341.86 (6294.66 - 20112.91)	17257.60 ± 1708.51 (13918.91 - 20709.31)	0.674	0.506	1.000	17073.84 ± 2019.81 (13952.77 - 20454.22)	17088.64 ± 2076.29 (13659.17 - 20679.38)	1.000	1.000	1.000
Left Crus II	13395.10 ± 1337.00 (9208.45 - 16246.67)	13146.82 ± 1305.75 (8863.41 - 15346.39)	12803.41 ± 1156.06 (10887.73 - 14996.43)	1.000	0.104	0.316	13387.16 ± 1196.79 (11158.75 - 15290.59)	13186.06 ± 1670.73 (10549.01 - 17237.68)	1.000	0.904	1.000
Vermis Crus II	543.66 ± 55.28 (391.92 - 638.49)	529.92 ± 45.00 (403.89 - 607.39)	522.30 ± 65.53 (376.5 - 656.91)	1.000	0.578	1.000	542.23 ± 47.17 (450.65 - 614.57)	542.46 ± 64.42 (435.51 - 645.48)	1.000	1.000	1.000
Right Crus II	12608.73 ± 1116.27 (10445.79 - 14676.75)	12274.48 ± 1089.25 (10011.93 - 14671.86)	11861.13 ± 1079.68 (10131.02 - 14323.13)	1.000	0.017	0.070	12273.34 ± 1317.10 (10251.54 - 15300.30)	11940.70 ± 1424.13 (9704.90 - 15349.59)	1.000	0.087	1.000
Left VIIb	6777.29 ± 640.83	6579.04 ± 654.86	6398.95 ± 679.80	1.000	0.077	0.225	6787.21 ± 622.39	6611.28 ± 854.09	1.000	0.443	1.000

	(5336.57 - 8326.35)	(5367.82 - 7808.39)	(5240.30 - 7874.31)				(5692.55 - 7935.25)	(5205.38 - 8710.29)			
Vermis VIIb	240.72 ± 36.27 (133.80 - 345.67)	220.32 ± 28.44 (117.39 - 263.82)	223.32 ± 35.17 (166.59 - 298.21)	0.189	0.250	1.000	236.14 ± 25.80 (196.04 - 271.23)	239.34 ± 39.05 (181.51 - 321.98)	1.000	0.811	1.000
Right VIIb	6836.78 ± 608.77 (5483.39 - 8184.08)	6688.17 ± 617.31 (5269.94 - 7660.55)	6418.02 ± 657.11 (5075.89 - 7784.29)	1.000	0.019	0.085	6760.85 ± 626.77 (5778.92 - 7736.56)	6528.72 ± 777.25 (5325.27 - 8459.36)	1.000	0.067	1.000
Left VIIIa	7059.44 ± 699.10 (4501.80 - 8682.68)	6834.44 ± 667.90 (4976.7 ± 7938.36)	6711.19 ± 721.78 (5492.14 - 8418.51)	1.000	0.139	0.798	7200.25 ± 715.96 (6229.92 - 8751.78)	6975.92 ± 825.73 (5607.87 - 8847.86)	1.000	0.865	0.914
Vermis VIIIa	1547.16 ± 188.00 (792.14 - 1925.24)	1457.86 ± 174.96 (890.25 - 1800.19)	1490.34 ± 165.81 (1228.61 - 1804.51)	0.088	0.408	1.000	1506.94 ± 126.00 (1258.32 - 1693.58)	1549.36 ± 226.27 (1228.84 - 1998.03)	1.000	1.000	1.000
Right VIIIa	6483.28 ± 688.87 (3506.01 - 7656.93)	6370.20 ± 680.84 (4092.09 - 7720.46)	6161.04 ± 614.52 (4962.37 - 7612.67)	1.000	0.092	0.333	6563.34 ± 567.68 (5818.53 - 7589.59)	6303.56 ± 684.68 (5259.21 - 7939.34)	1.000	0.558	0.689
Left VIIIb	5661.24 ± 580.55 (3111.71 - 6628.33)	5484.83 ± 551.13 (3802.79 - 6482.95)	5473.35 ± 573.10 (4418.24 - 6946.41)	1.000	0.611	1.000	5821.86 ± 575.93 (4878.75 - 6705.25)	5628.72 ± 657.75 (4691.71 - 7263.62)	1.000	1.000	0.895
Vermis VIIIb	776.80 ± 81.73 (428.63 - 940.87)	756.36 ± 90.65 (470.98 - 950.25)	748.00 ± 93.07 (562.37 - 950.37)	1.000	0.498	1.000	783.22 ± 58.82 (673.25 - 866.99)	785.73 ± 113.56 (616.57 - 1031.05)	1.000	1.000	1.000
Right VIIIb	5400.34 ± 502.96 (3105.79 - 6132.71)	5258.81 ± 499.73 (3352.77 - 6103.33)	5268.44 ± 537.08 (4194.79 - 6430.70)	0.708	0.681	1.000	5462.55 ± 498.92 (4510.07 - 6144.61)	5314.02 ± 569.56 (4434.56 - 6498.71)	1.000	1.000	1.000
Left IX	4369.81 ± 486.42 (2600.20 - 5269.52)	4283.77 ± 448.41 (3284.17 - 5259.15)	4254.31 ± 475.34 (3289.08 - 5293.86)	1.000	1.000	1.000	4359.53 ± 435.15 (3615.10 - 5052.50)	4282.48 ± 552.20 (3561.14 - 5390.65)	1.000	0.867	1.000

Vermis IX	915.68 ± 115.59 (504.41 - 1202.48)	878.48 ± 107.19 (651.55 - 1136.24)	884.64 ± 112.05 (709.8 - 1097.0)	1.000	1.000	1.000	923.62 ± 98.88 (770.64 - 1076.22)	923.81 ± 147.02 (737.62 - 1178.14)	1.000	1.000	1.000
Right IX	4571.85 ± 525.48 (2627.43 - 5465.87)	4431.04 ± 432.24 (3595.61 - 5367.82)	4448.26 ± 473.69 (3509.56 - 5598.73)	1.000	1.000	1.000	4526.81 ± 467.62 (3763.81 - 5440.52)	4548.00 ± 598.30 (3637.77 - 5591.70)	1.000	1.000	1.000
Left X	918.90 ± 100.54 (472.44 - 1122.37)	914.79 ± 98.05 (725.94 - 1100.64)	913.79 ± 93.75 (750.57 - 1097.82)	1.000	1.000	1.000	925.49 ± 109.02 (771.38 - 1166.27)	921.55 ± 99.34 (788.03 - 1179.11)	1.000	1.000	1.000
Vermis X	489.09 ± 68.21 (320.88 - 655.32)	507.85 ± 85.13 (338.21 - 709.38)	510.47 ± 69.02 (369.30 - 679.55)	0.645	0.547	1.000	544.71 ± 85.73 (391.78 - 714.88)	548.81 ± 115.37 (409.82 - 870.97)	0.104	0.094	1.000
Right X	902.45 ± 103.20 (468.89 - 1140.85)	901.31 ± 120.72 (422.06 - 1104.77)	910.27 ± 90.61 (734.38 - 1102.65)	1.000	1.000	1.000	909.77 ± 101.10 (714.02 - 1069.86)	921.69 ± 90.50 (795.22 - 1114.10)	1.000	0.974	1.000

Values (mm³) are reported as means ± standard deviations [min. value – max. value]. P values refer to age-, sex- and MR scanner-adjusted ANOVA models, followed by post-hoc pairwise comparisons, Bonferroni-corrected for multiple comparisons. Abbreviations: HC= healthy control; sMND= sporadic motor neuron disease; sFTD= sporadic frontotemporal dementia; gMND= genetic motor neuron disease; gFTD= genetic frontotemporal dementia.

eTable 10. Subcortical, hippocampal and cerebellar grey matter volumes in healthy controls and FTLN patients classified by clinical presentation and genotype.

	HC	sMND	C9-MND	SOD1	TARDBP	p ^{MND}	sFTD	C9-FTD	GRN	p ^{FTD}
Left Caudate	4307.65 ± 68.10 (4173.27 – 4442.04)	4233.82 ± 73.16 (4089.36 – 4378.28)	3864.43 ± 104.63 (3657.82 – 4071.04)	4467.71 ± 185.49 (4101.44 - 4834.00)	4093.39 ± 155.19 (3786.94 - 4399.83)	0.001	3795.91 ± 122.70 (3553.64 – 4038.18)	3653.68 ± 148.00 (3361.49 - 3945.864)	3910.89 ± 173.51 (3568.27 - 4253.51)	<0.001
Right Caudate	4612.60 ± 74.88 (4464.73 - 4760.46)	4527.55 ± 80.50 (4368.60 - 4686.50)	4203.81 ± 115.13 (3976.48 - 4431.14)	4897.08 ± 204.09 (4494.07 - 5300.09)	4291.27 ± 170.76 (3954.09 - 4628.45)	0.007	3898.10 ± 1345.00 (3631.53 - 4164.66)	3872.27 ± 162.81 (3550.78 - 4193.76)	4028.22 ± 190.90 (3651.24 - 4405.20)	<0.001
Left Putamen	6129.14 ± 106.70 (5918.44 - 6339.84)	5802.01 ± 114.70 (5575.51 - 6028.50)	5769.75 ± 164.05 (5445.82 - 6093.68)	6120.68 ± 290.83 (5546.41 - 6694.95)	5794.31 ± 243.32 (5313.84 - 6274.78)	0.127	5532.64 ± 192.36 (5152.79 - 5912.48)	5467.32 ± 232.00 (5009.21 - 5925.43)	5180.66 ± 272.04 (4643.48 - 5717.84)	0.001
Right Putamen	5999.96 ± 113.20 (5776.43 - 6223.50)	5810.34 ± 121.69 (5570.05 - 6050.63)	5812.01 ± 174.04 (5468.34 - 6155.67)	6045.98 ± 308.54 (5436.73 - 6655.24)	5700.60 ± 258.15 (5190.86 - 6210.34)	0.501	5161.65 ± 204.08 (4758.67 - 5564.64)	5586.28 ± 246.13 (5100.26 - 6072.29)	5230.31 ± 288.62 (4660.40 - 5800.22)	0.035
Left Pallidum	2327.81 ± 50.76 (2227.58 - 2428.05)	2392.86 ± 54.57 (2285.11 - 2500.60)	2207.37 ± 78.04 (2053.27 - 2361.46)	2411.67 ± 138.35 (2138.48 - 2684.86)	2391.33 ± 115.75 (2162.77 - 2619.9)	0.127	2116.23 ± 91.51 (1935.53 - 2296.93)	2151.36 ± 110.37 (1933.43 - 2369.29)	2153.55 ± 129.41 (1898.00 - 2409.09)	0.022
Right Pallidum	2324.39 ± 47.65 (2230.3 - 2418.48)	2334.04 ± 51.22 (2232.89 - 2435.18)	2187.33 ± 73.26 (2042.67 - 2331.99)	2440.47 ± 129.87 (2184.02 - 2696.92)	2295.78 ± 108.66 (2081.22 - 2510.35)	0.147	2102.96 ± 85.90 (1933.33 - 2272.58)	2102.08 ± 103.60 (1897.50 - 2306.65)	2109.89 ± 121.49 (1870.00 - 2349.78)	0.004
Left Thalamus	10214.62 ± 105.67 (10005.95 - 10423.29)	10140.60 - 113.560 (9916.29 - 10364.91)	9591.92 ± 162.46 (9271.11 - 9912.72)	10443.54 ± 288.02 (9874.81 - 11012.26)	10004.01 ± 240.97 (9528.18 - 10479.84)	<0.001	9214.83 ± 190.51 (8838.65 - 9591.00)	8997.07 ± 229.76 (8543.39 - 9450.76)	8799.17 ± 269.42 (8267.17 - 9331.16)	<0.001
Right Thalamus	9992.55 ± 109.99 (9775.36 - 10209.74)	9841.19 ± 118.24 (9607.72 - 10074.67)	9362.10 ± 169.10 (9028.19 - 9696.01)	10156.31 ± 299.78 (9564.35 - 10748.27)	9698.09 ± 250.82 (9202.82 - 10193.36)	0.001	8799.30 ± 198.29 (8407.76 - 9190.85)	8476.12 ± 239.14 (8003.90 - 8948.33)	8421.24 ± 280.42 (7867.52 - 8974.97)	<0.001
Left Hippocampus	4940.79 ± 86.46 (4770.06 - 5111.52)	4674.49 ± 92.94 (4490.96 - 4858.02)	4655.52 ± 132.93 (4393.04 – 4918.00)	5150.93 ± 235.65 (4685.60 - 5616.25)	4783.75 ± 197.16 (4394.44 - 5173.07)	0.199	4159.78 ± 155.87 (3852.00 - 4467.56)	4407.30 ± 187.99 (4036.09 - 4778.50)	3973.59 ± 220.43 (3538.32 - 4408.86)	<0.001

Right Hippocampus	4875.95 ± 91.01 (4696.25 - 5055.66)	4778.28 ± 97.83 (4585.09 - 4971.46)	4770.49 ± 139.92 (4494.21 - 5046.78)	5105.08 ± 248.05 (4615.28 - 5594.89)	4846.56 ± 207.53 (4436.76 - 5256.36)	0.876	4169.75 ± 164.07 (3845.77 - 4493.73)	4447.94 ± 197.88 (4057.21 - 4838.67)	4002.89 ± 232.03 (3544.72 - 4461.06)	0.001
Left Amygdala	1828.65 ± 35.68 (1758.20 - 1899.10)	1754.91 ± 38.35 (1679.19 - 1830.64)	1793.33 ± 54.85 (1685.02 - 1901.63)	1927.08 ± 97.24 (1735.08 - 2119.09)	1684.46 ± 81.35 (1523.82 - 1845.11)	0.091	1589.02 ± 64.32 (1462.02 - 1716.02)	1795.71 ± 77.57 (1642.55 - 1948.88)	1664.48 ± 90.96 (1484.87 - 1844.08)	0.078
Right Amygdala	1718.00 ± 43.85 (1631.42 - 1804.58)	1756.29 ± 47.13 (1663.22 - 1849.36)	1789.44 ± 67.41 (1656.33 - 1922.55)	1808.20 ± 119.50 (1572.22 - 2044.17)	1830.90 ± 99.99 (1633.47 - 2028.33)	0.931	1469.34 ± 79.05 (1313.26 - 1625.42)	1783.55 ± 95.33 (1595.31 - 1971.80)	1633.12 ± 111.79 (1412.37 - 1853.84)	0.117
Left I-IV	4224.53 ± 466.39 (2175.12 - 5128.73)	4101.63 ± 516.97 (1433.90 - 4798.41)	4060.73 ± 386.57 (3215.16 - 4648.53)	4337.49 ± 345.20 (3871.92 - 4896.71)	4158.52 ± 305.63 (3633.66 - 4752.55)	0.399	4235.49 ± 351.72 (3794.45 - 5055.45)	4303.60 ± 570.96 (3411.94 - 5160.87)	4207.25 ± 370.72 (3841.34 - 4804.46)	0.804
Right I-IV	4835.00 ± 454.31 (2810.96 - 5719.95)	4675.49 ± 520.08 (2121.51 - 5374.03)	4666.51 ± 416.10 (3734.50 - 5398.62)	4948.14 ± 428.11 (4405.01 - 5572.3)	4740.04 ± 350.92 (4089.25 - 5236.20)	0.401	4906.44 ± 455.01 (4279.04 - 5746.21)	4957.69 ± 648.90 (4072.83 - 5966.43)	4839.91 ± 447.24 (4456.97 - 5756.75)	0.732
Left V	5519.82 ± 637.48 (2396.54 - 6857.00)	5302.20 ± 716.17 (1432.51 - 6035.71)	5410.12 ± 536.24 (4560.93 - 6466.83)	5882.04 ± 536.55 (5210.63 - 6681.43)	5528.30 ± 487.04 (4456.44 - 6362.11)	0.165	5535.25 ± 507.60 (4827.28 - 6560.12)	5729.39 ± 845.54 (4673.10 - 7287.29)	5451.61 ± 486.34 (4837.93 - 6183.34)	0.534
Right V	5394.18 ± 556.73 (2686.64 - 6359.12)	5164.01 ± 646.51 (1769.32 - 5863.51)	5226.50 ± 494.01 (4283.84 - 6223.12)	5703.13 ± 483.12 (5036.87 - 6308.19)	5374.96 ± 493.97 (4453.04 - 6248.98)	0.097	5429.06 ± 541.44 (4730.82 - 6547.82)	5574.60 ± 733.52 (4819.29 - 6997.49)	5320.16 ± 447.14 (4857.91 - 6129.58)	0.576
Left VI	12238.89 ± 1483.53 (4570.48 - 15128.63)	11677.95 ± 1636.25 (3110.99 - 13296.96)	11761.03 ± 1263.72 (9546.33 - 14048.83)	12579.01 ± 1301.80 (10552.39 - 14083.73)	12100.87 ± 1261.78 (9705.91 - 14222.38)	0.369	12430.06 ± 1177.61 (11010.10 - 14900.47)	12265.46 ± 1712.16 (9821.44 - 14862.83)	12088.79 ± 1236.64 (10530.52 - 14262.05)	0.870
Vermis VI	2508.21 ± 288.01 (1194.72 - 3089.37)	2450.65 ± 294.26 (1102.68 - 2795.82)	2409.56 ± 237.69 (2052.08 - 2887.40)	2576.29 ± 254.66 (2248.89 - 2920.22)	2484.97 ± 269.22 (2132.50 - 2811.08)	0.730	2522.81 ± 224.72 (2195.92 - 2955.83)	2510.93 ± 264.99 (2173.59 - 2969.38)	2453.03 ± 246.48 (2138.37 - 2848.70)	0.825
Right VI	10669.18 ± 1141.67 (5130.54 - 12436.81)	10291.03 ± 1373.58 (3143.14 - 12226.63)	10506.24 ± 1128.38 (8126.65 - 13033.17)	11208.36 ± 1241.76 (9085.04 - 13001.97)	10701.24 ± 1031.93 (8974.93 - 12672.22)	0.274	10969.97 ± 1156.69 (9613.10 - 13816.94)	10822.71 ± 1476.24 (8706.82 - 13159.07)	10361.22 ± 962.83 (9375.87 - 11840.68)	0.493
Left Crus I	17988.07 ± 2144.14	17384.04 ± 2295.39	17213.59 ± 1614.21	18767.59 ± 1778.24	17511.53 ± 1558.31	0.457	17763.73 ± 1689.76	18003.79 ± 2399.18	17581.07 ± 1553.18	0.702

	(6579.83 - 21373.06)	(5667.15 - 20296.89)	(14215.08 - 20637.10)	(15881.17 - 20808.86)	(15537.62 - 20684.86)		(13774.84 - 20753.11)	(15136.47 - 22365.30)	(15693.68 - 19607.66)	
Vermis Crus I	27.38 ± 5.92 (16.01 - 40.41)	27.63 ± 4.86 (15.37 - 37.62)	27.29 ± 5.92 (15.60 - 40.54)	28.89 ± 5.84 (20.89 - 36.60)	32.28 ± 6.62 (21.92 - 42.93)	0.159	27.40 ± 6.37 (16.06 - 35.40)	31.15 ± 4.98 (24.13 - 41.28)	26.85 ± 2.23 (23.95 - 30.09)	0.214
Right Crus I	17517.67 ± 1713.27 (9367.11 - 19876.71)	17350.72 ± 2341.86 (6294.66 - 20112.91)	16957.10 ± 1554.86 (13918.91 - 20709.32)	18425.21 ± 1638.80 (15295.01 - 20590.42)	16911.63 ± 1543.43 (14894.19 - 19363.71)	0.329	17073.84 ± 2019.81 (13952.77 - 20454.22)	17157.07 ± 2074.49 (14122.34 - 20679.38)	16522.05 ± 1994.00 (13659.17 - 19668.27)	0.693
Left Crus II	13395.10 ± 1337.00 (9208.45 - 16246.67)	13146.82 ± 1305.75 (8863.41 - 15346.39)	12566.99 ± 997.33 (10887.73 - 14847.24)	13475.04 ± 1330.42 (11217.02 - 14996.43)	12871.95 ± 1096.92 (11450.44 - 14692.27)	0.193	13387.16 ± 1196.79 (11158.75 - 15290.59)	13488.13 ± 1810.46 (11698.63 - 17237.68)	12880.58 ± 1478.41 (10549.01 - 14908.25)	0.344
Vermis Crus II	543.66 ± 55.28 (391.92 - 638.49)	529.92 ± 45.00 (403.89 - 607.39)	505.41 ± 69.64 (376.50 - 656.91)	582.03 ± 54.34 (507.68 - 642.02)	531.05 ± 49.19 (461.22 - 595.19)	0.036	542.23 ± 47.17 (450.65 - 614.57)	544.87 ± 61.79 (474.61 - 645.49)	515.19 ± 60.19 (435.51 - 609.19)	0.425
Right Crus II	12608.73 ± 1116.27 (10445.79 - 14676.75)	12274.48 ± 1089.25 (10011.93 - 14671.86)	11593.72 ± 986.12 (10244.60 - 13671.81)	12322.57 ± 1379.74 (10131.02 - 14323.13)	11914.69 ± 744.48 (10756.49 - 13018.024)	0.033	12273.34 ± 1317.10 (10251.54 - 15300.30)	12395.29 ± 1457.97 (11045.84 - 15349.59)	11632.03 ± 1292.66 (9704.90 - 13495.74)	0.049
Left VIIb	6777.29 ± 640.83 (5336.57 - 8326.35)	6579.04 ± 654.86 (5367.82 - 7808.39)	6206.21 ± 587.81 (5240.30 - 7521.90)	6775.47 ± 872.22 (5394.68 - 7874.31)	6470.08 ± 606.51 (5698.26 - 7752.60)	0.053	6787.21 ± 622.39 (5692.55 - 7935.25)	6745.29 ± 917.48 (5739.96 - 8710.29)	6471.64 ± 794.39 (5205.38 - 7635.49)	0.214
Vermis VIIb	240.72 ± 36.27 (133.80 - 345.67)	220.32 ± 28.44 (117.39 - 263.82)	217.50 ± 35.79 (171.64 - 297.86)	250.21 ± 35.65 (197.73 - 298.22)	220.91 ± 36.34 (166.59 - 285.92)	0.093	236.14 ± 25.80 (196.04 - 271.23)	233.96 ± 44.93 (192.28 - 321.98)	227.53 ± 29.39 (181.51 - 273.91)	0.356
Right VIIb	6836.78 ± 608.77 (5483.39 - 8184.08)	6688.17 ± 617.31 (5269.94 - 7660.55)	6268.13 ± 664.35 (5075.89 - 7431.64)	6740.03 ± 819.71 (5433.13 - 7784.29)	6504.02 ± 465.88 (6025.50 - 7540.93)	0.027	6760.85 ± 626.77 (5778.92 - 7736.56)	6659.75 ± 824.34 (5875.21 - 8459.36)	6322.79 ± 687.47 (5325.27 - 7439.71)	0.058
Left VIIa	7059.44 ± 699.10 (4501.80 - 8682.68)	6834.44 ± 667.90 (4976.7 ± 7938.36)	6524.07 ± 629.27 (5492.14 - 7978.23)	7207.63 ± 891.48 (5801.93 - 8418.51)	6780.92 ± 673.31 (5833.40 - 8247.12)	0.091	7200.25 ± 715.96 (6229.92 - 8751.78)	6998.64 ± 908.81 (6059.38 - 8847.86)	6860.01 ± 779.90 (5607.87 - 7826.47)	0.508
Vermis VIIa	1547.16 ± 188.00 (792.14 - 1925.24)	1457.86 ± 174.96 (890.25 - 1800.19)	1445.03 ± 143.73 (1228.61 - 1752.10)	1677.29 ± 104.32 (1498.84 - 1804.51)	1479.34 ± 162.90 (1281.36 - 1788.95)	0.072	1506.94 ± 126.00 (1258.32 - 1693.58)	1554.55 ± 248.65 (1256.0 - 1998.03)	1478.84 ± 228.19 (1228.84 - 1783.48)	0.578
Right VIIa	6483.28 ± 688.87 (3506.01 - 7656.93)	6370.20 ± 680.84 (4092.09 - 7720.46)	6060.24 ± 662.50 (4962.37 - 7203.88)	6453.89 ± 685.57 (5149.08 - 7100.279)	6166.26 ± 389.72 (5535.06 - 7001.70)	0.200	6563.34 ± 567.68 (5818.53 - 7589.59)	6399.01 ± 748.29 (5595.70 - 7939.34)	6206.72 ± 781.71 (5259.21 - 7612.67)	0.447

Left VIIIb	5661.24 ± 580.55 (3111.71 - 6628.33)	5484.83 ± 551.13 (3802.79 - 6482.95)	5317.10 ± 509.17 (4418.24 - 6257.43)	5949.81 ± 746.85 (4737.90 - 6946.41)	5453.24 ± 496.45 (4723.33 - 6299.16)	0.070	5821.86 ± 575.93 (4878.75 - 6705.25)	5701.20 ± 695.62 (4833.50 - 7263.62)	5453.76 ± 637.77 (4691.71 - 6405.55)	0.348
Vermis VIIIb	776.80 ± 81.73 (428.63 - 940.87)	756.36 ± 90.65 (470.98 - 950.25)	733.09 ± 90.56 (562.37 - 950.38)	853.03 ± 63.83 (762.04 - 934.82)	733.37 ± 81.07 (608.17 - 871.32)	0.057	783.22 ± 58.82 (673.25 - 866.99)	787.69 ± 124.57 (635.50 - 1031.05)	749.38 ± 113.33 (616.57 - 929.78)	0.593
Right VIIIb	5400.34 ± 502.96 (3105.79 - 6132.71)	5258.81 ± 499.73 (3352.77 - 6103.33)	5176.61 ± 469.49 (4194.79 - 6155.92)	5712.63 ± 744.30 (4243.55 - 6430.70)	5185.79 ± 463.06 (4458.14 - 5813.90)	0.167	5462.55 ± 498.92 (4510.07 - 6144.61)	5360.07 ± 563.61 (4619.55 - 6498.71)	5140.91 ± 655.65 (4434.56 - 6271.02)	0.372
Left IX	4369.81 ± 486.42 (2600.20 - 5269.52)	4283.77 ± 448.41 (3284.17 - 5259.15)	4198.38 ± 399.02 (3667.94 - 5085.29)	4746.25 ± 501.93 (3935.96 - 5293.86)	4143.08 ± 417.18 (3435.61 - 4812.93)	0.108	4359.53 ± 435.15 (3615.10 - 5052.50)	4336.01 ± 642.13 (3289.08 - 5390.65)	4138.39 ± 586.46 (3561.14 - 5062.83)	0.426
Vermis IX	915.68 ± 115.59 (504.41 - 1202.48)	878.48 ± 107.19 (651.55 - 1136.24)	863.76 ± 103.58 (709.83 - 1080.14)	993.72 ± 111.80 (796.45 - 1097.06)	873.24 ± 105.98 (719.08 - 1053.17)	0.148	923.62 ± 98.88 (770.64 - 1076.22)	907.20 ± 159.22 (737.62 - 1178.14)	889.50 ± 122.64 (762.15 - 1078.91)	0.665
Right IX	4571.85 ± 525.48 (2627.43 - 5465.87)	4431.04 ± 432.24 (3595.61 - 5367.82)	4357.80 ± 388.46 (3884.43 - 5071.77)	5007.34 ± 505.67 (4089.76 - 5598.73)	4350.30 ± 446.97 (3509.56 - 5041.07)	0.058	4526.81 ± 467.62 (3763.81 - 5440.52)	4543.05 ± 600.48 (3849.01 - 5591.70)	4360.07 ± 656.05 (3637.77 - 5292.62)	0.511
Left X	918.90 ± 100.54 (472.44 - 1122.37)	914.79 ± 98.05 (725.94 - 1100.64)	883.89 ± 81.70 (752.37 - 1038.02)	961.86 ± 88.90 (849.81 - 1069.83)	934.04 ± 97.24 (763.28 - 1059.28)	0.426	925.49 ± 109.02 (771.38 - 1166.27)	916.73 ± 114.42 (750.57 - 1179.11)	930.81 ± 111.39 (788.03 - 1097.82)	0.991
Vermis X	489.09 ± 68.21 (320.88 - 655.32)	507.85 ± 85.13 (338.21 - 709.38)	494.47 ± 67.94 (369.30 - 627.86)	523.56 ± 80.00 (389.20 - 640.14)	528.70 ± 66.96 (436.70 - 679.55)	0.483	544.71 ± 85.73 (391.78 - 714.88)	573.39 ± 120.85 (460.83 - 870.97)	533.98 ± 104.87 (409.82 - 698.33)	0.051
Right X	902.45 ± 103.20 (468.89 - 1140.85)	901.31 ± 120.72 (422.06 - 1104.77)	897.81 ± 82.83 (785.87 - 1089.17)	965.98 ± 115.50 (776.83 - 1102.65)	898.39 ± 105.80 (734.38 - 1084.31)	0.825	909.77 ± 101.10 (714.02 - 1069.86)	922.59 ± 88.41 (801.87 - 1114.10)	923.71 ± 98.46 (795.22 - 1086.52)	0.693

Values (mm³) are reported as mean ± SD [max. value – min. value]. P values refer to age-, sex- and MR scanner-adjusted ANOVA models. Post-hoc pairwise comparisons are reported in **eTable 11**. Abbreviations: HC= healthy controls; sMND= sporadic motor neuron disease; sFTD= sporadic frontotemporal dementia; C9-MND= motor neuron disease with *C9orf72* mutation; C9-FTD= frontotemporal dementia with *C9orf72* mutation; SOD1= motor neuron disease due to *SOD1* mutation; TARDBP= motor neuron disease due to *TARDBP* mutation; GRN= frontotemporal dementia due to *GRN* mutation.

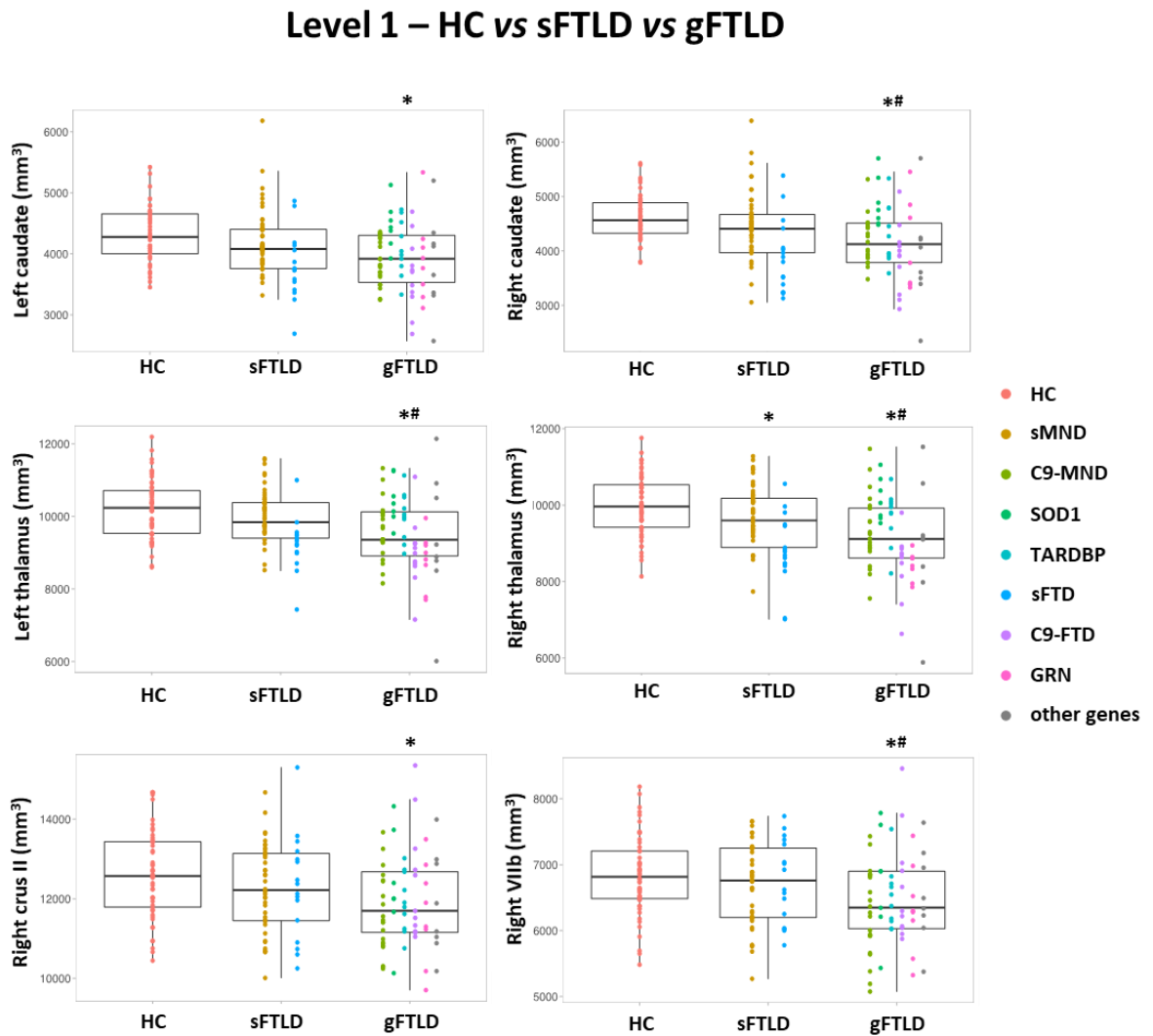
eTable 11. P values obtained from post-hoc pairwise comparisons of volumetric measures in healthy controls and FTLN patients classified by clinical presentation and genotype.

	p HC vs sMND	p HC vs C9-MND	p HC vs SOD1	p HC vs TARDBP	p sMND vs C9-MND	p sMND vs SOD1	p sMND vs TARDBP	p SOD1 vs TARDBP	p C9-MND vs SOD1	p C9-MND vs TARDBP	p HC vs sFTD	p HC vs C9-FTD	p HC vs GRN	p sFTD vs C9-FTD	p sFTD vs GRN	p C9-FTD vs GRN
Left caudate	1.000	0.010	1.000	1.000	<0.001	0.230	1.000	1.000	0.201	1.000	<0.001	0.001	0.037	1.000	1.000	1.000
Right caudate	1.000	0.042	1.000	1.000	0.083	0.250	1.000	1.000	0.331	1.000	<0.001	0.001	0.030	1.000	1.000	1.000
Left putamen	1.000	0.099	1.000	1.000	0.824	1.000	1.000	1.000	1.000	1.000	0.025	0.115	0.006	1.000	1.000	1.000
Right putamen	1.000	1.000	1.000	1.000	1.000	1.000	1.000	1.000	1.000	1.000	0.050	1.000	0.387	1.000	1.000	1.000
Left pallidum	0.234	1.000	1.000	1.000	0.113	1.000	1.000	1.000	1.000	1.000	0.047	0.733	0.279	1.000	1.000	1.000
Right pallidum	0.862	1.000	1.000	1.000	0.232	1.000	1.000	1.000	1.000	1.000	0.019	0.218	0.089	1.000	1.000	1.000
Left thalamus	1.000	<0.001	1.000	1.000	0.001	1.000	1.000	1.000	0.065	0.122	<0.001	<0.001	<0.001	1.000	1.000	1.000
Right thalamus	1.000	<0.001	1.000	1.000	0.005	1.000	1.000	1.000	0.063	1.000	<0.001	<0.001	<0.001	1.000	1.000	1.000
Left hippocampus	1.000	0.512	1.000	1.000	1.000	1.000	1.000	1.000	0.854	1.000	<0.001	0.061	<0.001	1.000	1.000	0.475
Right hippocampus	1.000	1.000	1.000	1.000	1.000	1.000	1.000	1.000	1.000	1.000	0.007	0.546	0.012	1.000	1.000	0.889
Left amygdala	0.324	1.000	1.000	0.279	1.000	1.000	1.000	0.603	1.000	1.000	0.067	1.000	1.000	0.659	1.000	1.000
Right amygdala	1.000	1.000	1.000	1.000	1.000	1.000	1.000	1.000	1.000	1.000	0.215	1.000	1.000	0.181	1.000	1.000
Left I-IV	1.000	1.000	1.000	1.000	0.948	1.000	1.000	1.000	1.000	1.000	1.000	1.000	1.000	1.000	1.000	1.000
Right I-IV	1.000	1.000	1.000	1.000	1.000	1.000	1.000	1.000	1.000	1.000	1.000	1.000	1.000	1.000	1.000	1.000
Left V	0.530	1.000	1.000	1.000	1.000	0.488	1.000	1.000	1.000	1.000	1.000	1.000	1.000	1.000	1.000	1.000
Right V	0.308	1.000	1.000	1.000	1.000	0.407	1.000	1.000	0.916	1.000	1.000	1.000	1.000	1.000	1.000	1.000
Left VI	0.810	1.000	1.000	1.000	1.000	1.000	1.000	1.000	1.000	1.000	1.000	1.000	1.000	1.000	1.000	1.000
Vermis VI	1.000	1.000	1.000	1.000	1.000	1.000	1.000	1.000	1.000	1.000	1.000	1.000	1.000	1.000	1.000	1.000
Right VI	0.638	1.000	1.000	1.000	1.000	1.000	1.000	1.000	1.000	1.000	1.000	1.000	1.000	1.000	1.000	1.000

Left Crus I	1.000	1.000	1.000	1.000	1.000	1.000	1.000	1.000	1.000	1.000	1.000	1.000	1.000	1.000	1.000	1.000
Vermis Crus I	1.000	1.000	1.000	1.000	0.488	1.000	0.141	1.000	1.000	0.300	1.000	0.216	1.000	1.000	1.000	1.000
Right Crus I	1.000	0.838	1.000	1.000	1.000	1.000	1.000	1.000	1.000	1.000	1.000	1.000	1.000	1.000	1.000	1.000
Left Crus II	1.000	0.204	1.000	1.000	0.568	1.000	1.000	1.000	1.000	1.000	1.000	1.000	0.595	1.000	1.000	0.563
Vermis Crus II	1.000	0.174	1.000	1.000	0.701	0.504	1.000	1.000	0.066	1.000	1.000	1.000	0.685	1.000	1.000	0.810
Right Crus II	1.000	0.030	1.000	1.000	0.106	1.000	1.000	1.000	1.000	1.000	0.787	1.000	0.056	1.000	1.000	0.249
Left VIIb	1.000	0.038	1.000	1.000	0.150	1.000	1.000	1.000	0.804	1.000	1.000	1.000	0.235	1.000	0.887	0.491
Vermis VIIb	0.648	0.309	1.000	1.000	0.953	1.000	1.000	1.000	1.000	1.000	1.000	1.000	0.565	1.000	1.000	1.000
Right VIIb	1.000	0.019	1.000	1.000	0.074	1.000	1.000	1.000	1.000	1.000	1.000	1.000	0.059	1.000	0.344	0.414
Left VIIa	1.000	0.087	1.000	1.000	0.565	0.186	1.000	1.000	0.131	1.000	1.000	1.000	0.916	1.000	0.969	1.000
Vermis VIIa	0.195	0.193	1.000	1.000	1.000	1.000	1.000	1.000	0.054	1.000	1.000	1.000	1.000	1.000	1.000	1.000
Right VIIa	1.000	1.000	1.000	1.000	1.000	1.000	1.000	1.000	0.529	1.000	1.000	1.000	0.730	1.000	0.834	1.000
Left VIIIb	1.000	1.000	1.000	1.000	1.000	0.211	1.000	0.213	0.079	1.000	1.000	1.000	0.789	1.000	0.540	1.000
Vermis VIIIb	1.000	1.000	1.000	1.000	1.000	1.000	1.000	1.000	1.000	1.000	1.000	1.000	1.000	1.000	1.000	1.000
Right VIIIb	1.000	1.000	1.000	1.000	1.000	0.904	1.000	1.000	1.000	1.000	1.000	1.000	0.571	1.000	0.647	1.000
Left IX	1.000	1.000	1.000	1.000	1.000	0.357	1.000	0.633	1.000	1.000	1.000	1.000	0.606	1.000	1.000	1.000
Vermis IX	1.000	1.000	1.000	1.000	1.000	0.448	1.000	1.000	1.000	1.000	1.000	1.000	1.000	1.000	1.000	1.000
Right IX	1.000	1.000	0.576	1.000	1.000	0.280	1.000	0.422	0.063	1.000	1.000	1.000	0.899	1.000	1.000	1.000
Left X	1.000	1.000	1.000	1.000	1.000	1.000	1.000	1.000	1.000	1.000	1.000	1.000	1.000	1.000	1.000	1.000
Vermis X	1.000	1.000	1.000	1.000	1.000	1.000	1.000	1.000	1.000	1.000	0.441	0.071	1.000	1.000	1.000	1.000
Right X	1.000	1.000	1.000	1.000	1.000	1.000	1.000	1.000	1.000	1.000	1.000	1.000	1.000	1.000	1.000	1.000

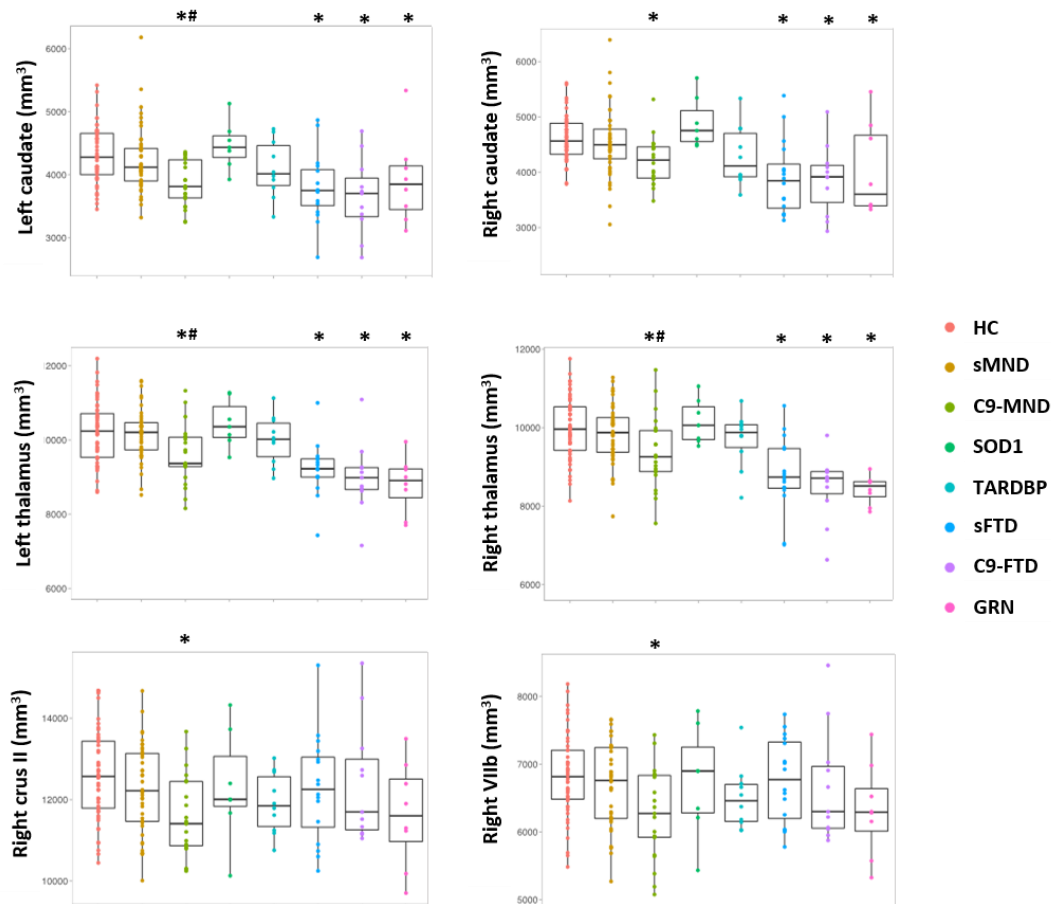
Values (mm³) are referred to age-, sex- and MR scanner-adjusted ANOVA models, Bonferroni-corrected for multiple comparisons. Abbreviations: HC= healthy controls; sMND= sporadic motor neuron disease; sFTD= sporadic frontotemporal dementia; C9-MND= motor neuron disease with *C9orf72* mutation; C9-FTD= frontotemporal dementia with *C9orf72* mutation; SOD1= motor neuron disease due to *SOD1* mutation; TARDBP= motor neuron disease due to *TARDBP* mutation; GRN= frontotemporal dementia due to *GRN* mutation.

eFigure 1. Box-plots reporting GM volumes of selected subcortical and cerebellar structures in gFTLD and sFTLD patients. Comparisons between groups were made using age-, sex- and MR scanner-adjusted ANOVA models, followed by post-hoc pairwise comparisons, Bonferroni-corrected for multiple comparisons. *Symbols:* * = $p < 0.05$ compared with HC; # = $p < 0.05$ compared with sFTLD. *Abbreviations:* FTL D= frontotemporal lobar degeneration; GM= grey matter; g= genetic; HC= healthy controls; s= sporadic.



eFigure 2. Box-plots reporting GM volumes of selected subcortical and cerebellar structures in FTLD patients according to genetic mutation. Comparisons between groups were made using age-, sex- and MR scanner-adjusted ANOVA models, followed by post-hoc pairwise comparisons, Bonferroni-corrected for multiple comparisons. *Symbols:* * = $p < 0.05$ compared with HC; # = $p < 0.05$ compared with sMND. *Abbreviations:* C9-FTD= frontotemporal dementia patients carrying a C9orf72 mutation; C9-MND= motor neuron disease patients carrying a C9orf72 mutation; FTD= frontotemporal dementia; GM= grey matter; HC= healthy controls; MND= motor neuron disease; s= sporadic.

Level 3 – HC vs sMND vs C9-MND vs SOD1 vs TARDBP / HC vs sFTD vs C9-FTD vs GRN



5.2. Amyotrophic lateral sclerosis-frontotemporal dementia: shared and divergent neural correlates across the clinical spectrum

OPEN

Neurology®

The most widely read and highly cited peer-reviewed neurology journal
The Official Journal of the American Academy of Neurology



Neurology Publish Ahead of Print
DOI: 10.1212/WNL.0000000000013123

Amyotrophic Lateral Sclerosis Frontotemporal Dementia: Shared and Divergent Neural Correlates Across the Clinical Spectrum

Author(s):

Camilla Cividini, MSc^{1,2}; Silvia Basaia, PhD¹; Edoardo G. Spinelli, MD^{1,2}; Elisa Canu, PhD¹; Veronica Castelnovo, MSc^{1,2}; Nilo Riva, MD, PhD³; Giordano Cecchetti, MD^{1,2,4}; Francesca Caso, MD, PhD⁴; Giuseppe Magnani, MD⁴; Andrea Falini, MD, PhD^{2,5}; Massimo Filippi, MD^{1,2,3,4,6}; Federica Agosta, MD, PhD^{1,2,4}

This is an open access article distributed under the terms of the Creative Commons Attribution-NonCommercial-NoDerivatives License 4.0 (CC BY-NC-ND), which permits downloading and sharing the work provided it is properly cited. The work cannot be changed in any way or used commercially without permission from the journal.

The following data have been published (Cividini et al., Neurology. 2021 Dec 1;10.1212/WNL.0000000000013123. doi: 10.1212/WNL.0000000000013123).

ABSTRACT

Objectives. A significant overlap between amyotrophic lateral sclerosis (ALS) and behavioral variant of frontotemporal dementia (bvFTD) has been observed at clinical, genetic and pathological levels. Within this continuum of presentations, the presence of mild cognitive and/or behavioral symptoms in ALS patients has been consistently reported, although it is unclear whether this is to be considered a distinct phenotype or, rather, a natural evolution of ALS. Here, we used mathematical modeling of MRI connectomic data to decipher common and divergent neural correlates across the ALS-FTD spectrum.

Methods. We included 83 ALS patients, 35 bvFTD patients and 61 healthy controls, who underwent clinical, cognitive and MRI assessments. ALS patients were classified according to the revised Strong criteria into 54 ALS with only motor deficits (ALS-cn), 21 ALS with cognitive and/or behavioral involvement (ALS-ci/bi), and 8 ALS with bvFTD (ALS-FTD). First, we assessed the functional and structural connectivity patterns across the ALS-FTD spectrum. Second, we investigated whether and where MRI connectivity alterations of ALS patients with any degree of cognitive impairment (i.e., ALS-ci/bi and ALS-FTD) resembled more the pattern of damage of one (ALS-cn) or the other end (bvFTD) of the spectrum, moving from group-level to single-subject analysis.

Results. As compared with controls, extensive structural and functional disruption of the frontotemporal and parietal networks characterized bvFTD (bvFTD-like pattern), while a more focal structural damage within the sensorimotor-basal ganglia areas characterized ALS-cn (ALS-cn-like pattern). ALS-ci/bi patients demonstrated an “ALS-cn-like” pattern of structural damage, diverging from ALS-cn with similar motor impairment for the presence of enhanced functional connectivity within sensorimotor areas and decreased functional connectivity within the “bvFTD-like” pattern. On the other hand, ALS-FTD patients resembled both structurally and functionally the bvFTD-like pattern of damage with, in addition, the structural ALS-cn-like damage in the motor areas.

Conclusions. Our findings suggest a maladaptive role of functional rearrangements in ALS-ci/bi concomitantly with similar structural alterations compared to ALS-cn, supporting the hypothesis that ALS-ci/bi might be considered as a phenotypic variant of ALS, rather than a consequence of disease worsening.

INTRODUCTION

Amyotrophic lateral sclerosis (ALS) is the most common clinical presentation of motor neuron disease, characterized by progressive neurodegeneration of upper and lower motor neurons. A growing body of evidence supports the notion of clinical, pathological and genetic overlap between ALS and the wide spectrum of frontotemporal dementia (FTD) (Burrell, Halliday et al., 2016). Indeed, at least 50% of ALS patients develop cognitive symptoms – mostly affecting executive functions – and behavioral alterations along the course of the disease, leading to a full-blown diagnosis of FTD in 5-25% of cases (Strong et al., 2017; Saxon, Thompson et al., 2017). Considering that comorbid cognitive impairment is a known negative prognostic factor associated with more rapid progression to death or tracheostomy in ALS patients (Calvo et al., 2017, Elamin, Bede et al., 2013), a better definition and understanding of this condition has clear clinical relevance.

The revised Strong criteria (Strong et al., 2017) established a recognized nomenclature for the ALS-FTD clinical continuum ranging from ALS cognitively normal (ALS-cn) to ALS with FTD (ALS-FTD), including ALS with cognitive impairment (ALSci), ALS with behavioural impairment (ALSbi), and ALS with combined cognitive and behavioural impairment (ALS-cbi). Nevertheless, there is currently great debate regarding the pathological underpinnings distinguishing ALS-cn from ALS-ci/bi and ALS-FTD cases, and whether this is to be considered a distinct phenotype or, rather, a natural evolution of ALS. Cross-sectional studies reported an increasing percentage of ALS-ci/bi in disease stages with more severe motor impairment (Chio, Moglia et al., 2019), and even a sequential cognitive staging system has been proposed for ALS (Lule, Bohm et al., 2018), mirroring regions involved in pathological stages of TDP-43 deposition (Brettschneider et al., 2013). However, findings of the few available longitudinal neuropsychological studies in ALS diverge, as some support a stability of cognitive and behavioral changes over time, when present (Kasper, Schuster et al., 2015, Kilani, Micallef et al., 2004), whereas others suggest a subtle progression of cognitive deficits (Beeldman, Govaarts et al., 2020, Castelnovo, Canu et al., 2021). The largest study in this context (Elamin et al., 2013) showed that patients who were cognitively impaired at baseline had a faster decline, in contrast with a tendency to remain cognitively intact in those who were cognitively unimpaired at study entry.

In this context, advanced magnetic resonance imaging (MRI) has provided a useful tool to investigate brain architecture in ALS and FTD. Several MRI studies evaluated patients with behavioral variant of FTD (bvFTD), using both conventional MRI (Gordon, Rohrer et al., 2016, Seeley et al., 2008, Trojsi et al., 2015, Whitwell, Jack et al., 2011) and connectomic approaches (Agosta, Sala et al., 2013c, Filippi et al., 2017), reporting specific patterns of structural and functional damage within frontoinsular and temporal networks. In ALS, widespread grey matter (GM) (Agosta et al., 2016, Alruwaili, Pannek et al., 2018, Illan-Gala, Montal et al., 2020) and white matter (WM) damage (Agosta et al., 2016, Alruwaili et al., 2018, Kasper, Schuster et al., 2014a) has been shown in patients cognitively impaired relative to ALS-cn patients, involving not only motor but also extra-motor areas, including frontotemporal, parietal, insular and cingulate regions. A recent study using a connectomic approach revealed widespread cerebral WM changes affecting frontotemporal regions in ALS-ci/bi patients relative to ALS-cn patients (van der Burgh, Westeneng et al., 2020). Available functional MRI studies have reported conflicting results, as executive dysfunction and behavioral disturbances in ALS have been associated with either enhanced functional connectivity in frontoparietal and temporal networks (Basaia, Agosta et al., 2020, Castelnovo, Canu et al., 2020, Schulthess, Gorges et al., 2016) or suppressed connectivity within frontoparietal, salience and executive networks (Mohammadi et al., 2009, Trojsi et al., 2015). However, in the current literature, there is a lack of MRI studies specifically assessing functional brain alterations in ALS with mild cognitive/behavioral decline, as only one study suggested an enhanced functional connectivity in patients with cognitive decline relative to ALS-cn (Hu, Hou et al., 2020).

To date, a direct evaluation of brain network reorganization in ALS-ci/bi compared with the opposite ends of the ALS-FTD spectrum (i.e., ALS-cn and full-blown FTD) is still needed. Moreover, no studies have combined the structural and functional information using graph analysis and connectomics to investigate neural correlates of cognitive and behavioral decline within patients of the spectrum. The aim of the present study was to bridge this gap, investigating structural and functional network correlates of cognitive/behavioral impairment in patients within the ALS-FTD continuum, who were fully characterized according to the revised Strong criteria (Strong et al., 2017). Using up-to-date MRI approaches, we assessed distinctive patterns of network disruption (i.e.,

“ALS-cn-like pattern” and “bvFTD-like pattern”) that may prove useful for accurate classification at a single-patient level.

METHODS

An overview of the Methods is provided in Figure 1.

Participants

Eighty-three ALS and 35 bvFTD patients were recruited at the IRCCS Ospedale San Raffaele, Milan, Italy, in the framework of an observational study (Fig. 1.I). Only sporadic patients (i.e., with no family history of dementia or motor neuron disease) who proved negative for mutations in the major genes associated with ALS/FTD (i.e., *C9ORF72*, *GRN*, *MAPT*, *TARDBP*, *SOD1*, *FUS*, *TBKI*, *TREM2*, *OPTN* and *VCP*) were included. The diagnosis of ALS was based on the revised El Escorial criteria (Brooks et al., 2000), whereas bvFTD was diagnosed according to Rascovsky criteria (Rascovsky et al., 2011). Patients underwent a comprehensive evaluation including neurological history, clinical assessment (Table 1), neuropsychological testing (eTable 1) and MRI scan. For ALS patients, the site of disease onset was recorded; disease severity was assessed using the ALSFRS-r (Cedarbaum et al., 1999); rate of disease progression was defined as [48–ALSFRS-r score]/time from symptom onset; and muscular strength was assessed by manual muscle testing based on the Medical Research Council (MRC) scale. ALS patients were receiving riluzole at study entry. For bvFTD patients, disease severity was assessed using the Clinical Dementia Rating scale (Knopman, Kramer et al., 2008).

Sixty-one healthy controls were recruited by word of mouth, based on the following criteria: no history of neurologic and psychiatric diseases, no family history of neurodegenerative diseases, and a normal neurological assessment (Table 1).

Exclusion criteria for all subjects were: (other) significant medical illnesses or substance abuse that could interfere with cognitive functioning; any (other) major systemic, psychiatric, or neurological illnesses; and other causes of focal or diffuse brain damage, including lacunae and extensive cerebrovascular disorders at routine MRI.

Cognitive and Behavioral Assessment

Patient classification (Fig. 1.I). Comprehensive multi-domain cognitive testing was performed by trained neuropsychologists unaware of MRI results. Tested cognitive

domains were: global cognitive functioning, memory, executive function, visuospatial abilities, fluency, language, mood and behaviors, as previously described (Basaia et al., 2020, Filippi et al., 2017) (eTable 1). According to the revised Strong criteria (Strong et al., 2017), patients with ALS were classified into 54 cases with motor impairment only (ALS-cn), 21 cases with cognitive and/or behavioral deficits (ALS-ci/bi) and 8 ALS patients with bvFTD (ALS-FTD).

MRI acquisition and pre-processing

MRI scans were obtained using a 3T Philips Medical Systems Intera machine scan. T1-weighted, T2-weighted, fluid-attenuated inversion recovery, diffusion tensor MRI (DT MRI) and resting-state functional MRI (RS fMRI) sequences were acquired. Full details of the MRI acquisition protocol are reported in eTable 2. MRI analyses were performed by experienced observers blinded to subjects' identity.

Connectome Reconstruction (Fig. 1.II). Brain parcellation, DT MRI and RS fMRI pre-processing, and construction of brain structural and functional connectome have been described previously (Basaia et al., 2020, Filippi et al., 2017). Briefly, brain was parcellated into 220 similarly-sized GM cortical and subcortical regions (eTable 3). Applying a graph theoretical approach, the 220 brain regions are represented as nodes and structural/functional connections linking each pair of nodes as edges. Edges for structural connectivity are represented by fractional anisotropy (FA), whereas functional edges are represented by Pearson's correlation coefficients between each pair of nodes. Once the structural macroscale connectome was reconstructed per each subject, we applied the structural connectome of an independent healthy control group as a comprehensive brain connection mask (Filippi et al., 2017). Then, the masked structural connectome of each subject was used as mask for the respective functional connectome, in order to investigate the functional alterations only where structural connections exist, enhancing the biological interpretation of the results (Schmidt, Verstraete et al., 2014).

Statistical analysis

Characterization of functional and structural connectivity across the ALS-FTD spectrum

Regional connectivity analysis (Fig. 1.III). We investigated structural and functional network features in the different subject groups at regional level. Network Based Statistic (NBS) (Zalesky et al., 2010a) was performed to assess regional structural and functional connectivity strength at the level of significance $p < 0.05$. All possible combinations of comparisons between groups were performed. The largest (or principal) connected component and the smaller clusters of altered connections were identified (Basaia et al., 2020, Zalesky et al., 2010a). A corrected p-value was calculated for each contrast using an age-, sex-, and education-adjusted permutation analysis (10000 permutations).

Investigation of ALS-cn-like or bvFTD-like patterns of alterations in ALS-ci/bi and ALS-FTD

The following analyses were focused firstly on identifying the specific structural and functional connectivity patterns that characterize the ends of the ALS-FTD spectrum (ALS-cn and bvFTD). Secondly, we investigated whether and where ALS-ci/bi and ALS-FTD patients showed an ALS-cn-like or a bvFTD-like connectivity pattern.

Distribution analysis (Fig. 1.IV). Distribution analysis was performed to assess the structural and functional connectivity alterations in patient groups. The connectivity values of each connection for each patient were normalized relative to controls as follows:

$$Z_{ij}^s = \frac{C_{ij}^s - \mu}{\sigma}$$

where C_{ij}^s is the structural/functional connectivity value of the connection between node i and j for subject s ; μ is the mean structural/functional connectivity value of the considered connection in the control group; and σ is the standard deviation of the structural/functional connectivity value of such connection in the control group. Subsequently, the 220 regions from both hemispheres were grouped into six anatomical macro-areas (hereafter referred to as brain areas): temporal, parietal, occipital, fronto-insular, basal ganglia, and sensorimotor. Per each patient group (ALS-cn, ALS-ci/bi, ALS-FTD, and bvFTD), the mean values of intra- and inter-area connectivity were calculated averaging the normalized structural/functional connections belonging to an area (intra) or linking two distinct areas (inter), respectively. The percentage of patients with connectivity value below the reference value (i.e., control mean value) was calculated per each intra- and inter-area network. Finally, the intra- and inter-area

connectivity values were compared between patient groups using age-, sex-, and education-adjusted analysis of variance models, followed by post hoc pairwise comparisons, Bonferroni-corrected for multiple comparisons ($p < 0.05$, SPSS Statistics 26.0 [SPSS Inc., Chicago, IL]).

Classification analysis (Fig. 1.V). Classification analysis was performed to define the characteristic structural/functional patterns of damage of the two ends of the spectrum (ALS-cn and bvFTD). For this purpose, we selected the structural and functional connectivity values only in those intra- and inter-area networks, where ALS-cn and bvFTD showed significantly different patterns in the distribution analysis. Receiver Operator Characteristic (ROC) curve analysis was performed in these selected networks. The area under the curve (AUC), as derived measure of accuracy, was considered to assign a specific set of structural/functional alterations to ALS-cn (ALS-cn-like pattern) or to bvFTD (bvFTD-like pattern). Per each intra- and/or inter-area connectivity value involved in one of the two patterns, Youden Index was calculated, providing the best tradeoff between sensitivity and specificity. Finally, patients of each group were classified in those with connectivity values above or below the identified optimal cut-offs.

Frequency analysis (Fig. 1.VI). Aiming to assess, at the single-subject level, whether and where ALS-ci/bi and ALS-FTD patients showed commonalities and differences with ALS-cn-like or bvFTD-like patterns, we performed a frequency analysis using the Chi-squared test ($p < 0.05$). Specifically, we identified and compared between groups the frequency of subjects with connectivity values above and below the optimal cut-offs belonging to the ALS-cn-like and the bvFTD-like pattern. ALS-cn group was excluded in the frequency analysis of the ALS-cn-like pattern, as well as the bvFTD group was not considered in the bvFTD-like pattern analysis.

Data availability

The dataset used during the current study will be made available by the corresponding author upon request to qualified researchers (i.e., affiliated to a university or research institution/hospital).

Standard Protocol Approvals, Registration, and Patient Consents

Local ethical standards committee on human experimentation approved the study protocol and all participants (or their caregivers) provided written informed consent.

RESULTS

Clinical and neuropsychological features

Demographic and clinical characteristics of study groups are reported in Table 1, while neuropsychological features in eTable 1. Relative to controls, ALS-cn and bvFTD patients showed a larger proportion of male individuals. In addition, ALS-ci/bi and bvFTD patients showed lower education relative to controls. ALS groups and bvFTD patients were different for disease duration at MRI, which was shorter in ALS patients. ALS groups were comparable in terms of disease severity, as assessed by ALSFRS-r and MRC global score, disease progression rate and site of clinical onset, although ALS-ci/bi were older than ALS-cn. The neuropsychological assessment did not reveal differences between controls and ALS-cn. bvFTD and ALS-FTD patients performed worse than controls and ALS-cn cases in all investigated cognitive domains. The ALS-ci/bi group performed worse than controls in naming (actions) and better than bvFTD and ALS-FTD patients in fluency tests, with additional higher performance in global cognition, verbal memory, and abstract reasoning compared to bvFTD group only (eTable 1).

Characterization of functional and structural connectivity across the ALS-FTD spectrum (Fig. 2)

Structural connectivity. Regional connectivity analysis showed alterations involving the connections within and among the sensorimotor network, basal ganglia, frontal, temporal and parietal areas, in addition to minimal involvement of the occipital connections, in ALS-cn patients relative to controls ($p=0.01$; Fig. 2A[1]). This structural pattern of damage was also found in ALS-ci/bi and ALS-FTD cases relative to controls ($p=0.02$ and $p=0.001$, Fig. 2A[2,3], respectively), with a more widespread disruption of the same networks in ALS-FTD reflecting increasing severity of impaired behavior and cognition (Fig. 2A[3]). ALS-FTD patients showed also a more severe structural damage, mainly within frontal areas, relative to ALS-cn cases ($p=0.01$; Fig. 2A[6]). Additionally, ALS-cn patients showed greater structural alterations relative to bvFTD ($p=0.03$; Fig. 2A[5]) in few connections within and among sensorimotor regions, parietal areas, and

basal ganglia, especially involving thalamus and those connections from pallidum and putamen towards precentral, postcentral and precuneus bilaterally. Patients with bvFTD showed a widespread structural damage relative to controls, ALS-cn and ALS-ci/bi patients across the whole brain ($p < 0.001$; Fig. 2A[4,7,8], respectively). No further differences were observed in the remaining comparisons.

Functional connectivity. NBS analysis did not show differences in functional connectivity in ALS groups relative to controls, although ALS-ci/bi patients showed a trend toward an enhanced functional connectivity relative to controls within frontal and basal ganglia areas ($p = 0.06$). On the other hand, bvFTD patients were characterized by reduced functional connectivity relative to controls ($p = 0.02$; Fig. 2B[1]), ALS-cn ($p = 0.01$; Fig. 2B[3]) and ALS-ci/bi ($p < 0.001$; Fig. 2B[4]) cases, mainly involving the connections within the frontotemporal regions and between frontal and sensorimotor areas. ALS-FTD relative to ALS-ci/bi patients showed reduced functional connectivity within and between the frontal, temporal and motor areas similarly to bvFTD cases ($p = 0.02$; Fig. 2B[2]). No further differences were observed in the remaining comparisons.

Investigation of ALS-cn-like and bvFTD-like patterns of alterations in ALS-ci/bi and ALS-FTD: structural connectivity (Fig. 3-4)

Distribution analysis. Compared with ALS-cn, bvFTD patients showed greater structural intra-area disruption within frontal, temporal and parietal areas (Fig. 3[1], Fig. 4[3,4] and eTable 4; $p < 0.05$) and inter-area disruption in the frontal, temporal and occipital connections toward parietal lobe ($p = 0.01$, Fig. 3[2] and Fig. 4[2,5]), in the frontal, basal ganglia and occipital connections toward temporal areas ($p = 0.002$, $p < 0.001$ and $p = 0.03$, Fig. 3[3] and Fig. 4[1,6] respectively), and in the connections between frontal and basal ganglia ($p < 0.001$) (Fig. 3[5] and eTable 4). Most of bvFTD patients (from 83 to 100%) were found severely disrupted in these networks (eTable 4). On the other hand, most of ALS-cn patients (81%) were characterized by a greater damage within the motor network, specifically among the sensorimotor – basal ganglia connections, relative to bvFTD cases ($p = 0.01$, Fig. 3[7]). Additionally, ALS-FTD patients showed structural connectivity alterations within the motor areas, resembling the ALS-cn damage. In particular, 88% of ALS-FTD revealed a significant structural disruption in the sensorimotor-basal ganglia connections compared with bvFTD ($p = 0.01$; Fig. 3[7] and

eTable 4). Among the other brain regions, ALS-ci/bi and ALS-FTD patients behaved differently. ALS-ci/bi patients showed significant structural connectivity differences within frontal and temporal lobe (Fig. 3[1] and Fig. 4[3]) and between frontal, temporal and basal ganglia areas compared to bvFTD ($p < 0.05$, (Fig. 3[3,5] and Fig. 4[1]), embracing a pattern of damage more like ALS-cn. On the other hand, ALS-FTD revealed a behavior more like bvFTD, showing a greater structural disruption within frontal ($p = 0.03$) and in frontal -sensorimotor connections ($p = 0.02$) compared to ALS-cn (Fig. 3[1,4] and eTable 4).

Classification analysis. From ROC curve analysis, two characteristic patterns of damage were identified: the “ALS-cn-like pattern” defined by a focal structural damage within sensorimotor-basal ganglia areas that distinguished ALS-cn from bvFTD patients (accuracy [AUC]=0.67, eFigure. 1A-blue line), and the “bvFTD-like pattern” characterized by structural alterations of the frontotemporal and parietal networks that discriminated bvFTD from ALS-cn cases with AUC ranging from 0.67 and 0.88 (eFigure. 1A-red lines). The best cutoff of structural connectivity per each significant network are reported in Table 2.

Frequency analysis. The ALS-cn-like pattern was identified more frequently in ALS-ci/bi and ALS-FTD compared with bvFTD patients (ALS-ci/bi vs bvFTD $p = 0.04$; ALS-FTD vs bvFTD non-significant trend $p = 0.07$) (eTable 5). On the other hand, the bvFTD-like pattern was found to be more frequent neither in ALS-ci/bi nor ALS-FTD compared to ALS-cn, except for a non-significant trend ($p = 0.08$) within frontal and among frontal-basal ganglia, temporal-occipital areas in ALS-FTD relative to ALS-cn cases (eTable 5).

Investigation of ALS-cn-like and bvFTD-like patterns of alterations in ALS-ci/bi and ALS-FTD: functional connectivity (Fig. 5)

Distribution analysis. Regarding functional connectivity distribution analysis, decreased functional connectivity within frontotemporal ($p = 0.001$) and between sensorimotor and parietal connections ($p < 0.02$) was found in bvFTD compared with ALS-cn patients (Fig. 5[1,2] and eTable 4). ALS-ci/bi patients showed significant enhanced functional connectivity relative to bvFTD in the frontal-sensorimotor connections ($p = 0.001$), parietotemporal connections ($p = 0.03$) and within sensorimotor areas ($p < 0.001$, Fig. 5[3,4,5] and eTable 4). Additionally, ALS-ci/bi showed increased

functional connectivity within sensorimotor areas relative to ALS-cn ($p < 0.04$, Fig. 5[4] and eTable 4). Of note, most ALS-ci/bi patients (a percentage ranging from 67 to 76%) revealed normalized values of functional connectivity greater than zero in these abovementioned networks (i.e., frontal-sensorimotor, parietotemporal and sensorimotor). Moreover, ALS-FTD patients showed a significant greater reduced functional connectivity in temporal-sensorimotor connections compared to ALS-cn ($p = 0.03$) and ALS-ci/bi ($p < 0.01$, Fig. 5[6] and eTable 4).

Classification analysis. The ROC curve analysis on functional connectivity data identified only a “bvFTD-like pattern” of functional damage, involving frontotemporal and sensorimotor-parietal connections, with an AUC of 0.77 and 0.67 in discriminating bvFTD from ALS-cn, respectively (eFigure. 1B-red lines). The best cutoff values of functional connectivity for each significant network are reported in Table 2.

Frequency analysis. Within frontotemporal connections, ALS-ci/bi patients were characterized by a greater proportion of cases showing bvFTD-like decreased functional connectivity compared with ALS-cn ($p = 0.03$; eTable 5), but a lower proportion compared with ALS-FTD ($p = 0.02$), who mostly showed a typical bvFTD-like pattern with a decreased functional connectivity relative to ALS-cn patients ($p < 0.001$; eTable 5).

DISCUSSION

The present multiparametric MRI study provides a comprehensive characterization of the neural correlates across the spectrum of ALS-FTD clinical presentations. A connectome-based approach was adopted, first, to identify the connectivity signatures of ALS-cn and bvFTD (i.e., the two ends of this spectrum) and, subsequently, to characterize the alterations underlying mild cognitive/behavioral deficits and full-blown dementia in ALS patients, with the aid of mathematical models and single-subject analysis. An ALS-cn-like pattern was defined by a focused structural damage within the motor areas. By contrast, a bvFTD-like pattern was delineated by a widespread structural damage and decreased functional connectivity, specifically in frontal, temporal and parietal areas. ALS-ci/bi patients showed a pattern of structural damage mostly overlapping with the ALS-cn-like pattern, whereas functional data diverged from ALS-cn for the presence of enhanced functional connectivity within the sensorimotor regions and decreased functional connectivity in the frontotemporal areas (i.e., mirroring a bvFTD-like pattern).

Finally, ALS-FTD resembled the bvFTD-like pattern of damage both structurally and functionally, with, in addition, the structural ALS-cn-like damage in the motor areas. Although connectivity data alone cannot fully address the homogeneity or heterogeneity of this spectrum, our findings suggest a maladaptive role of functional rearrangements in ALS-ci/bi concomitantly with similar structural alterations compared to ALS-cn, supporting the hypothesis that ALS-ci/bi might be considered as a phenotypic variant of ALS, rather than a consequence of disease worsening.

When considering the results of the present study, some limitations should be noted. Despite the robust size of the overall ALS cohort, some subgroups were small (i.e., ALS-FTD), although this is indicative of the relative incidence of cognitive alterations. This aspect has also influenced our choice to bring together patients with mild cognitive dysfunction (i.e., ALS-ci) and patients with mild behavioral disturbances (i.e., ALS-bi), to avoid dispersion of data and the reduced statistical power that would result. Furthermore, the lack of information of a definite pathological diagnosis for bvFTD patients is an important limitation of the present study, even though the aim of the work was to explore the neural correlates of the clinical rather than the pathological heterogeneity of the ALS-FTD spectrum. Another issue lies in the cross-sectional nature of the study. In this context, longitudinal studies are warranted to verify whether cognitive/behavioral dysfunction is a stable or progressive feature of the ALS trajectory, and to assess the evolution of associated network alterations over time.

The inherent limitations of MRI connectomic should also be acknowledged (Pandya, Kuceyeski et al., 2017, Reyes, Ortega-Merchan et al., 2018) including, among others, the lack of an optimal framework, i.e., a reference standard for the regional parcellation of brain MR imaging. It is also important to note that the accuracy of any attempt to model the connectome is biased by the intrinsic limitations of the imaging techniques used. For example, fibre tracking based on DT MRI is known to be poor at points where only limited information about the WM fibre direction is available such as where multiple tracts cross. This results in incomplete reconstruction of tracts and a general under-representation of long-distance connections in the brain. Despite these shortcomings, our study highlights the potential of multiparametric connectome-based approaches for providing novel pathophysiological insights and biomarkers of cognitive dysfunction in the context of ALS-FTD. A key point of our study was the demonstration of characteristic

brain structural damage and functional rearrangements across ALS cognitive phenotypes, as defined based on the application of revised Strong criteria to a sizeable monocentric cohort. Our conclusions were made possible by the extensive clinical and neuropsychological characterization of the sample, as well as by the multiparametric nature of this study. Current MRI literature has generally provided results based on the assessment of structural and functional alterations separately, at voxel or regional level, without a straightforward investigation of their relationship. Conversely, a connectomic approach gave us the potential to bridge the gap of the anatomo-functional link thanks to the application of the same parcellation system, connectome reconstruction framework and statistical approach. Whereas the capability of connectome-based approach to provide information on the brain network architecture was achieved by a group-level analysis, smoothing out the inter-individual variability, a further innovative aspect of our study was the transition to the single-level analysis by the help of mathematical models. Indeed, the study framework was able to identify the ALS-cn-like or bvFTD-like patterns of damage, and to characterize the type of damage that each ALS-ci/bi and ALS-FTD patient shared with such signatures of network alterations.

The selective involvement of motor WM regions in the ALS-cn sample is largely consistent with previous literature (Basaia et al., 2020, Illan-Gala et al., 2020, Muller, Lule et al., 2021), confirming a “signature” pattern of frank decline in FA of the subnetworks connecting primary motor, supplementary motor and premotor areas, as well as basal ganglia – specifically, the thalamus (Tu, Menke et al., 2018). The structural disruption of the sensorimotor network supports the current view of this network as the epicenter of degenerative process of the disease, in line with proposed neuropathological and MRI-based disease staging systems (Brettschneider et al., 2013, Meier, van der Burgh et al., 2020). As for the functional MRI findings, the current literature counts on a number of studies reporting reduced (Mohammadi et al., 2009, Trojsi et al., 2015) or increased functional connectivity in ALS patients (Basaia et al., 2020, Castelnovo et al., 2020, Schulthess et al., 2016), or even a mixed picture (Agosta et al., 2013a). Nevertheless, there is a shortage of MRI studies focusing on functional brain rearrangements in ALS related to cognitive status, and our findings contribute to fill this gap. Of note, both regional (i.e., NBS) and distribution analyses suggest that ALS-cn patients are

characterized by a quite preserved functional connectivity comparable to the functional healthy-brain organization.

The bvFTD-like pattern included a widespread brain structural disruption, with a predominant damage in the frontotemporoparietal network and the involvement of the striatum, and functional connectivity breakdown within the same networks. Our findings confirm previous evidence that see the disconnection of the frontoinsula and temporal regions as hallmark of the behavioral clinical syndrome of FTD both at structural and functional levels (Agosta et al., 2013c, Filippi et al., 2017, Gordon et al., 2016, Whitwell et al., 2011). Herein, we extend these results by highlighting the relative preservation of the motor areas in bvFTD, in contrast with a widespread structural and functional involvement of the anterior frontal lobes, as well as a differential involvement of the basal ganglia circuits when compared with ALS-cn (i.e., greater involvement of striatal connections in bvFTD, in contrast with thalamic involvement in ALS-cn). These findings are in line with previous reports (Bede, Omer et al., 2018, Tu et al., 2018), and support the notion of a diverging network vulnerability to disease pathology in the two opposite ends of the ALS-FTD spectrum.

The focus of the current study was on elucidating MRI connectomic underpinnings of mild or full-blown cognitive deficits in ALS, possibly addressing the long-standing debate on the nature of cognitive deficits in the course of the disease, as an early or, rather, a late-stage feature. Regarding the structural brain network, the presence of mild cognitive and/or behavioral impairment in ALS patients did not contribute significantly to an additional microstructural damage relative to ALS-cn with otherwise comparable clinical characteristics – including measures of motor impairment and disease duration. Although previous literature has suggested greater structural damage related to cognitive impairment in ALS (Agosta et al., 2016, Alruwaili et al., 2018, Illan-Gala et al., 2020, Kasper et al., 2014a, van der Burgh et al., 2020), such damage was generally subtle and possibly driven by the inclusion of ALS-FTD subjects. By contrast, our study highlighted shared structural damage between ALS-ci/bi and ALS-cn patients, involving mainly the motor networks. On the other hand, the analysis of functional connectivity alterations played an important role for the differentiation of ALS-ci/bi from ALS-cn. Indeed, ALS-ci/bi patients showed a rearrangement of the functional networks, which was divergent from ALS-cn, with enhanced functional connectivity within motor areas and decreased

connectivity in the frontotemporal networks. The concomitant absence of significant structural alterations, compared with the ALS-cn group, apparently supports a maladaptive role of such functional rearrangements in ALS-ci/bi, as previously hypothesized (Basaia et al., 2020, Menke et al., 2018). The biological underpinnings of such functional disequilibrium have been suggested to lie in the known excitatory/inhibitory imbalance due to interneuron pathology in ALS, causing a reduction in recurring inhibition that has been associated with disease severity (Crabe, Aimond et al., 2020, Van den Bos, Higashihara et al., 2018). We argue that functional imbalance between motor and extra-motor frontal networks might be particularly severe in ALS-ci/bi, causing mild cognitive disturbances even in early phases of the disease – consistent with the relatively short disease duration of the present cohort. Therefore, our data suggest that ALS-ci/bi might be considered as a phenotypic variant of ALS, rather than a consequence of disease worsening (Chio et al., 2019, Lule et al., 2018). These findings may find support in one of the few longitudinal neuropsychological studies in this context (Elamin et al., 2013), in which cognition decline was faster in patients who were already cognitively impaired at baseline, while normal cognition tended to remain intact with slower motor and cognitive progression. Of note, education levels of ALS-ci/bi patients were lower than ALS-cn in our sample, consistent with the recently highlighted influence of environmental factors that collectively constitute the cognitive reserve (i.e., education, occupation and physical activity) over an early development of cognitive symptoms in ALS (Costello, Rooney et al., 2021).

In contrast with ALS-ci/bi cases, when ALS patients had co-occurrent dementia (ALS-FTD), our study has outlined not only a pattern of microstructural damage involving the motor networks (i.e., the characteristic ALS-cn-like pattern), but also a disruption of frontal, temporal, parietal and striatal circuits, both from a structural and a functional point of view – therefore, resembling the bvFTD-like pattern (Saxon, Thompson et al., 2020). These findings agree with the pattern of widespread hypometabolism recently demonstrated in ALS cases with severe cognitive impairment (Canosa, Moglia et al., 2020), possibly mirroring the most advanced stages of TDP-43 neuropathological models which have been proposed both in ALS (Brettschneider et al., 2013) and bvFTD (Braak, Brettschneider et al., 2013), here sharing the same pathological signature (Omer, Finegan et al., 2017, Rohrer, Geser et al., 2010). Similar to ALS-ci/bi, ALS-FTD patients showed

similar severity of motor symptoms and disease duration when compared with ALS-cn, supporting a view of this clinical presentation as a specific phenotype within the frontotemporal lobar degeneration spectrum, characterized by a combined, severe involvement of both motor and extra-motor brain networks, rather than an evolution of either ALS or bvFTD.

Acknowledgements

Work performed by Dr Edoardo Gioele Spinelli was in partial fulfillment of the requirements for obtaining the PhD degree at Vita-Salute San Raffaele University, Milano, Italy.

References

Agosta F, Canu E, Valsasina P, Riva N, Prella A, Comi G, Filippi M (2013a) Divergent brain network connectivity in amyotrophic lateral sclerosis. *Neurobiology of aging* 34: 419-27

Agosta F, Ferraro PM, Riva N, Spinelli EG, Chio A, Canu E, Valsasina P, Lunetta C, Iannaccone S, Copetti M, Prudente E, Comi G, Falini A, Filippi M (2016) Structural brain correlates of cognitive and behavioral impairment in MND. *Human brain mapping* 37: 1614-26

Agosta F, Sala S, Valsasina P, Meani A, Canu E, Magnani G, Cappa SF, Scola E, Quatto P, Horsfield MA, Falini A, Comi G, Filippi M (2013b) Brain network connectivity assessed using graph theory in frontotemporal dementia. *Neurology* 81: 134-43

Alruwaili AR, Pannek K, Coulthard A, Henderson R, Kurniawan ND, McCombe P (2018) A combined tract-based spatial statistics and voxel-based morphometry study of the first MRI scan after diagnosis of amyotrophic lateral sclerosis with subgroup analysis. *Journal of neuroradiology = Journal de neuroradiologie* 45: 41-48

Basaia S, Agosta F, Cividini C, Trojsi F, Riva N, Spinelli EG, Moglia C, Femiano C, Castelnovo V, Canu E, Falzone Y, Monsurro MR, Falini A, Chio A, Tedeschi G, Filippi M (2020) Structural and functional brain connectome in motor neuron diseases: A multicenter MRI study. *Neurology* 95: e2552-e2564

Bede P, Omer T, Finegan E, Chipika RH, Iyer PM, Doherty MA, Vajda A, Pender N, McLaughlin RL, Hutchinson S, Hardiman O (2018) Connectivity-based characterisation of subcortical grey matter pathology in frontotemporal dementia and ALS: a multimodal neuroimaging study. *Brain Imaging Behav* 12: 1696-1707

Beeldman E, Govaarts R, de Visser M, Klein Twennaar M, van der Kooij AJ, van den Berg LH, Veldink JH, Pijnenburg YAL, de Haan RJ, Schmand BA, Raaphorst J (2020)

Progression of cognitive and behavioural impairment in early amyotrophic lateral sclerosis. *Journal of neurology, neurosurgery, and psychiatry* 91: 779-780

Braak H, Brettschneider J, Ludolph AC, Lee VM, Trojanowski JQ, Del Tredici K (2013) Amyotrophic lateral sclerosis--a model of corticofugal axonal spread. *Nature reviews Neurology* 9: 708-14

Brettschneider J, Del Tredici K, Toledo JB, Robinson JL, Irwin DJ, Grossman M, Suh E, Van Deerlin VM, Wood EM, Baek Y, Kwong L, Lee EB, Elman L, McCluskey L, Fang L, Feldengut S, Ludolph AC, Lee VM, Braak H, Trojanowski JQ (2013) Stages of pTDP-43 pathology in amyotrophic lateral sclerosis. *Annals of neurology* 74: 20-38

Brooks BR, Miller RG, Swash M, Munsat TL, World Federation of Neurology Research Group on Motor Neuron D (2000) El Escorial revisited: revised criteria for the diagnosis of amyotrophic lateral sclerosis. *Amyotroph Lateral Scler Other Motor Neuron Disord* 1: 293-9

Burrell JR, Halliday GM, Kril JJ, Ittner LM, Gotz J, Kiernan MC, Hodges JR (2016) The frontotemporal dementia-motor neuron disease continuum. *Lancet* 388: 919-31

Calvo A, Moglia C, Lunetta C, Marinou K, Ticozzi N, Ferrante GD, Scialo C, Soraru G, Trojsi F, Conte A, Falzone YM, Tortelli R, Russo M, Chio A, Sansone VA, Mora G, Silani V, Volanti P, Caponnetto C, Querin G et al. (2017) Factors predicting survival in ALS: a multicenter Italian study. *Journal of neurology* 264: 54-63

Canosa A, Moglia C, Manera U, Vasta R, Torrieri MC, Arena V, D'Ovidio F, Palumbo F, Zucchetti JP, Iazzolino B, Peotta L, Calvo A, Pagani M, Chio A (2020) Metabolic brain changes across different levels of cognitive impairment in ALS: a (18)F-FDG-PET study. *Journal of neurology, neurosurgery, and psychiatry*

Castelnovo V, Canu E, Calderaro D, Riva N, Poletti B, Basaia S, Solca F, Silani V, Filippi M, Agosta F (2020) Progression of brain functional connectivity and frontal cognitive dysfunction in ALS. *NeuroImage Clinical* 28: 102509

Castelnovo V, Canu E, Riva N, Poletti B, Cividini C, Fontana A, Solca F, Silani V, Filippi M, Agosta F (2021) Progression of cognitive and behavioral disturbances in motor neuron diseases assessed using standard and computer-based batteries. *Amyotrophic lateral sclerosis & frontotemporal degeneration*: 1-14

Cedarbaum JM, Stambler N, Malta E, Fuller C, Hilt D, Thurmond B, Nakanishi A (1999) The ALSFRS-R: a revised ALS functional rating scale that incorporates

assessments of respiratory function. BDNF ALS Study Group (Phase III). *J Neurol Sci* 169: 13-21

Chio A, Moglia C, Canosa A, Manera U, Vasta R, Brunetti M, Barberis M, Corrado L, D'Alfonso S, Bersano E, Sarnelli MF, Solara V, Zucchetti JP, Peotta L, Iazzolino B, Mazzini L, Mora G, Calvo A (2019) Cognitive impairment across ALS clinical stages in a population-based cohort. *Neurology* 93: e984-e994

Costello E, Rooney J, Pinto-Grau M, Burke T, Elamin M, Bede P, McMackin R, Dukic S, Vajda A, Heverin M, Hardiman O, Pender N (2021) Cognitive reserve in amyotrophic lateral sclerosis (ALS): a population-based longitudinal study. *Journal of neurology, neurosurgery, and psychiatry*

Crabe R, Aimond F, Gosset P, Scamps F, Raoul C (2020) How Degeneration of Cells Surrounding Motoneurons Contributes to Amyotrophic Lateral Sclerosis. *Cells* 9

Elamin M, Bede P, Byrne S, Jordan N, Gallagher L, Wynne B, O'Brien C, Phukan J, Lynch C, Pender N, Hardiman O (2013) Cognitive changes predict functional decline in ALS: a population-based longitudinal study. *Neurology* 80: 1590-7

Filippi M, Basaia S, Canu E, Imperiale F, Meani A, Caso F, Magnani G, Falautano M, Comi G, Falini A, Agosta F (2017) Brain network connectivity differs in early-onset neurodegenerative dementia. *Neurology* 89: 1764-1772

Gordon E, Rohrer JD, Fox NC (2016) Advances in neuroimaging in frontotemporal dementia. *Journal of neurochemistry* 138 Suppl 1: 193-210

Hu T, Hou Y, Wei Q, Yang J, Luo C, Chen Y, Gong Q, Shang H (2020) Patterns of brain regional functional coherence in cognitive impaired ALS. *The International journal of neuroscience* 130: 751-758

Illan-Gala I, Montal V, Pegueroles J, Vilaplana E, Alcolea D, Dols-Icardo O, de Luna N, Turon-Sans J, Cortes-Vicente E, Martinez-Roman L, Sanchez-Saudinos MB, Subirana A, Videla L, Sala I, Barroeta I, Valldeneu S, Blesa R, Clarimon J, Lleó A, Fortea J et al. (2020) Cortical microstructure in the amyotrophic lateral sclerosis-frontotemporal dementia continuum. *Neurology* 95: e2565-e2576

Kasper E, Schuster C, Machts J, Bittner D, Vielhaber S, Benecke R, Teipel S, Prudlo J (2015) Dysexecutive functioning in ALS patients and its clinical implications. *Amyotrophic lateral sclerosis & frontotemporal degeneration* 16: 160-71

Kasper E, Schuster C, Machts J, Kaufmann J, Bittner D, Vielhaber S, Benecke R, Teipel S, Prudlo J (2014) Microstructural white matter changes underlying cognitive and behavioural impairment in ALS--an in vivo study using DTI. *PloS one* 9: e114543

Kilani M, Micallef J, Soubrouillard C, Rey-Lardiller D, Demattei C, Dib M, Philippot P, Ceccaldi M, Pouget J, Blin O (2004) A longitudinal study of the evolution of cognitive function and affective state in patients with amyotrophic lateral sclerosis. *Amyotrophic lateral sclerosis and other motor neuron disorders : official publication of the World Federation of Neurology, Research Group on Motor Neuron Diseases* 5: 46-54

Knopman DS, Kramer JH, Boeve BF, Caselli RJ, Graff-Radford NR, Mendez MF, Miller BL, Mercaldo N (2008) Development of methodology for conducting clinical trials in frontotemporal lobar degeneration. *Brain : a journal of neurology* 131: 2957-68

Lule D, Bohm S, Muller HP, Aho-Ozhan H, Keller J, Gorges M, Loose M, Weishaupt JH, Uttner I, Pinkhardt E, Kassubek J, Del Tredici K, Braak H, Abrahams S, Ludolph AC (2018) Cognitive phenotypes of sequential staging in amyotrophic lateral sclerosis. *Cortex; a journal devoted to the study of the nervous system and behavior* 101: 163-171

Meier JM, van der Burgh HK, Nitert AD, Bede P, de Lange SC, Hardiman O, van den Berg LH, van den Heuvel MP (2020) Connectome-Based Propagation Model in Amyotrophic Lateral Sclerosis. *Annals of neurology* 87: 725-738

Menke RAL, Proudfoot M, Talbot K, Turner MR (2018) The two-year progression of structural and functional cerebral MRI in amyotrophic lateral sclerosis. *NeuroImage Clinical* 17: 953-961

Mohammadi B, Kollewe K, Samii A, Krampfl K, Dengler R, Munte TF (2009) Changes of resting state brain networks in amyotrophic lateral sclerosis. *Experimental neurology* 217: 147-53

Muller HP, Lule D, Roselli F, Behler A, Ludolph AC, Kassubek J (2021) Segmental involvement of the corpus callosum in C9orf72-associated ALS: a tract of interest-based DTI study. *The Adv Chronic Dis* 12: 20406223211002969

Omer T, Finegan E, Hutchinson S, Doherty M, Vajda A, McLaughlin RL, Pender N, Hardiman O, Bede P (2017) Neuroimaging patterns along the ALS-FTD spectrum: a multiparametric imaging study. *Amyotrophic lateral sclerosis & frontotemporal degeneration* 18: 611-623

Pandya S, Kuceyeski A, Raj A, Alzheimer's Disease Neuroimaging I (2017) The Brain's Structural Connectome Mediates the Relationship between Regional Neuroimaging Biomarkers in Alzheimer's Disease. *Journal of Alzheimer's disease : JAD* 55: 1639-1657

Rascovsky K, Hodges JR, Knopman D, Mendez MF, Kramer JH, Neuhaus J, van Swieten JC, Seelaar H, Dopper EG, Onyike CU, Hillis AE, Josephs KA, Boeve BF, Kertesz A, Seeley WW, Rankin KP, Johnson JK, Gorno-Tempini ML, Rosen H, Prioleau-Latham CE et al. (2011) Sensitivity of revised diagnostic criteria for the behavioural variant of frontotemporal dementia. *Brain* 134: 2456-77

Reyes P, Ortega-Merchan MP, Rueda A, Uriza F, Santamaria-Garcia H, Rojas-Serrano N, Rodriguez-Santos J, Velasco-Leon MC, Rodriguez-Parra JD, Mora-Diaz DE, Matallana D (2018) Functional Connectivity Changes in Behavioral, Semantic, and Nonfluent Variants of Frontotemporal Dementia. *Behav Neurol* 2018: 9684129

Rohrer JD, Geser F, Zhou J, Gennatas ED, Sidhu M, Trojanowski JQ, Dearmond SJ, Miller BL, Seeley WW (2010) TDP-43 subtypes are associated with distinct atrophy patterns in frontotemporal dementia. *Neurology* 75: 2204-11

Saxon JA, Thompson JC, Harris JM, Richardson AM, Langheinrich T, Rollinson S, Pickering-Brown S, Chaouch A, Ealing J, Hamdalla H, Young CA, Blackburn D, Majeed T, Gall C, Jones M, Snowden JS (2020) Cognition and behaviour in frontotemporal dementia with and without amyotrophic lateral sclerosis. *Journal of neurology, neurosurgery, and psychiatry* 91: 1304-1311

Saxon JA, Thompson JC, Jones M, Harris JM, Richardson AM, Langheinrich T, Neary D, Mann DM, Snowden JS (2017) Examining the language and behavioural profile in FTD and ALS-FTD. *Journal of neurology, neurosurgery, and psychiatry* 88: 675-680

Schmidt R, Verstraete E, de Reus MA, Veldink JH, van den Berg LH, van den Heuvel MP (2014) Correlation between structural and functional connectivity impairment in amyotrophic lateral sclerosis. *Human brain mapping* 35: 4386-95

Schulthess I, Gorges M, Muller HP, Lule D, Del Tredici K, Ludolph AC, Kassubek J (2016) Functional connectivity changes resemble patterns of pTDP-43 pathology in amyotrophic lateral sclerosis. *Scientific reports* 6: 38391

Seeley WW, Crawford R, Rascofsky K, Kramer JH, Weiner M, Miller BL, Gorno-Tempini ML (2008) Frontal paralimbic network atrophy in very mild behavioral variant frontotemporal dementia. *Arch Neurol* 65: 249-55

Strong MJ, Abrahams S, Goldstein LH, Woolley S, McLaughlin P, Snowden J, Mioshi E, Roberts-South A, Benatar M, HortobaGyi T, Rosenfeld J, Silani V, Ince PG, Turner MR (2017) Amyotrophic lateral sclerosis - frontotemporal spectrum disorder (ALS-FTSD): Revised diagnostic criteria. *Amyotroph Lateral Scler Frontotemporal Degener* 18: 153-174

Trojsi F, Esposito F, de Stefano M, Buonanno D, Conforti FL, Corbo D, Piccirillo G, Cirillo M, Monsurro MR, Montella P, Tedeschi G (2015) Functional overlap and divergence between ALS and bvFTD. *Neurobiology of aging* 36: 413-23

Tu S, Menke RAL, Talbot K, Kiernan MC, Turner MR (2018) Regional thalamic MRI as a marker of widespread cortical pathology and progressive frontotemporal involvement in amyotrophic lateral sclerosis. *Journal of neurology, neurosurgery, and psychiatry* 89: 1250-1258

Van den Bos MAJ, Higashihara M, Geevasinga N, Menon P, Kiernan MC, Vucic S (2018) Imbalance of cortical facilitatory and inhibitory circuits underlies hyperexcitability in ALS. *Neurology* 91: e1669-e1676

van der Burgh HK, Westeneng HJ, Walhout R, van Veenhuijzen K, Tan HHG, Meier JM, Bakker LA, Hendrikse J, van Es MA, Veldink JH, van den Heuvel MP, van den Berg LH (2020) Multimodal longitudinal study of structural brain involvement in amyotrophic lateral sclerosis. *Neurology* 94: e2592-e2604

Whitwell JL, Jack CR, Jr., Parisi JE, Knopman DS, Boeve BF, Petersen RC, Dickson DW, Josephs KA (2011) Imaging signatures of molecular pathology in behavioral variant frontotemporal dementia. *J Mol Neurosci* 45: 372-8

Zalesky A, Fornito A, Bullmore ET (2010) Network-based statistic: identifying differences in brain networks. *NeuroImage* 53: 1197-207

Table 1. Demographic and clinical features of healthy controls, bvFTD patients and ALS patient groups.

	Healthy controls	ALS-cn	ALS-ci/bi	ALS-FTD	bvFTD
N	61	54	21	8	35
Age [years]	63.04 ± 8.46 (43.36 – 81.81)	61.08 ± 9.96 (36.38 – 81.26)	67.99 ± 11.77 [^] (39.89 – 86.12)	60.28 ± 10.54 (44.68 – 70.06)	63.18 ± 9.13 (45.51 – 74.83)
Sex [women/men]	36/25	19/35*	11/10	5/3	12/23*
Education [years]	12.89 ± 4.79 (5.00 – 24.00)	11.06 ± 4.52 (5.00 – 24.00)	8.38 ± 3.72* (3.00 – 18.00)	11.50 ± 5.95 (4.00 – 18.00)	9.56 ± 3.65* (4.00 – 17.00)
Onset [limb/bulbar/limb+bulbar]	-	41/12/1	16/5/0	3/5/0	-
Disease duration [months]	-	23.76 ± 23.96# (4.00 – 136.00)	16.62 ± 12.11# (4.00 – 47.00)	23.25 ± 17.06 (7.00 – 56.00)	41.00 ± 29.63 (6.87 – 144.70)
ALSFRS-r [0-48]	-	38.31 ± 5.46 (23.00 – 47.00)	39.00 ± 5.72 (28.00 – 46.00)	35.63 ± 7.84 (24.00 – 45.00)	-
UMN score	-	11.22 ± 4.39 (0.00 – 16.00)	10.45 ± 3.78 (2.00 – 16.00)	12.67 ± 5.47 (2.00 – 16.00)	-
MRC global score	-	102.94 ± 15.39 (60.00 – 148.00)	101.20 ± 17.62 (71.00 – 127.00)	108.17 ± 8.33 (98.00 - 118)	-
Disease progression rate	-	0.64 ± 0.56 (0.04 – 2.67)	0.77 ± 0.67 (0.13 – 2.86)	0.57 ± 0.22 (0.33 – 1.00)	-
ADL	-	-	-	-	5.62 ± 0.85 (2.00 – 6.00)
IADL	-	-	-	-	4.77 ± 2.29 (1.00 – 8.00)
CDR	-	-	-	-	0.96 ± 0.57 (0.50 – 2.00)
CDR SB	-	-	-	-	4.81 ± 2.53 (1.00 – 9.50)

Values are numbers or means ± standard deviations (range). Disease duration was defined as months from onset to date of MRI scan. The rate of disease progression in ALS patients was defined as follows: (48–ALSFRS-r score)/time from symptom onset. P values refer to ANOVA models, followed by post-hoc pairwise comparisons (Bonferroni-corrected

for multiple comparisons), or Chi-squared test. *: $p < 0.05$ vs HC; #: $p < 0.05$ vs bvFTD; ^: $p < 0.05$ vs ALS-cn.

Abbreviations: ADL= Activities of Daily Living; ALS-ci/bi= ALS with cognitive and/or behavioral impairment; ALS-FTD= ALS with Frontotemporal Dementia; ALS-cn= Amyotrophic lateral sclerosis with only motor impairment; ALSFRS-r= Amyotrophic lateral sclerosis functional rating scale revised; bvFTD= behavioral variant of Frontotemporal Dementia; CDR= Clinical dementia rating; CDR sb= Clinical dementia rating sum of boxes; HC= healthy controls; IADL= Instrumental Activities of Daily Living; MRC= Medical Research Council; N= Number; UMN= Upper motor neuron.

Table 2. Classification (ROC curves) analysis for identification of the “ALS-cn-like pattern” and the “bvFTD-like pattern”.

Structural Connectivity			
Intra-area and Inter-areas connections	AUC bvFTD vs ALS-cn	AUC ALS-cn vs bvFTD	Best Cut-off (Youden’s index)
Frontal	0.88	0.12	-0.21 (0.68)
Frontal-Basal Ganglia	0.82	0.18	-0.67 (0.52)
Frontal-Parietal	0.71	0.29	-0.30 (0.37)
Frontal-Temporal	0.76	0.24	-0.20 (0.44)
Sensorimotor-Basal Ganglia	0.33	0.67	-0.55 (0.30)
Basal Ganglia-Temporal	0.78	0.22	-0.52 (0.45)
Basal Ganglia-Occipital	0.72	0.28	-0.47 (0.42)
Parietal	0.67	0.33	0.003 (0.31)
Parietal-Temporal	0.72	0.28	-0.36 (0.43)
Parietal-Occipital	0.69	0.31	-0.08 (0.35)
Temporal	0.75	0.25	-0.2 (0.41)
Temporal-Occipital	0.70	0.30	-0.40 (0.35)
Functional Connectivity			
Frontal-Temporal	0.77	0.23	-0.27 (0.48)
Sensorimotor-Parietal	0.67	0.33	-0.04 (0.34)

The Area Under the ROC curve represents the capability of the structural and functional connectivity damage within the reported intra- and inter-areas to discriminate bvFTD from ALS-cn and viceversa. Only intra-area and inter-areas connections significantly different between the two groups were considered. Bold values in the column “bvFTD vs ALS-cn” identify the “bvFTD-like pattern”. Bold values in the column “ALS-cn vs bvFTD” identify the “ALS-cn-like pattern”. The optimal cut-off per each connectivity distribution was calculated through the Youden’s index, maximizing sensibility and specificity. Cut-off= sensibility-(1-specificity). Abbreviations: ALS-cn= Amyotrophic lateral sclerosis with only motor impairment; AUC= Area Under the ROC curve; bvFTD= behavioral variant of Frontotemporal Dementia.

Figure 1. Study Framework. (I) Patient classification. Revised Strong's Criteria were applied. **(II) Connectome Reconstruction.** Connectomics was apply on DT MRI and RS fMRI, after parcellating the brain into 220 regions. Structural and functional connectomes of all subjects were reconstructed. **(III) Regional connectivity analysis.** Network based Statistics was performed. **(IV) Distribution analysis.** All connections per each patient were normalized relative to controls and grouped into 6 macro-areas. Intra-area and inter-area connectivity distribution were plotted and compared between groups. **(V) Classification analysis.** ROC curve analysis was performed to discriminate ALS-cn from bvFTD and vice versa. **(VI) Frequency analysis.** ALS-ci/bi and ALS-FTD cases were then subdivided in those under and above the optimal cutoff. Chi-squared test was performed in order to identify the behavior of these two groups. Abbreviations: ALS= Amyotrophic lateral sclerosis; ALS-ci/bi= ALS with cognitive and/or behavioral impairment; ALS-cn= ALS with motor impairment only; ALS-FTD= ALS with Frontotemporal Dementia; bvFTD= behavioral variant of Frontotemporal Dementia; DT MRI= diffusion tensor MRI; fMRI= functional MRI; HC= healthy controls; SBJ= subject.

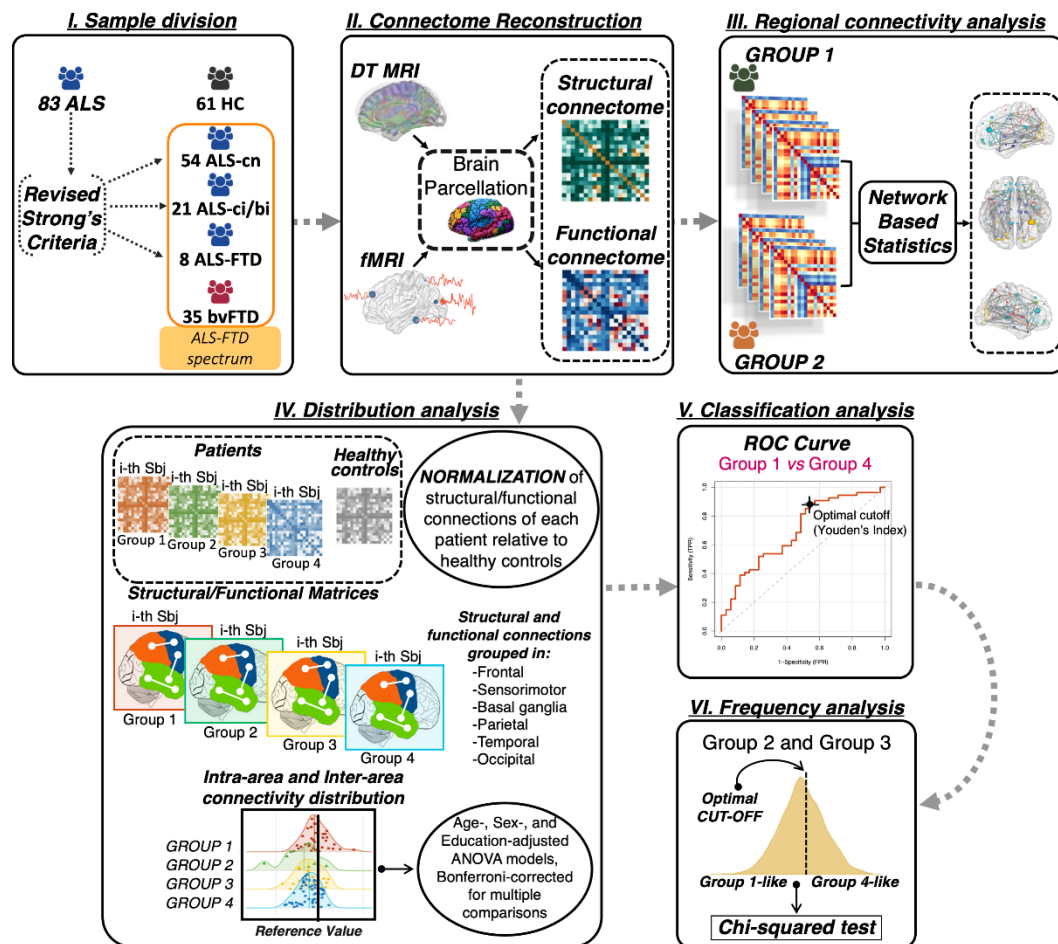


Figure 2. Alterations in structural and functional connectivity in ALS and bvFTD patients relative to healthy controls and each other. Altered structural (A) and functional (B) connections are represented per each significant contrast, respectively ($p < 0.05$). The comparisons were adjusted for age, sex and education. The node color represents its belonging to specific macro-areas (frontal, sensorimotor, basal ganglia, parietal, temporal and occipital). The node size is proportional to the number of affected connections (the higher the number of disrupted connections, the bigger the node). Abbreviations: A= anterior; ALS= Amyotrophic lateral sclerosis; ALS-ci/bi= ALS with cognitive and/or behavioral impairment; ALS-cn= ALS with motor impairment only; ALS-FTD= ALS with Frontotemporal Dementia; bvFTD= behavioral variant of Frontotemporal Dementia; FA= fractional anisotropy; HC= healthy controls; L= left; P= posterior; R= right.

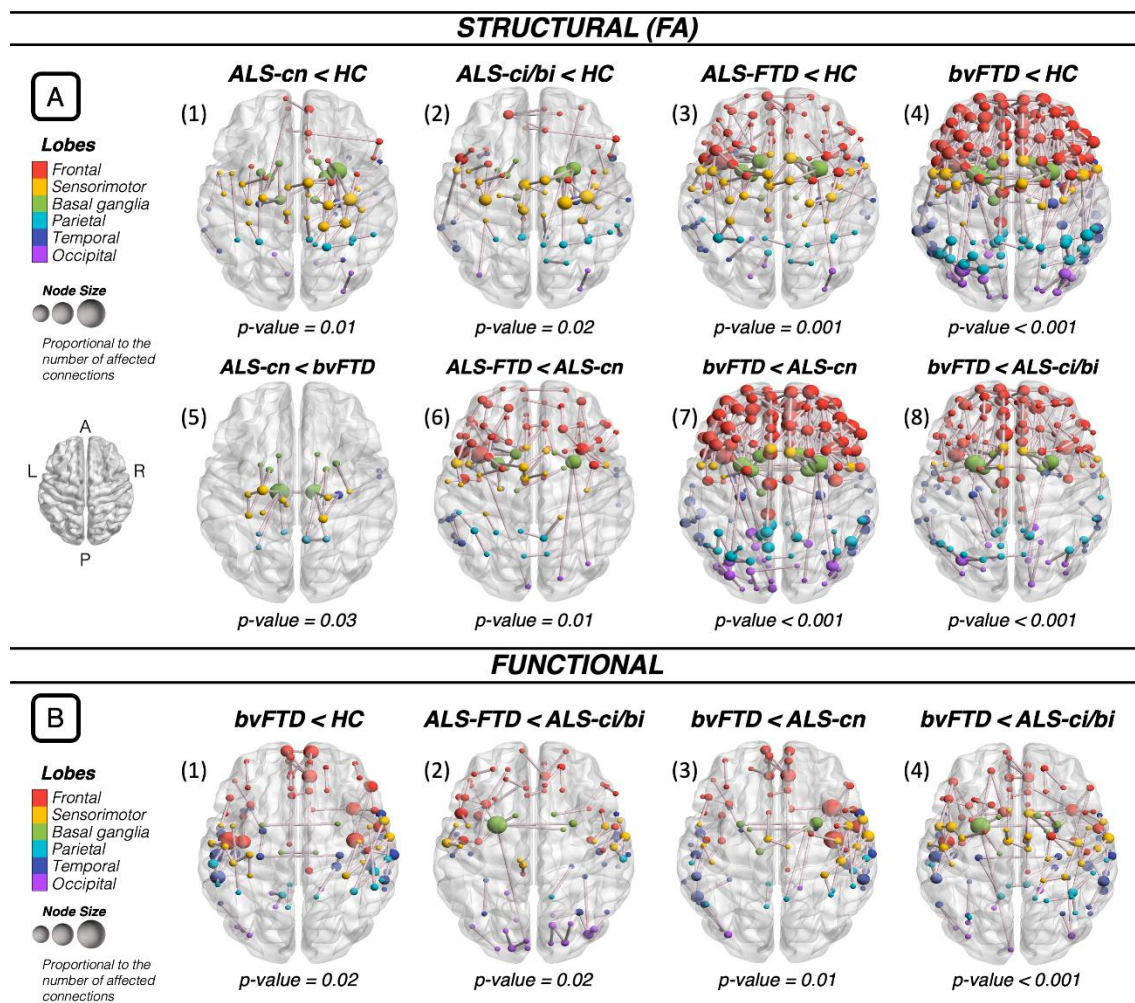


Figure 3. Distribution analysis of the structural connectivity damage in patient groups. The distribution of the structural connectivity alterations within frontal and motor areas and in the connections towards these areas is displayed. Distribution curves are normalized relative to control values. The more the curve is shifted towards negative values, the greater is the structural damage. All significant contrasts ($p < 0.05$) – displayed with colored stars – are reported according to age-, sex- and education-adjusted ANOVA models, Bonferroni-corrected for multiple comparisons. Abbreviations: ALS= Amyotrophic lateral sclerosis; ALS-ci/bi= ALS with cognitive and/or behavioral impairment; ALS-cn= ALS with motor impairment only; ALS-FTD= ALS with Frontotemporal Dementia; bvFTD= behavioral variant of Frontotemporal Dementia.

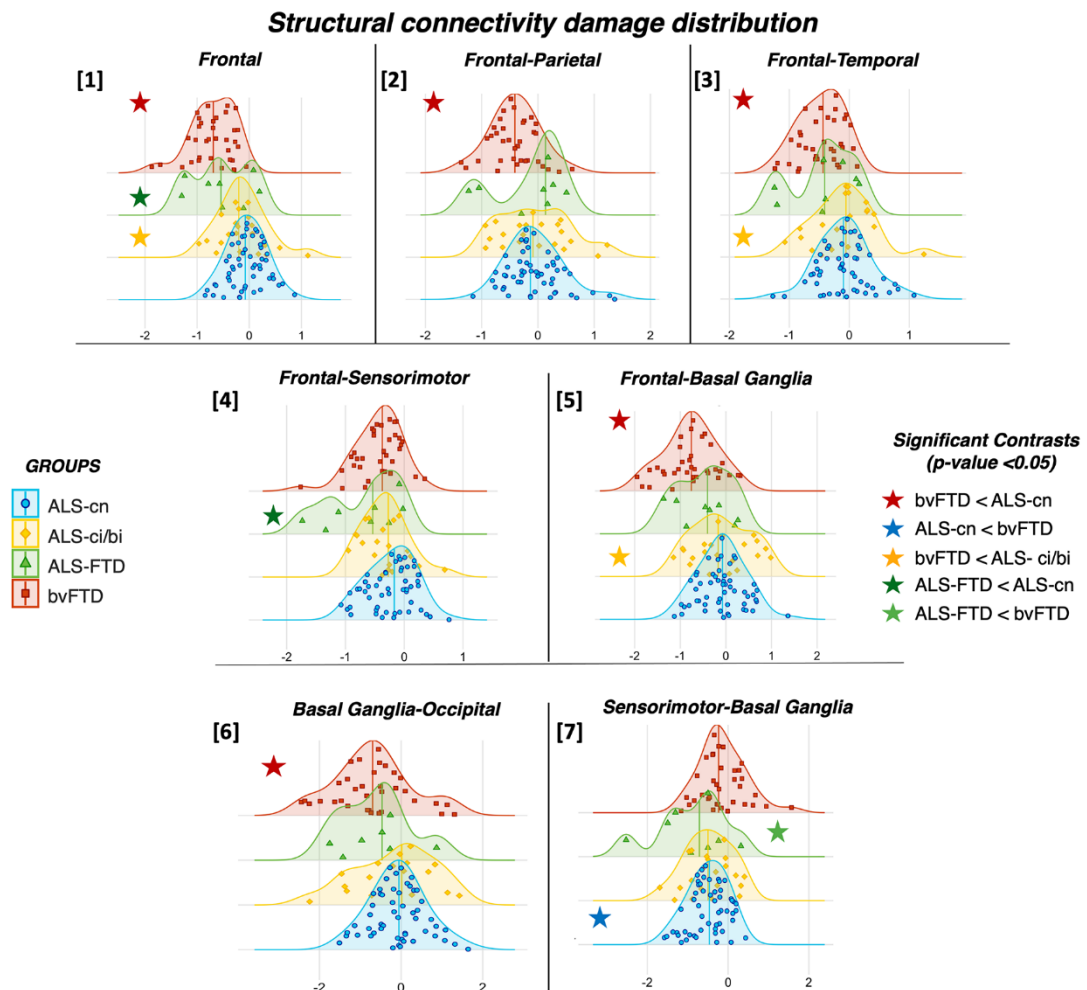


Figure 4. Distribution analysis of the structural connectivity damage in patient groups. The distribution of the structural connectivity alterations within parietal and temporal areas and in the connections towards these areas is displayed. Distribution curves are normalized relative to control values. The more the curve is shifted towards negative values, the greater is the structural damage. All significant contrasts ($p < 0.05$) – displayed with colored stars – are reported according to age-, sex- and education-adjusted ANOVA models, Bonferroni-corrected for multiple comparisons. Abbreviations: ALS= Amyotrophic lateral sclerosis; ALS-ci/bi= ALS with cognitive and/or behavioral impairment; ALS-cn= ALS with motor impairment only; ALS-FTD= ALS with Frontotemporal Dementia; bvFTD= behavioral variant of Frontotemporal Dementia.

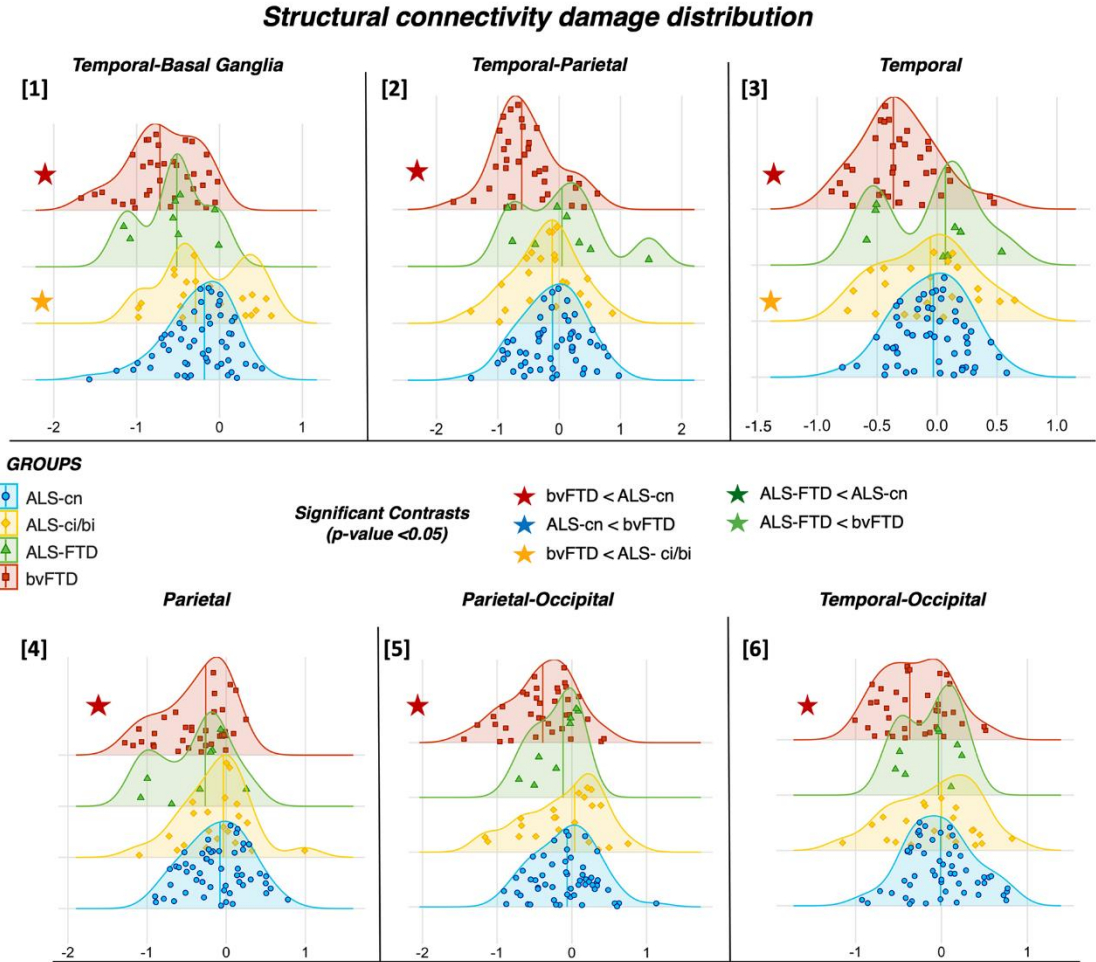
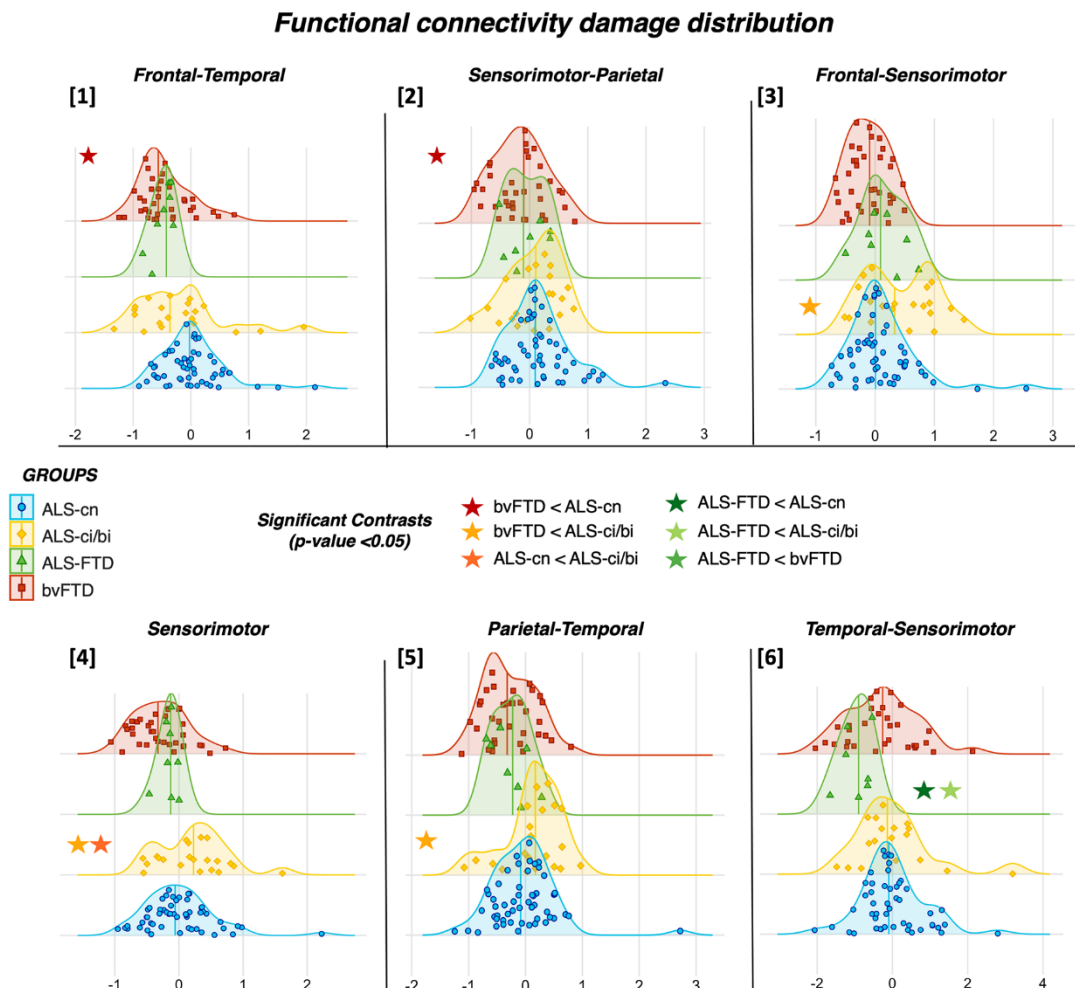


Figure 5. Distribution analysis of the functional connectivity damage in patient groups. Functional connectivity damage distribution within area and among areas is reported. Distribution curves are normalized relative to control values. The more the curve is shifted towards negative values, the more reduced is the functional connectivity. All significant contrasts ($p < 0.05$) – displayed with colored stars – are reported according to age-, sex- and education-adjusted ANOVA models, Bonferroni-corrected for multiple comparisons. Abbreviations: ALS= Amyotrophic lateral sclerosis; ALS-ci/bi= ALS with cognitive and/or behavioral impairment; ALS-cn= ALS with motor impairment only; ALS-FTD= ALS with Frontotemporal Dementia; bvFTD= behavioral variant of Frontotemporal Dementia.



SUPPLEMENTARY INFORMATION

eTable 1. Neuropsychological features of the healthy controls, ALS subgroups and bvFTD patients.

	HC	ALS-cn	ALS-ci/bi	ALS-FTD	bvFTD
Global cognition					
MMSE* ¹	29.34 ± 0.97 (26.00 – 30.00)	28.41 ± 1.65 (21.00 – 30.00)	27.43 ± 2.52 (20.00 – 30.00)	24.75 ± 3.15\$ (21.00 – 29.00)	22.81 ± 5.99\$#^ (8.00 – 29.00)
Memory					
Digit span forward ²	5.97 ± 0.99 (4.00 – 9.00)	4.75 ± 0.93 (4.00 – 9.00)	27.43 ± 2.52 (3.00 – 6.00)	4.67 ± 0.82 (4.00 – 6.00)	4.55 ± 1.03\$# (3.00 – 6.00)
RAVLT delayed ³	9.19 ± 3.32 (3.00 – 15.00)	9.02 ± 3.30 (1.00 – 15.00)	7.13 ± 2.42 (3.00 – 12.00)	5.14 ± 5.79\$## (0.00 – 14.00)	3.53 ± 3.24\$#^ (0.00 – 10.00)
Rey Figure recall ⁴	18.37 ± 5.90 (9.50 – 33.00)	-	-	-	8.17 ± 5.73\$ (0.00 – 26.00)
Executive function					
CPM ⁵	30.91 ± 3.41 (22.00 – 36.00)	29.54 ± 4.36 (20.00 – 36.00)	26.75 ± 5.26 (16.00 – 35.00)	22.14 ± 6.62\$ (14.00 – 33.00)	20.36 ± 8.08\$#^ (0.00 – 32.00)
Digit span backward ⁶	4.57 ± 1.07 (2.00 – 7.00)	4.06 ± 0.91 (2.00 – 6.00)	3.44 ± 1.03 (2.00 – 5.00)	2.43 ± 1.81\$ (0.00 – 6.00)	3.63 ± 0.96 (2.00 – 5.00)
CET ⁷	-	13.66 ± 3.84 (6.00 – 24.00)	14.86 ± 4.50 (10.00 – 23.00)	19.50 ± 3.87 (14.00 – 23.00)	-
Weigl's Test ⁸	-	12.45 ± 1.98 (8.00 – 15.00)	9.43 ± 4.15 (1.00 – 15.00)	7.50 ± 4.14# (4.00 – 15.00)	-
CST, perseverations** ^{9, 10}	0.11 ± 0.16 (0.00 – 0.83)	0.14 ± 0.14 (0.00 – 0.73)	0.16 ± 0.13 (0.04 – 0.40)	0.20 ± 0.18 (0.01 – 0.46)	-
Visuospatial Abilities					
Rey Figure copy ⁴	33.13 ± 2.46 (27.00 – 36.00)	-	-	-	19.35 ± 9.77\$ (1.50 – 36.00)
Language					
BADA (noun) ¹¹	29.79 ± 0.54 (28.00 – 30.00)	29.22 ± 0.99 (27.00 – 30.00)	28.00 ± 1.97 (24.00 – 30.00)	25.71 ± 5.94\$## (13.00 – 30.00)	-
BADA (action) ¹¹	27.68 ± 0.58 (26.00 – 28.00)	27.22 ± 1.07 (24.00 – 28.00)	24.88 ± 2.60\$ (20.00 – 28.00)	23.14 ± 4.48\$## (17.00 – 28.00)	-
Token Test ¹²	33.20 ± 2.10 (29.00 – 36.00)	-	-	-	27.47 ± 5.25\$ (13.00 – 36.00)
Fluency					
Phonemic fluency ¹³	38.50 ± 9.55 (18.00 – 55.00)	31.67 ± 9.71 (16.00 – 59.00)	26.55 ± 11.89 (5.00 – 55.00)	11.80 ± 5.54\$## (4.00 – 28.00)	14.38 ± 11.22\$#^ (0.00 – 37.00)
Index PF*** ¹⁴	4.68 ± 2.17 (2.60 – 12.05)	5.75 ± 2.54 (2.76 – 12.42)	9.34 ± 8.52 (2.64 – 35.00)	19.83 ± 12.56\$#^ (7.17 – 37.20)	-
Semantic fluency ¹³	43.74 ± 8.83 (27.00 – 60.00)	40.38 ± 9.04 (26.00 – 66.00)	34.20 ± 9.45 (20.00 – 55.00)	21.60 ± 4.88\$## (16.00 – 27.00)	22.59 ± 11.44\$#^ (0.00 – 48.00)
Index SF*** ¹⁴	3.89 ± 0.96 (2.49 – 6.50)	4.14 ± 1.43 (2.20 – 8.04)	6.73 ± 4.93 (2.63 – 22.22)	13.57 ± 6.85\$#^ (6.91 – 23.00)	-
Mood & Behavior					
BDI ¹⁵	5.00 ± 4.42 (0.00 – 15.00)	-	-	-	-
HDRS ¹⁶	-	6.34 ± 4.69 (0.00 – 22.00)	4.77 ± 3.44 (0.00 – 11.00)	6.60 ± 2.70 (3.00 – 10.00)	-

FBI total ¹⁷	-	2.11 ± 1.83 (0.00 – 7.00)	6.75 ± 7.21 (0.00 – 23.00)	9.75 ± 6.02 (4.00 – 18.00)	-
ALS-FTD-Q ¹⁸	-	8.35 ± 5.71 (2.00 – 20.00)	20.23 ± 14.29 (2.00 – 50.00)	5.00 ± 6.06 (1.00 – 14.00)	-
NPI ¹⁹	-	-	-	-	27.00 ± 15.83 (11.00 – 60.00)

Values are numbers or means ± standard deviations (range). Differences between patient groups and healthy controls were assessed using one-way ANOVA (statistical contrasts) corrected for age, sex and education. The number of patients performing each test is reported in table. \$: p<0.05 vs. HC; #: p < 0.05 vs. ALS-cn; ^: p < 0.05 vs. ALS-ci/bi. *= Ratio between the number of correct items and the maximum number of administered items; **= Perseverations are reported as the ratio between perseveration absolute number and the maximum number of cards provided during the test; ***= Verbal fluency indices were obtained as following: time for generation condition - time for control condition (reading or writing generated words)/total number of items generated. Abbreviations: ALS= Amyotrophic lateral sclerosis; ALS-ci/bi= ALS with cognitive/behavioral impairment; ALS-FTD= ALS with frontotemporal dementia; ALS-cn= ALS only with motor impairment; ALS-FTD-Q= ALS-FTD-questionnaire; BADA= Battery for aphasic deficit analysis; BDI= Beck Depression Inventory; bvFTD= behavioral variant of frontotemporal dementia; CET= Cognitive estimation test; CPM= Colored progressive matrices; CST= Card sorting tests; FBI= Frontal Behavioral Inventory; HDRS= Hamilton Depression Rating Scale; HC= Healthy controls; MMSE= Mini-Mental state examination; NPI= Neuropsychiatric inventory; PF= Phonemic fluency; RAVLT= Rey auditory verbal learning test; SF= Semantic fluency.

eReferences

- e1. Folstein MF, Folstein SE, McHugh PR. "Mini-mental state". A practical method for grading the cognitive state of patients for the clinician. *J Psychiatr Res* 1975;12:189-198.
- e2. Orsini A, Grossi D, Capitani E, et al. Verbal and spatial immediate memory span: normative data from 1355 adults and 1112 children. *Ital J Neurol Sci* 1987;8:539-548.
- e3. Carlesimo GA, Caltagirone C, Gainotti G. The Mental Deterioration Battery: normative data, diagnostic reliability and qualitative analyses of cognitive impairment. The Group for the Standardization of the Mental Deterioration Battery. *Eur Neurol* 1996;36:378-384.
- e4. Caffarra P, Vezzadini G, Dieci F, et al. Rey-Osterrieth complex figure: normative values in an Italian population sample. *Neurol Sci* 2002;22:443-447.
- e5. Basso A, Capitani E, Laiacona M. Raven's coloured progressive matrices: normative values on 305 adult normal controls. *Funct Neurol* 1987;2:189-194.
- e6. Monaco M, Costa A, Caltagirone C, et al. Forward and backward span for verbal and visuo-spatial data: standardization and normative data from an Italian adult population. *Neurol Sci* 2013;34:749-754.
- e7. Della Sala S, MacPherson SE, Phillips LH, et al. How many camels are there in Italy? Cognitive estimates standardised on the Italian population. *Neurol Sci* 2003;24:10-15.
- e8. Tognoni HSaG. Standardizzazione e Taratura Italiana di Test Neuropsicologici 1987.
- e9. Laiacona M, Inzaghi MG, De Tanti A, et al. Wisconsin card sorting test: a new global score, with Italian norms, and its relationship with the Weigl sorting test. *Neurol Sci* 2000;21:279-291.
- e10. Caffarra P, Vezzadini G, Dieci F, et al. Modified Card Sorting Test: normative data. *J Clin Exp Neuropsychol* 2004;26:246-250.
- e11. Miceli G, neuropsicologia UcdSCSd, psicologia CndrId. Batteria per l'analisi dei deficit afasici B.A.D.A: Servizio di neuropsicologia, Università cattolica del S. Cuore, 1994.
- e12. De Renzi E, Vignolo LA. The token test: A sensitive test to detect receptive disturbances in aphasics. *Brain* 1962;85:665-678.

- e13. Novelli G, Laiacona M, Papagno C, Vallar G, Capitani E, Cappa SF. Three clinical tests to research and rate the lexical performance of normal subjects. *Arch Psicol Neurol Psichiatr* 1986;47:477-506.
- e14. Abrahams S, Leigh PN, Harvey A, et al. Verbal fluency and executive dysfunction in amyotrophic lateral sclerosis (ALS). *Neuropsychologia* 2000;38:734-747.
- e15. Beck AT, Ward CH, Mendelson M, et al. An inventory for measuring depression. *Arch Gen Psychiatry* 1961;4:561-571.
- e16. Hamilton M. A rating scale for depression. *J Neurol Neurosurg Psychiatry* 1960;23:56-62.
- e17. Alberici A, Geroldi C, Cotelli M, et al. The Frontal Behavioural Inventory (Italian version) differentiates frontotemporal lobar degeneration variants from Alzheimer's disease. *Neurol Sci* 2007;28:80-86.
- e18. Raaphorst J, Beeldman E, Schmand B, et al. The ALS-FTD-Q: a new screening tool for behavioral disturbances in ALS. *Neurology* 2012;79:1377-1383.
- e19. Cummings JL, Mega M, Gray K, et al. The Neuropsychiatric Inventory: comprehensive assessment of psychopathology in dementia. *Neurology* 1994;44:2308-2314.

eTable 2. MRI acquisition parameters.

	Philips Medical System Intera 3T scan				
	T2-weighted SE	FLAIR	3D T1-weighted FFE	Pulsed-gradient SE echo planar with sensitivity encoding	T2*-weighted single-shot EPI sequence (resting state fMRI)
Repetition time (msec)	3500	11000	25	8986	3000
Echo time (msec)	85	120	4.6	80	35
Flip angle	90°	90°	30°	-	90°
Section thickness (mm)	5	5	-	2.5	4
No. of sections	22	22	220	55	30 for 220 volumes
Matrix	512x512	512x512	256x256	96x96	128x128
Field of view (mm²)	230x184	230x230	230x182	240x240	240x240
Diffusion gradient directions	-	-	-	32	-
<i>b</i> value sec/mm²	-	-	-	1000	-

Abbreviations: FFE= fast field echo; FLAIR= fluid-attenuated inversion recovery; FSE= fast spin echo; MRI= magnetic resonance imaging; msec= millisecond; mm= millimeter; No= number; SE=spin echo; sec=second

eTable 3. Brain nodes of the network.

N	Node	Lobe	N	Node	Lobe	N	Node	Lobe
1	Precentral_L_p1	SENSMOT	75	Insula_L_p2	FRONT-INS	149	Parietal_Inf_L_p1	PAR
2	Precentral_L_p2	SENSMOT	76	Insula_L_p3	FRONT-INS	150	Parietal_Inf_L_p2	PAR
3	Precentral_L_p3	SENSMOT	77	Insula_R_p1	FRONT-INS	151	Parietal_Inf_L_p3	PAR
4	Precentral_L_p4	SENSMOT	78	Insula_R_p2	FRONT-INS	152	Parietal_Inf_R_p1	PAR
5	Precentral_L_p5	SENSMOT	79	Cingulum_Ant_L_p1	FRONT-INS	153	Parietal_Inf_R_p2	PAR
6	Precentral_R_p1	SENSMOT	80	Cingulum_Ant_L_p2	FRONT-INS	154	SupraMarginal_L_p1	PAR
7	Precentral_R_p2	SENSMOT	81	Cingulum_Ant_R_p1	FRONT-INS	155	SupraMarginal_L_p2	PAR
8	Precentral_R_p3	SENSMOT	82	Cingulum_Ant_R_p2	FRONT-INS	156	SupraMarginal_R_p1	PAR
9	Precentral_R_p4	SENSMOT	83	Cingulum_Mid_L_p1	FRONT-INS	157	SupraMarginal_R_p2	PAR
10	Precentral_R_p5	SENSMOT	84	Cingulum_Mid_L_p2	FRONT-INS	158	SupraMarginal_R_p3	PAR
11	Frontal_Sup_L_p1	FRONT-INS	85	Cingulum_Mid_L_p3	FRONT-INS	159	Angular_L_p1	PAR
12	Frontal_Sup_L_p2	FRONT-INS	86	Cingulum_Mid_R_p1	FRONT-INS	160	Angular_L_p2	PAR
13	Frontal_Sup_L_p3	FRONT-INS	87	Cingulum_Mid_R_p2	FRONT-INS	161	Angular_R_p1	PAR
14	Frontal_Sup_L_p4	FRONT-INS	88	Cingulum_Mid_R_p3	FRONT-INS	162	Angular_R_p2	PAR
15	Frontal_Sup_L_p5	FRONT-INS	89	Cingulum_Post_L_p1	PAR	163	Precuneus_L_p1	PAR
16	Frontal_Sup_R_p1	FRONT-INS	90	Cingulum_Post_R_p1	PAR	164	Precuneus_L_p2	PAR
17	Frontal_Sup_R_p2	FRONT-INS	91	Hippocampus_L_p1	TEMP	165	Precuneus_L_p3	PAR
18	Frontal_Sup_R_p3	FRONT-INS	92	Hippocampus_R_p1	TEMP	166	Precuneus_L_p4	PAR
19	Frontal_Sup_R_p4	FRONT-INS	93	ParaHippocampal_L_p1	TEMP	167	Precuneus_L_p5	PAR
20	Frontal_Sup_R_p5	FRONT-INS	94	ParaHippocampal_R_p1	TEMP	168	Precuneus_R_p1	PAR
21	Frontal_Sup_Orb_L_p1	FRONT-INS	95	ParaHippocampal_R_p2	TEMP	169	Precuneus_R_p2	PAR
22	Frontal_Sup_Orb_R_p1	FRONT-INS	96	Amygdala_L_p1	TEMP	170	Precuneus_R_p3	PAR
23	Frontal_Mid_L_p1	FRONT-INS	97	Amygdala_R_p1	TEMP	171	Precuneus_R_p4	PAR
24	Frontal_Mid_L_p2	FRONT-INS	98	Calcarine_L_p1	OCC	172	Paracentral_Lobule_L_p1	SENSMOT
25	Frontal_Mid_L_p3	FRONT-INS	99	Calcarine_L_p2	OCC	173	Paracentral_Lobule_L_p2	SENSMOT
26	Frontal_Mid_L_p4	FRONT-INS	100	Calcarine_L_p3	OCC	174	Paracentral_Lobule_R_p1	SENSMOT
27	Frontal_Mid_L_p5	FRONT-INS	101	Calcarine_R_p1	OCC	175	Caudate_L_p1	BG
28	Frontal_Mid_L_p6	FRONT-INS	102	Calcarine_R_p2	OCC	176	Caudate_R_p1	BG
29	Frontal_Mid_L_p7	FRONT-INS	103	Calcarine_R_p3	OCC	177	Putamen_L_p1	BG
30	Frontal_Mid_R_p1	FRONT-INS	104	Cuneus_L_p1	OCC	178	Putamen_R_p1	BG
31	Frontal_Mid_R_p2	FRONT-INS	105	Cuneus_L_p2	OCC	179	Pallidum_L_p1	BG
32	Frontal_Mid_R_p3	FRONT-INS	106	Cuneus_R_p1	OCC	180	Pallidum_R_p1	BG
33	Frontal_Mid_R_p4	FRONT-INS	107	Cuneus_R_p2	OCC	181	Thalamus_L_p1	BG
34	Frontal_Mid_R_p5	FRONT-INS	108	Lingual_L_p1	OCC	182	Thalamus_R_p1	BG
35	Frontal_Mid_R_p6	FRONT-INS	109	Lingual_L_p2	OCC	183	Heschl_L_p1	TEMP
36	Frontal_Mid_R_p7	FRONT-INS	110	Lingual_L_p3	OCC	184	Heschl_R_p1	TEMP
37	Frontal_Mid_Orb_L_p1	FRONT-INS	111	Lingual_R_p1	OCC	185	Temporal_Sup_L_p1	TEMP
38	Frontal_Mid_Orb_R_p1	FRONT-INS	112	Lingual_R_p2	OCC	186	Temporal_Sup_L_p2	TEMP
39	Frontal_Inf_Oper_L_p1	FRONT-INS	113	Lingual_R_p3	OCC	187	Temporal_Sup_L_p3	TEMP
40	Frontal_Inf_Oper_R_p1	FRONT-INS	114	Occipital_Sup_L_p1	OCC	188	Temporal_Sup_R_p1	TEMP
41	Frontal_Inf_Oper_R_p2	FRONT-INS	115	Occipital_Sup_L_p2	OCC	189	Temporal_Sup_R_p2	TEMP

42	Frontal_Inf_Tri_L_p1	FRONT-INS	116	Occipital_Sup_R_p1	OCC	190	Temporal_Sup_R_p3	TEMP
43	Frontal_Inf_Tri_L_p2	FRONT-INS	117	Occipital_Sup_R_p2	OCC	191	Temporal_Sup_R_p4	TEMP
44	Frontal_Inf_Tri_L_p3	FRONT-INS	118	Occipital_Mid_L_p1	OCC	192	Temporal_Pole_Sup_L_p1	TEMP
45	Frontal_Inf_Tri_R_p1	FRONT-INS	119	Occipital_Mid_L_p2	OCC	193	Temporal_Pole_Sup_L_p2	TEMP
46	Frontal_Inf_Tri_R_p2	FRONT-INS	120	Occipital_Mid_L_p3	OCC	194	Temporal_Pole_Sup_R_p1	TEMP
47	Frontal_Inf_Tri_R_p3	FRONT-INS	121	Occipital_Mid_L_p4	OCC	195	Temporal_Pole_Sup_R_p2	TEMP
48	Frontal_Inf_Orb_L_p1	FRONT-INS	122	Occipital_Mid_R_p1	OCC	196	Temporal_Mid_L_p1	TEMP
49	Frontal_Inf_Orb_L_p2	FRONT-INS	123	Occipital_Mid_R_p2	OCC	197	Temporal_Mid_L_p2	TEMP
50	Frontal_Inf_Orb_R_p1	FRONT-INS	124	Occipital_Mid_R_p3	OCC	198	Temporal_Mid_L_p3	TEMP
51	Frontal_Inf_Orb_R_p2	FRONT-INS	125	Occipital_Inf_L_p1	OCC	199	Temporal_Mid_L_p4	TEMP
52	Rolandic_Oper_L_p1	FRONT-INS	126	Occipital_Inf_R_p1	OCC	200	Temporal_Mid_L_p5	TEMP
53	Rolandic_Oper_R_p1	FRONT-INS	127	Fusiform_L_p1	TEMP	201	Temporal_Mid_L_p6	TEMP
54	Rolandic_Oper_R_p2	FRONT-INS	128	Fusiform_L_p2	TEMP	202	Temporal_Mid_L_p7	TEMP
55	Supp_Motor_Area_L_p1	SENSMOT	129	Fusiform_L_p3	TEMP	203	Temporal_Mid_R_p1	TEMP
56	Supp_Motor_Area_L_p2	SENSMOT	130	Fusiform_R_p1	TEMP	204	Temporal_Mid_R_p2	TEMP
57	Supp_Motor_Area_L_p3	SENSMOT	131	Fusiform_R_p2	TEMP	205	Temporal_Mid_R_p3	TEMP
58	Supp_Motor_Area_R_p1	SENSMOT	132	Fusiform_R_p3	TEMP	206	Temporal_Mid_R_p4	TEMP
59	Supp_Motor_Area_R_p2	SENSMOT	133	Postcentral_L_p1	SENSMOT	207	Temporal_Mid_R_p5	TEMP
60	Supp_Motor_Area_R_p3	SENSMOT	134	Postcentral_L_p2	SENSMOT	208	Temporal_Mid_R_p6	TEMP
61	Olfactory_L_p1	FRONT-INS	135	Postcentral_L_p3	SENSMOT	209	Temporal_Pole_Mid_L_p1	TEMP
62	Olfactory_R_p1	FRONT-INS	136	Postcentral_L_p4	SENSMOT	210	Temporal_Pole_Mid_R_p1	TEMP
63	Frontal_Sup_Medial_L_p1	FRONT-INS	137	Postcentral_L_p5	SENSMOT	211	Temporal_Pole_Mid_R_p2	TEMP
64	Frontal_Sup_Medial_L_p2	FRONT-INS	138	Postcentral_R_p1	SENSMOT	212	Temporal_Inf_L_p1	TEMP
65	Frontal_Sup_Medial_L_p3	FRONT-INS	139	Postcentral_R_p2	SENSMOT	213	Temporal_Inf_L_p2	TEMP
66	Frontal_Sup_Medial_L_p4	FRONT-INS	140	Postcentral_R_p3	SENSMOT	214	Temporal_Inf_L_p3	TEMP
67	Frontal_Sup_Medial_R_p1	FRONT-INS	141	Postcentral_R_p4	SENSMOT	215	Temporal_Inf_L_p4	TEMP
68	Frontal_Sup_Medial_R_p2	FRONT-INS	142	Postcentral_R_p5	SENSMOT	216	Temporal_Inf_R_p1	TEMP
69	Frontal_Sup_Medial_R_p3	FRONT-INS	143	Parietal_Sup_L_p1	PAR	217	Temporal_Inf_R_p2	TEMP
70	Frontal_Mid_Orb_L_p2	FRONT-INS	144	Parietal_Sup_L_p2	PAR	218	Temporal_Inf_R_p3	TEMP
71	Frontal_Mid_Orb_R_p2	FRONT-INS	145	Parietal_Sup_L_p3	PAR	219	Temporal_Inf_R_p4	TEMP
72	Rectus_L_p1	FRONT-INS	146	Parietal_Sup_R_p1	PAR	220	Temporal_Inf_R_p5	TEMP
73	Rectus_R_p1	FRONT-INS	147	Parietal_Sup_R_p2	PAR			
74	Insula_L_p1	FRONT-INS	148	Parietal_Sup_R_p3	PAR			

Abbreviations: Ant= anterior; BG= basal ganglia; FRONT-INS= fronto-insular; Inf= inferior; L= left; Mid= middle; N= region number; Oper= operculum; OCC= occipital; Orb= orbital; p= part; PAR= parietal; Post= posterior; R= right; SENSMOT= sensorimotor; Sup= superior; Supp= supplementary; TEMP= temporal; Tri= triangularis

eTable 4. Structural and functional distribution measures of the normalized inter- and intra-area connectivity values in patient groups.

Structural Connectivity										
Intra-area and Inter-area connections	ALS-cn	ALS-ci/bi	ALS-FTD	bvFTD	p value ALS-cn vs bvFTD	p value ALS-cn vs ALS-ci/bi	p value ALS-cn vs ALS-FTD	p value ALS-ci/bi vs bvFTD	p value ALS-ci/bi vs ALS-FTD	p value ALS-FTD vs bvFTD
Frontal	-0.05 ± 0.37 (56%)	-0.13 ± 0.48 (67%)	-0.53 ± 0.56 (75%)	-0.70 ± 0.42 (100%)	<0.001	1.00	0.03	<0.001	0.09	1.00
Frontal-Sensorimotor	-0.22 ± 0.41 (65%)	-0.32 ± 0.39 (81%)	-0.70 ± 0.63 (100%)	-0.45 ± 0.40 (94%)	0.21	1.00	0.02	1.00	0.10	0.59
Frontal-Basal Ganglia	-0.09 ± 0.51 (61%)	-0.09 ± 0.64 (57%)	-0.48 ± 0.59 (75%)	-0.78 ± 0.57 (91%)	<0.001	1.00	0.44	<0.001	0.45	1.00
Frontal-Parietal	-0.06 ± 0.50 (63%)	-0.05 ± 0.63 (52%)	-0.17 ± 0.64 (38%)	-0.41 ± 0.43 (86%)	0.01	1.00	1.00	0.07	1.00	1.00
Frontal-Temporal	-0.09 ± 0.45 (59%)	-0.11 ± 0.52 (67%)	-0.44 ± 0.54 (75%)	-0.48 ± 0.36 (92%)	0.002	1.00	0.27	0.01	0.22	1.00
Sensorimotor-Basal Ganglia	-0.50 ± 0.48 (81%)	-0.49 ± 0.57 (81%)	-0.90 ± 0.88 (88%)	-0.13 ± 0.57 (66%)	0.01	1.00	0.48	0.17	0.47	0.01
Basal Ganglia-Temporal	-0.25 ± 0.42 (67%)	-0.16 ± 0.51 (57%)	-0.55 ± 0.41 (100%)	-0.68 ± 0.42 (100%)	<0.001	1.00	0.46	<0.001	0.11	1.00
Basal Ganglia-Occipital	-0.07 ± 0.68 (54%)	-0.17 ± 1.00 (43%)	-0.61 ± 0.87 (75%)	-0.69 ± 0.94 (80%)	0.01	1.00	0.77	0.20	1.00	1.00
Parietal	-0.11 ± 0.40 (59%)	-0.12 ± 0.44 (57%)	-0.41 ± 0.47 (88%)	-0.38 ± 0.42 (89%)	0.04	1.00	0.36	0.11	0.38	1.00
Parietal-Temporal	-0.11 ± 0.51 (57%)	-0.22 ± 0.55 (71%)	0.05 ± 0.75 (50%)	-0.53 ± 0.52 (83%)	0.01	1.00	1.00	0.14	1.00	0.052
Parietal-Occipital	-0.08 ± 0.42 (59%)	-0.12 ± 0.53 (48%)	-0.22 ± 0.30 (75%)	-0.40 ± 0.45 (89%)	0.01	1.00	1.00	0.14	1.00	1.00
Temporal	-0.05 ± 0.29 (54%)	-0.09 ± 0.39 (57%)	-0.07 ± 0.41 (38%)	-0.31 ± 0.32 (86%)	0.01	1.00	1.00	0.03	1.00	0.51
Temporal-Occipital	-0.02 ± 0.40 (56%)	-0.08 ± 0.50 (52%)	-0.12 ± 0.31 (63%)	-0.30 ± 0.39 (77%)	0.03	1.00	1.00	0.28	1.00	1.00

Functional Connectivity										
Frontal-Sensorimotor	0.11 ± 0.56 (48%)	0.41 ± 0.59 (33%)	0.14 ± 0.40 (50%)	-0.12 ± 0.33 (63%)	0.21	0.09	1.00	0.001	1.00	0.70
Frontal-Temporal	0.03 ± 0.55 (52%)	-0.19 ± 0.78 (67%)	-0.49 ± 0.19 (100%)	-0.45 ± 0.45 (83%)	0.001	1.00	0.13	0.06	0.44	1.00
Sensorimotor	0.003 ± 0.54 (53%)	0.23 ± 0.54 (29%)	-0.15 ± 0.14 (88%)	-0.28 ± 0.41 (74%)	0.12	0.04	1.00	<0.001	0.15	1.00
Sensorimotor-Parietal	0.17 ± 0.55 (37%)	0.06 ± 0.47 (43%)	-0.07 ± 0.34 (50%)	-0.17 ± 0.45 (69%)	0.02	1.00	1.00	0.34	1.00	1.00
Sensorimotor-Temporal	0.005 ± 0.83 (54%)	0.03 ± 1.06 (48%)	-0.98 ± 0.41 (88%)	-0.28 ± 0.94 (60%)	1.00	1.00	0.03	0.48	0.01	0.18
Parietal-Temporal	-0.04 ± 0.58 (52%)	0.13 ± 0.51 (24%)	-0.25 ± 0.33 (75%)	-0.28 ± 0.45 (71%)	0.26	1.00	1.00	0.03	0.35	1.00

Values are numbers or means ± standard deviations (percentage of people with normalized connectivity value below 0). Inter- and intra-area connectivity values significantly different in at least one comparison are reported. P values refer to ANOVA models, followed by post-hoc pairwise comparisons (Bonferroni-corrected for multiple comparisons). Significant p value < 0.05. Abbreviations: ALS-ci/bi= Amyotrophic lateral sclerosis with cognitive and/or behavioral impairment; ALS-FTD= ALS with frontotemporal dementia; ALS-cn= Amyotrophic lateral sclerosis with only motor impairment; bvFTD= behavioral variant of Frontotemporal Dementia

eTable 5. Classification (ROC curves) analysis for identification of the “ALS-cn-like pattern” and the “bvFTD-like pattern”.

Structural Connectivity			
Intra-area and Inter-areas connections	AUC bvFTD vs ALS- cn	AUC ALS-cn vs bvFTD	Best Cut-off (Youden’s index)
Frontal	0.88	0.12	-0.21 (0.68)
Frontal-Basal Ganglia	0.82	0.18	-0.67 (0.52)
Frontal-Parietal	0.71	0.29	-0.30 (0.37)
Frontal-Temporal	0.76	0.24	-0.20 (0.44)
Sensorimotor-Basal Ganglia	0.33	0.67	-0.55 (0.30)
Basal Ganglia-Temporal	0.78	0.22	-0.52 (0.45)
Basal Ganglia-Occipital	0.72	0.28	-0.47 (0.42)
Parietal	0.67	0.33	0.003 (0.31)
Parietal-Temporal	0.72	0.28	-0.36 (0.43)
Parietal-Occipital	0.69	0.31	-0.08 (0.35)
Temporal	0.75	0.25	-0.2 (0.41)
Temporal-Occipital	0.70	0.30	-0.40 (0.35)
Functional Connectivity			
Frontal-Temporal	0.77	0.23	-0.27 (0.48)
Sensorimotor-Parietal	0.67	0.33	-0.04 (0.34)

The Area Under the ROC curve represents the capability of the structural and functional connectivity damage within the reported intra- and inter-areas to discriminate bvFTD from ALS-cn and viceversa. Only intra-area and inter-areas connections significantly different between the two groups were considered. Bold values in the column “bvFTD vs ALS-cn” identify the “bvFTD-like pattern”. Bold values in the column “ALS-cn vs bvFTD” identify the “ALS-cn-like pattern”. The optimal cut-off per each connectivity distribution was calculated through the Youden’s index, maximizing sensibility and specificity. Cut-off= sensibility-(1-specificity). Abbreviations: ALS-cn= Amyotrophic lateral sclerosis with only motor impairment; AUC= Area Under the ROC curve; bvFTD= behavioral variant of Frontotemporal Dementia.

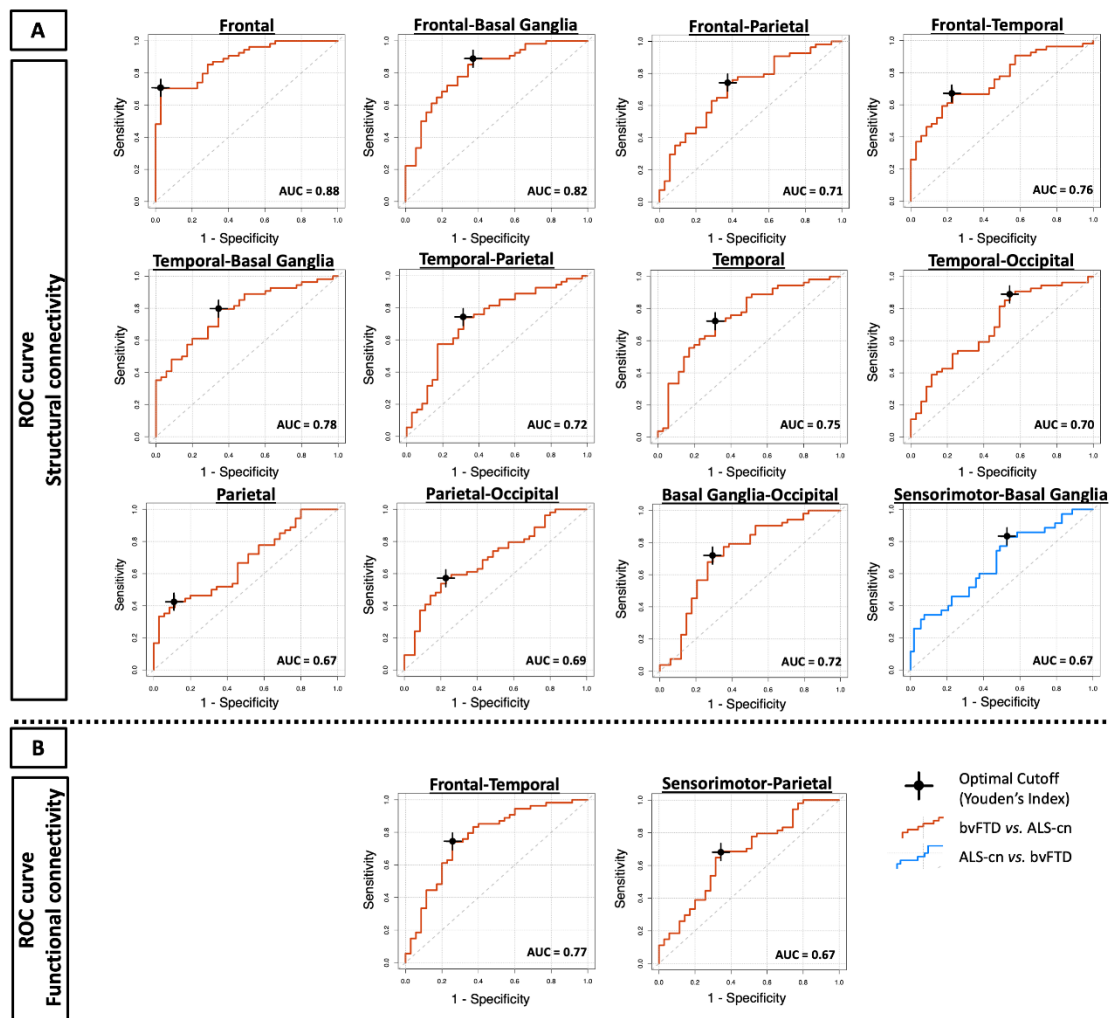
eTable 6. Frequency analysis for the identification of ALS-cn-like or bvFTD-like patterns in ALS-ci/bi and ALS-FTD patients.

Structural Connectivity									
Intra-area and Inter-area connections	N ALS-cn below cutoff (%)	N ALS-ci/bi below cutoff (%)	N ALS-FTD below cutoff (%)	N bvFTD below cutoff (%)	p: ALS-ci/bi vs ALS-cn	p ALS-ci/bi vs bvFTD	p: ALS-FTD vs ALS-cn	p: ALS-FTD vs bvFTD	p: ALS-ci/bi vs ALS-FTD
Frontal	16 (30%)	10 (48%)	5 (63%)	-	0.12	-	0.08	-	0.38
Frontal-Basal Ganglia	6 (11%)	5 (24%)	3 (38%)	-	0.15	-	0.08	-	0.38
Frontal-Parietal	14 (26%)	8 (38%)	2 (25%)	-	0.22	-	0.66	-	0.42
Frontal-Temporal	18 (33%)	9 (43%)	5 (63%)	-	0.31	-	0.12	-	0.43
Sensorimotor-Basal Ganglia	-	9 (43%)	4 (50%)	6 (17%)	-	0.04	-	0.07	0.53
Basal Ganglia-Temporal	11 (20%)	5(24%)	4 (50%)	-	0.48	-	0.09	-	0.18
Basal Ganglia-Occipital	15 (28%)	7 (33%)	3 (38%)	-	0.42	-	0.42	-	0.58
Parietal	31 (57%)	12 (57%)	7 (88%)		0.59	-	0.10	-	0.14
Parietal-Temporal	14 (26%)	8 (38%)	3 (38%)	-	0.22	-	0.38	-	0.66
Parietal-Occipital	23 (43%)	10 (48%)	4 (50%)	-	0.45	-	0.49	-	0.62
Temporal	15 (28%)	7 (33%)	3 (38%)	-	0.42	-	0.42	-	0.58
Temporal-Occipital	6 (11%)	6 (29%)	3 (38%)	-	0.07	-	0.08	-	0.48

Functional Connectivity									
Frontal-Temporal	14 (26%)	11 (52%)	8 (100%)	-	0.03	-	<0.001	-	0.02
Sensorimotor-Parietal	17 (31%)	8 (38%)	4 (50%)	-	0.39	-	0.26	-	0.43

Per each group, the number (N) and the respective percentage (%) of patients with structural/ functional connectivity values below the optimal cutoff are reported. Within ‘bvFTD-like pattern’, frequency analysis, using Chi-squared test was performed only between ALS groups, excluding the. Within ‘ALS-cn-like pattern’, frequency analysis was performed between bvFTD, ALS-ci/bi and ALS FTD, excluding ALS-cn group. Significant results are highlight in bold. Abbreviations: ALS-ci/bi= Amyotrophic lateral sclerosis with cognitive and/or behavioral impairment; ALS-FTD= ALS with frontotemporal dementia; ALS-cn= ALS with only motor impairment; AUC= Area Under the ROC curve; bvFTD= behavioral variant of Frontotemporal Dementia.

eFigure 1. Classification analysis. The ROC curves for the identification of the structural (A) and functional (B) characteristic patterns (ALS-cn-like and bvFTD-like) are shown. The curves in red represent the discriminative capability to distinguish bvFTD from ALS-cn (lower values of structural inter- and intra-area connectivity better identified bvFTD), while the curves in blue represent the opposite discriminative capability (lower values of structural inter- and intra-area connectivity better identified ALS-cn from bvFTD). Per each ROC curve, the area under the curve is reported as well as the optimal cutoff, obtained as Youden's index. Abbreviations: ALS-cn= ALS with motor impairment only; AUC= Area under the curve; bvFTD= behavioral variant of Frontotemporal Dementia.



6. GENERAL DISCUSSION

In this dissertation, I aimed to describe the patterns of neurodegeneration and the alterations of brain network connectivity in presentations of the FTLN spectrum. In the first part, the focus was on MND presentations, in particular on MRI multimodal biomarkers and predictors of disease evolution, in terms of both motor and cognitive impairment. Subsequently, we looked for volumetric MRI signatures and patterns of functional network reorganization propagating from the corresponding disease epicenter in FTD presentations (i.e., bvFTD, nfvPPA and svPPA variants). Finally, we provided further evidence supporting the notion of a continuum across FTD and MND, both in sporadic and in genetic presentations of FTLN, by means of volumetric and network-based MRI analyses. In the following paragraphs, the most relevant implications of each of the studies previously reported will be critically discussed, in order to draw some general conclusions.

Neuroimaging progression markers in motor neuron disease

In **Chapter 3.1**, I explored the comprehensive use of clinical, cognitive and multimodal MRI variables for the development of a prognostic survival model in a large cohort of patients with different MND presentations. The inclusion of quantitative measures of structural brain damage into a multivariable model based on clinical and cognitive data provided a significant increase of accuracy for survival prediction at 4-year follow-up across MND phenotypes and, specifically, in patients with a classic ALS presentation. The greatest improvement for a prognostic definition was provided by measures of frontal and temporal cortical atrophy, as well as DT MRI metrics of both motor and extra-motor white matter (WM) tracts. The novelty and, therefore, the relevance of this study lies on both methodological and factual aspects. Similar to a recent large multicenter study (Westeneng, Debray et al., 2018), which led to the development of the European Network to Cure ALS (ENCALS) survival model (<http://www.encalssurvivalmodel.org/>), we applied a data-driven approach for the identification of survival groups in MND. Here, we went a step further, including also the findings provided by advanced MRI techniques into a multimodal approach that, as we suggest, should be combined with clinical and cognitive features at an individual patient level. Moreover, the presence of corticospinal tract (CST) DT MRI measures among

survival predictors, consistent with previous studies in ALS patients (Agosta et al., 2010, Schuster et al., 2017), supports the translation of this measure of UMN damage to the clinical practice not only as a diagnostic, but also as a prognostic tool. Also, the relevant prognostic role of frontotemporal cortical regions and associative WM tracts suggests that the involvement of extra-motor brain regions in MND might reflect a more advanced pathological stage (Brettschneider et al., 2013), and therefore a more rapid progression to death/tracheostomy.

I then focused my attention on pure lower motor neuron (PLMN) phenotypes (**Chapter 3.2**), in order to investigate cerebral damage in these presentations which are expected to show minimal or absent CNS involvement. Amongst PLMN phenotypes, Kennedy's disease (KD) is an X-linked condition showing slow disease progression and normal or minimally reduced life expectancy that is often initially misdiagnosed as ALS. Our study demonstrated the absence of WM abnormalities in patients with KD and PLMN with a slow progression, in contrast with diffuse WM damage in ALS and focal CST degeneration in PLMN-fast. These findings have clear prognostic implications and support the use of DT MRI measures as powerful tools to differentiate fast- and slow-progressing MND, including KD. However, we also showed that more than one third of KD and PLMN patients did show some degree of mild cognitive and/or behavioral alterations on neuropsychological testing, in line with previous observations in these MND phenotypes (Phukan, Elamin et al., 2012, Raaphorst, de Visser et al., 2011, Spinelli et al., 2016). The absence of significant differences from healthy controls indicated by structural MRI analysis in KD and LMND-slow patients of the present study suggests that neuroanatomical correlates of cognitive and behavioral impairment in slow-progressing MND presentations should be sought in either functional rearrangements or very subtle structural alterations, not detectable using the standard volumetric and tractography techniques here applied.

In another study dedicated to the assessment of MRI outcomes and predictors of disease progression in ALS (**Chapter 3.3**), we performed a longitudinal follow-up of patients enrolled within one year from clinical diagnosis, who showed consequently mild disease severity at baseline. Whereas no significant grey matter (GM) cortical thinning was detected either at baseline or longitudinally, analysis of WM microstructure showed significant decrease of fractional anisotropy (FA) in motor and anterior frontal tracts of

ALS patients at baseline, as well as widespread progression of WM damage over 1 year. The rate of decline of the ALS Functional Rating Scale revised (ALSFRS-r) was associated with the rate of FA decrease in the body of the corpus callosum, suggesting that functional decline in ALS might at least partially derive from an interhemispheric disconnection between contralateral motor networks. Moreover, lower FA of the cerebral peduncle at baseline was associated with faster subsequent clinical progression, indicating the importance of this measure as a prognostic tool. Once again, our data suggest that a multiparametric approach including DT MRI measures of brain damage would provide an optimal method for an accurate stratification of ALS patients into prognostic classes.

In **Chapter 3.4**, we further extended our attention, using up-to-date graph analysis and connectomic MRI techniques to explore both structural and functional brain networks in different variants of the MND spectrum. Patients with ALS and primary lateral sclerosis (PLS) shared alterations of structural global and lobar network properties and regional connectivity, with a specific involvement of sensorimotor and extra-motor frontotemporal areas, whereas progressive muscular atrophy (PMA) patients showed preserved structural and functional connectomes. Moreover, in both ALS and PLS groups, alterations in structural connectivity correlated with measures of motor impairment, while functional connectivity disruptions were mostly related to executive dysfunctions and behavioral disturbances. Therefore, the application of advanced network-based neuroimaging techniques deepened previous findings of standard MRI techniques, providing additional information about how networks are embedded and interact in the brain of different phenotypes within the MND spectrum. Moreover, the use of a common parcellating system helped to bridge the gap between anatomical and functional connectivity data, allowing a straightforward comparison between the two types of information. Particularly, our findings were consistent with previous DT MRI studies that reported the presence of an impaired subnetwork including bilateral primary motor regions, supplementary motor areas and basal ganglia (Buchanan et al., 2015). Furthermore, our study highlights that affected extra-motor regions are structurally connected to the sensorimotor network, known to be the “epicenter” of the degenerative process of the disease (Brettschneider et al., 2013). This hypothesis is consistent with the pattern of progression of TDP-43 pathological burden described by Brettschneider et al.

(Brettschneider et al., 2013) in *post mortem* tissue, and supports a network-based degeneration model in ALS (Seeley, Crawford et al., 2009), although longitudinal MRI studies are needed to validate this hypothesis.

Taken collectively, the results of the studies reported in **Chapter 3** of the present dissertation strongly suggest that advanced MRI analyses hold the promise to provide an objective *in vivo* assessment of MND-related pathological changes across brain networks, delivering potential biomarkers for disease monitoring and prognostic stratification.

Tracking neurodegeneration in frontotemporal dementia variants

In a first study assessing FTD clinical presentations and neuroanatomical correlates underlying their intrinsic heterogeneity, we focused on nfvPPA (**Chapter 4.1**). In particular, we compared connected speech samples and MRI volumetric findings in monolingual English and Italian speakers with a diagnosis of nfvPPA, to validate our hypothesis that, despite a similar brain cortical damage, English-speaking nfvPPA patients might show higher number of distortions and motor speech errors, while Italian patients might show more morpho-syntactic difficulties. During connected speech samples, nfvPPA-E cases showed higher number of distortions, whereas nfvPPA-I had reduced mean length of sentences and showed greater difficulty in syntax comprehension. By contrast, both patient groups showed similar degree of GM atrophy of the left pars opercularis of the inferior frontal gyrus, premotor cortex, anterior insula, pre-SMA, angular gyrus, and striatum. These findings suggest that similar patterns of brain atrophy might be associated with different symptomatology depending on the patients native language. Therefore, applying current PPA sub-variants diagnostic criteria – conceived in an English-speaking cultural context (Gorno-Tempini et al., 2011) – to patients speaking languages with different features might lead to misdiagnosis or at least diagnostic confusion. Of note, our results also indicate that volume loss in GM structures of the speech production network (Mandelli, Welch et al., 2018) might be considered as a characteristic, “transcultural” signature of nfvPPA presentations.

Similar to our approach to the study of MND, we further enlarged our focus to all FTD presentations, including bvFTD, nfvPPA and svPPA patients in a study applying a novel RS-fMRI connectomic paradigm, i.e., stepwise functional connectivity (SFC) analysis (**Chapter 4.2**). Here, I explored the pattern of rearrangements of functional connectivity

at increasing topological distance from the disease epicenters of FTD clinical variants. Selecting the peaks of atrophy of an independent cohort of patients with high confidence of FTLD pathology as the seed regions for a subsequent whole-brain SFC analyses, all patient groups showed extensive reductions of functional connectivity in brain regions with direct and intermediate connections with the respective seed regions. In addition to this, FTD patients also showed more localized increases of functional connectivity involving either short-range direct connections or more distant indirect connections. In the case of svPPA, we also demonstrated a relationship between SFC architecture of the healthy brain from the disease epicenter and the regional distribution of atrophy in patients. These findings open fundamental insights supporting the notion of FTD variants as “disconnection syndromes”, providing also promising perspectives to understand the physiopathological underpinnings and to model disease progression in these complex clinical presentations.

Neurodegeneration patterns across the ALS/FTD continuum

Finally, in **Chapter 5** of this dissertation, advanced MRI techniques were used to explore brain structural and functional changes across different presentations of the ALS/FTD continuum, with the ultimate goal of mapping spatiotemporal patterns of converging and diverging network alterations underlying the clinical, genetic and pathological overlap of these conditions.

In **Chapter 5.1**, I focused on GM volumetric signatures of genetic presentations within the ALS/FTD continuum. Of note, genetically determined FTLD patients (i.e., both FTD and MND presentations) consistently showed greater GM disruption, compared with sporadic cases who were matched for clinical presentation and degree of functional and cognitive impairment. In particular, the involvement of parietal cortices, thalami and posterior cerebellar regions was observed consistently in genetic FTLD cases, in contrast with sporadic FTD showing atrophy mostly affecting fronto-temporo-insular regions and basal ganglia, and sporadic MND displaying focal damage of motor cortical regions. I also described distinctive patterns of atrophy that associate with each specific mutation, identifying the reduction of thalamic and caudate volumes as mostly indicative of *C9orf72*-mutated cases, in particular for patients presenting with MND. The inverse correlation between thalamic volumes and behavioral impairment in genetic FTLD

patients, which was mostly driven by *C9orf72* mutation carriers, also supports a significant influence of such characteristic neuroanatomical damage over the progression of neurobehavioral impairment in *C9orf72*-related FTL, consistent with the involvement of the thalami in cognition and complex behavior (Wolff & Vann, 2019). Therefore, our results strongly point towards the use of measures of deep GM involvement as useful markers of *C9orf72*-related disorders, regardless of the clinical presentation within the FTL spectrum. More in general, this study also provided interesting insights into the pathophysiology of genetic FTL, suggesting possible neuroimaging markers of underlying pathology that may help to disentangle the heterogeneity of FTL disorders, and possibly serve as outcome measures in clinical trials targeting specific genetic mutations.

Finally, the multiparametric MRI study reported in **Chapter 5.2** assessed sporadic patients with ALS/FTD clinical presentations. A connectome-based approach was adopted, first, to identify the connectivity signatures of ALS-cognitively normal (ALS-cn) and bvFTD (i.e., the two ends of this spectrum) and, subsequently, to characterize the alterations underlying mild cognitive/behavioral deficits (i.e., ALS-ci/bi) and full-blown dementia in ALS patients, with the aid of mathematical models and single-subject analysis. Patients with ALS-ci/bi displayed an ALS-cn-like pattern of structural damage, whereas functional data showed enhanced functional connectivity within the sensorimotor regions and decreased functional connectivity in the frontotemporal areas (therefore, mirroring a bvFTD-like pattern). Finally, ALS-FTD resembled the bvFTD-like pattern of damage both structurally and functionally, with, in addition, the structural ALS-cn-like damage in the motor areas. Although connectivity data alone cannot fully address the homogeneity or heterogeneity of this spectrum, our findings suggest a maladaptive role of functional rearrangements in ALS-ci/bi concomitantly with similar structural alterations compared to ALS-cn, supporting the hypothesis that ALS-ci/bi might be considered as a phenotypic variant of ALS, rather than a consequence of disease worsening.

Conclusions

Taken together, the results of the studies reported in this dissertation suggest that the assessment of network connectivity in the ALS/FTD spectrum by means of a

multiparametric MRI approach is useful in improving our understanding of the mechanisms that link protein deposition and consequent neuronal damage to motor and cognitive symptoms in these patients. In fact, we were successful in identifying neuroanatomical markers and potential predictors of aggressive disease progression in MND, mirroring progression through the motor system and the additional pathological involvement of extra-motor brain networks, which overlap with those involved in pure FTD presentations. At the same time, we demonstrated characteristic alterations of structural and functional brain networks in bvFTD and PPA syndromes, propagating from selective vulnerable regions (disease epicenters) in “target” networks to “off-target” connected regions (Seeley et al., Neuron 2009). We also succeeded in combining structural and functional MRI to detect brain signatures of damage related to pathological spreading across the continuum of ALS/FTD presentations, further characterizing genetic (e.g., *C9orf72* mutations) and cognitive overlap (i.e., ALS-ci/bi) between the two opposite ends of this spectrum. A more profound knowledge of such mechanisms will allow a better stratification of patients and an improved prognostic definition that will be vital in future clinical trials with disease modifying drugs.

References

- Agosta F, Pagani E, Petrolini M, Sormani MP, Caputo D, Perini M, Prella A, Salvi F, Filippi M (2010) MRI predictors of long-term evolution in amyotrophic lateral sclerosis. *Eur J Neurosci* 32: 1490-6
- Brettschneider J, Del Tredici K, Toledo JB, Robinson JL, Irwin DJ, Grossman M, Suh E, Van Deerlin VM, Wood EM, Baek Y, Kwong L, Lee EB, Elman L, McCluskey L, Fang L, Feldengut S, Ludolph AC, Lee VM, Braak H, Trojanowski JQ (2013) Stages of pTDP-43 pathology in amyotrophic lateral sclerosis. *Ann Neurol* 74: 20-38
- Buchanan CR, Pettit LD, Storkey AJ, Abrahams S, Bastin ME (2015) Reduced structural connectivity within a prefrontal-motor-subcortical network in amyotrophic lateral sclerosis. *Journal of magnetic resonance imaging : JMRI* 41: 1342-52
- Gorno-Tempini ML, Hillis AE, Weintraub S, Kertesz A, Mendez M, Cappa SF, Ogar JM, Rohrer JD, Black S, Boeve BF, Manes F, Dronkers NF, Vandenberghe R, Rascovsky K, Patterson K, Miller BL, Knopman DS, Hodges JR, Mesulam MM, Grossman M (2011) Classification of primary progressive aphasia and its variants. *Neurology* 76: 1006-14
- Mandelli ML, Welch AE, Vilaplana E, Watson C, Battistella G, Brown JA, Possin KL, Hubbard HI, Miller ZA, Henry ML, Marx GA, Santos-Santos MA, Bajorek LP, Fortea J, Boxer A, Rabinovici G, Lee S, Deleon J, Rosen HJ, Miller BL et al. (2018) Altered topology of the functional speech production network in non-fluent/agrammatic variant of PPA. *Cortex* 108: 252-264
- Phukan J, Elamin M, Bede P, Jordan N, Gallagher L, Byrne S, Lynch C, Pender N, Hardiman O (2012) The syndrome of cognitive impairment in amyotrophic lateral sclerosis: a population-based study. *J Neurol Neurosurg Psychiatry* 83: 102-8
- Raaphorst J, de Visser M, van Tol MJ, Linssen WH, van der Kooij AJ, de Haan RJ, van den Berg LH, Schmand B (2011) Cognitive dysfunction in lower motor neuron disease: executive and memory deficits in progressive muscular atrophy. *J Neurol Neurosurg Psychiatry* 82: 170-5
- Schuster C, Hardiman O, Bede P (2017) Survival prediction in Amyotrophic lateral sclerosis based on MRI measures and clinical characteristics. *BMC Neurol* 17: 73
- Seeley WW, Crawford RK, Zhou J, Miller BL, Greicius MD (2009) Neurodegenerative diseases target large-scale human brain networks. *Neuron* 62: 42-52

Spinelli EG, Agosta F, Ferraro PM, Riva N, Lunetta C, Falzone YM, Comi G, Falini A, Filippi M (2016) Brain MR Imaging in Patients with Lower Motor Neuron-Predominant Disease. *Radiology* 280: 545-56

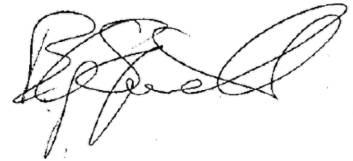
Westeneng HJ, Debray TPA, Visser AE, van Eijk RPA, Rooney JPK, Calvo A, Martin S, McDermott CJ, Thompson AG, Pinto S, Kobeleva X, Rosenbohm A, Stubendorff B, Sommer H, Middelkoop BM, Dekker AM, van Vugt J, van Rheenen W, Vajda A, Heverin M et al. (2018) Prognosis for patients with amyotrophic lateral sclerosis: development and validation of a personalised prediction model. *Lancet Neurol* 17: 423-433

Wolff M, Vann SD (2019) The Cognitive Thalamus as a Gateway to Mental Representations. *J Neurosci* 39: 3-14

7. ADDITIONAL PUBLICATIONS

1. Basaia S, Filippi M, **Spinelli EG**, Agosta F. White Matter Microstructure Breakdown in the Motor Neuron Disease Spectrum: Recent Advances Using Diffusion Magnetic Resonance Imaging. *Front Neurol*. 2019 Mar 5;10:193. doi: 10.3389/fneur.2019.00193. PMID: 30891004; PMCID: PMC6413536. *Review*.
2. Falzone YM, Radaelli M, Agosta F, Domi T, Guerrieri S, **Spinelli EG**, Pozzi L, Carrera P, Ferrari M, Comi G, Filippi M, Quattrini A, Riva N. Concurrence of NMOSD and ALS in a patient with hexanucleotide repeat expansions of C9orf72. *Amyotroph Lateral Scler Frontotemporal Degener*. 2019 Aug;20(5-6):449-452. doi: 10.1080/21678421.2019.1604761. Epub 2019 Apr 22. PMID: 31007077.
3. Filippi M, **Spinelli EG**, Cividini C, Agosta F. Resting State Dynamic Functional Connectivity in Neurodegenerative Conditions: A Review of Magnetic Resonance Imaging Findings. *Front Neurosci*. 2019 Jun 20;13:657. doi: 10.3389/fnins.2019.00657. PMID: 31281241; PMCID: PMC6596427. *Review*.
4. De Marchi F, Carrarini C, De Martino A, Diamanti L, Fasano A, Lupica A, Russo M, Salemme S, **Spinelli EG**, Bombaci A; SIgN. Cognitive dysfunction in amyotrophic lateral sclerosis: can we predict it? *Neurol Sci*. 2021 Jun;42(6):2211-2222. doi: 10.1007/s10072-021-05188-0. Epub 2021 Mar 27. PMID: 33772353; PMCID: PMC8159827. *Review*.
5. Santangelo R, Agosta F, Masi F, **Spinelli EG**, Cecchetti G, Caso F, Mandelli A, Cardamone R, Barbieri A, Furlan R, Magnani G, Filippi M. Plasma neurofilament light chain levels and cognitive testing as predictors of fast progression in Alzheimer's disease. *Eur J Neurol*. 2021 Sep;28(9):2980-2988. doi: 10.1111/ene.14999. Epub 2021 Jul 23. PMID: 34176186.
6. Scamarcia PG, Agosta F, **Spinelli EG**, Basaia S, Stojković T, Stankovic I, Sarasso E, Canu E, Markovic V, Petrović I, Stefanova E, Pagani E, Kostic VS, Filippi M. Longitudinal White Matter Damage Evolution in Parkinson's Disease. *Mov Disord*. 2021 Nov 22. doi: 10.1002/mds.28864. Epub ahead of print. PMID: 34806799.

7. Filippi M, Cecchetti G, **Spinelli EG**, Vezzulli P, Falini A, Agosta F. Amyloid-Related Imaging Abnormalities and Amyloid-Targeting Antibodies - A Systematic Review. *JAMA Neurol.* 2022 (in press). *Review.*

A handwritten signature in black ink, appearing to read 'E. G. Spinelli', located in the right-center of the page.